Site C0002[1]

H. Tobin, T. Hirose, D. Saffer, S. Toczko, L. Maeda, Y. Kubo, B. Boston, A. Broderick, K. Brown, A. Crespo-Blanc, E. Even, S. Fuchida, R. Fukuchi, S. Hammerschmidt, P. Henry, M. Josh, M.J. Jurado, H. Kitajima, M. Kitamura, A. Maia, M. Otsubo, J. Sample, A. Schleicher, H. Sone, C. Song, R. Valdez, Y. Yamamoto, K. Yang, Y. Sanada, Y. Kido, and Y. Hamada[2]

Chapter contents

Operations

Transit from Shimizu, Japan (port)

Integrated Ocean Drilling Program (IODP) Expedition 348 began on 13 September 2013 when the D/V *Chikyu* left the port of Shimizu en route for Site C0002. Typhoon Man-yi's approach on 14 September set the *Chikyu* into waiting on weather (WOW) status; the *Chikyu* remained in WOW until 16 September and then returned to Site C0002, arriving on 17 September. Upon return to Hole C0002F, the remotely operated vehicle (ROV) dove, and the seabed survey and transponder deployment was completed on 18 September. The ROV then checked the wellhead at Hole C0002G to observe the Long Term Borehole Monitoring System CORK.

Hole C0002M

The riser joints required pressure tests when the riser running equipment was rigged down to prepare for testing the small-diameter rotary coring barrel (SD-RCB) assembly, which continued until 19 September 2013. Although designated the "small-diameter" coring tool, the SD-RCB core is actually larger than standard RCB cores (7.3 versus 6.6 cm inner diameter [ID]); the bit itself has a smaller diameter (8½ inches versus the standard 10½ inch [or larger] drill bits) (see the **"Methods"** chapter [Tobin et al., 2015]). The guide horn was rigged up and the job completed by 20 September. The coring bottom-hole assembly (BHA) (Table **T1**) was made up on the rig floor and run into the hole (RIH) on 19 September. The *Chikyu* began drifting to the proposed well center, the center bit was dropped, and the BHA was washed down 30 m; Hole C0002M drilling began from 30.5 meters below seafloor (mbsf) (1996.5 meters below rig table [m BRT]). By 21 September, the BHA had drilled ahead to 475 mbsf, and coring began from that depth (Tables **T2, T3**), cutting 4 cores and ending at 512.5 mbsf (total depth [TD]). After coring operations were completed, 50 m^3 of kill mud (1.30 sg) was spotted in the hole, and the BHA was pulled out of hole and recovered to the surface on 22 September.

Hole C0002F

The riserless guide horn assembly rig down began, and the rig up for riser running started; the ROV dove to deploy 3 transponders. This was completed, and the *Chikyu* moved to the well center.

---

[1] Tobin, H., Hirose, T., Saffer, D., Toczko, S., Maeda, L., Kubo, Y., Boston, B., Broderick, A., Brown, K., Crespo-Blanc, A., Even, E., Fuchida, S., Fukuchi, R., Hammerschmidt, S., Henry, P., Josh, M., Jurado, M.J., Kitajima, H., Kitamura, M., Maia, A., Otsubo, M., Sample, J., Schleicher, A., Sone, H., Song, C., Valdez, R., Yamamoto, Y., Yang, K., Sanada, Y., Kido, Y., and Hamada, Y., 2015. Site C0002. *In* Tobin, H., Hirose, T., Saffer, D., Toczko, S., Maeda, L., Kubo, Y., and the Expedition 348 Scientists, *Proc. IODP,* 348: College Station, TX (Integrated Ocean Drilling Program). doi:10.2204/iodp.proc.348.103.2015

[2] **Expedition 348 Scientists' addresses.**

Pressure tests of riser joints continued until the risers and test plug were secured for another standby off Shionomisaki for WOW until 25 September. The *Chikyu* left Shionomisaki for the helicopter meeting point, for crew changes. The *Chikyu* then returned to the Site C0002 blow-out preventer (BOP) running point, 15 mi northwest of Site C0002, and prepared to run the BOP and riser. From 26 September 2013, the BOP was run down while low-pressure (300 psi) tests of the auxiliary line (kill and choke lines) began. The tests failed, so troubleshooting began, continuing with various connectors, riser joints, and other procedures. On 28 September, all lines passed low-pressure and high-pressure (5000 psi) tests. The BOP was landed on the BOP cart, and moonpool hoses were recovered for transit to Mikawa Bay on 29 September to pick up a repaired riser joint. The *Chikyu* reached the anchorage point on 30 September and, once loading was completed, returned to the Site C0002 BOP running point. On 1 October, however, the approach of Tropical Storm Fitow returned the *Chikyu* to WOW until the storm track and an unrelated weather front were observed. The logging-while-drilling (LWD) tools were loaded from the supply boat on 2 October during WOW.

Full operations resumed on 5 October. The BOP and riser were run, with subsea vibration data loggers for vortex-induced vibration (VIV) monitoring installed on slick joints. After running Joint 9 on 6 October, auxiliary line pressure tests were carried out. While running the BOP and riser, the ship drifted at 0.2 kt to Site C0002. The termination joint and last subsea vibration data loggers were installed on 9 October. BOP landing began after running the last sets of joints, on 10 October. The landing was successfully completed, followed by pressure tests of the 20 inch casing and wellhead connector.

On 11 October, a tropical depression developed into a typhoon and was predicted to approach the drill site. Therefore, the lower marine riser package (LMRP) was disconnected on 12 October, and the vessel moved to the stand-by site 17 mi north-northwest of Site C0002. WOW continued until Typhoon Wipha passed the site on 16 October, with the LMRP hung near the seafloor. Even after Typhoon Wipha passed, WOW continued because of the forecast of another strong typhoon reaching the area in a week. Therefore, riser pipe and LMRP recovery began on 16 October and continued to 19 October. The LMRP pick-up was suspended because of bad weather but was completed by 20 October. WOW continued until 25 October, when the *Chikyu* moved to the Site C0002 BOP running location. Typhoon Francesco's course was similar to that of Wipha and approached the site on 25 October; the *Chikyu* resumed operations on 26 October.

The LMRP was run into the water on 26 October, following the earlier procedure. A dummy landing was carried out when the vessel was 50 m west of Hole C0002F on 31 October. The vessel moved to the well center (1967.5 m BRT [1939 meters below sea level [mbsl]), and the LMRP was successfully landed on the BOP and locked by 31 October. After the BOP isolation test tool was run, Yellow BOP control pod (POD) pressure tests and Blue POD function tests of the BOP were conducted on 1 November.

The 17 inch LWD and GeoPilot BHA was made up and run in the hole on 2 November. Running the BHA in the hole while pumping and washing down continued until reaching the estimated top depth of the Number 2 shallow cement plug at 348.4 mbsf, but there was no indication of any decrease (45 kN) in weight on bit (WOB). The top of the Number 1 cement plug, however, was indicated by a clear decrease (15 kN) in WOB at 765.5 mbsf on 3 November. Drilling continued to 850.5 mbsf, and we conducted a pressure test of the 20 inch casing.

Hole C0002N

After circulation for hole cleaning, the sidetrack for Hole C0002N began at 860.3 mbsf on 4 November 2013. Sidetracking continued until the drilling inclination and azimuth reached 5° and 0°, respectively. On 5 November at 1191.5 mbsf, inclination was changed to 0°. Drilling continued to 1219 mbsf, followed by sweeping with 10 m^3 of Hi-vis mud. During drilling in Hole C0002N, several episodes of overpull continued to occur. On 7 and 8 November during pulling out of hole (POOH) for maintenance, two overpull intervals were observed: (1) 240 kN at 1632.5 mbsf and (2) 200–250 kN between 1579.5 and 1577.5 mbsf (Table T4). On 10 November, when the LWD BHA was POOH for WOW stand-by, overpull, drag, and slack intervals were observed:

- Drag (100–240 kN) between 2008.5 and 1404.5 mbsf,
- Overpull (320 kN),
- Slack (222 kN) at 1804.5 mbsf, and
- Drag (100–250 kN) from 1545.2 mbsf.

After TD (2330 mbsf) was reached on 13 November, POOH during a wiper trip had two overpull intervals: (1) >300 kN between 2330 and 2023.5 mbsf and (2) ~300 kN between 2023.5 and 1807.5 mbsf. On 14 November after two sets of Hi-vis mud sweeping at 2327.5 mbsf, POOH began with two overpull events:

(1) 2311.5 mbsf (400 kN) and (2) 2289.5 mbsf (500 kN). Pumping cleared these overpull intervals and no additional drag was observed.

Drilling paused on 9 November because the real-time measurement-while-drilling (MWD) signal was lost. After several attempts to recover the signal, the Operations Superintendent, Operation Liaison, and Expedition Project Manager agreed to continue drilling without real-time monitoring to 2008.5 mbsf. On 10 November, the LWD BHA was POOH to rig floor to remove the GeoPilot from the BHA, LWD memory data dumping, MWD pulser replacement, and mud-pump maintenance. The new 17 inch LWD BHA was run in the hole, and drilling resumed from 2008.5 mbsf on 11 November. Soon after, an active volume drop causing 48 m^3/h of mud loss at 2036.5 mbsf was observed. Lost circulation material (LCM) and Hi-vis mud were spotted and mud-loss rates decreased to 1 m^3/h by 12 November. Drilling resumed with another short interruption and spotting LCM due to reoccurring mud loss (27 m^3/h) at 2117.5 mbsf. POOH continued until the BHA reached the 20 inch casing shoe. The LWD BHA was run back to the bottom to check and clean the hole; washing and reaming continued until 14 November.

On 15 November, the LWD BHA was POOH to 836 mbsf and resumed after flow check and BOP function test. The LWD BHA was laid down, and LWD memory data were successfully downloaded. Preparations to run and cement the 13⅜ inch casing began. After troubleshooting the flush-mount grip spider and power tong, running casing continued all day. On 18 November, the casing hanger joint was picked up and the 13⅜ inch casing was run with 5⅞ inch drill pipe from 341.5 to 501.5 mbsf, and the insert was changed to 6⅝ inch drill pipe after taper seating against the primary elevator insert was checked. Running 13⅜ inch casing on the 6⅝ inch landing string continued to 1993.5 mbsf without observing significant drag.

While running the casing string, tight spots were encountered at 2014.5 and 2027.5 mbsf and a pressure buildup was observed; the pipe became stuck at 2024.5 mbsf. The casing was pulled up to 1993.5 mbsf after working the pipe slowly with overpull, but pack-off indication was observed. This continued while pulling back to 1802.5 mbsf, but on 19 November pressure and return flow rate returned to normal while pulling back to 1774.5 mbsf. At 1799.5 mbsf, the pump rate was increased to 50–100 strokes/min at pump pressure of 3.4–6.2 MPa to clean the annulus. Running casing resumed, although minor mud loss and tight spots were again encountered at 1954.5 mbsf. The tight spots were passed by increasing the flow rate; however, mud loss increased to 40 m^3/h after the flow rate was again reduced. Working pipes, adjusting flow rate, and spotting LCM were repeated without success to push the casing beyond 2041.5 mbsf due to mud loss up to 50 m^3/h. At the end, we decided to pull out the 13⅜ inch casing, shorten it, and run it again. POOH started on 20 November.

A new pressure-assisted drill pipe running tool assembly was made up and casing handling tools were rigged up on 21 November. Twenty-five joints of 13⅜ inch casing pipes were laid down, and running the shortened 13⅜ inch casing pipes began. No drag larger than 100 kN was observed while running to 1502 mbsf; however, minor mud loss (5–10 m^3/h) was observed at 1994.5 mbsf. Working pipes and increasing flow rate allowed the casing to pass these tight spots. Landing the casing hanger onto the wellhead was completed on 22 November. The bottom depth of the 13⅜ inch casing was 2010 mbsf. Cementing the casing was followed by a 5500 psi pressure test. The BOP's Blue POD function and pressure test was carried out successfully, ending on 24 November. Following in-line blowout protector and Hydrarack power swivel (HPS; National Oilwell Varco) rotary hose pressure tests, the 12¼ inch drill-out cement (DOC) BHA was made up and RIH. The cement top was tagged at 1897.7 mbsf on 25 November, although standby for WOW (cold-front passage) began. The drill string was pulled out to above the BOP, and mud in the riser was displaced with seawater. After WOW, operations resumed from displacing riser with 1.13 sg drilling mud. The top of cement was tagged again, circulated bottoms up, and rigged up for a casing pressure test. The pressure test was completed, and the test joint was rigged down to prepare for drilling out cement. On 27 November, drilling ahead confirmed the presence of cement at 2008.5 mbsf, and rig up for the shoe bond test began. The test was successful, pressurized to equivalent mud weight of 1.25 sg for 5 min. Drilling out cement recommenced, but when drilling reached 2028.4 mbsf, WOB and the HPS torque became unstable, fluctuating and suddenly increasing. It became clear that the pipe was stuck, and attempts to free the pipe by jarring began. Jarring was only paused for derrick inspection. The Schlumberger free point indicator tool (FPIT) was rigged up and run to survey for the drill string stuck point. The FPIT indicated that the stuck point was inside the 13⅜ inch casing, right above the Number 2 centralizer. The FPIT was recovered, and a dummy run of the back-off tool was run in hole on 29 November. The back-off tool planned to break the drill string above the Number 2 centralizer, between the Number 1 and 2 drill pipes. Wireline calibration with the casing collar locator (CCL) was used to correct the estimated colliding depth, as determined by wireline and drill pipe length. The back-off tool broke the drill pipe at 1886.35 mbsf, confirmed by torque changes (–37 to 0 kN/m) and a one-quarter rotation observed in the drill pipe at the rig floor. The colliding tool was recovered to the surface, and circulation with bottoms up was performed. The drill string was POOH to surface on 30 November, and the back-off point was confirmed and examined. No damage was observed on the bottom drill pipe pin connection, but the pipe joint was marked and removed from use. The fishing BHA was made up and run in hole, and by 1 December the fishing BHA reached and was screwed into the top of the fish. After pumping, checking hook load, and increasing torque, work continued on trying to work the stuck pipe. By 2 December, the fish had been jarred 724 times up and 173 times down. The Schlumberger FPIT was rigged up again and confirmed the free pipe measure to 1963 mbsf. A second FPIT run on 3 December confirmed a drill collar connection at 1969.88 mbsf. A dummy run with a 2.3 inch gauge also confirmed the drill collar connection. The back-off/colliding tool was prepared and RIH to 1960.58 mbsf, calibrated the firing depth with the CCL, and fired. The back-off tool was recovered to the surface, and free pipe was confirmed by monitoring hook load (4150 kN) after picking up 2 m. Circulation and bottoms up from 4 December was completed while the Schlumberger wireline tools were rigged down. The collided drill collar was recovered on deck on 5 December, and pin end examination of the drill collar found that the outer diameter had expanded by $\frac{9}{16}$ inch (8½ to $9\frac{1}{16}$ inches in size), while the pin thread was also expanded and cracked. A 12¼ inch BHA was made up and RIH to tag the top of the remaining fish; it tagged the top (slack off weight = 30 kN) at 1960.4 mbsf. The decision was made to kick off through the casing and begin a new sidetrack to continue drilling. The BHA was POOH to surface, after which a scraper BHA was made up and RIH.

The scraper BHA tagged the fish at 1960.5 mbsf and started scraping the interior of the casing. The BHA was POOH and laid down to rig up for wireline runs with the Schlumberger cement bond log tool began. The cement bond log tool was run on 7 December and surveyed between 1958.5 and 1299.5 mbsf, confirming cement to 1352.5 mbsf. A junk basket run recovered ~600 g of cement, after which the bridge plug/CCL wireline run was rigged up and RIH; the bridge plug was set at 1950 mbsf. The wireline running tool was recovered, and a flat-bottom mill BHA was made up and RIH to confirm the bridge plug setting depth. The mill BHA tagged the bridge plug at 1948 mbsf on 8 December. Circulation and bottoms up completed with POOH for the BHA. The slight discrepancy (~2 m) in bridge plug depths necessitated another run with the CCL wireline assembly, which was rigged up and RIH. The CCL tagged the bridge plug and confirmed the top of plug depth at 1949.5 mbsf. Wireline recovery and rig down was completed early on 9 December.

The next operation was a BOP pressure test, running ~11 successful pressure tests. The weather began to pick up, and at 0230 h a planned emergency disconnect sequence was successfully carried out. The vessel moved 1.1 mi north of the well center by 0700 h. After this, the HPS was dismantled for a magnetic particle inspection of the main shaft of the main power unit; inspection passed. The vessel at this point was 1.2 mi northwest of the Hole C0002F well center, and we began rigging up the riser running tool. The *Chikyu* began drifting to well center as the LMRP running and landing tools were made up and RIH. On 11 December, the vessel had reached well center and, guided by the ROV, landed the LMRP on the BOP. Riser running tools were rigged down and began to displace the riser with KNPP (KCl-NaCl/polymer/PPG) mud, finishing on 12 December. The BOP was pressure tested again. There was a short 1 h break to service the HPS on 13 December, and running into the hole continued. The top of the bridge plug was tagged at 1948.5 mbsf, circulation and bottoms up was completed, and the simulation BHA was POOH to surface. The whipstock assembly was made up and attached to the BHA and RIH. The whipstock BHA was set at 1945.5 mbsf on 14 December, and milling out the window in the 13⅜ inch casing began.

Hole C0002N mud program

A primary difference between riser operations and riserless drilling is the use of weighted mud to prevent wellbore failure and to balance or control formation pore pressures (e.g., Saffer, McNeill, Byrne, Araki, Toczko, Eguchi, Takahashi, and the Expedition 319 Scientists, 2010; Strasser, Dugan, Kanagawa, Moore, Toczko, Maeda, and the Expedition 338 Scientists, 2014). Continuous monitoring of mud weight, annular pressure, mud losses, and other circulation data during riser drilling can provide useful constraints on formation pore fluid pressure and state of stress (e.g., Zoback, 2007). Problems related to mud weight or hole collapse may impact successful drilling or casing of the borehole itself, as well as the ability to conduct downhole measurements or to achieve postdrilling scientific objectives including observatory installations and active source seismic experiments. Because riser drilling remains relatively new in IODP, we follow on recent proceedings from

IODP Expeditions 319 and 338 to describe key observations related to downhole (borehole) pressure, mud weight, and hole conditions while drilling Hole C0002N.

In general, mud weight is selected such that the pressure of the mud column in the borehole is sufficient to balance formation fluid pressure but remains below the fracture pressure (approximately equal to the least principal stress plus the tensile strength of the formation at a given depth). The initial mud weight for a section of hole is typically chosen on the basis of constraints on the fracture pressure from direct measurement by leak-off testing or extended leak-off testing at casing set points or from predrilling estimates based on models or seismic velocity information (e.g., Zoback, 2007). If mud weight is too low (an underbalanced condition), formation fluid may enter the borehole. This can be observed as "kicks" in mud gas or as increased annular pressure at times when pumping stops for pipe connections.

If mud weight is too high (overbalanced condition), the pressure of the mud in the borehole can cause fracturing of the formation and/or mud losses. The ensuing loss of circulation can reduce the effectiveness of cuttings circulation, potentially leading to pack-offs or hole collapse. If mud weight is too low, wellbore failure and cavings can lead to hole collapse and/or pack-offs; additionally, if the formation is overpressured, formation fluids can enter the borehole and lead to pressure or gas kicks.

In order to assess hole conditions, LWD annular-pressure-while-drilling (APWD) tools are commonly used, and the data are both recorded and pulsed to the surface in real time. The measured borehole pressures are typically reported both as absolute pressures (psig or equivalent) and as an equivalent circulating density (ECD; in g/cm^3), computed as the total pressure divided by the product of depth below a reference datum (e.g., the rig floor) and gravitational acceleration.

Mud program operations

After drilling out cement at the 20 inch casing shoe at 2840 m BRT (872.5 mbsf) and sidetracking, we drilled to 4297.5 m BRT (2330 mbsf) in riser mode. We collected MWD data, including APWD) during these operations, providing a direct measurement of mud pressure at the bit (Fig. F1). During drilling, the mud weight was 1.12 g/cm^3 in the upper part of the hole (to ~3640 m BRT) and was increased to 1.13 g/cm^3 from that depth to TD. Mud was sampled and tested regularly by a service company to confirm the mud weight and chemical composition going in to the riser and exiting after circulation up the annulus.

Over the interval from 2800 to ~3200 m BRT, the ECD computed from APWD measurements gradually increased from 1.144 to 1.162 g/cm^3 (Fig. F1B). Between ~3200 and ~3950 m BRT, ECD remained relatively constant and ranged between 1.156 and 1.164 g/cm^3, with a few peaks as high as 1.168 g/cm^3. At ~3950 m BRT, ECD increased sharply and remained between 1.17 and 1.18 g/cm^3 to TD. The increase in ECD at ~3950 m BRT corresponds to an increase in rate of penetration (ROP) from ~20 to 35 m/h for most of the section above and to ~45–50 m/h below. The pumping rate during drilling remained constant at ~950 gal/min.

The measured pressures correspond to values of ECD up to 0.05 greater than the nominal mud weight mixed at the surface, likely due to the combination of cuttings load in the annulus and dynamic pressures generated during drilling and pumping. Throughout drilling, annular pressure was consistently smaller than the lithostatic stress, but close to or slightly in excess of the leak-off pressure of ~1.15 g/cm^3 ECD determined from a leak-off test (LOT) conducted at 2841.5 m BRT during Expedition 338 (Strasser, Dugan, Kanagawa, Moore, Toczko, Maeda, and the Expedition 338 Scientists, 2014) (Fig. F1).

Large mud losses occurred on 11–12 November while drilling the lowermost ~300 m of the hole, including losses of up to 48 m^3/h when the bit depth was 4004 m BRT and up to ~15 m^3/h when bit depth was 4083 m BRT (Fig. F2). The first major mud loss was noted at ~2355 on 11 November, with an initial loss rate of 48 m^3/h during pumping (i.e., dynamic mud loss), which decreased to 15 m^3/h over ~30 min of circulation and drilling (Fig. F2A, F2B). Following this, mud losses were monitored after shutting the pumps off for ~20 min (static mud loss) and then during pumping at 400 gal/min. Both the static mud loss rate and the dynamic rate measured at 400 gal/min were 6 m^3/h. The ECD at the time of these mud losses ranged from 1.16 to 1.172 g/cm^3. After spotting LCM, the mud losses were significantly reduced to 1–5 m^3/h during drilling to 4083 m BRT. During this leg of the drilling, ECD ranged from 1.158 to 1.165 g/cm^3 with pumps off (for pipe connections) to 1.164–1.172 g/cm^3 during circulation and drilling ahead (Fig. F2C, F2D). In comparison, prior to the onset of mud loss, ECD was 1.15–1.16 g/cm^3 with pumps off and ~1.16–1.164 g/cm^3 while circulating. After additional mud losses were noted when the bit depth was 4083 m BRT, LCM was again added to the mud, mud loss stopped (<1 m^3/h), and drilling resumed. During drilling of the lowermost hole from 4083 to 4297 m BRT, ECD ranged from 1.167 g/cm^3 with pumps off to >1.17 g/cm^3 while circulating.

After drilling and cleaning the hole, we attempted to run and land a 13⅜ inch casing string to 4279.5 m BRT. However, while running the casing past ~3990 m BRT, large mud losses (45–50 m^3/h) occurred while circulating. Ultimately, the mud losses limited our ability to clear cuttings and cavings from the hole while lowering the casing by either increasing pumping rate or mud weight, and we pulled out of the hole and shortened the casing string.

Clear responses to mud losses in the riser hole were recorded in a long-term borehole observatory installed at Hole C0002G, located ~110 m west-southwest of Hole C0002N (Fig. F3) (Kopf, Araki, Toczko, and the Expedition 332 Scientists, 2011). These signals include changes in pore fluid pressure, tilt, and strain (Fig. F4) and provide additional constraints on the location and timing of the mud loss in the riser hole.

Discussion

The entire depth of the riser hole (2840–4297 m BRT) was drilled using a nominal mud weight (1.12–1.13 g/cm^3) less than, but near, the leak-off pressure at the 2840 m BRT 20 inch casing shoe (ECD of ~1.15 g/cm^3). The APWD data show that the pressure during circulation ranged from ~1.14 g/cm^3 to values as high as ~1.18 g/cm^3. For most of the hole, the difference in downhole pressure between drilling ahead (pumps on) and at pipe connections (pumps off) is consistently equivalent to a difference in ECD of ~0.01 g/cm^3 (Fig. F2). The remainder of the difference between the nominal mud weight and measured ECD can therefore be attributed to cuttings load. This component of the downhole pressure ranges from 0.014 g/cm^3 at the top of the riser hole (~2840–2950 m BRT) to ~0.04 g/cm^3 in the lower portion of the hole (Fig. F1).

The clear increase in ECD at ~3900 m BRT coincides with an increase in ROP and cuttings load in the annulus as described above. This is consistent with the general observation that increased ROP is associated with higher ECD, because for a constant pumping (circulation) rate of mud in the riser, a higher ROP will lead to a larger concentration of cuttings (Fig. F5). Thus, the increased ECD in this zone could simply be caused by a higher ROP associated with drilling through a weaker formation. It is also possible that formation overpressure could have contributed to both the increased ROP by weakening the rock and to the ECD by flow of fluid from the formation into the borehole. However, throughout drilling there is no evidence of ballooning or of fluid influx or gas kicks when pumps were shut down during pipe connections (Fig. F2). This suggests that formation overpressures exceeding the mud weight are unlikely.

Both static and dynamic mud losses incurred while drilling the interval from 4004 to 4083 m BRT indicate that the leak-off pressure was likely equivalent to an ECD of ~1.162 g/cm^3 (Fig. F2). Above this value, mud losses were observed, and when pumps were off, both mud and pressure losses were noted (Fig. F2A, F2B). At the time of maximum mud loss, pressure in the annulus decreased even while pumping (Fig. F2A). At circulating pressures below an ECD of ~1.155–1.16 g/cm^3, no losses were observed (Fig. F2E). After the addition of LCM, drilling at slightly higher pressures (corresponding to an ECD of 1.167–1.172 g/cm^3) was possible without substantial mud loss but was likely near or slightly above the leak-off pressure (Fig. F2C, F2D).

Pore-pressure monitoring in the Kumano Basin section and the uppermost accretionary wedge at the observatory Hole C0002G document a clear and rapid response to mud loss in the riser hole (Fig. F3). These responses include a gradual rise in pore pressure within both intervals following mud loss while drilling at 4004 and 4083 m BRT and a rapid rise in pressure following mud loss while running the 13⅜ inch casing. Increases in pressure following the mud losses while drilling are clear in both the Kumano Basin and upper accretionary prism intervals. The pressure history in the Kumano Basin monitoring interval is well fit by a transient pump-test model, consistent with small but continuous mud losses while drilling the interval from 4004 to 4083 m BRT. The pressure record in the upper accretionary prism follows a similar trend but is not as well fit by a simple pump-test model. A large pressure increase in response to mud loss during casing operations is observed only in the Kumano Basin monitoring interval. Following a sharp increase, the pressure decays and is mirrored by a gradual pressure rise in the accretionary prism monitoring interval.

Based on the rapid responses to mud loss in the riser hole observed in monitoring zones at 757–780 (in the Kumano Basin strata) and 937–980 mbsf (upper accretionary prism), we interpret that mud loss in the riser hole was localized at or near the casing shoe at 2840 m BRT. This is also consistent with the observation that pressure increased only in the Kumano Basin monitoring interval following mud loss during casing operations and with the expectation that the lowest leak-off point (LOP) pressure should be at shallow depth in the basin fill, where the horizontal principal stresses are less than the overburden. Together with the observed ECD at the time of mud loss, these observations suggest that mud loss was triggered by exceeding the LOP very slightly at the 2840 m BRT 20 inch casing shoe. After addition of LCM, drilling could continue at pressures slightly above the LOP without large losses.

Hole C0002P

Hole C0002P began at the top of the window, at 1936.5 mbsf. Milling out the casing window continued to 1954.5 mbsf, when dressing the window and reaming began. The window was checked to ensure that the drill string would pass through without hanging up. The drill string was then pulled up into the 13⅜ inch casing in preparation for a LOT. Two LOTs were set up and run to test the strength of the formation (see **"Downhole measurements"**). The tests were completed, and circulation began to increase mud weight to 1.18 sg. The milling BHA was POOH and laid down. The kick-off BHA was made up and run into the hole on 16 December 2013. Once at 1952.5 mbsf, the kick-off BHA began rotating and drilling out the 12¼ inch sidetrack hole. Mud weight was raised to 1.23 sg while the BHA was alternately rotated and slid forward to increase inclination and therefore offset from Hole C0002N. Drilling the kick-off continued, with one short stuck pipe incident at 1045 h on 17 December. Jarring broke the hold the formation had on the drill pipe, and it was freed. Reaming up to the casing window was completed, and then the drill string was pulled into the casing so that the drilling mud could be conditioned and weight increased to 1.28 sg. Drilling resumed, reaching 2067.7 mbsf on 18 December. A short 45 min period of stuck pipe occurred again, but the pipe was freed after another short session of jarring. The kick-off BHA was POOH to above the BOP because of rough weather; WOW continued until 19 December. The kick-off BHA was run back to the bottom on 20 December, and drilling resumed. The kick-off inclination reached up to 3.9° by 2107.5 mbsf (16.35 m above the bit) and then started to drop by 2162.5 mbsf. After sweeping out the hole with 10 m^3 of Hi-vis mud, the kick-off BHA was POOH to the rig floor on 21 December. The 10⅝ inch RCB BHA (Table T1) was run in the hole on 22 December. RCB coring ran from 22 to 24 December; the coring interval was 2163.0–2218.5 mbsf (6 cores; Tables T2, T3). The RCB BHA was POOH to the rig floor and laid down on 25 December. Routine BOP testing and HPS maintenance (25.5 h) were completed on 26 December before LWD operations began. The 12¼ inch LWD BHA was made up, RIH, and continued until 27 December. The hole was washed down from 2149.5 to 2152.5 mbsf, 10 m above the top of the coring interval, and then opened from 10⅝ to 12¼ inches over the coring interval with the MWD/LWD BHA. Drilling ahead with MWD/LWD continued on 28 December; however, when the bit depth reached 2263 mbsf, MWD data telemetry stopped. All attempts to resolve the problem failed; therefore, the OSI, Co-Chief Scientists, and EPM agreed to drill ahead without real-time monitoring from 0215 h on 28 December. Drilling resumed and proceeded to 2601.5 mbsf with relatively stable hole conditions by 29 December. A wiper trip back to 2148 mbsf found no excess drag. Drilling resumed and proceeded to 3058.5 mbsf by 31 December. The hole was swept out with 10 m^3 of Hi-vis mud, and a wiper trip to 2582.5 mbsf was conducted.

Hole C0002P also had hole condition problems: overpulls of 200 kN at 3000.5 mbsf and 250 kN at 2993.5 mbsf; HPS stall, partial pack-off, and bleed-off stand pipe pressure at 2944.5 mbsf; and two tight spots at 2755.5–2753.5 and 2716.5–2710.5 mbsf. Mud weight was increased from 1.28 to 1.30 sg to improve hole conditions, and a large amount of cavings was recovered on the shale shaker. While running the LWD BHA back to the bottom from 2582.5 mbsf, hole conditions worsened; the BHA stuck twice, once at 2973.5 and again at 3041.5 mbsf. Each time, the pipe was freed after dropping pumping pressure and working the drill pipe. Reaming downward continued, reaching 3058.5 mbsf by 1 January 2014; a heavy load of cavings continued to be seen on the shale shakers. The HPS stalled three times while working pipe to make connections, so mud weight was increased to 1.32 sg. While racking back stands during POOH, two overpull events were observed: 450 kN at 2980.5 mbsf and 200 kN at 1945.5 mbsf. After working the drill string, there was no more overpull past the same interval.

On 2 January, the LWD BHA was recovered on deck, and downloading memory data began. Gamma radiation, pressure while drilling, and resistivity were downloaded by 0545 h and XBAT data were recovered by 0615 h, but the AFR data recovery port was damaged, preventing data download, therefore requiring shipping to the Halliburton base in Thailand for data recovery.

Reaming out the open hole was the next phase in operations. The 14½ inch Anderreamer underreamer BHA, with no logging tools, was made up and RIH, passing the BOP and casing window with no indications of drag. The underreamer was activated and, after confirming activation, reaming the 12¼ inch hole to 14½ inches from 1963.5 mbsf began. Reaming down operations were occasionally paused for mud-pump maintenance. Hole opening continued, with no excess drag observed over the next several days of reaming. Traces of gas and cavings were encountered throughout this period of drilling. From 8

January, several episodes of HPS stalling at 2867.5 mbsf from heave increase were noted. The approach of a cold front weather system required another POOH for WOW to above the BOP for standby. The cold front passed, and WOW continued until 9 January. Between 0930 and 2045 h on 10 January, drillers reamed up and down 9 times between 2877.2 and 2907.2 mbsf, with frequent HPS stalls, tight spots, and one hole pack-off at 2902.5 mbsf. The pack-off initially had no mud return, but continuous working the pipe and reduction in pumping pressure first resulted in a gradually strengthening return; HPS speed was increased and the pipe was confirmed freed by 1500 h. Backreaming from 2879.5 to 2849.5 mbsf and then again reaming down through 2879.5–2906.5 mbsf while circulating mud resulted in a decrease in cuttings volume and also a stabilization in HPS torque. Hole opening resumed from 2045 h with a 2 h pause from 2330 h to perform more maintenance on the Number 1 mud pump. Hole opening resumed from 0130 h on 11 January, opening the hole from 2912.5 to 2960.5 mbsf. The hole packed off at 0645 h while reaming up to 2934.5 mbsf, but the drill string was freed by 0715 h. Another pack-off occurred at 1345 h when back down at 2960.5 mbsf and was freed by 1530 h. Sweeping out the hole with 40 m^3 of Hi-vis mud was carried out in three sessions between 1530 and 2115 h. At that point, troubleshooting the HPS torque wrench was required after the torque wrench die slipped while trying to break a connection between the saver sub and the drill pipe. Once fixed, the drill string was POOH to 2728.5 mbsf. Drag was observed while pulling out to 2936.5 mbsf, but no stuck pipe incidents occurred. The Anderreamer underreamer BHA was recovered on deck on 12 January; examination of the reamer cutters found excessive wear and damage. The BHA was laid down, and a new underreamer BHA was rigged up and RIH. After a short pause to cut and slip the drilling line, the BHA was RIH on 13 January. Once reaching 1957.5 mbsf, the Anderreamer was activated. A series of issues with the mud pumps started impacting drilling, with frequent pauses in drilling to swab out and replace cylinders of the mud pumps. Reaming down resumed and by 14 January had reached 2960.5 mbsf. Hole opening had progressed 4 m when the hole packed off, leaving the drill pipe stuck in the hole. Operations to free the pipe began immediately, pumping Hi-vis mud downhole more than 8 times. Attempts to fire the jars met with no success, leading the drillers to speculate that the stuck point was located above the jars in the hole. A 1 h pause to swab and change the Number 1 and 2 cylinder of the Number 2 mud pump was followed by more attempts to free the drill pipe. Spotting 6 m^3 of clean lube at 1800 h was again followed by working the pipe near maximum overpull. It was noticed that the overpull began to decrease with each attempt, and after setting the tension to neutral and applying 30 kNm of torque, the pipe was freed. Sweeping the hole began and circulation and bottoms up was finished by 15 January. The BHA was pulled back to 1928.5 mbsf for a series of wiper trips; no excess drag was observed while passing through the 13⅜ inch casing window. From 0830 to 1915 h, reaming advanced without much trouble, until taking 160 kN WOB at 2925.5 mbsf. Reaming to 2964.5 mbsf encountered numerous tight spots before reaching 2964.5 mbsf by 2130 h. Circulation and bottoms up to clean the hole began and continued until 16 January. Hi-vis mud (30 m^3) was spotted, and the underreamer was POOH to surface. The mechanical jar, Anderreamer underreamer, float sub, and bit were laid down by 1800 h.

It was decided to end reaming and drilling and move ahead with running and cementing the 11¾ inch liner casing. Rig up continued until 18 January, when the liner was run to 966.5 m MSL while setting the guide shoe joint, float collar joint, landing collar joint, and the 3.5 inch ball in the float collar joint. The 11¾ inch liner casing hanger and packer assembly were picked up and made to the casing joints. No drag was observed while running casing to 2922.5 mbsf. Slack was checked and weight picked up before circulating after breaking pipe to drop the 1¾ inch ball. Setting the liner hanger began when the 2¼ inch ball was dropped and chased; the first three attempts to set the hanger failed. After picking up 1 m and applying pressure, confirmation that the setting tool had released the hanger was made. Attempts to circulate failed, with no mud return; the liner-casing packer had accidentally set during the attempts to set the hanger. Pressure tests confirmed that the annulus pressure was holding (up to 7.8 MPa), and there was no communication with the formation below. Two LOTs were performed; the second ended in an injection test. The liner packer was pressure tested at 5000 psi for 5 min and then at 4000 psi for 15 min; both tests passed. After the LOTs, the liner hanger running tool was POOH to surface, laying out the cement stand on 19 January. A cement diverter assembly was made up and RIH and passed through the top of the 11¾ inch liner without taking any drag. The first of 2 cement "squeezes" was completed early on 20 January, pumping 120.5 bbl of cement. The second began from 0500 h and pumped a total of 94 bbl of cement. Once completed, the diverter was circulated clean, and then POOH to 1632.5 mbsf when 7.9 m^3 of Hi-vis mud was spotted. Once the circulation was complete, the diverter assembly was POOH to surface. The cement plug was pressure tested on 21 January.

Preparations to recover the risers began, and the Blue POD on the BOP was unlatched and the BOP disconnected from the wellhead on 22 January, while the ROV dove to set the corrosion cap and recover transponders. Riser joint recovery operation began once the vessel was 50 m offset from Hole C0002F well center. By 23 January, the gooseneck and termination joints had been recovered and riser joints proper began to be recovered as the vessel continued to drift north-northwest. The BOP was recovered and set on the BOP cart over the moonpool by 25 January. The ROV dove to complete transponder recovery. Once complete, the ROV was recovered to the surface, while riser-handling tools were rigged down. The riser tensioners were tested on 27–28 January while general rig equipment services were performed. The *Chikyu* left the site on 29 January for facilities in Irago, Aichi Prefecture, Japan.

Lithology

Evaluation of lithology was conducted on core samples from Holes C0002M (475–512.5 mbsf) and C0002P (2163–2217.5 mbsf), as well as observations on cuttings from Holes C0002N (875.5–2325.5 mbsf) and C0002P (1965.5–3058.5 mbsf). Based on the integration of geological, geophysical, geochemical, and LWD data available from the cores and cuttings, together with the results from previously drilled Holes C0002A (Expedition 314 Scientists, 2009), C0002B (Expedition 315 Scientists, 2009), C0002F, C0002H, C0002I, C0002K, and C0002L (Strasser et al., 2014b), we identified four lithologic units and seven subunits (Fig. F6; Table T5). Units III–V were previously defined based on the evaluation of cuttings from Hole C0002F (Strasser et al., 2014b).

Hole C0002M

Four cores were recovered in Hole C0002M between 475 and 512.5 mbsf, with an average core recovery of ~43.8% (see "Operations"). Based on comparisons with core descriptions from Holes C0002B (Expedition 315 Scientists, 2009), C0002K, and C0002L (Strasser et al., 2014b), the cored interval (475–512.5 mbsf) is situated in the previously defined lithologic Unit II.

Lithologic variation description

The dominant lithology in Hole C0002M is greenish gray silty claystone. Minor lithologies include thin interbeds of silty sandstone and siltstone (Fig. F7). The silty claystone is typically homogeneous. No major sedimentary structures were identified, but locally horizontal to gently inclined plane-parallel laminae and incipient fissility were observed (Fig. F8). The silty interbeds are usually <5 cm thick and show normal grain size gradation, fining upward to silty claystone. Their bases are defined by sharp surfaces (locally erosive), and their tops are diffuse. Such features are typical of fine-grained turbidites.

A siliciclastic assemblage of clay, silt, and sandstone dominates with quartz and feldspar as main minerals. Minor grains include micas (biotite and muscovite), glauconite, volcanic glass, and an extensive diversity of dense minerals, based on smear slide observations (Figs. F9, F10; also see Site C0002 smear slides in "Core descriptions"). Lithic fragments are generally observed but are most abundant in the sandy siltstone. Carbonate is primarily present in the form of nannofossils, foraminifers, and silt-size anhedral calcite. Organic matter is seen throughout the cores and is locally observed as <2 mm nodules, commonly pyritized.

Mineralogical and geochemical analyses

X-ray diffraction (XRD) patterns show average total clay content of 51 wt%, quartz content of 26 wt%, and feldspar content of 20 wt% (Fig. F11; Table T6). Calcite abundance determined by XRD is generally present in low amounts of 3 wt% on average; however, three samples show relatively high contents of up to 15 wt%. A comparison of all XRD data including cuttings and core in Holes C0002B, C0002F, C0002K, C0002L, C0002H, and C0002M is shown in summary Figure F12.

X-ray fluorescence (XRF) analyses performed on 11 samples do not show specific trends (Table T7). Average values for this data set are

Na_2O = 2.37 wt%,
MgO = 2.30 wt%,
Al_2O_3 = 16.57 wt%,
SiO_2 = 63.63 wt%,
P_2O_5 = 0.14 wt%,
K_2O = 3.13 wt%,
CaO = 4.10 wt%,
TiO_2 = 0.72 wt%,
MnO = 0.08 wt%,
Fe_2O_3 = 6.39 wt%, and
Loss on ignition (LOI) = 7.8 wt%.

A comparison of all XRF data of cuttings and core in Holes C0002F, C0002K, C0002L, C0002H, and C0002M is shown in summary Figure F13.

Biological features

Calcareous nannofossils are abundant throughout the cored interval (Fig. **F9**). Foraminifers, diatoms, and fragmented siliceous bioclasts (including sponge spicules and radiolarians) occur in trace amounts. Bioturbation of moderate severity was observed throughout the sequence, but no particular trace fossil could be identified (Fig. **F8**). Mottled textures, small (millimeter scale) burrows filled with sandy material, and disturbed bedding are the most common bioturbation features. A few networks of burrows are well imaged in the X-ray computed tomography (XRCT) images.

Authigenic components

Few authigenic components were identified in the silty claystone. Pyrite is widely distributed through the cores, occurring as framboids, and in the above-noted <2 mm nodules of organic matter (Sections 348-C0002M-1R-2, 16 cm; 1R-2, 117 cm; and 4R-3, 86 cm) (Fig. **F10**). Pyrite precipitation was also observed along a 5.5 cm vein in interval 348-C0002M-1R-2, 11–16 cm.

Interpretation

Lithologic Unit II was previously interpreted as the lower forearc succession of the Kumano Basin, dominated by the hemipelagic mud of distal turbidites (Expedition 315 Scientists, 2009; Strasser et al., 2014b). The four cores recovered from Hole C0002M are in agreement with this interpretation. Strasser et al. (2014b) suggested the presence of two coarsening-upward packages of thin turbidites between 480 and 460 mbsf and from 460 mbsf to the top of Unit II. The more common occurrence of slightly coarser sand interbeds in the upper Hole C0002M core sections may correspond to the proposed lower cycle.

Holes C0002N and C0002P

The lithologic unit and subunit boundaries determined in cuttings from Holes C0002N and C0002P are defined primarily on the basis of variations in percent sandstone versus percent silty claystone (Fig. **F14;** Table **T8**). Figures **F15, F16, F17, F18,** and **F19** show representative lithologies and mineralogy as seen in the cuttings.

In Holes C0002N and C0002P, three units and seven subunits were defined. Hole C0002N was drilled between 860.5 and 2330 mbsf, and Hole C0002P was drilled between 1965.5 and 3058.5 mbsf. Lithologic units and subunits in Hole C0002N are in agreement with the boundaries determined during Expedition 338 in Hole C0002F (Strasser et al., 2014b), with few minor offsets in specific boundary depths that can be explained by the mixing of cuttings due to the usage of the underreamer in Hole C0002F (Strasser et al., 2014b) and/or the steep bedding.

Unit III (lower part of Kumano forearc basin)

Interval: cuttings Samples 348-C0002N-3-SMW through 24-SMW
Depth: ~875.5–975.5 mbsf
Lithology: greenish gray silty claystone

Hole C0002N drilling began within Unit III below the 20 inch casing shoe (860.3 mbsf), with collection of cuttings samples starting at ~875.5 mbsf (Sample 348-C0002N-3-SMW). The base of Unit III was first defined in Hole C0002A by LWD data (Expedition 314 Scientists, 2009) and by core and seismic integration at 915.5 mbsf (Expedition 315 Scientists, 2009). In Hole C0002F (Strasser et al., 2014b), the lithologic boundary is at 1025 mbsf. In Hole C0002N, the lithologic boundary is at 975.5 mbsf (Sample 24-SMW), with the first occurrence of sand and changes in mineralogy (Fig. **F14;** Table **T5**). The LWD boundary is set at 915 mbsf (see **"Logging"**). The discrepancies between the lithologic boundaries observed during Expeditions 338 and 348 are most likely due to the usage of the underreamer during Expedition 338, the relative uncertainty of cuttings descriptions, and the steep bedding as detected in LWD data.

Between 875.5 and 915.5 mbsf (Samples 3-SMW through 12-SMW), cuttings consist of ~40% fragments of cement derived from the earlier well completion (Strasser et al., 2014b) (Fig. **F14**). The cement contamination decreases with depth and disappears at 965.5 mbsf (Sample 22-SMW). A more detailed description of cement contamination in cuttings is in "Physical properties" in Strasser et al. (2014b).

The lithology in the formation cuttings is greenish gray silty claystone (Fig. **F15;** Table **T8;** also see macroscopic descriptions in VCDSCAN in **"Supplementary material"**). Locally, trace amounts of very fine, loose sand occur, some of which could also be disaggregated cement pieces. The silty claystone is semiconsolidated (i.e., compacted, but mechanically weak). In terms of mineralogy, quartz is the dominant mineral, glauconite minerals are present, and fossils are absent to rare and some are pyritized (Fig. **F17A**).

Unit IV (upper accretionary prism)

Interval: cuttings Samples 348-C0002N-24-SMW through 175-SMW
Depth: 975.5–1665.5 mbsf
Lithology: dominant greenish gray silty claystone, minor sandstone

In Hole C0002N, the Unit III/IV boundary is defined by the first occurrence of sandstone at 975.5 mbsf. In Hole C0002B (Expedition 315 Scientists, 2009), the Unit III/IV boundary is defined in cores by a relatively abrupt change in structural style and a shift in lithology from condensed silty claystone above to underlying interbeds of silty claystone, siltstone, and very fine to fine sandstone. In Hole C0002F (Strasser et al., 2014b), the Unit III/IV boundary is also defined by the first occurrence of sandstone, albeit in very small amounts, at 1025.5 mbsf (Sample 338-C0002F-45-SMW). The difference between Holes C0002F and C0002N likely occurs because of simultaneous drilling by the bit and the underreamer tool during Expedition 338 (see "X-ray diffraction mineralogy" and "Operations" in Strasser et al., 2014b). Another explanation could be the steep bedding of the rock formation.

Within Unit IV, five subunits are defined on the basis of the occurrence and absence of sand and sandstone (Fig. F14; Table T1). This is in accordance with LWD data interpretations and is consistent with the boundaries defined during Expedition 338 (Strasser et al., 2014b). Increasing and decreasing sand content characterizes the following subunits:

- Subunit IVA: 975.5–1045.5 mbsf (Samples 348-C0002N-24-SMW through 39-SMW).
- Subunit IVB: 1045.5–1125.5 mbsf (Samples 39-SMW through 54-SMW).
- Subunit IVC: 1125.5–1345.5 mbsf (Samples 54-SMW through 107-SMW).
- Subunit IVD: 1345.5–1525.5 mbsf (Samples 107-SMW through 146-SMW).
- Subunit IVE: 1525.5–1665.5 mbsf (Samples 146-SMW through 175-SMW).

In Subunit IVA, the dominant lithology is greenish gray silty claystone with sandstone as a minor lithology (Fig. F15; Table T8; also see macroscopic descriptions in VCDSCAN in "Supplementary material"). The silty claystone is semiconsolidated, and the cuttings shapes are subangular to angular. Sandstone cuttings are generally loose or very weakly consolidated (i.e., soft). Their typical shape is round to subangular. Loose quartz grains are the dominant component in the dispersed >63 µm sand-sized fraction.

The main mineralogy in Subunit IVA can be summarized as follows (Fig. F17A):

Quartz = dominant.
Feldspar = few.
Lithic fragments = few to common.
Mica = absent.
Volcanic glass = rare to common (but mostly as a few grains).
Pyrite = common.
Organics (including wood) = common.
Fossils = rare.

In Subunit IVB, the major lithology is greenish gray silty claystone. Only few grains of loose sand were detected in this subunit, in contrast to the description for Hole C0002F in which ~30% sand was observed (Strasser et al., 2014b). In Subunit IVC, the major lithology is greenish gray silty claystone (average = ~70%), and the minor lithology is loose sand (average = ~30%). In Subunit IVD, the major lithology is greenish gray silty claystone (average = ~65%). In Subunit IVE, the major lithology is greenish gray silty claystone showing a progressive increase in the amount of sand with depth. Mineralogy in Subunits IVB–IVE can be summarized as follows (Fig. F17A):

- Pyrite decreases from few in Subunits IVB–IVD to rare in Subunit IVE.
- Organic material/wood/lignite is common to locally abundant in Subunits IVB–IVD and decreases to few in Subunit IVE.
- Fossils are rare in all subunits.
- Glauconite is rare in Subunits IVB and IVC and is absent in Subunits IVD and IVE.

Examples of some of these minerals are shown in Figure F18.

Unit V (trench or Shikoku Basin hemipelagic deposits)

Intervals: cuttings Samples 348-C0002N-175-SMW through 327-SMW and 348-C0002P-9-SMW through 300-SMW
Depths: Hole C0002N = 1665.5–2330 mbsf; Hole C0002P = 1965.5–3058.5 mbsf
Lithology: dominant greenish gray silty claystone and fine silty claystone; minor fine sandstone

Unit V was drilled in Holes C0002N and C0002P. In Hole C0002N, the Unit IV/V boundary is defined by a lithologic change from sand and sandstone to silty claystone between 1655.5 and 1677.5 mbsf (Samples 348-C0002N-173-SMW through 177-SMW). In Hole C0002F (Strasser et al., 2014b), the Unit IV/V transition is a gradual decrease of sand, with its complete disappearance at the base of this interval.

In Hole C0002N, only Subunit VA was drilled within Unit V (Fig. F14; Table T5). Based on macroscopic observations of cuttings in Hole C0002N, Subunit VA is composed almost entirely of greenish gray silty claystone with a minor mineralogy of gray sandstone (Fig. F16; Table T8; also see macroscopic descriptions in VCDSCAN in "Supplementary material"). The silty claystone is semiconsolidated, and cuttings shape is subangular to angular. The >63 µm sand-sized fraction (Fig. **F17A**) contains quartz as the dominant mineral. Feldspar decreases from common to few with depth, lithic fragments are few, mica is rare to absent, volcanic glass is always rare, pyrite is common at the top of Subunit VA and then decreases to few, wood is mostly few and only locally common, and fossils are rare and become few at 1955.5 mbsf (Sample 274-SMW). Where present, fossils are commonly pyritized (Figs. **F17A, F18**). Glauconite is always rare.

Within Unit V in Hole C0002P, two subunits (VA and VB) were drilled. The subunits are defined on the basis of the occurrence of sandstone, silty claystone, and fine silty claystone observed in the cuttings (Fig. **F14;** Table **T5**):

- Subunit VA: 1960.5–2625.5 mbsf (Samples 348-C0002P-9-SMW through 200-SMW).
- Subunit VB: 2625.5–3058.5 mbsf (Samples 200-SMW through 300-SMW)

Between 1965.5 and 2015.5 mbsf (Samples 9-SMW through 28-SMW), cuttings consist of 30%–10% fragments of cement derived from sidetracking the well through the cemented casing. Cement contamination decreases with depth and disappears at 2025.5 mbsf (Sample 28-SMW). However, metal pieces from milling the casing persist in the samples downhole to 2195.5 mbsf (Sample 81-SMW).

In Hole C0002P, Unit V is dominated by greenish gray to medium gray silty claystone with minor amounts of sandstone (Figs. **F14, F16;** Table **T8;** also see macroscopic descriptions in VCDSCAN in **"Supplementary material"**). The silty claystone is locally firm to hard, and cuttings shapes are subangular to angular throughout. The sandstone is fine-grained and friable but locally also consolidated (cemented). Silty claystone alternates with several sandstone packages until 2625.5 mbsf. Below this depth, sandstone is observed in very small amounts. From 2360.5 mbsf, the fine-grained content increases in the silty claystone, providing a much finer texture. At 2625.5 mbsf, fine silty claystone is the dominant lithology. This depth marks the Subunit VA/VB boundary based on the observed change into a finer grained silty claystone and scarcity of sandstone interbeds. In Subunit VB, the fine silty claystone is sticky at certain depths, especially when wet (hygroscopic behavior). Few hard pieces of lithified fine silty claystone are observed throughout Unit V. These commonly exhibit polished internal shear surfaces with slickenlines and incipient fissility (see **"Structural geology"**).

The >63 µm sand-sized fraction (Fig. **F17B**) shows quartz as the dominant mineral, with feldspar decreasing from abundant to common/few with depth and few micas. Lithic fragments are rare until 2350 mbsf and are not observed below that depth. Volcanic glass is locally observed but always in small amounts (rare to few). Glauconite is rarely observed and was generally not detected below 2550 mbsf.

Smear slide observations

In Hole C0002N, 148 smear slides made from cuttings were examined at 10 m sampling intervals (Figs. **F18, F19;** also see Hole C0002N smear slides in SMEARSLD in **"Supplementary material"**). Quartz grains are common throughout the cuttings. Micas and heavy minerals are estimated to be few in Unit III and at certain depths within Subunit VA. Carbonate minerals are common in Unit III and Subunit IVC and are commonly observed in the upper part of Unit III, most likely because of cement contamination of the uppermost 100 m (20%–40% of Sample 348-C0002N-3-SMW to 1%–3% of Sample 24-SMW). Clay mineral clusters are dominant throughout the hole. Volcanic glass is generally scarce to common but is not observed in the lower part of Subunit VA (Samples 213-SMW through 241-SMW and 302-SMW through 327-SMW). Pyrite is commonly observed in Units III and IV and decreases slightly in Unit V. Glauconite is locally rare in Unit III and between Subunits IVD and VA. Sedimentary lithics are common throughout, and volcanic lithics are rarely observed in Unit V. Nannofossils, foraminifers, and diatoms are abundant in Unit III to Subunit IVC (Samples 5-SMW through 101-SMW) but are rarely seen in Subunits IVD–VA. Organic matter abundance generally decreases with depth.

In Hole C0002P, 115 smear slides were examined (Fig. **F19;** also see Hole C0002P smear slides in SMEARSLD in **"Supplementary material"**). Quartz is common to abundant throughout the drilled interval. Heavy minerals are rare to scarce at all depths. Carbonate minerals are common in Subunit VA but less so in Subunit VB. Clay minerals are usually abundant to dominant at all depths. Volcanic glass and volcanic lithics vary between few and common but are locally not observed. Pyrite is few to common at all depths. Sedimentary lithics are common to abundant. Organic matter is few to common throughout the hole.

Mineralogical and geochemical analyses

X-ray diffraction analysis

Bulk powder XRD results show the relative abundance of total clay minerals, quartz, feldspar, and calcite (Fig. **F12;** Table **T9**). Summary Figure **F12** shows XRD data of cuttings from the 1–4 mm size fraction of Holes C0002F (Strasser et al., 2014b), C0002N, and C0002P, together with core data from

Holes C0002B (Expedition 315 Scientists, 2009) and C0002H, C0002J, C0002K, and C0002L (Strasser et al., 2014b). In cuttings from Holes C0002N and C0002P, no significant differences in lithology are observed between the 1–4 and >4 mm cuttings size fractions; consequently, we use only cuttings from the 1–4 mm size fraction for further documentation, which is also in line with standard oil industry cuttings routines.

In Hole C0002N, XRD data were routinely measured starting at 875.5 mbsf (Sample 348-C0002N-3-SMW). The uppermost few measurements still show contamination by cement based on the relative high weight percentage of calcite, especially in the >4 mm size fraction. We observe a gradual increase between 875.5 and 1025.5 mbsf (Samples 3-SMW through 34-SMW) in total clay, quartz, and feldspar, as well as a large decrease in calcite from ~39 to 0.1 wt%. Because of this gradual change, together with the first occurrence of sandstone, the Unit III/IV boundary is defined at 975.5 mbsf (Sample 24-SMW). A corresponding boundary is defined in LWD data at ~915 mbsf (see **"Logging"**), whereas Expedition 315 observed an abrupt reduction in calcite content at the discordance at 922 mbsf (Expedition 315 Scientists, 2009). This shift was explained during Expedition 315 as an abrupt change of the depositional site from below (Unit IV) to above the carbonate compensation depth (Unit III). Similar but more gradual shifts in calcite content were also recorded at Ocean Drilling Program Sites 1175 and 1176 (Shipboard Scientific Party, 2001a, 2001b; Underwood et al., 2003).

In Hole C0002N, Unit IV shows two cycles of decreasing and then increasing total clay content downhole that correspond reasonably well to the subunit boundaries (Fig. **F12**). The amount of quartz (weight percent) increases slightly and then decreases in Subunits IVD and IVE. Feldspar shows similar changes as quartz throughout Unit IV. Calcite content determined by XRD generally remains low (~0.1 wt%) in Subunit IV, with a slight increase in Subunits IVC and IVD.

The Unit IV/V boundary at 1665.5 mbsf (Sample 175-SMW) is associated with a downhole increase in total clay content and a slight decrease in feldspar in Subunit VA. Quartz remains constant in Subunit VA, whereas calcite decreases from 2.3 to 0.1 wt% until 1885.5 mbsf (Sample 226-SMW), where it increases again to an average of ~4 wt% before decreasing at 1955.5 mbsf (Sample 239-SMW) to an average of ~0.1 wt%. Total clay and feldspar contents slightly decrease and then increase several times. Quartz content slightly increases and then decreases.

In Hole C0002P, cuttings samples were routinely analyzed starting at 1965.5 mbsf (Sample 348-C0002P-9-SMW) and overlap with Hole C0002N to 2325.5 mbsf (Sample 129-SMW). Total clay, quartz, feldspar, and calcite contents correlate well between Holes C0002P and C0002N in this overlap interval. Total clay starts decreasing from 2325.5 to 2425.5 mbsf (Sample 155-SMW), whereas both quartz and feldspar slightly increase. Between 2425.5 and 2705.5 mbsf (Sample 219-SMW), total clay content increases again. Quartz and feldspar contents remain approximately the same. Between 2705.5 and 2945.5 mbsf (Sample 273-SMW), total clay content decreases first and then starts to increase from 2825.5 mbsf (Sample 247-SMW), whereas quartz and feldspar have exactly the opposite trend compared with total clay. Calcite content still remains low at ~0.1 wt% throughout the whole depth range.

X-ray fluorescence

In order to characterize compositional trends in Holes C0002N and C0002P, XRF analysis was undertaken on cuttings samples (Fig. **F13;** Table **T10**). Major and minor element contents (SiO_2, Al_2O_3, CaO, K_2O, Na_2O, Fe_2O_3, MgO, TiO_2, P_2O_5, and MnO) were analyzed and complemented by LOI measurements. To compare the composition of cuttings sizes, both 1–4 and >4 mm cuttings size fractions were analyzed, with no significant differences, except for K_2O (the >4 mm fraction shows a higher content than the 1–4 mm fraction) and MgO (the 1–4 mm fraction slightly exceeds the >4 mm fraction downhole to 1200 mbsf). Therefore, further analysis of Holes C0002N and C0002P only involved the 1–4 mm cuttings size fraction.

The compositional changes observed in the upper intervals of both Holes C0002N and C0002P are mainly due to the mixing of cement with formation. Based on CaO content, the lowest depth of cuttings contaminated by cement may be at ~955.5 mbsf in Hole C0002N (Sample 348-C0002N-20-SMW) and ~2045.5 mbsf in Hole C0002P (Sample 348-C0002P-32-SMW). Results for MnO are not shown because of the very small weight percentages. LOI within the zone of cement contamination shows 17.8 wt%, and such samples are not used in assessing averages.

In Hole C0002N below the cement contamination, CaO remains fairly constant (>3.0 wt%) throughout the profile. LOI and P_2O_5 decrease from Unit III to IV, whereas SiO_2, Al_2O_3, K_2O, Na_2O, Fe_2O_3, MgO, and TiO_2 increase. Most of the elements do not change significantly in Unit IV. Slight decreases in LOI and MgO are visible in Subunits IVD and IVE. LOI, Al_2O_3, Fe_2O_3, MgO, TiO_2, and K_2O decrease at the boundary between Units IV and V, and P_2O_5 and SiO_2 increase. K_2O increases throughout Unit V, whereas Na_2O content slightly decreases. TiO_2 increases slightly, but for the other elements the average values are about the same in Units IV and V. At the Subunit VA/VB boundary, there is a small offset in all the elements. In Subunit VA, MgO slightly increases and then decreases. K_2O increases slightly, whereas the other elements seem constant. No significant changes are visible for most of the elements, except that there is a slight offset for Al_2O_3, Fe_2O_3, and MgO. The averages throughout Units IV and V are

MgO = 2.19 wt%,
Al_2O_3 = 16.06 wt%,
SiO_2 = 65.44 wt%,
P_2O_5 = 0.09 wt%,
CaO = 3.03 wt%,
Fe_2O_3 = 5.44 wt%, and
LOI = 7.33 wt%.

In Unit IV, the averages are

K_2O = 3.39 wt%,
TiO_2 = 0.64 wt%, and
Na_2O = 2.55 wt%.

In Unit V, the averages are

K_2O = 3.71 wt%,
TiO_2 = 0.67 wt%, and
Na_2O = 2.30 wt%.

Hole C0002P only penetrates Unit V and overlaps with Hole C0002N from 1965.5 to 2330 mbsf. Along the overlapping interval, Na_2O, MgO, Fe_2O_3, P_2O_5, and LOI correlate well with the data from Hole C0002N. However, for SiO_2, K_2O, Al_2O_3, TiO_2, and CaO, there are offsets between 1965.5 and 2045.5 mbsf for data from Holes C0002N and C0002P, which result from the cement contamination mentioned above. SiO_2, K_2O, and Al_2O_3 remain relatively constant throughout Unit V at ~65, 3.5, and ~16 wt%, respectively. P_2O_5 and LOI similarly are invariable with depth (~0.07 and ~6 wt%, respectively). Fe_2O_3 and TiO_2 contents are also fairly constant throughout (~5 and ~0.65 wt%, respectively), except for a cluster of samples between 2445.5 and 2525.5 mbsf (Samples 348-C0002P-159-SMW, 163-SMW, 168-SMW, 172-SMW, and 176-SMW), which are anomalously higher than the average. These values may be related to the presence of iron titanium–rich minerals. Na_2O content averages ~2.3 wt% but is more scattered than other compositional elements, fluctuating between 2.1 and 2.4 wt%. K_2O increases slowly with depth from 3.2 to 3.8 wt%, which may be related to smectite-illite transformation. MgO content generally decreases with depth from 2.1 to 1.9 wt% but exhibits a peak of higher values between 2585.5 and 2705.5 mbsf. A peak is also observed at the same depth interval for CaO content (maximum 2.4 wt% at 2665.5 mbsf; Sample 210-SMW). Apart from this interval, CaO content decreases with depth from ~1.8 to ~0.9 wt%.

Limitations of sediment cuttings analyses

In comparison to Expedition 338 (Strasser et al., 2014b), the cuttings data collected during this expedition correlate reasonably well with LWD and other data (see **"Logging," "Physical properties," "Structural geology,"** and **"Geochemistry"**), with depth shifts of ~10–40 m. However, specific lithologic variations that are normally observed and documented in cores cannot be recognized in cuttings.

An important limiting factor on the reliability of cuttings is the amount of their stratigraphic mixing. For example, the collapse of wall rock into the drilling mud (cavings) results in vertical mixing of lithologies, making it difficult to accurately reconstruct stratigraphic relationships. In Hole C0002N, several circumstances may have caused caving contamination, such as hole cleaning (1205–1221 mbsf), WOW (1662–1678 and 1992–2008 mbsf), and mud-loss treatment (2022–2038 mbsf). Sand was recovered in cuttings and drilling fluid as mostly unconsolidated material, and the >63 µm sand-sized fraction was separated during washing and sieving. Because of temperature, drilling mud circulation speed and viscosity, pH values, and chemical supplements added to the drilling mud, the lithified sediment is partly disaggregated. This makes it difficult to differentiate the drilling mud and disaggregated mud from mudstone or sand from sandstone.

In Holes C0002N and C0002P, defining units and subunits by the occurrence or disappearance of a different lithology (e.g., the appearance of sandstone) is the most reasonable approach. Because of slight smearing effects created by general circulation of cuttings fragments, the base of a unit or subunit can be defined only in a relatively imprecise way.

Hole C0002P cored interval

Six cores were taken in Hole C0002P, with an average recovery of 56.9% (minimum recovery of 4.2% for Core 348-C0002P-1R and maximum of 86.0% for Core 4R; see **"Operations"**). The cored interval (2163–2218.5 mbsf) was entirely within Unit V, as per the unit depths and descriptions established from Hole C0002N cuttings (Fig. **F20A, F20B**).

Lithologic variation

The main lithologies identified in the cored interval of Hole C0002P are greenish gray silty claystone and fine-grained sandstone (Figs. **F20, F21**). Minor lithologies include medium-gray fine silty claystone (Section 348-C0002P-6R-4) and black organic matter–

rich interbeds and laminations. Bedding is very steep to vertical and generally planar but locally wavy. The silty claystones are firm to hard, have developed incipient fissility in places, and typically exhibit color banding, thin dark laminae, lenses, and irregular patches of sand. Mottled textures are locally observed, which may be related to possible postdepositional bioturbation. The sandstones are fine grained and friable but slightly cemented in places. They often show grain size gradation, fining into silty claystone. Sharp contact surfaces (locally erosive) between silty claystone and sandstone are common. This sediment is interpreted to be fine-grained turbidites.

A fault zone made up of highly fractured and deformed rock material (fault gouge) is identified in between intervals 348-C0002P-5R-4, 30–90 cm, and 5R-5, 0–30 cm (see **"Structural geology"**). Precipitation of calcite and other carbonate minerals occurred along localized veins (i.e., Section 5R-4, 58 cm). Slight lithologic changes are observed below this fault zone in both macro- and microscopic descriptions. The silty claystone is slightly sticky in places, and sandstone interbeds are less common.

Smear slides observation

Thirty-six smear slides were prepared and examined from the cored interval. A siliciclastic assemblage of clay, silt, and sand grains with quartz and feldspar dominates these lithologies. Clay minerals, micas (biotite and muscovite), diverse dense minerals, and lithic fragments are common components (Figs. **F22**, **F23**; also see SMEARSLD in **"Supplementary material"**).

Quartz is common to dominant at all depths. Feldspar and mica are few in all samples and rare or not observed in and near the fault zone. Heavy minerals are common in and close to Core 348-C0002P-3R. Carbonate minerals are rarely observed above the fault zone and are few below the fault zone, but there are calcite veins within the fault zone. Clay minerals are common to abundant. Volcanic glass is commonly observed in sandstone and below and in the fault zone. Pyrite is generally observed but is only rare in the fault zone. Sedimentary lithics vary from common to dominant, depending on the lithology. Volcanic lithics are generally observed below Core 4R-1. Pelagic grains including nannofossils, foraminifers, and diatoms are only observed in Cores 1R and 2R and below the fault zone. Organic matter is commonly observed in the black beds and laminations but is only rare in the fault zone.

Mineralogical and geochemical analyses

Bulk powder XRD results show the relative abundance of total clay minerals, quartz, plagioclase, and calcite throughout the core. The data are plotted in Figures **F12** and **F24** and in Table **T11**. Among the major minerals, total clay, quartz, and feldspar show some heterogeneity in the uppermost sections of the core. Total clay shows the greatest amount of variation throughout the core, ranging from ~58 to 62 wt%. Quartz, feldspar, and calcite do not show significant variations throughout the core. The fault zone at 2205 mbsf also shows no changes in sedimentary matrix mineralogy. Cuttings from Holes C0002N and C0002P show similar trends as the core. Interestingly, the cuttings from Hole C0002P have slightly lower total clay values and higher quartz values than the core and the cuttings from Hole C0002N. One possible reason could be the change in the drill mud composition.

XRF composition shows no major changes within the core, except a slight decrease of average SiO_2 and CaO and a slight increase of average MgO and Al_2O_3 (Fig. **F25**; Table **T12**). No significant changes in the fault zone at 2205 mbsf are recognized. The overall trends of the XRF core composition are similar to those observed in cuttings from Holes C0002N and C0002P. However, the cuttings taken in the same hole as the core show consistently lower values in MgO, Al_2O_3, and Fe_2O_3 and higher values in SiO_2, K_2O, Ca_2O, and LOI. One reason could again be a change in the drill mud composition.

Bulk elemental compositional variation across the fault zone in Sections 348-C0002P-5R-4, 35–91 cm, and 5R-5, 0–59 cm, was examined using XRF core scanning (Fig. **F26**). The fault zone shows significantly higher values of Fe_2O_3 and lower values of K_2O between the lower half of Section 5R-4 and the upper half of Section 5R-5 (see **"Structural geology"**). The veins encountered in the fault zone are enriched in CaO and MnO.

Biological features

Calcareous nannofossils, foraminifers, and diatoms are observed in the uppermost sections of the core and below the fault zone. Organic matter is abundant in the black laminations, beds, and isolated specks but rare within the fault zone. Mild bioturbation were locally observed within the silty claystones, but no particular ichnotaxa were identified. Mottled textures and small burrows (millimeter-scale tubes) preserved by carbonate material (Fig. **F21B**) are the most common bioturbation features. Burrows are very clear in the XRCT images.

Authigenic components

Few authigenic components were identified in the silty claystones and sandstones. Pyrite was generally observed throughout the cores, occurring as framboids and in <2 mm nodules.

Comparison of core and cuttings

We compared rock composition and sedimentologic features from the core interval between 2163 and 2218.5 mbsf with cuttings (Samples 348-C0002P-71-SMW through SMW-86; Fig. F27). The main lithologies can be identified in both the cores and the cuttings; both show greenish gray silty claystone and fine-grained sandstone. In the cuttings, however, the sand fraction is often disaggregated and appears as loose sand. Firmer cuttings of sandstone are detected in the >4 mm size fractions (Fig. F27A). Minor lithologies like black organic matter–rich interbeds and laminations in the core can also be observed in the cuttings, as well as occasional sedimentary structures like bedding and bioturbation (Fig. F27B). Calcite veins that occur in Core 348-C0002P-5R-4 can be found in the form of small pieces in the cuttings. Although best observed in cores, shear features can also be recognized in cuttings. Common hard silty claystone cuttings exhibit polished shear surfaces with distinct slickenlines. Calcite vein pieces also show these striations (see "Structural geology").

Mineralogical and geochemical comparison

X-ray diffractometry

XRD data from the core intervals of Holes C0002M and C0002P and cuttings from Holes C0002N and C0002P were compared with XRD data from Expeditions 338 (Holes C0002K, C0002L, C0002J, and C0002H; Strasser et al., 2014b) and 315 (Hole C0002B; Expedition 315 Scientists, 2009) (Fig. F12; Table T9). The data display the mineral variation with depth throughout all units identified at Site C0002.

Total clay content in cores between 200.9 and 506.5 mbsf (Holes C0002J, C0002K, C0002L, and C0002M) averages ~55 wt%, whereas total clay in Hole C0002B core has slightly lower average values of ~45 wt%. At the Unit III/IV boundary at ~915 mbsf, total clay increases to ~65 wt% in Hole C0002B core. This increase is also visible in core from Hole C0002H. The cuttings from Hole C0002N show similar higher average total clay values of ~60–65 wt%, which also correlate well with cuttings from Hole C0002F and cuttings and core data from Hole C0002P. At the Subunit IVC/IVD boundary, total clay decreases slightly to an average of ~58–60 wt% and stays almost constant to the bottom of the hole at 3058.5 mbsf. Samples taken from Hole C0002P core show a wider range of total clay content, but their average is consistent with cuttings values from Holes C0002N and C0002P.

The average content of quartz in Hole C0002J, C0002K, C0002L, and C0002M cores is ~30 wt% and decreases at the Unit III/IV boundary to ~18 wt% in Hole C0002B core. In Units IV and V, quartz increases slightly with depth to ~30 wt%. Similarly, feldspar increases slightly from an average content of 18 wt% in Hole C0002J, C0002K, C0002L, and C0002M cores to ~25 wt% in Hole C0002B core and decreases at the Unit III/IV boundary back to ~18 wt% until the end of the hole at 3058.5 mbsf. Hole C0002J, C0002K, C0002L, C0002M, and C0002B cores show highly scattered calcite content between 0.1 and 30 wt%. This is similar to observations made in Hole C0002B (Expedition 315 Scientists, 2009), where calcite abundance ranges from 0.63 (trace) to 27.16 wt% with an average of 14.21 wt%. Apart from these values, calcite remains at ~0.1–2 wt% with no significant change between data from core and cuttings. Exceptional areas are those data with higher values from possible cement contamination. The XRD cuttings data are relatively homogeneous compared with the core data because of the preferential preservation of the fine-grained (more consolidated) sediment in the silty claystone (1–4 mm size fraction) with respect to coarse-grained (less consolidated) sandy sediment.

There are weight percent differences between calcite analyzed by XRD and calcium carbonate from coulometric analysis (see "Geochemistry" for carbonate data). Although XRD results show trace values of calcite, the carbonate coulometry data are consistently higher. This is probably because the normalization procedure used in the XRD analyses usually underestimates mineral content when it is <5%. In addition, XRD analyses only provide relative abundances by using singular value decomposition computations, considering only total clay minerals, quartz, feldspar, and calcite.

X-ray fluorescence

XRF data from the cored intervals of Holes C0002M and C0002P and cuttings of Holes C0002N and C0002P are compared with XRF data from Expedition 338 (Holes C0002K, C0002L, C0002J, C0002H; Strasser et al., 2014b) (Fig. F13; Table T10). The data display mineral variations with depth throughout all units identified at Site C0002.

SiO_2 content remains relatively constant at ~65–70 wt% throughout all drilled sections at Site C0002. Al_2O_3 exhibits the same trend with depth, staying between ~15 and 18 wt%. The cores in shallower

Holes C0002K, C0002L, C0002J, and C0002M show an average of 3 wt% for K_2O. Analysis of deeper cuttings from Holes C0002F, C0002N, and C0002P reveal a slight increase of K_2O from 3.1 to 3.6 wt%, which may be related to a beginning smectite-illite transformation. Hole C0002J, C0002K, and C0002P cores show slightly lower average K_2O values but exhibit a similar increasing trend with depth. Average MgO values in the upper cores are highly scattered between 1 and 3 wt%. MgO contents in cuttings decrease with depth from ~2.5 to ~1.8 wt%. Hole C0002J and C0002H cores show significantly lower average values than cuttings from greater depth, whereas Hole C0002P core data are mainly in agreement with the cuttings. Na_2O values for the upper cores average ~2.5 wt%. Cuttings data decrease in Na_2O content to ~2000 mbsf and remain constant at ~2.1 wt% below that depth. Hole C0002H core data show lower values. Scattering between 0.4 and 0.85 wt% is observed in the upper cores for TiO_2. The cuttings show a slight decrease in TiO_2 in Unit IV from 0.7 to 0.6 wt% and then remain constant throughout Unit V. There are two areas of anomalous TiO_2 content at ~2000 mbsf (average = 0.5 wt%) and ~2500 mbsf (average = 0.88 wt%). Hole C0002P core data scatter between 0.2 and 0.75 wt%. The upper cores and Hole C0002J core show highly scattered values of CaO content between 0.1 and 20 wt%. Apart from these scattered values, CaO remains at ~0.1 to 2 wt% with no significant change between data from core and cuttings, except in areas with cement contamination.

Interpretation of drilled stratigraphy

Unit III, consisting of silty claystone with trace amounts of sandy material, is interpreted as the fill of the lowermost part of the Kumano forearc basin and potentially prism slope basins (Expedition 315 Scientists, 2009). The composition of detrital grains is consistent with sediment supply from erosion of the exposed sedimentary and metasedimentary rock units within the Outer Zone of Japan, including the Shimanto Belt (e.g., Taira et al., 1988; Isozaki and Itaya, 1990).

Expedition 315 Scientists interpreted Unit III as forearc or supra-accretionary prism slope deposits that accumulated above the carbonate compensation depth, both prior to and during the early stages of formation of the Kumano Basin (Expedition 315 Scientists, 2009). Sediment-starved conditions were accompanied by a diverse assemblage of infauna. Local cementation of the sediment surface (by glauconite, possibly with phosphates and carbonates) was favored by slow sediment accumulation rates and exposure to oxygenated seawater (Strasser et al., 2014b). The base of Unit III was proposed to be a depositional contact between accreted trench-wedge sediment (Unit IV) and the initial deposits of hemipelagic silty claystone on the lowermost trench slope (Unit III) (Expedition 315 Scientists, 2009).

Seismic reflection profiles show complicated geometries with angular discordances and contrasts in structural style across the boundary. Expedition 315 Scientists interpreted the pronounced unconformity at ~922 mbsf as a manifestation of uplift along a system of out-of-sequence (splay) faults that occurred at ~5 Ma (Expedition 315 Scientists, 2009). Whether the uplift triggered erosion of accreted strata or favored slow sediment accumulation above the prism cannot be resolved without higher resolution biostratigraphy.

Unit IV represents the uppermost part of the older accretionary prism sediment, with silty claystone as the major lithology. Sandstone consists of mainly quartzo-feldspatic material, including common heavy-mineral assemblages and volcanic glass and variable but generally small amounts of organic/woody material. This assemblage is consistent with proximity to a volcanic source (Strasser et al., 2014b).

During Expedition 315, the depositional environment of Unit IV was difficult to interpret because of poor core recovery and a strong tectonic overprint characterized by intense fracturing, scaly fabric in mudstone, and fragmentation of sandstone beds (Expedition 315 Scientists, 2009).

Unit IV consists of the most sandstone rich deposits recovered in Holes C0002F and C0002N. The most likely depositional environment is that of older accretionary prism slope basin fill or accreted submarine-fan deposits that accumulated in either a paleotrench or the Shikoku Basin.

The Unit IV/V boundary is set at 1665.5 mbsf. XRD and XRF analyses show a significant shift in mineralogy and element oxides at this interface, similar to what was identified during Expedition 338 in Hole C0002F (Strasser et al., 2014b).

Unit V consists essentially of silty claystone, the finest grained deposits within any unit in Holes C0002F and C0002N, and is also associated with the highest gamma radiation values (see "Logging"). Late Miocene age and sedimentology suggest that it is a candidate correlative unit to the lower hemipelagic Unit III drilled at subduction inputs Sites C0011 and C0012 (Expedition 322 Scientists, 2010a, 2010b), albeit possibly internally thrust duplicated and folded.

Structural geology

Structural analyses at Site C0002 included description of cuttings in Holes C0002N (875.5–2330 mbsf) and C0002P (1939.5–3058.5 mbsf) and analyses of cores in Holes C0002M (475–512.5 mbsf) and C0002P (2163.0–2218 mbsf).

Cuttings description

Sampling and quality control of intact cuttings

In Holes C0002N and C0002P, deformation structures in cuttings from both the 1–4 and >4 mm size fractions were investigated from 875.5 to 2330 and 1939.5 to 3058.5 mbsf. It should be noted that in the shallow portion of the hole, intact cuttings that are apparently internally undisturbed by drilling processes represent only a small fraction of the initial amount of the sample prior to hard washing (see the **"Methods"** chapter [Tobin et al., 2015]).

For the coarser fraction (>4 mm), the total number of cuttings per sample was generally <100 in the upper section, and the maximum number of intact cuttings counted was 100 (Fig. **F28**). In some samples, all of the initial cuttings disaggregated entirely. The ~200 cm^3 initial amount present prior to hard washing was taken throughout the section from 1200 to 3058.5 mbsf in Holes C0002N and C0002P. In the section above 1200 mbsf, the volume of the initial sample was small (frequently ~20 cm^3), and few intact cuttings were retained after hard washing.

WOW or drilling operations that add additional time between the initial drill bit penetration and sampling can have some implications for the retrieval of cuttings. Indeed, during this downtime, some cuttings and cavings can become detached from the borehole walls and fall along the mud column. The denser intact cuttings should fall more rapidly than the drilling-induced aggregates (see **"Physical properties"**). As a consequence, the amount of intact cuttings (and cavings) retrieved after these incidents often increases dramatically. In Hole C0002N, these incidents occurred at 1219, 1677.5, 2008.5, and 2036 mbsf (Fig. **F28**) and are associated with a corresponding increase of retrieved intact cuttings, although the increase of the cuttings observed at ~1200 mbsf is less pronounced than the others, probably due to the relatively short down time. In Hole C0002P, similar occurrences took place at 2067.7, 2163.0, 2218.5, and 2601.5 mbsf. The increases in volume at 2163.0 and 2218.5 mbsf are likely due to coring operations, but no influence is observed due to the WOW incident that took place at 2067.7 mbsf. At 2601.5 mbsf, the intact cutting recovery is high, and the influence of the wiper trip cannot be observed.

As a whole, the amount of examined intact cuttings increases from 1045.5 to 3058.5 mbsf (Fig. **F28**). Shallower than 1045.5 mbsf it was not possible to retain any material at all after washing.

Distribution of deformation structures in intact cuttings samples

Observed deformation structures besides drilling-induced disturbance in intact cuttings (from here onward called "cuttings") from the 1–4 and >4 mm size fractions include slickenlined surfaces, scaly fabric, deformation bands, opaque bands, minor faults, and mineral veins.

Figure **F29** shows the percentage of deformed cuttings obtained by dividing the number of cuttings that show deformation structures by the total number of retrieved cuttings as a function of depth for both Holes C0002N and C0002P. Because of the highly variable number of retrieved intact cuttings, three categories are represented: >40 cuttings, >20 cuttings, and at least 1 cutting.

For the >4 mm size cuttings, the percentages based on 21–40 or >41 cuttings are similar, but the percentages based on very few cuttings are more scattered, in particular above 1500 mbsf in Hole C0002N. Accordingly, we consider the percentages based on >20 cuttings as representative of the actual distribution of the deformation. In that case, in Hole C0002N, the percentage of deformed cuttings varies mainly between 5% and 25%, and the mean percentage reaches 16%. In Hole C0002P, the rate of deformed cuttings identified is more frequent than in Hole C0002N, and the percentage of deformed cuttings varies mainly between 10% and 30%. The mean is ~21% for Hole C0002P.

In the >4 mm size cuttings in Hole C0002N, four intervals deviate from the mean value of 16%. A clear peak appears at 1235.5 mbsf, but it is defined by relatively few samples (maximum of 52% deformed cuttings) recovered from a position a few tens of meters after a hole cleaning (1219 mbsf). Accordingly, although the observation is correct in terms of percentage, the exact depth of the cuttings is perhaps not precise, and some may be cavings. A second deviation from the mean can be observed from 1565.5 to 1695.5 mbsf, with a maximum of 27% deformed cuttings. A third peak is present between 1870.5 and 1905.5 mbsf (maximum of 38% deformed cuttings). These two increases are not influenced by waiting on weather, hole cleaning, or mud loss treatment incidents. Finally, a fourth increase can be observed between 2015.5 and 2145.5 mbsf (maximum of 27% deformed cuttings). In this case, the upper part of this broad peak could have been influenced by the waiting on weather and mud loss treatment just before retrieval of these cuttings, at least in terms of exact position of the sample.

In Hole C0002P, the percentages of deformed cuttings of the >4 mm size fraction show a variable trend with peaks of >35%. No localized deformation zone can be clearly shown based on high percentage distribution of the deformation around a particular depth.

From both holes, the relationships between the deformation percentages in the >4 and 1–4 mm fractions are not clear. For the 1–4 mm size cuttings in Hole C0002N, the ratio of deformation increases with depth shallower than 1235.5 mbsf. The percentage reached 30%, although it is generally ~8%. By contrast, in sections where a high percentage of deformation was observed in the >4 mm size cuttings, the 1–4 mm size fraction has a high percentage of undeformed cuttings. Indeed, in the 1–4 mm fraction, the size of the cuttings is perhaps too small to exhibit any type of distributed deformation structures. In Hole C0002P, the deformation seems to be penetrative, as it can also be observed even in the 1–4 mm size cuttings. In the intervals where observation was possible, a similar variable trend of the percentage of deformation is observed, but no correspondence between size fractions can be established.

Type of deformation structures as a function of depth

Figure F29 shows depth distribution of cuttings with deformed structures: slickenlined surfaces, scaly fabric, deformation bands, opaque bands, minor faults, and mineral veins. Cuttings with slickenlines were observed throughout the entire section below 1045.5 mbsf. In Hole C0002P below 2430.5 mbsf, the slickenlined surfaces are so abundant in the cuttings that a scaly fabric develops in almost all the samples. In Hole C0002N, in the >4 mm size fraction, a cluster of deformation band observations is noted around a peak of deformed cuttings at 1235.5 mbsf. The abundance of such structures is scattered but they continue to appear downhole to 2215.5 mbsf. In Hole C0002P, these structures appear below 2380.5 mbsf, although they are not frequently observed. The first appearance of veins is at 1245.5 mbsf (Hole C0002N). They appear irregularly below this depth to 2225.5 mbsf, but below that depth they are present regularly in Hole C0002N and in all of Hole C0002P. Rarely, arrays of minor faults were identified below 2410.5 mbsf.

Description of deformation structures

All observed deformation structures except for clearly drilling-induced ones are summarized in CUTTINGS STRUCTURE.XLSX in STRUCTUR in **"Supplementary material."** In this file, we differentiated the lithology in which the different types of deformation structures were observed. We also counted the number of the cuttings of different lithologies in each sample, including nondeformed cuttings. Both 1–4 and >4 mm size cuttings include slickenlined surfaces, scaly fabric, deformation bands, opaque bands, minor faults, and mineral veins.

Slickenlined surfaces

Cuttings with slickenlined surfaces were observed throughout the entire section below 1045.5 mbsf. A slickenlined surface is the polished surface of a cutting that shows striations. At shallow depths, the cuttings of silty claystone with slickenlines generally show a shiny planar surface with very fine striations (in Fig. F30A at 1235.5 mbsf). Striations on surfaces in similar lithology can be easily observed with increasing depth (in Fig. F30B, F30C, F30D at 1665.5, 2095.5, and 2560.5 mbsf, respectively). Lens-shaped cuttings are commonly observed, surrounded by slickenlined surfaces. Under the optical microscope, clay mineral–rich zones are observed along these surfaces, reaching 200 µm thick (Fig. F30E). It is has been suggested that the thickness of such zones can increase with depth, together with the preferred alignment of clay minerals (Strasser et al., 2014b). This is confirmed by scanning electron microscope (SEM) images (see **"SEM description"**). Slickenlines are commonly associated with steps (Fig. F30F) from which the sense of shear can be inferred (e.g., Petit, 1987). The appearance of the slickenlined surfaces also depends on the lithology of the affected rock. In quartz-rich silty sandstone, the slickenlines are not coated by clay minerals (Fig. F31A, F31B). Stepped slickenlines can also be observed, but they are very tiny (<10 µm between steps; Fig. F31C). Under the optical microscope, deformation is very localized near the slickenlined surface. In one example, only a band of ~120 µm is affected by brittle shear that displaced opaque bands, which acquired an en echelon geometry (Fig. F31D). Figure F31E shows a detail of this band, where a plagioclase grain shows undulose extension probably due to the shearing along the slickenlined surface. A broken and displaced quartz grain indicates the sense of shear, dextral in the present position of the thin section (Fig. F31F).

Scaly fabric

Scaly fabric was observed in Hole C0002P from 2430.5 mbsf downhole. It broadly corresponds to the relative enrichment in clayey materials of the sediment (see **"Lithology"**). At the cuttings scale, the scaly fabric appears related to slickenlined surfaces (Fig. **F32**). It also corresponds to reorientation of clay particles into preferred alignment (see **"SEM description"**).

Deformation bands

Deformation bands (Maltman et al., 1993) are not frequent, but they appear from the top to the bottom of the studied section of Holes C0002N and C0002P (see CUTTINGS STRUCTURE.XLSX in STRUCTUR in **"Supplementary material"**). These structures were observed in silty claystones at 1235.5 mbsf and in silty sandstones at 2380.5 mbsf. Their distribution along Holes C0002N and C0002P is shown in Figure **F32.**

In the cuttings, the deformation bands are characterized by thin planar dark gray bands (Fig. **F33A–F33D**), which in some cases show slickenlined surfaces (Fig. **F33A, F33C**) or stepovers (Fig. **F33B**). These bands generally do not appear as single planes but as a set of bands of variable orientation, which define a web structure (Byrne, 1984) (Fig. **F33A, F33C, F33D**). In thin section, the deformation bands have a thickness of >100 µm and are composed of dark brown clay minerals and angular quartz or feldspar grains in which it is not possible to recognize any preferred orientation (Fig. **F33E, F33F**). In Figure **F33F,** a quartz grain adjacent to the fault does not show any deformation.

Opaque bands

When thin sections were made to study the cuttings with a microscope, a type of structure not visible with binocular magnifying glass was revealed in a sample of silty claystone from 2015.5 mbsf (Sample 348-C0002N-259-SMW). Two systems of apparent veins of opaque material go through the whole sample (Fig. **F34A–F34C**), although primarily in the more clayey lithology of the thin section. The two systems define an apparent angle of 40° between them. They are very thin (no more than 5 µm thick), and no material other than opaque minerals can be seen within them. Geometries reminiscent of stepovers can be observed (Fig. **F33D**). This suggests that they could be microfaults, separating lenses, or rhombs of rocks within which no deformation is observed (Fig. **F34A–F34C**). In that case, their appearance is very different from the deformation bands described in the previous paragraph.

Minor faults

Arrays of minor faults were observed in a few samples below 2410.5 mbsf. The faults exhibit spacing of 0.5 mm or less and displacement of the same order of magnitude (Fig. **F35A**). Figure **F35B** shows that each minor fault is in turn a fault zone, constituted by various coalescing microfaults.

Mineral veins

Veins appear in all the lithologies observed in Holes C0002N and C0002P (Fig. **F36A, F36B**). They were also observed rarely as individual cuttings, as they are probably more resistant than other materials to the drilling and washing processes. The distribution of these veins in Holes C0002N and C0002P is shown in Figure **F39.**

The veins are generally less than a few millimeters wide and most commonly consist of carbonate minerals (Fig. **F36A**), although veins composed of pyrite were sometimes observed (Fig. **F36B**). Occasionally, open veins appear and are lined by carbonate minerals (Fig. **F36C**). In some cases, these veins are formed by fibers, occasionally stepped (Fig. **F36D**), which suggests shear deformation during vein formation. This is consistent with the orientation of some veins perpendicular to the slickenlines. Locally, wall rocks were brecciated during vein formation, and both the fibers of the vein and the slickensides of the wall rocks indicate the same direction, which suggests a common sense of shear (Fig. **F36E**). A few samples show veining and repeated brecciation, reminiscent of hydraulic fracturing processes (Fig. **F36F**).

Core description

Hole C0002M

Observation of the Hole C0002M cores and XRCT images revealed few structures in the lower part of the Kumano Basin deposits (lithologic Unit II). The orientation of seven bedding planes and one vein were measured on core from Hole C0002M. Because of the limited number of structures and oversized diameter of SD-RCB cores for the onboard cryogenic magnetometer, reorientation using paleomagnetic measurement was skipped for cores from Hole C0002M.

Bedding

Several bedding planes and laminations were identified in Hole C0002M (lower Kumano Basin sediment; lithologic Unit II; see **"Lithology"**). The bedding planes were identified at the bottoms of sandstone layers corresponding to the base of muddy distal turbidites. Their attitudes are almost horizontal; all bedding planes dip less than 5° (Fig. F37).

Faults and veins

In the cored interval in the Kumano Basin lithologic Unit II (Hole C0002M), faults were not observed by visual core description or XRCT observation. One vein composed of precipitated pyrite was observed in interval 348-C0002M-1R-2, 11–16 cm (476.52–476.57 mbsf; Fig. F38). The XRCT image shows that this vein has a planar shape as a whole, but in detail it shows a wavy, ptygmatic form. The origin of this vein is unknown. The ptygmatic shape suggests that the vein was deformed during compaction (lithification). In that case, it developed during an early stage. A possible genesis through bioturbation could be invoked, although the planar shape of the vein suggests it formed as a vein along a crack in shallow sediment.

Hole C0002P

Observations of Hole C0002P cores and associated XRCT images revealed bedding and other structures. A total of 41 bedding planes, 27 minor faults, and 4 carbonate veins were measured from the cored interval (2163.0–2217.5 mbsf). A wide fault zone between 2204.9 and 2205.8 mbsf was also observed.

Bedding

In most of the cored interval, bedding dips steeply (>75°) (Fig. F39). In some places, a group of layers was traceable in adjacent biscuits of the core. In that case, the attitude of the bedding was measured using only one segment to avoid duplicate measurements. Some boundaries between sandstone and silty claystone show flame structures and load cast indicative of younging direction. Sand layer grading was also used to determine the polarity of the bedding, indicating that most of layers are upright. Postcruise paleomagnetic research will hopefully permit restoration of the attitudes of the bedding planes in true azimuthal coordinates.

Faults

A total of 27 faults were observed in the core (Fig. F39). They are discrete planes that bear slickenlines (Fig. F40A, F40B). Sense of movement was deduced from slickensteps, the offsets of bedding, and asymmetric scratching and grooving along fault surfaces. The designation of reverse or normal faulting is based on the structure's present-day position, but because the current bedding dips are very steep, the original attitude at the time of deformation is generally unknown.

There are 12 faults with an apparent reverse sense of faulting and 15 faults with apparent normal sense of faulting in their current orientation. The apparent normal faults appear scattered in the hanging wall of the fault zone, whereas the apparent reverse faults are distributed around the main fault zone, ~10 m above and below it. Interestingly, the main fault zone at ~2205 mbsf has a normal sense of motion (Fig. F39). One apparent reverse fault far from that fault zone lies at 2178 mbsf. The normal and reverse faults dip 23°–78° and 31°–70°, respectively. In one case, a cross-cutting relationship between both types of faults was observed: a normal fault cuts two conjugated reverse faults (2177.14–2177.27 mbsf; Fig. F40C, F40D). The mixing of apparent normal and reverse faults suggests at least two phases of deformation have occurred with possible bed rotation to steep angles occurring between them. This makes a simple kinematic interpretation of this region difficult.

Brittle fault zone

A brittle fault zone characterized by fault breccia appears between Sections 348-C0002P-5R-4, 30 cm, and 5R-5, 30 cm (2204.9–2205.8 mbsf; Fig. F41). The light brown matrix (~50%) involves angular brecciated clasts, generally <2 mm. Scaly fabric characterizes most of the clasts.

A few slickensteps observed along discrete minor faults in the fault zone were measured. With respect to the present core coordinates, the slickenlines show a high rake (~60°). Moreover, the 3-D XRCT images show that the observed surface of the working/archive half is oriented at a high angle (40°–60°) to the fault plane, which is adequate for determining the movement along the fault zone.

The shape and geometric distribution of clasts is highly asymmetric (Fig. F41), indicative of the apparent normal faulting sense of the fault in its current orientation. The few slickensteps observed along discrete minor faults in the fault zone are also coherent with the apparent normal faulting sense.

Some calcite veins were identified in the fault zone and appear at the top and bottom of the fault zone and near a 2 cm deformed sandstone clast (Fig. F42). The XRCT image shows that the geometry of these veins is not planar; rather they are generally curviplanar. Also, the veins are imbricated (Fig. F42). Given these occurrences and their limited distribution developed only inside the fault zone, the veins apparently developed during the faulting and have been partially disrupted by later movement.

SEM description

Hole C0002N: shallow section (850–2330 mbsf)

SEM images were made of broken surfaces of intact cuttings. We tried to image "exposures" as close as possible to the striated surfaces. However, cuttings often broke in a variety of orientations, and not all internal surfaces had striation orientations that were parallel to those visible on the outer surfaces. Compaction fabrics with grain alignment are weakly developed at 850–2100 mbsf in undeformed cuttings away from obvious shear zones (Fig. **F43**). Local collapse and alignment of the clay fabric initiated at ~1500–2000 mbsf but does so in an irregular box-framework pattern enclosing uncollapsed and poorly oriented subregions. Locally, siliceous microfossils that remained intact during burial and deformation are present at least to 1225.5 mbsf. Little evidence exists for opal diagenesis, suggesting in situ temperature is low (<80°C at 1225.5 mbsf), which is consistent with the estimated thermal gradient of Spinelli and Harris (2011). The lack of strong compaction foliation may occur because the beds, or parts of them, rotated during accretion and are now dipping at a high angle, as measured in Hole C0002P (mostly >60°) and in the LWD resistivity imaging data from both C0002F and C0002P. This would cause a superposition of compaction strains that limits ultimate grain alignment.

Surface images of striated microfaults in cuttings reveal that striations occur at all scales down to the micrometer level. Examples are shown in Figure **F44A** and **F44B** from a variety of depths. Striations occur in all lithologies from silty clay to sands. Striated surfaces of sand-rich inclusions often show polished glassy surfaces that may contain poorly resolved broken grains/cements. Shear surfaces have a microlayered internal texture, but individual shear surfaces are generally thin (<1–5 µm; Fig. **F44A–F44D**). In silty clays, the striations on shear surfaces can occur in extremely localized shear zones ≤1 µm thick, in which grain alignment is intense to the point of it being difficult to resolve individual clay grains at the highest resolution of the shipboard SEM (0.1–1 µm generally, depending on sea state) (Fig. **F44B–F44F, F44G–I, F44K**).

Typically, shears in silty clays form distributed anastomosing incipient scaly fabric networks enclosing interiors of lenticular phacoids composed of poorly oriented clays and silt grains (Fig. **F44G–F44I**). This lack of a strong consistent internal clay alignment away from the "nano-thin" shears appears typical of many of the deformed cuttings from the shallow to intermediate depths of the part of the wedge transected by Hole C0002N and may signify distributed low-intensity bulk strain. In other, rarer, cases, more penetrative foliation of clays along thicker slickensided microshear zones is apparent. An example from 2205.5 mbsf (Fig. **F44E**), the same depth as the cored fault zone (2204.9–2205.8 mbsf), has an intense scaly fabric forming a broad shear zone a few millimeters thick. These zones comprise many individual thin shear zones (<<1 µm thick) and represent full scaly fabric development. The location of the scaly clay cuttings sample shown in Figure **F44E** at the depth of the fault zone in the cores is probably not a coincidence, but such scaly fabrics also become generally more common with depth below 2000 mbsf (see below).

Hole C0002P: cores and deeper section (1939–3058 mbsf)

Examples of the deformation fabrics revealed in specimens from the cored section (2163.0–2217.5 mbsf in Hole C0002P) are shown in Figure **F45.**

The cores show a variably deformed hanging wall sequence overlying the main fault zone identified in Section 348-C0002P-5R-4. Bedding is steeply oriented (generally >75°), as are the measured faults (mostly between 40° and 70°) within the cores (Fig. **F39**). SEM images were taken from a portion of Section 2R-3 (2176.28–2177.70 mbsf) in the hanging wall from the interstitial water whole round excavated during retrieval of material for pore water sampling (see **"Geochemistry"**). The strata in this section are dismembered to form lenticular sandstone blocks in a clay-rich matrix with scaly fabrics (Fig. **F45**). Observations on SEM images of the edges of lenticular sand-rich blocks suggest that they are dismembered by the generation of a deformed outer rind that is progressively sheared off into the surrounding matrix. For example, Figure **F46** shows a series of increasingly higher magnification images of a deformed rind of a muddy sandstone block in which many individually thin (<0.1–1 µm), spaced, clay-dominated shears develop, with intervening less deformed ~40 µm thick panels containing the sand grains and more weakly aligned clays. The progressive localization of the shear zones into the clays suggests mechanical control. The ~40 µm spacing of the shear zones is quite regular and may have been dictated by the average size of sand grains, resembling the spaced cleavage seen in the early stages of cleavage development in low-grade metamorphic rocks. However, in this case a simple shear component dominates, given the common development of striations on the shear planes in the scaly fabrics and asymmetric fabrics in some locations (Fig. **46F**).

Toward the base of the hole below 2625 mbsf, more clay-rich sediment dominates the lithology. The percentages of deformed, striated, and scaly (Figs. F29, F47) cuttings are consistently elevated, suggesting distributed deformation is pervasive in this unit. SEM images indicate that apparently unsheared or undeformed cuttings at binocular microscope scale also exhibit a progressively developing penetrative clay alignment fabric at SEM scale. SEM views roughly perpendicular to the pervasive clay alignment fabric in a sample at 2980 mbsf illustrate this (Fig. F48). The flattening fabric can presumably be attributed to compaction. Porosities (uncorrected for any clay-bound water) fall below 20% by the base of the hole, and such compaction fabrics are to be expected in deeply buried sediments. XRD studies will reveal if the progressive development of pervasive clay alignment fabrics is associated with recrystallization of smectite to illite.

Together with the compaction fabrics, clay alignment in shear zones might be expected to also intensify with depth (e.g., Fig. F47) through the development of dense low-porosity shear fabrics, although such shear fabrics may also just represent regions with elevated shear strains. However, there are numerous clear examples of single <0.1–1 µm shear zones that cut directly across quite intense preexisting clay-compaction fabrics with almost no wall-damage zone, other than bending the ends of clays that intersect minor shears at a high angle (Fig. F48). This implies extreme strain localization.

Preliminary interpretations

The key observations made on cuttings in Holes C0002N and C0002P, along with structural analyses of cores retrieved in Hole C0002P are as follows:

1. The main structures observed in intact cuttings include slickenlined surfaces, scaly fabric, deformation bands, minor faults, and mineral veins. Slickenlines are observed throughout the whole interval, but scaly fabric is increasingly observed below ~2400 mbsf. The other types of structures are scattered throughout the whole section.
2. SEM images in the upper part of Hole C0002N show little evidence for opal diagenesis, implying that in situ temperatures are <60°–80°C at 1225.5 mbsf. In Hole C0002N, the fabric lacks a strongly preferred orientation in clay-rich materials, except along striated microfaults formed by clays. These zones are extremely localized and a few micrometers or less thick. Only in the deeper part of Hole C0002N do these microfaults reach a few millimeters thick, and even then they are composed of many individual ≤1 µm thick shear zones. In Hole C0002P below 2200 mbsf, SEM images show the development of regularly spaced fabric in sandstones, constituted by thin (<0.1–1 µm), clay-dominated shear planes. Toward the base of the hole below 2625 mbsf, compaction fabrics in clay-rich materials can be observed. This fabric is commonly cut by very thin shear zones with almost no wall-damage zone.
3. A 90 cm thick fault zone with 2 mm angular clasts is present in one of the cores (2204.9–2205.8 mbsf). In its present position, the brittle fault zone is associated with a normal faulting sense. It is unclear if this represents an early prerotation thrust or a late normal fault.

Structural features observed in Holes C0002N and C0002P are characteristic of relatively shallow deformation processes, consistent with deformational features identified from modern accretionary wedges and other shallowly buried accretionary prisms (Taira et al., 1992; Maltman et al., 1993; Yamamoto et al., 2005). The overall character of the deformation (independent particulate flow with limited evidence for cataclastic deformation) is suggestive of a relatively shallow environment (~0–4 km in burial depth).

Biostratigraphy and paleomagnetism

Biostratigraphy

Preliminary biostratigraphy for Holes C0002M, C0002N, and C0002P is based exclusively on the examination of calcareous nannofossils. Abundance and preservation of calcareous nannofossils varies throughout the section. A general preservational pattern of well- to moderately preserved nannofossils was observed in the upper part of the site (475.09–985.50 mbsf), with moderate to poor preservation observed below 985.50 mbsf. Assemblages recovered from Hole C0002M (475.09–506.68 mbsf) are Pleistocene in age, and assemblages from Holes C0002N and C0002P (875.50 and 3058.50 mbsf) indicate late Pliocene to late Miocene age.

Calcareous nannofossils

Shipboard nannofossil stratigraphy for this site is based on the recognition of the events reported in Table T8 in the “Methods” chapter (Tobin et al., 2015). Nannofossils are continuously present throughout the sequence. Their abundance decreases significantly downhole; however, a good biostratigraphic framework was established for the entire succession. A total of 25 samples containing calcareous nannofossils from Sections 348-C0002M-1R-1, 9 cm, to 4R-3, 86 cm, and 287 cuttings samples from 348-

C0002N-3-SMW to 327-SMW and 348-C0002P-9-SMW to 300-SMW were examined. In addition, 25 samples from Sections 348-C0002P-1R-CC, 20 cm, to 6R-CC, 10 cm, were examined.

Hole C0002M

Cores collected in Hole C0002M from 475.00 to 512.50 mbsf yield well-preserved and abundant calcareous nannofossils that exhibit Pleistocene age for the upper part of this interval. Table T13 summarizes the calcareous nannofossil assemblages found in Hole C0002M. Section 348-C0002M-1R-1, 9 cm, from 475.09 mbsf contains *Pseudoemiliania lacunosa,* which indicates a minimum age of 0.44 Ma based on its last occurrence (LO). The presence of *P. lacunosa* indicates nannofossil Zone NN20. The LO of *Helicosphaera sellii* was detected in Section 348-C0002M-1R-3, 64 cm, at 478.47 mbsf. *Gephyrocapsa* spp. (>3.5 µm) was found at 506.68 mbsf, indicating a maximum age of 1.67 Ma for Sample 4R-3, 86 cm, based on the LO of *Gephyrocapsa* spp. (>3.5 µm). Comparison of the ages found in Hole C0002M can be made with Hole C0002B. The LO of *H. sellii* was found in Hole C0002B between 485.98 and 495.37 mbsf (Expedition Scientists 315, 2009), whereas this nannofossil event occurs at a shallower depth of 478.47 mbsf in Hole C0002M. In Hole C0002L, the LO of *H. sellii* was found at 502.74 mbsf (Strasser et al., 2014b).

Holes C0002N and C0002P

Cuttings and core samples from Holes C0002N and C0002P from 875.50 to 3058.5 mbsf contain assemblages ranging in age from the late Pliocene to late Miocene (Table T14). There is a difference in both preservation and abundance of calcareous nannofossils between Holes C0002N and C0002P. Generally, abundance of calcareous nannofossils is lower in Hole C0002P, and assemblages are also less well preserved. Samples collected from the same depths have different preservation and abundances in Holes C0002N and C0002P. In Hole C0002P, abundance of calcareous nannofossils tends to be lower where there is a greater percentage of sand in the sample. Preservation of calcareous nannofossils is also generally poorer where the samples have a higher percentage of sand. Specimens of the genus *Discoaster* are poorly to moderately preserved, commonly with broken rays, making identification to the species level difficult.

Preliminary examination of the cuttings and core samples from Holes C0002N and C0002P revealed good to poor preservation of calcareous nannofossils, with assemblages having relatively low species diversity. Dissolution or deformation occurred, leading to barren or poor occurrence of nannofossils in certain intervals. Several of the zonal markers of the zonation by Raffi et al. (2006) were identified in the sedimentary sequence. The nannofossils identified in Holes C0002N and C0002P are listed in Table T14, and biostratigraphy is summarized in Table T15. Biostratigraphic events observed in Holes C0002N and C0002P are presented in Figure F49.

The uppermost sample from Holes C0002N and C0002P contains *P. lacunosa,* assigning Sample 348-C0002N-3-SMW at 875.50 mbsf to a maximum age of 3.92 Ma. At 905.50 mbsf, *Discoaster brouweri* is present, therefore indicating an age of older than 2.06 Ma and the top of the late Pliocene Zone NN19 for Sample 9-SMW based on the age of its LO. *Discoaster pentaradiatus* is present in Sample 14-SMW, indicating the top of Zone NN18 and an age range of 2.393–2.512 Ma at 925.50 mbsf. Sample 24-SMW (975.50 mbsf) contains specimens of *Sphenolithus* spp., which has a LO of 3.6 Ma and indicates the top of Zone NN17. An age of older than 3.79 Ma can be assigned to Sample 34-SMW (1025.50 mbsf) because it contains *Reticulofenestra pseudoumbilicus* (LO at 3.79 Ma). The presence of *R. pseudoumbilicus* also indicates the bottom of Zone NN16. *Discoaster asymmetricus* is present in Sample 46-SMW, designating Zones NN14–NN15 and an age of older than 4.13 Ma at 1085.50 mbsf. Sample 85-SMW (1245.50 mbsf) contains *Amaurolithus primus* (LO at 4.5 Ma), indicating an age of older than 4.5 Ma. An age of older than 5.59 Ma is indicated by the presence of *Discoaster quinqueramus* in Sample 125-SMW (1436.50 mbsf) because of its LO, marking the top of Zone NN12. The first occurrence of *A. primus* was identified in Sample 192-SMW (1735.50 mbsf), giving an age range of at least 7.362–7.424 Ma and indicating late Miocene Subzone NN11b. Sample 287-SMW (2145.50 mbsf) contains the LO of *Discoaster hamatus,* indicating Subzone NN10a and an age of 9.56 Ma. In Sample 348-C0002P-111-SMW (2245.5 mbsf), *D. hamatus* was last observed downhole, therefore indicating its first occurrence (FO), dated at 10.541 Ma and marking the top of Zone NN9. In Sample 348-C0002P-273-SMW (2945.5 mbsf), *D. brouweri* is present, therefore indicating a maximum age range of 10.734–10.764 Ma at this depth because its FO is at that age range. The presence of *D. brouweri* indicates Zone NN9. Samples analyzed between 2955.5 and 3055.5 mbsf did not yield any calcareous nannofossil zonal marker species; therefore, the deepest section of Holes C0002N and C0002P cannot be dated.

In Hole C0002F, nannofossil events was observed at shallower depths than in Holes C0002N and C0002P (Strasser et al., 2014b). For example, *R. pseudoumbil-*

icus and *Sphenolithus* spp. was observed at 935.5 mbsf in Hole C0002F (Strasser et al., 2014b), whereas *Sphenolithus* spp. was first found at 975.5 mbsf and *R. pseudoumbilicus* was observed at 1025.5 mbsf. *Sphenolithus* spp. was observed at a shallower depth of 906.85 mbsf in Hole C0002J (Strasser et al., 2014b).

Calcareous nannofossil assemblages can provide some insight into paleoceanographic conditions. Species abundance is generally common to rare. In the Pliocene and late Miocene, sediment contains warm-water genera such as *Discoaster* and *Sphenolithus*.

Paleomagnetism

Hole C0002P

Remanent magnetization of archive-half sections from Hole C0002P were measured at demagnetization levels of 0, 5, 10, 15, and 20 mT peak fields to identify characteristic directions. Demagnetizations of 10–15 mT successfully removed low-coercivity components, and magnetic directions after the demagnetizations indicate stable constant directions (Fig. **F50**). Declination, inclination, and intensity profiles with depth after 20 mT demagnetization are shown in Figure **F51.** The declination profile represents widely scattered directions, which is indicative of "biscuiting" of cores created during RCB coring operations. The inclination profile reveals that data are of dominantly positive inclination, and the degrees of the positive inclination in each interval are not constant. For example, the calculated mean inclinations using the method proposed by Arason and Levi (2010) are 34.22° for the interval between 2172.450 and 2174.955 mbsf, 61.83° for the interval between 2194.005 and 2196.985 mbsf, and 36.50° for the interval between 2210.0 and 2215.0 mbsf. Some intervals show steep negative inclinations, which occur in relatively short intervals. Interestingly, the interval between 2205.195 and 2205.515 mbsf, which shows a clear negative inclination, corresponds to the brittle fault zone (see **"Structural geology"**). This suggests a different timing of magnetization for this interval from that of the intervals lying above and below. In order to elucidate the lock-in timing of those magnetizations, careful evaluation referencing structural analysis (e.g., bedding) results is required for postcruise study.

Geochemistry

Hole C0002M

Interstitial water chemistry for core samples

One whole-round sample of 20 cm length was collected from each of the four Hole C0002M cores (348-C0002M-1R-1, 87–107 cm; 2R-2, 111–131 cm; 3R-1, 90–110 cm; and 4R-2, 113–133 cm). Interstitial water (IW) was obtained with a 55 mm diameter Manheim squeezer. The squeezing method used for this experiment differs from the standard squeezing method (see **"Geochemistry"** in the "Methods" chapter [Tobin et al., 2015]). Because the cores were not processed until 72 days after they were collected, the data are not useful for geochemical interpretations, but the cores were used to test the new squeezers to determine maximum squeezing pressure to use for future IW sampling. Increasing pressures up to 60,000 lb (corresponding to an applied pressure of 112 MPa) with different time steps were applied for assessing the effect of high pressure on the measured value of chlorinity, and IW was sampled at each different time interval. The squeezing sequences and their corresponding aliquots of IW and chlorinity results are listed in Table **T16.**

All samples were squeezed first according to standard hydraulic press Recipes 1–3 (Table **T16;** up to 20,000 lb [37 MPa] applied force), and Aliquot A was collected. The core samples were squeezed according to recipes 4–6 (up to 25,000 lb applied force [47 MPa]), and Aliquot B was collected. Finally, for samples from Sections 1R-1 and 2R-2, a force of 60,000 lb (112 MPa) was reached in four increments and Aliquot C was collected. For samples from Sections 3R-1 and 4R-2, an additional aliquot of fluid (Aliquot C′) was collected at 50,000 lb (94 MPa) just before ramping applied force up to 60,000 lb (112 MPa). This force was held for 12 h, and then Aliquot C″ was collected.

Results of chlorinity measurements for different applied pressures are reported in Figure **F52.** Overall, results show a freshening of the fluid when the same sample was squeezed at higher pressure and for a longer time. With the exception of the highest pressure water sampled from Section 3R-1, chlorinity values are higher than those observed at the same depth interval (475–504.41 mbsf) during Expedition 338. This is likely due to contamination by higher chlorinity mud water while the cores were stored. During the pressure experiments, freshening increased with increasing pressure. The signal is strongest with core samples squeezed at pressures above 25,000 lb (47 MPa). In all four experiments, the first two squeezing steps yielded water with the same chlorinity value within error. Relative to the average of the first two steps, the long, highest pressure step (~60,000 lb [112 MPa] for 12 h) shows chlorinity decreases of 3% for samples from Sections 1R-1, 2R-2, and 4R-2 and 7% for Section 3R-1. The mechanism that induces the freshening of IW at high pressure is not yet understood, and later shore-based experiments will be conducted.

Organic geochemistry

Carbonates, organic carbon, and total nitrogen

Carbon values were analyzed for 15 samples from the four cores from Hole C0002M (Fig. F53; Table T17). Calcium carbonate content ranges from 4.26 to 13.67 wt% (median = 6.24 wt%). The highest point value of 13.67 wt% is from 478.70 mbsf (Sample 348-C0002M-1R-3, 87–89 cm), whereas Core 348-C0002M-4R has the highest average value. Carbonate content at this depth interval in Hole C0002M is higher than the highest and average values determined in the same interval in Hole C0002L obtained during Expedition 338, which were 6.1 and 1.4 wt%, respectively. Total organic carbon (TOC) is low, ranging from 0.46 to 0.82 wt%, and decreases slightly with depth. Hole C0002M TOC values are similar to those observed during Expedition 338 at the same depth interval. Total nitrogen (TN) is also low in Hole C0002M, similar to Expedition 338, and low TOC/TN values in Hole C0002M indicate a marine origin for the organic matter.

Comparison of XRD and coulometric data shows that the relative trends are the same, but XRD underestimated the abundance of carbonates (see "Lithology").

Gas chemistry from cores

Headspace gas samples were taken from the four cores in Hole C0002M. Methane, ethane, and propane concentrations in the headspace gas were measured by a gas chromatograph–flame ionization detector (GC-FID) (see "Gas analysis in core samples" in the "Methods" chapter [Tobin et al., 2015]).

The concentrations of methane and ethane are shown in Table T18 and Figure F54. Propane was not detected in the core samples. The concentrations are shown in parts per million by volume (ppmv) and moles per kilogram, which is the concentration of gas molecules dissolved in 1 kg of interstitial water, as calculated by the equation in "Gas analysis in core samples" in the "Methods" chapter (Tobin et al., 2015). The concentrations of methane and ethane are 2532–7355 and 5.4–9.9 ppmv, respectively. Although variable, the concentrations generally increase with increasing depth.

Temperature estimation from headspace gas and total organic carbon

A cross plot of $C_1/(C_2 + C_3)$ ratios and temperature is commonly used to get quick information about the origin of the hydrocarbons (i.e., to distinguish between biogenic gas and gas migrated from a deeper source of thermogenic hydrocarbon). A very high $C_1/(C_2 + C_3)$ ratio indicates in situ gas formation by microbiological process. On the other hand, the occurrence of major amounts of $C_2 + C_3$ in shallow depths is associated with thermogenic hydrocarbon generation and migration. In general, the $C_1/(C_2 + C_3)$ ratio consistently decreases with burial depth, resulting in a consistent (normal) decrease in the $C_1/(C_2 + C_3)$ with increasing temperature. Anomalously low $C_1/(C_2 + C_3)$ ratios suggest the presence of migrated thermogenic hydrocarbons. The separation pattern of normal versus anomalous zones was suggested by Stein et al. (1995) and JOIDES Pollution Prevention and Safety Program (PPSP; 1992) and is shown in Figure F55. Temperature estimations are based on heat probe and LWD data (JOIDES PPSP, 1992). Also shown by the solid lines is the approximate influence of different levels of organic carbon content (i.e., TOC). Sediment showing high C_1 concentrations is characterized by relatively high organic carbon contents and high sedimentation rates because the decomposition of the organic matter is dominated by anaerobic microbial processes under these conditions (Claypool and Kvenvolden, 1983). Although this diagram was initially established for safety purposes, it is used here to estimate approximate temperatures in the borehole using TOC in cuttings (>4 mm) and the $C_1/(C_2 + C_3)$ ratio in drilling mud-gas data obtained during Expedition 348. Following this approach, it seems that the $C_1/(C_2 + C_3)$ ratios are too low for the given TOC concentrations and thus would result in unrealistically high temperatures (Table T19). Most likely, hydrocarbon gas concentrations are not only generated in situ but are also influenced by gas migration. Consequently, the temperature-$C_1/(C_2 + C_3)$-TOC relationship is not suitable for estimating formation temperature (JOIDES PPSP, 1992).

Holes C0002N and C0002P

Interstitial water chemistry for core samples

Five whole-round samples varying from 10 to 41.5 cm were collected from Cores 348-C0002P-2R through 6R over the 2176.28–2211.31 mbsf depth interval (see "Geochemistry" in the "Methods" chapter [Tobin et al., 2015]). Recovery in Core 1R was insufficient for an IW sample. Traditional squeezing methods did not produce any IW because of sediment consolidation, so all samples were processed to obtain pore water (GW) using the ground rock interstitial normative determination (GRIND) method used during Expedition 338 (Wheat et al., 1994). Data are summarized in Table T20, after correction of dilution based on the water content determined at 60° and 105°C, with the exceptions of salinity (refractive index) and pH.

Salinity values obtained by the standard GRIND method, including determination of IW percentage by drying samples at 105°C, show a large range paralleled by chlorinity values, which range from 387 to 848 mM (Fig. F56). The lowest value of the chlorinity range is similar to values obtained in Kumano Basin sediment, either from the standard or GRIND method (Strasser et al., 2014a). Chlorinity in Section 348-C0002P-4R-2 samples is >50% higher than average seawater (551 mM). The standard drying temperature of 105°C to determine GW content could give erroneously high estimates of IW by also releasing some of the clay-bound water. If estimates of pore water obtained using a lower drying temperature of 60°C are considered; however, the chlorinity values are significantly higher for three of five samples (Sections 2R-3, 4R-2, and 6R-2).

Chlorinity values show a downhole variation of alternating high and low values paralleled by several other major and minor ions, including Br^-, NH_4^+, Na^+, K^+, Mg^{2+}, Ca^{2+}, Li, Mn, Ba, Si, B and Sr (Figs. F56, F57). Although the possibility of localized brines in the formation cannot be excluded, it is unlikely that such large fluctuations in concentrations could occur in samples taken only 10 m apart with respect to depth. It is more likely that the variations in concentrations are related to lithology or mineralogy, core retrieval, and sample processing of the GRIND method. Crushing the samples may have damaged clay minerals and increased their capacity to absorb water. Also, addition of water in the sample produces a paste that is also subject to water loss during the transfer process. Both of these processing steps could induce artifacts in measured values of chlorinity.

Cross plots of Na^+, K^+, and Ca^{2+} versus chlorinity in GW, along with concentrations in mud water, show trends indicating that most of the variation in compositions is related to changes in salinity (Fig. F58). The plots show that mud contamination can be eliminated as the cause of this salinity increase, as no mixing trend between a lower saline fluid and the mud-water concentrations is observed except for Sample 2R-3, for which a slight trend toward mud potassium values exists. KCl was a significant additive to the mud fluids and K^+ in mud-water samples is almost 1–2 orders of magnitude higher than in GW, whereas Cl in mud water is only ~4 times the GW values (Table T21). Moreover, the perfluorocarbon (PFC) tracer data indicate that mud-water contamination is possibly 5% in this sample (Table T22; Fig. F59).

The cause of the salinization trends in Hole C0002P cores is not clear. The increase in concentrations might be related to uptake of freshwater by hydrous clay minerals, occurring in response to unloading during the wireline trip of the core barrel back to the surface, which took ~2 h. Uptake could also occur during the milling process of preparing GRIND samples. The differences in salinity increases would then be related to differences in clay mineral abundance or clay mineralogy in the different cores. This will be investigated further with shore-based research.

To examine whether signals related to diagenesis or other geological processes are present in GW data from the cores, the concentrations were normalized to chlorinity and plotted relative to depth for selected ions (Fig. F60). This assumes that actual chlorinity values do not vary substantially over the cored interval or the processes effecting the concentration data was a simple addition or subtraction of water from the pore space that equally impacted all ions (e.g by simple hydration/dehydration of hydrous clays as one example). Clearly, chlorinity variations can occur, so the following observations can only be considered as approximations.

Normalization of concentrations to chlorinity significantly reduces the scatter in the data for many elements, although it does not completely eliminate the alternating pattern of high and low values observed in the concentration data (Table T23; Fig. F61). K and Ca show significant variation after normalization. The variations are in the range of those observed in shallower parts of Site C0002. The highest normalized K value could reflect some contamination by drilling mud, which has high K contents. However, the other alkali metals, Rb and Cs, also show high values in this core (not present in any quantity in the mud), and thus the large values are more likely to reflect diagenetic or other natural processes occurring at this depth. The range of normalized K and Rb suggests variations related to clay mineral diagenesis, such as might be expected for the conversion of smectite to illite. Normalized Ca and Sr values also show ranges that suggest variation related to carbonate diagenesis. Core 5R exhibits large carbonate veins associated with a fault zone in Section 5R-4.

The results of trace element concentrations extracted by the GRIND method are plotted in Figure F62 and listed in Table T20. Most of the minor and trace elements fall in the range of concentrations obtained from the standard squeezing method on cores from Holes C0002B and C0002J (lithologic Unit III/IV; Strasser et al., 2014b). Trends similar to salinity are observed for Rb and Cs, and presumably Zn, despite missing data for Section 5R-2 (not detected during analysis). Mo shows remarkably high concentrations that are 10 times greater than those from Expedition 338 (Strasser et al., 2014b). One explanation could be contamination by the grease used to connect drilling pipes, but core contamination is generally not indicated by the PFC test. Cs concentrations are also two times higher than in Holes C0002B and C0002J. Pb decreases with depth comparably to SO_4^{2-}. As previously observed in GRIND results from Expedition 338 (Strasser et al., 2014b), no Fe was detected with the inductively coupled plasma–mass spectrometry except in Section 6R-2, with a concentration of 2.04 mM after correction with the water content at 60°C. It is likely that Fe was oxidized by the grinding process and adsorbed on mineral surfaces.

Organic geochemistry

Carbonates, organic carbon, and total nitrogen

Carbonates as $CaCO_3$, TOC, and TN were determined from the 1–4 and >4 mm size fractions of the cuttings from Holes C0002N and C0002P and in Hole C0002P cores. TOC was calculated by the difference of total carbon (TC) and inorganic carbon (IC) (see **"Geochemistry"** in the "Methods" chapter [Tobin et al., 2015]. Results are plotted in Figure **F63** and listed in Tables **T24** and **T25.** Contamination by cement from drilling operations was observed in $CaCO_3$ and CaO profiles of XRF data (Fig. **F13B**) from 870.5 to 950.5 mbsf (Sample 348-C0002N-20-SMW) in Hole C0002N and from 1960.5 to 2040.5 mbsf (Sample 348-C0002P-32-SMW) in Hole C0002P. Those data were therefore not plotted in the figure and are not discussed in the following section.

$CaCO_3$ in cuttings varies from 0.46 to 9.61 wt% with a median of 3.2 wt%. Scattered data are mostly observed in cuttings from Hole C0002N, whereas those from Hole C0002P show a narrower range of values. A prominent peak is observed at ~1900 mbsf, where $CaCO_3$ is as high as 7.94 wt%. Plots of the data from the drilling mud seem to follow the same trend and could reflect an uptake of carbonates in the mud. The peak is also reflected by CaO in XRF data (see **"Lithology"**). A wider peak at ~2650 mbsf shows $CaCO_3$ values as high as 5.80 wt%. Despite occurrences of carbonate veins recovered in the fault zone at 2205 mbsf, no increase in $CaCO_3$ is visible at that depth in the core samples or the cuttings.

TOC varies between 0.47 and 2.07 wt%, with a median of 0.9 wt%. The trend shows a gradual downhole decrease with local minor variations along the profile (e.g., a small peak at ~1790.5 mbsf [Sample 348-C0002N-205-SMW]). The range of values at the bottom of Hole C0002N between 2040 and 2320 mbsf does not strictly match those at the beginning of Hole C0002P, even though data for $CaCO_3$ and TN match in the overlapping interval. Data from core samples in Hole C0002P agree with those of cuttings from Hole C0002P more than with cuttings from Hole C0002N.

TN varies between 0.024 and 0.064 wt% with a median of 0.053 wt%. TN does not show any particular trend in cuttings from Hole C0002N. A shift toward higher values is observed around 2600 mbsf in cuttings from Hole C0002P. Most of the core samples have higher TN values than cuttings of both holes, except for two core samples (Sections 2R-4 and 5R-5) that have lower values

The C/N ratio that depicts marine (4~10) or terrestrial (>10) origin of organic matter varies from 7.58 to 35.58 with a median of 17.53. Therefore, most of the organic matter in Holes C0002N and C0002P is considered to be of terrestrial origin. However, core samples seem to tend toward to marine origin except for two samples (Sections 2R-4 and 6R-4), highlighting possible contamination from mud water in cuttings. The decreasing trend of the C/N ratio and the variations within match those observed in the TOC profile.

Gas chemistry from cores

Concentrations of methane (CH_4), ethane (C_2H_6), and propane (C_3H_8) in the headspace gas collected from core in Hole C0002P (2160–2220 mbsf) are shown in Table **T26** and Figure **F64.** Methane is the predominant hydrocarbon in all core samples, and ethane and propane were detected in all samples. The concentration of methane varies between 1,704 and 10,676 ppmv, except for two peaks at 2176.7 mbsf (20,183 ppmv) and 2183.4 mbsf (23,455 ppmv). The concentrations of ethane and propane are 57.5–346.9 and 24.6–351 ppmv, respectively, and increase slightly with increasing depth. The Bernard parameter ratio (i.e., $C_1/(C_2 + C_3)$ is also shown in Table **T26** and Figure **F64.** The $C_1/(C_2 + C_3)$ ratio varies between 7 and 68, and its trend mostly resembles methane concentrations. At 2205.5 mbsf, where the fault zone was identified (see **"Structural geology"**), the concentrations of ethane and propane decrease slightly relative to methane, and the $C_1/(C_2 + C_3)$ ratio increases.

Comparison between headspace gas data and drilling mud-gas data obtained by gas chromatograph–natural gas analyzer (GC-NGA) and GeoServices analysis shows that the concentrations of methane, ethane, and propane in the drilling mud are much lower than those in the headspace gas (Fig. **F65**). The highest methane concentration in the drilling mud is 696.7 ppmv at 2174 mbsf. The gas recovery rate by

GC-NGA analysis is up to 27% at 2174 mbsf. Methane concentration estimated by GeoServices analysis is also lower (<750 ppmv) than headspace gas, with a recovery rate up to 6%. The highest ethane and propane concentrations are 7.1 ppmv (2180.4 mbsf) and 2.81 ppmv (2164.5 mbsf), respectively, and the recovery rate of these gases is 8% by GC-NGA analysis. This underestimate is likely caused by the high mud density and low rate of penetration during coring. Despite the different concentrations, relative changes in methane are similar, with the highest methane values in Cores 348-C0002P-2R and 3R and an overall decrease in concentrations with increasing depth. Within the cores, ethane and propane variations are similar; ethane and propane start to increase with Core 5R, but the drilling mud-gas concentrations decline.

The $C_1/(C_2 + C_3)$ ratios calculated using GC-NGA and GeoServices data are higher than the headspace data (36–124 and 15–47, respectively) (Fig. F66). Figure F67 shows the Bernard diagram, which is usually used to distinguish between thermogenic and biogenic sources of hydrocarbon gas (Bernard et al., 1978). Microbial origin methane has $\delta^{13}C\text{-}CH_4$ values <55‰ Vienna Peedee belemnite (VPDB) (Rice and Claypool, 1981), and $C_1/(C_2 + C_3)$ ratios as high as 1000 (Bernard et al., 1978). Thermogenic methane has $\delta^{13}C\text{-}CH_4$ values between –50‰ and –25‰ VPDB (Schoell, 1983) and $C_1/(C_2 + C_3)$ ratios lower than 100. The headspace methane sampled from Hole C0002P core samples primarily falls in the region of thermogenic origin (Figs. F66, F67).

Comparison with other data sets

Plotting the C_2/C_1 ratios of headspace gas samples versus $\delta^{13}C\text{-}CH_4$ from the methane carbon isotope analyzer (MCIA) data set (Fig. F68) indicates normal maturation of organic matter rather than migration or diffusion of thermogenic gas. Figure F69 shows moisture and density (MAD)-derived porosity versus total headspace gas volume. In general, higher gas concentrations are expected for elevated porosities. Two outliers with exceptionally high gas concentrations at a porosity of ~0.2 are at a horizon where faults were identified (see **"Structural geology"**). Such high concentrations were not observed in the drilling mud-gas data, however. The significance of Rn data generated during coring and hole opening by underreaming are ambiguous. Although ^{222}Rn in Hole C0002N is only present in traces, coring and drilling Hole C0002P revealed concentrations up to ~200 and 250 Bq/m^3, respectively (Fig. F70).

Mud-gas chemistry

Overview of mud-gas composition

Continuous drilling mud-gas monitoring took place while drilling Holes C0002N and C0002P from 838 to 2330 mbsf and 1954 to 3058.5 mbsf, respectively. Two autonomous data sets were generated during the operation: a Rn data set available from the stand-alone Rn monitoring instrument (see **"Online radon analysis"** in the "Methods" chapter [Tobin et al., 2015]) and one from the SSX database, which was compiled with data from the GeoServices and scientific mud-gas monitoring systems on the *Chikyu* (hereafter referred to as "SciGas system"; see **"Onboard mud-gas monitoring system"** in the Methods chapter [Tobin et al., 2015]). The latter provided data from the GC-NGA, MCIA, and process gas mass spectrometer (PGMS). Gas concentrations determined by the MCIA, GC-NGA, and PGMS differ from those measured by GeoServices, most likely due to having a different degasser configuration of the onboard system during drilling of Hole C0002N (Strasser et al., 2014b). For Hole C0002P, the scientific degasser system and location were changed, which resulted in similar concentrations to the GeoServices' system (Figs. F65, F71; see also **"Geochemistry"** in the "Methods" chapter [Tobin et al., 2015]). For the PGMS, this is only of secondary importance because the concentrations of different gases were normalized to 100%. Nevertheless, the individual data sets include data from different instruments, measurement techniques, and sampling intervals, and all data are influenced by drilling operations (e.g., rate of penetration, mud pump activity, and mud weight).

In the GeoServices data set, the total hydrocarbon gas volume content range from ≤0.0001% (i.e., below detection limit) to 8.2% at ~1305 mbsf. At a similar depth, methane has a maximum concentration of 8.1%. Overall, methane trends resemble the concentrations of total gas, and methane dominates the gas show. Ethane and propane are only present in minor concentrations, with the highest values at 979 (0.05% ethane) and 1302 mbsf (0.02% propane), respectively. Higher homologs (i.e., *n*-butane, *i*-butane, *n*-pentane, and *i*-pentane) typically stay below 0.01% and do not add significantly to the total gas composition. In Hole C0002N, absolute gas concentrations determined by the SciGas system are significantly lower than those from the GeoServices data set, except for ethane. However, relative changes in gas concentration in the SciGas data are similar to GeoServices with maxima between 1320 and 1405 mbsf (Figs. **F71, F72, F73**). In Hole C0002P, the new degasser configuration led to absolute gas concentrations for methane and propane on the same order of magnitude as the GeoServices instruments (Figs. **F65, F74, F75**). Ethane values from GeoServices remain higher by a factor of ~10.

For nonhydrocarbons, the PGMS data set is dominated by nitrogen (~77.6%) and oxygen (~20.7%), whereas the concentrations of the remaining nonhydrocarbons rang from 1.15 × 10^{-6} percent for CO_2 to 0.99% for Ar (Fig. **F76**). Absolute concentrations determined with the PGMS are influenced by sensitivity checks and calibration, which lead to sudden concentration shifts, and therefore the data might be biased (see **"Online gas analysis by process gas mass spectrometer"** in the "Methods" chapter [Tobin et al., 2015]). In addition, depth intervals for which the ion current of the PGMS was unstable were removed from the data set. The concentrations of He, H_2, and Xe usually remain below the detection limit. H_2 was detected with the GC-NGA only in Hole C0002P (1954–3058 mbsf), with values up to 0.78% (Fig. **F77**). ^{222}Rn concentrations usually stay below 450 Bq/m^3 (Fig. **F78**).

Hydrocarbon gas distribution with depth

From 838 to 983 mbsf in Hole C0002N, total gas concentration stays below 2% and then abruptly increases to ~6.4% (Fig. **F71**). Gases in this interval are mainly hydrocarbons. Between 983 and 1500 mbsf, total gas concentration remains between 0.01% and 8.2%. Below 1500 mbsf, the values decrease sharply and stay less than 3.0%, except at 2145 mbsf, where the concentration increases to 3.2%. In Hole C0002P, total gas concentrations follow similar trends but are ~1 order of magnitude smaller compared to the Hole C0002N data set (Fig. **F65**). Starting at ~2170 mbsf, total gas concentrations in Hole C0002P decreases sharply to <0.2%, followed by an increase to ~0.9% at ~2184 mbsf. Farther downhole, no change in trend is visible.

As mentioned above, the gas show is dominated by methane (Figs. **F71, F72**). Data quality for ethane and propane from 838 to 1560 mbsf is poor, with most of the values below detection limit. Both ethane and propane show distinct peaks at ~980 mbsf with a sudden increase to 0.05% and 0.01%, respectively. Between 980 and 1560 mbsf, ethane concentrations remain less than 0.03%, whereas propane concentrations further increase with a maximum of 0.02% at 1320 mbsf. Below 1560 mbsf, data quality increases as ethane and propane concentrations rise above the detection limit. However, ethane values stay less than 0.03%, and propane decreases to concentrations less than 0.01%. Intervals relatively enriched in ethane and ethane + propane were found between 1825 and 1970 mbsf and between 2070 and 2220 mbsf, respectively. The sudden increase in propane from 0.001% to 0.01% between 1990 and 2000 mbsf is exceptional in the hydrocarbon gas show. Similar to the total gas/methane concentrations, ethane and propane in Hole C0002P are up to 2 orders and 1 order of magnitude smaller, respectively, compared to gas concentrations in Hole C0002N (Figs. **F65, F74, F75**). Relative changes, however, are similar. At ~2170 mbsf, ethane and propane decrease below detection limit for the GeoServices instruments, whereas the GC-NGA-reported concentrations are <10 ppm. Starting at 2200 mbsf, all data sets show a continuous increase of higher hydrocarbons (ethane and propane) with depth.

Distribution of nonhydrocarbon gas data with depth

^{222}Rn values detected by the stand-alone Rn monitor show an increase with depth with some scatter (Fig. **F78**). In Hole C0002P between 1954 and 2330 mbsf, ^{222}Rn values are almost twice as high as in Hole C0002N. Also, the significant decrease in Hole C0002N between 1835 and 2000 mbsf is absent in Hole C0002P. Overall, the Hole C0002P data follow the trend starting at 1835 mbsf in Hole C0002N, and concentrations increase to values >300 Bq/m^3 at ~2500 mbsf. Below 2500 mbsf, ^{222}Rn data show no trend but are highly scattered between 56 and 692 Bq/m^3.

Nonhydrocarbons detected by the PGMS show major variations only at points when calibration or sensitivity checks were carried out (Fig. **F76**). With averages of 77.6%, 20.7%, and 0.96% for N_2, O_2, and Ar, respectively, concentrations are similar to atmospheric values. CO_2 shows a slightly negative trend downhole from ~838 to 1300 mbsf. With an average of 0.0005%, concentrations of CO_2 stay below atmospheric values, except for ~1677 mbsf, where a single peak of 0.16% occurs, and below 2600 mbsf, where values >0.2% were encountered. In Hole C0002N, He and Xe values are as high as 0.06% and 0.02%, respectively (3 orders of magnitude higher than atmospheric values). Starting at 2600 mbsf, He and Xe have even higher concentrations, to 3% and 2.9%, respectively. Overall, He and Xe show a slightly positive trend in Hole C0002P.

H_2 data detected by the GC-NGA are relatively constant downhole and stay below 0.075%. At two exceptional peaks at 1969 and 3043.5 mbsf, H_2 reaches values to 0.34% and 0.78%, respectively.

Comparison with data from Expedition 338, Hole C0002F

The gas data from 838 to 2007 mbsf in Hole C0002N and from 1954 to 2007 mbsf in Hole C0002P are compared with the gas show from Hole C0002F (Strasser et al., 2014b). Comparison between the three mud-gas data sets reveals the following (Figs. F71, F76, F78, F79, F80, F81, F82):

1. Gas show: in all holes, gas show is dominated by methane.
2. Total gas and methane: the prominent gas kick of total gas and methane in Hole C0002F between 918 and 1000 mbsf is absent in Hole C0002N. By contrast, a small gas kick occurs in Hole C0002N between 1300 and 1460 mbsf, whereas no excursion is visible in Hole C0002F. The overall total gas/methane concentrations in Hole C0002N remain slightly higher downhole. Between 1950 and 2010 mbsf, data from Hole C0002P became available. Overall concentrations are lower, and the peak at ~1993 mbsf is absent in the Hole C0002F data (Fig. F79).
3. Ethane: overall, ethane concentrations in all boreholes are less than 0.05%. Between ~900 and 1500 mbsf, the two data sets show no apparent correlation. The gas kick in Hole C0002N at ~980 mbsf correlates well with the lower boundary of the gas kick in methane from Hole C0002F but has no corresponding signal in ethane from Hole C0002F. Between 1250 and 1460 mbsf in Hole C0002N, there is no sudden shift to higher concentrations in ethane, contrary to Hole C0002F. Between 1500 and 1700 mbsf, ethane concentrations show no significant deviation. Between 1700 and 1800 mbsf, ethane concentrations in Hole C0002F increase, contrary to the concentrations in Hole C0002N. Below 1800 mbsf, ethane concentrations drop in Hole C0002F but rise in Hole C0002N. In Hole C0002P, the few data points show concentrations ~1 order of magnitude lower compared to data from Hole C0002F (Fig. F79).
4. Propane: overall, propane concentrations in both Holes C0002F and C0002N remain very low (<0.008%). The elevated concentrations starting at ~980 mbsf are absent in Hole C0002F. Between ~1250 and ~1500 mbsf, propane concentrations in Hole C0002N are high, whereas a decline is visible in Hole C0002F. Below ~1500 mbsf, propane concentrations in Hole C0002N are similar to those in Hole C0002F. In Hole C0002P, propane is only present in trace amounts (Fig. F79). Concentrations are similar to Hole C0002F.
5. $\delta^{13}C$-CH_4: except for some outliers, data from Holes C0002N and C0002P match data from Hole C0002F. At ~1700 mbsf, a shift to more thermogenic methane is indicated by values greater than or equal to –60‰ (Fig. F80).
6. Other nonhydrocarbon gases: comparison between the two mud-gas data sets obtained by the PGMS (both data sets are normalized to 100%) and the ^{222}Rn data sets reveal the following (Figs. F78, F81, F82):
    a. ^{222}Rn: above 1835 mbsf, ^{222}Rn concentrations in Hole C0002N are significantly lower than in Hole C0002F (Figs. F78). Except for the peak between 918 and 1000 mbsf in the Hole C0002F data, relative changes in concentrations are the same. Between 1835 and 2007 mbsf, both data sets correspond well in absolute values and relative changes in concentration. The same is true for data from Hole C0002P (Fig. F81).
    b. Despite some problems with the ion current, data quality from the PGMS improved (Figs. F76, F82). Fewer calibrations were necessary, which decreased the number of data shifts in the Expedition 348 data set.
    c. All data sets are dominated by atmospheric gases ($O_2 + N_2 = 98.3\%$).
    d. N_2 and O_2 concentrations in Hole C0002F are slightly higher and lower (Fig. F82), respectively, when compared to the values from Expedition 338. Ar values are higher in Hole C0002P, whereas Hole C0002N data resemble the Hole C0002F concentrations. CO_2 is highest in Hole C0002N and lowest in Hole C0002P. At ~1930 mbsf, a CO_2 peak in Hole C0002F corresponds to elevated values in Hole C0002N. A limited increase in CO_2 at ~1985 mbsf is reproduced in Hole C0002P.
    e. Values of Xe are similar, whereas at depths shallower than 1200 mbsf, He concentrations are lower, and at depths deeper than 1600 mbsf, He concentrations are higher (Fig. F76). Between 1200 and 1600 mbsf, the apparently higher He concentrations are most likely caused by calibration of the PGMS during monitoring. Overall, concentrations in Holes C0002N and C0002P are higher compared to Hole C0002F (Figs. F76, F82).

Influence of drilling parameters and comparison with other data sets

The drilling mud-gas data can be easily influenced by drilling, or operational, parameters. For example, degassing is less effective when the mud level drops in the return mud trough, which can produce mud gas "artifacts" in gas data. The movement of the BHA up and down ("swabbing") within already drilled sections can also produce mud-gas anomalies, which underlines the importance of correlating operational procedures with mud gas analyses. This movement of the BHA can produce an effect similar to "pumping," as the movement of the BHA acts similarly to a piston in the borehole and can draw in mud gas from the formation, influencing mud-gas concentration analyses.

The influence of changes in drilling parameters becomes obvious when comparing the concentrations of hydrocarbon gases between drilling mud-gas data and in headspace gas data from the cored section of Hole C0002P; drilling mud-gas data from Hole C0002P were 1 order of magnitude lower. Propane in both Holes C0002N and C0002P are 1 order of magnitude lower compared to the headspace gas concentrations. It remains possible that the use of progressively higher mud weights in Hole C0002P compared to Hole C0002N (1.12 to 1.32 sg) could reduce the intake of higher hydrocarbons, and at the surface, hydrocarbons are likely to be retained in the cold, dense drilling mud (Ablard et al., 2012). As a consequence, the difference is most likely caused by underestimation of hydrocarbons in the drilling mud gas.

Two more examples of drilling operation artifacts occur at ~1320 and ~1954 mbsf. The prominent gas peaks correspond clearly to a time when the drill string was moved up and down several times and thus are interpreted as "trip gas" or "swab gas" rather than a true increase in formation gas concentration. An example of swab gas is visible between 30 December 2013 and 1 Jan 2014. When swabbing took place at ~4916.0 and 5010.7 m BRT, gas concentrations in drilling mud increased abruptly (total gas >3.5% and methane >28000 ppmv). The swabbing effect of upward movement of the drill string induced a temporary reduction of pressure in borehole. If the hydrostatic pressure at the bottom of the borehole decreases below the formation pressure of a gas-bearing formation, gas would be introduced into the borehole. Breakouts, possibly caused by temporary underpressure in the borehole, are also suggested by the presence of "pressure cuttings." The first major total gas peak clearly corresponds to swabbing at ~4915 m BRT and is within the expected lag time (i.e., ~135 min at this depth) for a constant mudflow rate. The next major peak occurs after swabbing at ~5015 m BRT between 2200 and 2300 h (i.e., after 2345 h), with the bit moving up and down in smaller steps. At this time the role of the mudflow rate remains unclear. Although the time difference is understandable given the low mudflow rate during swabbing, it is still within the expected lag time. Large volumes of gas tend to move upward faster than the drilling mud, and this upward movement increases with decreasing depth. Alternatively, if changes in flow rate are taken into account, swabbing at more shallow depths could be responsible as well.

The influence of changes in drilling parameters becomes obvious when comparing the concentrations of hydrocarbon gases in the drilling mud-gas data with the concentrations found in headspace-gas data from Hole C0002P (Fig. **F65**). Although drilling mud-gas data from Hole C0002N showed concentrations for methane and ethane similar to those in headspace gas from Hole C0002P, drilling mud-gas data from Hole C0002P are 1 order of magnitude lower. Propane in both Holes C0002N and C0002P are 1 order of magnitude lower compared to the headspace gas concentrations. Higher hydrocarbons are present in headspace gases at up to 49 ppmv (for *i*-butane) (Table **T26**). Subsequently, the Bernard parameter based on headspace gases indicates a slightly more thermogenic regime (Fig. **F67**). Reasons for this discrepancy are manifold, including the use of a higher mud weight in Hole C0002P and changing degasser efficiency (i.e., how much gas could be extracted from the drilling mud). Higher mud density would reduce the intake of higher hydrocarbons in the borehole, and at the surface, hydrocarbons are likely to be retained in the cold, dense drilling mud (Ablard et al., 2012). As a consequence, the difference is most likely caused by underestimation of hydrocarbons in the drilling mud gas.

In addition, the distributions of hydrocarbon gas expelled from Hole C0002P (1966.5–2780.2 mbsf) during widening of Hole C0002P (reaming gas) is different compared to that obtained during drilling. Concentrations of methane and ethane in the reaming gas are similar to gas concentrations encountered during drilling at shallower depths. However, methane and ethane found during drilling increased more steeply with depth. Concentrations of propane in the reaming gas hardly change with depth profile. At the same time, propane increased with increasing depth during drilling and became higher than the reaming gas at ~2400 mbsf. To estimate the difference of those hydrocarbon gas characteristics, these data are plotted on the Bernard diagram. Whereas gas concentration ratios obtained from drilling plot in a mixing area, reaming gas concentration ratios indicate a strong thermogenic regime.

Based on the overall changes detected in hydrocarbons in the GeoServices and SSX data sets, 3 boundaries (4 gas packages) are defined (Fig. **F83**). The first boundary, separating log Unit III from IV, is set at 983 mbsf, where a minor gas increase exists. The overall drop in hydrocarbon gas concentrations at

1500 mbsf is considered a second boundary. The third boundary is set at ~2200 mbsf, where the total gas concentrations increase overall. Considering other shipboard data allows correlation of some gas geochemical data to log unit boundaries at 915 mbsf (Unit III/IV boundary), 1514 mbsf (Subunit IVd/IVe boundary), and 2191 mbsf (Subunit Vb/Va boundary). Between 860 and 2008 mbsf, 7 hydrocarbon gas packages were defined during Expedition 338 (Strasser et al., 2014a), of which the Package 1/2 boundary at 918 mbsf and Package 4/5 boundary are close to the gas package boundaries defined during Expedition 348. The fact that none of the gas-package boundaries precisely match the log unit boundaries might be related to hydrocarbon gas diffusion and the uncertainties related to drilling mud-gas monitoring. Later postcruise research might elucidate the cause of these differences.

Similar to the data from Expedition 338 (Strasser et al., 2014a), the causes of nonhydrocarbon-gas data shifts at ~900, 1190, 1650, 2008, and ~2200 mbsf are not fully resolved. Most of the anomalies in the PGMS data correlate well with periods in which sensitivity checks or calibrations were carried out (Fig. F76).

Nonhydrocarbon gases are clearly dominated by atmospheric components. Although N_2 can also originate from various sources, including clay-rich sedimentary rock (e.g., Krooss et al., 1995; Mingram et al., 2005) the N_2/Ar ratio < 100 (Jenden et al., 1988; Krooss et al., 1995), and the overall constant He/Ar and Xe/Ar support an atmospheric source (Fig. F84). Additionally, the stable O_2/Ar ratio rules out oxidation processes at the drill bit. It remains unclear if the overall data scatter is related to a real change in gas composition. Postcruise noble gas studies will shed light on this issue.

The presence of H_2 in Hole C0002P can have various sources (Fig. F77). The low concentrations of H_2 compared to hydrocarbon gas concentrations suggest organic sources (Wiersberg and Erzinger, 2008, and references therein). δD analyses could help with a clear distinction of source. Alternatively, H_2 can be a product of artificial processes, such as electrolytic products released by interaction of the drilling fluid products and the drilling equipment, or by processes related to metal-to-metal friction.

Classification of hydrocarbons

Clear classification of the hydrocarbon gases proved to be difficult, mainly due to the conflicting data sets (Fig. F80). Above 1000 mbsf, $\delta^{13}C\text{-}CH_4$ has values less than or equal to –60‰. Combined with a $C_1/(C_2 + C_3)$ ratio of 1557 based on GC-NGA data, this indicates a bacterial source of methane. By contrast, the Bernard parameter based on the GeoServices data set indicates a thermogenic to mixed regime in this interval, with ratios between 75 and 377. Farther downhole, the Bernard parameter indicates the presence of mixed gases from bacterial and thermogenic regimes. Starting at 1500 mbsf, this pattern becomes more prominent as ethane and propane concentrations stay above the detection limit. At the same time, $\delta^{13}C\text{-}CH_4$ steadily declines. The $\delta^{13}C\text{-}CH_4$ ratio, Bernard parameter, and $C_1/(C_2 + C_3)$ ratios from the GC-NGA point to an increase in thermogenically derived hydrocarbon gases below 1700 mbsf. This trend stops at ~2025 mbsf. Farther downhole, $\delta^{13}C\text{-}CH_4$ values stay almost constant at an average of –48‰, whereas the Bernard parameter averages 91.2 for the drilling mud-gas data and ~23.3 for the headspace gas. Between ~2325 and 2600 mbsf, $\delta^{13}C\text{-}CH_4$ declines again, and the Bernard parameter drops to values >50, indicating an early mature thermogenic regime (e.g., Whiticar, 1994). Below 2600 mbsf, the Bernard parameters from GeoServices and GC-NGA data remain at 21 and 40, respectively, and methane carbon isotope ratios remain at an average of –43‰.

By using a Bernard diagram (i.e., Bernard parameter versus $\delta^{13}C\text{-}CH_4$; see also Bernard et al., 1978; Whiticar et al., 1994), it is possible to further evaluate the hydrocarbon gas composition (Fig. F67). Plotting the data in the Bernard diagram indicates that the gas show in Hole C0002N is influenced by secondary effects like mixing, diffusion, and/or microbial oxidation (Whiticar et al., 1994). Following the procedure of Prinzhofer and Pernaton (1997), it is possible to qualitatively estimate if the gas show is affected by mixing or diffusion fractionation in Hole C0002N (Fig. F85). Hydrocarbon data from GeoServices, however, show no clear trend, and although the data from the GC-NGA might indicate mixing, the low number of data points precludes further interpretation. Below 2325 mbsf in Hole C0002P a clear change to thermogenic gas is evident (Figs. F67, F85). Later onshore analysis will focus on the $\delta^{13}C\text{-}CH_4$ of ethane and propane, so it will be possible to calculate a proper mixing model for the gases present in the accretionary prism (Whiticar et al., 1994).

The diagram of $C_1/(C_2 + C_3)$ ratio and temperature relationship is also used to get quick information about the origin of the hydrocarbons (i.e., to distinguish between biogenic gas and gas migrated from a deeper source of thermogenic hydrocarbon). A very high $C_1/(C_2 + C_3)$ ratio indicates in situ gas formation by microbiological process. On the other hand, the occurrence of high amounts of C_2 and C_3 at shallow depths is associated with thermogenic hydrocarbon generation. The separation pattern of normal versus anomalous zones was suggested by Stein et al. (1995) and Shipboard Scientific Party (1995), as shown in Figure F86. Stein et al. (1995) estimated the sediment temperature following temperature gradients given by JOIDES PPSP (1992). Also shown by the two solid lines is the approximate influence of different organic carbon content (i.e., TOC). Sediment showing high C_1 concentrations is characterized by relatively high organic carbon contents and high sedimentation rates because the decomposition of the organic matter is dominated by anaerobic microbial process under these conditions (Claypool and Kvenvolden, 1983).

We plot values for TOC in >4 mm cuttings (with some 1–4 mm cuttings data) and the $C_1/(C_2 + C_3)$ ratios in drilling mud-gas data obtained during Expeditions 338 and 348 (Fig. F86; Table T27). The $C_1/(C_2 + C_3)$ ratio is calculated using data measured by the GC-NGA. The $C_1/(C_2 + C_3)$ ratio is high (>1000) at shallow levels and decreases normally with increasing depth. Below 2200 mbsf, the $C_1/(C_2 + C_3)$ ratio decreases to 100, and the Bernard diagram plots indicate that the majority of methane is thermogenic (Fig. F67). Therefore, the diagram cannot be used to estimate the temperature in the borehole deeper than 2200 mbsf.

Physical properties

During Expedition 348, physical property measurements were performed on core samples from Holes C0002M and C0002P and cuttings samples from Holes C0002N and C0002P. MAD, *P*-wave velocity, and electrical resistivity measurements were conducted on discrete samples taken from cuttings and the working half of cores. Thermal conductivity was measured on working halves using a half-space probe. The full suite of whole-round multisensor core logger (MSCL-W) and color spectroscopy logger (MSCL-C) measurements were conducted on whole-round core samples and archive halves, respectively. On cuttings, only measurements of natural gamma radiation (NGR) using the MSCL-W system and magnetic susceptibility using a Kappabridge system were conducted. Dielectric permittivity and electrical conductivity were only conducted on cuttings from Hole C0002N.

Moisture and density measurements

Cuttings

MAD measurements were made on 617 cuttings samples from 870.5 to 3058.5 mbsf to provide a detailed characterization of grain density, bulk density, and porosity. A total of 265 samples from both the 1–4 and >4 mm fraction size were measured at 10 m intervals (Table T28; Fig. F87). In addition, 111 intact cuttings, 12 caving samples, and 3 drilling-induced cohesive aggregates (DICAs) and pillow cuttings were separately handpicked from the >4 mm size fraction at various depths from 1222.5 to 3058.5 mbsf (Tables T29, T30, T31). MAD measurements on 1–4 and >4 mm size fractions and handpicked intact cuttings were conducted every 20–40 m between 2105.5 and 2855.5 mbsf in Hole C0002P.

Grain density values for the 1–4 and >4 mm size fractions are in close agreement throughout the cuttings interval (Fig. F87A). The grain density has considerable scatter from 870.5 to 940.5 mbsf with values ranging from 2.24 to 2.70 g/cm³ due to mixing with artificial cement. The scatter diminishes below 940.5 mbsf, and the grain density slightly increases from 2.68 g/cm³ at 950.5 mbsf to 2.72 g/cm³ at 3058.5 mbsf.

In contrast to the grain density values, bulk density and porosity for the two size fractions maintain close agreement only above 1600.5 mbsf. Below this depth, the trends for the two size fractions begin to sharply diverge. Bulk density for the 1–4 mm size fraction is consistently lower (porosity is higher) than that for the >4 mm size fraction while maintaining a similar value with depth to 3058.5 mbsf (Fig. F87B, F87C). The sharp increase in bulk density and decrease in porosity from 870.5 to 970 mbsf are probably caused by cement mixing (see "Lithology"). In general, bulk density of bulk cuttings increases from 1.9 to 2.0 g/cm³ and porosity decreases from 50% to 40% with depth in both size fractions. Exceptionally higher bulk density (and lower porosity) values are observed in intervals 1680–1690 and 2010.5–2090.5 mbsf in Hole C0002N and 2162.5–2220.5 and 2601.5 mbsf in Hole C0002P (see "Effects of operation on MAD measurements"). Taking a closer look at the data, bulk density increases and porosity decreases above 1600 mbsf, followed by a gradual decrease in bulk density and increase in porosity toward ~2000 mbsf. Below 2000 mbsf, bulk density shifts to slightly higher values and porosity to lower values and stays almost constant above 2550 mbsf. Below 2550 mbsf, bulk density values decrease, with an apparent porosity increase, and stay almost constant from 2750 to 3058.5 mbsf.

Handpicked intact cuttings and remolded cuttings

Visual observation suggests that three types of cuttings, intact cuttings, DICAs, and pillow cuttings, are present with different degrees of induration or strength (see "Operations"). Unexpectedly high porosity and low bulk density values seem to be caused by the presence of DICAs and pillow cuttings, which are formation materials remolded during the drilling and recovery process. Therefore, we separately hand picked intact cuttings and DICAs/pillow cuttings from the >4 mm size fractions in addition to MAD measurements on the bulk cuttings (Tables T29, T30).

Grain density, bulk density, and porosity values for handpicked intact samples were measured within the 1222.5–3058.5 mbsf interval (Figs. F87, F88). Some intact samples from Hole C0002P were separated according to lithology when possible (mud or silt/sand) (Table T29). Grain density measurements for the handpicked intact cuttings are consistent with the bulk cuttings, including both the 1–4 and >4 mm size fraction. However, handpicked intact cuttings show a consistent decrease in porosity and increase in bulk density when compared to the bulk cuttings (Fig. F87). Grain density slightly increases from 2.66 to 2.70 g/cm^3, and bulk density exponentially increases from 2.05 to 2.41 g/cm^3 throughout the entire interval.

Porosity and bulk density values of handpicked intact samples are generally offset from the bulk measurements. Porosity of the intact samples decreases from 37.0% to 26.9% at 1222.5 to 1800.5 mbsf, stays constant at ~27% from 1800.5 to 2000.5 mbsf, and decreases to 22.2% at 2245.5 mbsf in Hole C0002N (Figs. F87C, F88C). Porosity of the intact samples from Hole C0002P is slightly offset from the trend in Hole C0002N and decreases from 22.7% to 20.3% at 1960.5-2162.5 mbsf. Porosity stays constant at ~21.0% to 2660.5 mbsf and slightly decreases to 17.3% at 3058.5 mbsf. No significant differences in porosity between lithologies are observed when compared with the other handpicked intact samples.

Bulk density, porosity, and grain density of the DICAs/pillow cuttings at 1225.5, 1505.5, and 2090.5 mbsf are consistent with the 1–4 and >4 mm size fraction trends (Fig. F87). This suggests that the presence of DICAs/pillow cuttings does not affect the grain density measurements on bulk cuttings, but they do seem to influence the bulk density and porosity measurements reported above. The grain density agreement suggests that the measurements are of good quality, and the differences in porosity and density are real, but values from the bulk samples are affected strongly by artifacts of the drilling process. Thus, the bulk density and porosity data on handpicked intact cuttings better represent formation properties.

Effects of operation on MAD measurements

In some intervals, including 1680–1690 and 2010.5–2090.5 mbsf in Hole C0002N and 2162.5–2220.5 and 2601.5 mbsf in Hole C0002P, bulk cuttings, particularly of the >4 mm size fraction, show sharp increases in bulk density and decreases in porosity close to the handpicked intact cuttings values (Figs. F87, F89). This feature seems to be strongly related to drilling operations in these intervals, including WOW, hole cleaning, mud pump circulation, and RCB coring (Fig. F87). In the interval from 2010.5 to 2090.5 mbsf, for example, bulk cuttings increase sharply in bulk density and decrease in porosity followed by a gradual recovery with depth (Figs. F87, F89A). In this interval, there was a 50 h long WOW at 2008 mbsf and an 8 h mud circulation period for mud loss treatment at 2038 mbsf (see "Operations"). The size of cuttings in this interval is generally larger, and thus the size of >4 mm bulk cuttings was measured by visual observation of the long axis (Fig. F90A). The average cuttings size in the >4 mm fraction quickly increases with depth, reaches a maximum at 2055.5 mbsf, and then gradually decreases with depth. A rough correlation with increasing cuttings size and decreasing porosity is seen throughout this interval (Fig. F90B). The sudden decrease in apparent porosity and increase in the apparent bulk density with larger cuttings size are probably due to WOW and hole cleaning in this interval.

In the coring interval between 2163 and 2218.5 mbsf, cuttings were collected three times during (1) RCB coring, (2) drilling with a polycrystalline diamond compact drill bit, and (3) opening with an underreamer (Fig. F89B, F89C). In this interval, the bulk cuttings in the >4 mm fraction during coring and the subsequent hole opening with the polycrystalline diamond compact drill bit in both size fractions show lower porosity. This implies that the RCB coring BHA produces a larger amount of better quality cuttings.

Furthermore, cuttings sampled during reaming between 2105.5 and 3050.5 mbsf in Hole C0002P are of much better quality with fewer DICAs and no pillow cuttings present. This results in reasonable values of MAD measurements on bulk cuttings. The porosity of bulk cuttings in both size fractions during reaming is also lower and is similar to that of the handpicked intact cuttings (Figs. F87, F89C).

Discrete cores and porosity-depth trend

A total of 67 discrete core samples from Holes C0002M and C0002P were measured for MAD. All MAD data from Expedition 348 cores are summarized in Figure F88 and Table T32. In Hole C0002M between 475.85 and 507.2 mbsf, bulk density ranges from 1.87 to 2.03 g/cm^3, grain density ranges from 2.68 to 2.82 g/cm^3, and porosity ranges from 41.6% to 49.8%. Porosity, bulk density, and grain density are consistent with results from Holes C0002B and C0002L on core samples in the same depth interval (Expedition 315 Scientists, 2009; Strasser et al., 2014b). The scatter present could correspond to the occurrence of sand layers that yield lower porosity and higher bulk density; these layers become less common with depth.

In Hole C0002P between 2163 and 2217 mbsf, bulk density ranges from 2.16 to 2.42 g/cm^3, grain density ranges from 2.68 to 2.77 g/cm^3, and porosity ranges from 18.0% to 32.6% (Figs. F87, F89D; Table T32). At 2205 mbsf, a fault zone was observed, and grain density decreases to 2.64 g/cm^3, bulk density decreases to 1.96 g/cm^3, and porosity sharply increases to 42.6%. Below the fault zone, both grain density and bulk density increase back to ~2.71 and ~2.34 g/cm^3 at 2217 mbsf, respectively, whereas porosity decreases back to a trend that is offset from the trend seen above the fault zone. Porosity ranges from 21.7 to 31.5% between 2206 and 2217 mbsf.

Combined with MAD measurements on handpicked cuttings and discrete core samples including data from previous expeditions, porosity generally decreases with depth at Site C0002 (Fig. F88). The porosity data can be fit well by an exponential function (Athy, 1930):

$$\phi = \phi_0 \times \exp(-a \times z),$$

where z is the depth below seafloor, a is an empirical constant (4.26×10^{-4}), and ϕ_0 is reference porosity (59.1%). It should be noted that good data fit by Athy's model can be coincidental because the model is suitable for locations where the loading condition does not change and is monotonically progressive with the burial depth (e.g., in a sedimentary basin). This fit may not be applicable for an accretionary prism setting where the loading condition and history may be different with depth. Future postexpedition research, including laboratory experiments, borehole breakout analysis, and microstructural analyses will shed light on the evolution of porosity in the inner accretionary wedge.

Electrical conductivity and *P*-wave velocity measurements on discrete samples and cuttings

Electrical conductivity and *P*-wave velocity (V_P) measurements were conducted on 8 cubic samples collected from the working half of cores taken from 476–507 mbsf in Hole C0002M. Discrete samples could not be collected from RCB cores in this depth interval in Hole C0002B during Expedition 315 due to sample disturbance. Section 348-C0002M-4R-1, collected with the SD-RCB, shows similar types of disturbance as cores from Hole C0002B, with wavy open cracks and soft-sediment intervals. Overall, the samples were very fissile and tend to crack under load. As a result, the samples exhibited high attenuation associated with the *P*-wave analysis.

Electrical conductivity of both core and cuttings samples was measured at 10 kHz to allow direct comparison with Expedition 315 measurements. Electrical conductivity values measured during Expedition 338 were recalculated from raw data for 10 kHz and are reported in Table T33.

Electrical conductivities of samples from Hole C0002M appear lower than those recovered at deeper intervals from the same lithologic Unit II (Kumano Basin fill) in Hole C0002B, although porosity decreases with depth. Both chlorinity and salinity display a broad minimum at ~400 mbsf, and the variations in chlorinity and salinity with depth are a possible explanation for the lower conductivity values. In the 476–507 mbsf interval, samples from Hole C0002M decrease in electrical conductivity with depth (Fig. F91). This may be due to decreasing porosity with depth and lithologic variations implied from an apparent increase in NGR and clay content within the same interval. Anisotropy is observed with similar horizontal components and is systematically lower in the vertical component (Fig. F92). The range of vertical plane anisotropy is comparable to that observed deeper in lithologic Unit II. Anisotropy related to clay compaction fabric is expected to increase progressively with depth (Henry et al., 2003). The scatter in anisotropy values and the lack of an obvious trend with depth suggest that the presence of cracks influences the anisotropy of these samples.

P-wave velocity measurements on Hole C0002M cores could not be systematically done because of high attenuation. Five samples show velocities ≤1550 m/s, probably due to the presence of gas/air within the sample (Table T33; Fig. F93). Three samples have relatively high velocities in the horizontal directions, from 1830 to 1950 m/s, and the velocity along the z-axis ranges from 1583 to 1738 m/s. When combined with Expedition 315 data, these measurements define a trend for lithologic Unit II below 475 mbsf:

$$V_{\mathrm{Px,y}} = 0.8865z + 1384.4;\ R^2 = 0.553582 \text{ and}$$

$$V_{\mathrm{Pz}} = 0.9516z + 1212.8;\ R^2 = 0.66806.$$

Vertical-plane anisotropy could be reliably measured on only two samples and appears to be as high as 9% and 16%, which might be expected for samples bearing fractures in the x-y plane (Table T33).

In Holes C0002N and C0002P, electrical conductivity and *P*-wave velocity were measured on discrete core samples and on cuttings from the corresponding depth interval (Tables **T33, T34, T35**). Preparation of cubes for *P*-wave and electrical conductivity anisotropy was difficult in Core 348-C0002P-5R and in the uppermost two sections of Core 6R due to the presence of dense fracturing attributed to the fault in Section 5R-4 (see **"Structural geology"**).

Electrical conductivity for discrete samples from the 2163–2216.87 mbsf coring interval in Hole C0002P is generally greatest in the *z* (vertical)-direction. This can be explained by the subvertical strata that generally exceed 45° dip (Fig. **F91**). It is also observed that when two axes of measurements lie near the stratification plane (e.g., *z* and *y* or *z* and *x*), the values obtained in these two directions are similar and consistently higher than the other direction. This further suggests that the stratification is the primary source of anisotropy within the samples. The ratio of the maximum and minimum conductivities measured on such samples varies between 1.2 and 2. The least anisotropic sample (348-C0002P-2R-4, 73–77 cm; 2177.46 mbsf) contains high amounts of sand. Systematic variations in the average conductivity are observed with depth, with a minimum at 2182 mbsf and a maximum at 2175 mbsf. Lithologic variations in the samples remain a possible explanation for the differences in electrical conductivity. Measurements on cuttings are compared with values from discrete core samples (Fig. **F94;** Table **T34**). Most cuttings in the cored interval lie within the lower range of measurements done on discrete core samples. This may be likely because most cuttings platelets are prepared parallel to stratification, or fissility, over this interval. When all data from this expedition are compared with those from previous expeditions, they define a broad trend of decreasing conductivity with depth (Fig. **F94**), as may be expected considering that the evolution of conductivity is broadly approximated well by an exponential Archie's law. However, conductivity on cuttings appears relatively scattered. The range of variations (0.15–0.9 S/m) for both silt/clay and sandstone lithologies is broad in the interval from 2000 to 2020 mbsf and may reflect the large variability of porosity measurements on core samples from Hole C0002P. Below 2020 mbsf, sandstone cuttings display a larger amount of scatter and greater variability with depth when compared to the mudstone cuttings. The sandstone cuttings measured in the upper part of Hole C0002P (2000–2200 mbsf) plot in the same conductivity range as the mudstones, but these sandstones are generally fine grained and silty. The coarser sandstone cuttings sampled below 2400 mbsf have higher conductivity than the fine-grained sediment, but this contrast appears to decrease with depth. The conductivity of the mudstone cuttings shows a small offset between 2650 and 2720 mbsf. Mean conductivity is 0.23 ± 0.05 S/m between 2100 and 2700 mbsf and 0.17 ± 0.04 S/m below 2700 mbsf.

Water content of cuttings samples was obtained from wet and dry weight on all the platelets after impedance measurements, and porosity was estimated assuming a grain density of 2700 kg/m^3. For discrete core samples, porosity data are available from MAD measurements on a separate discrete sample collected next to the cubic samples. When conductivity, σ, is plotted versus porosity, ϕ, it appears that most samples plot above Archie's law:

$$\sigma = \sigma_f \, \phi^2,$$

assuming fluid conductivity, σ_f, is either equal to the fluid used for sample preparation (NaCl solution; 5.28 S/m at 21.5°C) or approximating a possible in situ fluid conductivity (4 S/m, corresponding to a chlorinity of 420 mM; see **"Geochemistry"**) (Fig. **F95**). No strong difference between the electrical properties of sand-rich and clay-rich lithologies is observed in this depth interval, with most of the sandstone data plotting in the upper range of conductivity at a given porosity. It appears that the relatively high conductivity of the sandstones in the 2400–2800 mbsf interval results from the combined effect of higher porosity values and a different porosity-conductivity relationship.

In the *P*-wave velocity measurements, traveltime was first determined by automatic picking in the Geotek system. Systematic manual repicking was needed for cuttings and Hole C0002P core samples, as the automatic picking method is sensitive to variations of signal frequency and appears to overestimate the range of *P*-wave variations because attenuation of high-frequency *P*-waves in the samples reduced the central frequency of the transmitted signal. Variations in sample attenuation increase the scatter of the automated picking, and the delay for the zero distance appears to be overestimated when performing the standard calibration with the 500 kHz transducers.

The traveltime was manually determined using the first maximum of the second derivative of the waveform, referenced to the signal recorded with the transducers in contact for delay time. Values obtained on discrete samples show scatter between 1900 and 2900 m/s, but the following features seem to emerge from the data set (Fig. **F96;** Table **T35**):

1. Measurements on cuttings appear slightly higher but compatible with those measured on cores, perhaps reflecting the likelihood that the se-

lected cuttings are probably biased toward the stronger parts of the formation.

2. *P*-wave velocity sharply increases with depth above the cored interval between 1990 and 2150 mbsf and decreases between 2150 and 2250 mbsf throughout the cored interval. These velocity variations appear to be related to differences in formation physical properties above and below the fault zone rather than to the fault zone itself, considering the length scale at which this variation is observed and the absence of measurements within the fault zone.
3. On average, velocity increases below 2250 mbsf. A number of high-velocity outliers (V_P = ~4 km/s or more) are observed and correspond to unusually hard cuttings samples, which is likely the result of the presence of natural cements. A change in the depth trend of velocity toward lower values is observed at ~2700 mbsf, evidence supporting the hypothesis that a lithologic or diagenetic change occurs at this depth interval.

Thermal conductivity

Thermal conductivity was measured on the working half of cores from Holes C0002M and C0002P using a half-space probe. All data are summarized in Figure **F97** and Table **T36**, along with data from Expeditions 315 and 338 (Expedition 315 Scientists, 2009; Strasser et al., 2014b). Thermal conductivity ranges from 1.44 to 1.58 W/(m·K) from 477 to 507 mbsf in Hole C0002M and 1.59 to 1.82 W/(m·K) from 2173.0 to 2214.6 mbsf in Hole C0002P. Thermal conductivity in Hole C0002M is consistent with the data from Expeditions 315 and 338. Overall, thermal conductivity increases with depth; however, its rate of increase is much less in the accretionary prism below ~1000 mbsf when compared to that of the Kumano Basin.

The correlation between thermal conductivity and porosity is shown in Figure **F98**. The theoretical values of thermal conductivity are calculated for different grain thermal conductivities (k_s) based on a geometric mean mixing model:

$$k = k_w^{\phi} \times k_s^{(1-\phi)},$$

where k_w is water thermal conductivity. The relationship between thermal conductivity and porosity of the prism sediment from Hole C0002P and previous expeditions follows the extrapolation from the data of Kumano Basin sediment at Site C0002 or Shikoku Basin sediment at Sites C0011 and C0012 (Expedition 315 Scientists, 2009; Expedition 322 Scientists, 2010a; 2010b; Expedition 333 Scientists, 2012a; 2012b; Strasser et al., 2014b). The grain thermal conductivity ranges from 2.1 to 3.4 W/(m·K) and is centered at 2.6 W/(m·K).

MSCL-W (whole-round cores)

Whole-round SD-RCB cores from Hole C0002M and RCB cores from Hole C0002P were analyzed by the MSCL-W. The results of gamma ray attenuation (GRA) density, magnetic susceptibility, NGR, and electrical resistivity measurements (see **"Physical properties"** in the "Methods" chapter [Tobin et al., 2015]) on whole-round cores are summarized in Figure **F99**. The data for Hole C0002M are shown together with Expedition 315 and 338 data (Expedition 315 Scientists, 2009; Strasser et al., 2014b). MSCL-W *P*-wave measurements are not presented here because they exhibit an extreme amount of noise due to poor contact between liner and sediment with voids. Magnetic susceptibility and electrical resistivity on Core 348-C0002M-3R (493.50–496.06 mbsf) are not available due to the presence of an aluminum core liner.

Overall, all MSCL-W data in Hole C0002M are consistent with the previous expedition results, except for NGR, which shows higher values than the previous expeditions. This is probably caused by the larger diameter, and thus volume, of the SD-RCB cores (inner diameter of 73 mm for SD-RCB core liner and 66 mm for regular RCB core liner) and by the use of a different calibration curve (see discussion in **"Natural gamma radiation (cuttings)"** for details). In Hole C0002P, all MSCL-W data are almost constant in the coring interval of 2163–2218.5 mbsf. Extremely high magnetic susceptibility is observed at 2183 mbsf (interval 348-C0002P-3R-1, 56–64 cm), where a metal piece derived from the core catcher was found in the core liner. Magnetic susceptibility shows a slight offset across the fault at 2205 mbsf (Section 348-C0002P-5R-4); it is ~2.5 × 10^{-4} SI above the fault and ~1.5 × 10^{-4} SI below it. Electrical resistivity increases right below the fault in Section 5R-5, which might have been disturbed during pulling out from the core barrel.

Color spectroscopy (archive halves)

The results of color reflectance measurements using the MSCL-C are summarized in Figure **F100**. In Hole C0002M between 475 and 507.57 mbsf, L* ranges from 19 to 48, a* ranges from –2.3 to 1.4, and b* ranges from –1.3 to 6.0. All values show no significant difference from cores collected during Expeditions 315 and 338 (Expedition 315 Scientists, 2009; Strasser et al., 2014b). In Hole C0002P between 2163.0 and 2217.5 mbsf, L* ranges from 20 to 66, a* ranges from –4.1 to 8.5, and b* ranges from –8.0 to 4.6.

Natural gamma radiation (cuttings)

Unwashed cuttings were collected in the core cutting area and packed in a 12 cm long core liner. The liner filled with cuttings was scanned with the MSCL-W to determine the NGR of the cuttings. The NGR of a liner filled with water was measured as a background reference, yielding a value of 34.8 counts/s.

NGR generally increases with depth (Fig. **F101**). In Hole C0002N, a sharp increase in NGR from 17.6 counts/s at 875.5 mbsf to ~40 counts/s at 975.5 mbsf is probably caused by a decrease in mixing with borehole cement in the cuttings. NGR slightly increases with depth to ~42 counts/s at 1825.5 mbsf and then is shifted toward a slightly higher value of ~45 counts/s and keeps increasing with depth to ~48 counts/s at the bottom of Hole C0002N (2325.5 mbsf). In Hole C0002P, NGR increases from 38 counts/s at 1965.5 mbsf to 47 counts/s at 2095.5 mbsf, followed by a sharp decrease to 40 counts/s at 2115.5 mbsf. The low NGR values in the upper portion of the hole probably reflect mixing with cement and metal in the cuttings. Below 2115.5 mbsf, NGR increases with depth toward ~50 counts/s at 2445.5 mbsf, shifts slightly to a lower value of 43.5 counts/s, and increases again with depth to ~50 counts/s at the bottom of Hole C0002P.

In addition to the unwashed cuttings, we attempted to measure NGR on lightly washed cuttings from Hole C0002P to understand the effect of mud water. Washed cuttings were collected separately with unwashed cuttings in the core cutting area. NGR values on the lightly washed cuttings show a similar trend to those of unwashed cuttings, but with a greater scatter (Fig. **F101B**).

It should be noted that NGR values of unwashed cuttings measured during Expedition 348 are higher by ~6 counts/s than those measured during Expedition 338. This is probably caused by the usage of different calibration curves between expeditions, because NGR values of a liner filled with water and granite measured for quality checks during Expedition 348 are consistently higher than those run during Expedition 338. Also, there is no difference in NGR values between mud water collected during Expedition 338 and Expedition 348 when calibrated with the curve used for Expedition 348 (Table **T37**).

Magnetic susceptibility (cuttings)

Magnetic susceptibility was measured on 148 vacuum-dried cuttings samples from both the 1–4 and >4 mm size fractions. Sample weight varied between the two cuttings sizes, so we calculated the mass magnetic susceptibility (MMS) from measured raw data magnetic susceptibility (bulk susceptibility) by

$$\text{MMS (m}^3\text{/kg)} = \text{(magnetic susceptibility} \times \text{sample volume [m}^3\text{])/(sample weight [kg])}.$$

The MMS in the >4 mm fraction is generally less scattered, ranging from 7.88×10^{-8} to 1.2×10^{-6} m^3/kg in the 1–4 mm fraction and from 9.69×10^{-8} to 4.05×10^{-7} m^3/kg in the >4 mm fraction between 875.5 and 3000.5 mbsf (Fig. **F102**). The depth trend of MMS values closely matches lithology. MMS decreases from 4.52×10^{-7} to 9.6×10^{-8} m^3/kg between 875.5 and 975.5 mbsf, which corresponds to lithologic Unit III. MMS is almost constant at ~1.2×10^{-7} m^3/kg in Subunit IVA (975.5–1045.5 mbsf) and sharply increases at 1045.5 mbsf (Subunit IVA/IVB boundary). MMS gradually decreases from 5.4×10^{-7} m^3/kg at 1045.5 mbsf to 1.2×10^{-7} m^3/kg at 1215.5 mbsf. High MMS probably corresponds to abundant volcanic glass observed in these intervals (see **"Lithology"**). MMS is almost constant at ~1.1×10^{-7} m^3/kg below 1215.5 mbsf to the Subunit IVD/IVE boundary and slightly increases with depth to 1.3×10^{-7} m^3/kg at 1765.5 mbsf. Below 1765.5 mbsf, MMS is almost constant at ~1.1×10^{-7} m^3/kg, except for scatter near 2000 and 2200 mbsf, possibly due to contamination of metal from window milling.

Dielectric permittivity and electrical conductivity (washed cuttings)

Approximately 150 cuttings samples were collected from 875 to 2325 mbsf at 10 m intervals in Hole C0002N, and ~120 samples were retrieved from 2325 to 3058 mbsf at 10 m intervals from Hole C0002P. During the expedition, only samples from Hole C0002N were tested because Hole C0002P samples were recovered too late in the expedition and will be used onshore for postexpedition analysis. Real and imaginary relative dielectric permittivity was measured in the frequency range from 300 kHz to 3 GHz, but some of the data were rejected due to experimental errors, instrument performance and calibration, and poor coupling with the sample. An example of the raw dielectric data is provided in Figure **F103** for Sample 348-C0002N-312-SMW (2255.5 mbsf). The example dielectric spectra show that the real dielectric permittivity (blue) monotonically declines smoothly at all frequencies above ~30 MHz, but below that frequency the data rapidly vary between high and low values. This occurs because of instrumental errors and is not related to the sample. More conductive samples are typically less affected. We have rejected all data with values <100 MHz for this reason. The imaginary dielectric data presented in Figure **F103** are less affected by these issues across the entire frequency range presented and show real relative dielectric values ε'_r = 35–50 in the frequency range from 100 MHz to 3 GHz, which is consistent with wet clays. Pure water has a real relative dielectric permittivity of ε'_r = 80, and ultradry clay would typically be ε'_r = ~5–6.

The 100 and 300 MHz and 1 and 3 GHz data were extracted from the dielectric spectra for each sample. We chose 100 MHz because it is the lowest frequency of the acceptable data that is common to all of the samples and 3 GHz because it is the highest. 300 MHz and 1 GHz data were also selected to provide two additional frequencies evenly distributed in (frequency) log space. In Figure **F104,** the 300 MHz data are plotted against depth to create a pseudo-log. In addition to the dielectric data, we also provide the conductivity of the water decanted from the paste sample after centrifugation (see **"Physical properties"** in the "Methods" chapter [Tobin et al., 2015]) and the water content of the residual paste at the time of dielectric analysis. Water content analysis was done on ~55 of the samples because the water content affects the dielectric permittivity of the paste.

A simple appraisal of the dielectric analysis results suggests that there are possible step change boundaries at 1050 and 1250 mbsf. Loss-angle logs at four spot frequencies were created by dividing the imaginary dielectric permittivity by the real dielectric permittivity (Fig. **F105**). These logs indicate a number of additional boundaries and features that are not as easily identified in the primitive (real and imaginary) logs. One zone containing upper and lower boundaries at 1000 and 1080 mbsf, respectively, is marked in yellow and dark blue. This boundary is more apparent at 100 and 300 MHz than at 3 GHz; however, the reverse is true for another subtle boundary at 2180 mbsf (dark green). A possible feature occurring at 1520 mbsf (light green) consists of two adjacent measurements that are higher than the surrounding values. LWD data recorded downhole included gamma ray and resistivity logs, and these typically correlate favorably with dielectric logs (Hizem et al., 2008). In Figure **F106,** we present the typical dielectric analysis logs against the downhole logs along with the log units (see **"Logging"**).

A a step increase in the gamma ray log at ~1650 mbsf indicates that the hole has passed from a less (low gamma radiation) to a more clay-rich unit (high gamma radiation). There is also a trend in the (39 and 27 inch) resistivity logs: these increase with depth from a starting value of ~1 Ωm at 900 mbsf to ~2 Ωm at 1600 mbsf. Below 1600 mbsf, the trend remains at a nearly constant value of ~2 Ωm. The same trend in resistivity logs is observed in the real and imaginary dielectric cuttings logs and in the water conductivity logs.

Downhole measurements

Leak-off test

After Hole C0002P was sidetracked out of Hole C0002N from 1936.5 mbsf (3904.0 m BRT), two LOTs were carried out at 1954.5 mbsf (3922.0 m BRT). The tests were conducted to determine the maximum mud density that could be used for the drilling of Hole C0002P. Additionally, LOTs can in principle be used to provide constraints on the magnitude of the least horizontal principal stress (see **"Downhole measurements"** in the "Methods" chapter [Tobin et al., 2015]). The sidetrack section leading to Hole C0002P was ~18 m in length from the kickoff point at 1936.5 mbsf. This exposed a zone from a few meters to 18 m of formation outside the cement during the two LOTs (Fig. **F107**).

The two tests were conducted at 0.20–0.32 and 0.7–0.8 bbl/min injection rates (Fig. **F108A, F108B**). The first pressure cycle injected 4.1 bbl of drilling mud for ~14 min and reached a downhole pressure of ~53 MPa. The downhole pressure increased steadily throughout this test until shut-in. In the second test, a downhole pressure of ~54 MPa was achieved after injecting 4.7 bbl of drill mud over a period of 6.5 min. The pressure slowly increased during the last 10 s of the second test, and a peak pressure value was possibly reached at 54 MPa, which is expected to be fairly close to the formation breakdown pressure. (Fig. **F108C**).

The pressure-volume curves show that the two tests follow a similar trend (Fig. **F109A, 109B**). This suggests that there is little rate dependence in the pressure-volume relation, that there is no significant time-dependent fluid leakage during the tests, and that the elastic response of the wellbore system was repeatable to first order. However, a nonlinear trend is observed with the pressure-volume relation in the pressure build-up rate data of the second test (dP/dV; Fig. **F109B, F109C**), which makes it difficult to pick a distinct LOP. The linear decrease in dP/dV with volume, as observed in the first test and most of the second test, suggests that there is slight mud fluid loss into the formation at a constant permeability (Todd and Mays, 2005). dP/dV decreases linearly with volume because the rate at which the mud fluid is lost is proportional to the increase in downhole pressure observed at a constant formation permeability. In such cases, the LOP can be recognized as the point where the linearly decreasing trend breaks in the dP/dV record. In the first pressure cycle (Fig. **F109B**), we do not observe any change in the decreasing trend of dP/dV, suggesting that the LOP was not reached during this test. In the second pressure cycle (Fig. **F109C**), dP/dV starts to decrease faster at an injected volume of around 3.3 bbl. We interpret this as the onset of a sudden increase in system volume, which corresponds to a LOP of 52.2 MPa.

The LOP pressure of 52.2 MPa corresponds to an equivalent mud density of 1.36 specific gravity (sg), higher than the 1.15 sg mud density value derived from the LOP pressure of 32 MPa observed at 872.5 mbsf in Hole C0002F (Strasser et al., 2014b). Although the exact relation between LOP pressures and least horizontal principal stress is still unclear (Raaen et al., 2006; Zoback, 2007), if we consider a stress gradient based on the LOP pressure observations, we see an increase from 14.9 to 17.1 MPa/km relative to the seafloor in the interval between 872.5 and 1954.5 mbsf (Fig. **F110**).

Logging

Log data acquisition

LWD data included NGR, electrical resistivity logs, electrical resistivity images, sonic velocity, and sonic caliper logs. These data were collected together with MWD data from 859.5 to 2329.3 mbsf (2827.0–4296.8 m BRT) in Hole C0002N (Table **T38**) and from 2162.5 to 3058.5 mbsf (4130–5026 m BRT) in Hole C0002P (Table **T39**). Detailed description of the tools and the bottom-hole assembly (BHA) configuration are provided in **"Logging"** in the "Methods" chapter (Tobin et al., 2015).

In Hole C0002N, LWD data were collected in two runs separated by a WOW event (Table **T40;** Fig. **F111A**). Data from the two runs overlapped between 1962.6 and 2008.5 mbsf (between 3930.2 and 3976 m BRT); the data from the earlier run were chosen over the later run when merging the data. The target ROP was set to an average of 40 m/h to optimize the quality of the LWD data collected during drilling. ROP was initially low, <10 m/h, from 872.5 to ~960 mbsf, as the hole drilled through the cemented section of Hole C0002F to kick-off Hole C0002N. Otherwise, ROP was maintained mainly between 30 and 50 m/h to the bottom of logged data in Hole C0002N (2329.3 mbsf; Fig. **F111A**). Annular pressure measured during drilling shows that the ECD increased from ~1.145 to ~1.18 g/cm^3 with depth.

In Hole C0002P, LWD data were collected after coring from 2163 to 2218.5 mbsf (4130.5–4186 m BRT) (Fig. **F111B**). The cored interval was logged as the borehole was reamed and enlarged from 10 5/8 to 12¼ inches in diameter, and then the formation below was logged as the borehole was newly drilled. The target ROP was 30 and 40 m/h in the cored and newly drilled section, respectively. Throughout Hole C0002P, ROP fluctuated between 5 and 40 m/h but was maintained mostly between 10 and 30 m/h with an average of ~18 m/h. Downhole annular pressure data show that ECD initially increased steadily with depth from ~1.31 to 1.33 g/cm^3 to ~2550 mbsf but stabilized within 1.32–1.33 g/cm^3 during the rest of the drilling.

Data quality

Overall quality of the data is satisfactory over the logged section of the well. However, several quality issues need to be taken into account in order to properly interpret the processed log data (Table **T40**). Exposure time is the time it takes for the LWD tools to reach the drilled formation after being penetrated by the drill bit and was provided in the log data relative to the position of the electromagnetic wave resistivity tools. Exposure times were typically between 30 min and 2 h during normal drilling operations but were as high as 50 h when incidents such as WOW or extended mud circulation occurred. Long exposure times cause degradation of the borehole condition (i.e., caving, drilling-mud invasion, etc.) before the logging tools measure the petrophysical properties of the formation; therefore, data quality can be compromised at such depth ranges.

There were several periods when drilling Hole C0002N was halted temporarily due to WOW or borehole condition concerns, which caused some intervals of the LWD well logs to be measured after long exposure times. Also, the absolute magnitudes of the NGR and shallow resistivity data do not properly reflect the formation petrophysical properties in Hole C0002N despite the mud and borehole size corrections, which corrected for the discrepancy between the LWD 12¼ inch calibration and the 17 inch Hole C0002N bore size. In Hole C0002P, resistivity data in the cored interval show possible signs of slight mud filtrate invasion and/or wellbore failure (Fig. **F111B**).

There were four major occurrences of long exposure times during the drilling of Hole C0002N (Fig. **F111;** Table **T40**). Those drilling intervals between 1205–1221 and 2022–2038 mbsf are both related to periods of extended mud circulation for borehole treatments, whereas those occurring at 1662–1678 and 1992–2008 mbsf were caused by temporary termination of drilling activities due to WOW. Resistivity log data at these depth ranges are both noisy and anomalously low (Fig. **F111A**), which indicates that the borehole conditions were worse compared to the formation logged both above and below these intervals. As a result, these data are not suitable for interpretation. Evidence of compromised borehole condition at these intervals also suggests that the cuttings collected right below the long-exposure time intervals may include more caving material when compared to cuttings collected during normal drilling operations.

Because the borehole diameter (17 inches) in Hole C0002N was larger than the standard borehole size range covered by the available LWD tools used during the drilling, there was more drilling fluid present in the annulus between the LWD tools and the formation. The effect of having more drilling mud present was corrected for by proprietary algorithms, but these may not always work optimally outside of the standard specification range of the tools (i.e., dual gamma ray [DGR] range is 12¼ inches and electromagnetic wave resistivity [EWR]-PHASE4 range is 10½ to 14¾ inches) (Fig. **F112**). As a result, the final corrected gamma ray data from Hole C0002N were, on average, 10–15 gAPI units lower than those measured from Hole C0002F at the same depth range (Fig. **F113**). It is also noted that the third-party contractors and logging tools were different between the two holes. These differences in tool calibration standards may also contribute to this discrepancy. Therefore, comparison of NGR data between boreholes is only possible in a qualitative sense. As for the resistivity data, we observe that the shallower measurements (e.g., 9 and 15 inch resistivity) show especially low resistivity values. This is likely due to the fact that the shallow measurements are sampling the highly conductive drilling fluid present in the large gap between the tool and the formation. Therefore, we only considered the two deep measurements (e.g., 27 and 39 inch resistivity) to represent the formation resistivity in our interpretations.

In Hole C0002P, exposure times are consistently low because of the steady drilling operation, which only stopped twice, once for 5.5 h during a scheduled wiper trip operation at 2601.5 mbsf and once during a >66 h interval between coring from 2163 to 2218.5 mbsf and subsequent logging of the same interval with the LWD BHA (Table **T40**). However the separation between the two resistivity curves is particularly large at the cored interval and largest between 2200 and 2208 mbsf where fault-zone rocks were recovered in Core 348-C0002P-5R, as shown by the ratio of the deepest to shallowest resistivity data (e.g., 48 inch data divided by 16 inch data; Fig. **F111B**). This indicates possible mud filtrate invasion or wellbore failure in this interval. Considering that the time between the last coring run (Core 6R) and the start of reaming was >66 h, it is possible that the formation was affected by invasion or wellbore failure to a deeper extent than was cut by the reaming operation. Nonetheless, the ratio of deep to shallow resistivity measurements is small compared to that observed in Hole C0002N (i.e., up to 5.5 at long exposure-time intervals), thus data quality was not significantly affected.

The sonic caliper data show that the borehole diameter is generally stable throughout the wellbore, thus borehole collapse does not appear to have been a severe issue for log data acquisition (Fig. **F111B**). The mean value of the average ellipse diameter is 12.42 inches along the well, indicating a slight increase in borehole diameter. Borehole enlargement is most pronounced at the top section of the borehole between ~2135 and 2210 mbsf, which corresponds to the depth ranges where the borehole was already cut by previous drilling/coring, then reamed to a larger diameter where the LWD data were collected. Borehole diameter is larger in this interval probably because of the longer exposure time (>66 h) of the formation before the interval was imaged by the azimuthal focused resistivity (AFR) tool. The eccentricity of the borehole shape, defined by the ratio of the maximum to minimum ellipse diameter, is also relatively large in this reamed section. If we ignore the occasional spikes in the eccentricity data, eccentricity is 1.04–1.2 in the reamed section, whereas it is generally <1.05 at lower depths.

The quality of the AFR tool resistivity image log was good. In the data collected by the high-resolution sensor, 36.8% of the data were missing due to occasional instantaneous high ROP and rotations per minute during drilling and the likely associated stick-slip movements of the drilling bit. With standard filtering and interpolation procedures, a high-quality smoothed image of the borehole was produced.

Hole C0002N

Logging data characterization and interpretations

The near-seafloor portion of Hole C0002F, and thus Hole C0002N, was drilled during Expedition 326 in 2010; however, logging data were not collected. Log Units I–III were identified during previous Expeditions 314 and 332 for Holes C0002A and C0002G (Expedition 314 Scientists, 2009; Expedition 332 Scientists, 2011). Expedition 338 extended Hole C0002F (Strasser et al., 2014b) and identified the bottom section of Unit III. The lowermost section of Unit III is the first unit drilled in Hole C0002N during Expedition 348. The log units presented below for Hole C0002N correlate with Hole C0002F and allow for the full suite of LWD from Hole C0002F to help interpret the geology in Hole C0002N (Figs. **F112, F113**). Average values of gamma radiation and resistivity are shown in Table **T41.**

Unit III (from beginning of LWD acquisition at 872.0–915.0 mbsf)

The log Unit II/III boundary was not drilled and therefore is not recorded on LWD logs for Expedition 348. Additionally, correlation with Holes C0002A and C0002G puts the top of Unit III above the kickoff point of Hole C0002N at 865.5 mbsf (2833 m BRT). Logging through Unit III started with drilling out the cement plug placed during Expedition 338 at 860.5 mbsf and cannot be properly characterized by the log response. This resulted in lower gamma ray values near the top of the hole (between 860.5 and 872.0 mbsf; Fig. **F113**). After the cement plug was drilled, gamma ray values increased by 11 gAPI at 873.5 mbsf. Fluctuation in the log response occurring in ~2 m intervals is thought to be from alternating silty/sandy layers to clay-rich layers, with gamma ray variations up to 9 gAPI. Resistivity in the deep, medium, and shallow logs exhibits similar trends and shows a decrease of ≤0.3 Ωm, which corresponds to the same fluctuation intervals seen in the gamma ray logs reported above.

Unit III has an average gamma ray value of 61.6 gAPI and shows a general trend of gamma ray increase of ~20 gAPI downhole to the basal boundary at 915.0 mbsf, where a decrease of ~25 gAPI occurs. The decrease is interpreted as a change in lithology from a clay-dominated sediment at the base of Unit III to a sandy hemipelagic sediment at the top of Unit IV. This change defines the boundary between Units III and IV and was correlated between the other LWD data from Holes C0002F, C0002A, and C0002G (Strasser et al., 2014b; Expedition 314 Scientists, 2009; Expedition 332 Scientists, 2011). The lowermost 10 m of Unit III is likely a clay-dominated section based on high gamma ray values averaging 73 gAPI with small sections of silty to sandy hemipelagic sediment. However, overall variations in resistivity are modest.

Unit IV (915.0–1656.3 mbsf)

Gamma ray and resistivity data show the largest variability in log Unit IV, with average gamma ray values of 66.5 gAPI (Fig. **F113**). We define five subunits based on overall trends in log response and comparison with the subunits defined during Expedition 338 in Hole C0002F on the basis of a complete data set of LWD data including images. The base of Unit IV is marked by a sharp increase in the values of average natural radioactivity.

The top of Unit IV (Subunit IVa) shows a gradual increase in gamma ray values. This subunit starts with average gamma ray values of ~61 gAPI and increases to a maximum of ~83 gAPI. The uppermost 13 m of the section contains alternating higher to lower excursions of gamma radioactivity, which could indicate alternating sandy and silty layers every ~2 m. At 928 mbsf, there is an increase to 65 gAPI that we interpret as an indication of increasing clay content. Fluctuations within the log data values are minor through ~974 mbsf (72 gAPI). Then gamma ray values decrease slightly, with changes of up to ~20 gAPI and four additional sequences of increasing–decreasing radioactivity that we interpret as indication of slight increases and decreases in clay. The log-sequence thicknesses are 5–20 m. The uppermost section of Subunit IVa is interpreted as coarsening upward and the lowermost as coarsening downward if higher gamma ray values respond to increasing clay and lower gamma ray values to silty/sandy sediment, as inferred from the lithology recovered and described from cuttings (see **"Lithology"**). The lower section of Subunit IVa (1032–1036.5 mbsf) is interpreted to consist of interlayered sandy layers or beds 2–4 m thick.

At 1036.5 mbsf (top of Subunit IVb), the gamma radiation changes with depth from downhole decreasing to increasing values. Between 1044 and 1048 mbsf is the largest change in the subunit, of ~40 gAPI. Less variation is seen throughout the rest of Subunit IVb, compatible with a homogeneous lithology with only slight fluctuations in gamma ray values that could be related to small changes in proportion of clay and silt. Resistivity decreases slightly from the bottom to the top of the subunit, which also defines the log properties for this section.

Between 1099.4 and 1360.5 mbsf (Subunit IVc), the average gamma ray values have a slightly higher range when compared to the average for Unit IV (>65 gAPI), and resistivity values are within a range of 2 Ωm. The resistivity logs show a notable feature between 1150 and 1175 mbsf, where there is a steady increase in resistivity values above a sharp decrease. For this depth interval, the gamma ray log exhibits variations of radioactivity that could be interpreted in terms of changing abundance of sand-silt and clay. The high resistivities seen here are interpreted to be a well-cemented sand-rich interval. The gamma ray log below the high-resistivity section shows alternating higher and lower radioactivity at 1 to 5 m intervals. Variations in the gamma radiation within this subunit can be compared with increased sand described in the lithology section (see **"Lithology"**). A sharp downhole decrease in gamma ray values and downhole increase in resistivity define the boundary between Subunits IVc and IVd.

The abrupt changes in resistivity and gamma ray values observed at the top of Subunit IVd at 1360.5 mbsf can be interpreted in terms of increased sand content, taking into account the lithology end-members defined on cutting samples (see **"Lithology"**). We identified two sand-rich sections from 1360.5 to 1377.7 mbsf and from 1426 to 1432 mbsf. Also notable is a section with increased radioactivity from 1385 to 1426 mbsf that is interpreted to be more clay rich. The boundary with Subunit IVe is characterized by a sharp downhole increase in gamma ray values followed by a decreasing downhole trend.

From the upper boundary with Subunit IVd to the lower boundary with log Unit V, Subunit IVe (1514.0–1656.3 mbsf) generally shows a downhole decrease in gamma ray response and increase in resistivity. We observed that sand content increases slightly in this section with depth. The highest resistivity of 5.5 Ωm is found at 1639.4 mbsf within the lowermost 20 m section, which can also be correlated with the decrease in gamma ray values. The cause of this response is unknown, but it could be the result of high sand content and/or low porosity. The Unit IV/V boundary at 1656.3 mbsf corresponds to a gamma ray change of ~20 gAPI and a resistivity spike (Figs. **F112, F113**). Data quality of this region is poor due to WOW (Fig. **F111A**).

Unit V (1656.3 mbsf to total depth)

Log Unit V is interpreted to be homogeneous and clay rich overall based on the relatively small fluctuation of log responses and the relatively higher gamma ray values (Fig. **F112, F113**), which is in agreement with the descriptions of core cuttings lithologies (see **"Lithology"**).

Three subunits are defined based on variations in log responses (Fig. **F113**). Gamma ray values average ~87 gAPI throughout this unit, with variations of up to 28 gAPI. The Unit IV/V boundary at 1656.3 mbsf is marked by a shift of ~20 gAPI in the gamma ray data and a local spike in resistivity. Distinctive features of Unit V, when compared with Unit IV, have a rather homogeneous log response, increased radioactivity, and show similar average resistivity values with depth within each of the subunits.

Subunit Va is characterized by downhole-increasing gamma ray values until ~1730 mbsf, followed by near-constant values of 80–90 gAPI. Resistivity values decrease moderately toward the base of Subunit Va. The boundary between Subunits Va and Vb was placed at a sharp downhole decrease in gamma ray and resistivity values at 1942.5 mbsf. From the top of Subunit Vb to the base, resistivity increases with depth and gamma radiation decreases with depth.

A shift in resistivity values and gamma ray variation at 2191.0 mbsf was interpreted as an abrupt change in rock composition. Subunit Vc is characterized by an increase in gamma radioactivity and decrease in the baseline resistivity values relative to Subunit Vb.

Subunits Va and Vb were defined in Hole C0002F and correlate with Hole C0002N (Fig. **F113**). Subunit Vc was defined in Hole C0002N and was not reached by drilling in Hole C0002F.

Correlation with previous Site C0002 LWD data

We correlate LWD data from Hole C0002F with data from Hole C0002N (Fig. **F113**). Differences in data can be due to the use of different tools, causing differences in data quality, resolution, and accuracy among logs. The comparison and correlation are based on the measurements that are common to all the holes of Site C0002, which are natural gamma radioactivity and resistivity (Table **T41**). Resistivity images with bedding and structural interpretation were only available for Holes C0002A and C0002F. Furthermore, because units are highly deformed and steeply dipping at depth (Units IV and V), some depth variations are expected even given the small distances between the holes.

The Unit III/IV boundary was correlated between holes based on a marked downhole shift to decreased gamma ray values. Depth of the boundary only varies by 3.5 m between Holes C0002F and C0002N but varied as much as ~20 m between Holes C0002G and C0002A (Expedition 332 Scientists, 2011). No LWD data recorded the top of Unit III in Holes C0002F and C0002N; therefore, the actual thickness of this unit is poorly constrained. Measurements of bedding in Holes C0002A and C0002F suggest that the boundary between Units III and IV is an unconformity, as discussed for previous expeditions (Expedition 314 Scientists, 2009; Strasser et al., 2014b).

Because Unit IV had more variability in log response, due to the complex geology and relatively variable lithology (from predominantly claystone to silt and sand), it was difficult to correlate units in detail, but overall trends were consistent in all the data sets. The Subunit IVa/IVb boundary was not reached from the total depth in Hole C0002G. However, gamma radiation does show an increase in the top of the section, which is seen in the other holes as well.

Structural analysis derived from both bedding and fracture measurements made on resistivity images from Hole C0002F (Strasser et al., 2014b) shows rather complex geometry and deformation features, with large changes in the orientations of bedding. Furthermore, the Subunit IVa/IVb boundary were interpreted as a change in bedding dip and increase in gamma ray response. The top of Subunit IVc is similar in all holes, with a slight increase in gamma ray values followed by a decrease. Subunit IVd is marked by a decrease in gamma radiation at the top. An increase in sonic velocity observed in Hole C0002F indicates this transition, and Subunit IVe may have lower porosities. The bottom of Subunit IVd is not reached in Hole C0002A. The Subunit IVd/IVe boundary between Holes C0002N and C0002F is offset by 14 m. The boundary is marked by a sharp increase in gamma ray values in both holes followed by a gradual decrease.

The top of log Unit V is a very sharp boundary for both Holes C0002N and C0002F. Both holes are marked by a ~20 gAPI shift in gamma ray values and changes in resistivity response. The boundary is offset by 18.3 m between the two holes. Image logs reveal a heavily deformed section around this boundary with the offset being potentially structurally related. Subunit Va shows a slight increase in gamma ray values followed by a small but sharp decrease at the Subunit Va/Vb boundary. The bottom of Subunit Vb and all of Subunit Vc are not present in Hole C0002F.

Hole C0002P

Logging data characterization and interpretations

Hole C0002P logging data record variations in log responses, which were characterized on the available measurements by inspection of the gamma ray, compressional acoustic velocity, and phase resistivity log responses (Figs. F114, F115, F116, F117). Subunits were defined based on variations in trend lines and log character (Table T42). Depth intervals (>200 m in all cases) displaying similar log responses were designated as log subunits, following criteria established during previous NanTroSEIZE expeditions (Kinoshita, M., Tobin, H., Ashi, J., Kimura, G., Lallemant, S., Screaton, E.J., Curewitz, D., Masago, H., Moe, K.T., and the Expedition 314/315/316 Scientists, 2009; Strasser, Dugan, Kanagawa, Moore, Toczko, Maeda, and the Expedition 338 Scientists, 2014), consistent with what was described for Holes C0002N and Hole C0002F. Resistivity image data acquired with the AFR tool were also processed and interpreted to complete Hole C0002P characterization. A preliminary interpretation of bedding, structures, and stress indicators has been integrated with shipboard interpretation results.

No major or abrupt change was identified in the logging data acquired in Hole C0002P; therefore, changes in trends of log response and values are interpreted as minor changes and designated as subunits. Subunits Vc′–Ve display distinctive trends.

From top to bottom in the section, LWD tools indicate that gamma radiation increases (from 75 to 95 gAPI) and resistivity decreases, followed by an increasing trend in resistivity toward the bottom. The compressional acoustic slowness/velocity shows constant or decreasing velocity from top to bottom. Within shorter intervals, the overall decrease in velocity is punctuated by different steps to higher–lower velocities that can be observed in Figure F114. The most prominent drops in velocity can be identified toward the bottom of Subunit Ve.

The subunits boundaries we define in Hole C0002P are suggested based on the log character and relative values for the same depth intervals and in the absence of significant compositional changes described from cuttings (see "Lithology"). We interpreted the background lithology as hemipelagic silty claystone with relatively high gamma ray values. Variations in the overall trend shown as excursions and spikes of low gamma ray values were observed and interpreted based on the sonic and resistivity data (Fig. F117). Low gamma radiation, low velocity, and low resistivity were interpreted as permeable sand within Subunit Vc′. Low gamma radiation and high resistivity were interpreted as possible ash within Subunit Vd. Low gamma radiation, high velocity, and high resistivity peaks were interpreted as carbonate/silica veins or cemented sandstone within Subunit Ve.

The proposed description and interpretation of Subunit Vc′ is based on log subunits and comparison with the log response of the subunits defined in Hole C0002N. The depth intervals for subunits are shown on Table T42 together with the average, minimum, and maximum values of gamma radioactivity, resistivity, and acoustic slowness/velocity.

Subunit Vc′ (2163–2365.6 mbsf)

In Hole C0002P, Subunit Vc′ radioactivity shows variations in gamma ray values (from 58 to 94 gAPI) and an average value of 84 gAPI. Acoustic slowness values are from 83 to 110 µs/ft with an average value of 94 µs/ft. Formation resistivity varies between 1.3 and 3.2 Ωm, and the average value is 2.2 Ωm.

The uppermost interval of the logs boundary for Subunit Vc′ is characterized by an increasing trend in gamma ray values and a decrease in sonic velocities and resistivity (Fig. F114). A defining character of

Subunit Vc′ is five ≤15 m thick local minima found in gamma radiation, resistivity, and sonic velocity at ~2205, 2223, 2281, 2332, and 2365 mbsf. Variations are up to ~30 gAPI, ~1.4 Ωm, and ~570 m/s in gamma radiation, resistivity, and sonic velocity, respectively. These responses were interpreted as permeable sands, with the low resistivity resulting probably from mud invasion or from high-salinity formation fluids in the sandy layers. Typically, sharp increases in gamma radiation, velocity, and resistivity are observed at the top and bottom of these levels, potentially caused by a change from coarser grained sediment within the minima zones to a background consisting of hemipelagic silty claystone. Between 2210 and 2217 mbsf, a decrease in sonic velocity to <2900 m/s does not correspond to decreases in gamma ray values or resistivity. The uppermost sandy intervals (2221–2230 and 2203–2208 mbsf) show patterns that suggest a gradual transition from clay to sand at the base, whereas the lowermost permeable intervals (2279–2282, 2332.5–2339, and 2360–2365 mbsf) show a pattern possibly reflecting a relatively gradual transition from sand to clay (from lower to higher gamma radiation) at the top. The observations of the log properties and shapes are consistent with the interpretation of turbiditic deposits and interbedding of sandy layers in hemipelagic silty claystone (see **"Lithology"**). Possible normal grading trends at the base and reverse grading at the top are observed in the log data. Postexpedition interpretation of borehole resistivity images will help define the structures described in the cored section (see **"Lithology"** and **"Structural geology"**).

Subunit Vd (2365.6–2753 mbsf)

Below sharp but small downhole increases in gamma radiation and resistivity, which may be interpreted as a change from coarser grained sediment to background hemipelagic silty claystone, this subunit (2365.6–2753 mbsf) exhibits rather constant trends (average values for gamma radiation, resistivity, and acoustic slowness are 87 gAPI, ~2 Ωm, and 93 µs/ft, respectively). The gamma ray values progressively increase from the top, with average values of ~80 gAPI, to the bottom, reaching maximum values of 101.75 gAPI and a minimum of 69 gAPI. The minor fluctuations around this trend line suggest silt–sand alternation within the dominant hemipelagic mud.

The most striking features in this section are the subtle but continuous increasing trend in gamma radioactivity and decreasing trend in resistivity from top to bottom followed by a sharp increase near the bottom (Fig. **F114**). The compressional acoustic velocity displays a trend of decreasing velocity followed by a slight increase in velocity at 2685 mbsf.

At a finer scale, high-value resistivity spikes (e.g., from 2 to 4.5 Ωm at 2497–2502 mbsf) correspond to slightly lower gamma ray and acoustic velocity values. The comparison of four phase-shift resistivities (RH16PC to RH48PC; Fig. **F116**) suggests invasion of the layers based on the slightly differing responses of the shallow and deep measurements. A similar log character was identified in Hole C0011A (Expedition 322 Scientists, 2010a). There, the different intervals with a similar thickness from 1 to 4 m based on the resistivity and gamma ray log characteristics and core descriptions, were identified as ash and volcaniclastic layers. The log features observed in Hole C0002P similarly could be related to the possible presence of ash and volcaniclastic layers (Fig. **F117**). The first such possible layers were identified at 2385 mbsf, and the most prominent occurrence was identified at 2499 mbsf. Other thin intervals with similar features were identified at 2444, 2450, 2527, 2532, and 2535 mbsf. Although no ash layers were identified by cuttings analyses (see **"Lithology"**), our interpretation is based on correlation of the log response with logs and lithologies observed in Hole C0011A. Detailed analysis of resistivity images may help to interpret these features.

From 2585 to 2640 mbsf and 2664 to 2713.54 mbsf, variation in resistivity readings from different depths of investigation indicates the absence of separation of between curves, a possible indication of impermeable formations. Within the upper section of the subunit and downhole to 2507 mbsf, no distinctive features are recognized on the gamma ray log. In the lower section, there is correspondence in the log response among low gamma radiation, high resistivity, and increased velocity. Sharp and prominent spikes in resistivity and compressional velocity values at 2697 mbsf (Fig. **F114**) need further examination.

Subunit Ve (2753–3058.5 mbsf)

The top of this interval is characterized by a sharp downhole decrease followed by a gradual increase in gamma radioactivity, decrease of velocity values, and a gradual increase of resistivity values (2–3 Ωm). An increasing trend from the top of this interval to 2882 mbsf is followed by a decreasing trend from to 3041 mbsf in both resistivity and velocity values. Average gamma ray values are 95 gAPI, with minimum and maximum of 81.3 and 104.3 gAPI, respectively. Acoustic compressional slowness average values are 94.2 µs/ft, with minimum and maximum values of 79.7 and 106.2 µs/ft, respectively. The average value for resistivity within this section is 2.6 Ωm, and minimum and maximum values are 1.9 and 4.0 Ωm, respectively.

Prominent local maxima in resistivity values related to lower gamma radiation and higher acoustic velocity were identified at 2765–2768, 2800–2806, 2887–2898, and 2942–2966 mbsf. Based on the log response on the shipboard logs (gamma radioactivity, resistivity, and acoustic velocity), these features were interpreted as cemented layers and/or vein-rich intervals related to possible deformational structures. Postexpedition analysis of resistivity images will help to refine the interpretation of these features.

Also noticeable is the sharp drop in velocity observed between 2896.5 and 2941.2 mbsf associated with relatively low resistivity values. This drop is followed by a sharp increase at the lower boundary of this interval. The gamma ray log does not indicate relevant compositional changes at this level. One likely interpretation is the existence of a low-velocity interval bounded by highly resistive and higher velocity levels associated with tectonic structures. These features might be associated with fault-related structures seen in cuttings (see **"Structural geology"**). Below this interval, a sharp increase in velocity with a broader (~10 m) decrease is found, followed by a general decrease with small spikes.

Resistivity images interpretation

The AFR images are of good quality throughout, although very noisy and locally affected by distortion resulting from drilling difficulties during acquisition and borehole wall damage. In the uppermost interval (2149.7–2216.8 mbsf), image quality suggests bad hole conditions (Figs. **F117, F118**). The section from 2149.7 to 2163 mbsf was drilled previous to coring at the depth interval below, and the hole condition is worse than the cored section between 2163 and 2218.5 mbsf.

Standard image processing and smoothing routines improved image quality for interpretation and provided correct orientations and angles of bedding and tectonic structures (fractures and faults). Hole azimuth and deviation values used for image interpretation were obtained from the drilling deviation survey. For image display and interpretation, the high-resolution image (lower transmitter) has been used.

Bedding and tectonic structures

Bedding planes are easily identified on the processed images for most of the logged section. Bedding plane orientation could be measured and characterized nearly continuously with depth (Fig. **F118**). Gaps of measured bedding dips occur only at zones of bad hole conditions, commonly at strongly deformed zones. The alternation of layers with slight contrasts in texture and composition favor resistivity contrast, and the good definition of bedding planes seen on the resistivity images show orientation that can easily be measured to define the orientation of bedding and planar structures.

The resistivity images predominantly display northwest-dipping steep bedding (varying from 60° to 90°). Locally, south–southeast-dipping beds are also present, especially along the section between 2600 and 2750 mbsf (Figs. **F117, F118**). Because of the severity of dip changes and the high density of fractures and faults, we interpret this section as strongly tectonically deformed (Fig. **F117**). Dips decreased from 2860 (very steep; ~90°) to 3040 mbsf (~60°) at the bottom of the logged section (Fig. **F118**).

Locally highly resistive features following bedding structures were identified within Subunits Vd and Ve and require further investigation and postexpedition analysis. Tentatively, these could be interpreted as cemented layers, but other interpretations (e.g., ash layers, resistive fluids) should be considered as well. Highly conductive layers aligned parallel to bedding surfaces also occur locally, especially in Subunit Vc′. These may possibly indicate hydraulically active structures with higher water content.

Preliminary interpretation of structures, both fractures and faults, is shown in Figure **F118.** A detailed structural analysis will be carried out postexpedition. Both fractures and faults could be characterized on the resistivity images. Fractures and faults show a wide range of orientations that are generally steeply dipping, with a range of dips between ~30° and 90°. Fracture density varies with depth, with the highest concentration in the lower section of Subunit Vd and uppermost section of Subunit Ve (Figs. **F117, F118**).

Wellbore failures

Numerous wellbore failures were observed in the AFR image log. The resistivity image was the primary source of information for identifying potential wellbore failures and classification. As the wellbore failures were examined closely, we characterized the position, orientation, vertical extent, and width of the feature and classified whether a feature was a breakout or a drilling-induced tensile fracture. Most features in this data set were identified as breakouts, which appeared as dark, vertically continuous features in pairs with 180° separation in the resistivity image. The sonic caliper borehole cross-section was also used to help decide the classification for features that were not continuous and less clear. When it was still unclear whether a feature was a breakout or a drilling-induced tensile fracture, we recorded the feature as unidentified.

The most prominent features are concentrated in the uppermost 67 m in Hole C0002P, where the borehole was exposed by previous drilling and coring activity (Fig. **F119**). From 2150 to 2163 mbsf, the borehole is nearly washed out, although the preferential development of the breakout in the northwest–southeast direction can be seen in the resistivity image (Fig. **F120**). This section was drilled before coring took place and thus had been exposed for 6.5 days before being imaged with resistivity logging tools. Breakout widths average 95° and reach an observed maximum of 140°. In the cored section between 2163 and 2218.5 mbsf, clear continuous breakout features were observed in the same northwest–southeast direction as the depths above but with moderate angular widths (average = 70°). Here, the borehole cross-section derived from sonic caliper data showed enlargement of borehole diameter in the azimuth consistent with the breakouts identified in the image log. However, we note that such correspondence is not persistent, and there are depth ranges where the cross-section does not necessary match the pattern expected by the presence of breakouts in the image log.

Below 2163 mbsf, occurrences of wellbore failures were sparse, and their widths were much smaller (average = 23°) compared to the depth ranges above. With the exception of several features identified above 2600 mbsf, it was not possible to conclusively classify these features as breakouts even with the aid of sonic caliper data, although their azimuthal directions were consistent with those observed at the cored section of the well (Fig. **F120**). Also, some narrow wellbore failures observed toward the bottom of the well appear different from the breakouts above and may possibly be drilling-induced tensile fractures (Fig. **F120**). Without conclusive evidence, which is currently unavailable, many of the features below the cored section are classified as unidentified.

If we limit the discussion to the depths above and within the cored section (<2218.5 mbsf), the length-weighted average value of the breakout azimuths is in the N35°W/S35°E direction. This suggests that the direction of the maximum horizontal principal stress in the upper 65 m of the imaged well is in the northeast–southwest direction.

References

Ablard, P., Bell, C., Cook, D., Fornasier, I., Poyet, J.-P., Sharma, S., Fielding, K., Lawton, L., Haines, G., Herkommer, M.A., McCarthy, K., Radakovic, M., and Umar, L., 2012. The expanding role of mud logging. *Oilfield Rev.,* 24(1): 24–41. **http://www.slb.com/resources/publications/industry_articles/oilfield_review/2012/or2012spr03_mudlog.aspx**

Arason, P., and Levi, S., 2010. Maximum likelihood solution for inclination-only data in paleomagnetism. *Geophys. J. Int.,* 182(2):753–771. **doi:10.1111/j.1365-246X.2010.04671.x**

Athy, L.F., 1930. Density, porosity, and compaction of sedimentary rocks. *AAPG Bull.,* 14(1):1–24.

Bernard, B.B., Brooks, J.M., and Sackett, W.M., 1978. Light hydrocarbons in recent Texas continental shelf and slope sediments. *J. Geophys. Res.: Oceans,* 83(C8):4053–4061. **doi:10.1029/JC083iC08p04053**

Blum, P., 1997. Physical properties handbook: a guide to the shipboard measurement of physical properties of deep-sea cores. *ODP Tech. Note,* 26. **doi:10.2973/odp.tn.26.1997**

Byrne, T., 1984. Early deformation in melange terranes of the Ghost Rocks Formation, Kodiak Islands, Alaska. *In* Raymond, L.A. (Ed.), *Melanges: Their Nature Origin, and Significance.* Spec. Pap.—Geol. Soc. Am., 198:21–52. **doi:10.1130/SPE198-p21**

Claypool, G.E., and Kvenvolden, K.A., 1983. Methane and other hydrocarbon gases in marine sediment. *Annu. Rev. Earth Planet. Sci.,* 11(1):299–327. **doi:10.1146/annurev.ea.11.050183.001503**

Expedition 314 Scientists, 2009. Expedition 314 Site C0002. *In* Kinoshita, M., Tobin, H., Ashi, J., Kimura, G., Lallemant, S., Screaton, E.J., Curewitz, D., Masago, H., Moe, K.T., and the Expedition 314/315/316 Scientists, *Proc. IODP,* 314/315/316: Washington, DC (Integrated Ocean Drilling Program Management International, Inc.). **doi:10.2204/iodp.proc.314315316.114.2009**

Expedition 315 Scientists, 2009. Expedition 315 Site C0002. *In* Kinoshita, M., Tobin, H., Ashi, J., Kimura, G., Lallemant, S., Screaton, E.J., Curewitz, D., Masago, H., Moe, K.T., and the Expedition 314/315/316 Scientists, *Proc. IODP,* 314/315/316: Washington, DC (Integrated Ocean Drilling Program Management International, Inc.). **doi:10.2204/iodp.proc.314315316.124.2009**

Expedition 322 Scientists, 2010a. Site C0011. *In* Saito, S., Underwood, M.B., Kubo, Y., and the Expedition 322 Scientists, *Proc. IODP,* 322: Tokyo (Integrated Ocean Drilling Program Management International, Inc.). **doi:10.2204/iodp.proc.322.103.2010**

Expedition 322 Scientists, 2010b. Site C0012. *In* Saito, S., Underwood, M.B., Kubo, Y., and the Expedition 322 Scientists, *Proc. IODP,* 322: Tokyo (Integrated Ocean Drilling Program Management International, Inc.). **doi:10.2204/iodp.proc.322.104.2010**

Expedition 332 Scientists, 2011. Site C0002. *In* Kopf, A., Araki, E., Toczko, S., and the Expedition 332 Scientists, *Proc. IODP,* 332: Tokyo (Integrated Ocean Drilling Program Management International, Inc.). **doi:10.2204/iodp.proc.332.104.2011**

Expedition 333 Scientists, 2012a. Site C0011. *In* Henry, P., Kanamatsu, T., Moe, K., and the Expedition 333 Scientists, *Proc. IODP,* 333: Tokyo (Integrated Ocean Drilling Program Management International, Inc.). **doi:10.2204/iodp.proc.333.104.2012**

Expedition 333 Scientists, 2012b. Site C0012. *In* Henry, P., Kanamatsu, T., Moe, K., and the Expedition 333 Scientists, *Proc. IODP,* 333: Tokyo (Integrated Ocean Drilling

Program Management International, Inc.). **doi:10.2204/iodp.proc.333.105.2012**

Henry, P., Jouniaux, L., Screaton, E.J., Hunze, S., and Saffer, D.M., 2003. Anisotropy of electrical conductivity record of initial strain at the toe of the Nankai accretionary wedge. *J. Geophys. Res.: Solid Earth,* 108(B9):2407. **doi:10.1029/2002JB002287**

Hizem, M., Budan, H., Deville, B., Faivre, O., Mosse, L., and Simon, M., 2008. Dielectric dispersion: a new wireline petrophysical measurement [presented at 2008 SPE Annual Technical Conference and Exhibition, Denver, CO, 21–24 September]. (SPE-116130-MS) **doi:10.2118/116130-MS**

Isozaki, Y., and Itaya, T., 1990. Chronology of Sanbagawa metamorphism. *J. Metamorph. Geol,* 8(4):401–411. **doi:10.1111/j.1525-1314.1990.tb00627.x**

Jenden, P.D., Newell, K.D., Kaplan, I.R., and Watney, W.L., 1988. Composition and stable-isotope geochemistry of natural gases from Kansas, midcontinent, USA. *Chem. Geol.,* 71(1–3):117–147. **doi:10.1016/0009-2541(88)90110-6**

JOIDES Pollution Prevention and Safety Panel, 1992. Ocean Drilling Program guidelines for pollution prevention and safety. *JOIDES J.,* 18(7):24. **http://www.odplegacy.org/PDF/Admin/JOIDES_Journal/JJ_1992_V18_No7.pdf**

Kinoshita, M., Tobin, H., Ashi, J., Kimura, G., Lallemant, S., Screaton, E.J., Curewitz, D., Masago, H., Moe, K.T., and the Expedition 314/315/316 Scientists, 2009. *Proc. IODP,* 314/315/316: Washington, DC (Integrated Ocean Drilling Program Management International, Inc.). **doi:10.2204/iodp.proc.314315316.2009**

Kopf, A., Araki, E., Toczko, S., and the Expedition 332 Scientists, 2011. *Proc. IODP,* 332: Tokyo (Integrated Ocean Drilling Program Management International, Inc.). **doi:10.2204/iodp.proc.332.2011**

Krooss, B.M., Littke, R., Müller, B., Frielingsdorf, J., Schwochau, K., and Idiz, E.F., 1995. Generation of nitrogen and methane from sedimentary organic matter: implications on the dynamics of natural gas accumulations. *Chem. Geol.,* 126(3–4):291–318. **doi:10.1016/0009-2541(95)00124-7**

Lurcock, P.C., and Wilson, G.S., 2012. PuffinPlot: a versatile, user-friendly program for paleomagnetic analysis. *Geochem., Geophys., Geosyst.,* 13(6):Q06Z45. **doi:10.1029/2012GC004098**

Maltman, A.J., Byrne, T., Karig, D.E., and Lallemant, S., 1993. Deformation at the toe of an active accretionary prism: synopsis of results from ODP Leg 131, Nankai, SW Japan. *J. Struct. Geol.,* 15(8):949–964. **doi:10.1016/0191-8141(93)90169-B**

Mingram, B., Hoth, P., Lüders, V., and Harlov, D., 2005. The significance of fixed ammonium in Palaeozoic sediments for the generation of nitrogen-rich natural gases in the North German Basin. *Int. J. Earth Sci.,* 94(5–6):1010–1022. **doi:10.1007/s00531-005-0015-0**

Petit, J.P., 1987. Criteria for the sense of movement on fault surfaces in brittle rocks. *J. Struct. Geol.,* 9(5–6):597–608. **doi:10.1016/0191-8141(87)90145-3**

Prinzhofer, A., and Pernaton, É., 1997. Isotopically light methane in natural gas: bacterial imprint or diffusive fractionation? *Chem. Geol.,* 142(3–4):193–200. **doi:10.1016/S0009-2541(97)00082-X**

Raaen, A.M., Horsrud, P., Kjørholt, H., and Økland, D., 2006. Improved routine estimation of the minimum horizontal stress component from extended leak-off tests. *Int. J. Rock Mech. Min. Sci.,* 43(1):37–48. **doi:10.1016/j.ijrmms.2005.04.005**

Raffi, I., Backman, J., Fornaciari, E., Pälike, H., Rio, D., Lourens, L., and Hilgen, F., 2006. A review of calcareous nannofossil astrobiochronology encompassing the past 25 million years. *Quat. Sci. Rev.,* 25(23–24):3113–3137. **doi:10.1016/j.quascirev.2006.07.007**

Rice, D.D., and Claypool, G.E., 1981. Generation, accumulation, and resource potential of biogenic gas. *AAPG Bull.,* 65(1):5–25. **doi:10.1306/2F919765-16CE-11D7-8645000102C1865D**

Saffer, D., McNeill, L., Byrne, T., Araki, E., Toczko, S., Eguchi, N., Takahashi, K., and the Expedition 319 Scientists, 2010. *Proc. IODP,* 319: Tokyo (Integrated Ocean Drilling Program management International, Inc.). **doi:10.2204/iodp.proc.319.2010**

Schoell, M., 1983. Genetic characterization of natural gases. *AAPG Bull.,* 67(3):546. **doi:10.1306/03B5B4C5-16D1-11D7-8645000102C1865D**

Shipboard Scientific Party, 1995. Site 909. *In* Myhre, A.M., Thiede, J., Firth, J.V., et al., *Proc. ODP, Init. Repts.,* 151: College Station, TX (Ocean Drilling Program), 159–220. **doi:10.2973/odp.proc.ir.151.107.1995**

Shipboard Scientific Party, 2001a. Site 1175. *In* Moore, G., Taira, A., Klaus, A., et al., *Proc. ODP, Init. Repts.,* 190: College Station, TX (Ocean Drilling Program), 1–149. **doi:10.2973/odp.proc.ir.190.106.2001**

Shipboard Scientific Party, 2001b. Site 1176. *In* Moore, G., Taira, A., Klaus, A., et al., *Proc. ODP, Init. Repts.,* 190: College Station, TX (Ocean Drilling Program), 1–149. **doi:10.2973/odp.proc.ir.190.107.2001**

Spinelli, G.A., and Harris, R.N., 2011. Thermal effects of hydrothermal circulation and seamount subduction: temperatures in the Nankai Trough Seismogenic Zone Experiment transect, Japan. *Geochem., Geophys., Geosyst.,* 12(12). **doi:10.1029/2011GC003727**

Stein, R., Brass, G., Graham, D., Pimmel, A., and the Shipboard Scientific Party, 1995. Hydrocarbon measurements at Arctic Gateways sites (ODP Leg 151). *In* Myhre, A.M., Thiede, J., Firth, J.V., et al., *Proc. ODP, Init. Repts.,* 151: College Station, TX (Ocean Drilling Program), 385–395. **doi:10.2973/odp.proc.ir.151.112.1995**

Strasser, M., Dugan, B., Kanagawa, K., Moore, G.F., Toczko, S., Maeda, L., and the Expedition 338 Scientists, 2014. *Proc. IODP,* 338: Yokohama (Integrated Ocean Drilling Program Management International, Inc.). **doi:10.2204/iodp.proc.338.2014**

Strasser, M., Dugan, B., Kanagawa, K., Moore, G.F., Toczko, S., Maeda, L., Kido, Y., Moe, K.T., Sanada, Y., Esteban, L., Fabbri, O., Geersen, J., Hammerschmidt, S., Hayashi, H., Heirman, K., Hüpers, A., Jurado Rodriguez, M.J., Kameo, K., Kanamatsu, T., Kitajima, H., Masuda, H., Milliken, K., Mishra, R., Motoyama, I., Olcott, K., Oohashi, K., Pickering, K.T., Ramirez, S.G., Rashid, H., Sawyer, D., Schleicher, A., Shan, Y., Skarbek, R., Song, I., Takeshita, T., Toki, T., Tudge, J., Webb, S., Wilson, D.J., Wu, H.-Y., and Yamaguchi, A., 2014a. Methods. *In* Strasser, M., Dugan, B., Kanagawa, K., Moore, G.F., Toczko, S., Maeda, L., and the Expedition 338 Scientists, *Proc. IODP,* 338: Yokohama (Integrated Ocean Drilling Program). **doi:10.2204/iodp.proc.338.102.2014**

Strasser, M., Dugan, B., Kanagawa, K., Moore, G.F., Toczko, S., Maeda, L., Kido, Y., Moe, K.T., Sanada, Y., Esteban, L., Fabbri, O., Geersen, J., Hammerschmidt, S., Hayashi, H., Heirman, K., Hüpers, A., Jurado Rodriguez, M.J., Kameo, K., Kanamatsu, T., Kitajima, H., Masuda, H., Milliken, K., Mishra, R., Motoyama, I., Olcott, K., Oohashi, K., Pickering, K.T., Ramirez, S.G., Rashid, H., Sawyer, D., Schleicher, A., Shan, Y., Skarbek, R., Song, I., Takeshita, T., Toki, T., Tudge, J., Webb, S., Wilson, D.J., Wu, H.-Y., and Yamaguchi, A., 2014b. Site C0002. *In* Strasser, M., Dugan, B., Kanagawa, K., Moore, G.F., Toczko, S., Maeda, L., and the Expedition 338 Scientists, *Proc. IODP,* 338: Yokohama (Integrated Ocean Drilling Program). **doi:10.2204/iodp.proc.338.103.2014**

Taira, A., Hill, I., Firth, J., Berner, U., Brückmann, W., Byrne, T., Chabernaud, T., Fisher, A., Foucher, J.-P., Gamo, T., Gieskes, J., Hyndman, R., Karig, D., Kastner, M., Kato, Y., Lallement, S., Lu, R., Maltman, A., Moore, G., Moran, K., Olaffson, G., Owens, W., Pickering, K., Siena, F., Taylor, E., Underwood, M., Wilkinson, C., Yamano, M., and Zhang, J., 1992. Sediment deformation and hydrogeology of the Nankai Trough accretionary prism: synthesis of shipboard results of ODP Leg 131. *Earth Planet. Sci. Lett.,* 109(3–4):431–450. **doi:10.1016/0012-821X(92)90104-4**

Taira, A., Katto, J., Tashiro, M., Okamura, M., and Kodama, K., 1988. The Shimanto Belt in Shikoku, Japan: evolution of Cretaceous to Miocene accretionary prism. *Mod. Geol.,* 12:5–46.

Tobin, H., Hirose, T., Saffer, D., Toczko, S., Maeda, L., Kubo, Y., Boston, B., Broderick, A., Brown, K., Crespo-Blanc, A., Even, E., Fuchida, S., Fukuchi, R., Hammerschmidt, S., Henry, P., Josh, M., Jurado, M.J., Kitajima, H., Kitamura, M., Maia, A., Otsubo, M., Sample, J., Schleicher, A., Sone, H., Song, C., Valdez, R., Yamamoto, Y., Yang, K., Sanada, Y., Kido, Y., and Hamada, Y., 2015. Methods. *In* Tobin, H., Hirose, T., Saffer, D., Toczko, S., Maeda, L., Kubo, Y., and the Expedition 348 Scientists, *Proc. IODP,* 348: College Station, TX (Integrated Ocean Drilling Program). **doi:10.2204/iodp.proc.348.102.2015**

Todd, D.K., and Mays, L.W., 2005. *Groundwater Hydrology* (3rd ed.): Hoboken, NJ (John Wiley & Sons).

Underwood, M.B., Moore, G.F., Taira, A., Klaus, A., Wilson, M.E.J., Fergusson, C.L., Hirano, S., Steurer, J., and the Leg 190 Shipboard Scientific Party, 2003. Sedimentary and tectonic evolution of a trench-slope basin in the Nankai subduction zone of southwest Japan. *J. Sediment. Res.,* 73(4):589–602. **doi:10.1306/092002730589**

Wheat, C.G., Boulègue, J., and Mottl, M.J., 1994. A technique for obtaining pore water chemical composition from indurated and hydrothermally altered sediment and basalt: the ground rock interstitial normative determination (GRIND). *In* Mottl, M.J., Davis, E.E., Fisher, A.T., and Slack, J.F. (Eds.), *Proc. ODP, Sci. Results,* 139: College Station, TX (Ocean Drilling Program), 429–437. **doi:10.2973/odp.proc.sr.139.234.1994**

Whiticar, M.J., 1994. Correlation of natural gases with their source. *In* Magoon, L.B., and Dow, W.G. (Eds.), *The Petroleum System—From Source to Trap.* AAPG Mem., 60:261–283.

Wiersberg, T., and Erzinger, J., 2008. Origin and spatial distribution of gas at seismogenic depths of the San Andreas Fault from drill-mud gas analysis. *Appl. Geochem.,* 23(6):1675–1690. **doi:10.1016/j.apgeochem.2008.01.012**

Yamamoto, Y., Mukoyoshi, H., and Ogawa, Y., 2005. Structural characteristics of shallowly buried accretionary prism: rapidly uplifted Neogene accreted sediments on the Miura-Boso Peninsula, central Japan. *Tectonics,* 24(5):TC5008. **doi:10.1029/2005TC001823**

Zoback, M.D., 2007. *Reservoir Geomechanics:* Cambridge, UK (Cambridge Univ. Press).

Publication: 29 January 2015
MS 348-103

Figure F1. **A.** Annular pressures measured at the bit during drilling, as a function of depth (referenced to the rig floor). The leak-off pressure measured by a leak-off test during Expedition 338 and hydrostatic and lithostatic pressures are shown for reference. Hydrostatic pressure was computed assuming a mean seawater and pore water density of 1.03 g/cm^3. DOC = drilling out cement, RIH = run in hole, csg = casing. **B.** Annular pressures shown in terms of equivalent circulating density (ECD) as a function of depth. The nominal mud weights used during drilling are shown for reference (gray dashed lines). Mud losses occurred when the bit was at 4004 and 4083 m BRT.

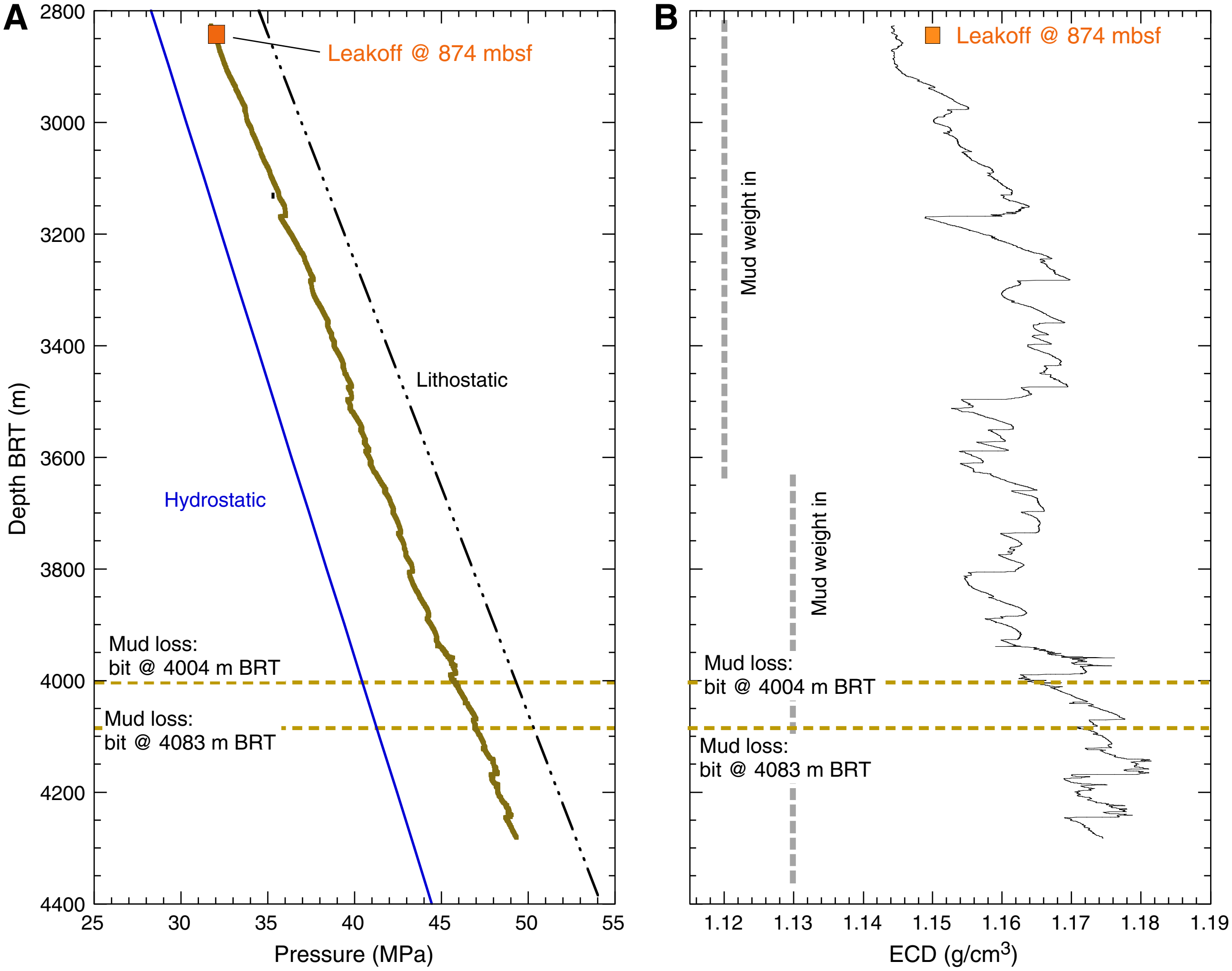

Figure F2. Equivalent circulating density (ECD) from measured annular pressure while drilling at Site C0002 as a function of time, showing changes in pressure during pipe connections as the pumps were turned off and on: **A.** Drilling from 3976 to 4004 m BRT, including a time when large mud losses were observed (gray shaded area); **B.** Detailed view of a pipe connection immediately preceding the mud losses at bit depth of 4004 m BRT. **C, D.** Detailed views of pipe connections while drilling from 4004 to 4083 m BRT after mud losses and addition of lost circulation material (LCM). **E.** Example of a pipe connection prior to mud losses while drilling from 3752 to 3819 m BRT. **F.** Example of pipe connection while drilling the deepest part of the hole after further mud losses at 4083 m BRT and addition of more LCM.

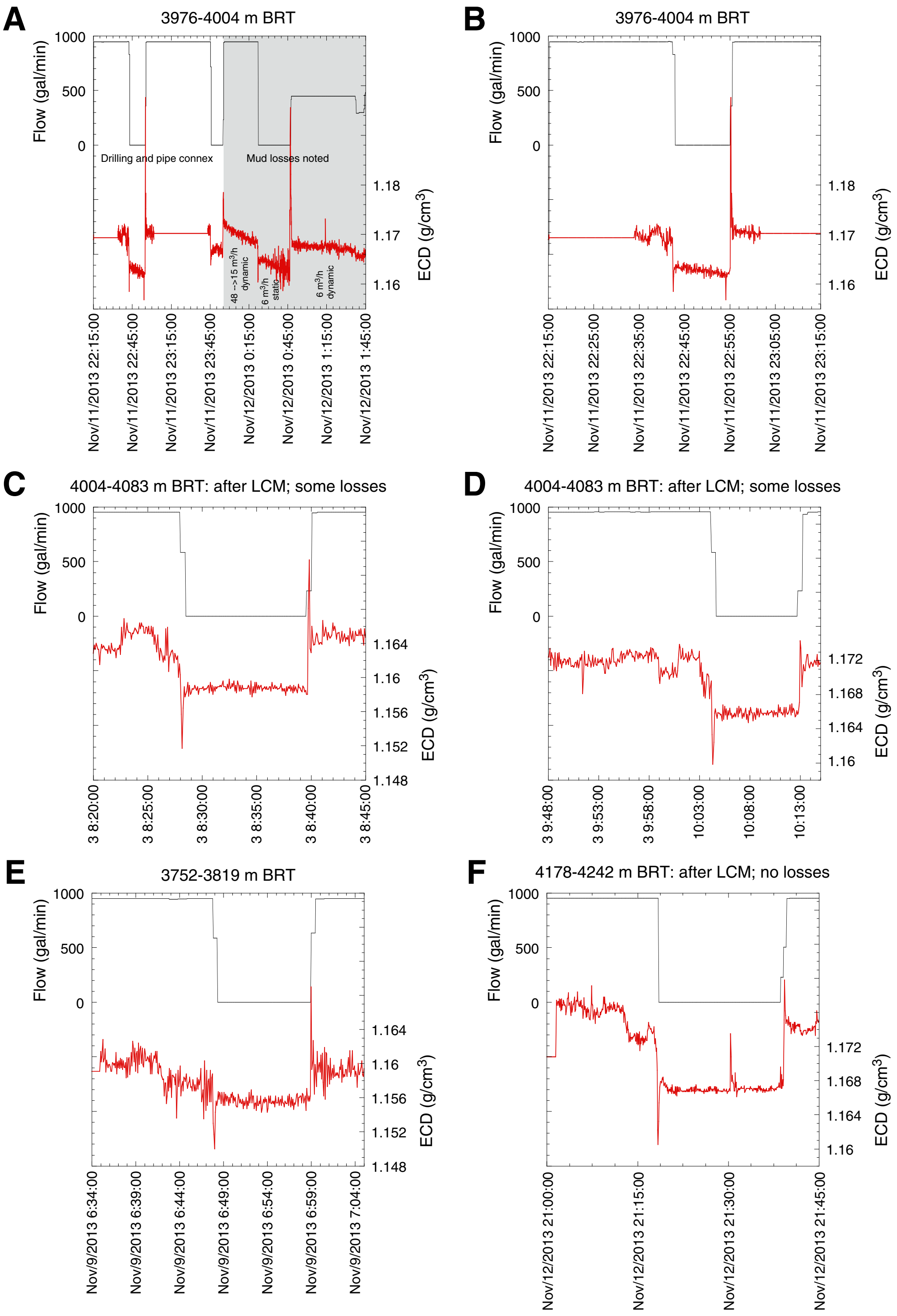

Figure F3. Bathymetric map of all holes drilled at Site C0002. Holes C0002M (red circle), C0002N (blue dashed line), and C0002P (green dashed line) were drilled during Expedition 348. Contours in meters below sea level.

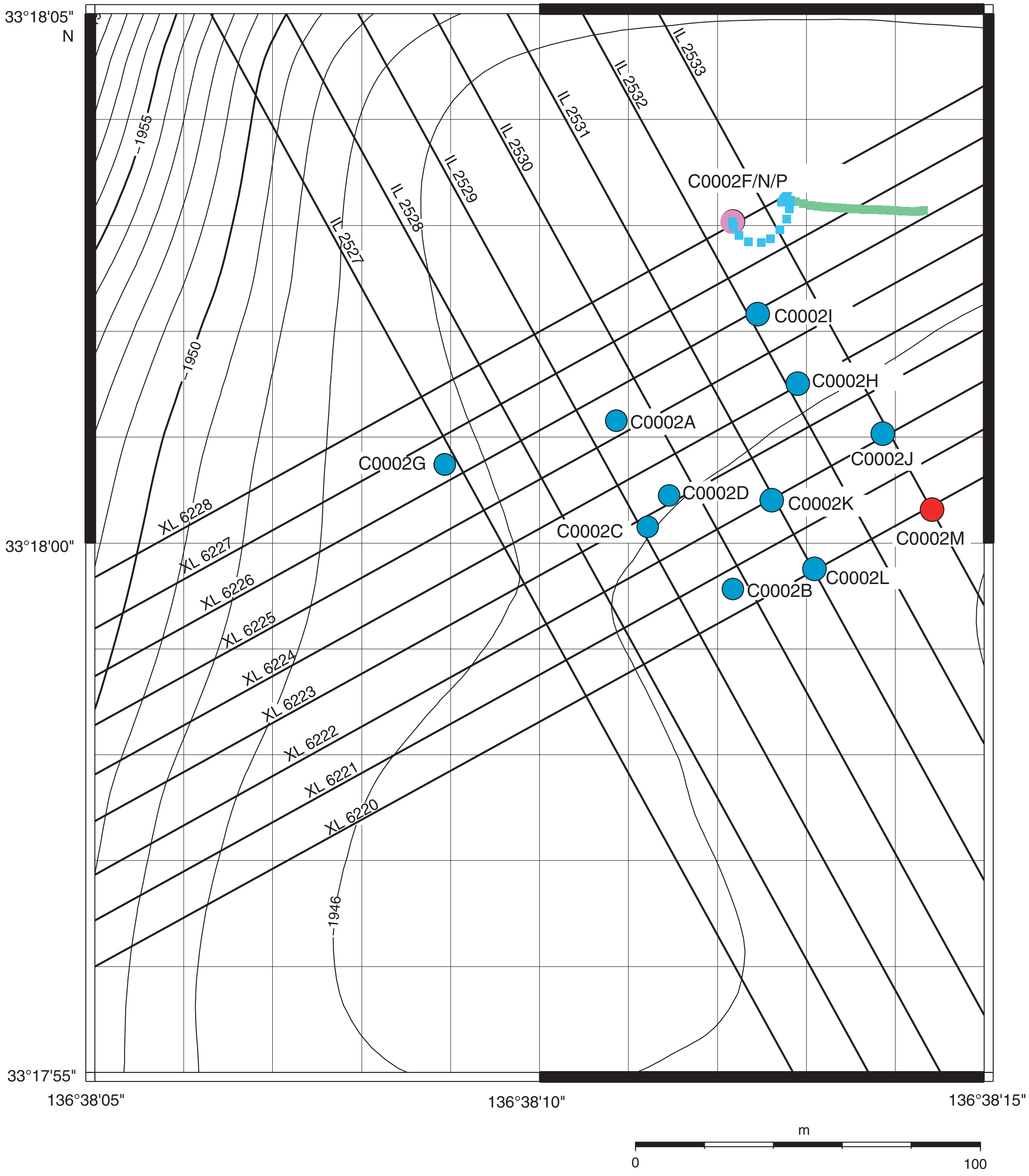

Figure F4. (**A**) Raw and (**B**) de-tided pore fluid pressures recorded in the borehole observatory in Hole C0002G. Pore pressure was monitored in a screened interval at 757–780 mbsf in Kumano Basin sediment (red), and in an open hole from 937 to 980 mbsf in the uppermost accretionary prism (brown). Seafloor hydrostatic pressure is shown for reference (blue). The formation pressures exhibit clear responses to drilling activity and mud losses in the riser Hole C0002F and sidetracked Hole C0002N.

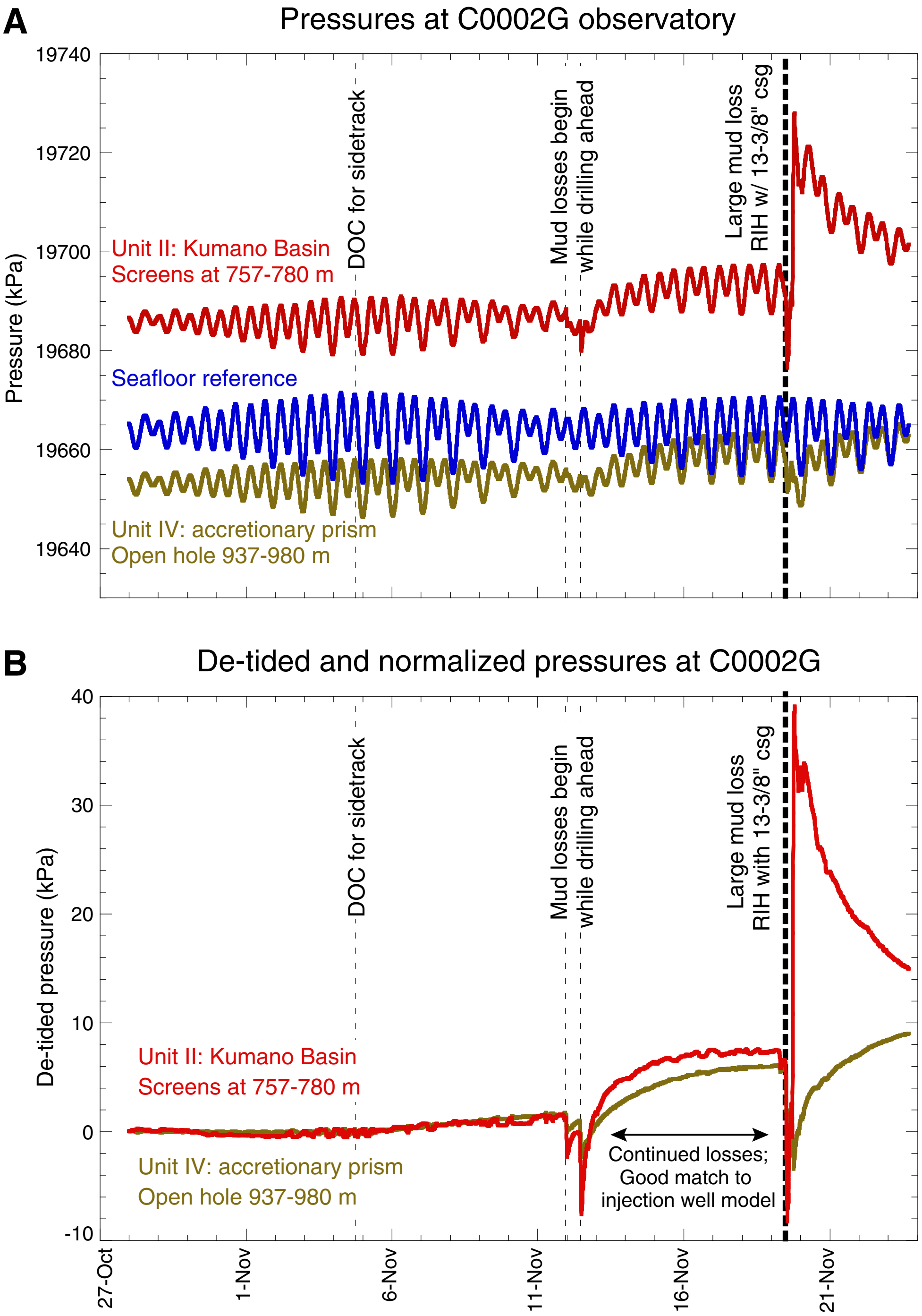

Figure F5. Data for entire period of riser operations in Hole C0002N showing the relationship between equivalent circulating density (ECD) and rate of penetration.

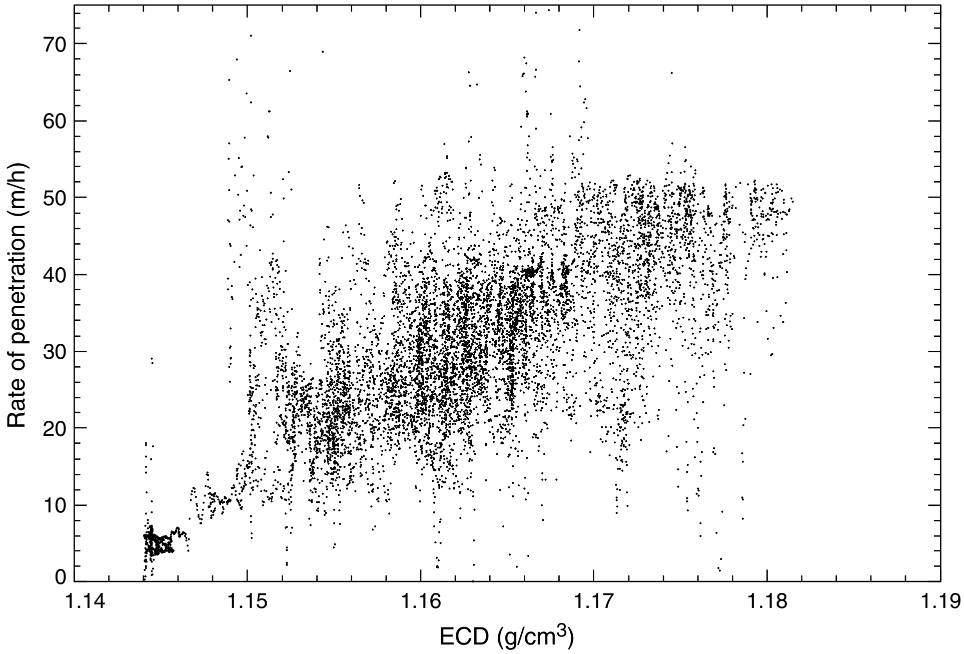

Figure F6. Depth intervals from which cores and cuttings were taken and lithologic unit boundaries (roman numerals), Expedition 348. Cuttings sampling intervals from Expedition 338 (Hole C0002F) are also included for comparison.

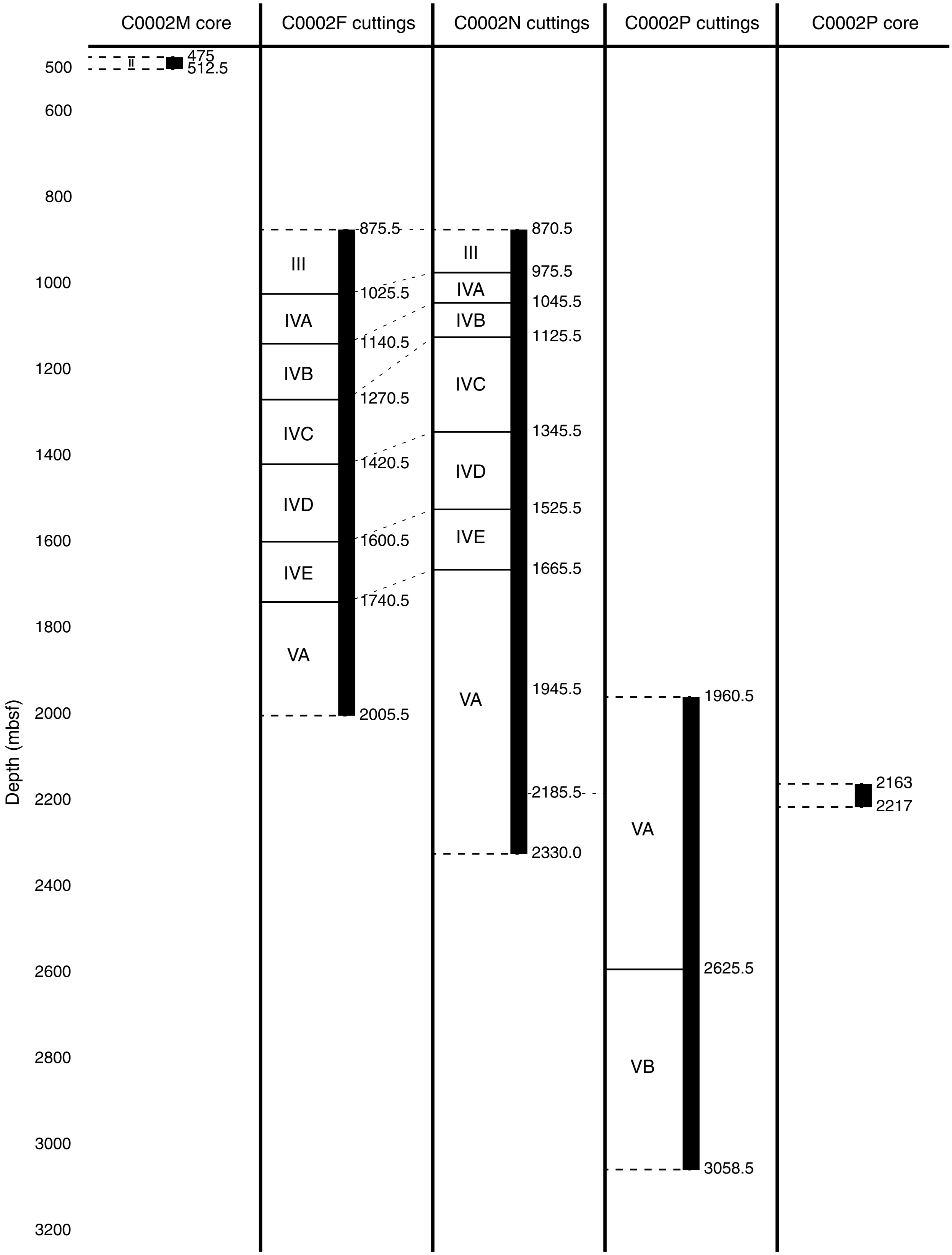

Figure F7. A–D. Lithologic columns, Cores 348-C0002M-1R through 4R. WR = whole-round sample.

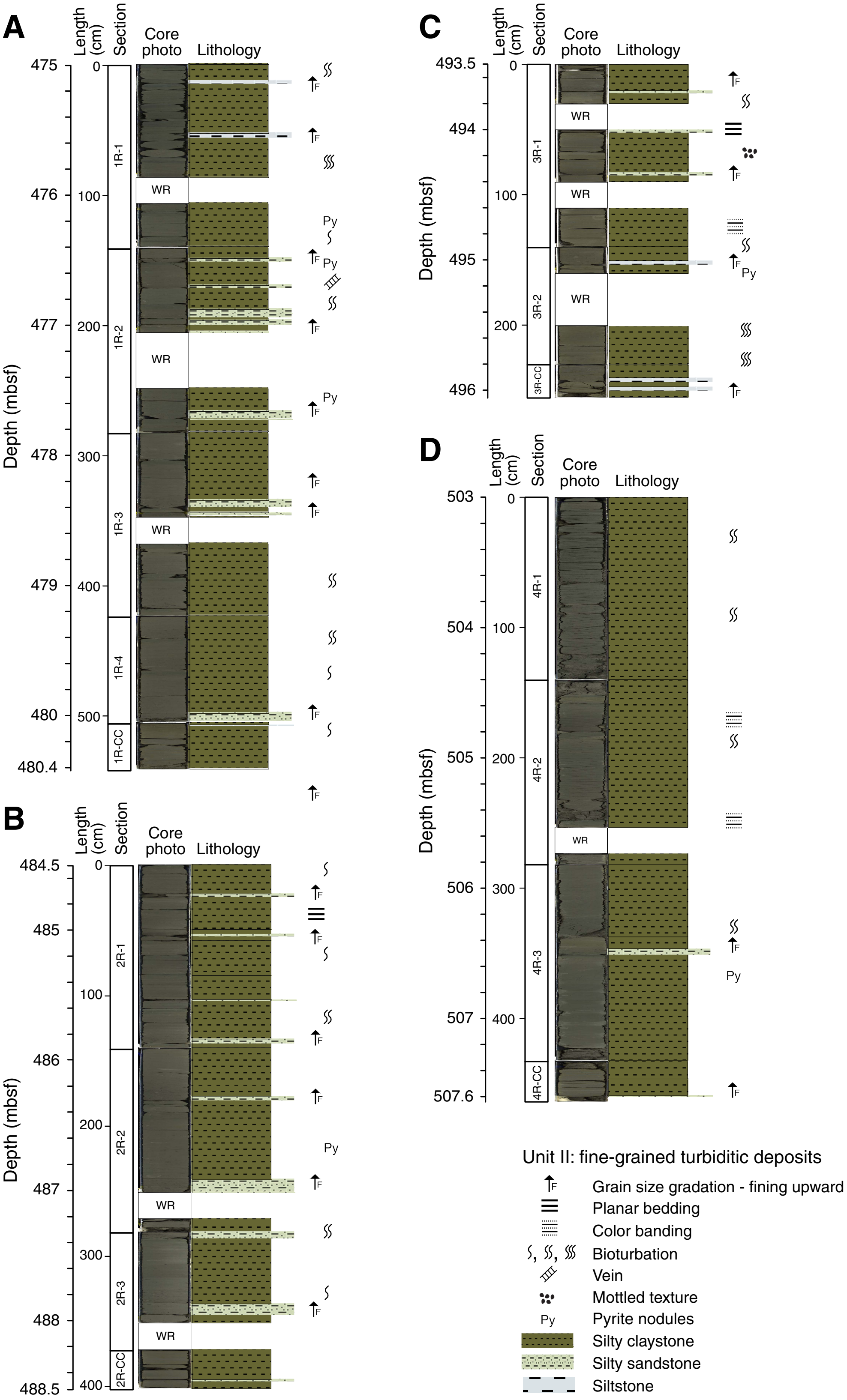

Figure F8. Lithologies in Hole C0002M cores. **A–C.** Fine-grained turbiditic intervals of silty claystone, sandy siltstone, and fine-grained sandstone, with fining-upward gradation. **D, E.** Silty claystone with mottled structures due to bioturbation; pyrite nodules and fossiliferous lenses are common throughout the core.

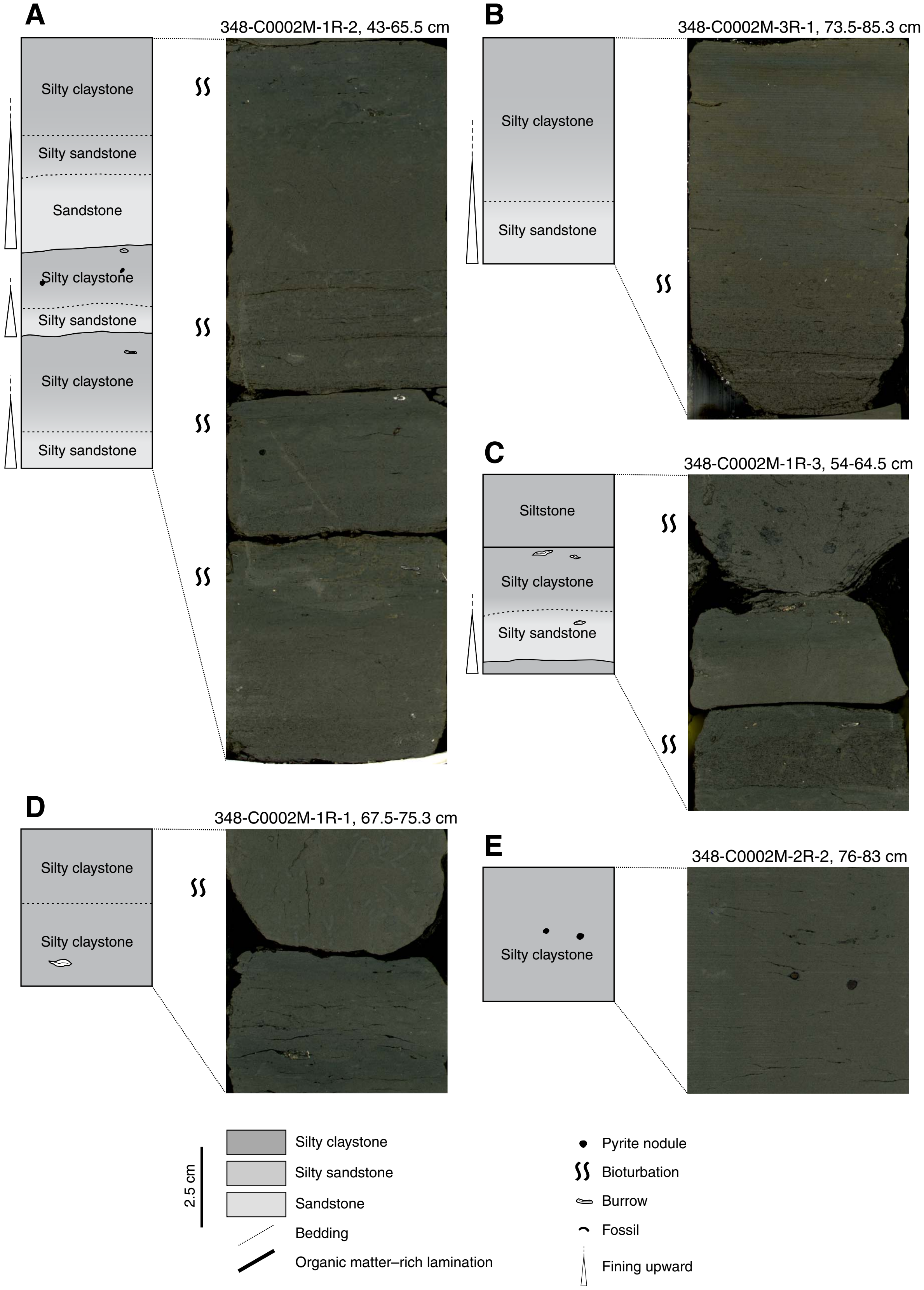

Figure F9. Smear slide mineral abundance trends, Hole C0002M.

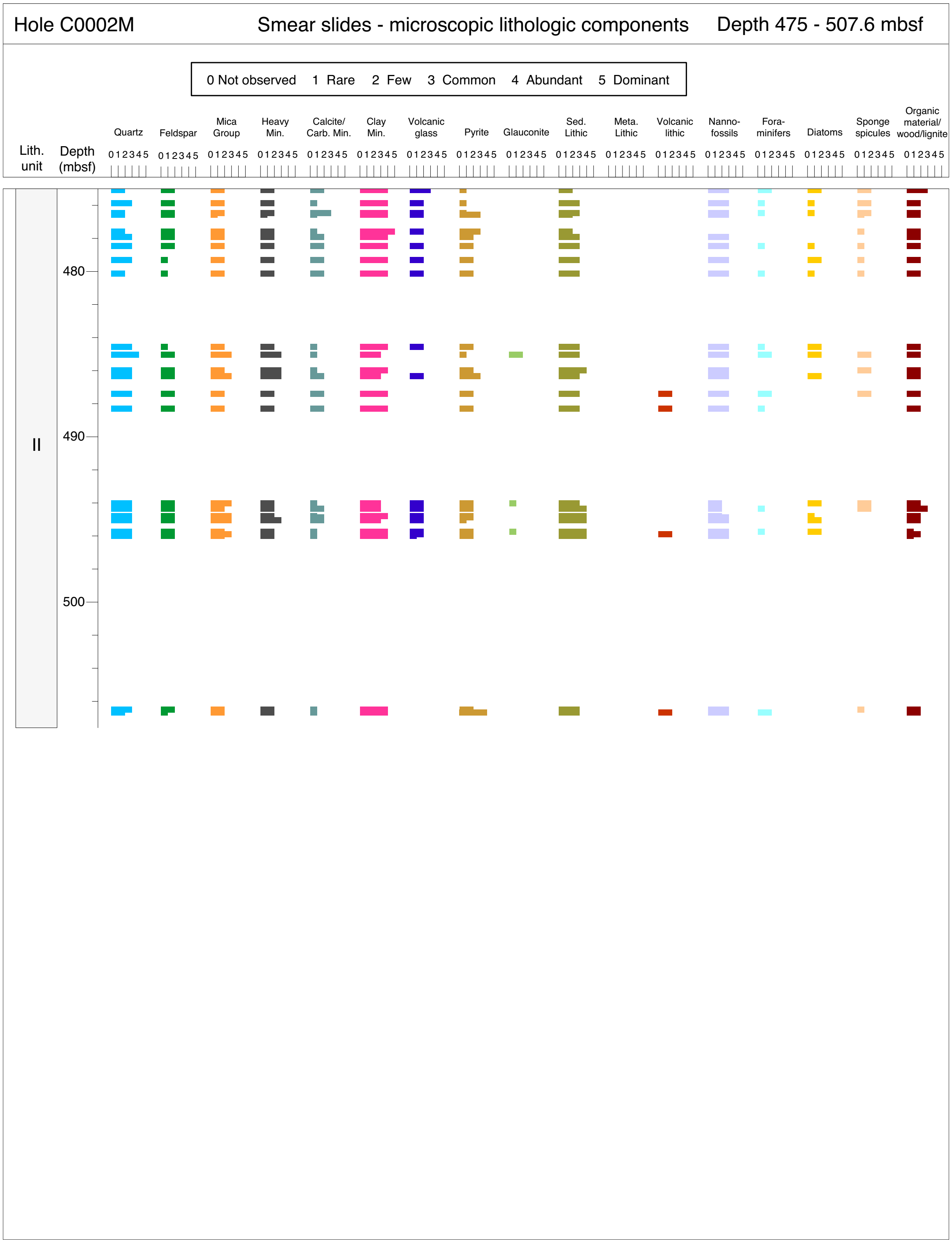

Figure F10. Smear slide mineralogy in core samples, Hole C0002M (plane-polarized light). **A.** Representative quartz (Sample 348-C0002M-1R-3, 64 cm; 478.47 mbsf). **B.** Mudstone (Sample 2R-1, 6 cm; 484.56 mbsf). **C.** Volcanic glass (Sample 1R-1, 86 cm; 475.86 mbsf). **D.** Pyrite (Sample 1R-2, 16 cm; 476.57 mbsf). **E.** Glauconite (Sample 1R-1, 86 cm; 475.86 mbsf). **F.** Hornblende (Sample 2R-1, 6 cm; 484.56 mbsf).

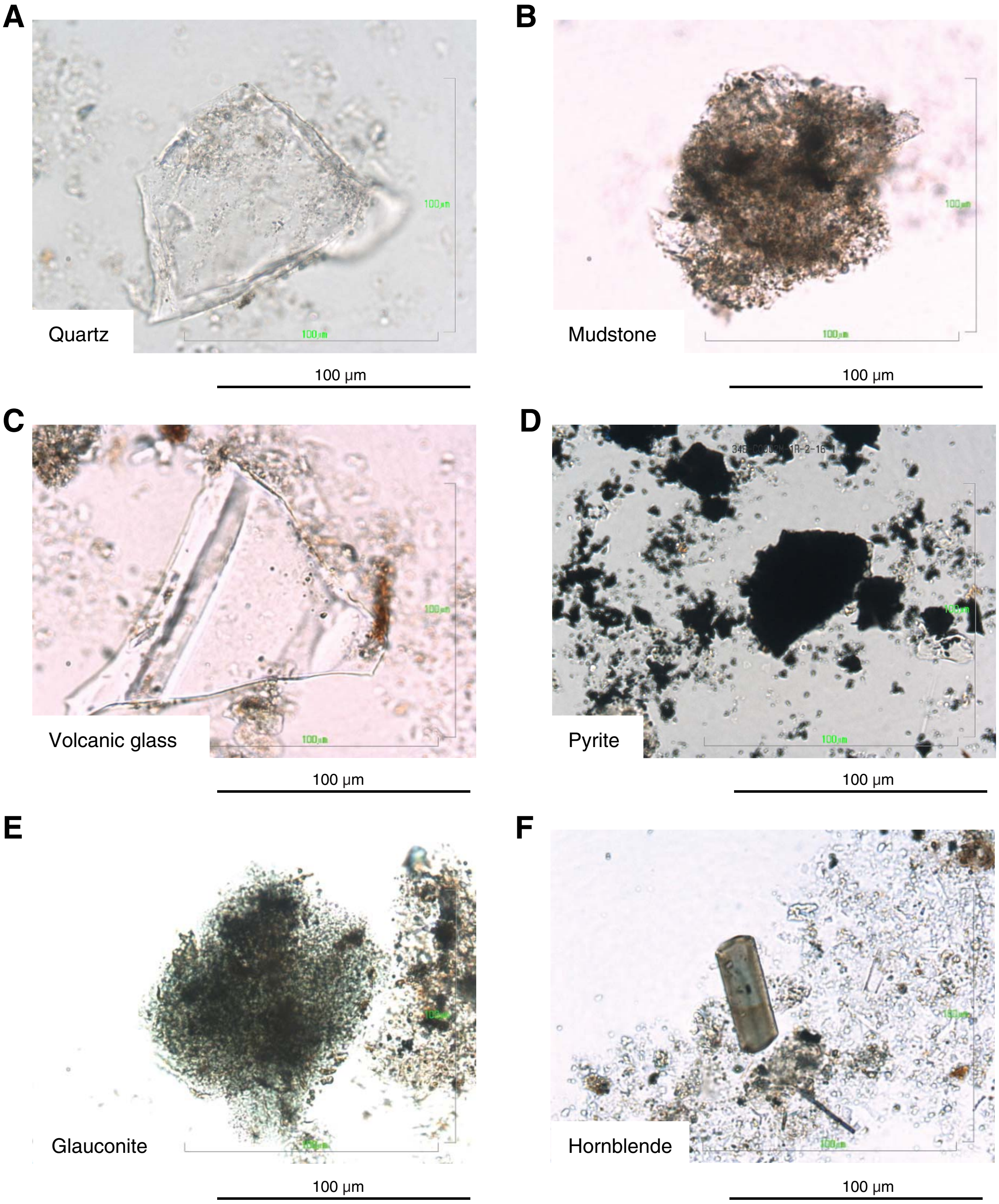

Figure F11. Summary of mineralogy from bulk powder X-ray diffraction analyses, Hole C0002M.

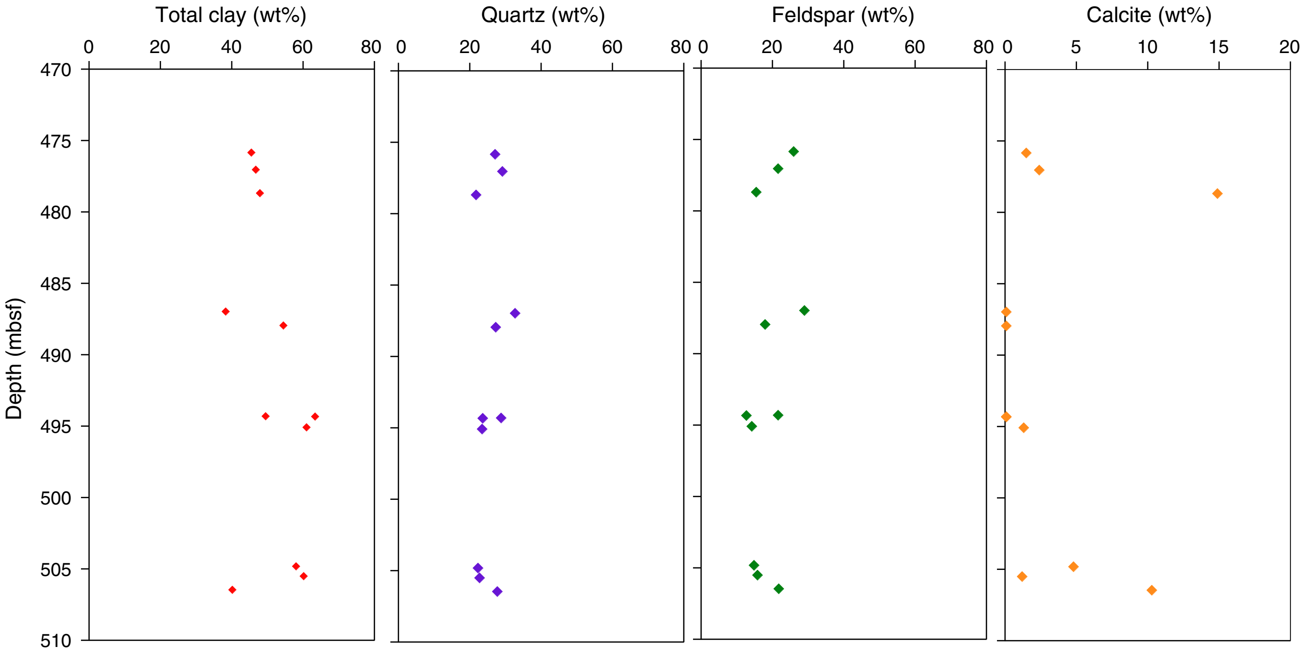

Figure F12. Summary of lithology and bulk powder X-ray diffraction analyses for 1–4 mm cuttings size fraction of samples from Site C0002. Data are included from Holes C0002B (Expedition 315 Scientists, 2009) and C0002F (Strasser et al., 2014b).

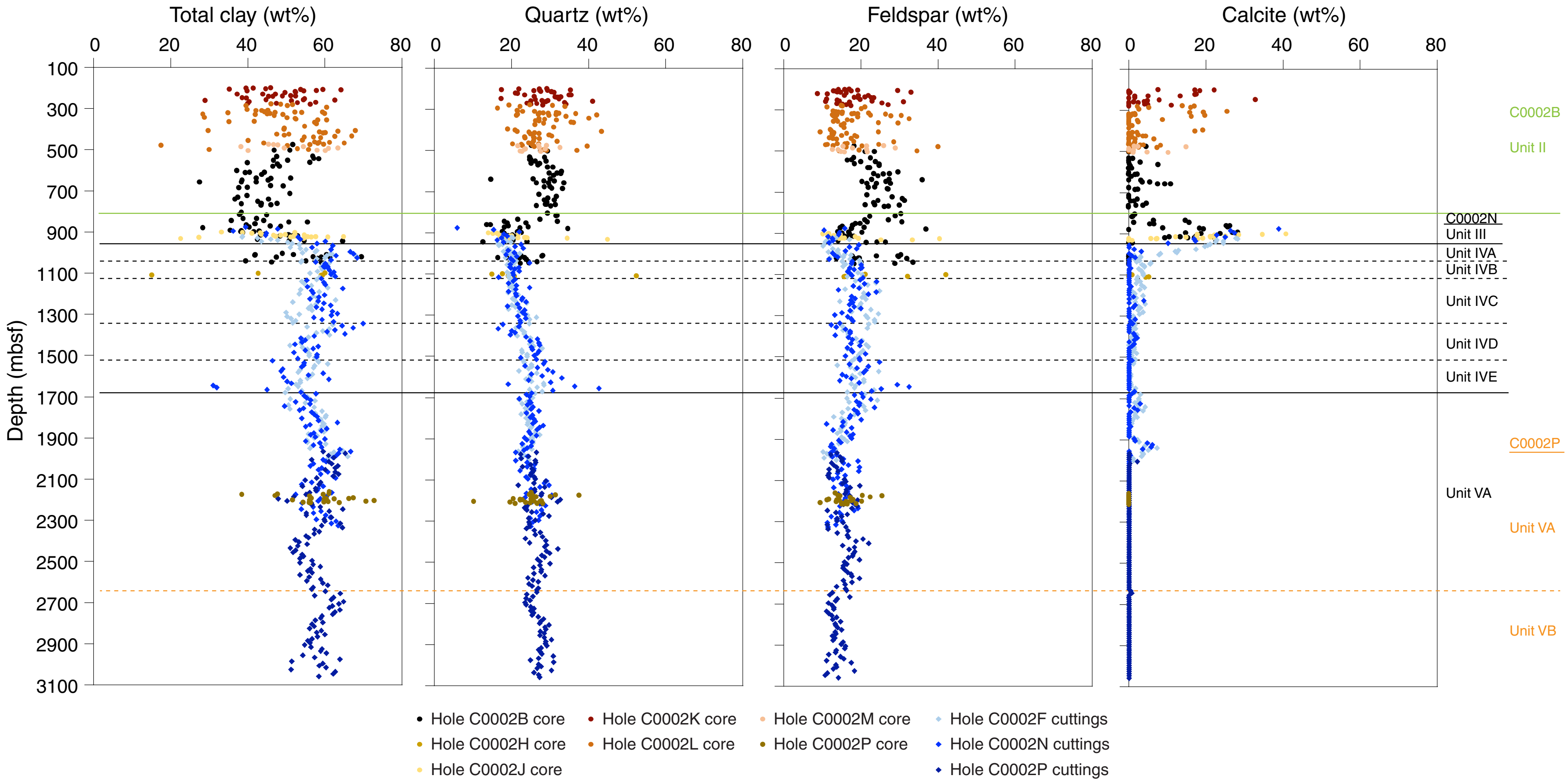

Figure F13. Summary of lithology and bulk powder X-ray fluorescence analyses for 1–4 mm cuttings size fraction of samples from Site C0002. Data are included from Holes C0002B (Expedition 315 Scientists, 2009) and C0002F (Strasser et al., 2014b). (Continued on next page.)

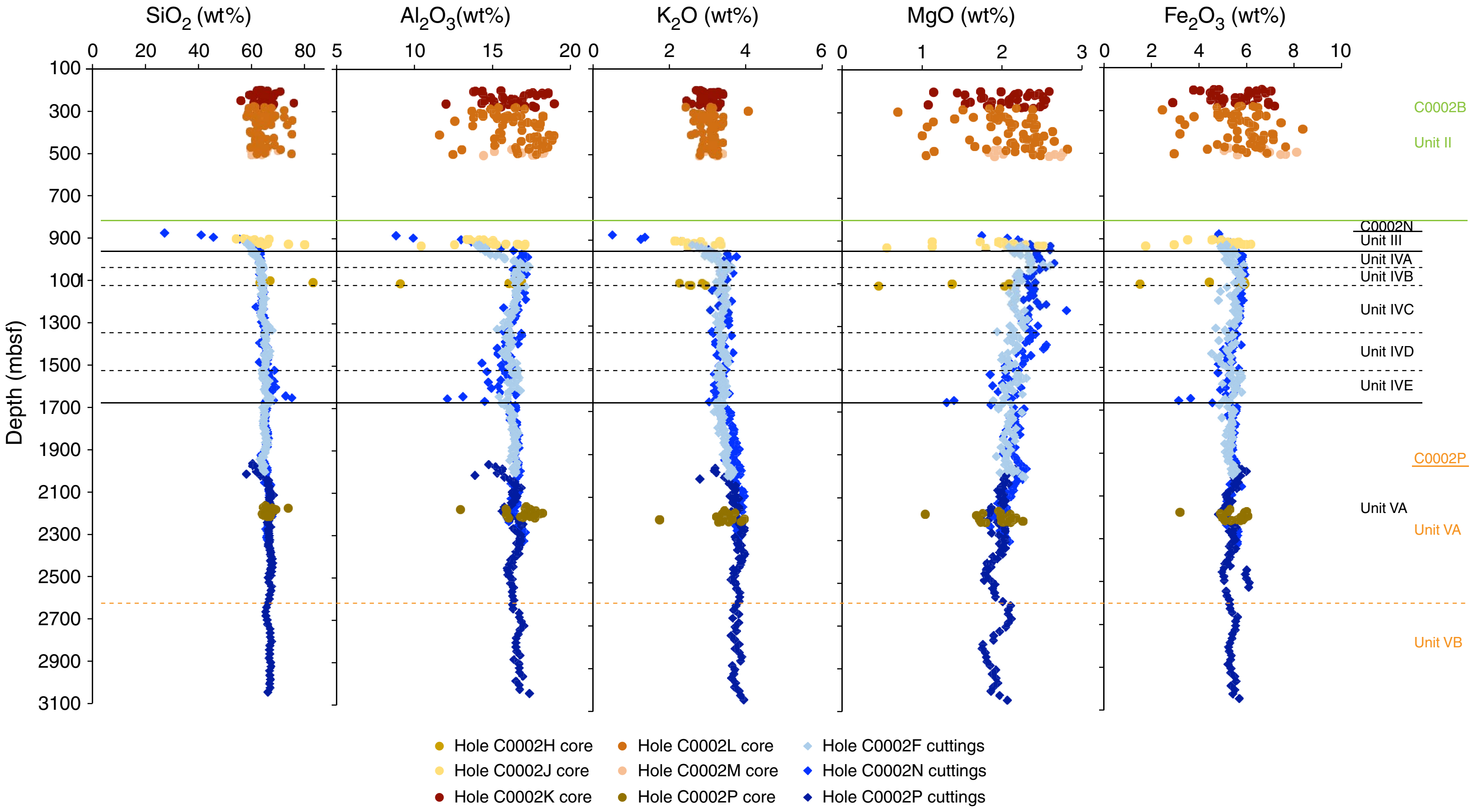

Figure F13 (continued). LOI = loss on ignition.

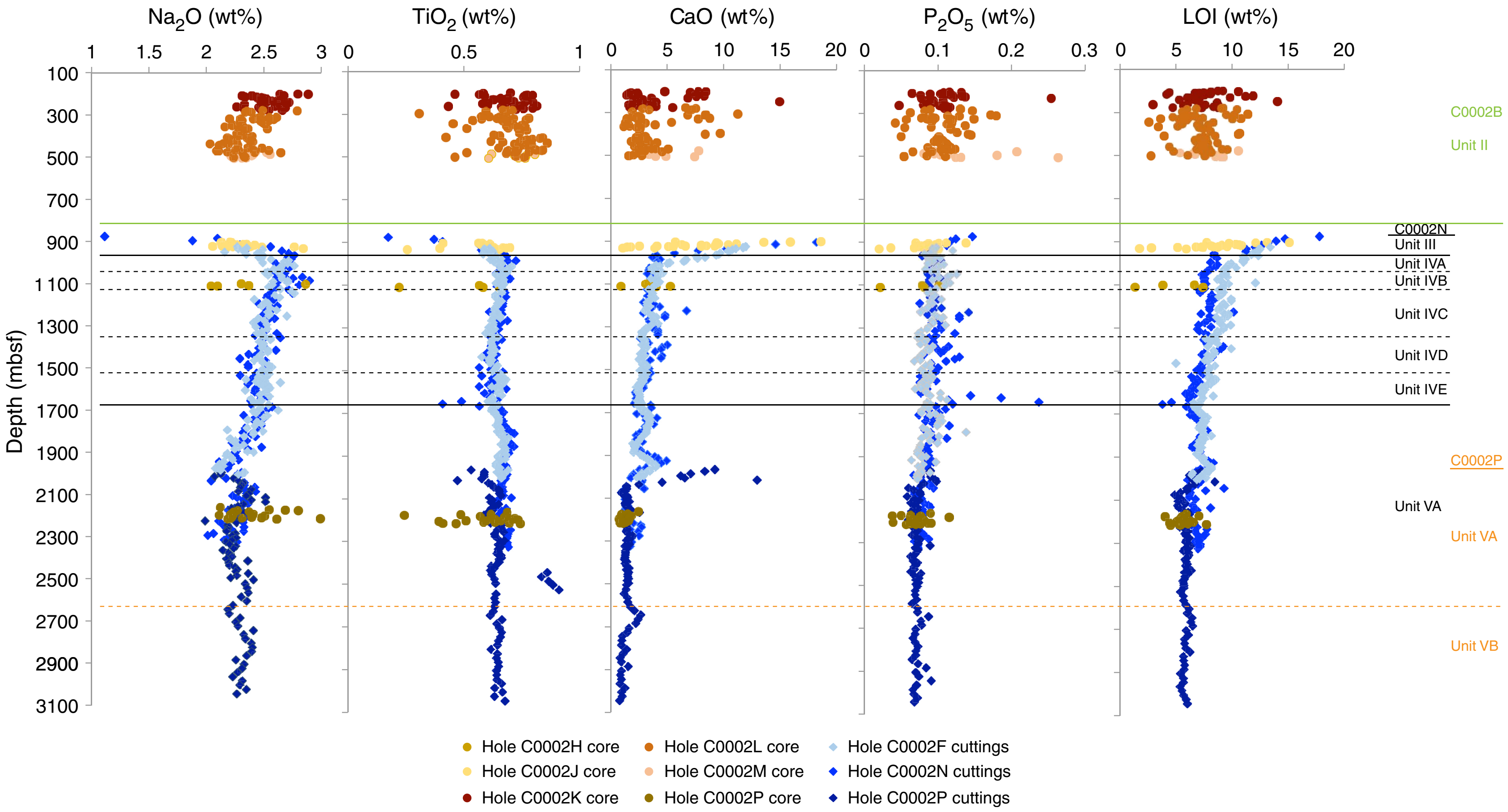

Figure F14. Percent sandstone vs. silty claystone vs. claystone, Holes C0002N and C0002P. See Table T5 for details of lithologic units and subunits.

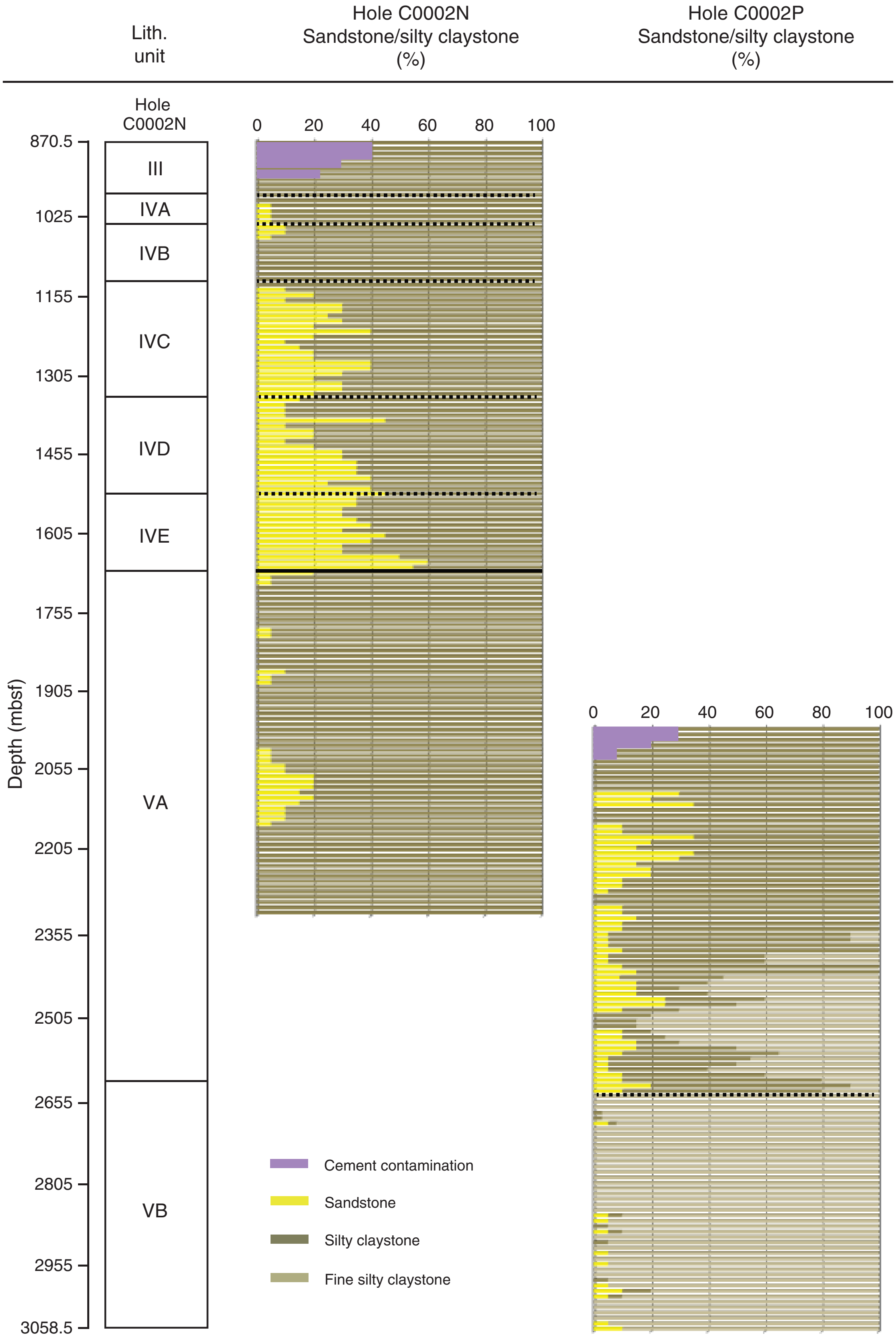

Figure F15. **A–F.** Dominant lithologies in lithologic Unit III and Subunits IVA–IVE, Holes C0002N and C0002P.

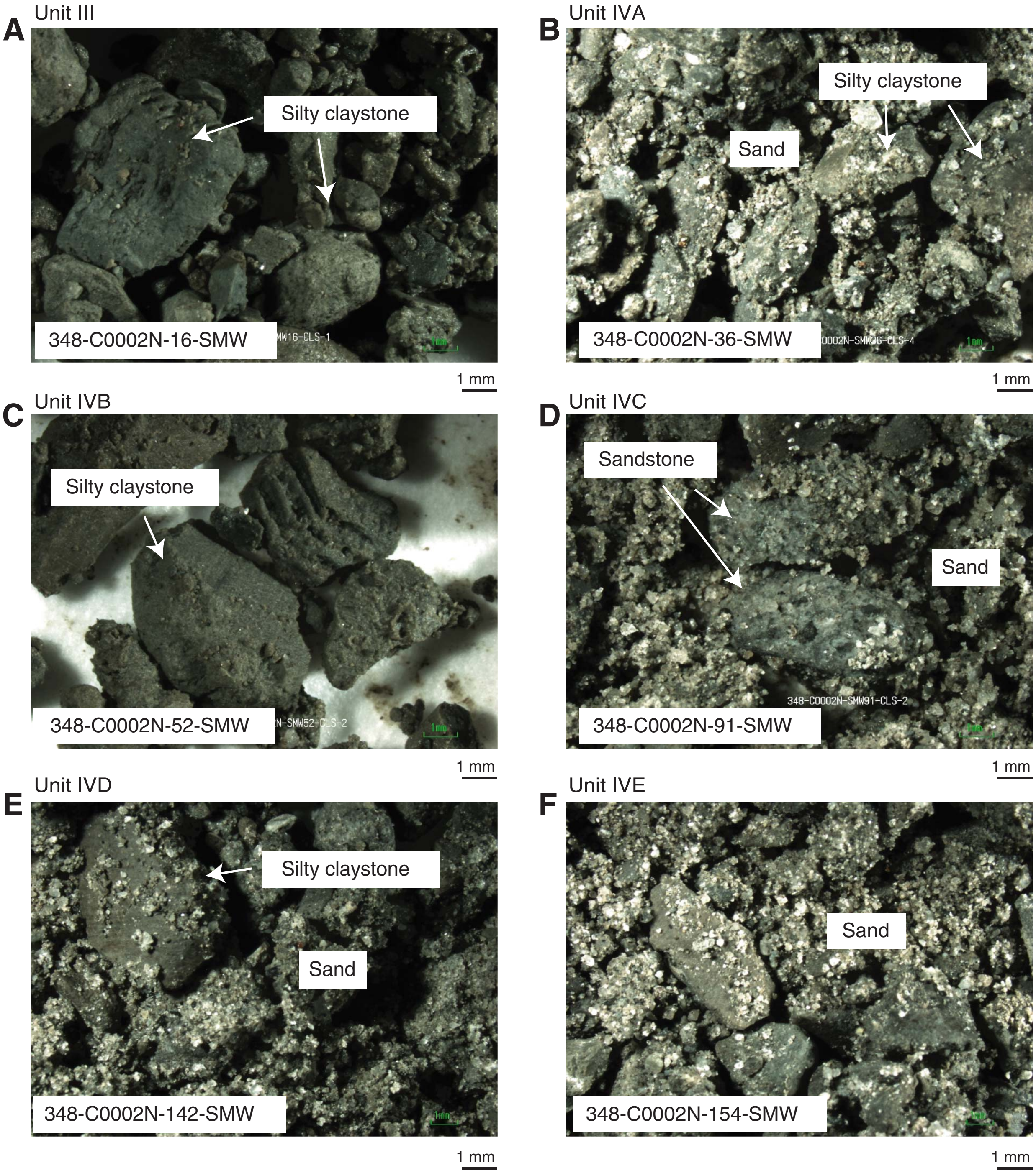

Figure F16. **A–F.** Dominant lithologies in lithologic Subunits VA and VB, Holes C0002N and C0002P.

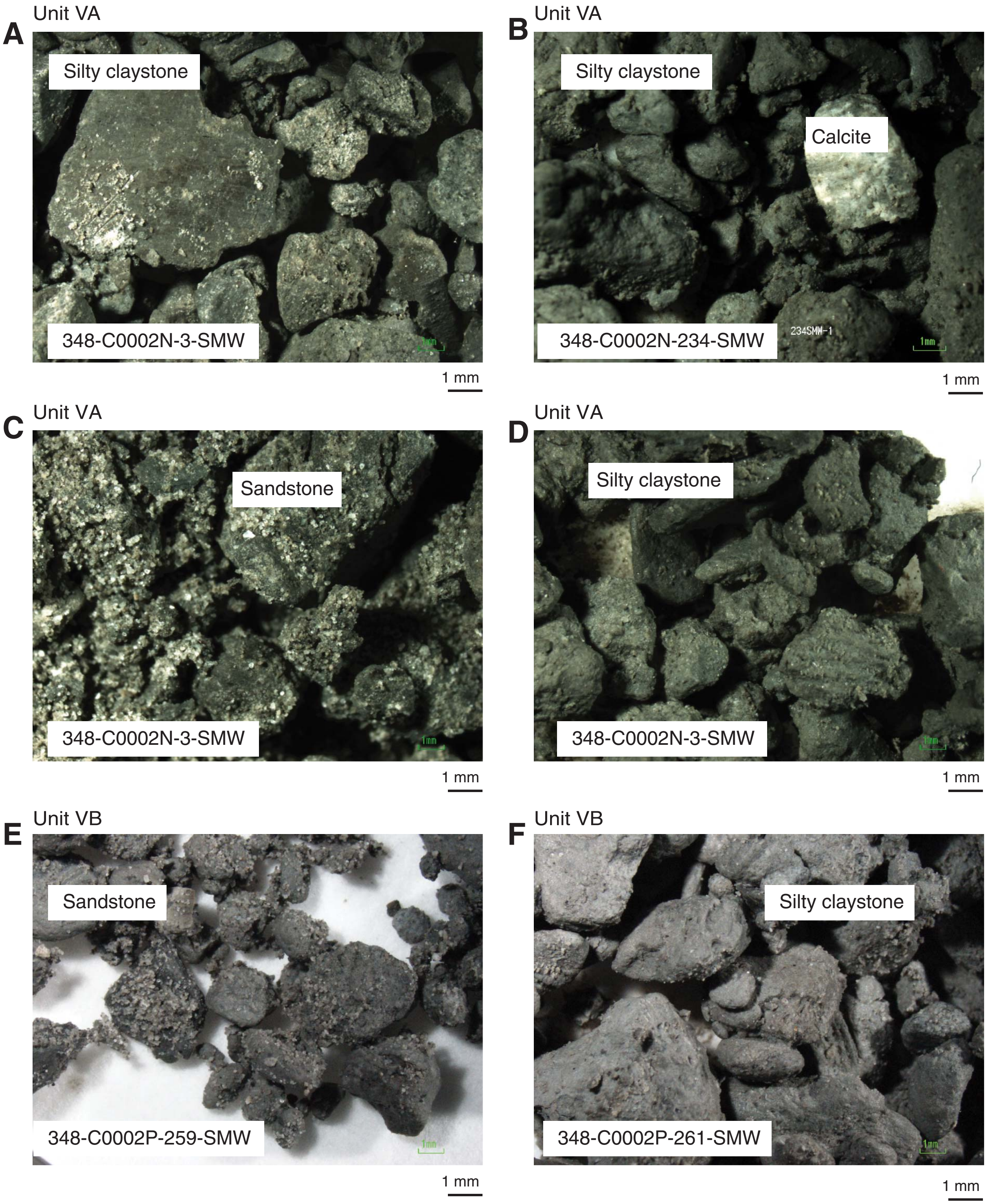

Figure F17. Microscopic cuttings characterization of lithologic components for >63 µm sieved sand fraction. **A.** Hole C0002N. (Continued on next page.)

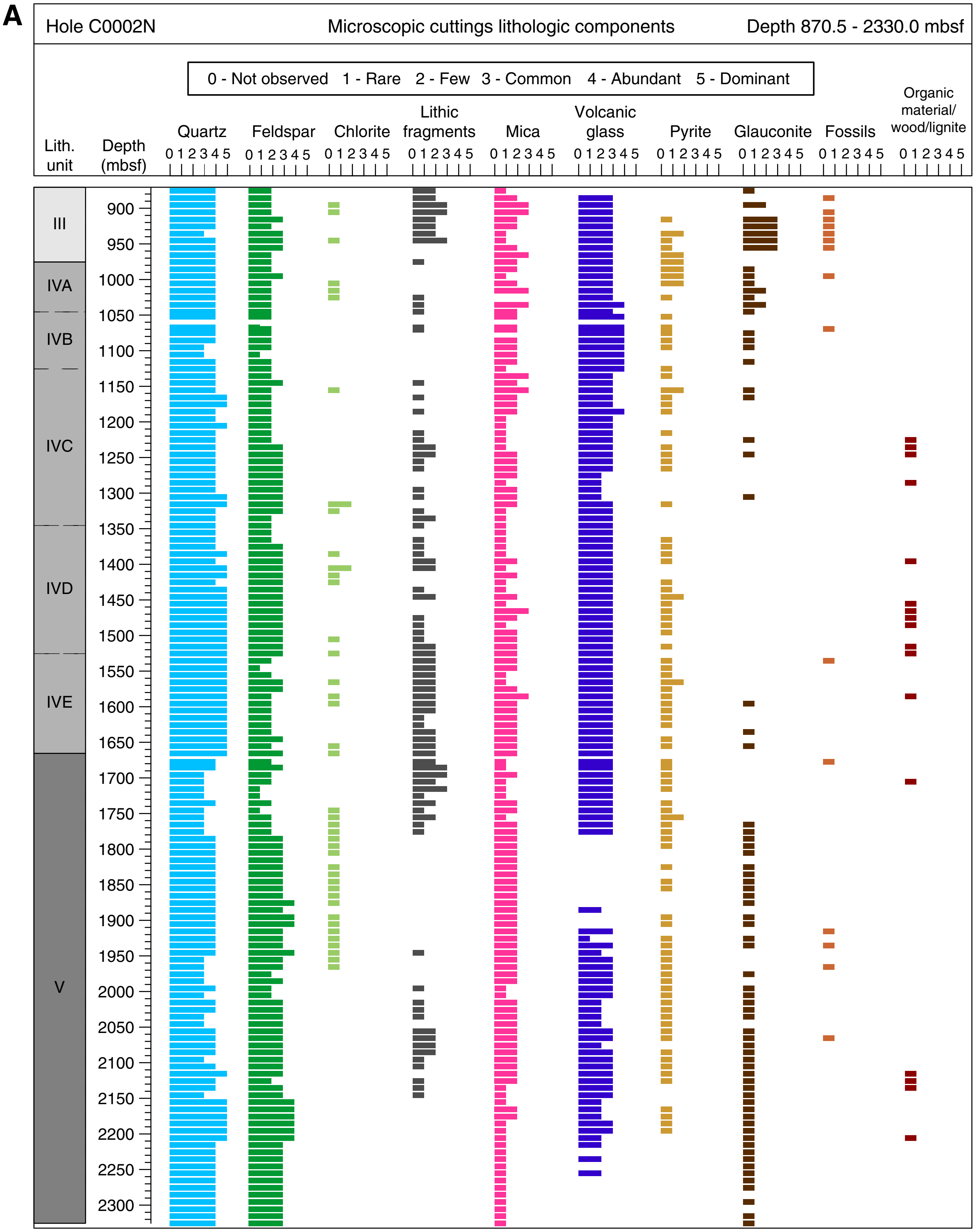

Figure F17 (continued). B. Hole C0002P.

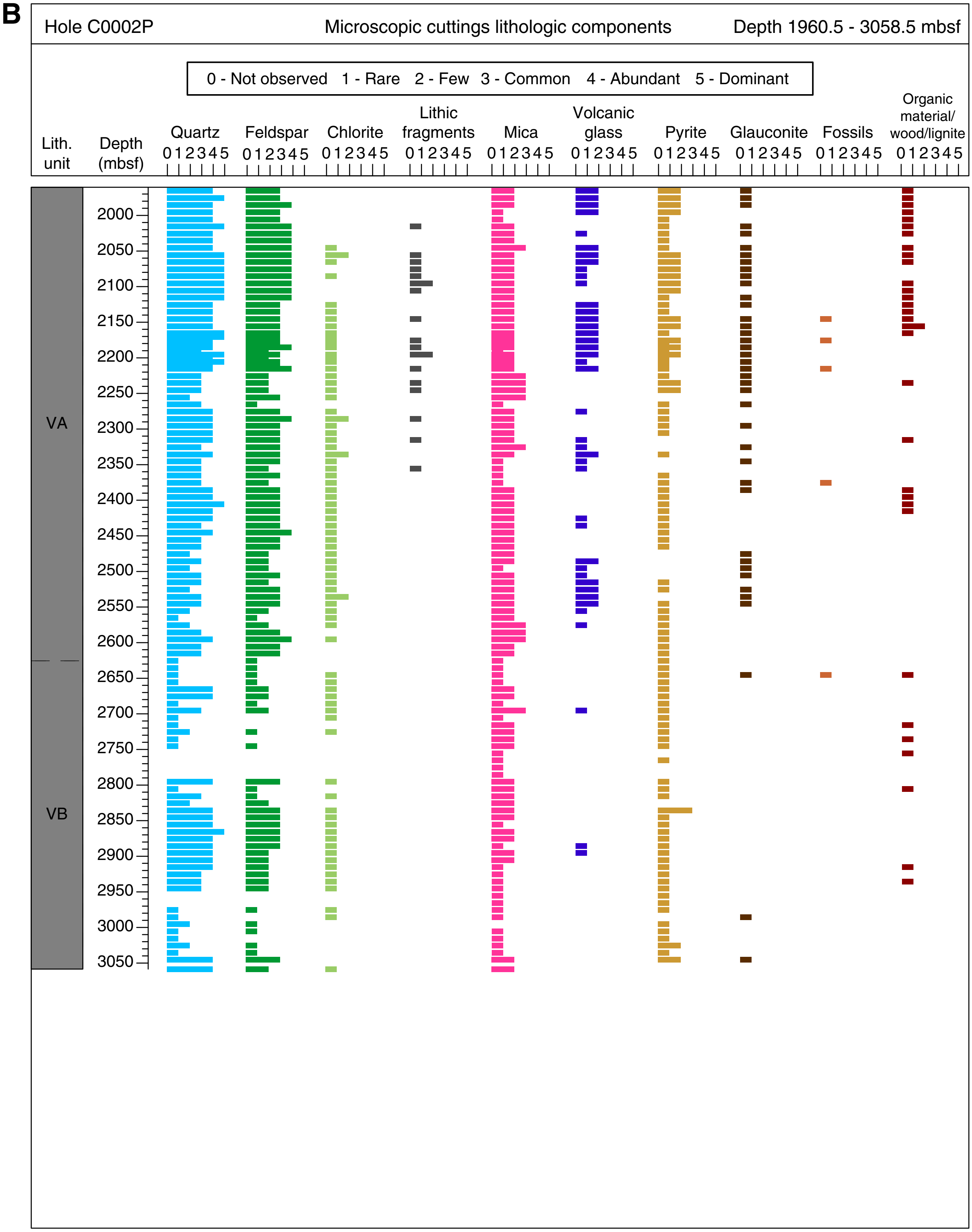

Figure F18. Smear slide mineralogy in cuttings samples from Hole C0002N (plane-polarized light). **A.** Representative chlorite. **B.** Altered volcanics. **C.** Pyrite. **D.** Volcanic glass. **E.** Lithic fragment. **F.** Glauconite.

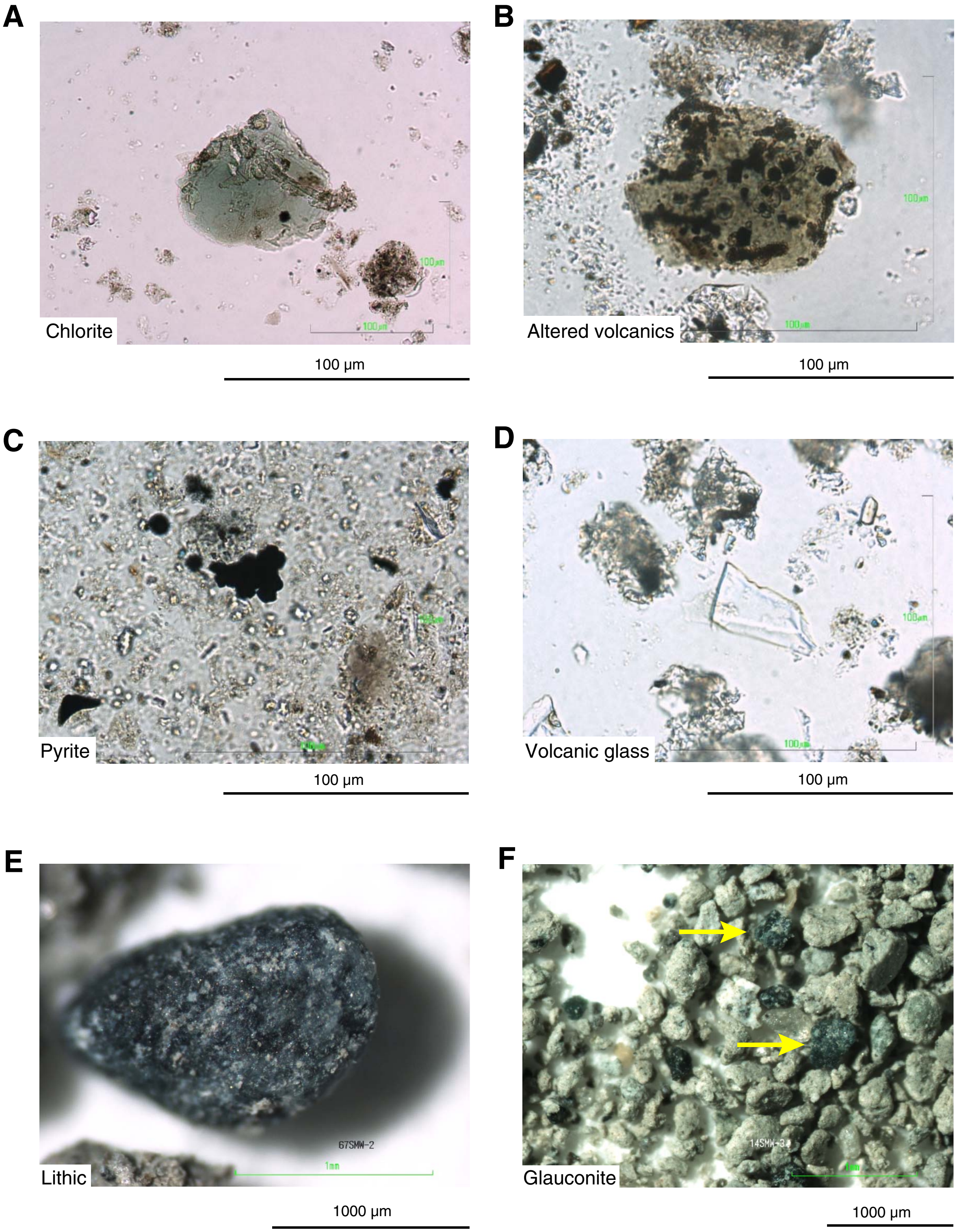

Figure F19. Smear slide mineralogy in cuttings samples from Hole C0002P. **A.** Glauconite (Sample 348-C0002P-SMW-181-SS_1; plane-polarized light [PPL]). **B.** Microlitic glass (Sample SMW-196; SS2_3; PPL). **C.** Zircon (Sample SMW-196; SS2_5; cross-polarized light [XPL]). **D.** Calcite (Sample SMW-273; SS_2; XPL). **E.** Volcanic glass (Sample SMW-111; SS_4; PPL). **F.** Chert (Sample SMW-141; SS_5; XPL).

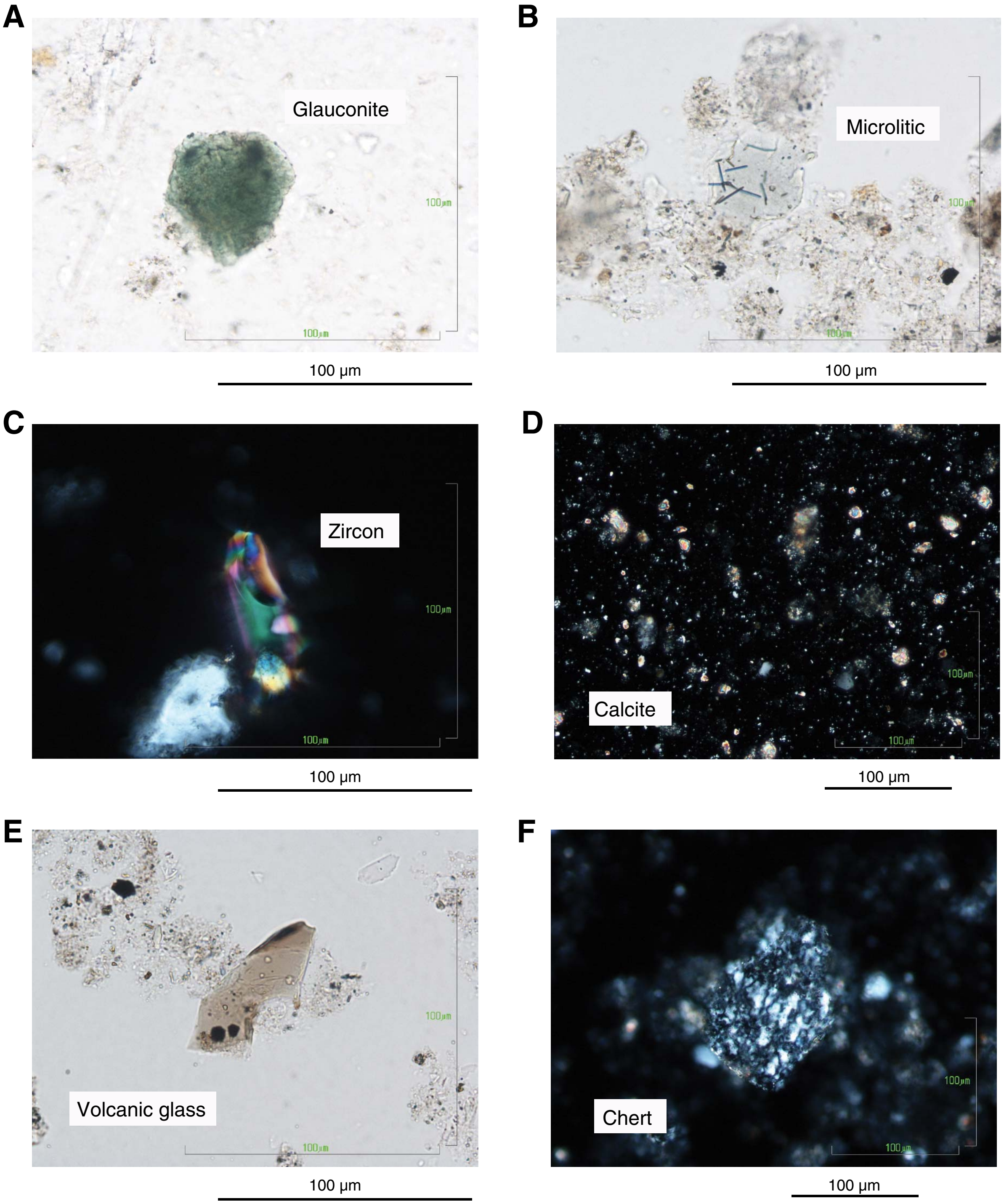

Figure F20. Lithologic columns, Hole C0002P. PAL = paleontology sample, WR = whole-round sample. **A.** Core 348-C0002P-1R. **B.** Core 2R. **C.** Core 3R. (Continued on next two pages.)

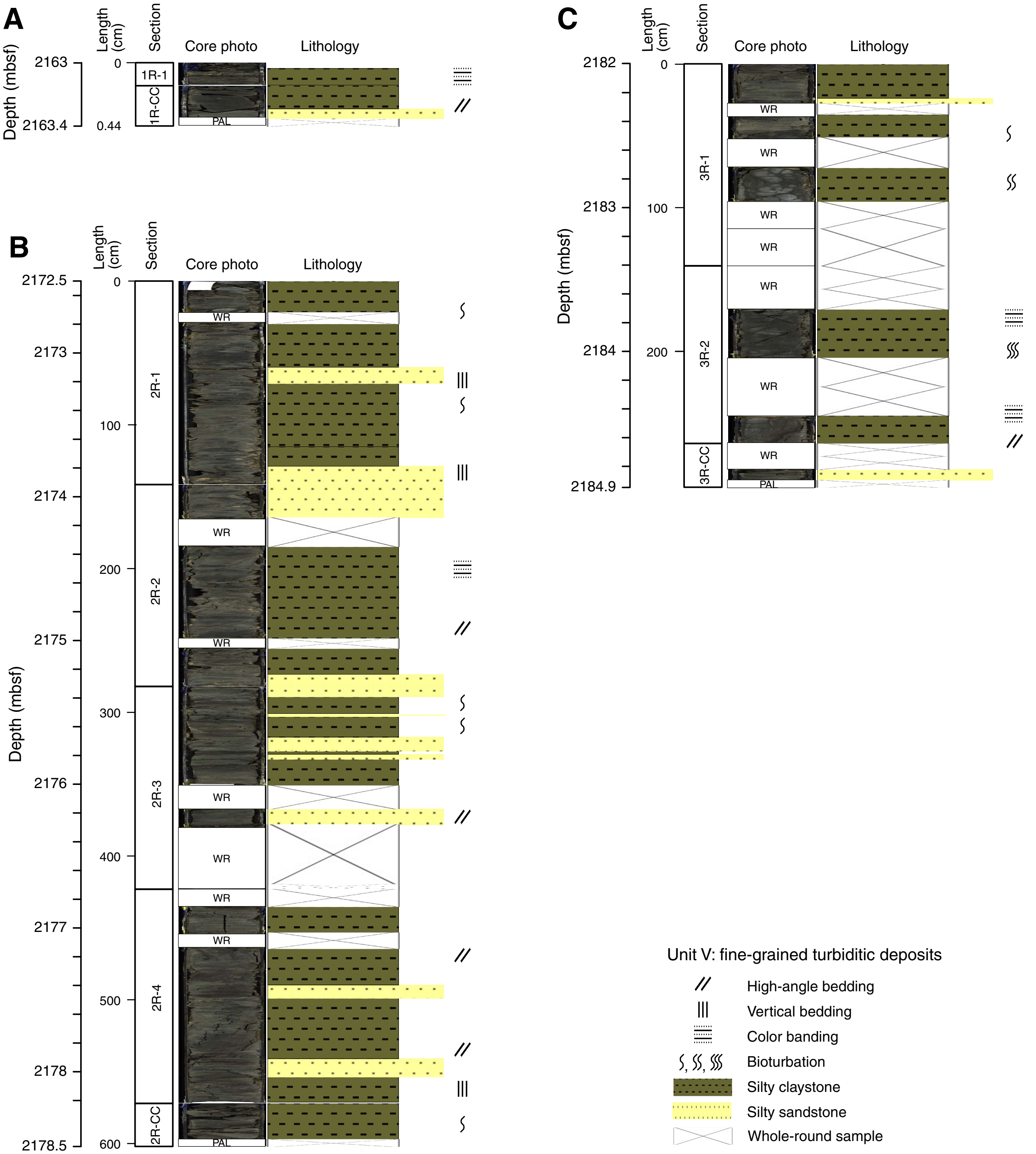

Figure F20 (continued). D. Core 348-C0002P-4R. E. Core 5R. (Continued on next page.)

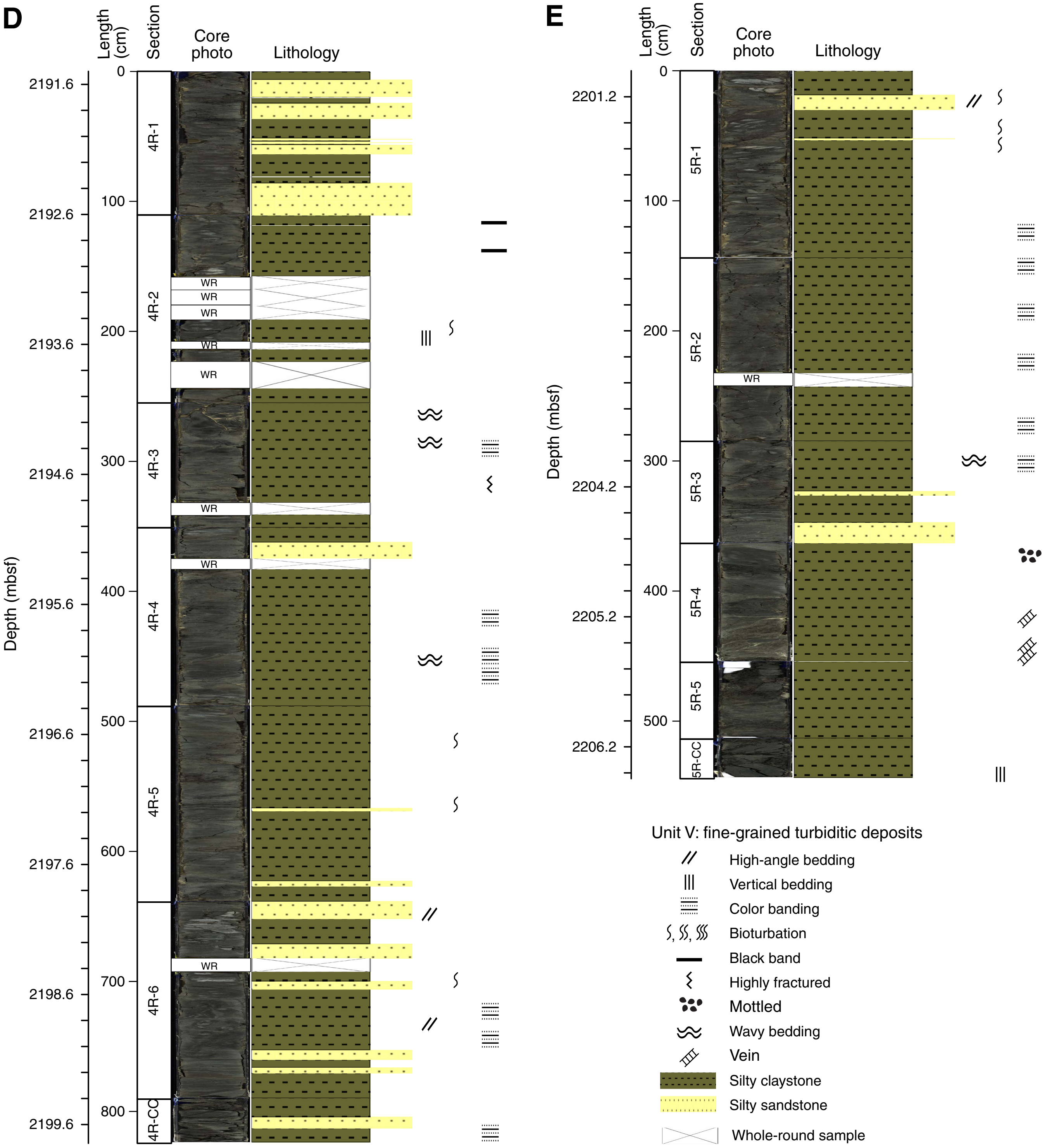

Figure F20 (continued). F. Core 348-C0002P-6R.

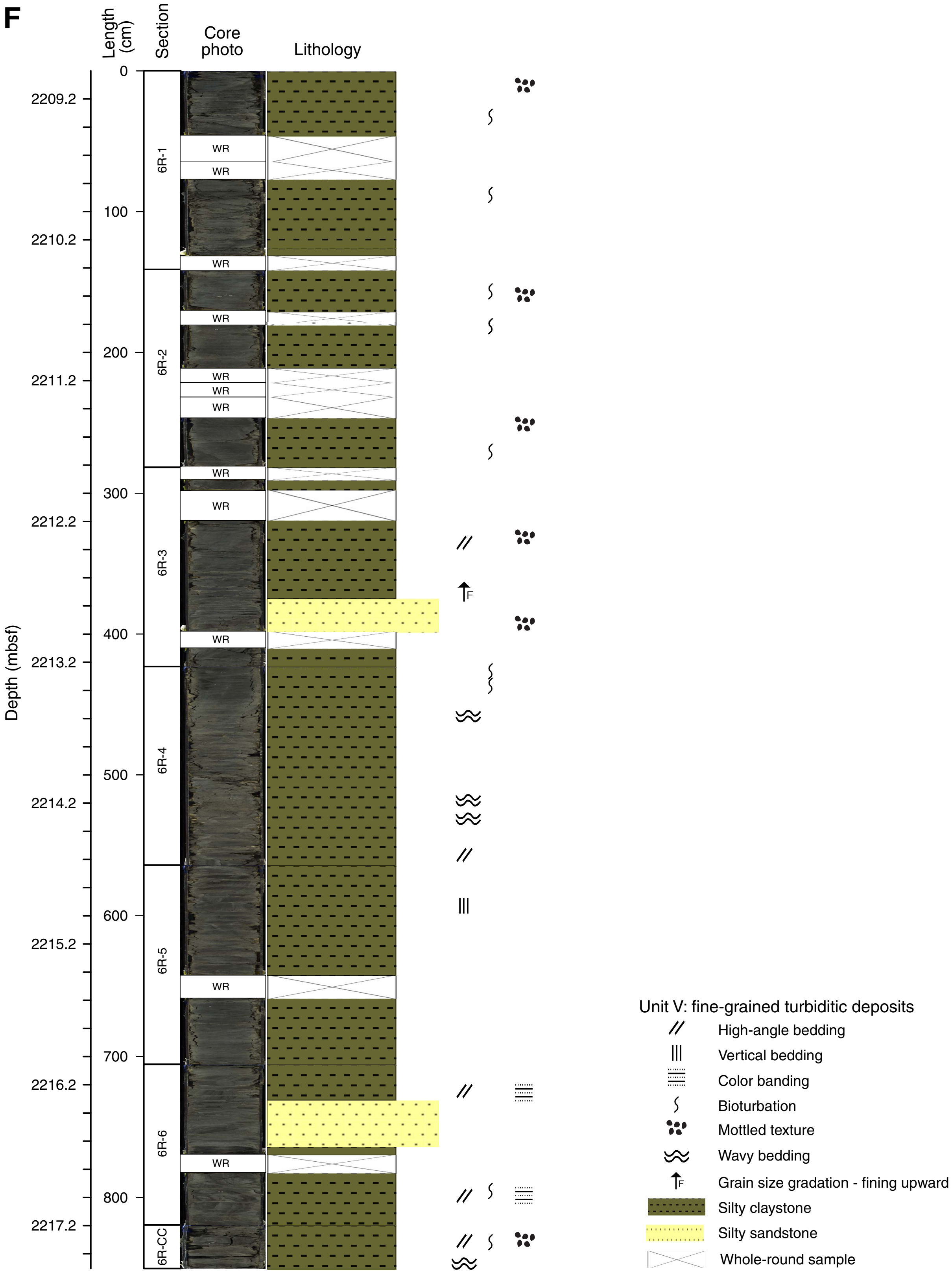

Figure F21. Lithologies in Hole C0002P cores. **A.** Silty claystone and very fine sandstone contact; sandstone shows deformation bands. **B.** Wavy beds of laminated silty claystone and sandstone; sandstone lens observed within silty claystone. **C.** Grain size gradation; fine sandstone grading into silty claystone. **D.** Rotated drilling biscuits of laminated silty claystone and organic matter–rich bands, showing very steep bedding. (Continued on next page.)

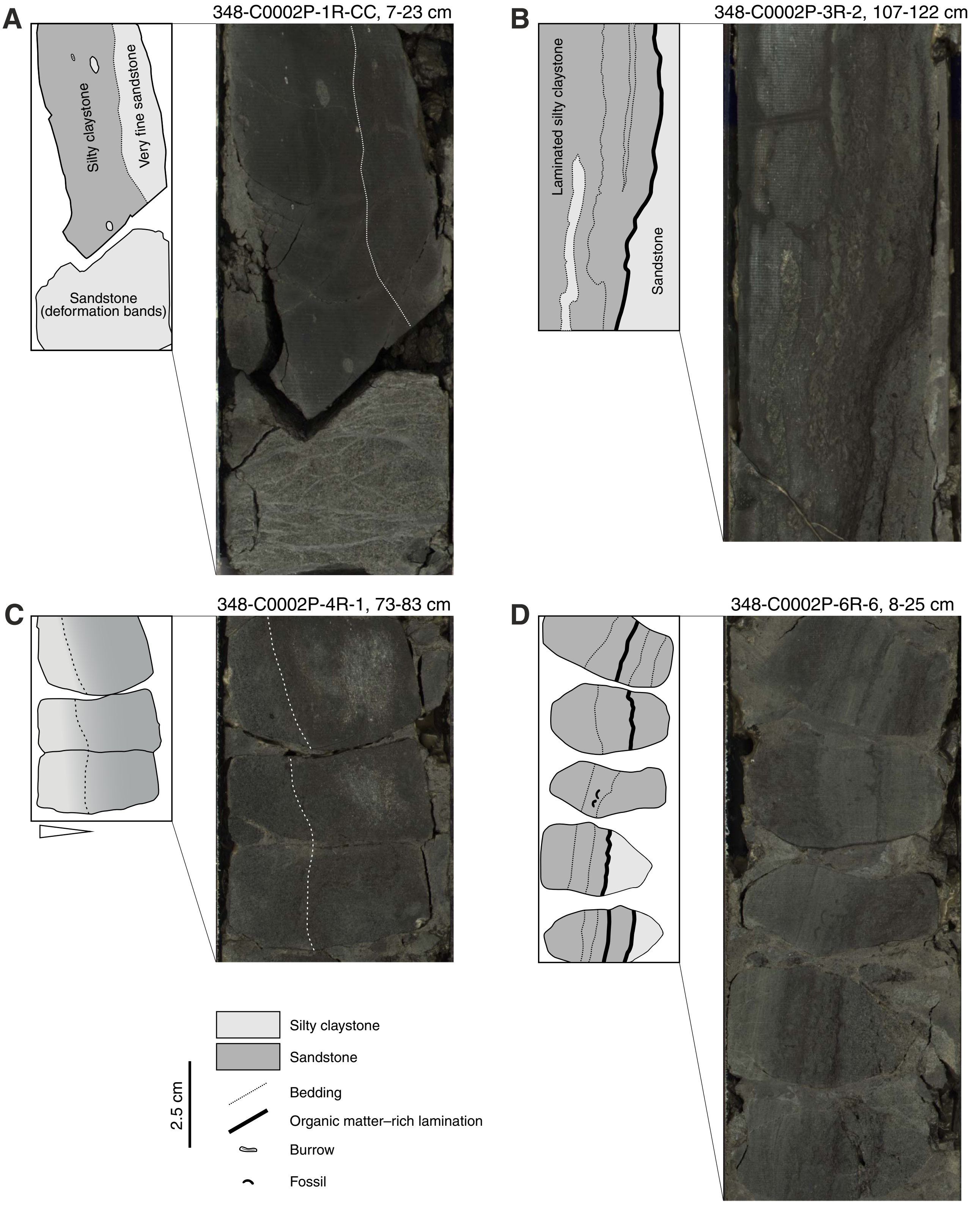

Figure F21 (continued). **E.** Mottled texture in silty claystone and sharp contact with sandstone. **F.** Fining upward turbiditic sequence. **G.** Steep and faulted bedding. **H.** Sandstone clast in silty claystone. **I.** Fine silty claystone with bioturbation (worm tubes?). **J.** Bioturbation in silty claystone (worm tubes?). **K.** Organic matter–rich bed.

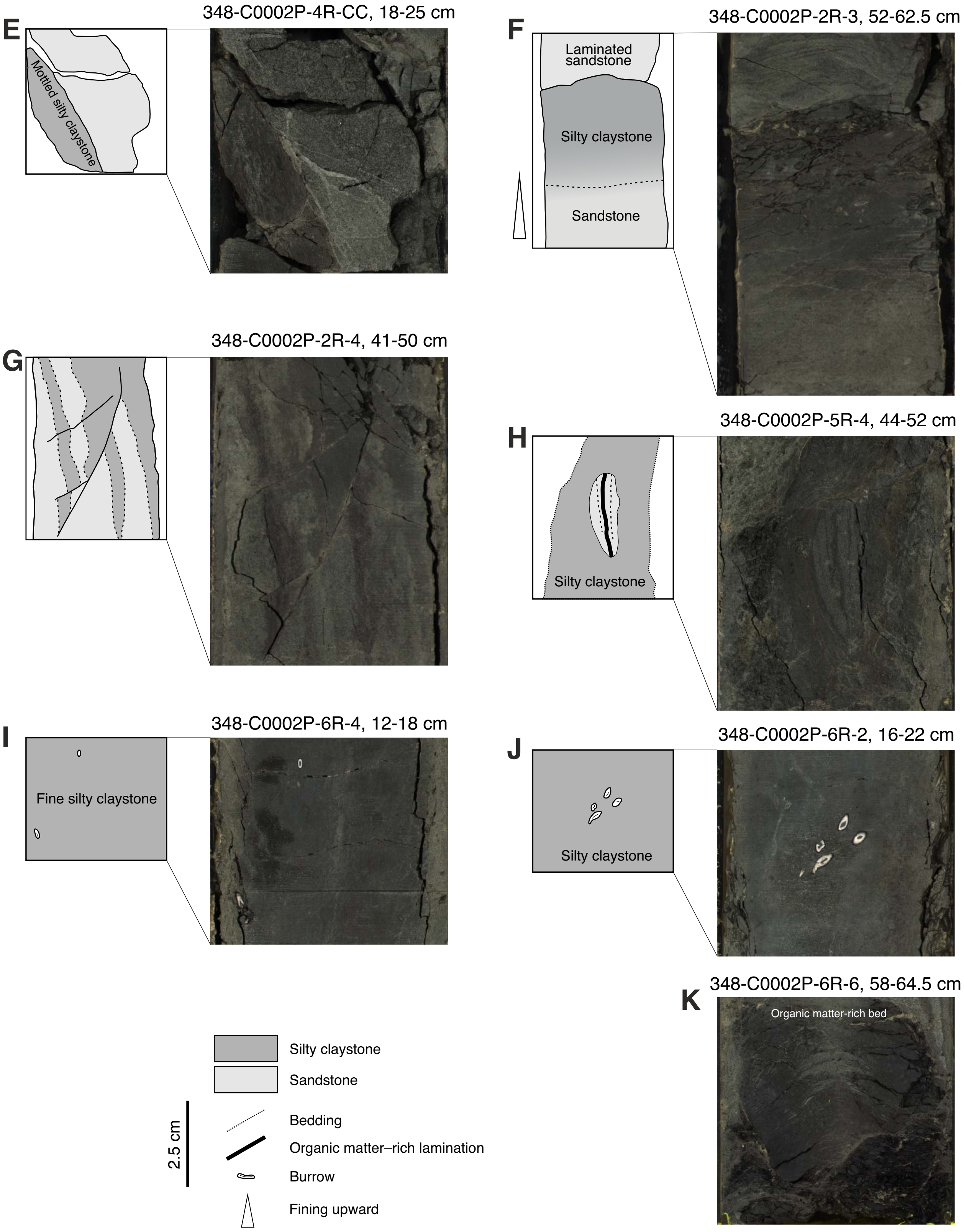

Figure F22. Smear slide mineral abundance trends, Hole C0002P.

Figure F23. Smear slide mineralogy, Hole C0002P. **A.** Zircon (Sample 348-C0002P-1R-1, 10.5 cm; SS_2; cross-polarized light [XPL]). **B.** Glauconite (Sample 2R-1, 17.5 cm; SS_2; plane-polarized light [PPL]). **C.** Volcanic glass (Sample 2R-1, 17.5 cm; SS_8; PPL). **D.** Tourmaline (Sample 5R-2, 127 cm; SS_4; PPL). **E.** Calcite (Sample 5R-4, 58 cm; SS_4; XPL). **F.** Microlitic glass (Sample 6R-1, 53 cm; SS_2; PPL).

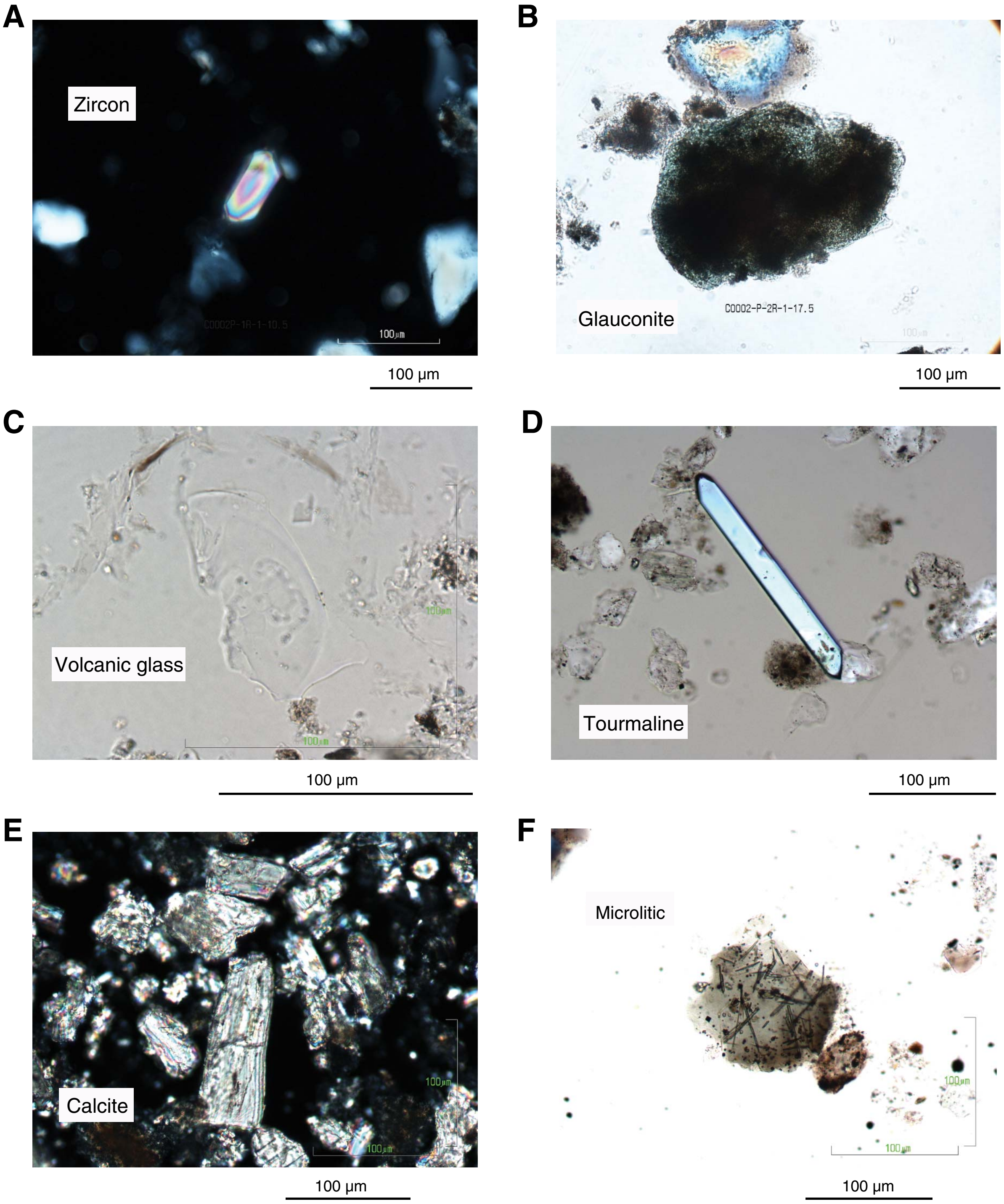

Figure F24. Mineralogical bulk compositions determined by X-ray diffraction analysis of core and cuttings samples, Hole C0002P. Note that the cutting samples are relatively homogeneous in composition across depth because of mixing across the drilled interval.

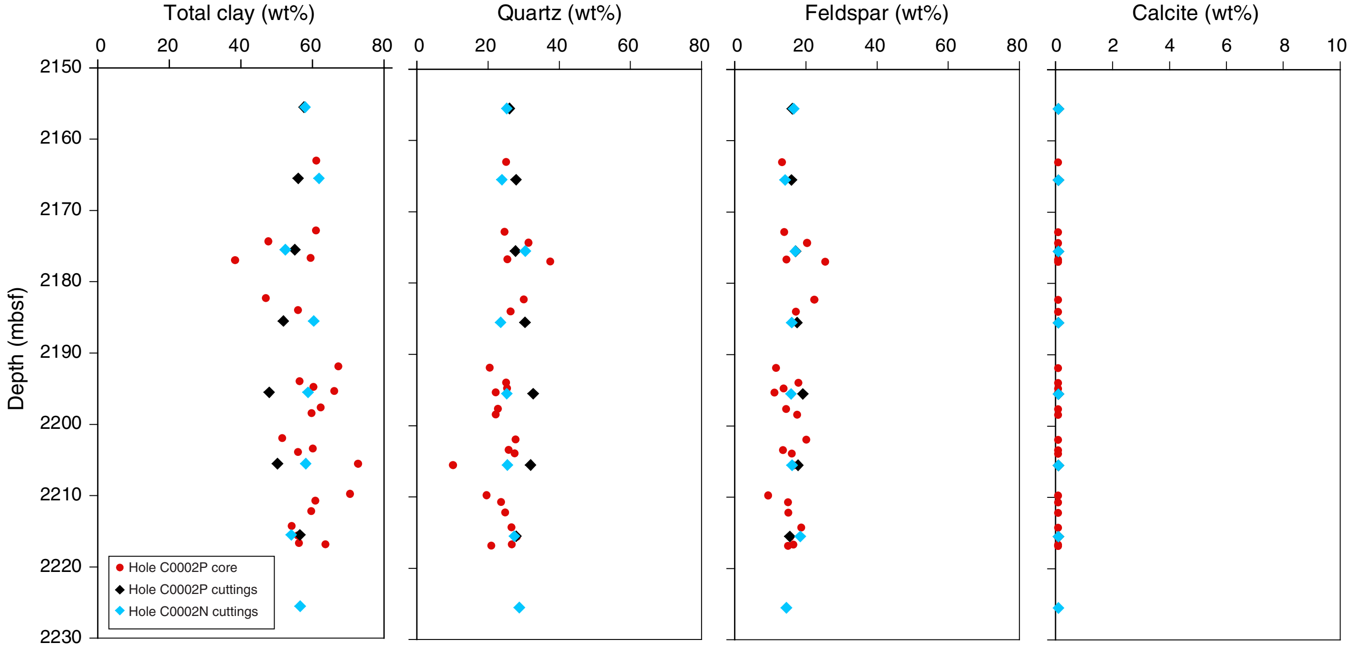

Figure F25. Bulk chemical compositions determined by X-ray fluorescence analyses of core and cuttings samples, Hole C0002P. LOI = loss on ignition.

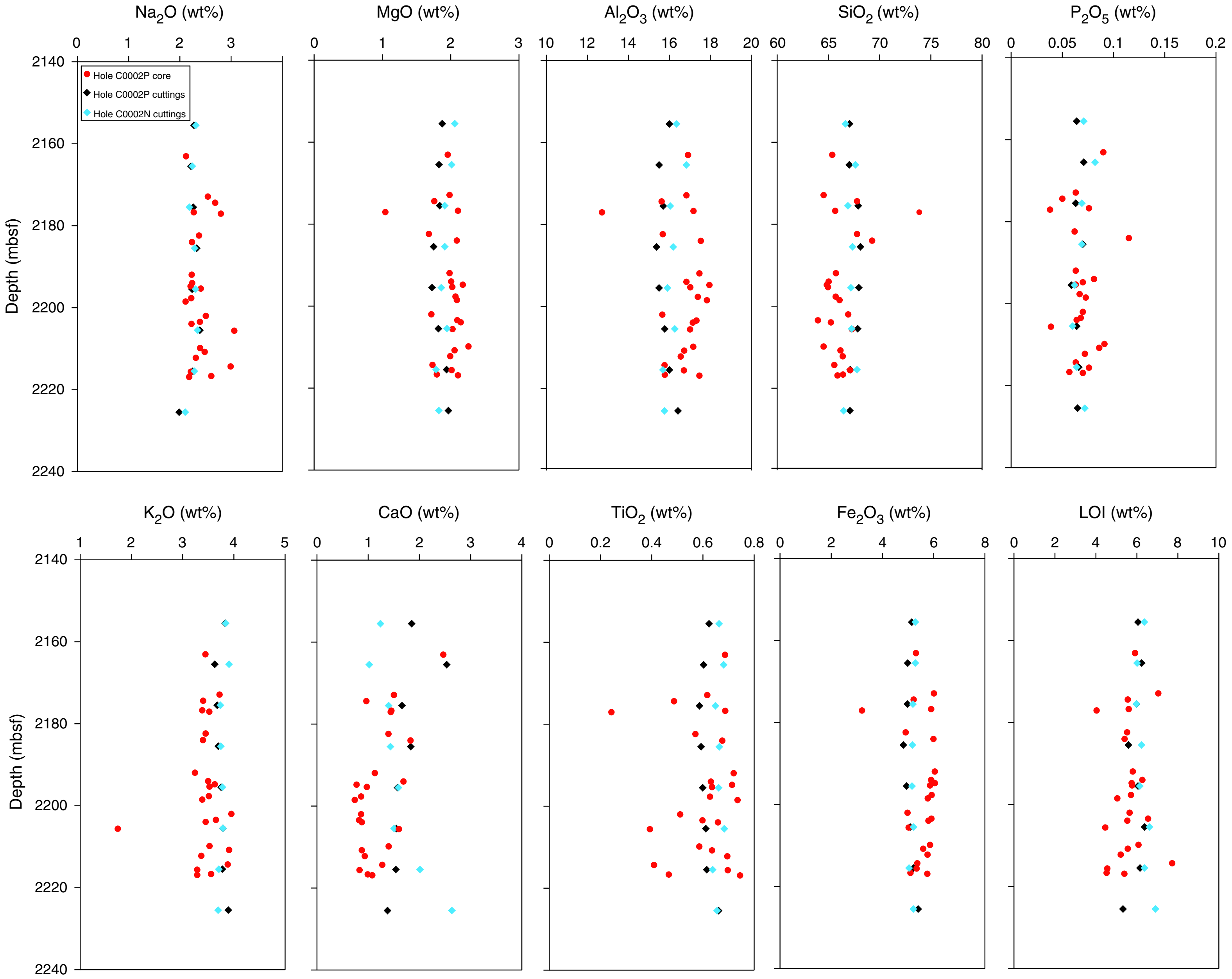

Figure F26. X-ray fluorescence core scanner image of Section 348-C0002P-5R-4. ms % = mass percent.

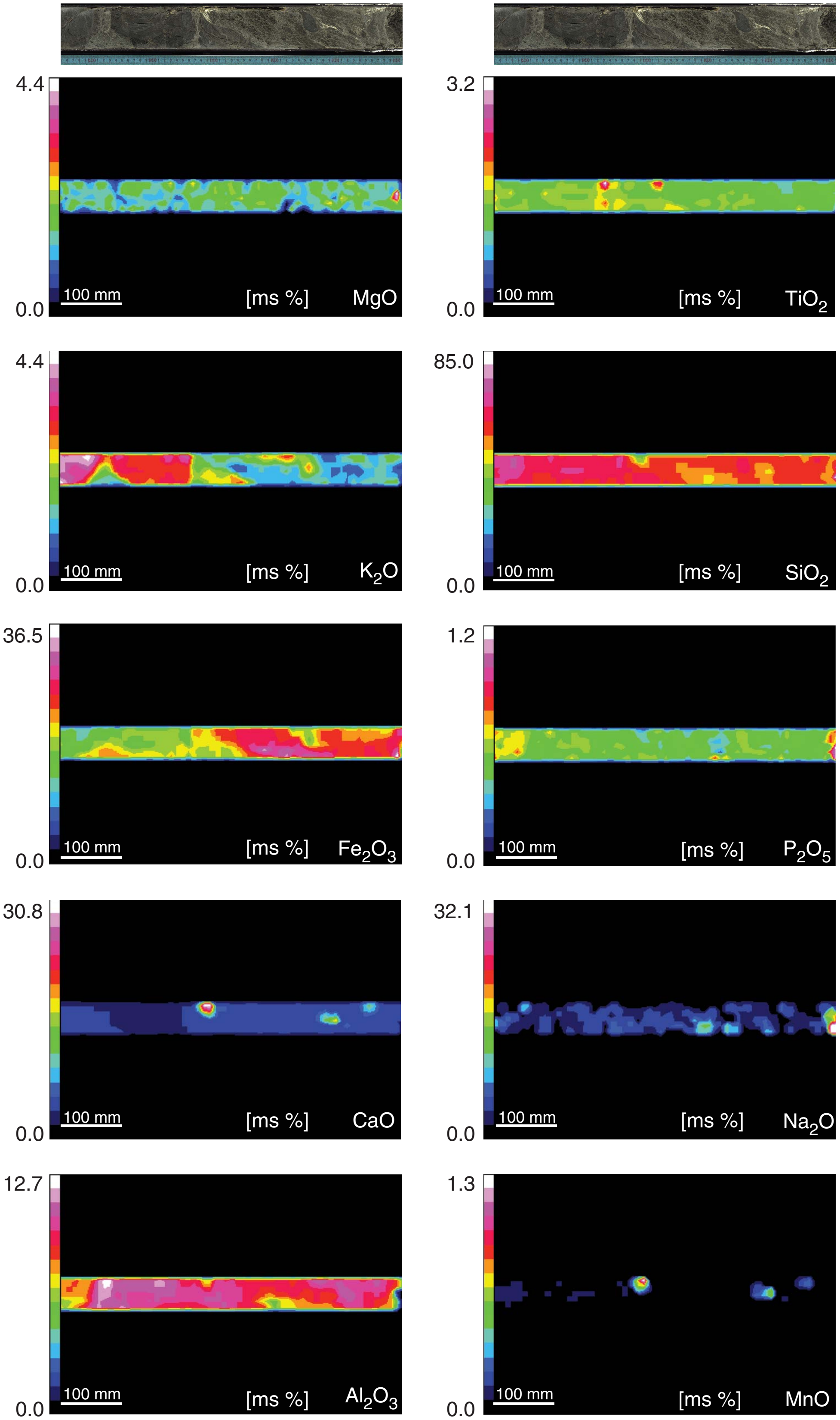

Figure F27. Comparison of lithologic features observed in core and cuttings and mineralogy (smear slides) of selected areas. (Continued on next page.)

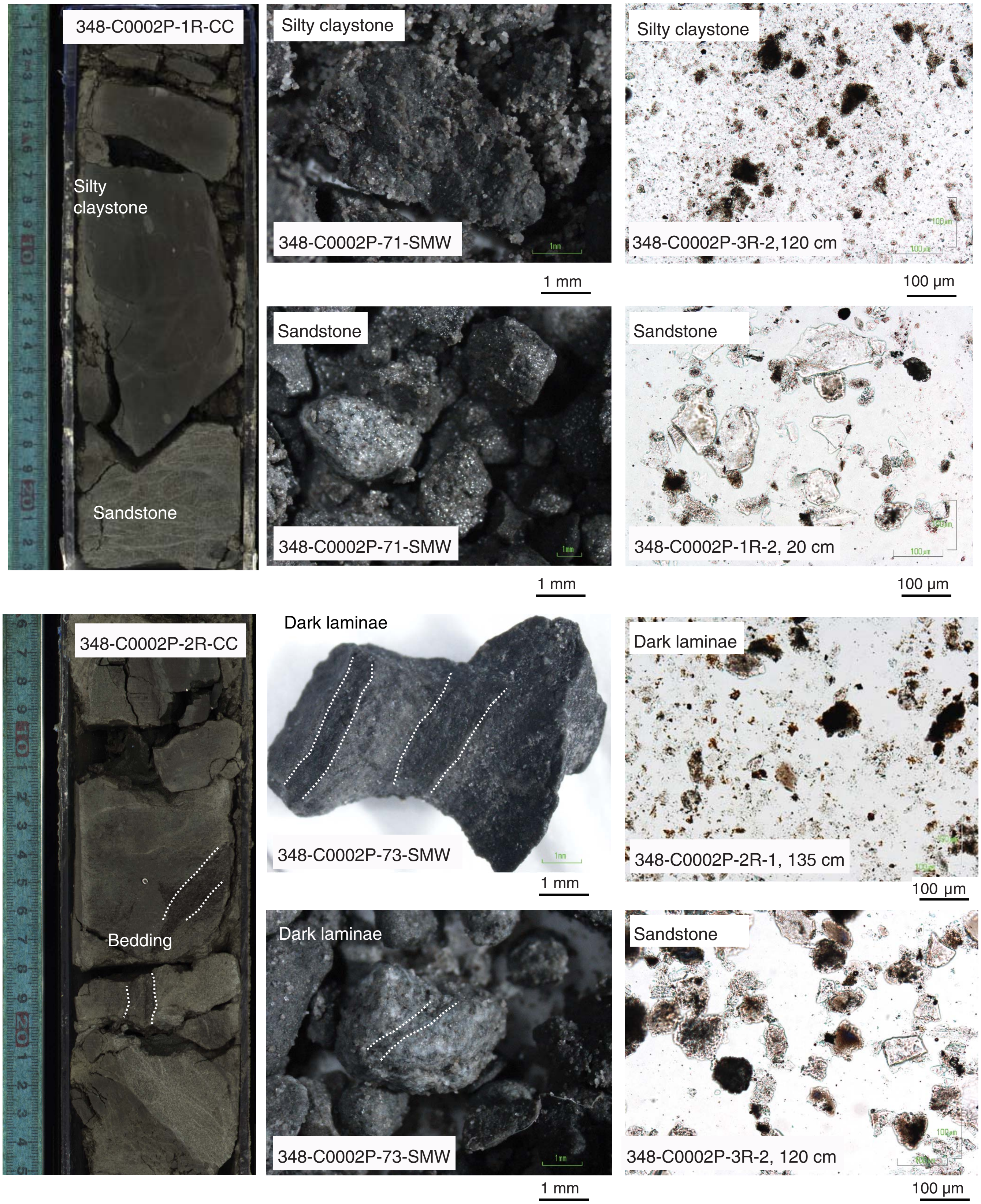

Figure F27 (continued).

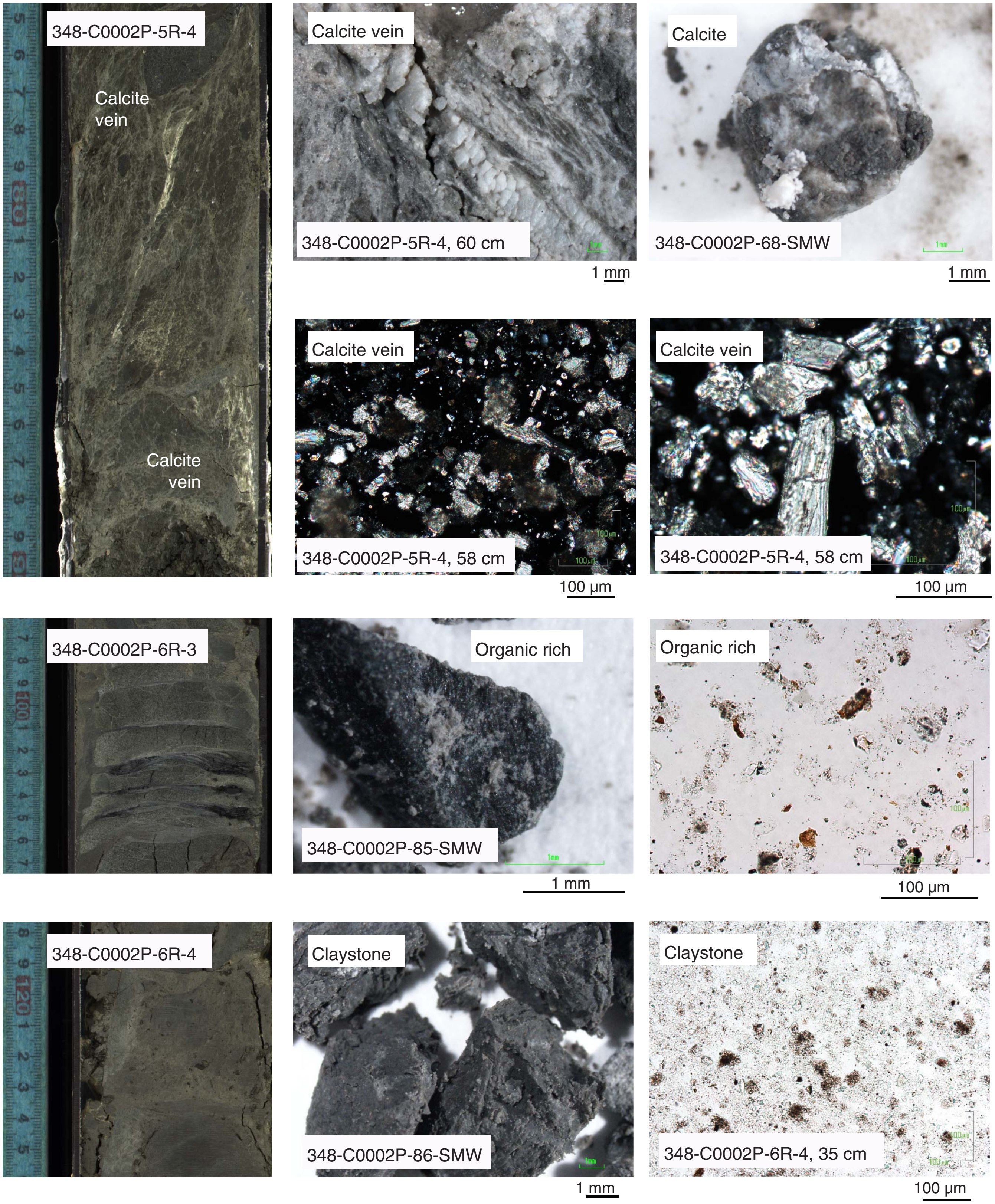

Figure F28. Quantity of retrieved intact cuttings (>4 mm) examined after hard washing of the samples for structural description, Holes C0002N and C0002P. The maximum number of intact cuttings counted was 100. Drill bit depth during waiting on weather (WOW) or drilling operations, which caused additional time between drilling and retrieval of cuttings, is indicated.

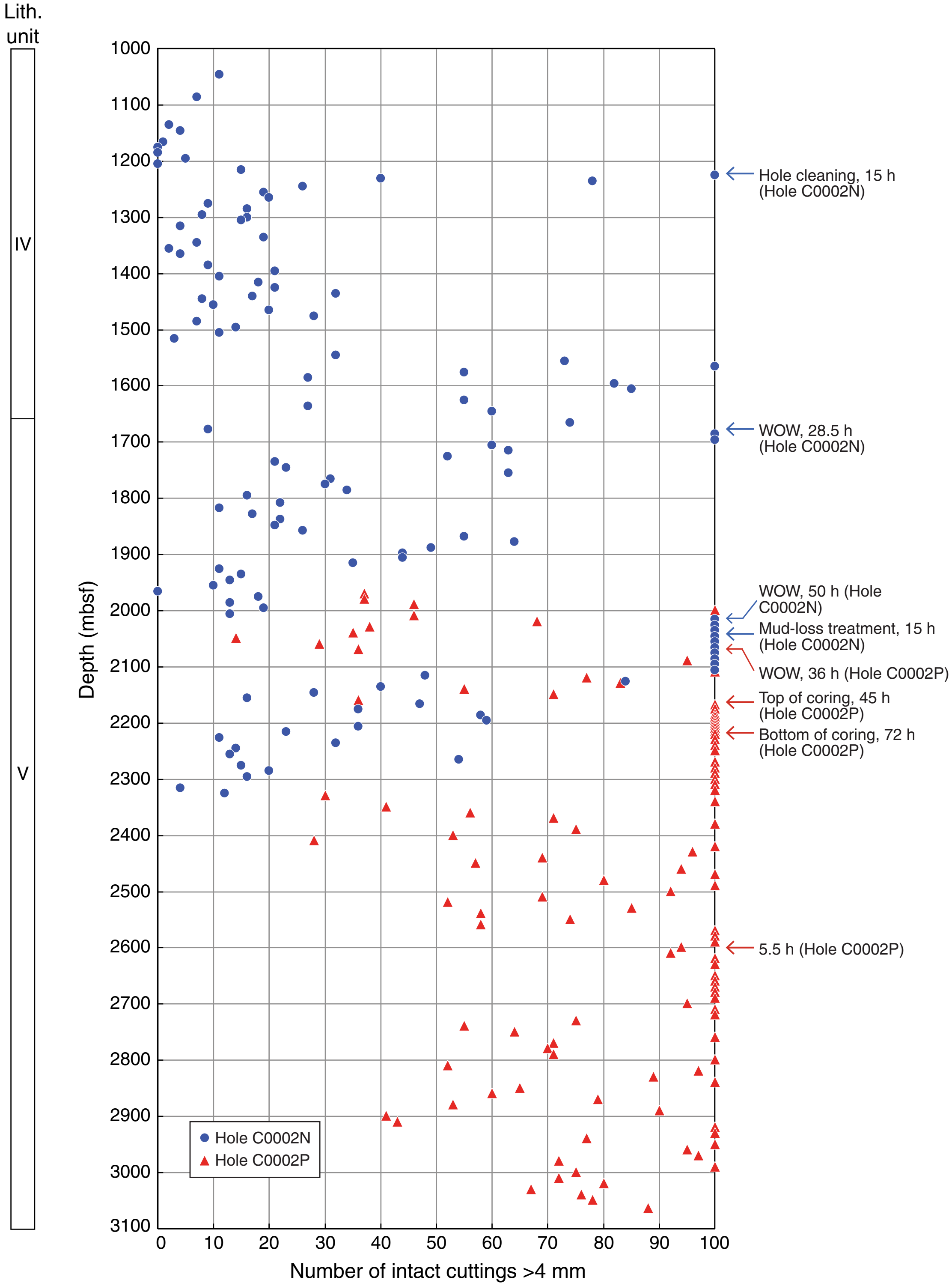

Figure F29. A, B. Depth distribution of percentage of deformation structures in intact cutting samples, Holes C0002N and C0002P. For each depth, this percentage is obtained by dividing the number of cuttings that show any deformation structures by the number of investigated cuttings. In turn, the relative contribution of slickenlines, veins, deformation bands, scaly fabric, and minor faults is represented as a percentage of the deformed cuttings along the bar that represents each sample. Dashed line is the mean value of percentage of deformation structures calculated from samples with >20 cuttings of retrieved intact cuttings (16% for Hole C0002N and 21% for Hole C0002P).

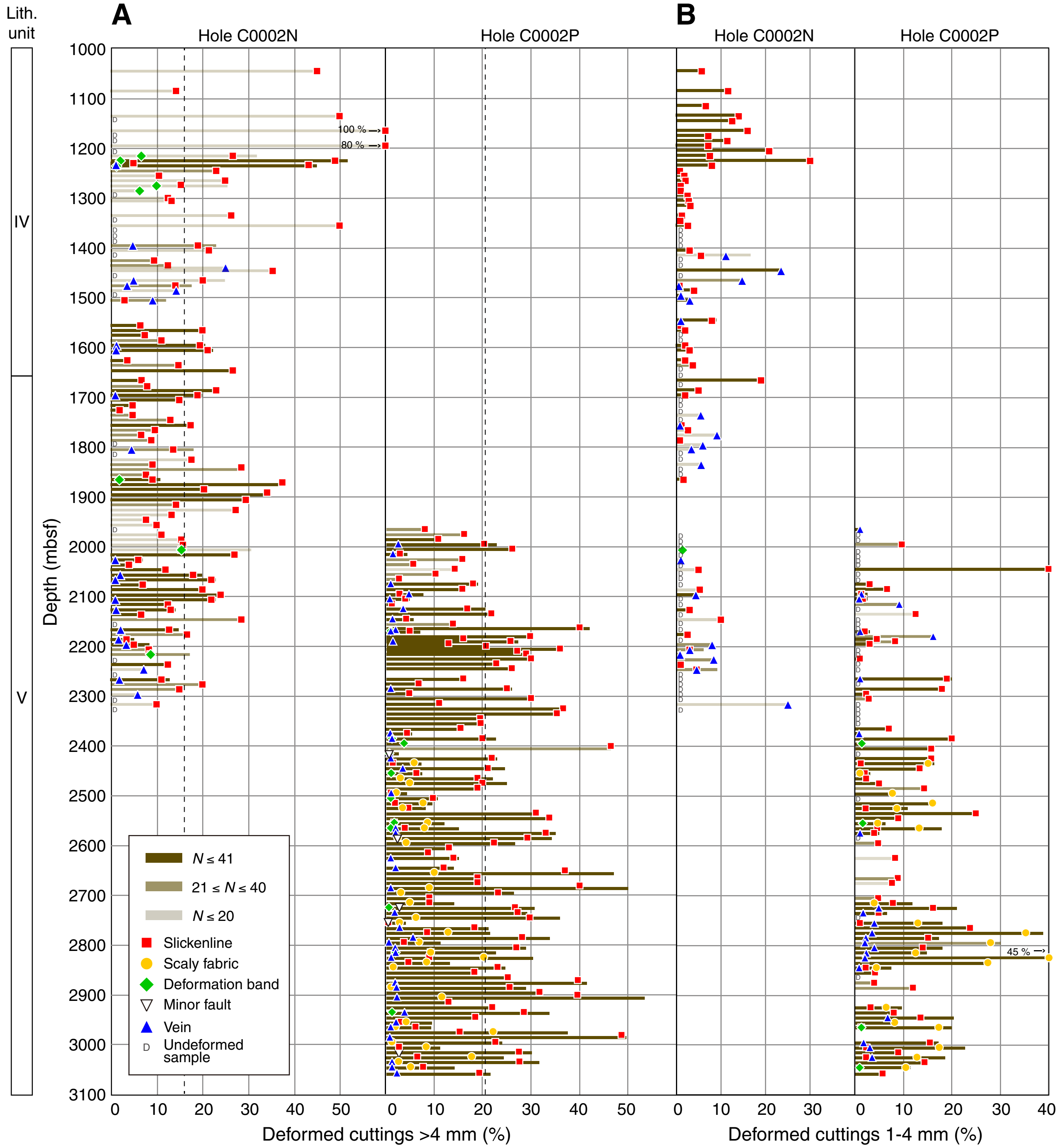

Figure F30. Characteristic examples of slickenlined surfaces in intact cuttings (>4 mm) formed by silty claystone. **A.** Sample 348-C0002N-083-SMW (1235.5 mbsf). **B.** Sample 175-SMW (1665.5 mbsf). **C.** Sample 276-SMW (2095.5 mbsf). **D.** Sample 185-SMW (2570.5 mbsf). **E.** Photomicrograph of cross-section of slickenlined surface (thin section was made perpendicular to the slickenlined surface in the upper part of the image). Note the preferred alignment of clay minerals parallel to the slickenlined surface, constituting a 100 µm thick band (Sample 259-SMW; 2015.5 mbsf). **F.** Stepped slickenlined surface (Sample 160-SMW; 1595.5 mbsf).

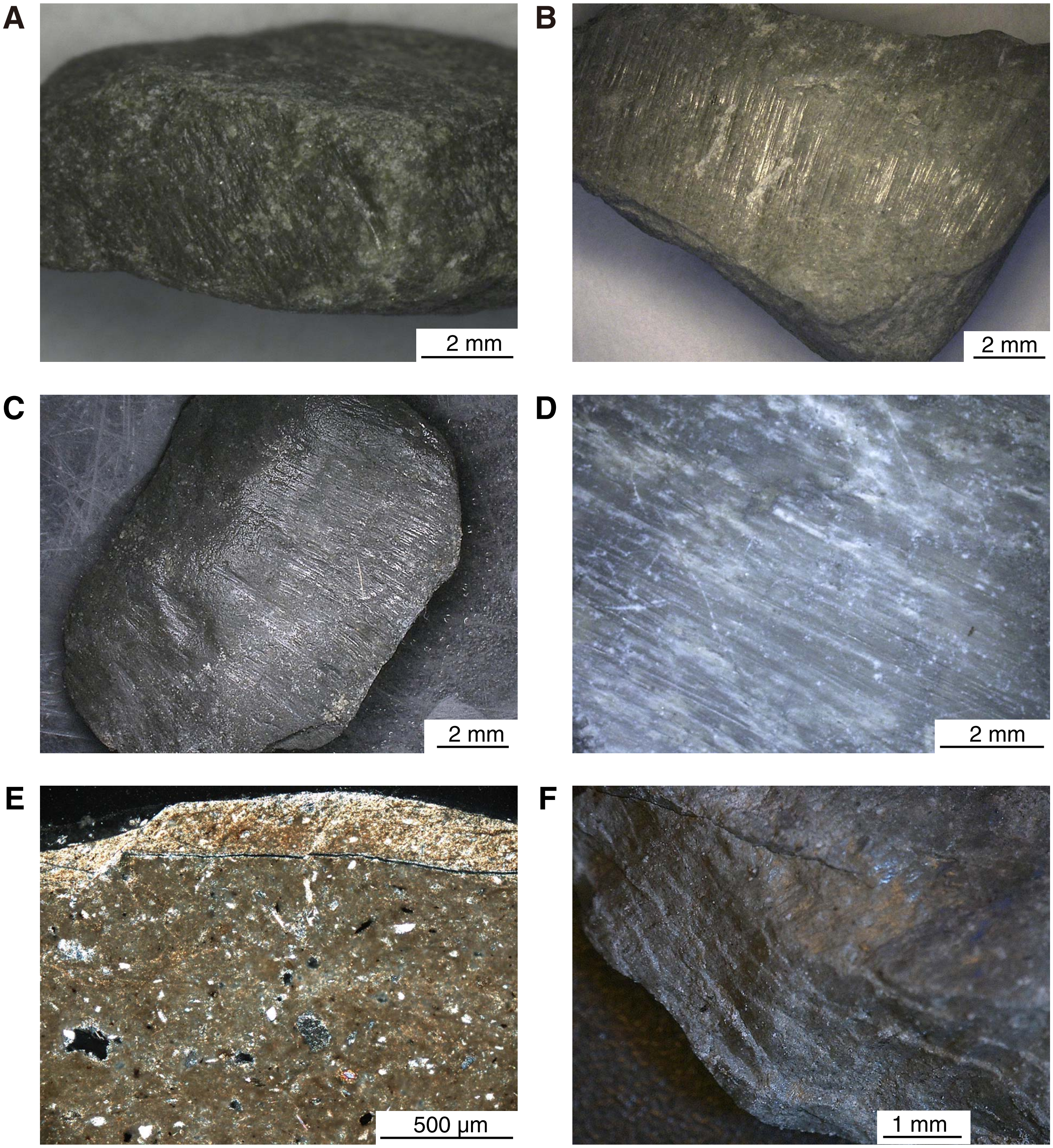

Figure F31. **A–C.** Characteristic examples of slickenlined surfaces in intact cuttings (>4 mm), formed by silty sandstone (Sample 348-C0002N-296-SMW; 2175.5 mbsf). B and C are enlargement of parts of the cutting reproduced in A. In C, note the very tiny stepped slickenlines. **D–F.** Cross-section of slickenlined surface in silty sandstone (thin section was made perpendicular to the slickenlined surface in the upper part of the photograph; Sample 304-SMW; 2215.5 mbsf). Note the staircase geometry of opaque layers in a 120 µm thick zone in the vicinity of the slickenline surface. E shows the undulose extinction of a feldspar grain near the slickenline surface (enlargement of D). F shows a broken quartz grain dextrally displaced by secondary fractures associated with shear along the slickenlined surface.

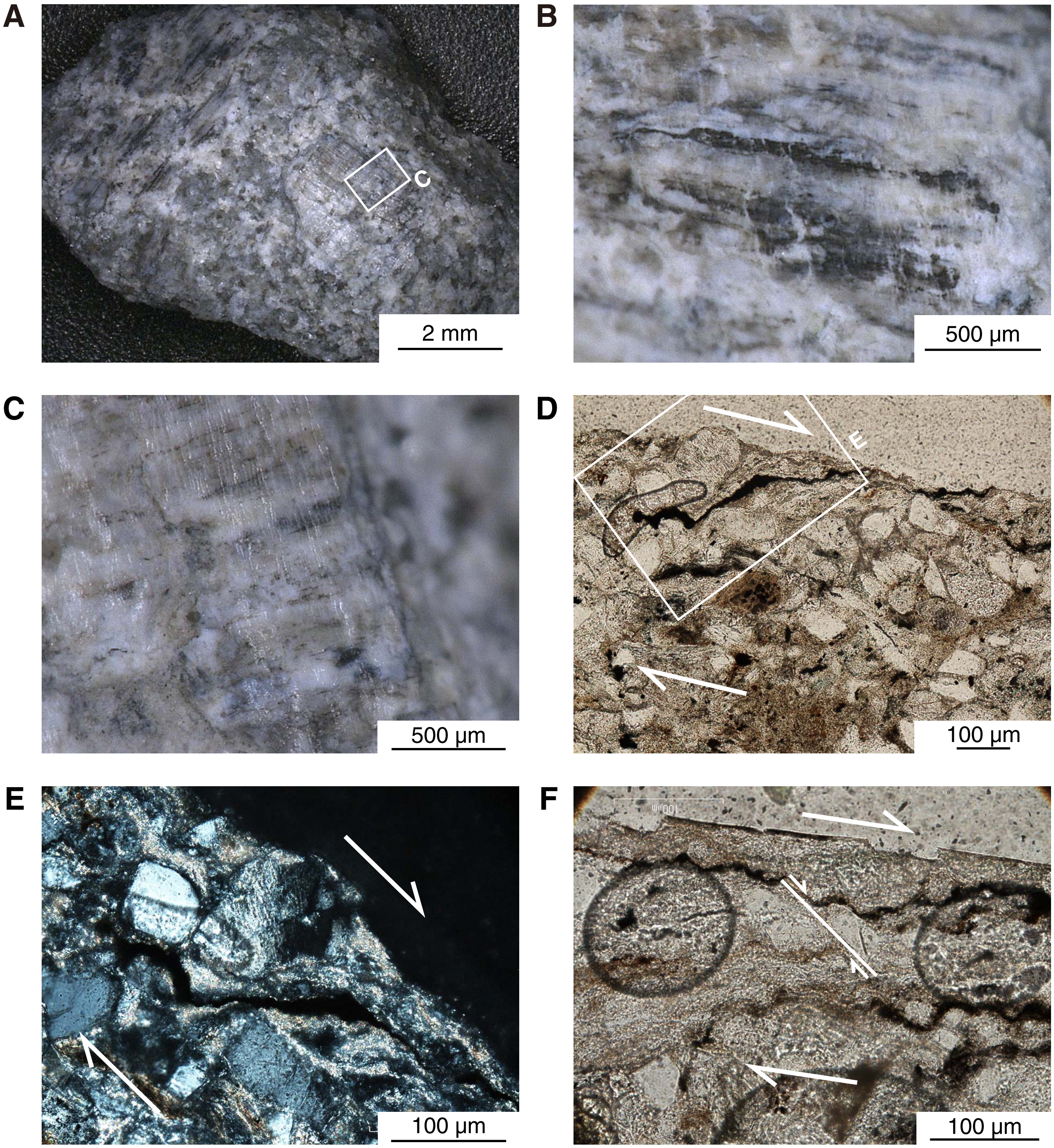

Figure F32. Characteristic examples of scaly fabric. **A.** Sample 348-C0002P-157-SMW (2430.5 mbsf). **B.** Sample 247-SMW (2820.5 mbsf).

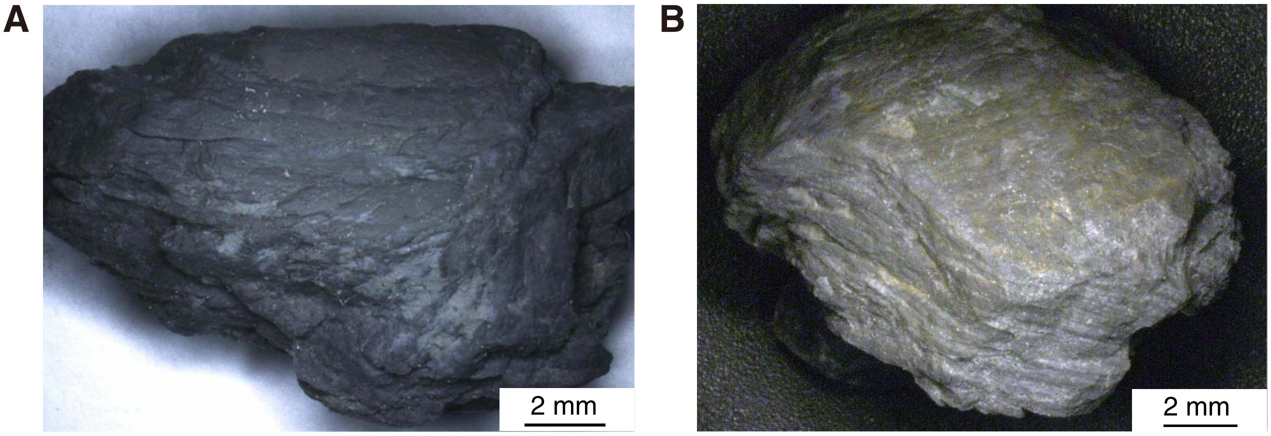

Figure F33. A–D. Characteristic examples of deformation band in intact cuttings (>4 mm). B is an enlargement of part of the cutting reproduced in A. Web structure is present in samples in C and D. (A, B) Sample 348-C0002N-220-SMW (1860.5 mbsf); (C) Sample 304-SMW (2215.5 mbsf); (D) Sample 145-SMW (2390.5 mbsf). **E.** Deformation band of the cutting shown in A. **F.** Enlargement of E.

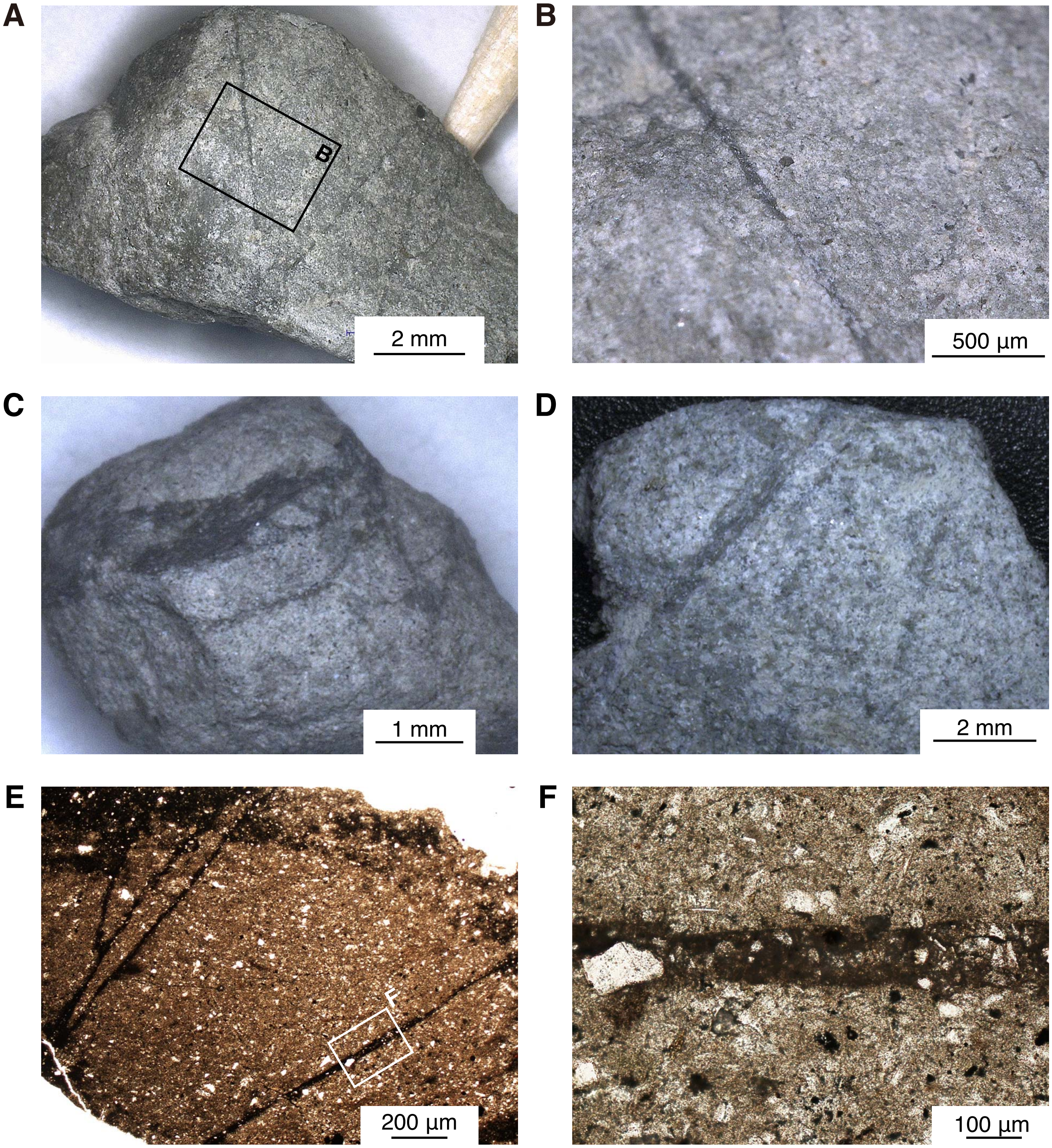

Figure F34. A–F. Distribution and geometry of opaque bands (Sample 348-C0002N-259-SMW; 2015.5 mbsf).

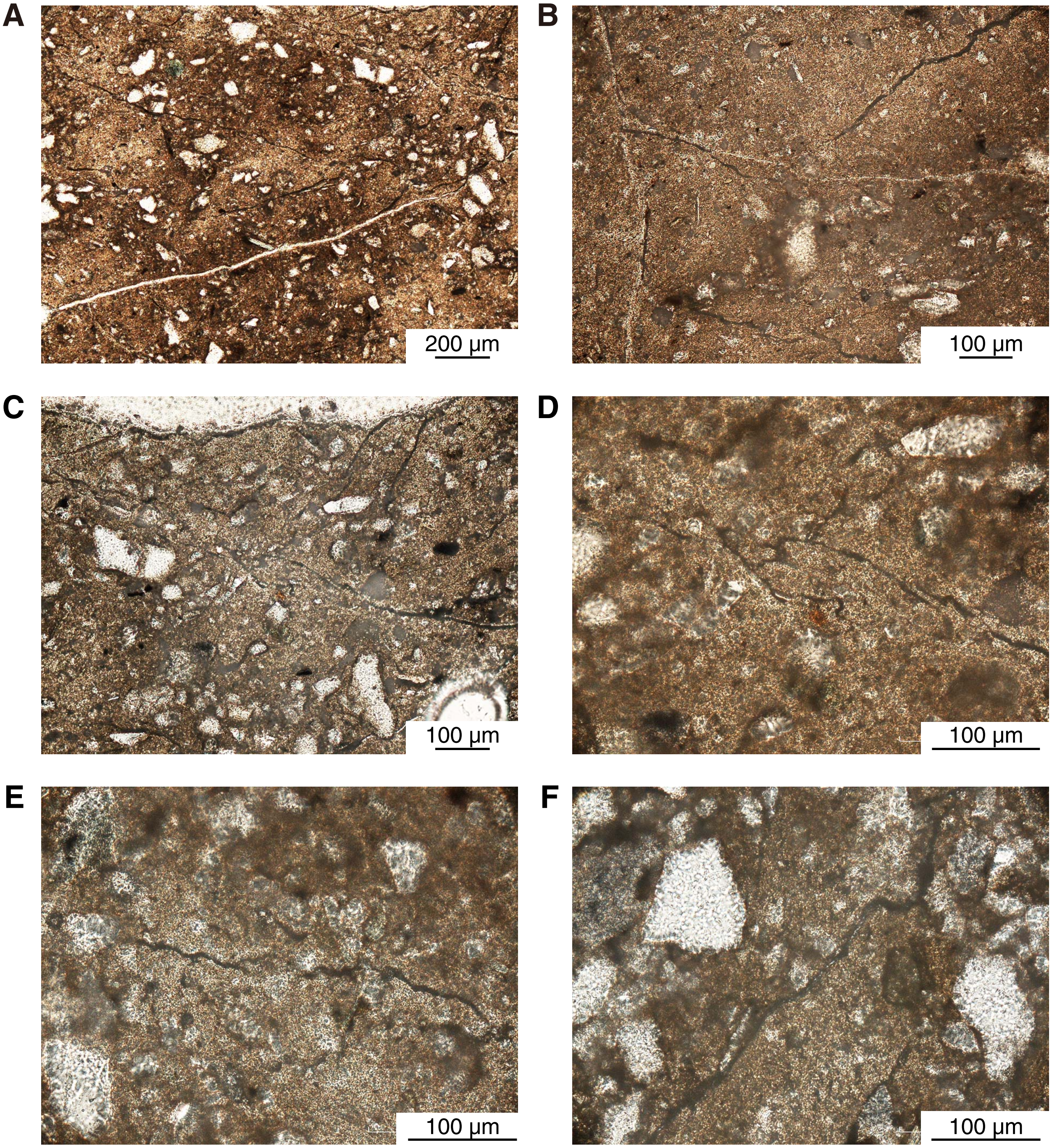

Figure F35. A, B. Minor fault array (Sample 348-C0002P-151-SMW; 2410.5 mbsf) observed in cuttings.

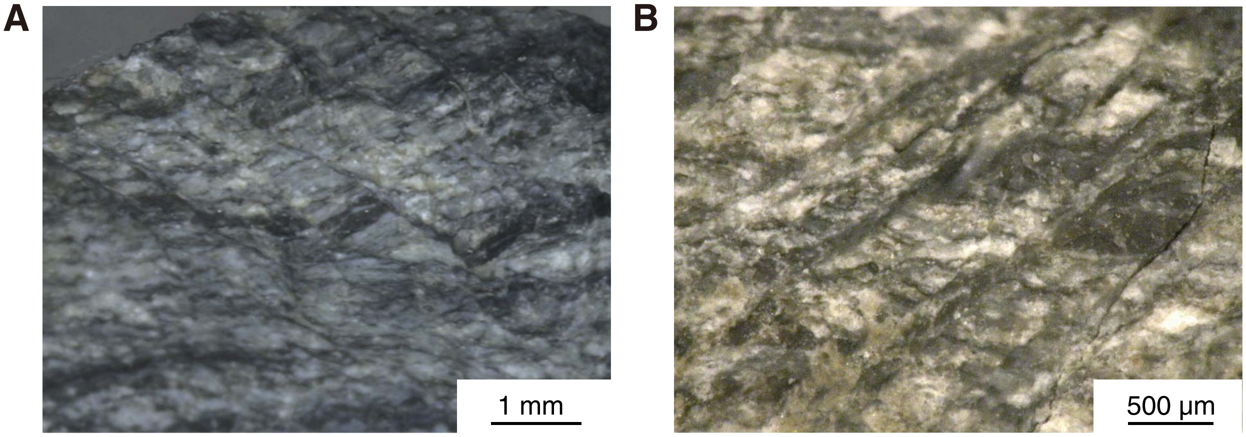

Figure F36. Characteristic examples of veins in intact cuttings (>4 mm). **A.** Carbonate vein (Sample 348-C0002N-140-SMW; 1505.5 mbsf). **B.** Pyrite vein. Note the slickenline subperpendicular to the vein (Sample 348-C0002P-018-SMW; 1990.5 mbsf). **C.** Carbonate minerals in open vein (Sample 018-SMW; 1990.5 mbsf). **D.** Stepped fibers of carbonate minerals (Sample 242-SMW; 2800.5 mbsf). **E.** Brecciation of wall rock (Sample 348-C0002N-162-SMW; 1605.5 mbsf). **F.** Veining and brecciation (Sample 072-SMW; 2165.5 mbsf).

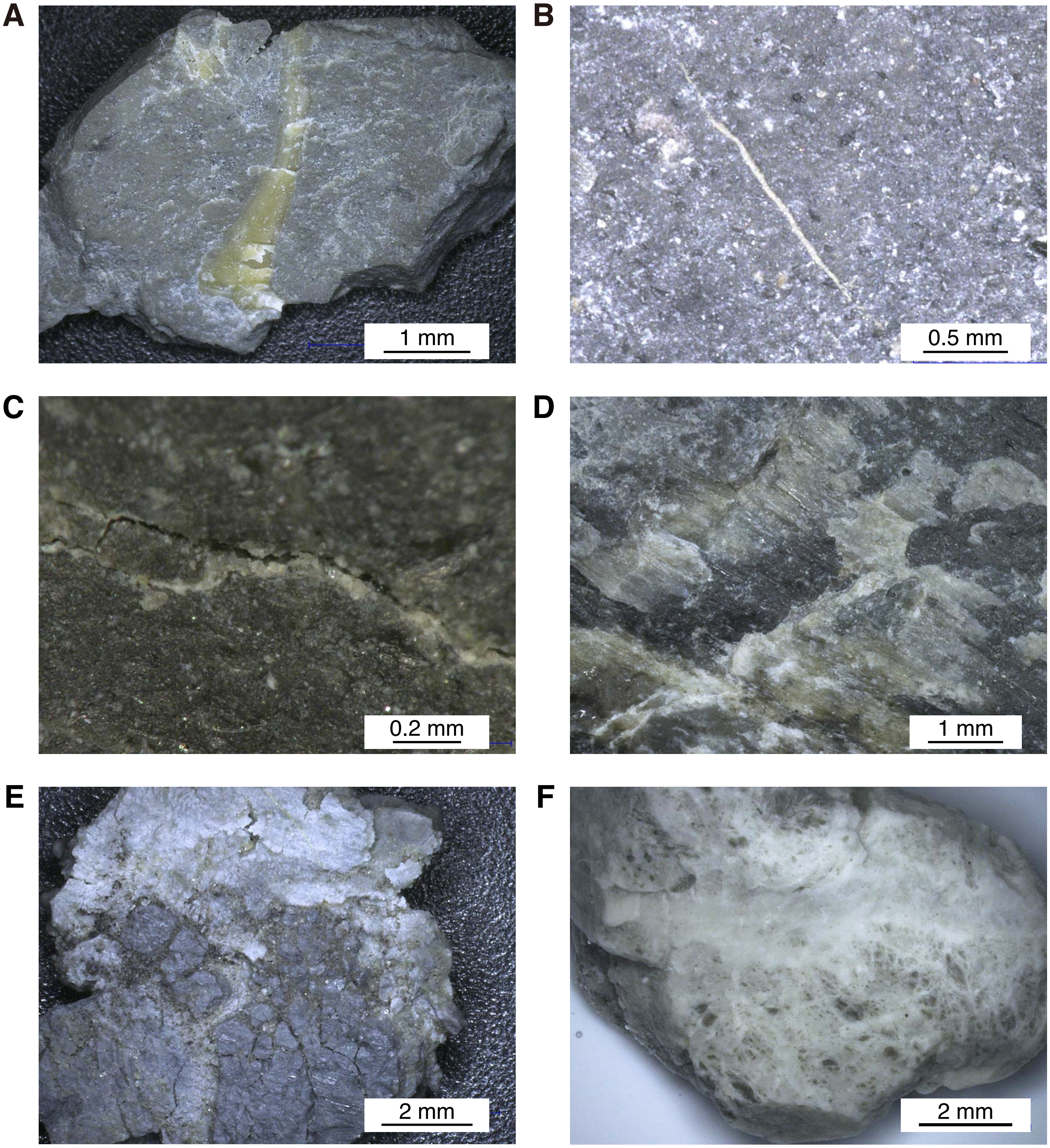

Figure F37. Dip angle variation of bedding (circles) and a vein (triangle) at 475–512.5 mbsf, Hole C0002M.

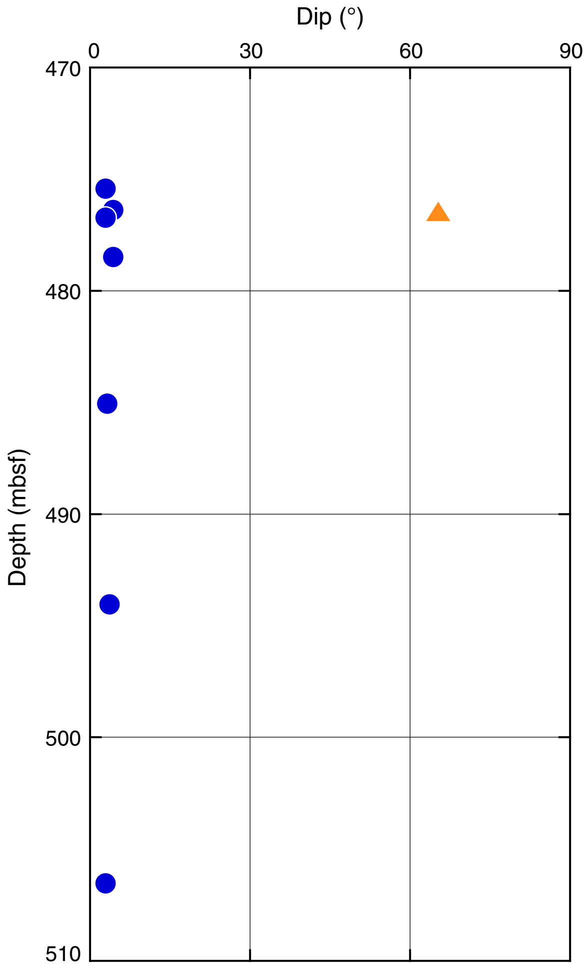

Figure F38. Pyrite vein in interval 348-C0002M-1R-2, 11–16 cm (476.52–476.57 mbsf). **A.** X-ray computed tomography images of horizontal (left) and vertical (right) cross-sections of the vein. Bar indicates the position of the horizontal cross-section. **B.** The vein in the core section.

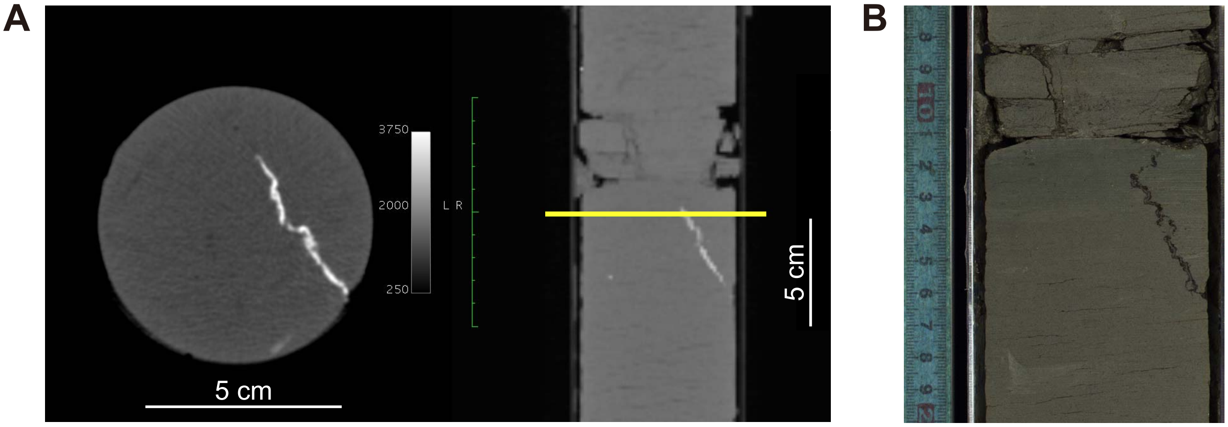

Figure F39. Depth distribution of dip angle variation measured in cores, Hole C0002P. **A.** Bedding. **B.** Minor faults, veins, and deformation band.

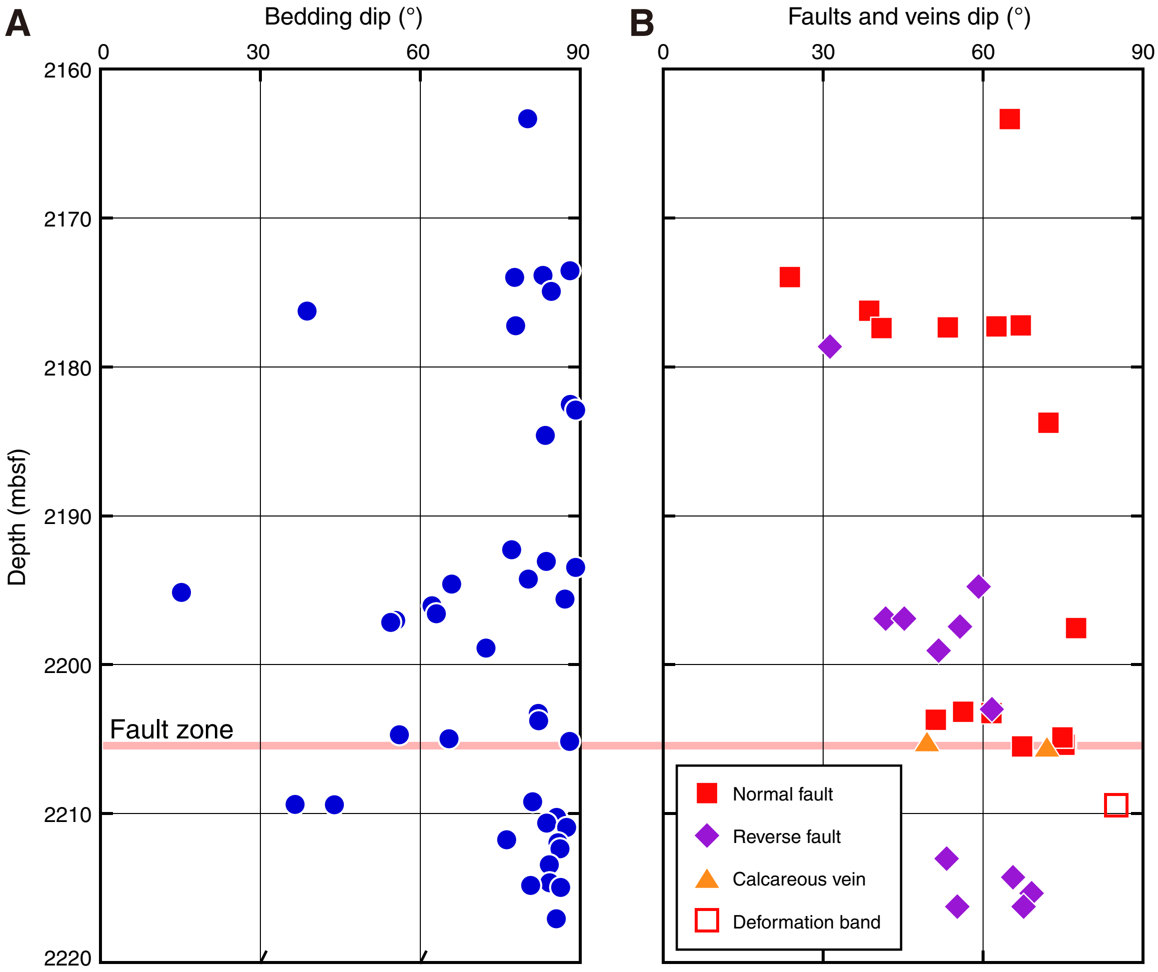

Figure F40. Characteristic examples of minor faults in cores, Hole C0002P. **A.** Slickenlines on a fault plane (2163.22–2163.36 mbsf). **B.** Slickenlines and scratched structures on a fault plane (2183.71–2183.80 mbsf). **C.** Cross-cutting relationship of minor faults (2177.14–2177.27 mbsf). Apparent normal fault cuts conjugate apparent reverse faults. **D.** Sketch of C. The younging direction of the bedding is indicated by the arrow.

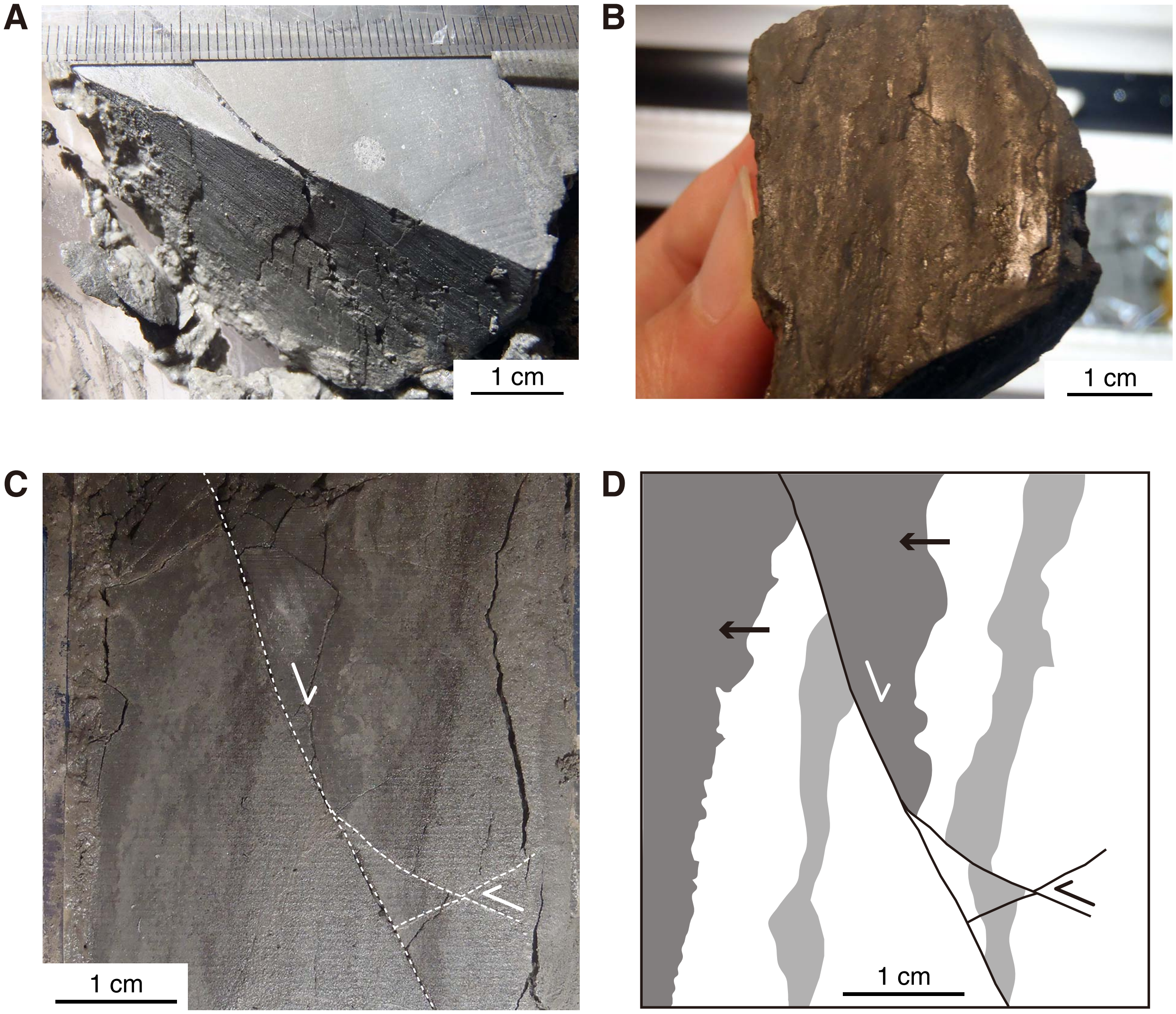

Figure F41. Part of the fault zone in cores retrieved from Hole C0002P (2205.22–2205.56 mbsf). **A.** Core sample (working half). **B.** X-ray computed tomography imaging of core sample. **C.** Sketch of the fault zone.

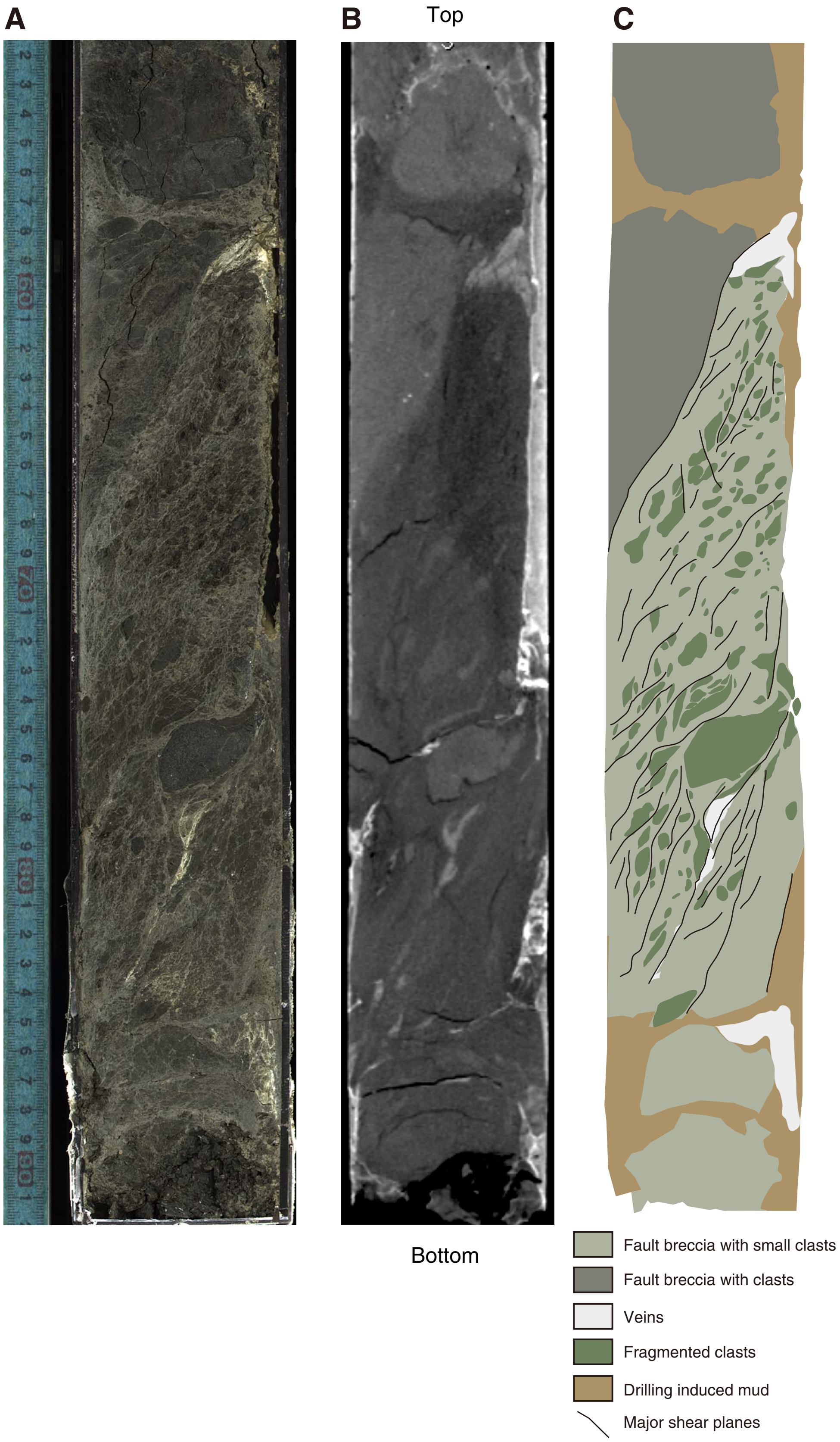

Figure F42. Detail of the fault zone (archive half), Hole C0002P. Note the asymmetric shape of the sandstone clast (left of the photograph), the domino-like structure of the clasts (right of the photograph), and the imbrications of the veinlets. All these criteria indicate a dextral sense of shear.

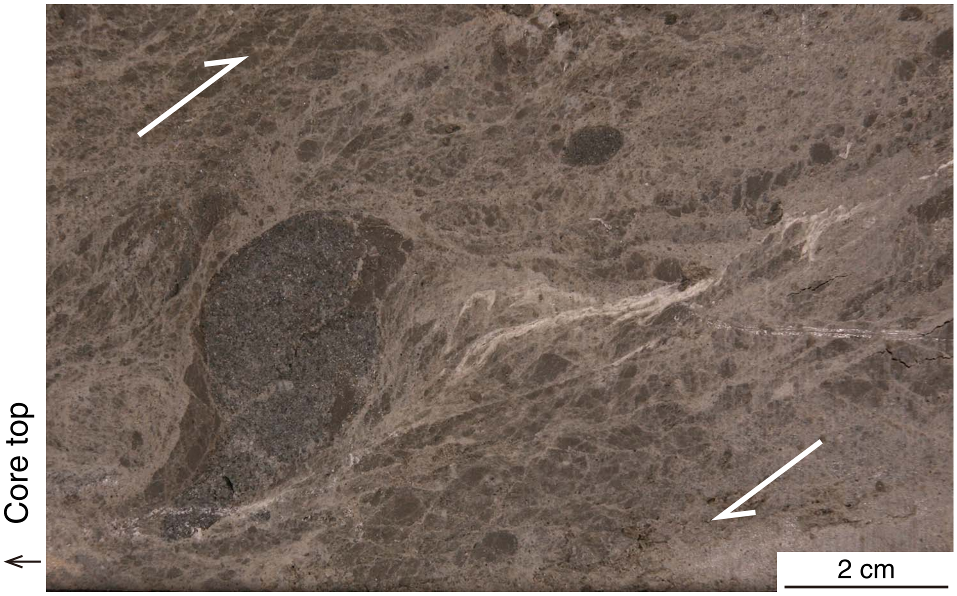

Figure F43. Scanning electron microscope photographs of intact cuttings (>4 mm) indicating the (A, H) characteristics of the clay fabric, (A–E) siliceous microfossils that remained intact, and (F, G) framboidal pyrite. **A–G.** Sample 348-C0002N-81-SMW (1225.5 mbsf). **H.** Sample 302-SMW (2205.5 mbsf).

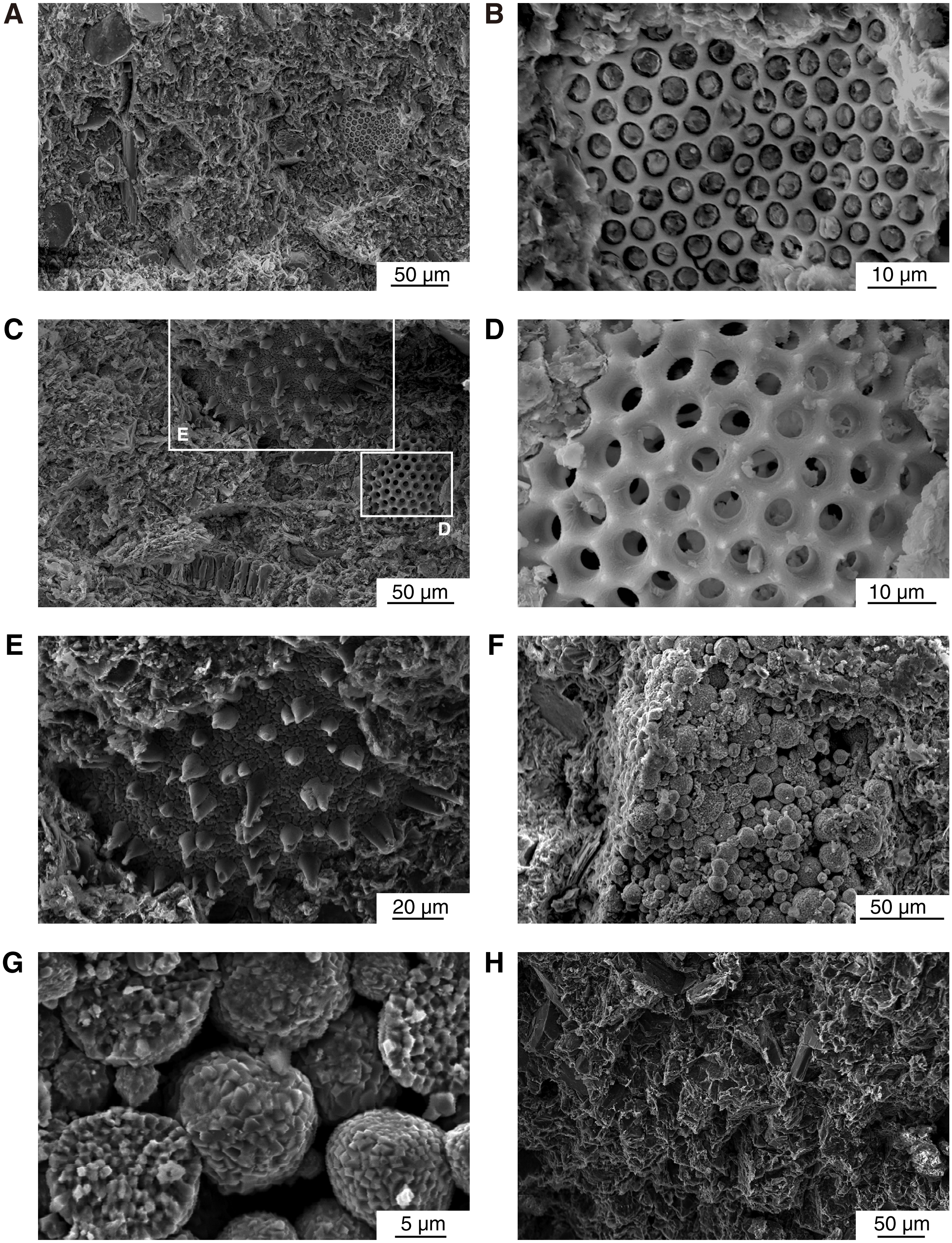

Figure F44. A–F. Intact cuttings (>4 mm) showing the characteristics of slickenlined surfaces. (A, B, D) Sample 348-C0002N-81-SMW (1225.5 mbsf); (C, E, F) Sample 302-SMW (2205.5 mbsf). (Continued on next page.)

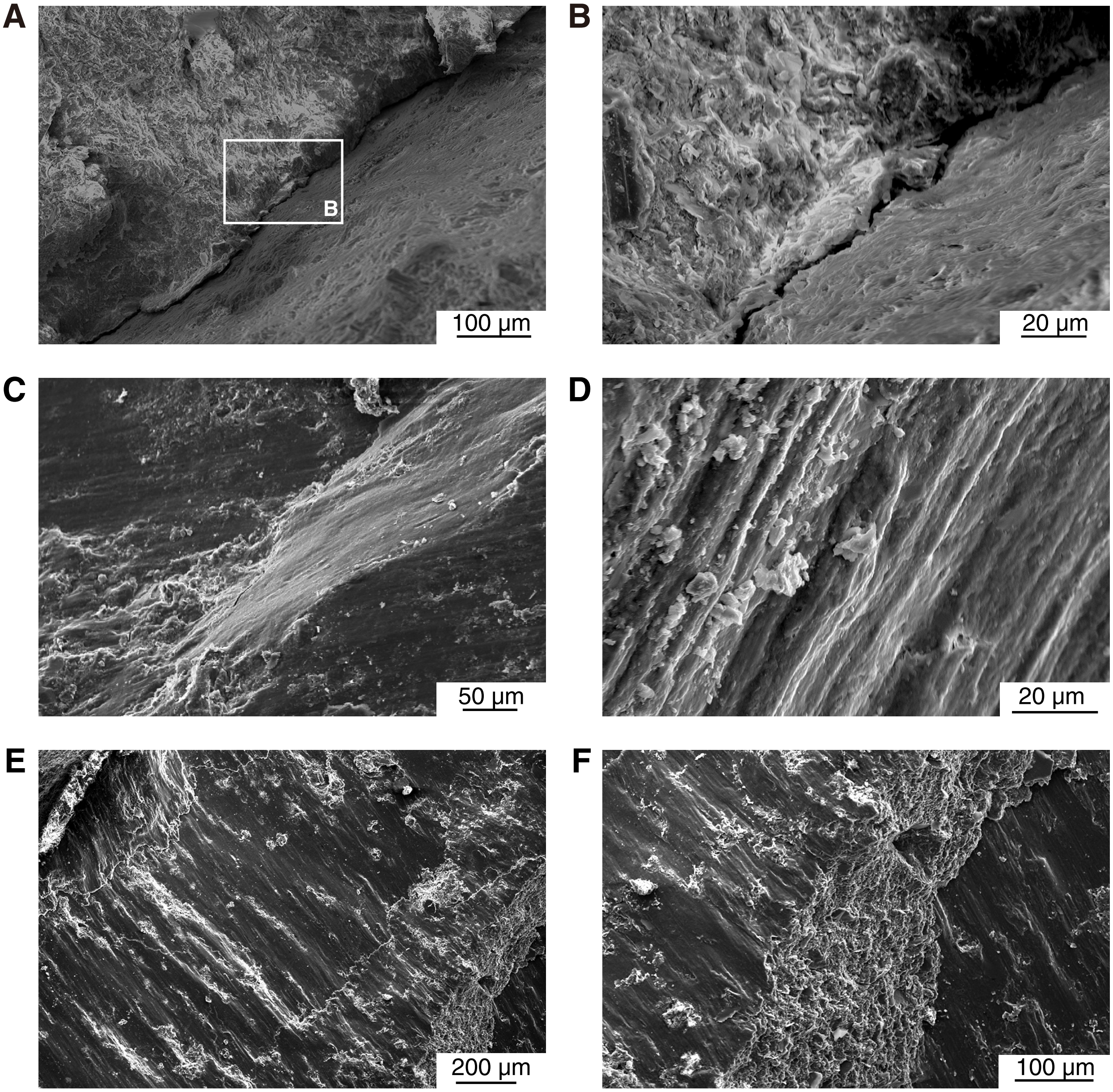

Figure F44 (continued). G–K. Intact cuttings (>4 mm) showing the geometry of microfault distribution. (G–I) Sample 348-C0002N-175-SMW (1665.6 mbsf); (J, K) Sample 81-SMW (1225.5 mbsf).

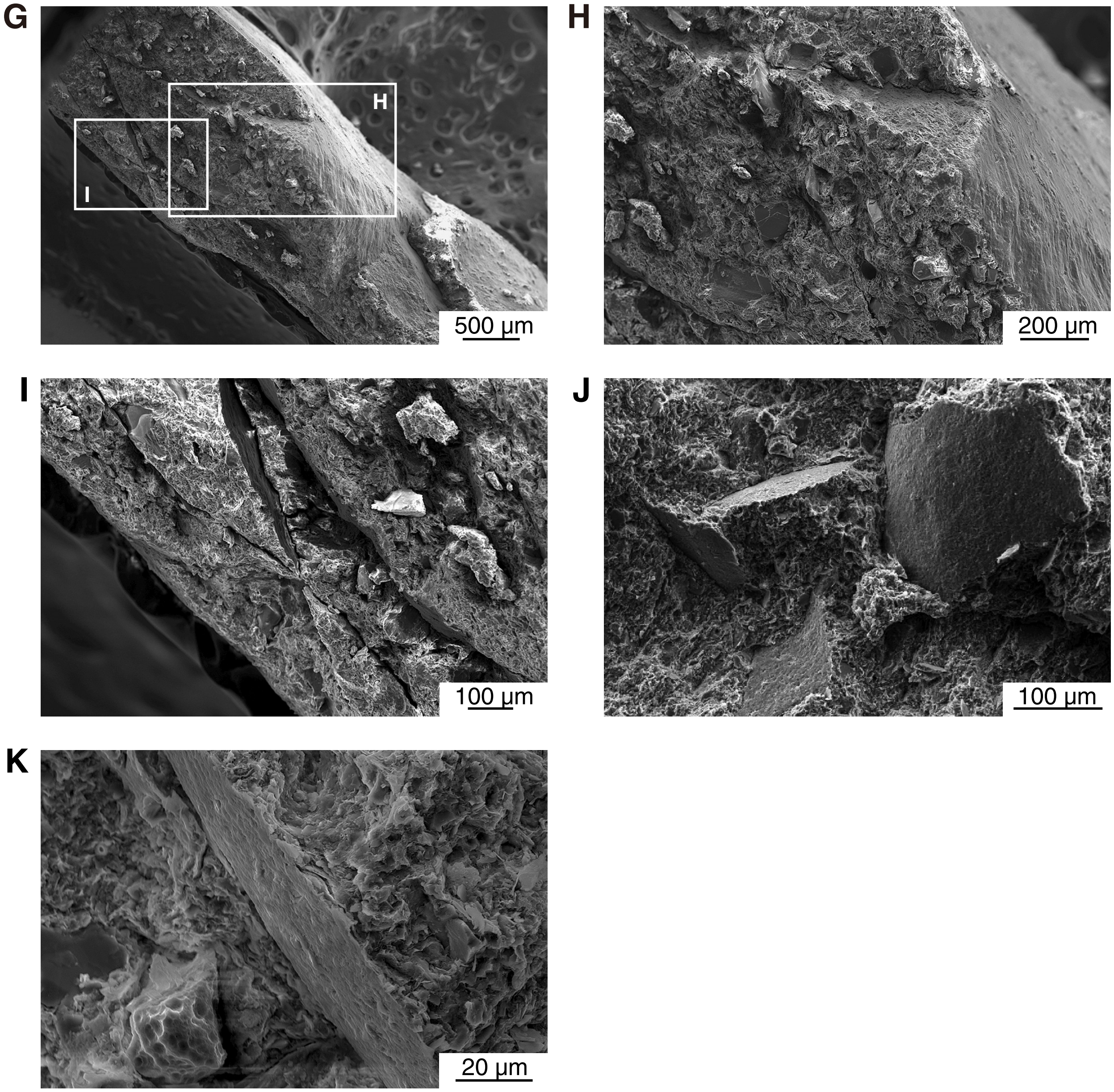

Figure F45. Saw-cut sections through lenticular sandstone blocks, Section 348-C0002P-2R-3 (2176.2 mbsf). The interior of the blocks show original laminations disrupted by (**A, B**) planar and (**C**) highly irregular weblike faults. The blocks are surrounded by scaly, striated, clay-rich sediment.

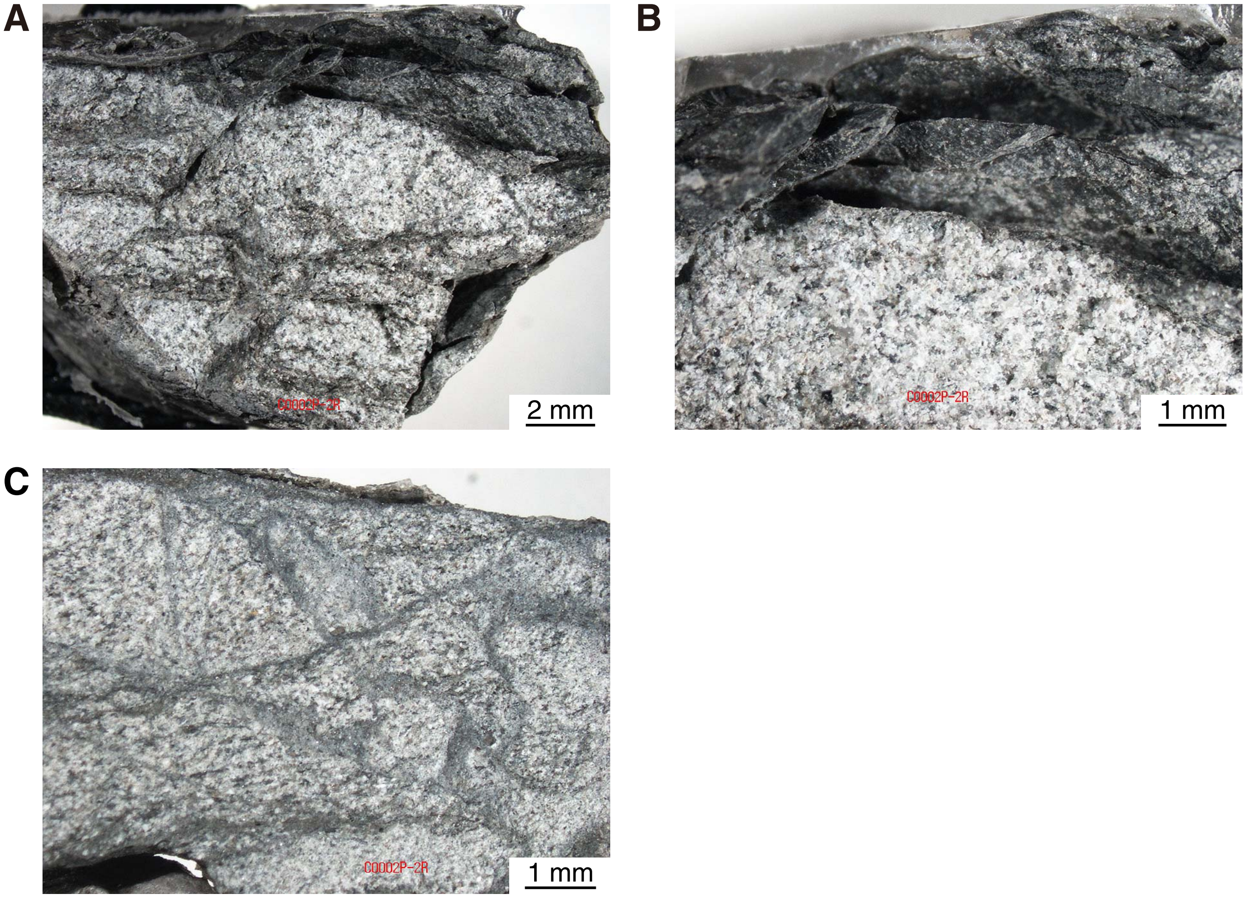

Figure F46. **A.** Binocular microscope photo of an indurated lenticular inclusion in the foliated broken formation, excavated during the interstitial water sample extraction undertaken in Section 348-C0002P-2R-3 (2176.2 mbsf). The inclusion is surrounded by scaly fabric. The arrow denotes a small fold. **B.** Fabric on the edge of a sand inclusion in the foliated material (position shown as inset in A). **C.** Fabric on the edge of a sand inclusion in the foliated material (position shown as inset in B). Note distribution of sand grain sizes and general spacing of discrete shears separating less deformed panels (position shown as inset in C). **D.** Spaced discrete shears and less deformed panel structure (position shown as inset in C). **E.** Spaced discrete shears and less deformed panel structure (position shown as inset in D). **F.** Asymmetric fabrics between microshear zones. Note the section is somewhat oblique to the striations on the microfault in the background.

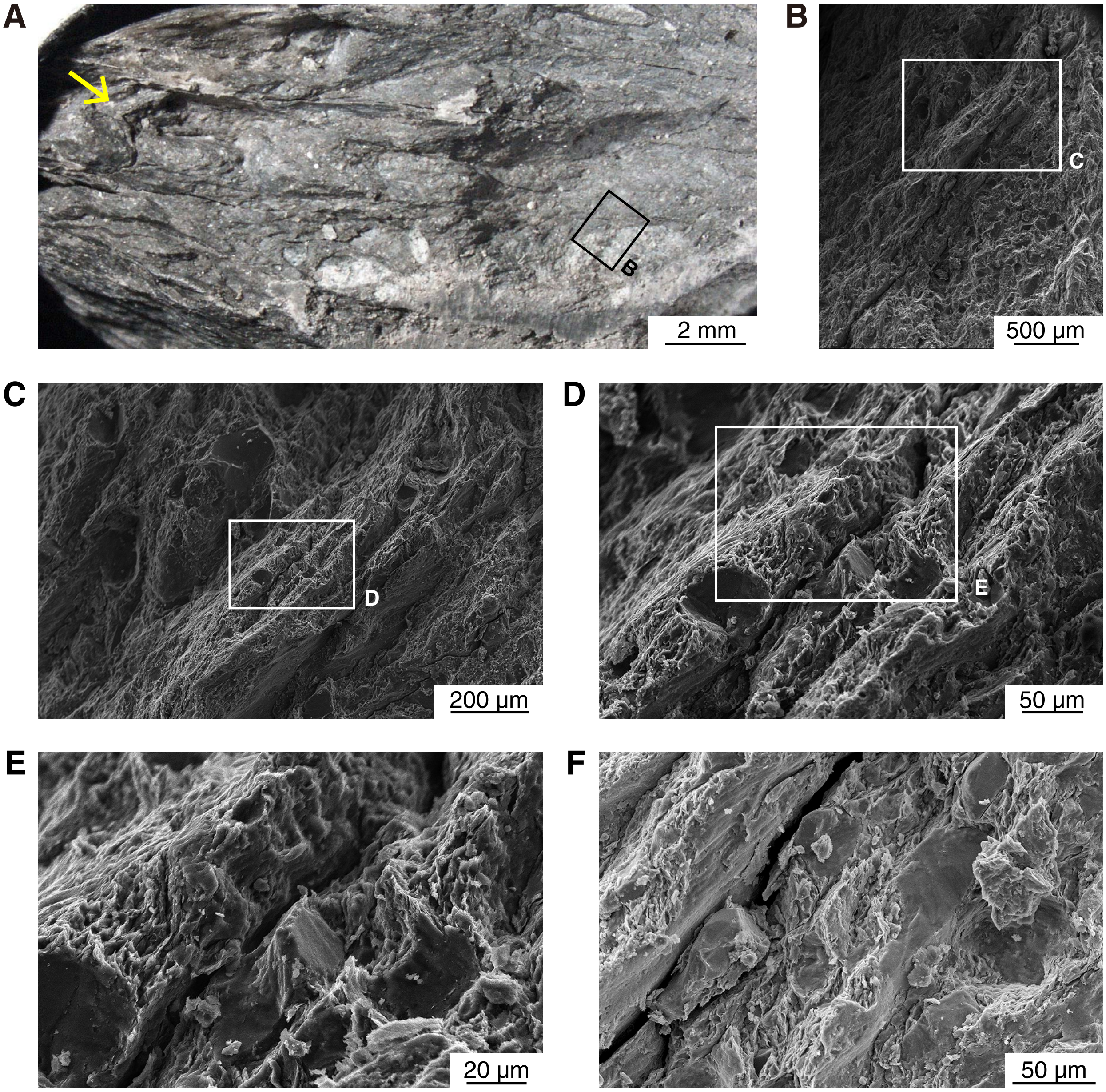

Figure F47. **A.** Striated surfaces of the scaly fabrics in a shear zone at 2115.5 mbsf (Sample 348-C0002N-281-SMW). **B.** Inset in A. Note the incipient oblique grain-alignment fabric between the thin shear zones. **C.** Striated surfaces of the scaly fabrics in a shear zone at 1990.5 mbsf (Sample 348-C0002P-18-SMW). **D.** Inset in C. Note extremely thin zone of grain-alignment fabric just below slickenlined surface (arrow).

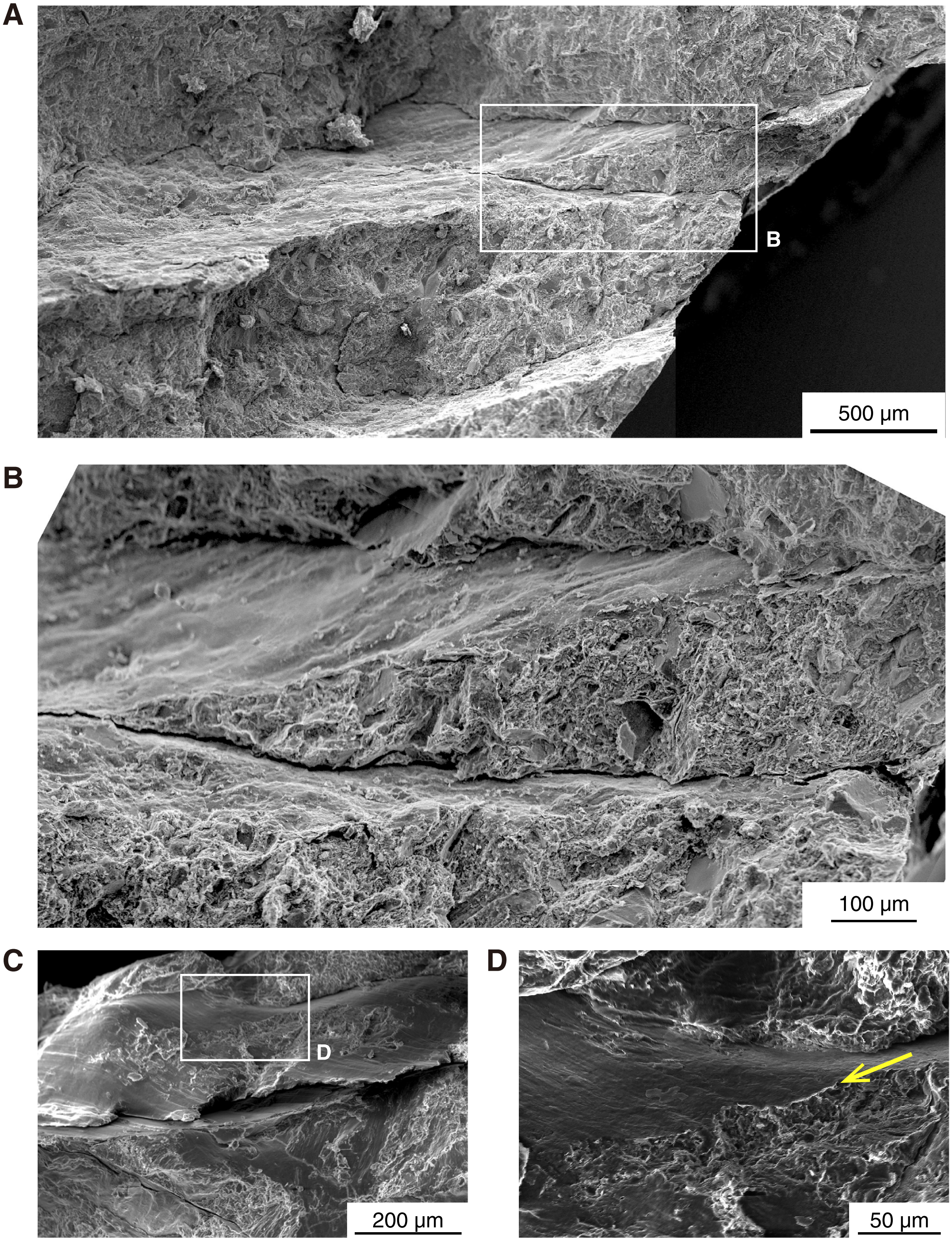

Figure F48. **A–C.** Foliation surface of the penetrative grain-alignment foliation at 2980.5 mbsf (Sample 348-C0002N-283-SMW). **D–F.** Foliation cross-section of the penetrative clay-alignment foliation of the same sample. Note the cross-cutting striated microfault in D with little deflection of the adjoining highly oblique clay fabric (bottom right).

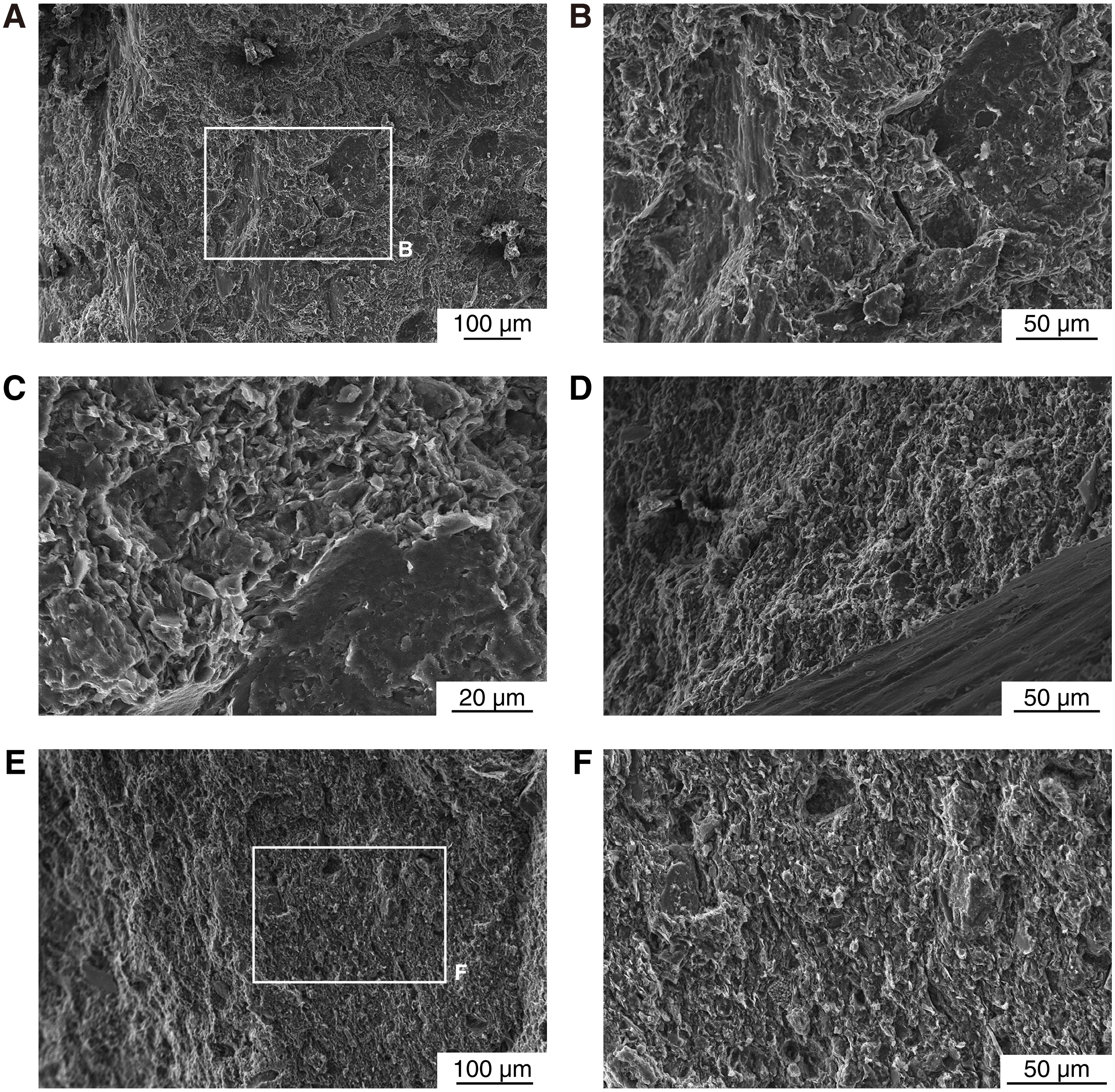

Figure F49. Biostratigraphic events identified in Holes C0002N and C0002P. LO = last occurrence, FCO = first common occurrence, FO = first occurrence.

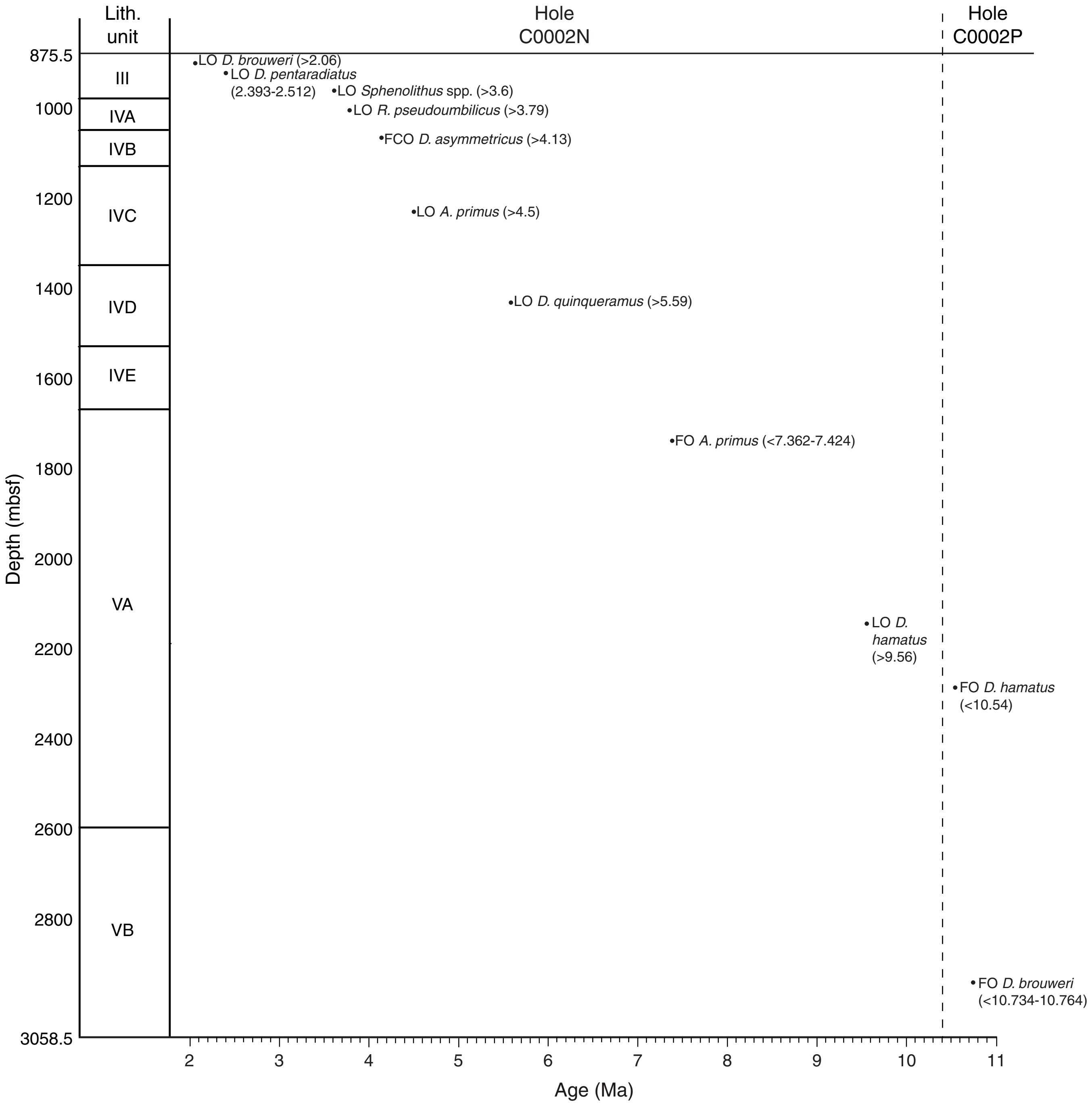

Figure F50. **A, B.** Normalized change in intensity of magnetization. **C, D.** Stereoplot diagrams showing remanent magnetization. Solid and open squares correspond to the lower and upper hemisphere equal area projection, respectively. **E, F.** Progressive alternating field demagnetization (AFD) displayed by vector endpoint diagrams. Data points = magnetization vector for individual demagnetization steps projected onto horizontal (solid squares) and vertical (open squares) plane. Figures were prepared with PuffinPlot (Lurcock and Wilson, 2012).

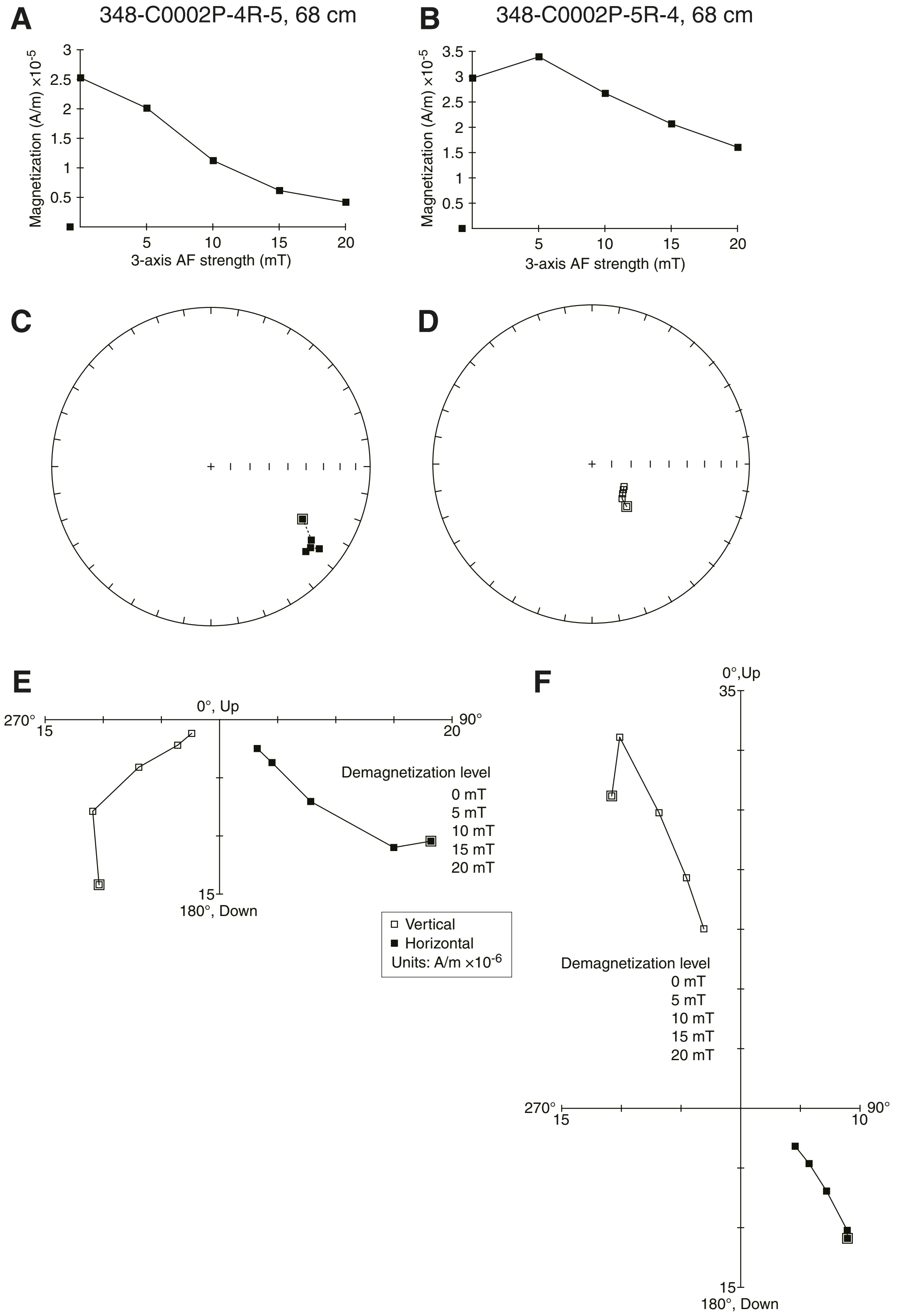

Figure F51. Paleomagnetic inclination, declination, and intensity after 20 mT demagnetization, Hole C0002P. Shaded area represents the brittle fault zone (2204.9–2205.8 mbsf).

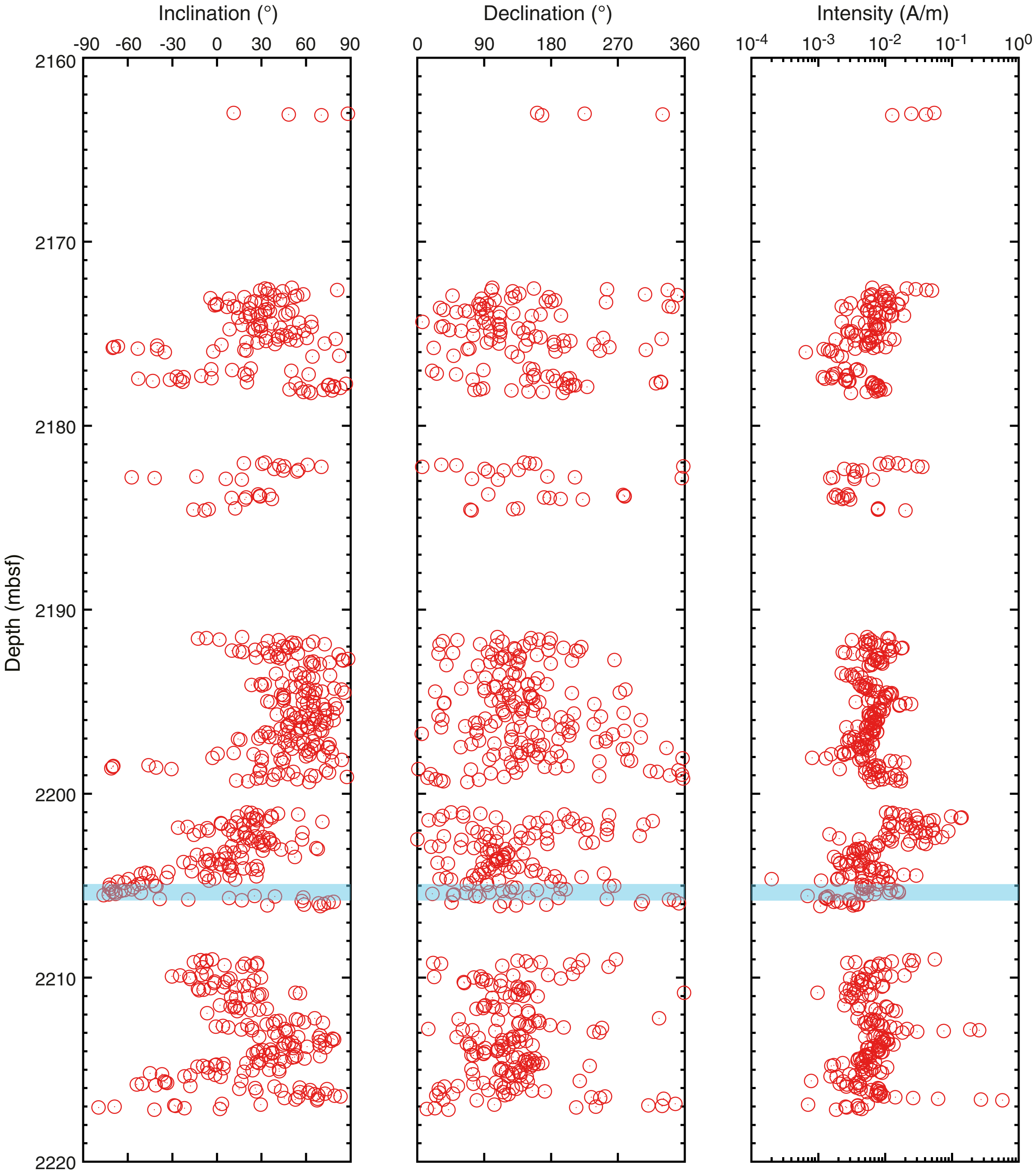

Figure F52. Chlorinity data, Hole C0002M. Measured chlorinity values for different squeezing pressure steps are shown. Data represent separate water aliquots from sequential squeeze steps of A through C″.

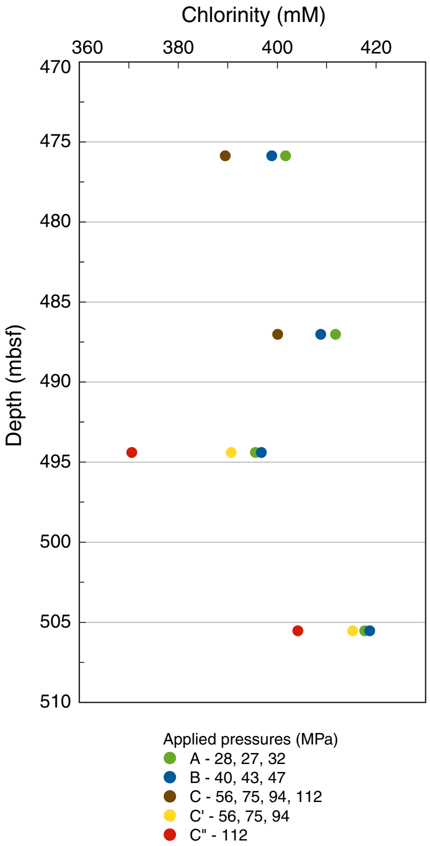

Figure F53. Carbonate ($CaCO_3$), total organic carbon (TOC), and total nitrogen (TN) data, Hole C0002M.

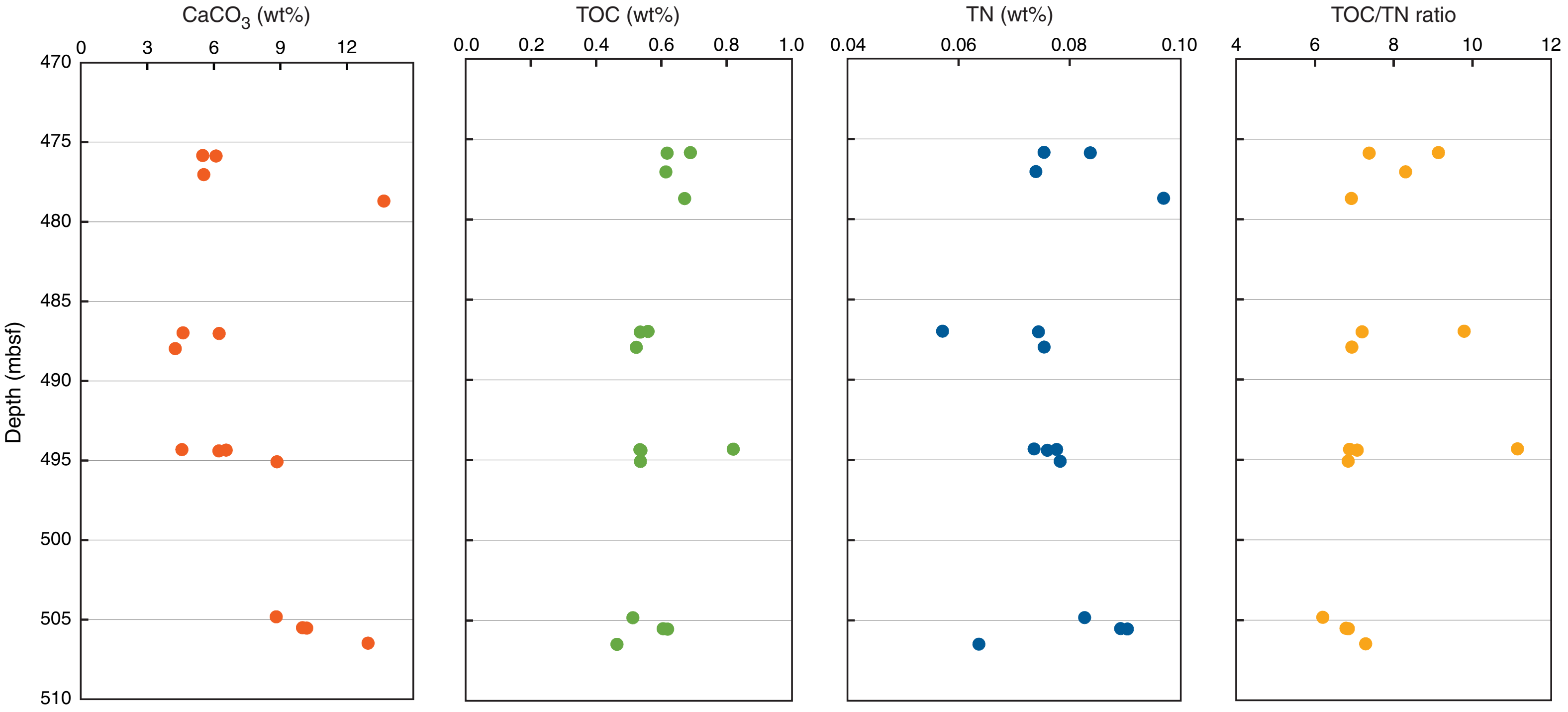

Figure F54. Variations in methane (C_1) and ethane (C_2) concentrations with depth, Hole C0002M.

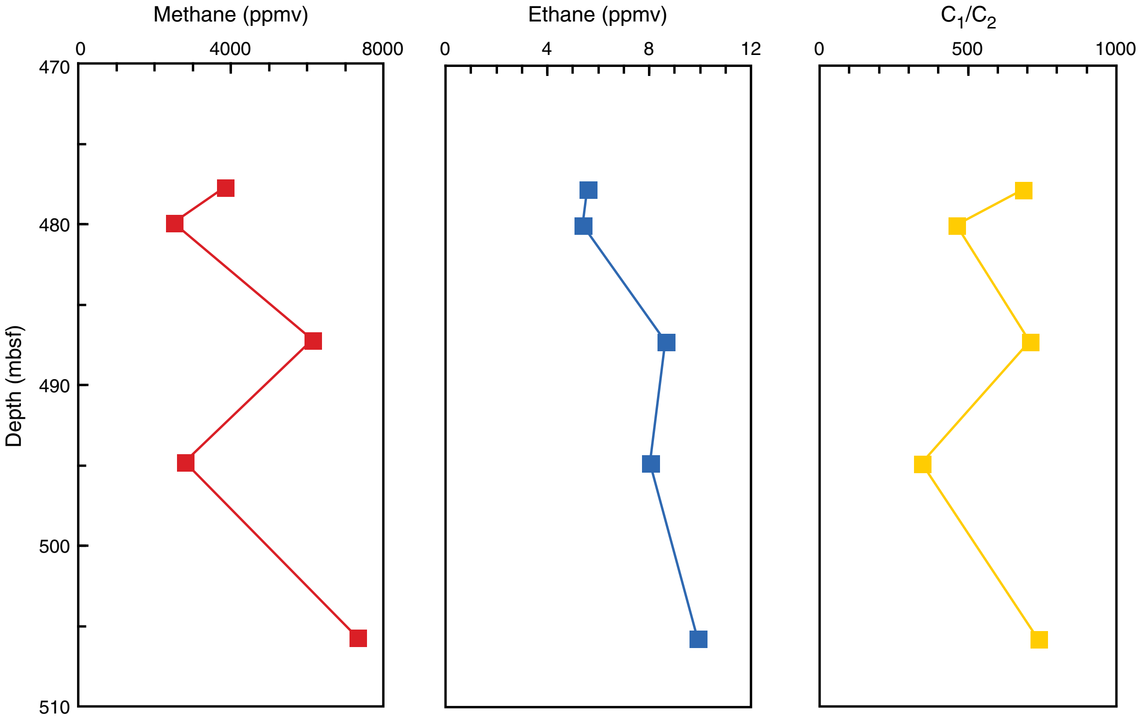

Figure F55. Temperature estimates using methane/ethane ratios and total organic carbon (TOC) data from cores, Hole C0002M.

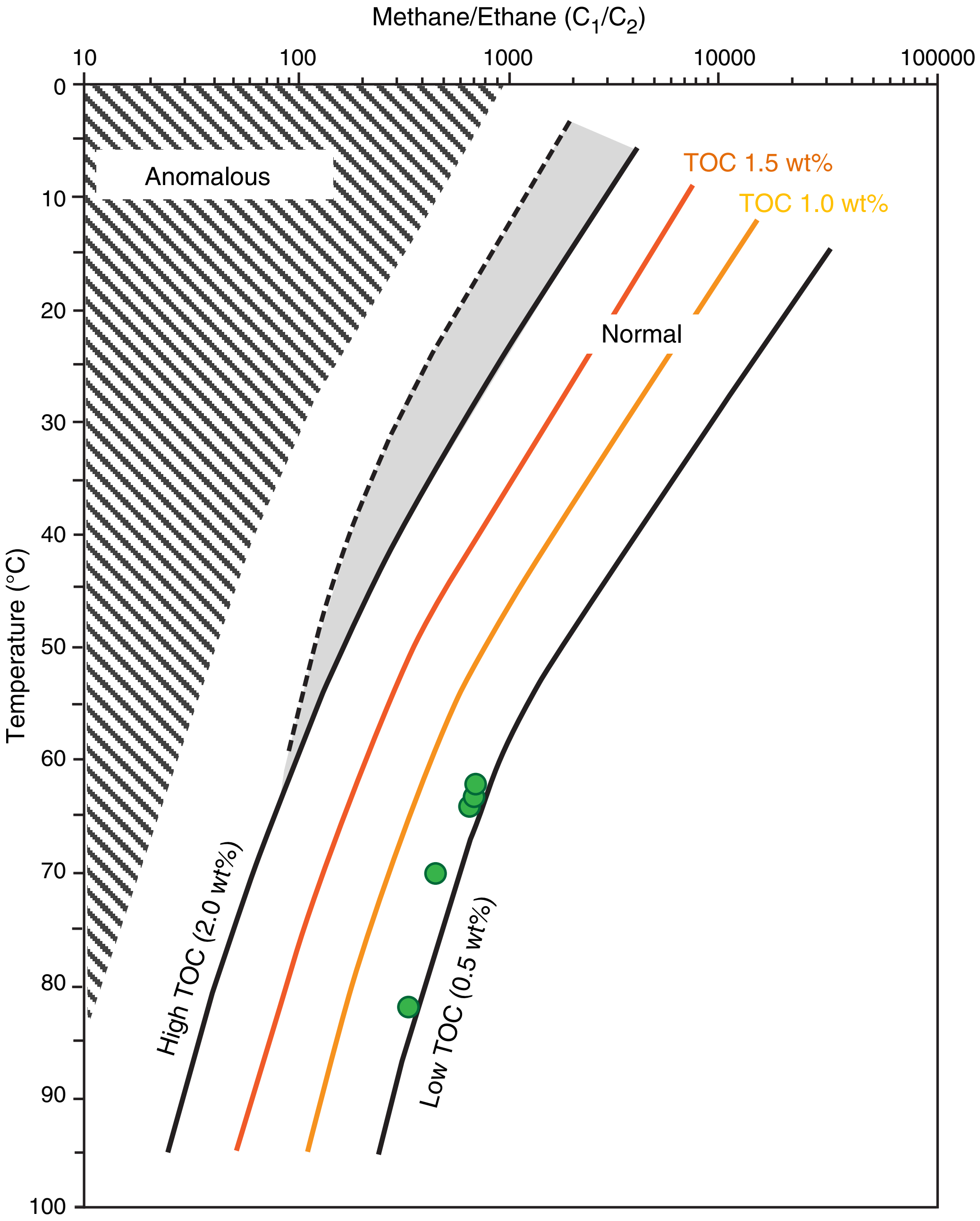

Figure F56. Salinity, pH, and downhole concentrations of chlorinity, bromide, sulfate, and ammonium in Hole C0002P cores determined by the ground rock interstitial normative determination (GRIND) method.

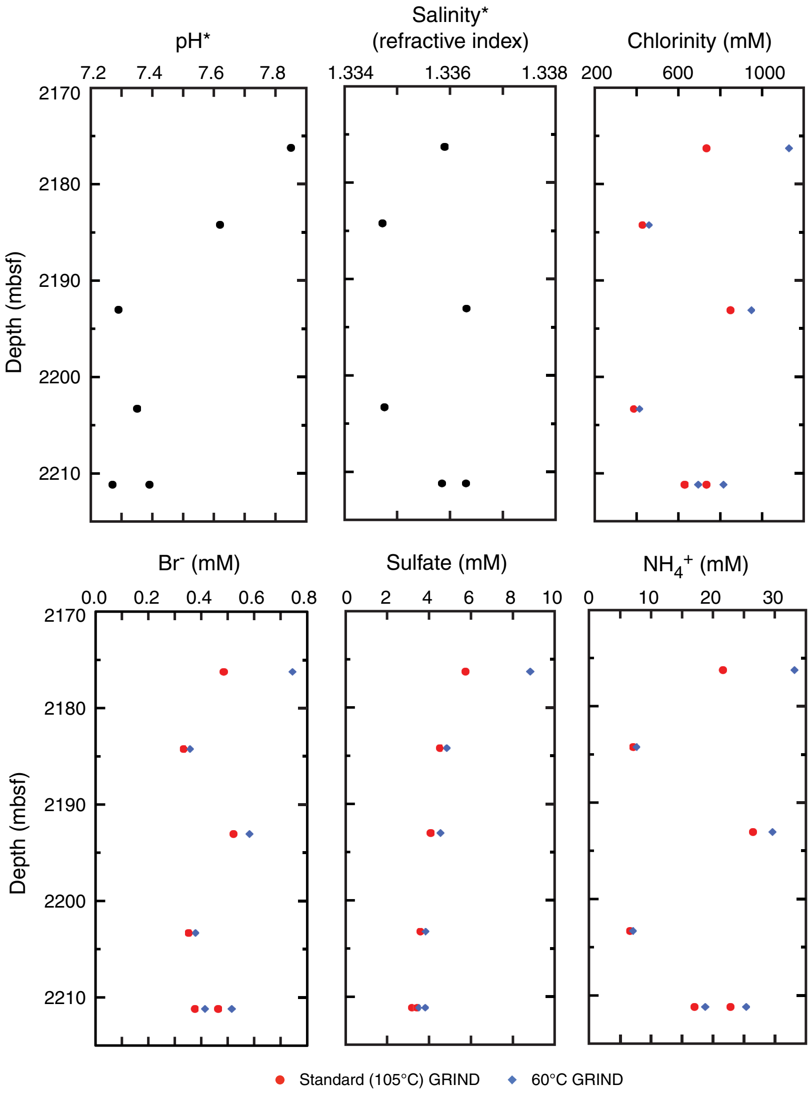

Figure F57. Concentrations of sodium, potassium, magnesium, calcium, barium, silica, boron, lithium, manganese, and strontium in Hole C0002P cores determined by the ground rock interstitial normative determination (GRIND) method. See Figure F56 for symbol definitions.

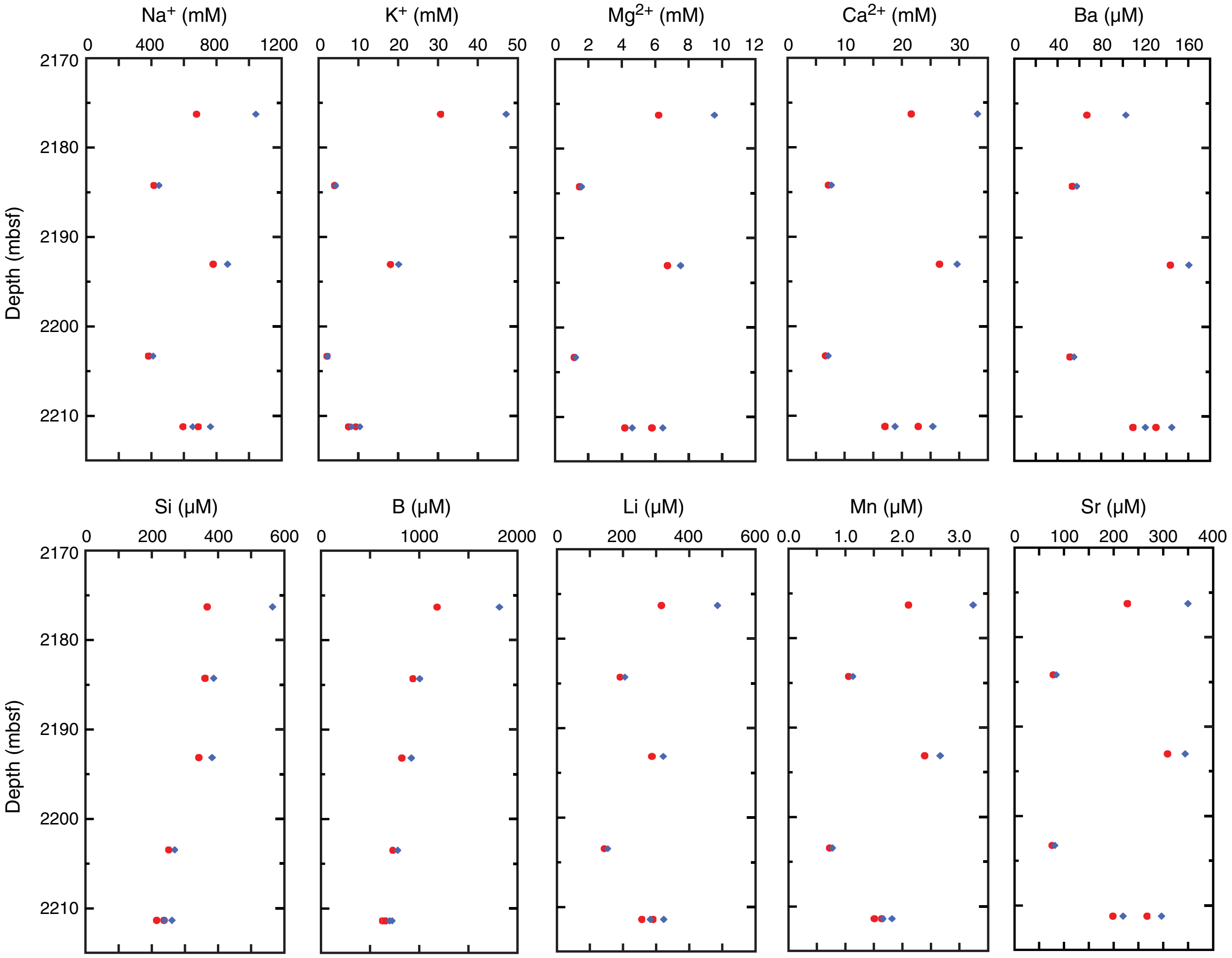

Figure F58. Cross-plots of ion concentrations in Hole C0002P cores determined by the ground rock interstitial normative determination (GRIND) method. Compositions of GRIND water (GW) and mud water (MW) are shown in each plot.

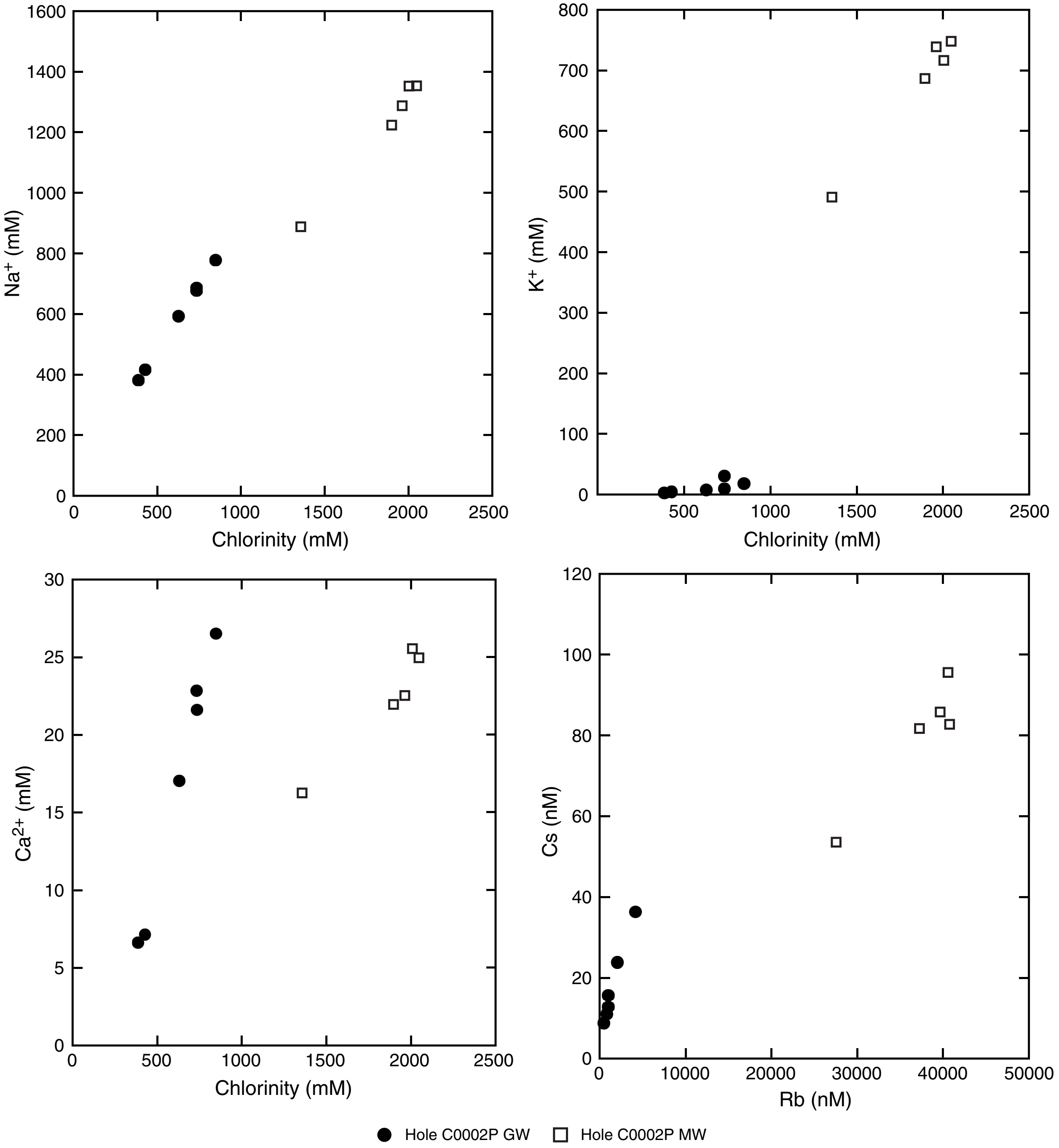

Figure F59. Downhole variations in percentage contamination in interstitial water (IW) as determined from perfluorocarbon (PFC) concentrations in cores and liquid in core liner (LCL) fluids. The only IW core with significant contamination is from Section 348-C0002P-2R-3. PFC in LCL from Core 1R was 56 µg/L, but no IW sample was taken from this core.

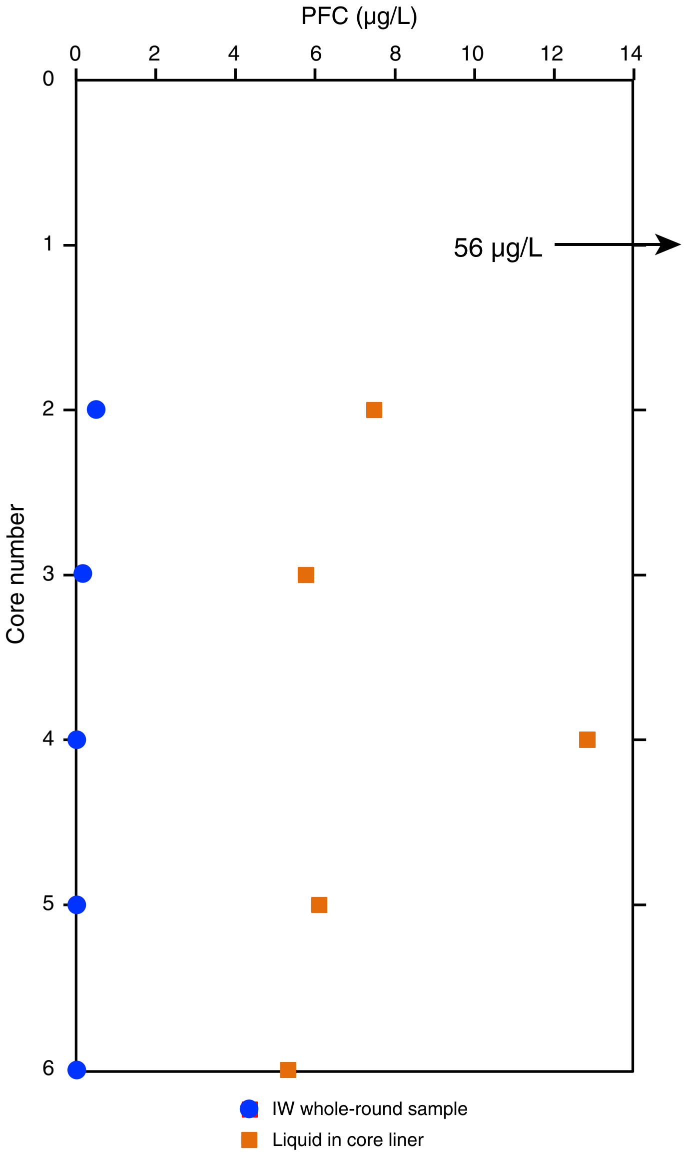

Figure F60. Comparison of concentrations of sodium and magnesium to chlorinity-normalized values, Site C0002. GRIND = ground rock interstitial normative determination.

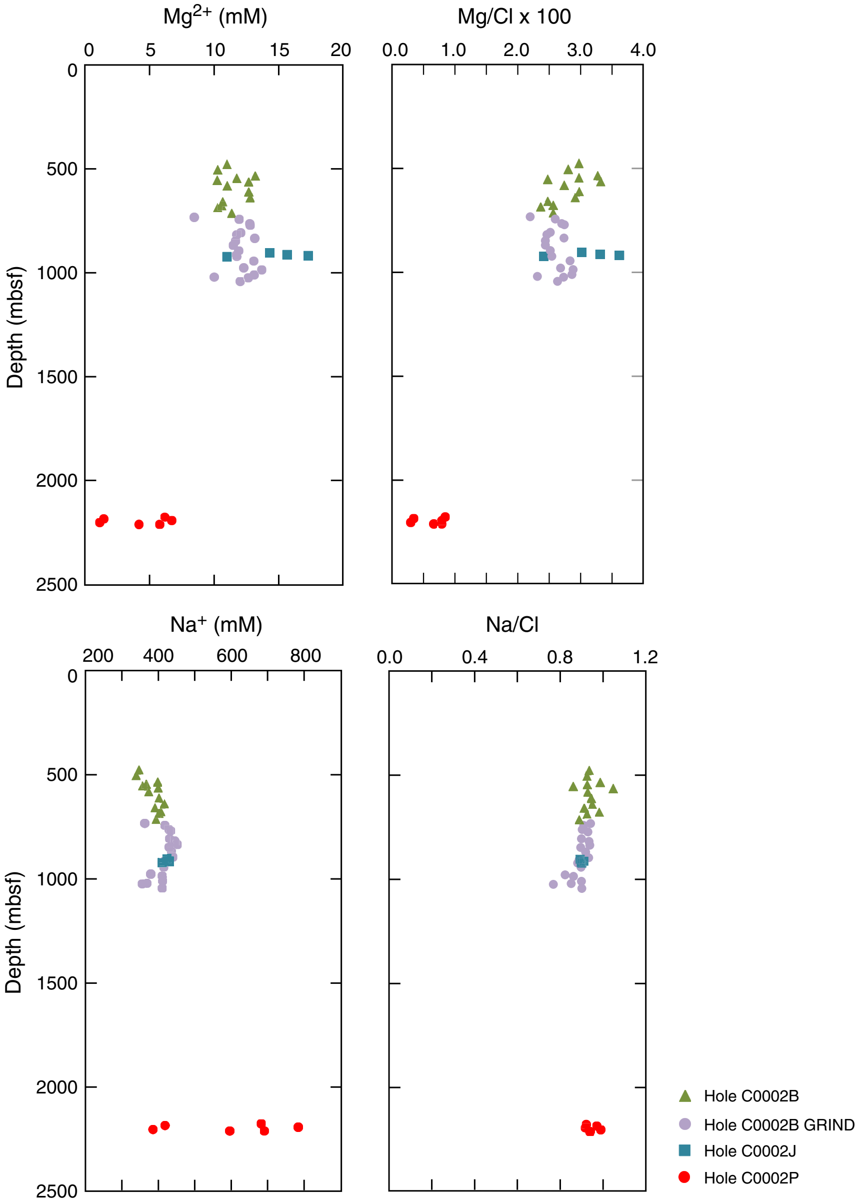

Figure F61. Variations of selected ion concentrations compared to ion concentrations normalized to chlorinity values, Site C0002. For these plots, concentrations using pore water estimates determined by drying interstitial water core fractions at 105°C were used, to be consistent with previous expeditions. GRIND = ground rock interstitial normative determination.

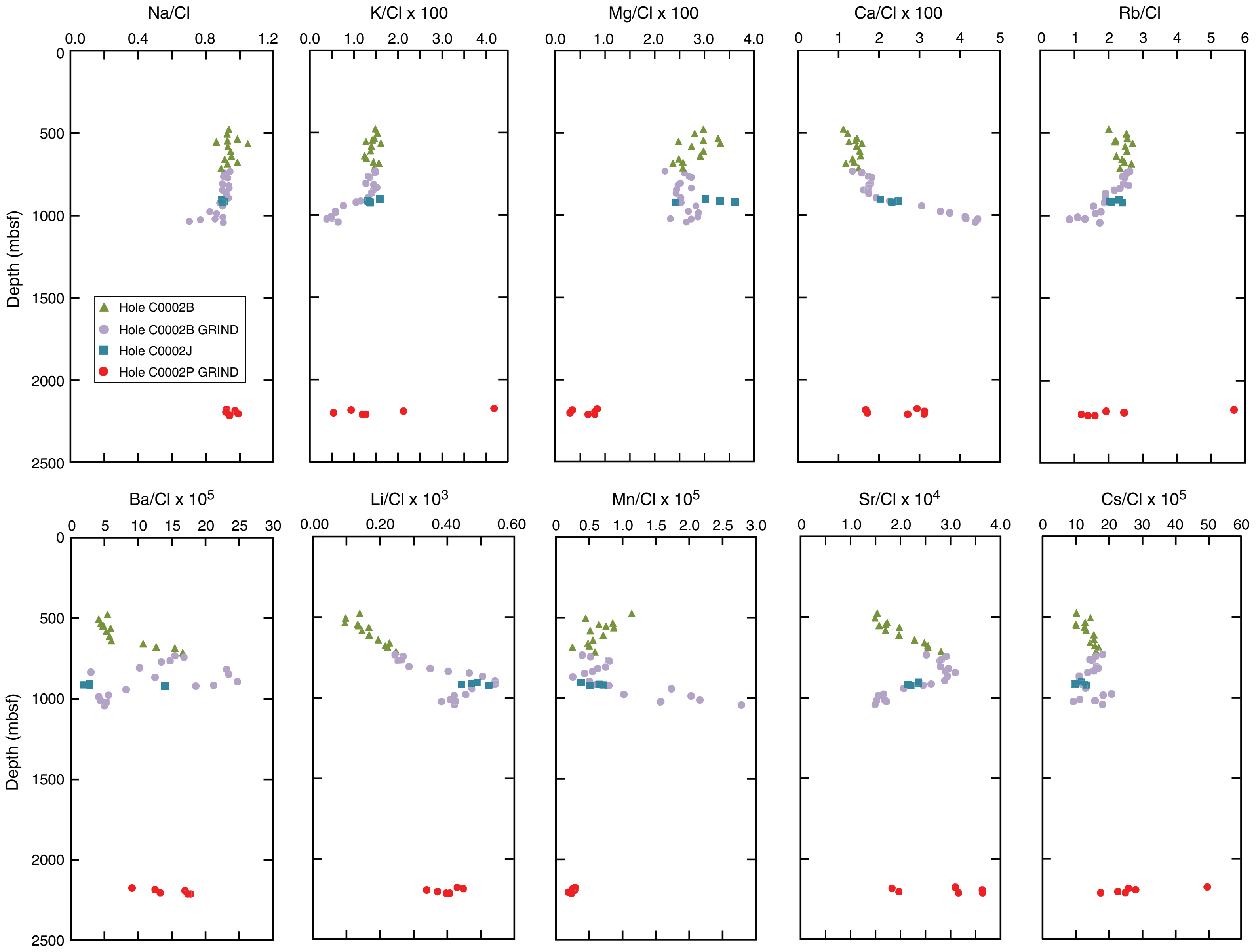

Figure F62. Trace element data, Holes C0002N and C0002P. See Figure F56 for symbol definitions.

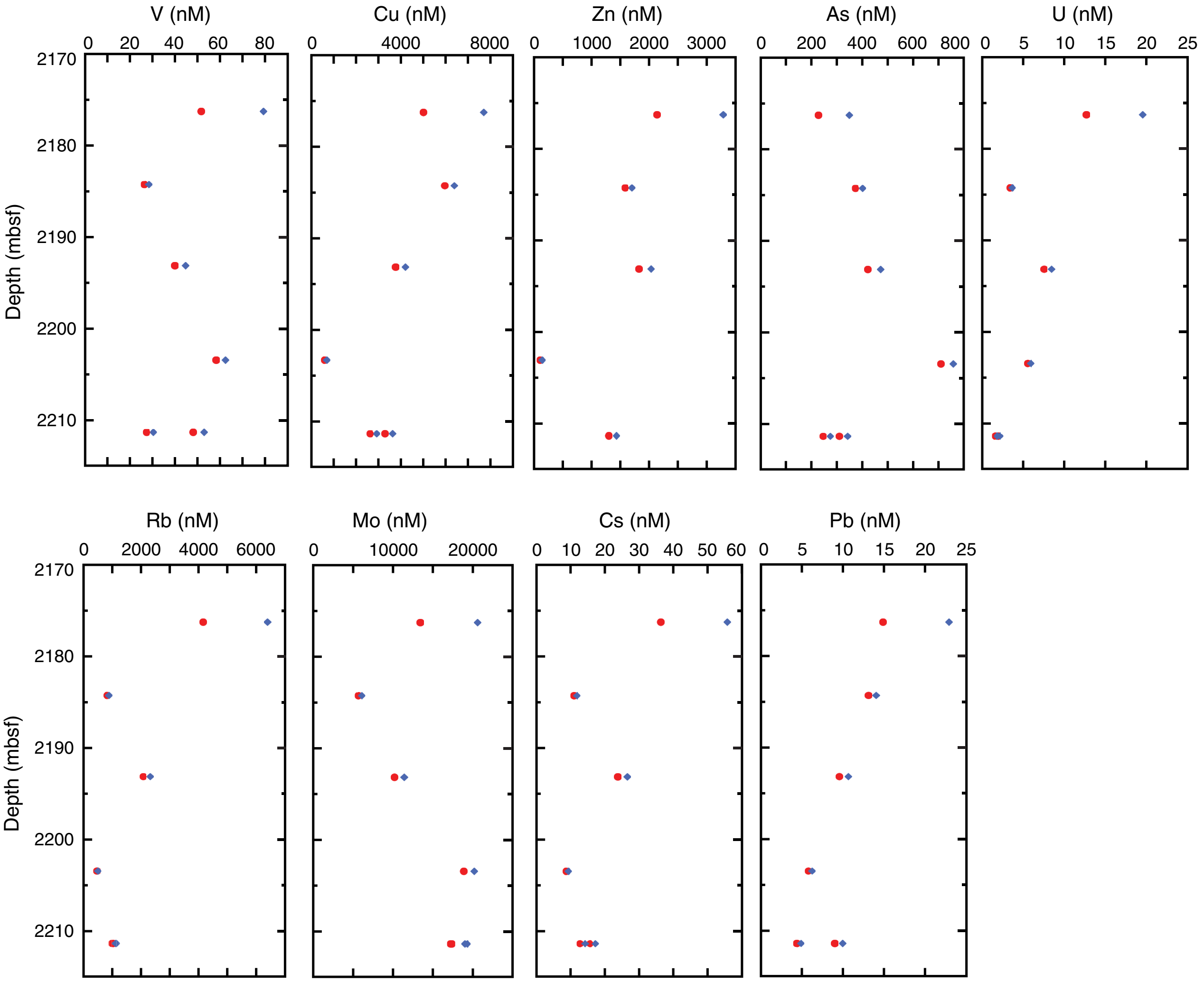

Figure F63. Carbonate ($CaCO_3$), total organic carbon (TOC), and total nitrogen (TN) data, Holes C0002N and C0002P.

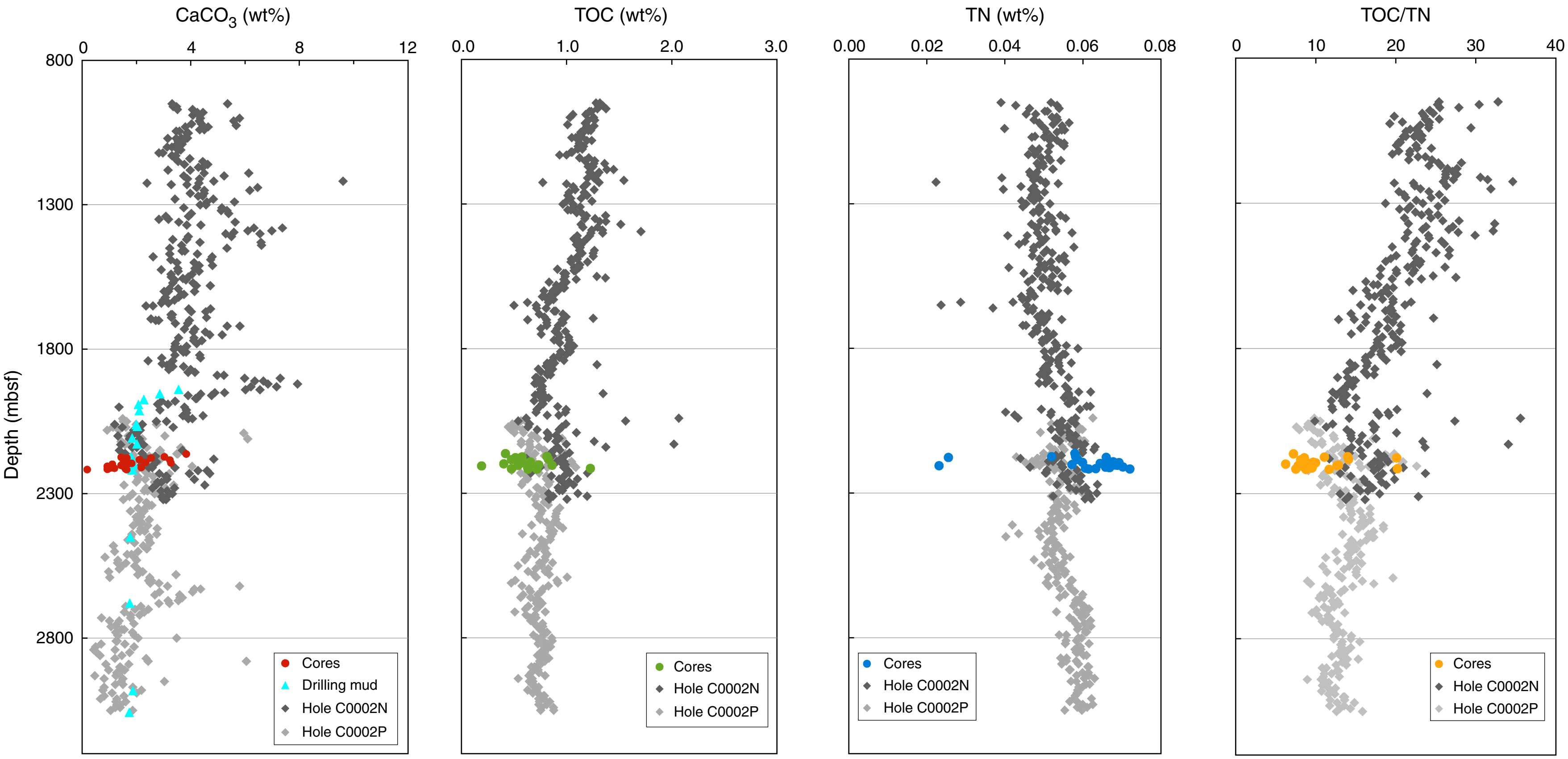

Figure F64. Vertical profiles of methane (CH_4), ethane (C_2H_6), and propane (C_3H_8) concentrations in headspace gas samples from cores, Hole C0002P.

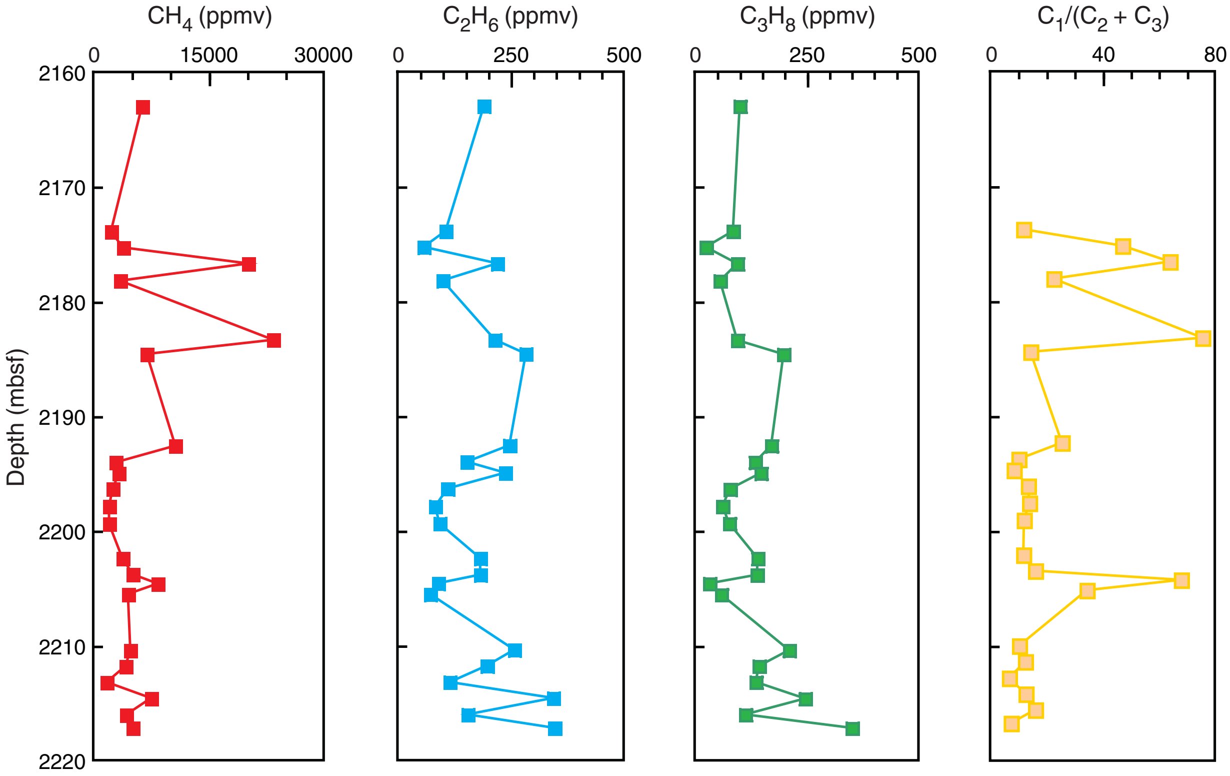

Figure F65. Overview of hydrocarbon gas and total gas concentrations determined by GeoServices, Holes C0002N and C0002P. Triangles = results from the headspace gas analysis on core from Hole C0002P (note change of scale).

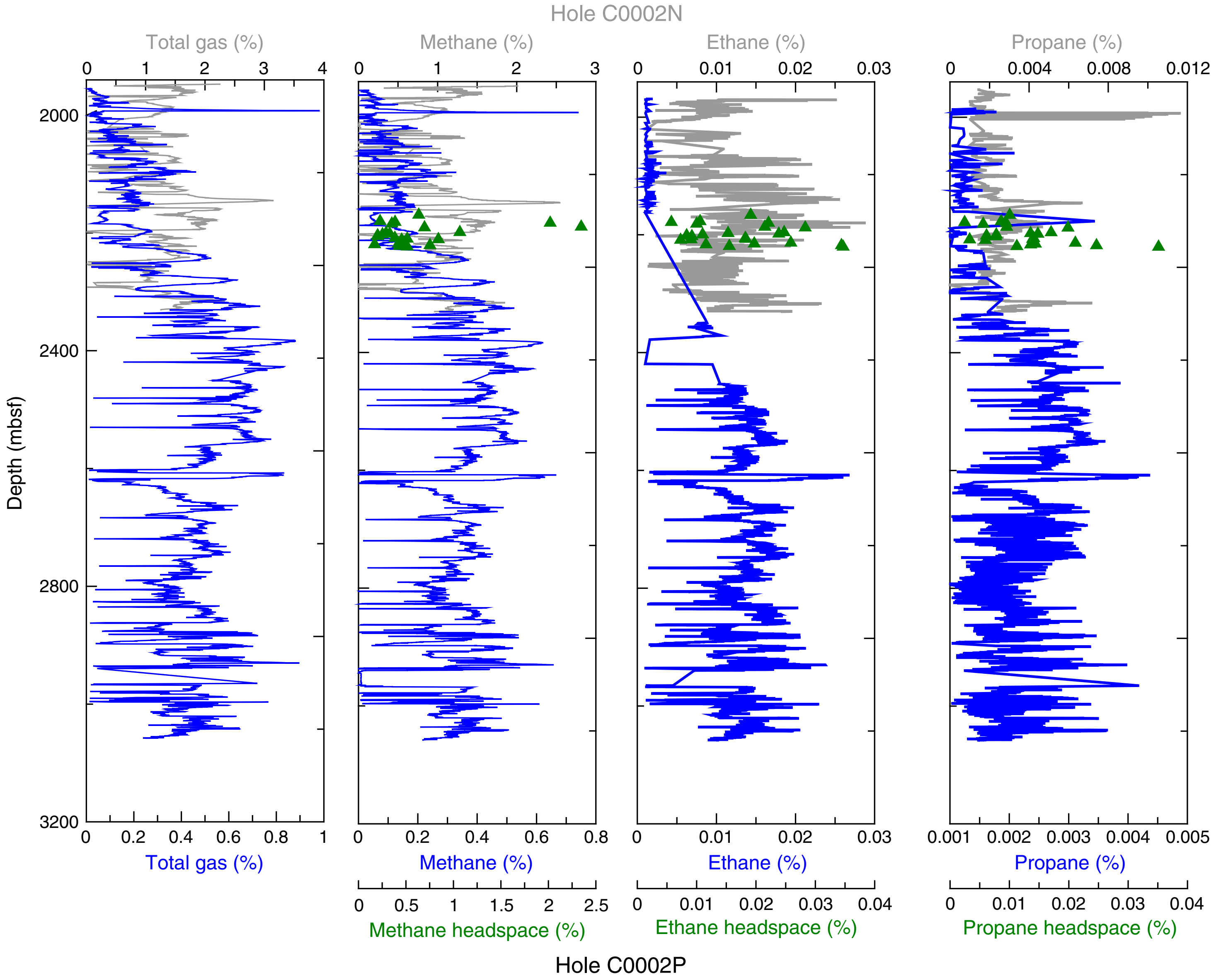

Figure F66. **A.** Bernard parameter from GeoServices and gas chromatograph–natural gas analyzer (GC-NGA) data sets and headspace gas analysis for the cored interval in Hole C0002P. **B.** $\delta^{13}C\text{-}CH_4$ values obtained from the methane carbon isotope analyzer (boundaries after Whiticar, 1994).

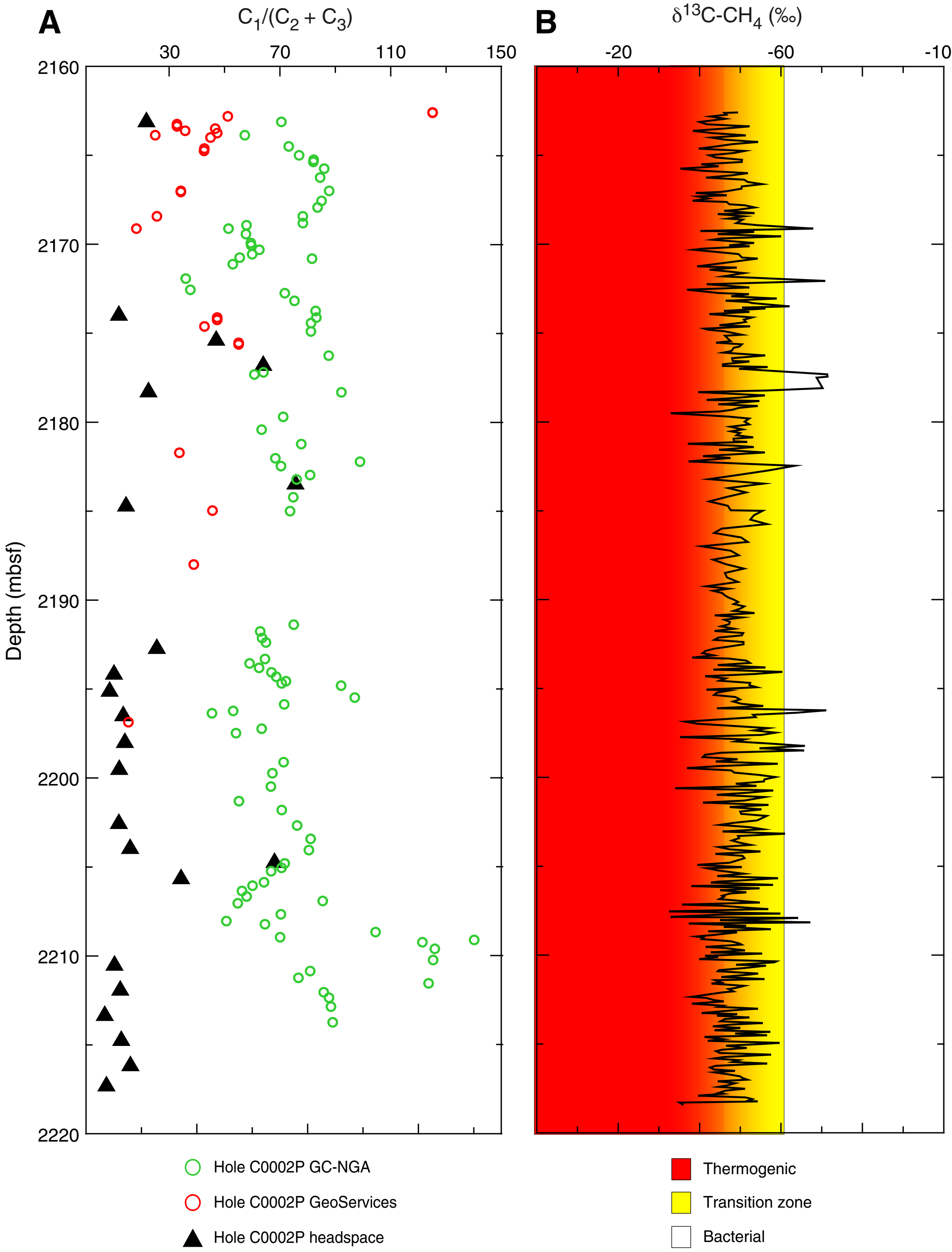

Figure F67. Bernard parameter vs. $\delta^{13}C\text{-}CH_4$ values plotted in a Bernard diagram (modified from Bernard et al., 1978; Whiticar, 1994), Holes C0002N and C0002P.

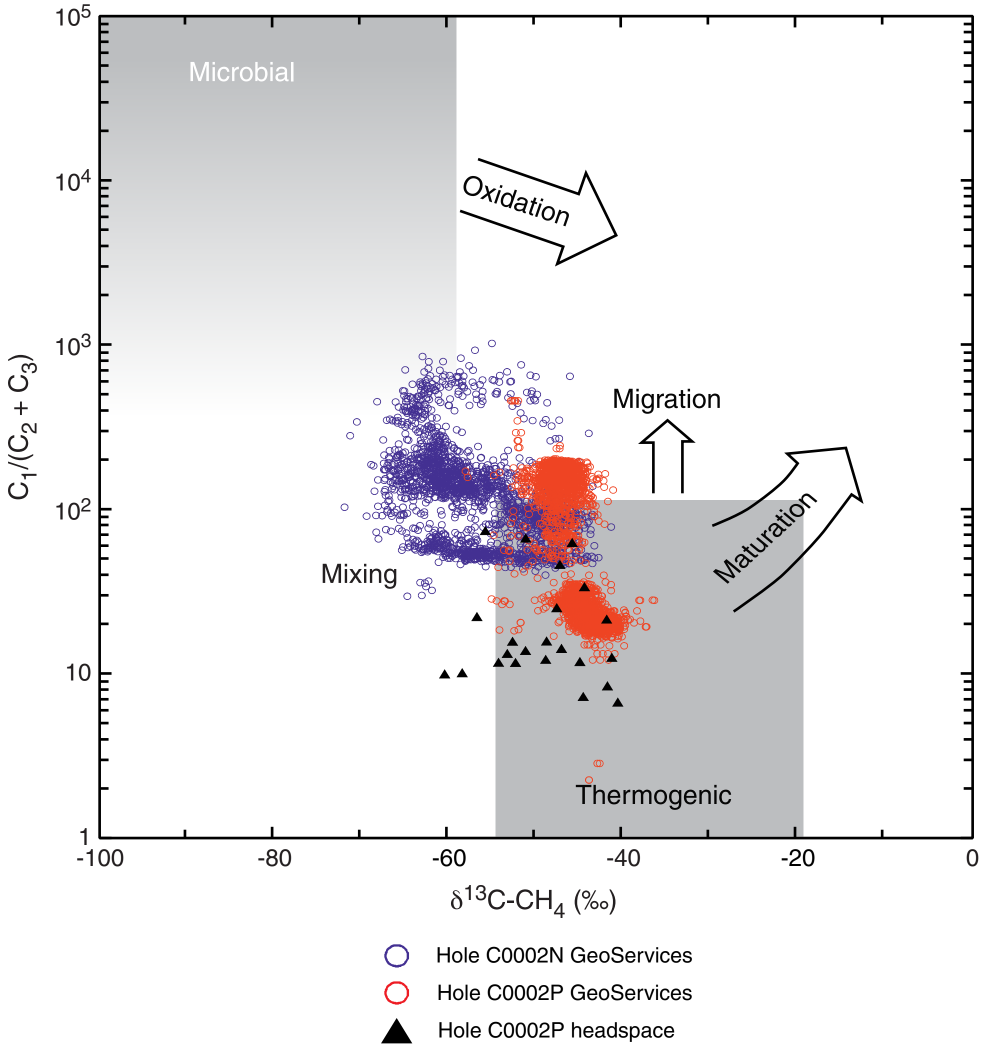

Figure F68. C_2/C_1 ratios plotted against $\delta^{13}C\text{-}CH_4$ for the cored interval in Hole C0002P to qualitatively elucidate possible diffusion fractionation vs. mixing of gases from different sources (after Prinzhofer and Pernaton, 1997). C_2/C_1 ratios were determined from headspace gas results and gas chromatograph–natural gas analyzer (GC-NGA) data.

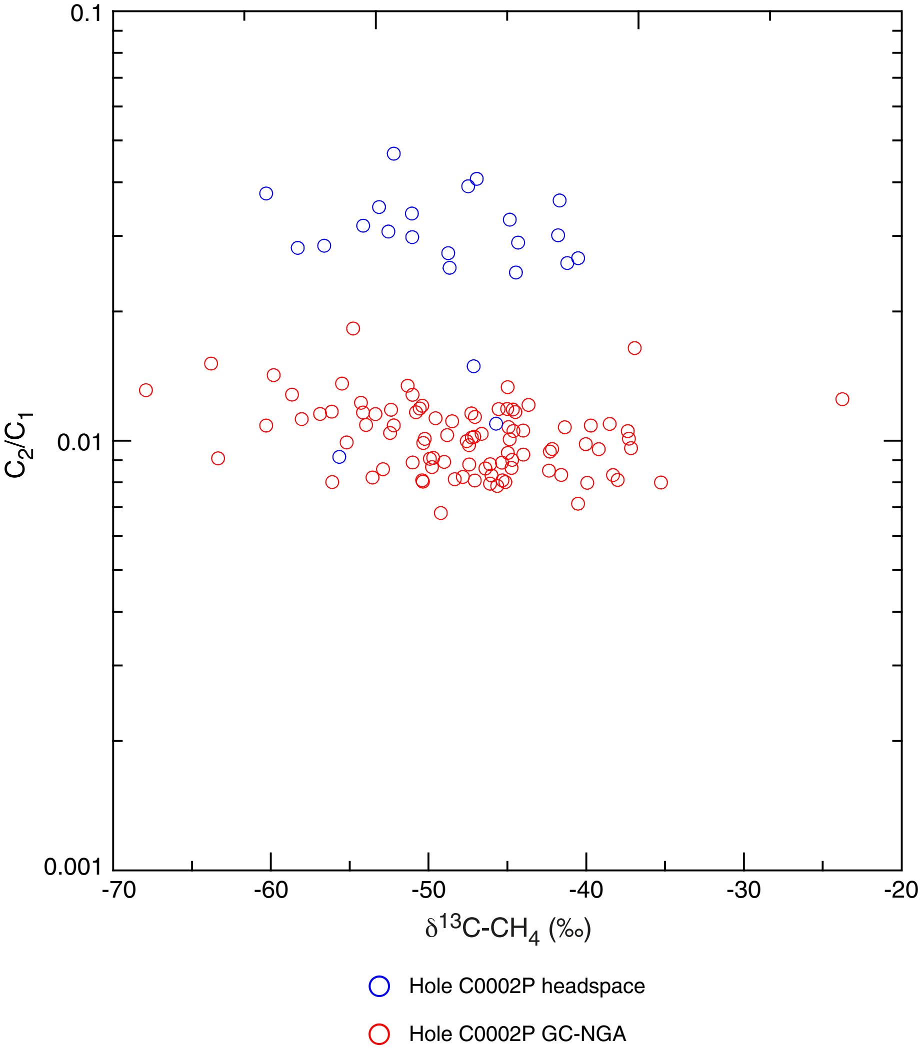

Figure F69. Total gas from headspace gas analysis in Hole C0002P vs. porosity from moisture and density analysis on cores.

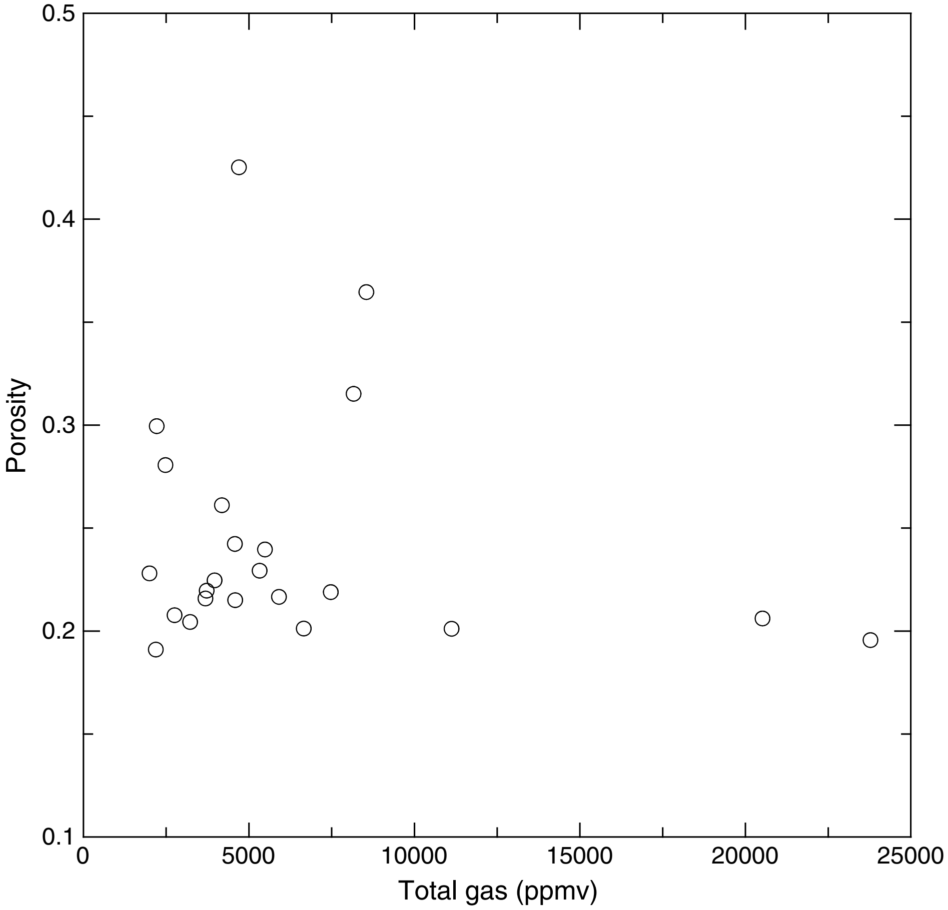

Figure F70. ^{222}Rn data determined during coring and reaming (i.e., hole widening) of Hole C0002P and during drilling of Hole C0002N.

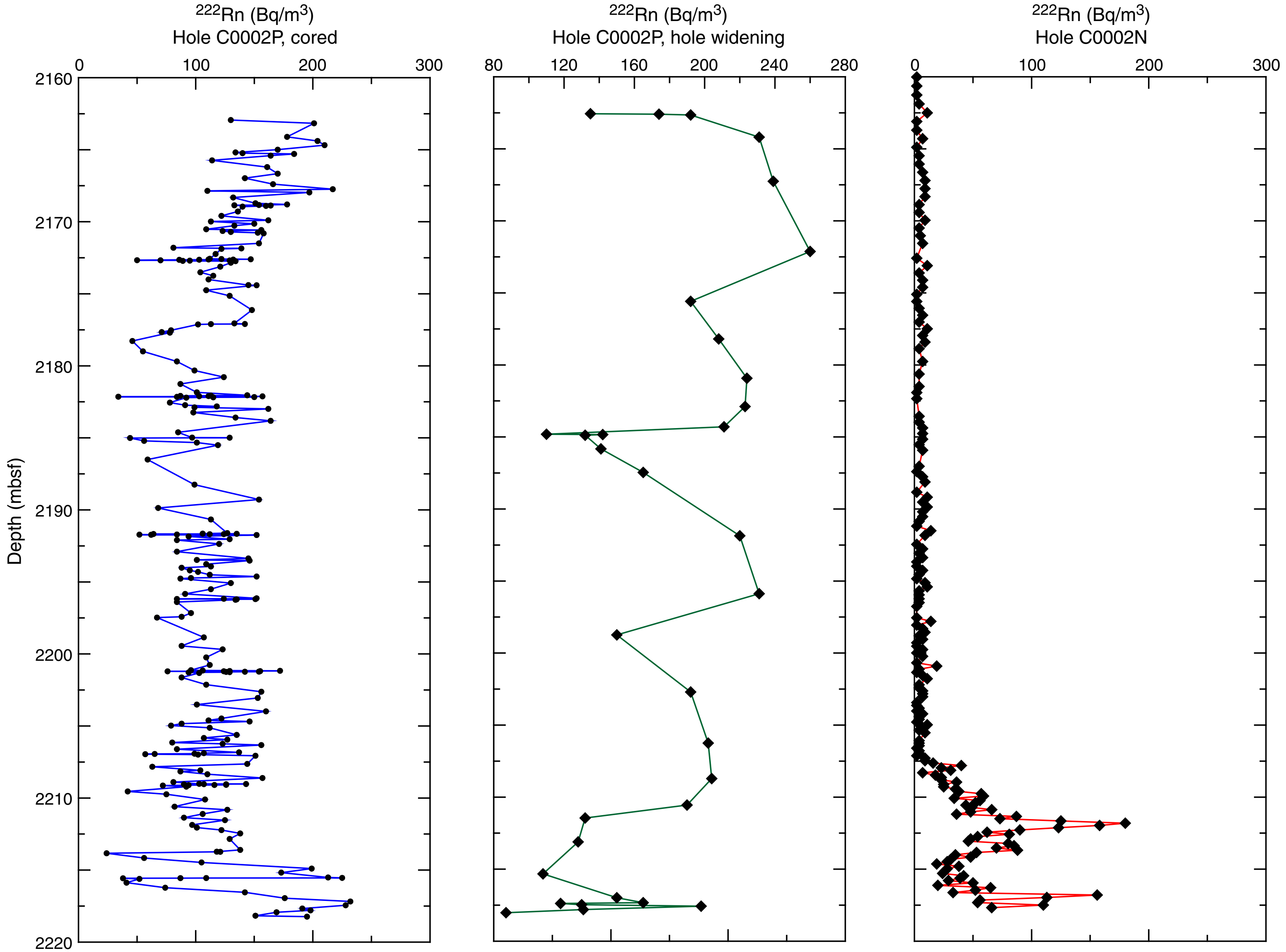

Figure F71. Overview of hydrocarbon gas and total gas concentrations in Hole C0002N as determined by GeoServices compared with data from Hole C0002F.

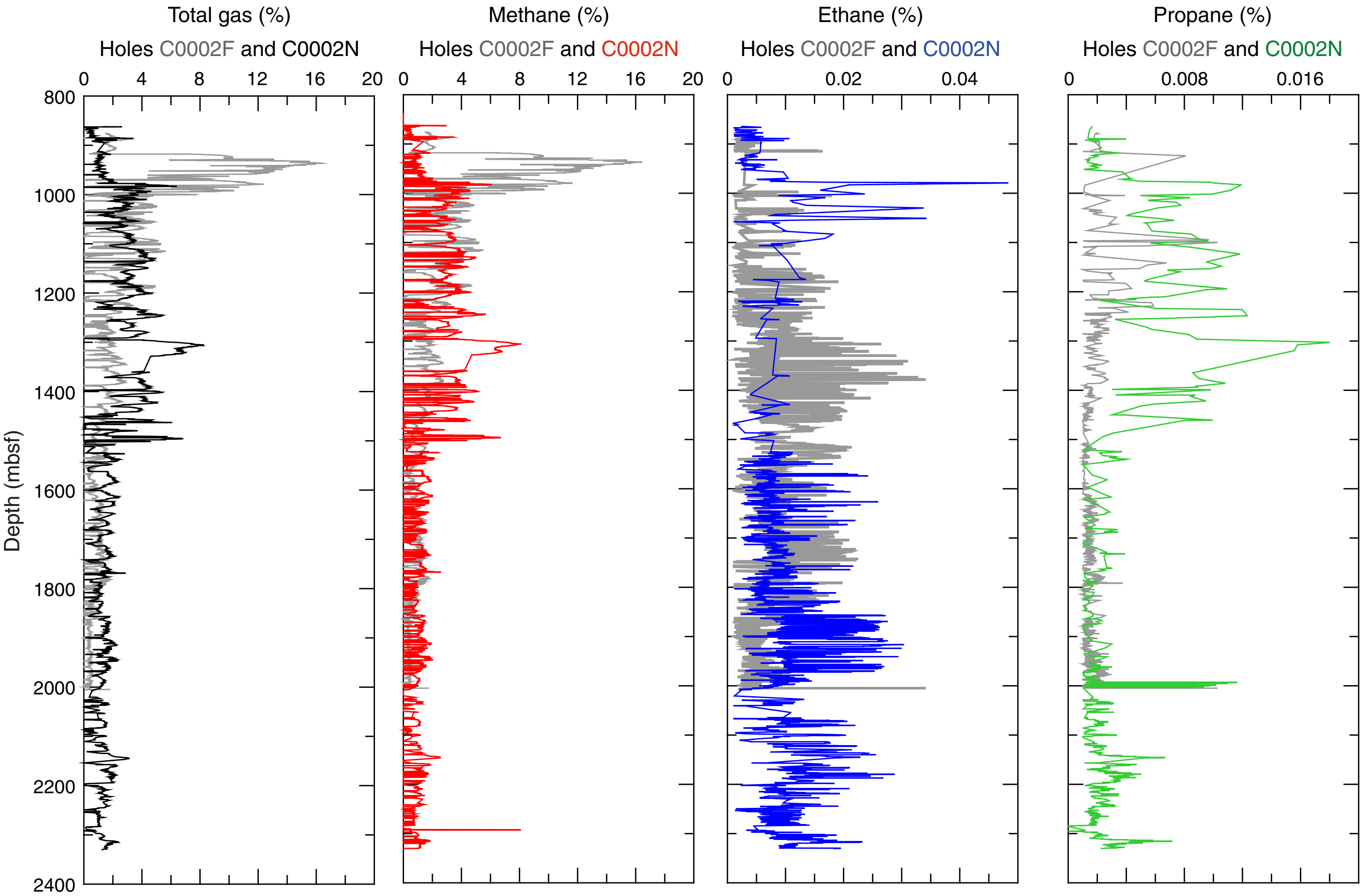

Figure F72. Methane concentrations determined by the GeoServices and SciGas systems, Hole C0002N. MCIA = methane carbon isotope analyzer, PGMS = process gas mass spectrometer, GC-NGA = gas chromatograph–natural gas analyzer.

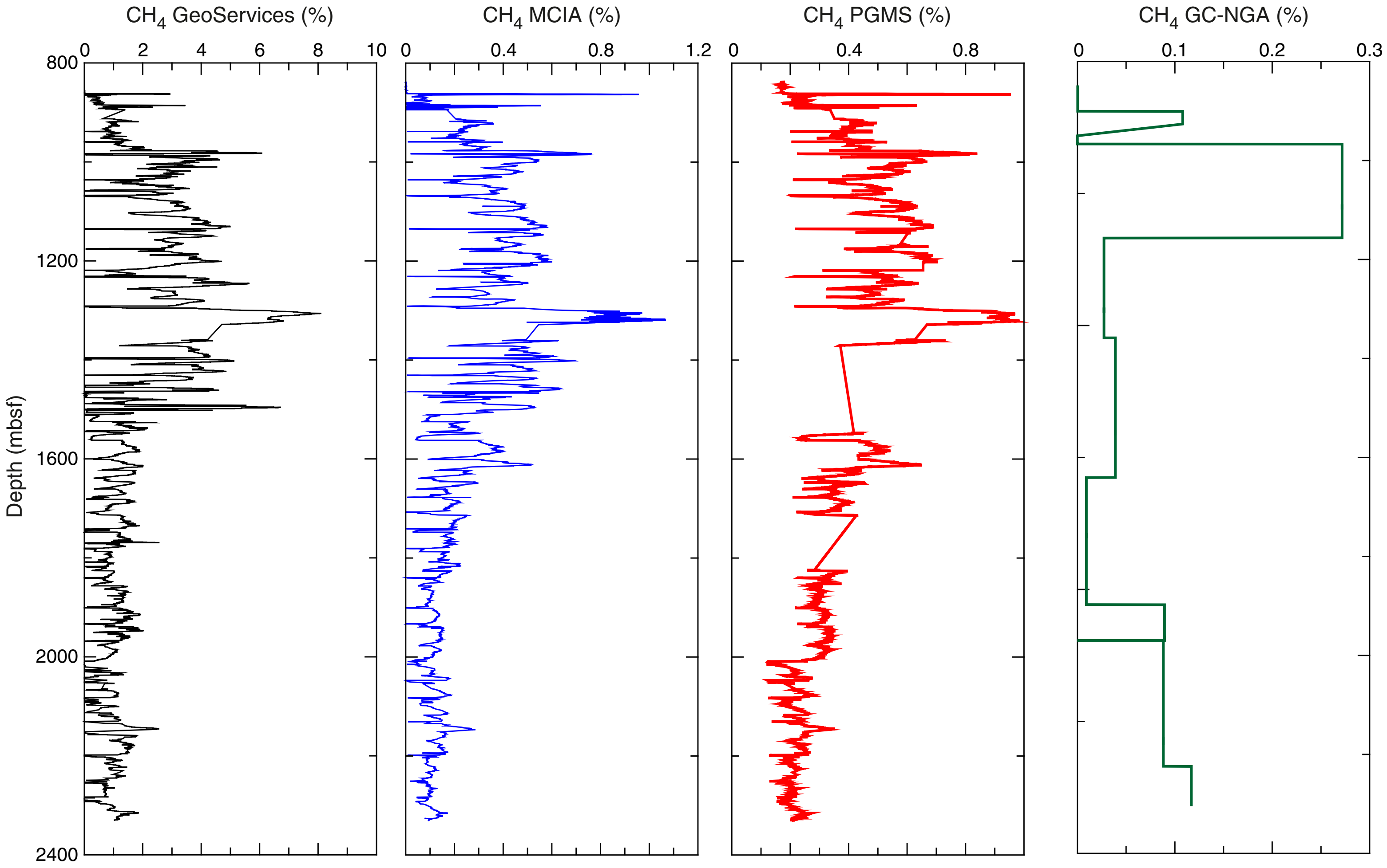

Figure F73. Ethane and propane data determined by gas chromatograph–natural gas analyzer (GC-NGA) from the SciGas system and the data set provided by GeoServices, Hole C0002N.

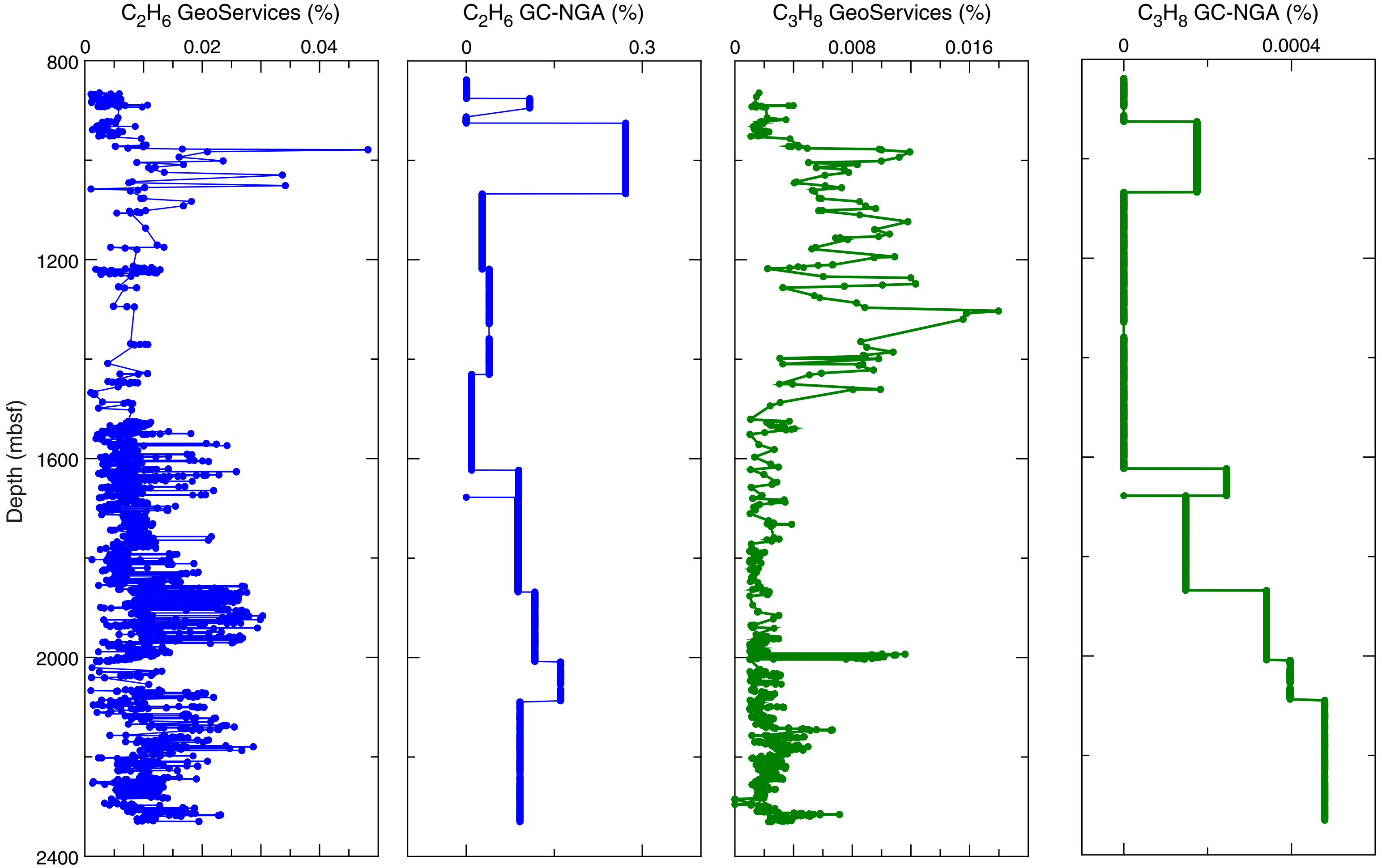

Figure F74. Methane concentrations determined by different measurement techniques from the onboard SciGas system, Holes C0002N and C0002P. MCIA = methane carbon isotope analyzer, PGMS = process gas mass spectrometer, GC-NGA = gas chromatograph–natural gas analyzer.

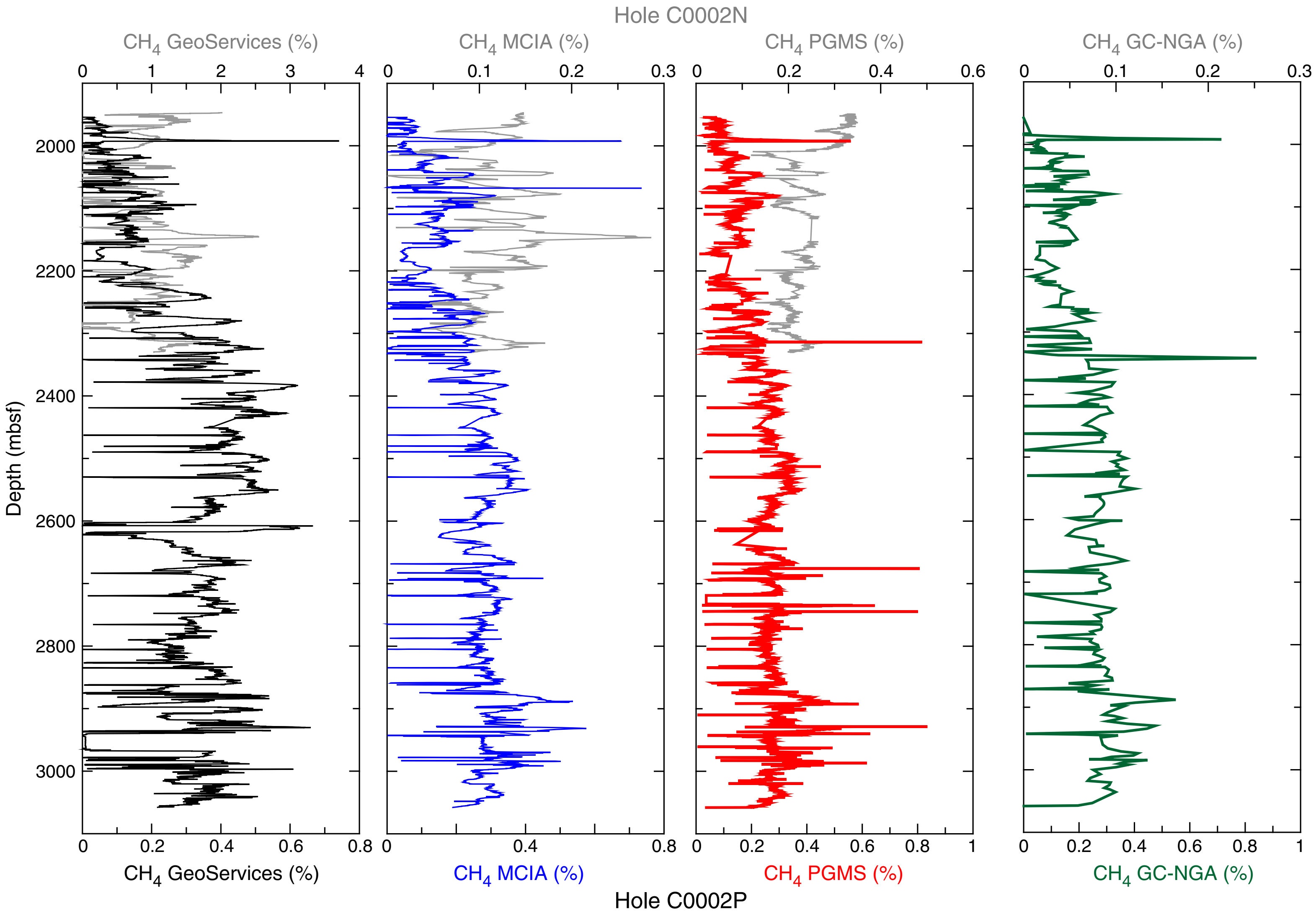

Figure F75. Ethane and propane data determined by gas chromatograph–natural gas analyzer (GC-NGA) from the SciGas system and the data set provided by GeoServices, Holes C0002N and C0002P.

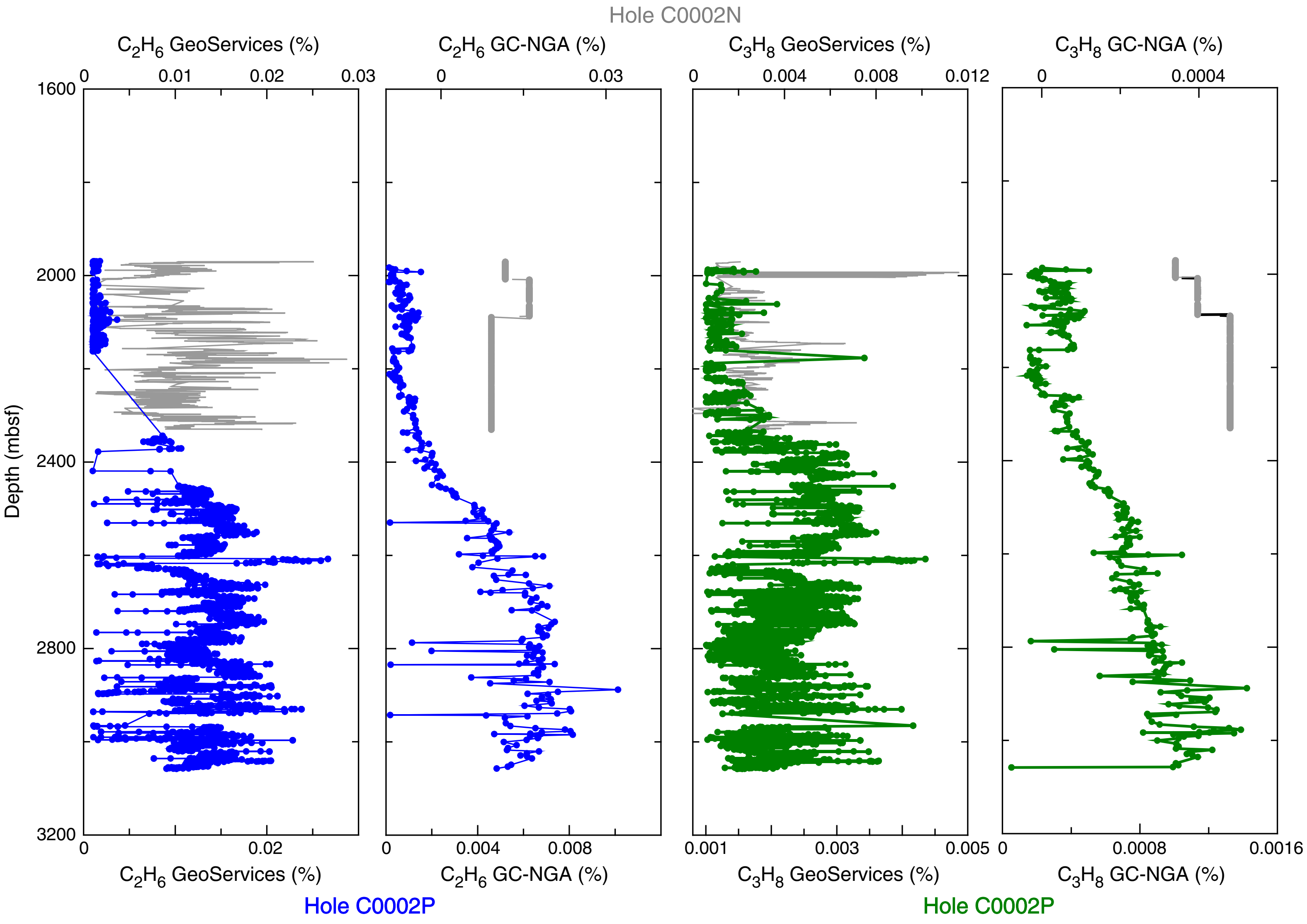

Figure F76. Process gas mass spectrometer data, Holes C0002F, C0002N, and C0002P.

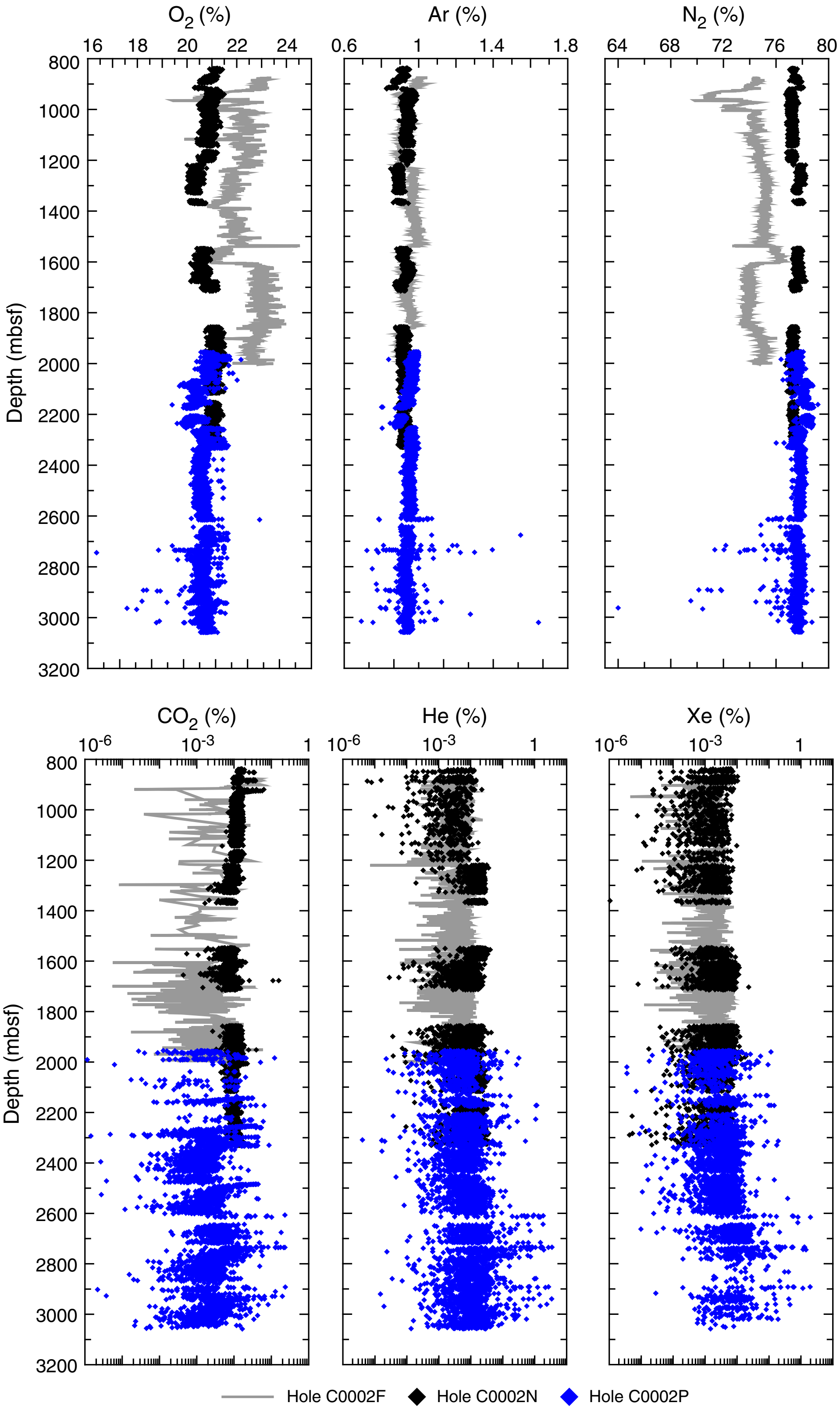

Figure F77. Hydrogen values in drilling mud gas, Hole C0002P.

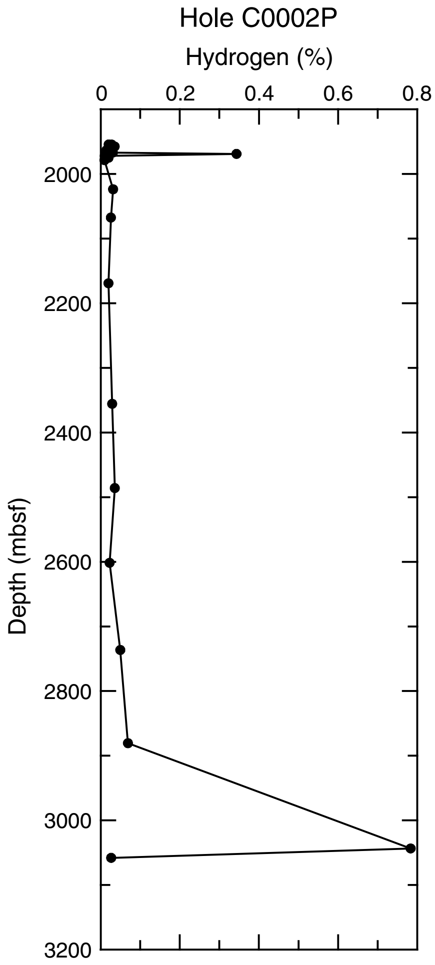

Figure F78. ^{222}Rn data recorded by the stand-alone Rn monitoring instrument for Holes C0002F, C0002N, and C0002P.

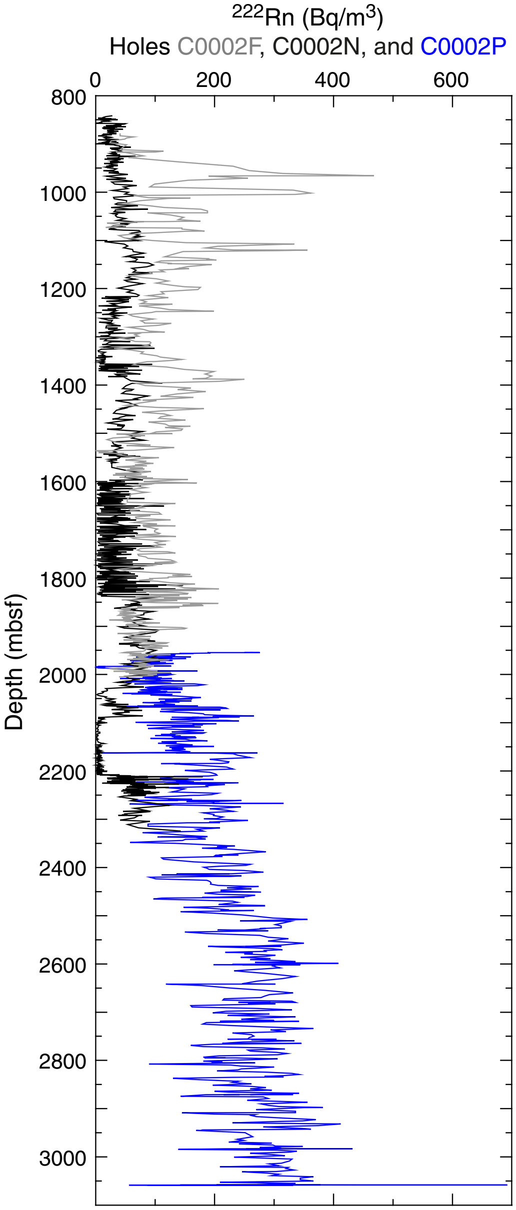

Figure F79. Hydrocarbon gas and total gas concentrations for 1940–2010 mbsf determined by GeoServices, Holes C0002F, C0002N, and C0002P.

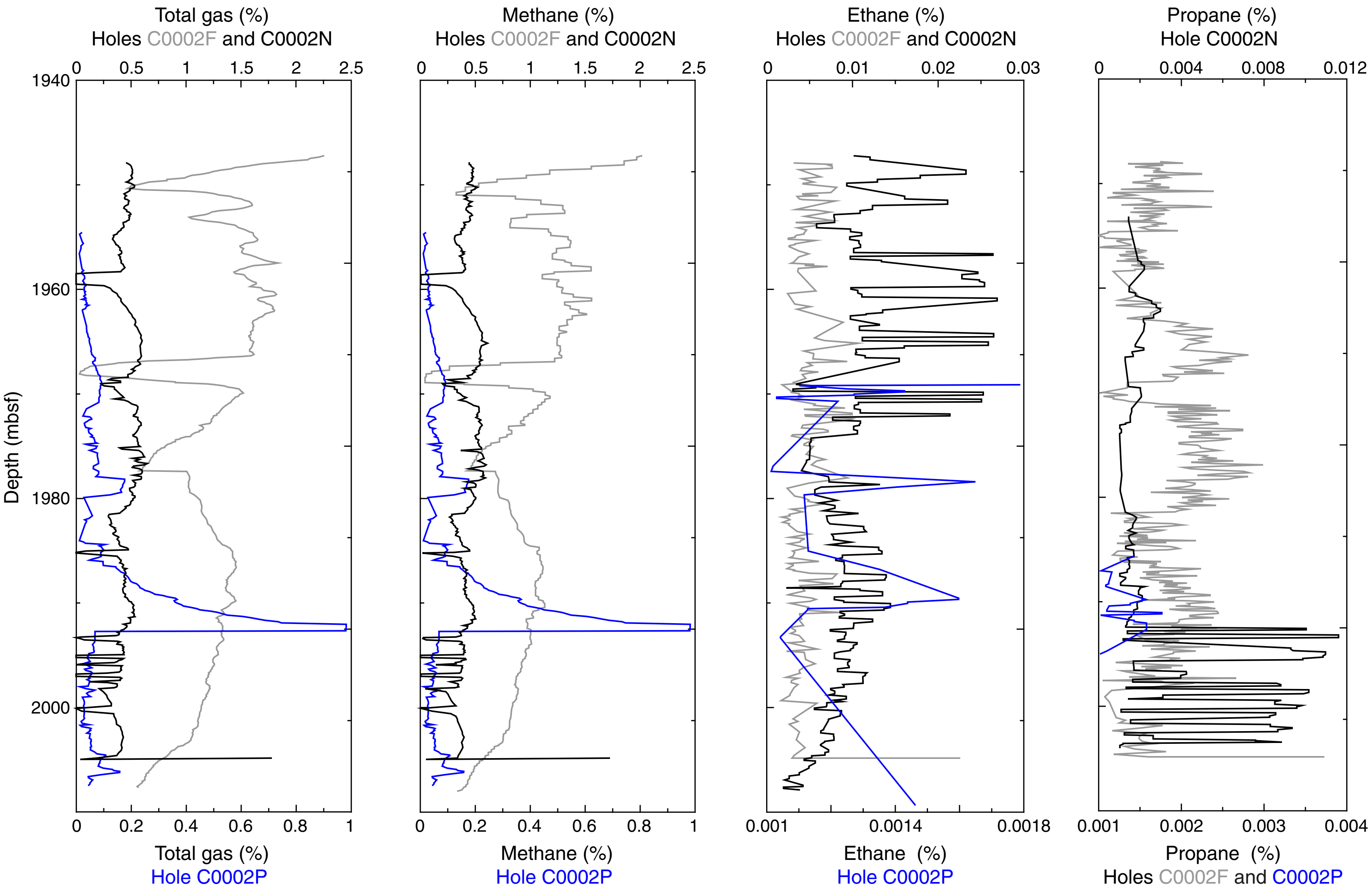

Figure F80. **A.** Bernard parameter from GeoServices and gas chromatograph–natural gas analyzer (GC-NGA) data sets in Holes C0002N and C0002P, as well as from headspace gas analysis from core material from Hole C0002P. **B.** $\delta^{13}C\text{-}CH_4$ values obtained from the methane carbon isotope analyzer in Holes C0002F, C0002N, and C0002P (boundaries after Whiticar, 1994).

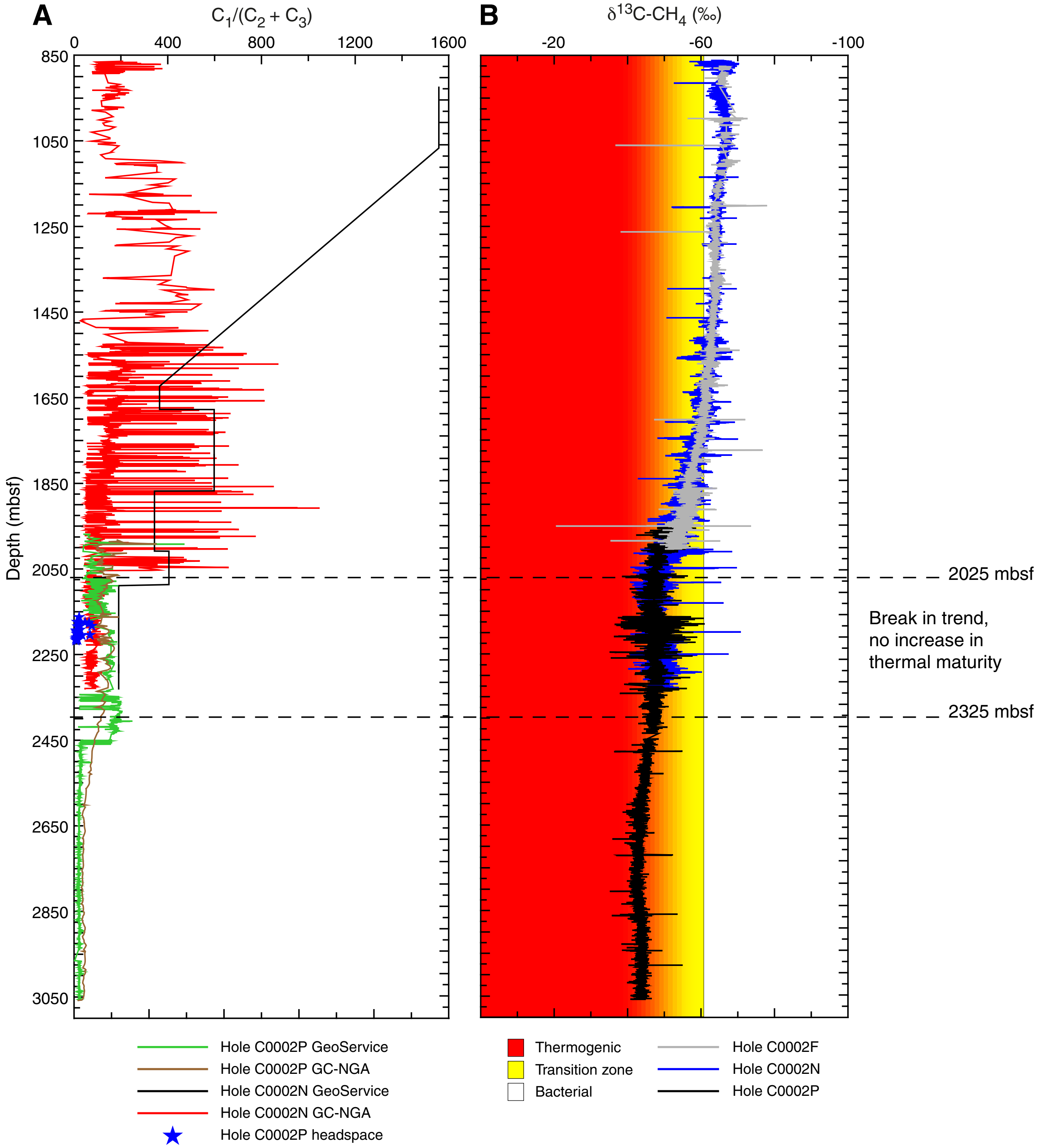

Figure F81. Detail of ^{222}Rn data recorded in the hole overlap zone by the stand-alone Rn monitoring instrument, Holes C0002F, C0002N, and C0002P.

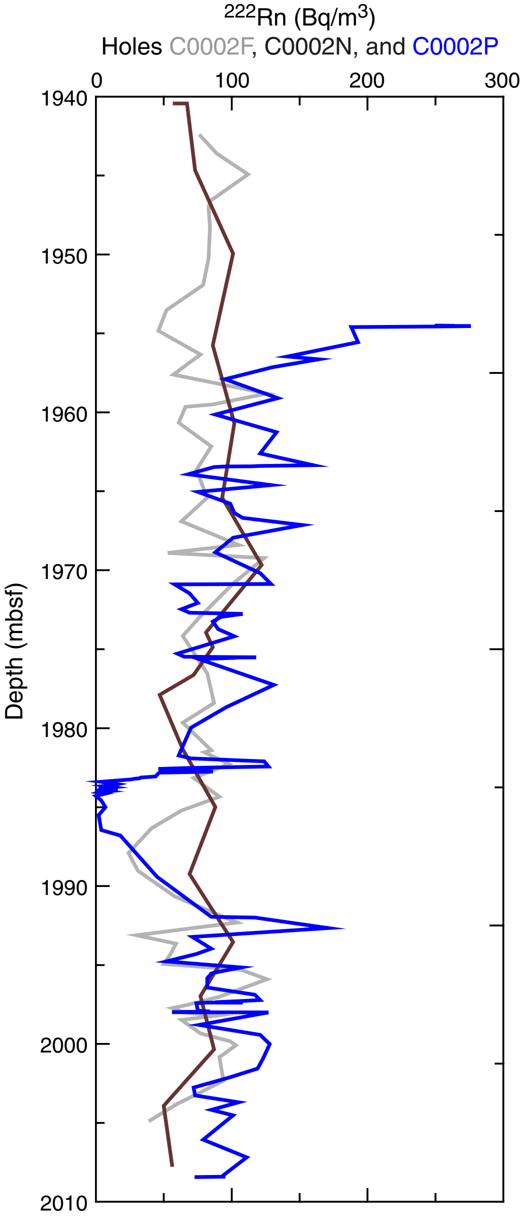

Figure F82. Close-up of process gas mass spectrometer data, Holes C0002F, C0002N, and C0002P.

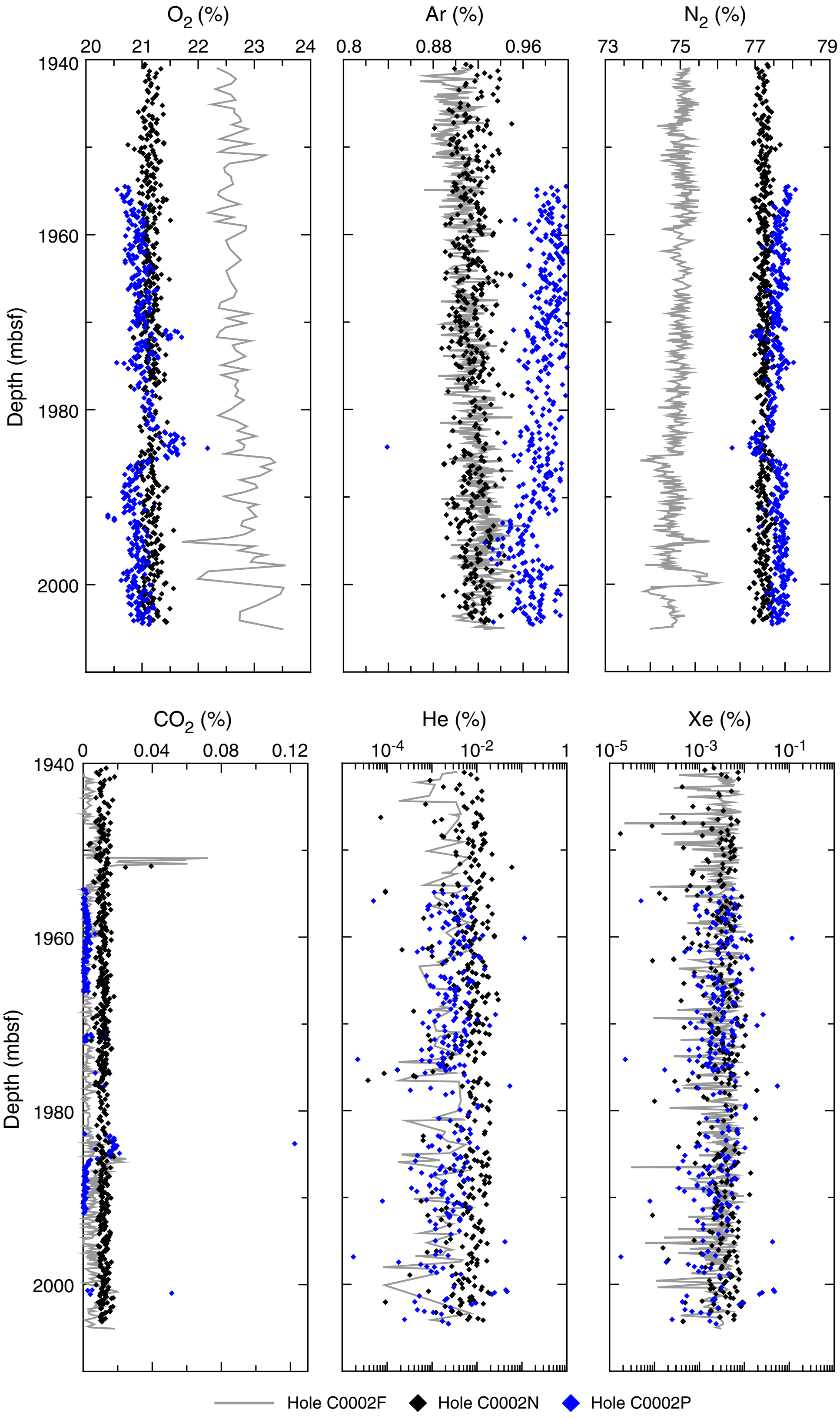

Figure F83. Log unit boundaries correlated with hydrocarbon (HC) gas package boundaries from Holes C0002N and C0002F (Strasser et al., 2014b).

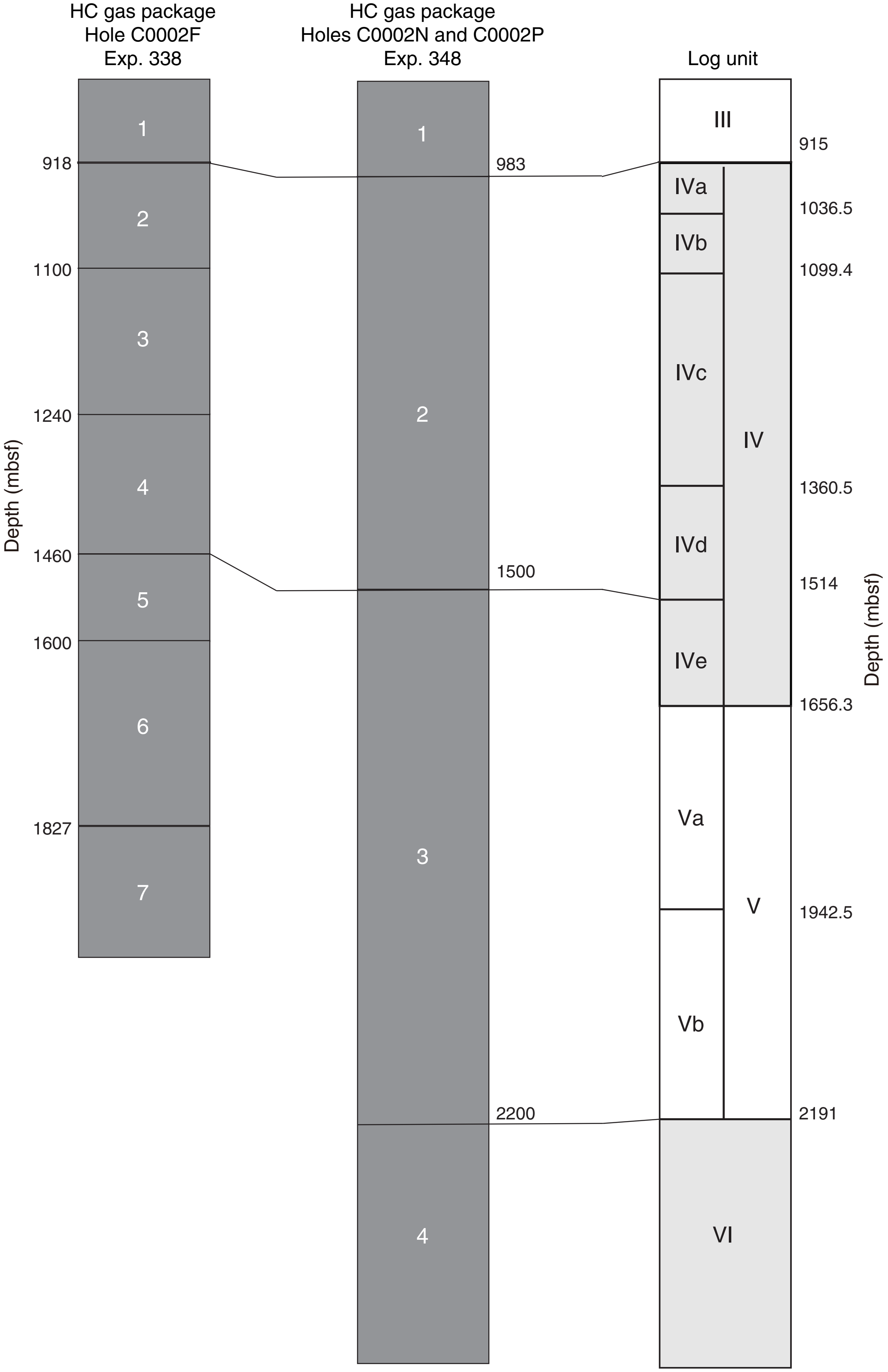

Figure F84. O_2/Ar, N_2/Ar, He/Ar, and Xe/Ar ratios based on the process gas mass spectrometer data set, Holes C0002N and C0002P.

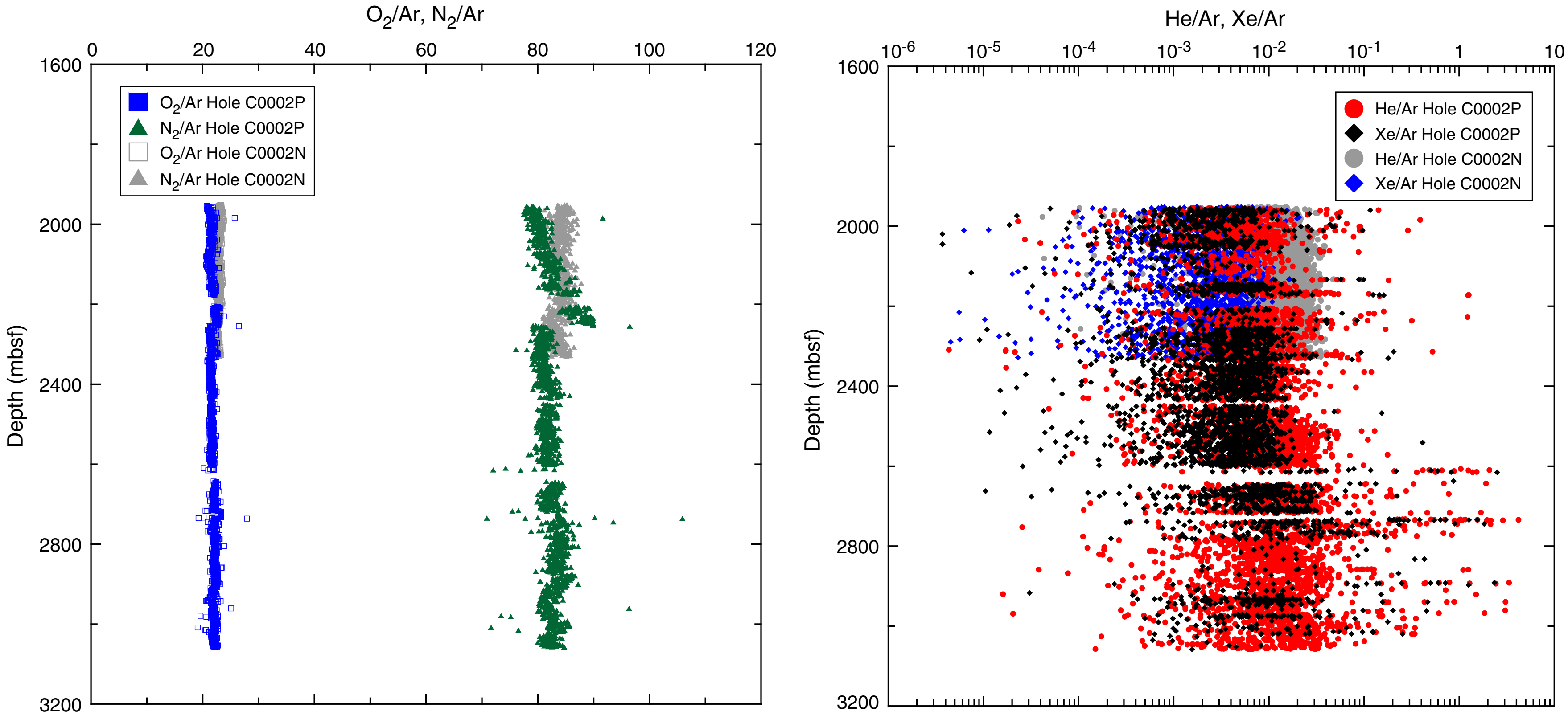

Figure F85. C_2/C_1 ratios plotted against $\delta^{13}C\text{-}CH_4$ to qualitatively elucidate possible diffusion fractionation vs. mixing of gases from different sources (after Prinzhofer and Pernaton, 1997). Data from Holes C0002F (Strasser et al., 2014b) and C0002N. GC-NGA = gas chromatograph–natural gas analyzer.

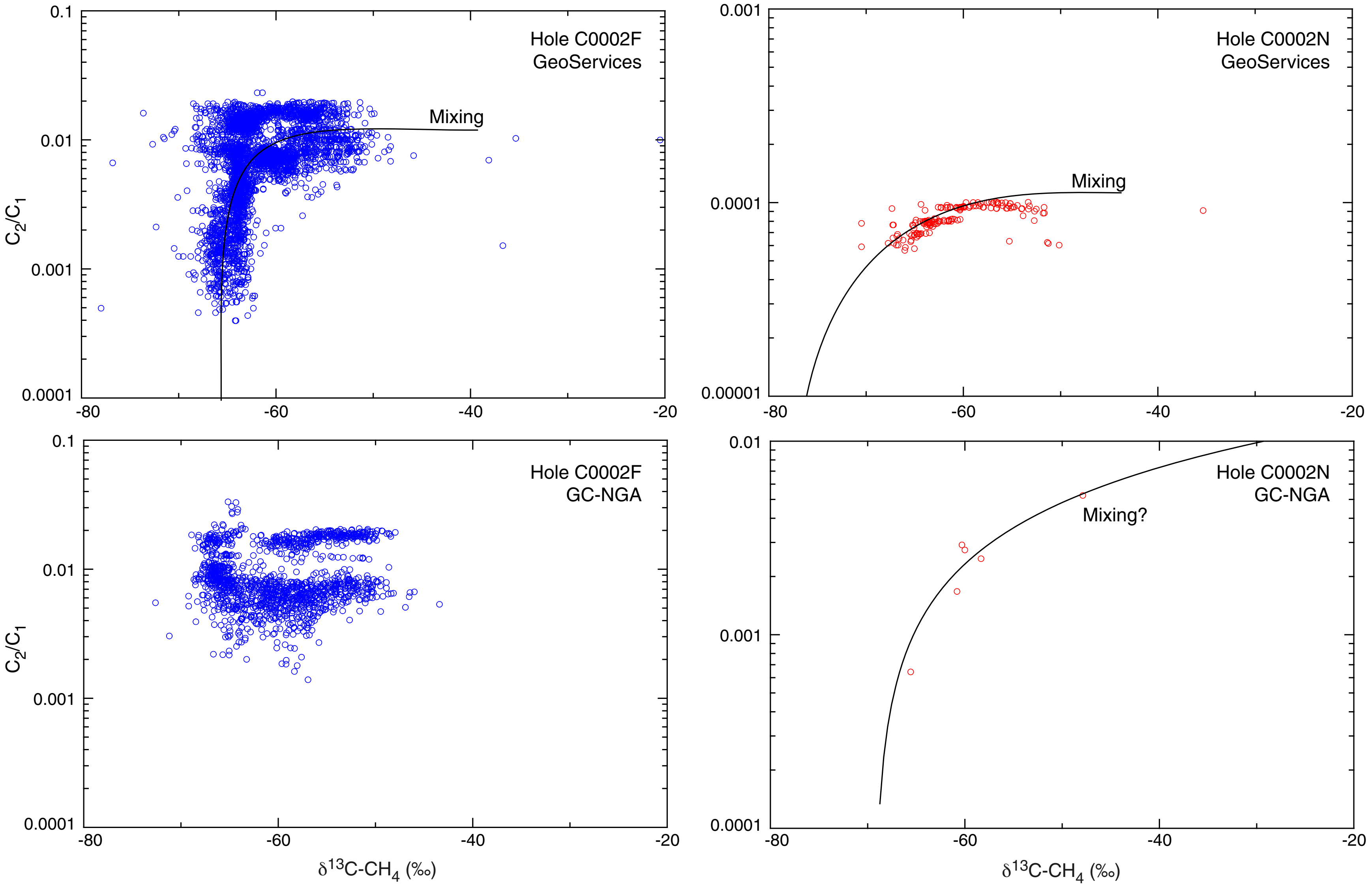

Figure F86. $C_1/(C_2 + C_3)$ ratios, total organic carbon (TOC), and temperature relationship based on Expedition 338 (Strasser et al., 2014b) and 348 data (after Stein et al., 1995).

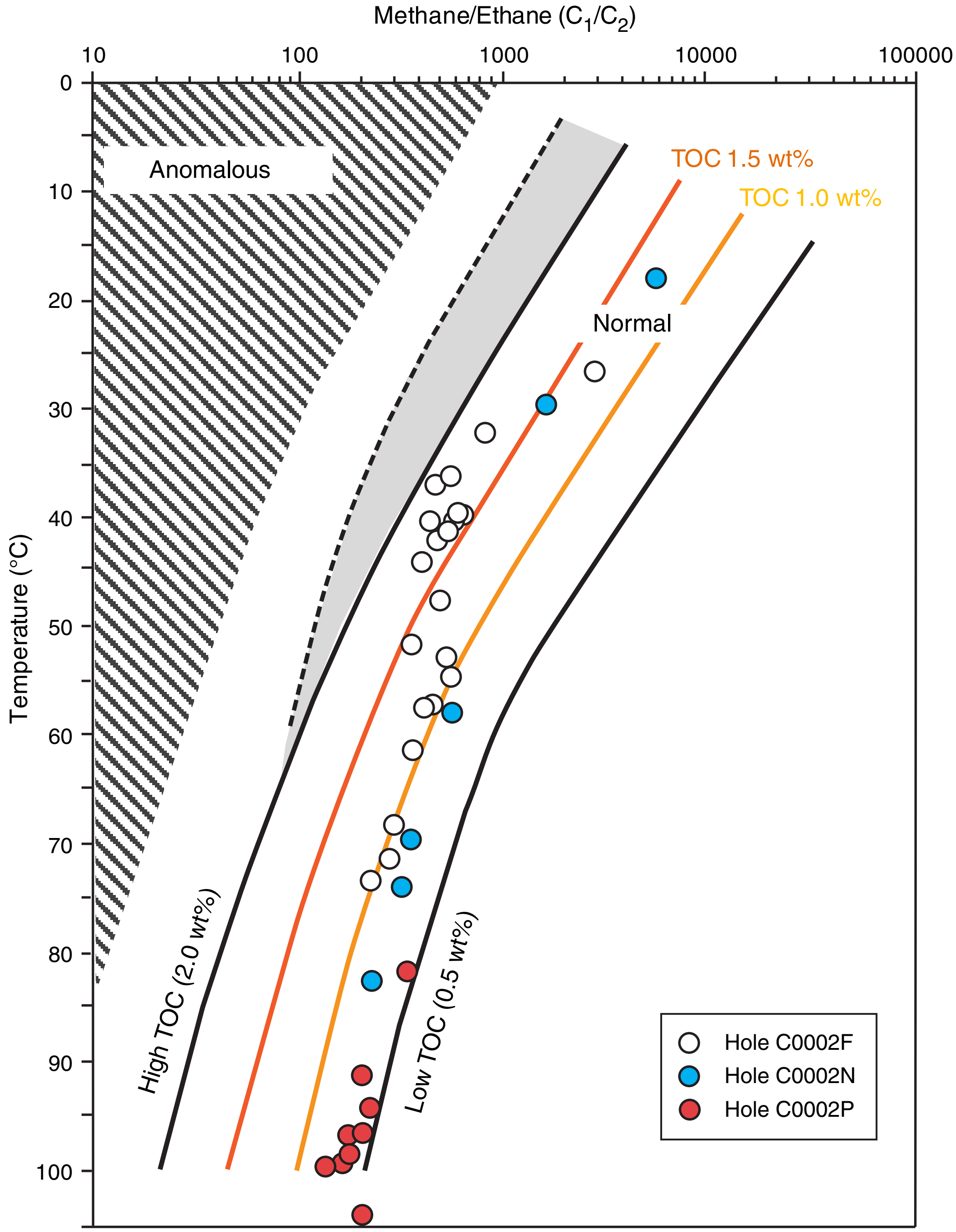

Figure F87. A–C. Moisture and density measurements on 1–4 and >4 mm bulk cuttings, handpicked intact cuttings, drilling-induced cohesive aggregates (DICAs)/pillow cuttings, and caving cuttings, Holes C0002N and C0002P. Porosity is consistently lower and bulk density is consistently higher for the handpicked intact cuttings in comparison with bulk cuttings. The depths of hole cleaning (HC) and waiting on weather (WOW) are indicated by black arrows for Hole C0002N and blue arrows for Hole C0002P. The dashed lines indicate the cored interval.

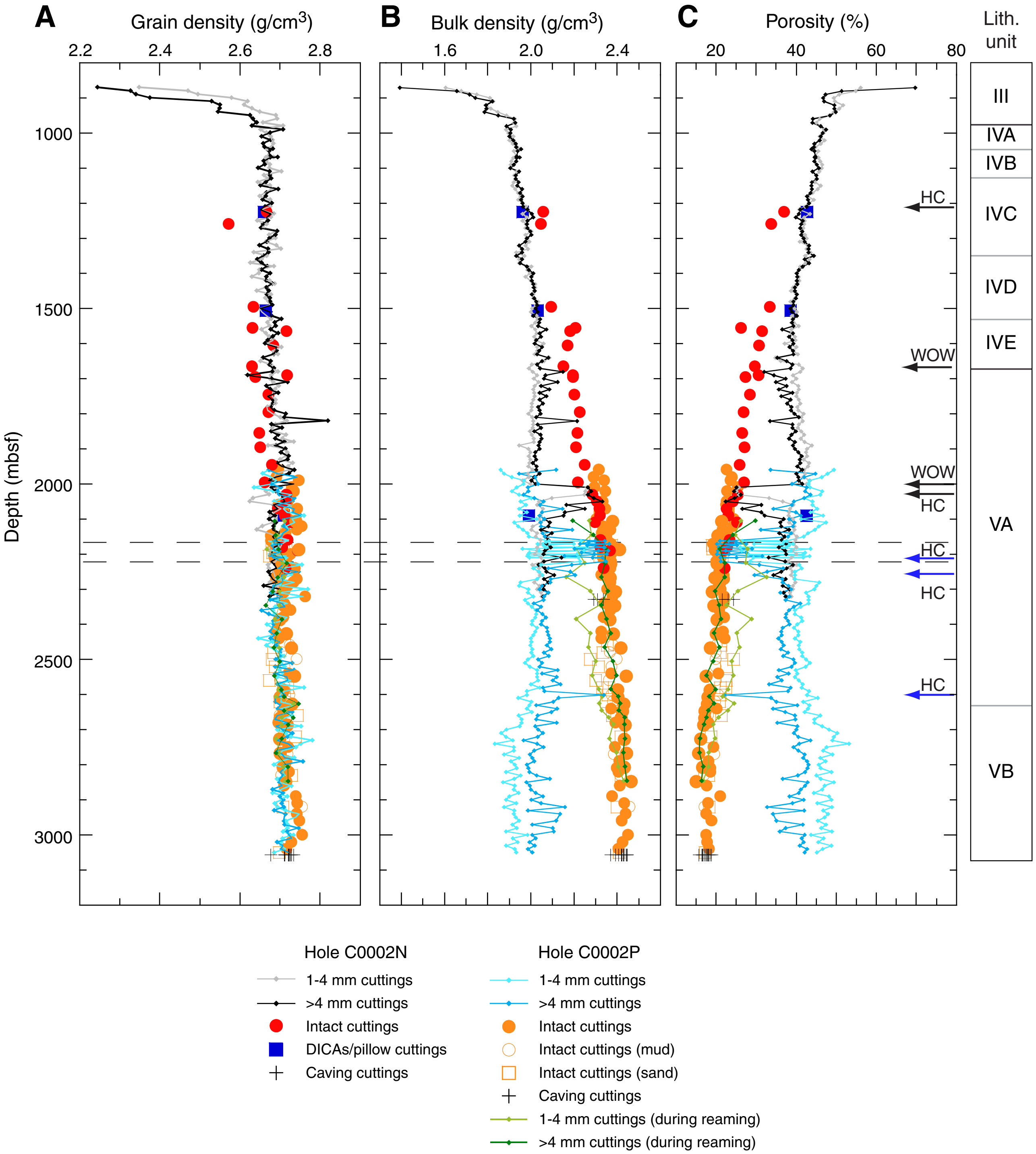

Figure F88. A–C. Selected moisture and density measurements, Holes C0002N and C0002P. The dashed line in C is Athy's porosity-depth model.

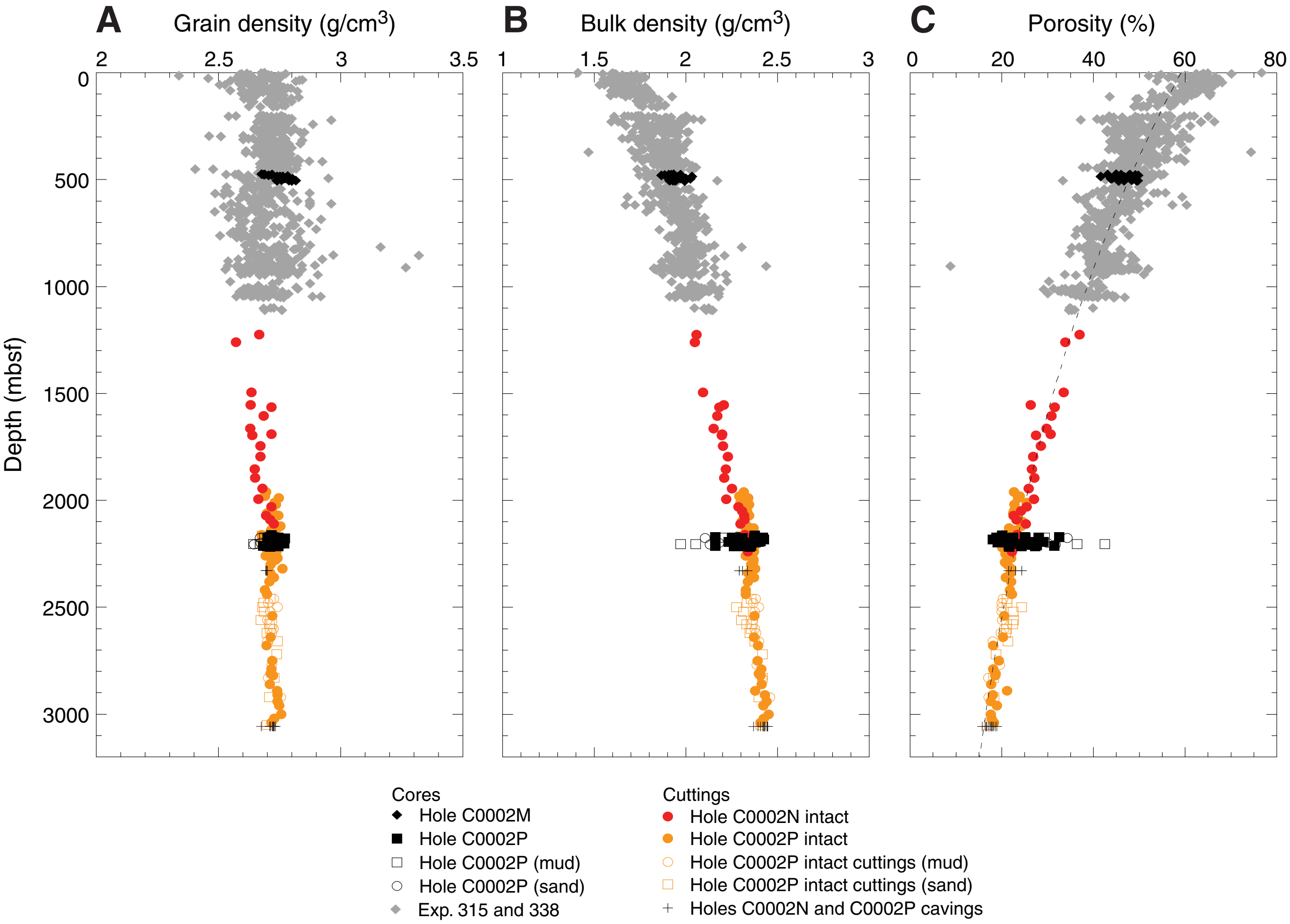

Figure F89. A–D. Porosity for discrete core samples and cuttings, Holes C0002N and C0002P. The dashed line indicates the fault zone at 2205 mbsf.

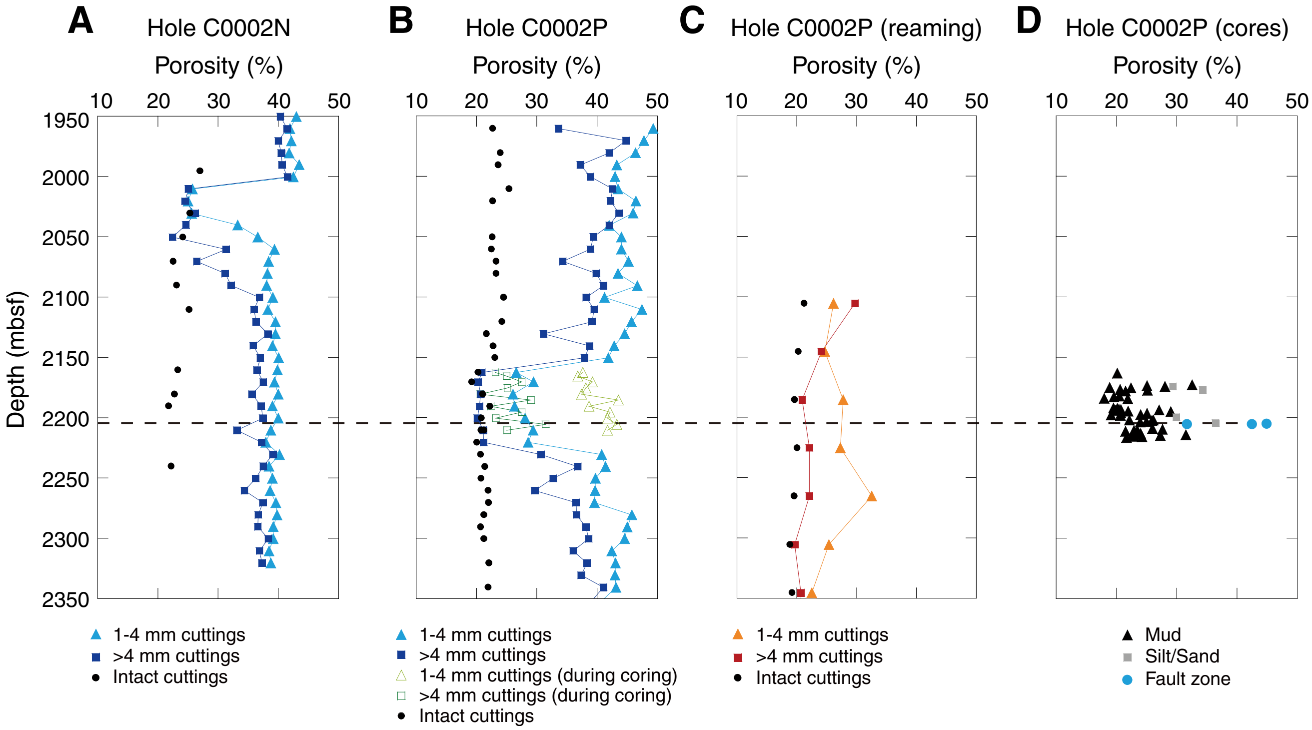

Figure F90. A. Cuttings size vs. cumulative abundance for >4 mm cuttings size samples collected in the 2010.5–2090.5 mbsf interval, Hole C0002N. **B.** Porosity as a function of mean cuttings size, showing a rough correlation with increasing cuttings size and decreasing porosity.

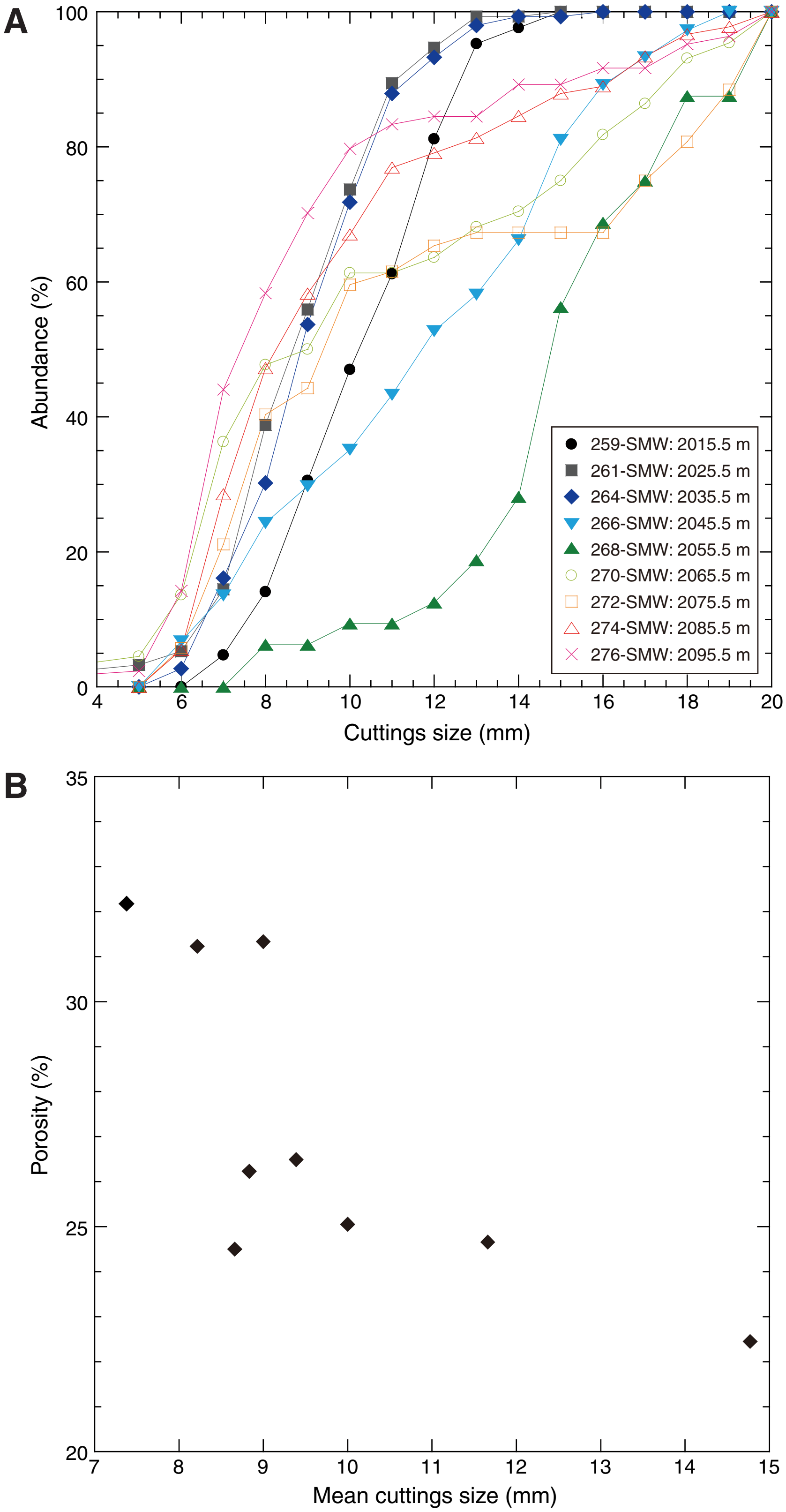

Figure F91. Electrical conductivity on discrete cube samples from (**A**) Holes C0002B and C0002M and (**B**) Hole C0002P.

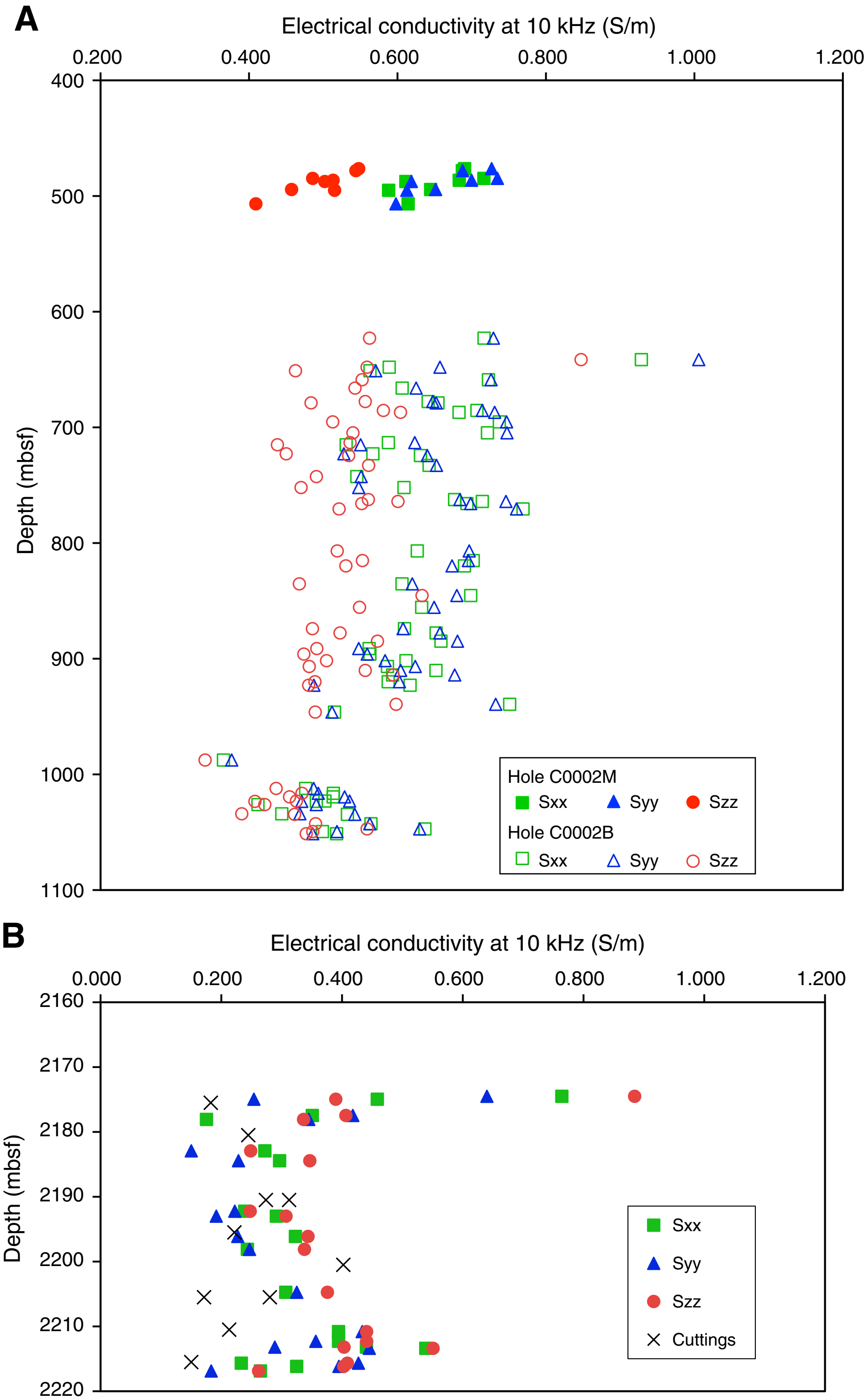

Figure F92. Anisotropy of electrical conductivity on discrete cube samples, Holes C0002B and C0002M.

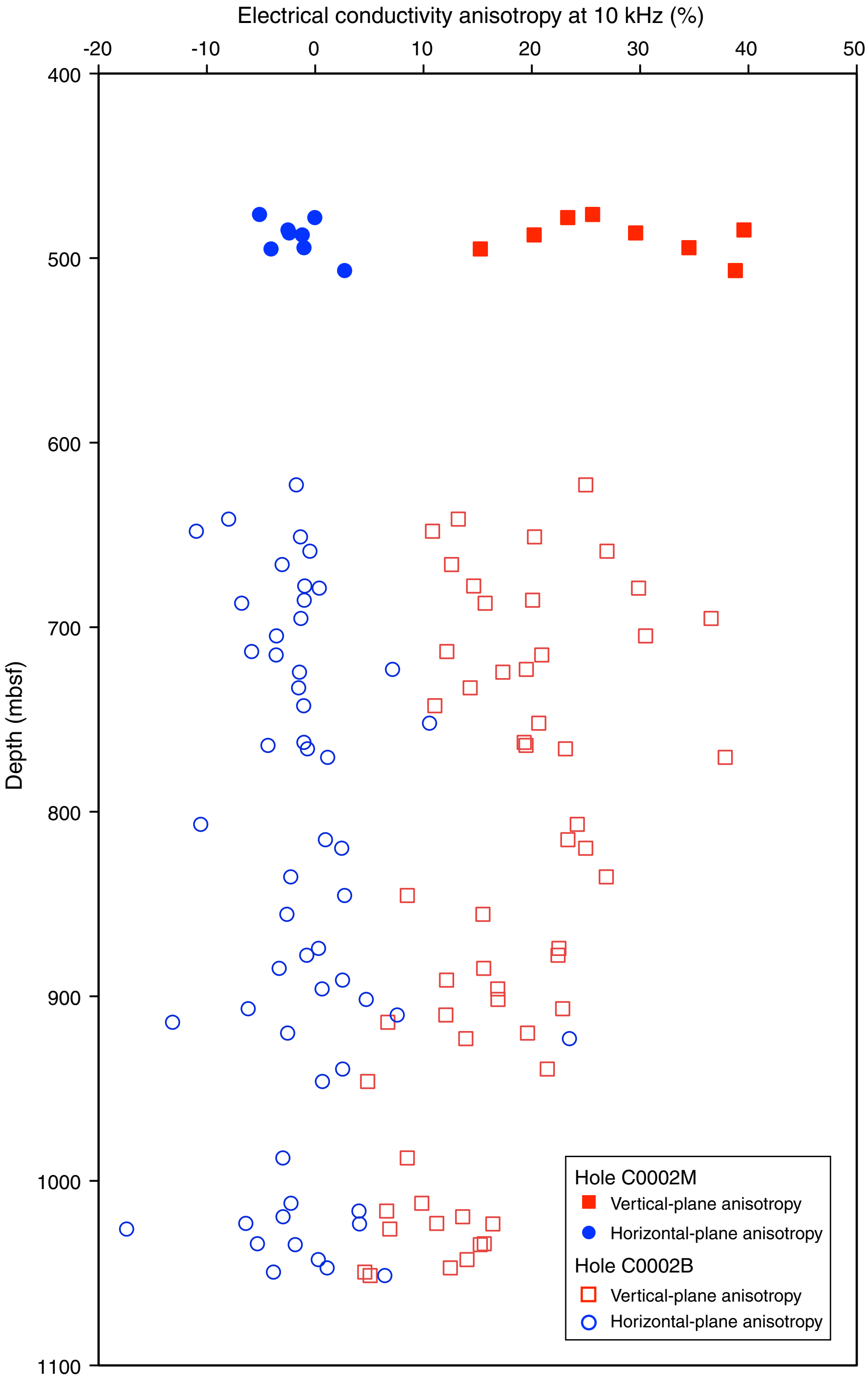

Figure F93. *P*-wave velocity on discrete cube samples from (**A**) Holes C0002B, C0002H, C0002J, and C0002M and (**B**) Hole C0002P.

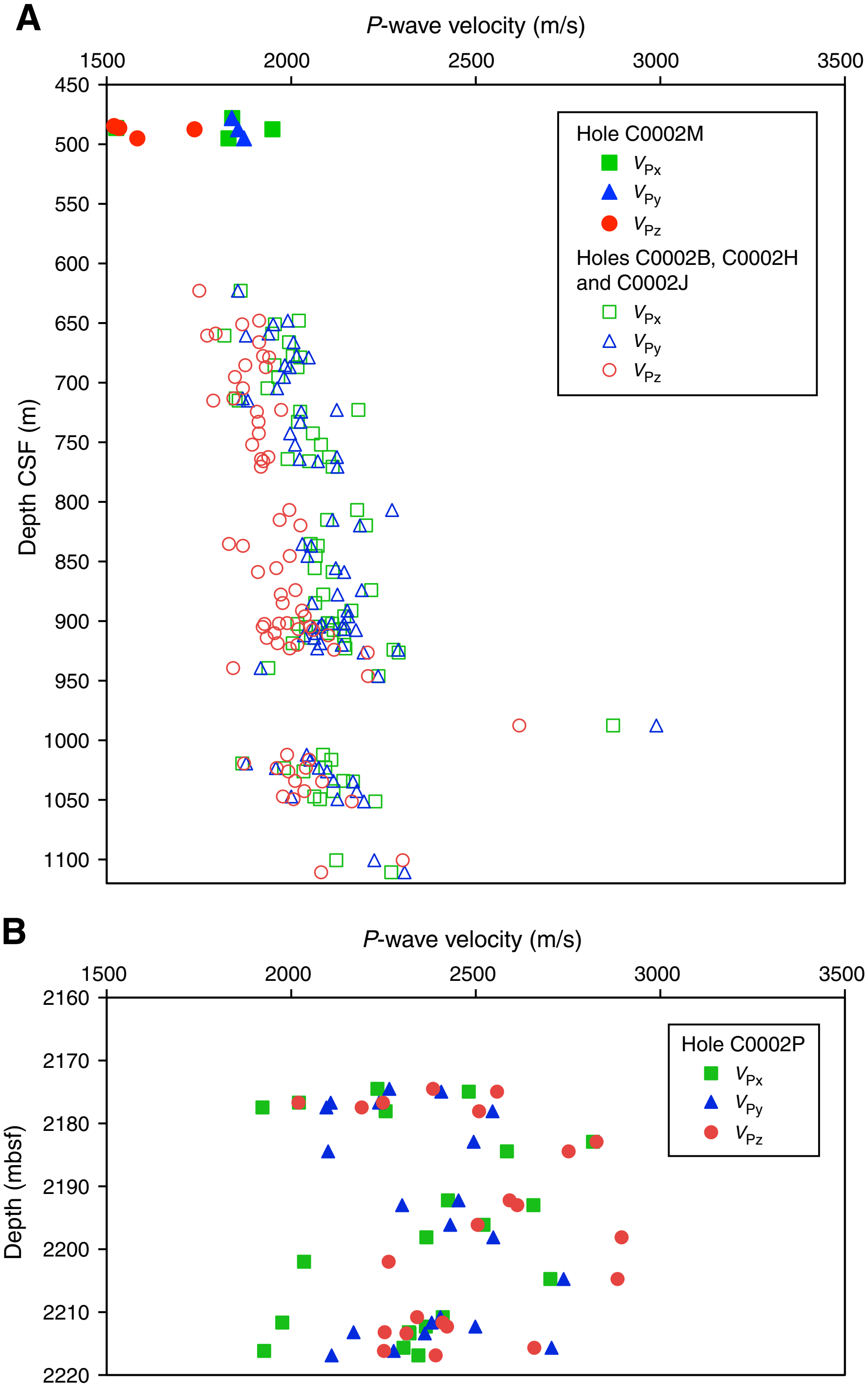

Figure F94. Electrical conductivity on discrete cube samples from Holes C0002B, C0002H, C0002J, C0002M, and C0002P and cuttings from Holes C0002N and C0002P. S_{min} = minimum conductivity, S_{max} = maximum conductivity.

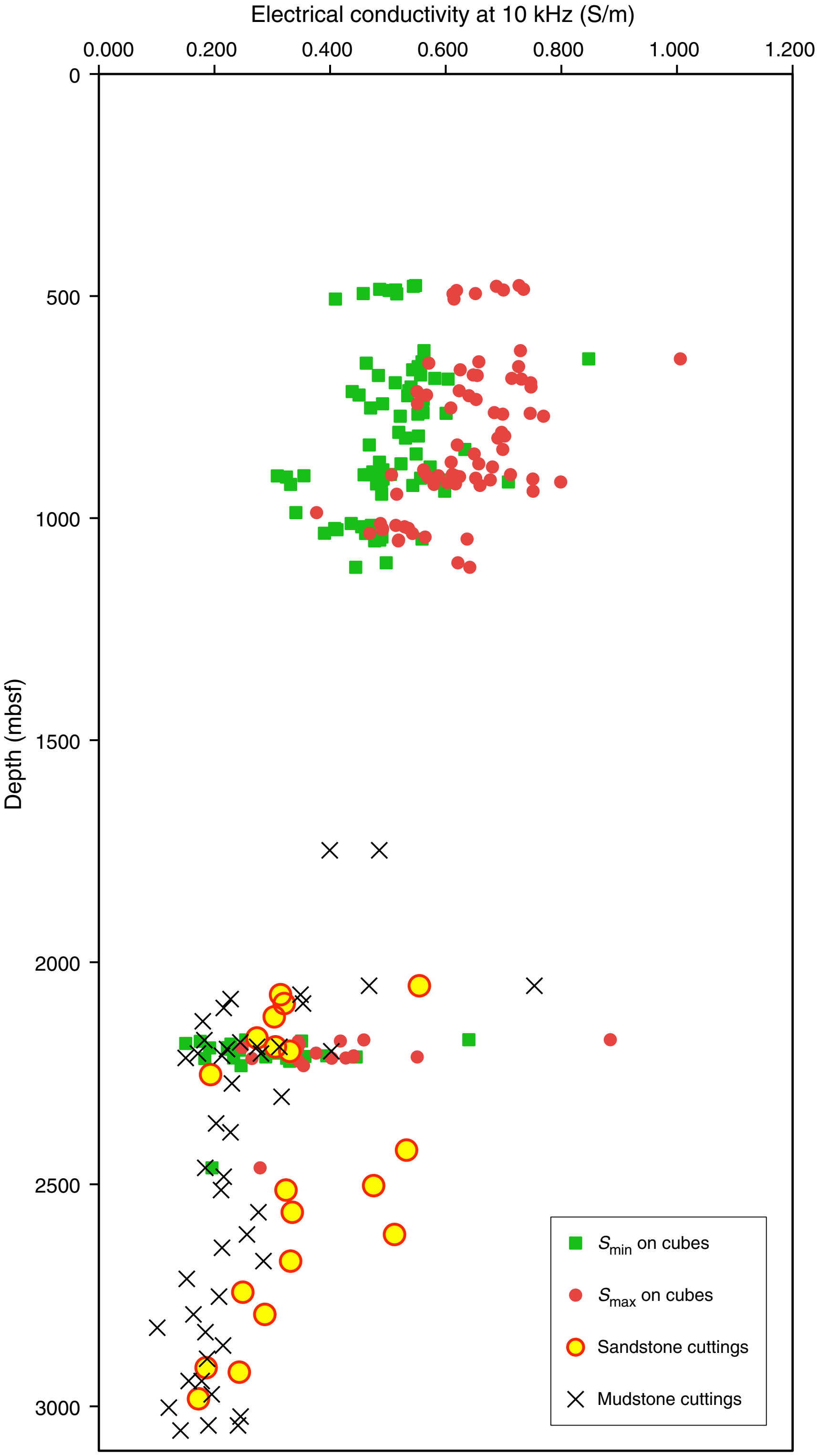

Figure F95. Relationship between electrical conductivity and porosity. Reference relationships based on Archie's law with fluid conductivities (σ_f) of 4 S/m (red curve) and 5.28 S/m (black curve) are also shown.

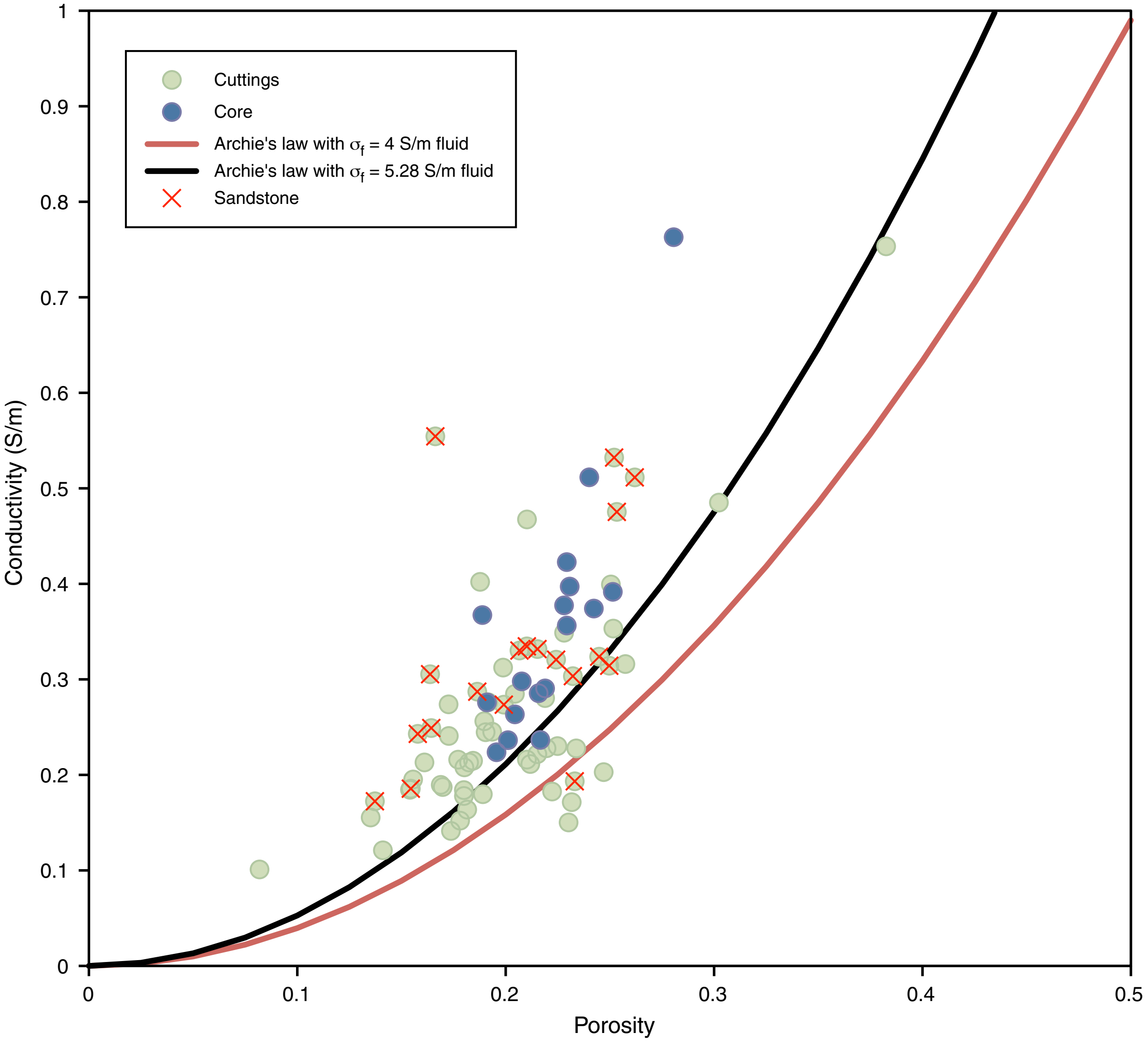

Figure F96. *P*-wave velocity on discrete cube samples and cuttings samples, Holes C0002N and C0002P. The errors for manual picking were calculated for uncertainties on sample length and traveltime measurements.

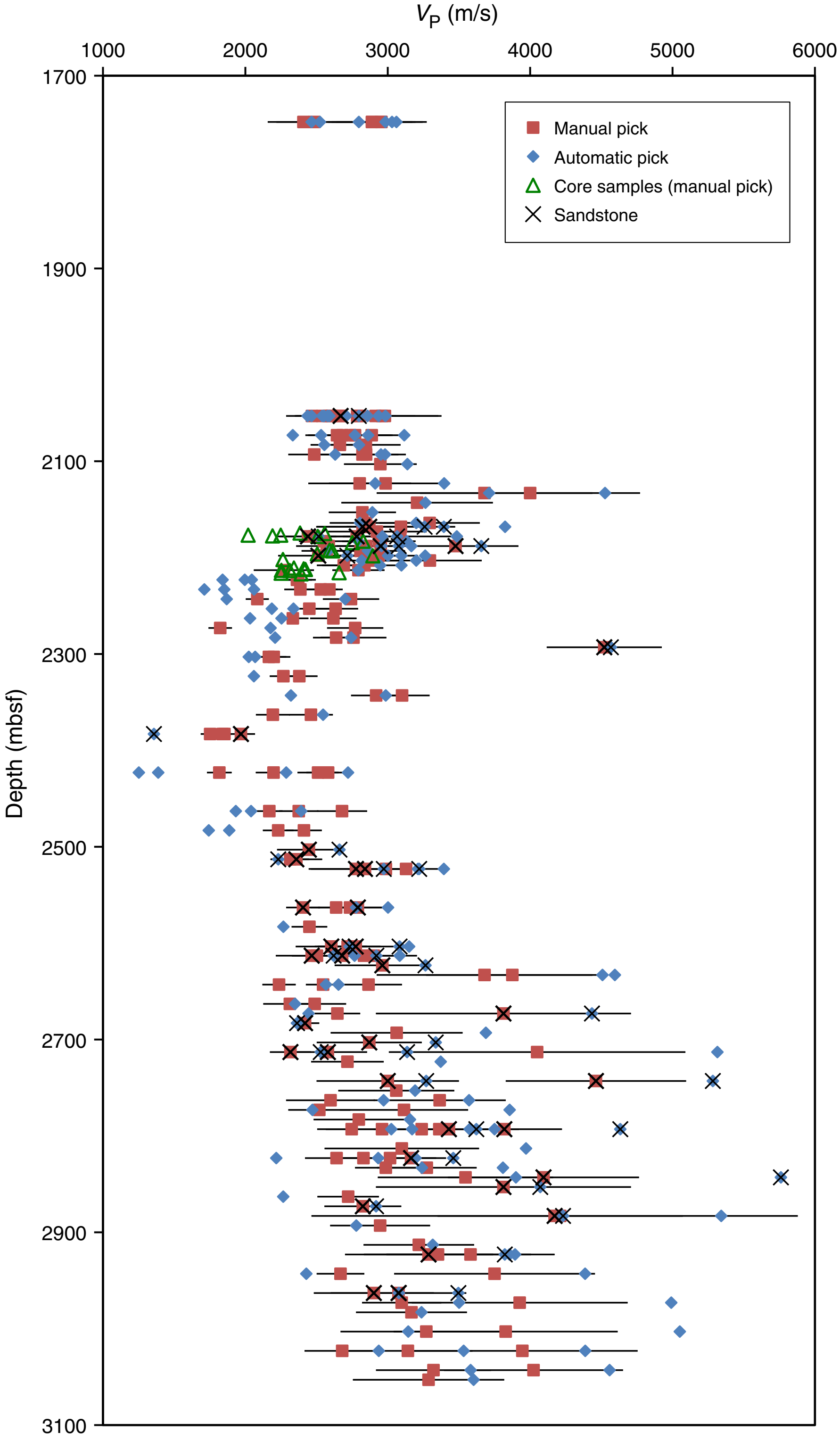

Figure F97. Thermal conductivity, Site C0002.

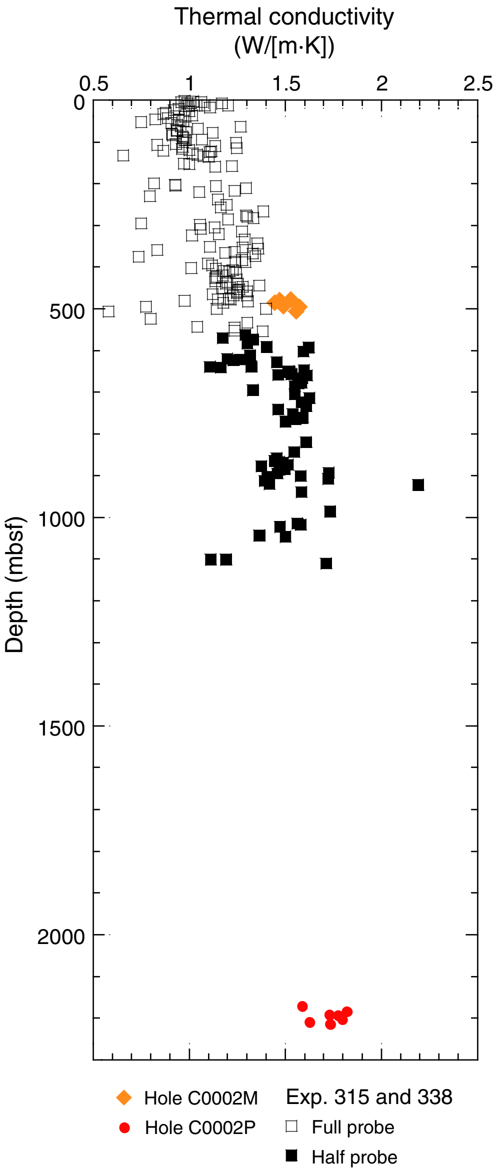

Figure F98. Porosity vs. thermal conductivity, Holes C0002M and C0002P and Sites C0011 and C0012. Open symbols = full probe, closed symbols = half probe. Dashed and solid lines represent theoretical values for different grain thermal conductivity (k_s) based on a geometric mean mixing model.

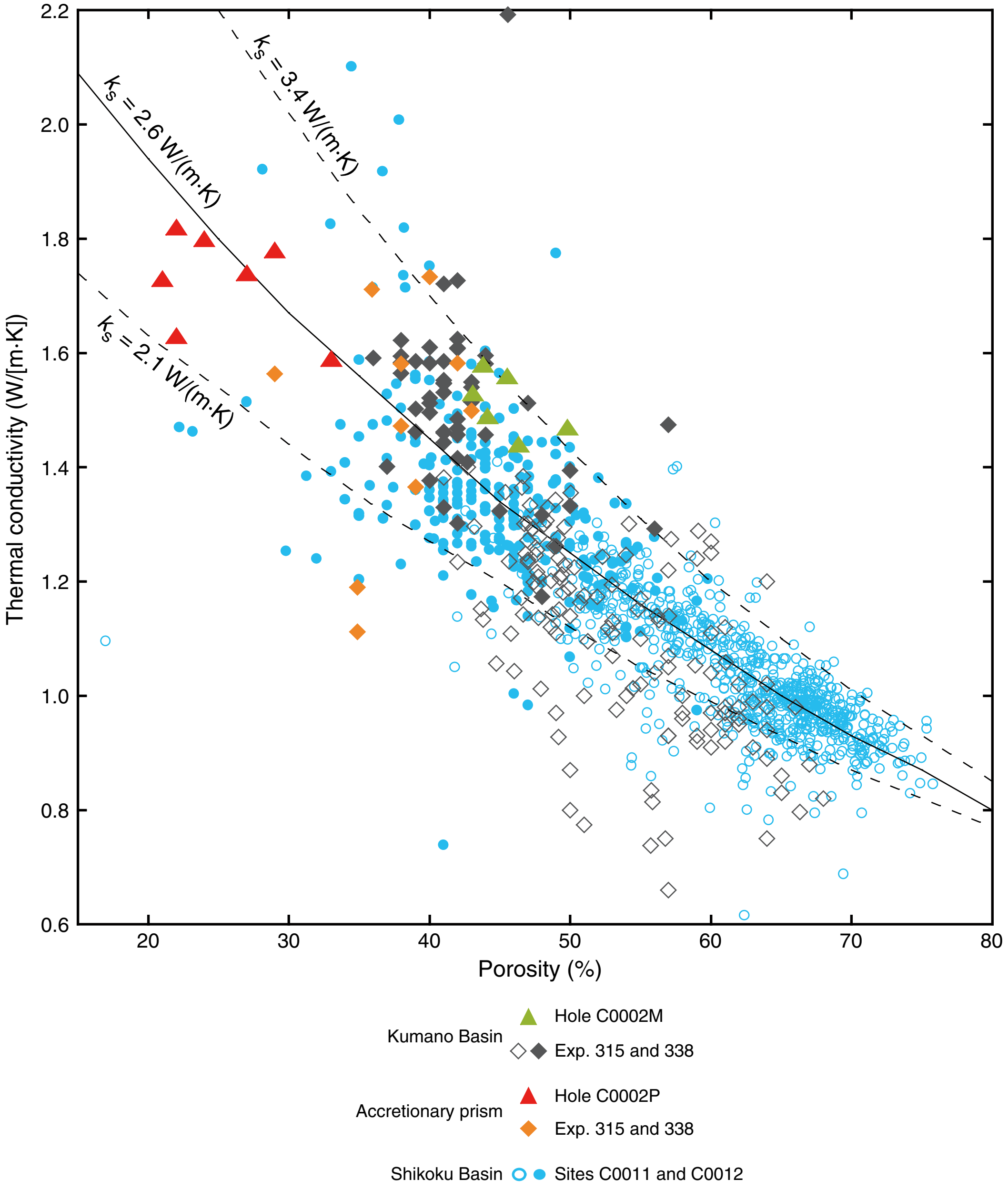

Figure F99. Whole-core multisensor logger measurements, Holes (**A**) C0002M and (**B**) C0002P. The dashed line in B indicates the fault observed at 2205 mbsf (Section 348-C0002P-5R-4). GRA = gamma ray attenuation; NGR = natural gamma radiation. Red = Expedition 348 data, black= Expedition 315 data, gray = Expedition 338 data.

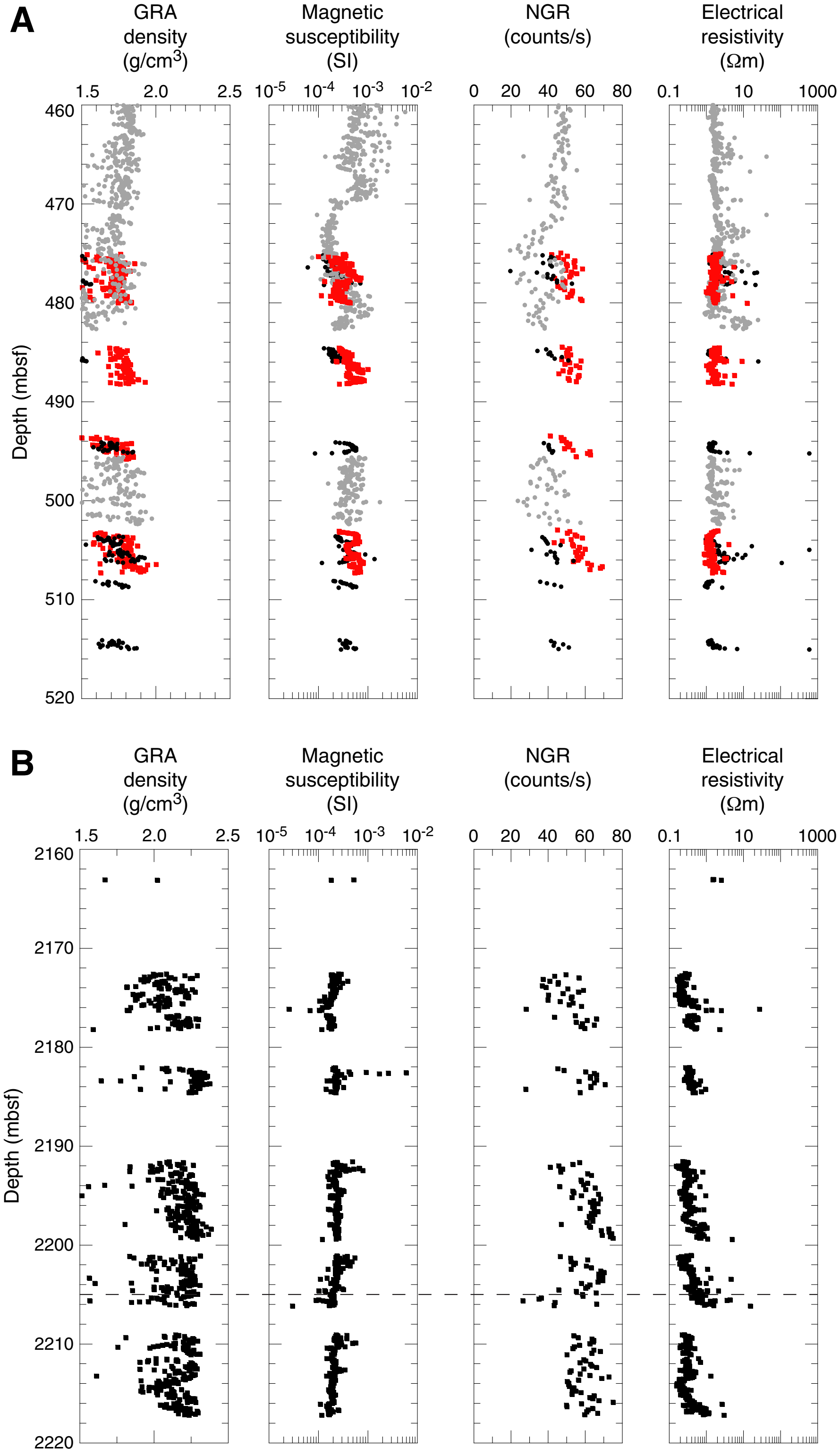

Figure F100. Color reflectance data, Holes (**A**) C0002M and (**B**) C0002P. L* = lightness; a* and b* = chromaticity variables (see Blum, 1997, for details). The dashed line in B indicates the fault observed at 2205 mbsf (Section 348-C0002P-5R-4). Red = Expedition 348 data, black = Expedition 315 data, gray = Expedition 338 data.

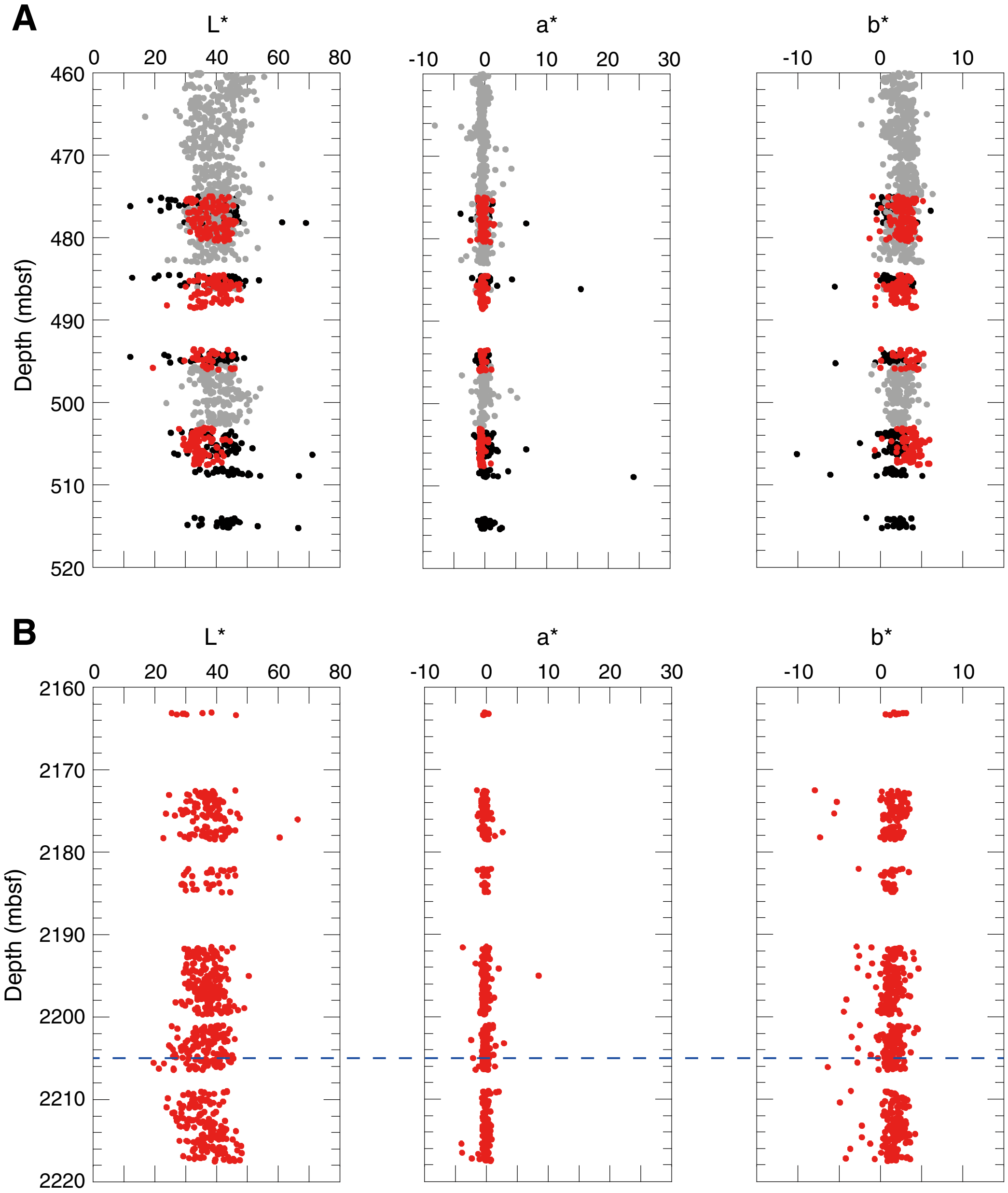

Figure F101. Multisensor core logger (MSCL) natural gamma radiation (NGR) values for (**A**) unwashed and (**B**) washed cuttings.

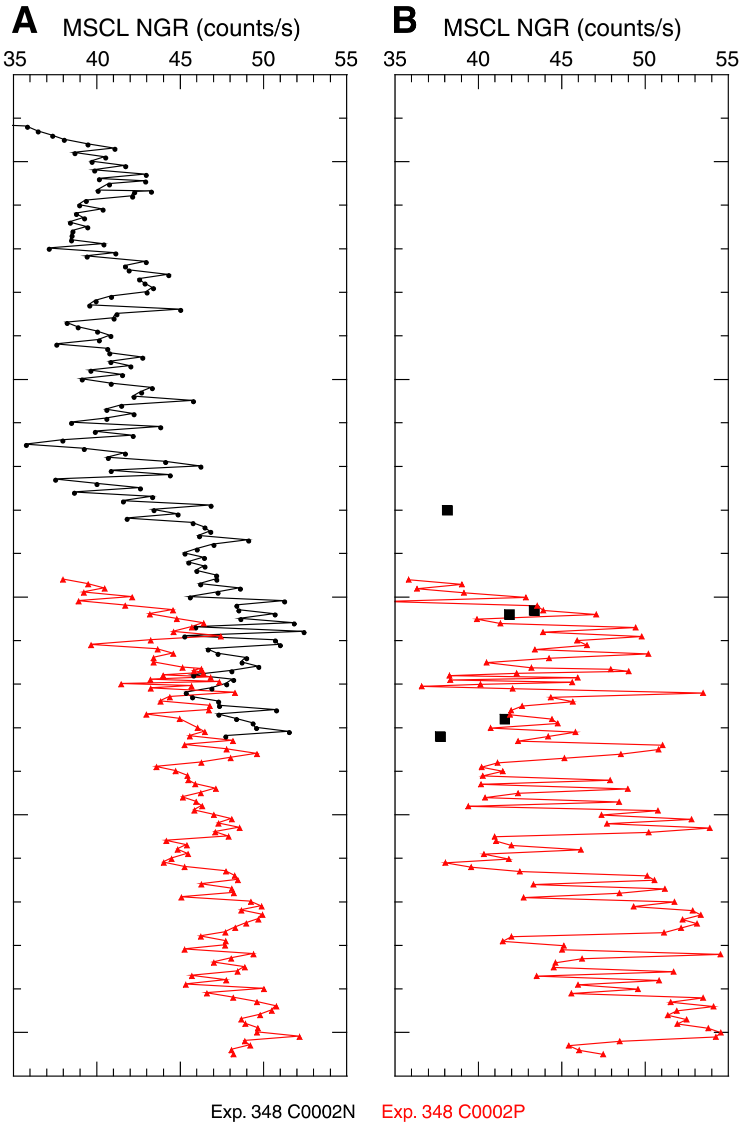

Figure F102. Mass magnetic susceptibility, Holes C0002N and C0002P.

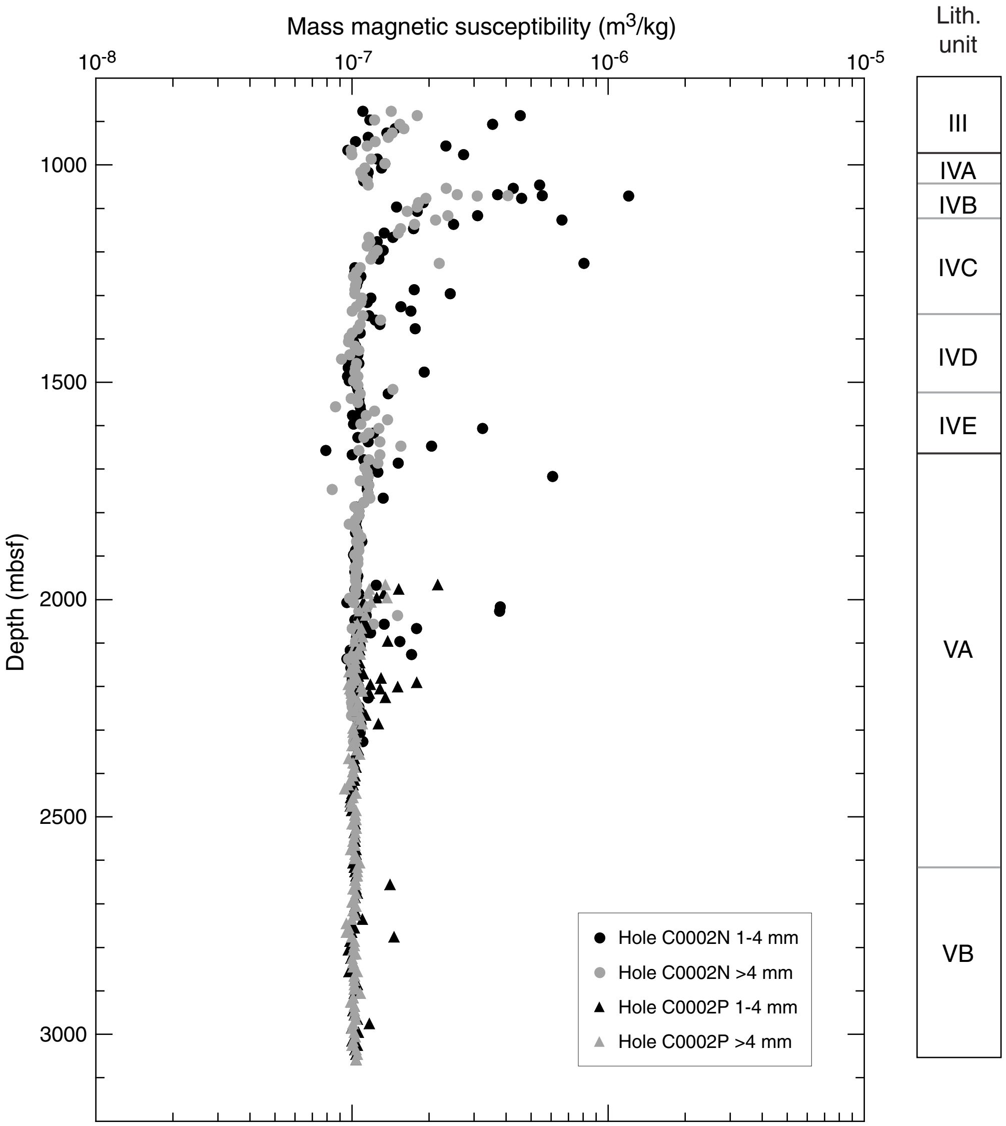

Figure F103. Raw data from dielectric analysis of the paste made from Sample 348-C0002N-312-SMW (2255.5 mbsf).

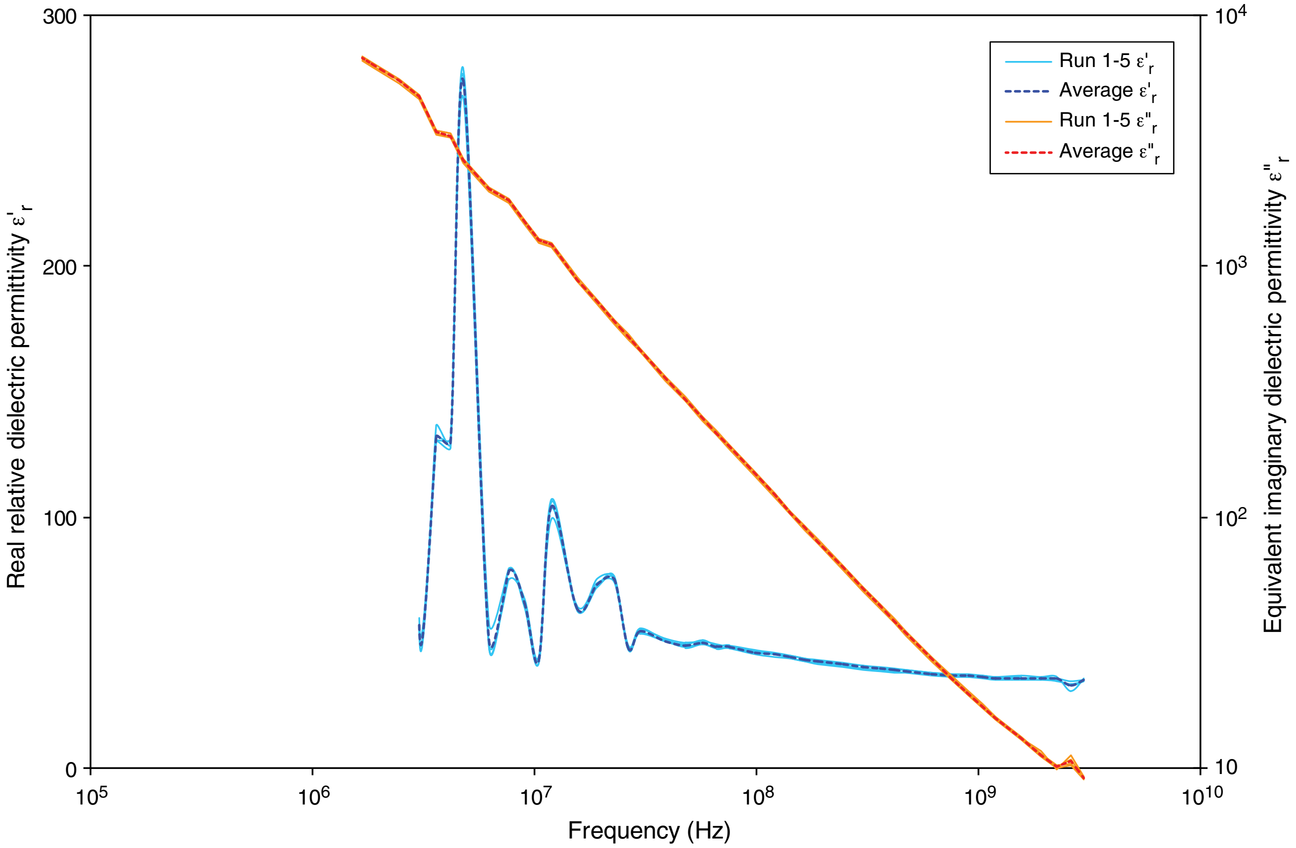

Figure F104. Drill cuttings dielectric analysis, Hole C0002N. Real relative dialectric permittivity and apparent conductivity are at 300 MHz. Apparent equivalent conductivity includes contributions from the conductivity and the relative imaginary dielectric permittivity. Colored lines are boundaries discussed in text.

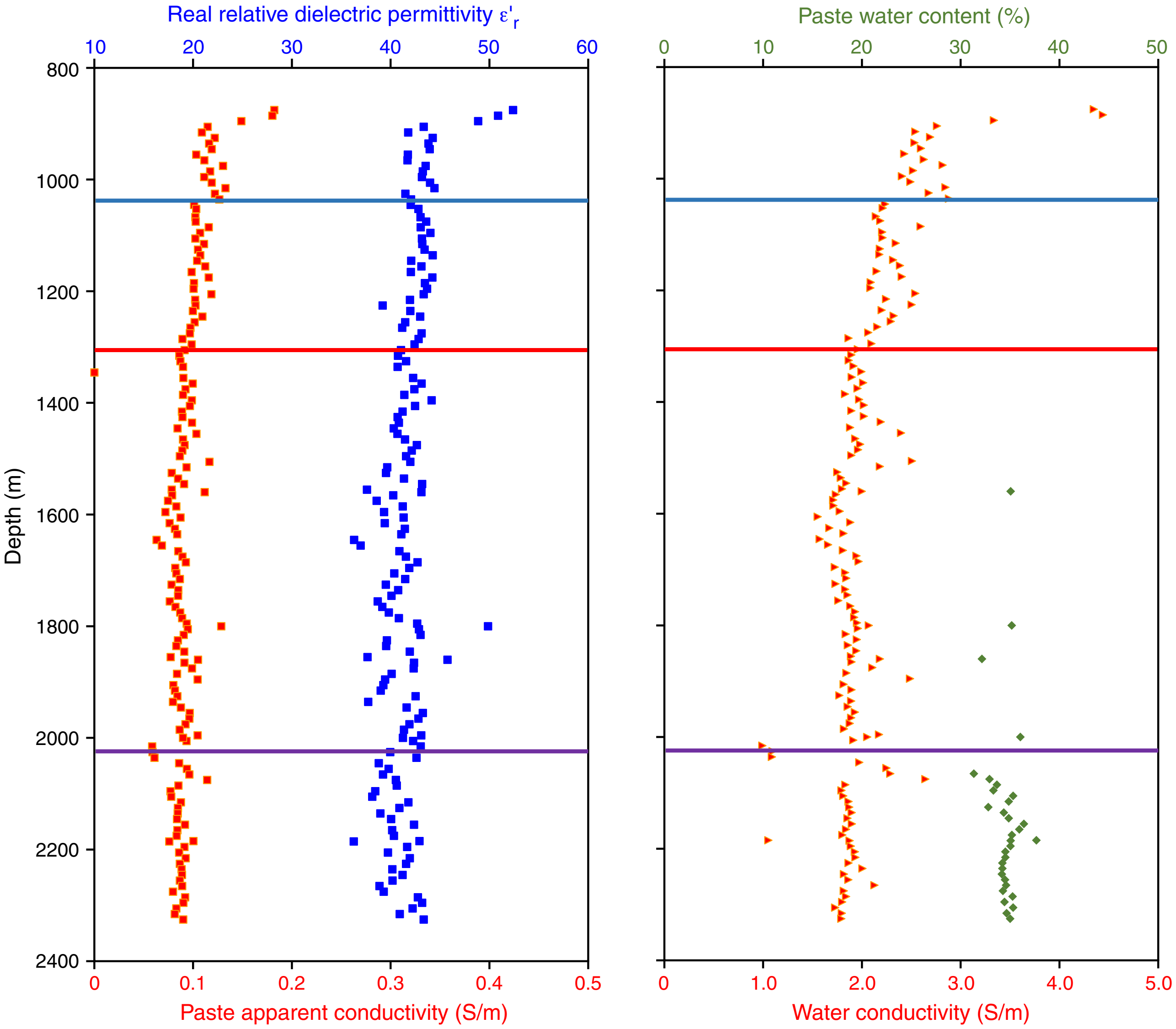

Figure F105. Loss angle values as a function of sample depth, Holes C0002N and C0002P.

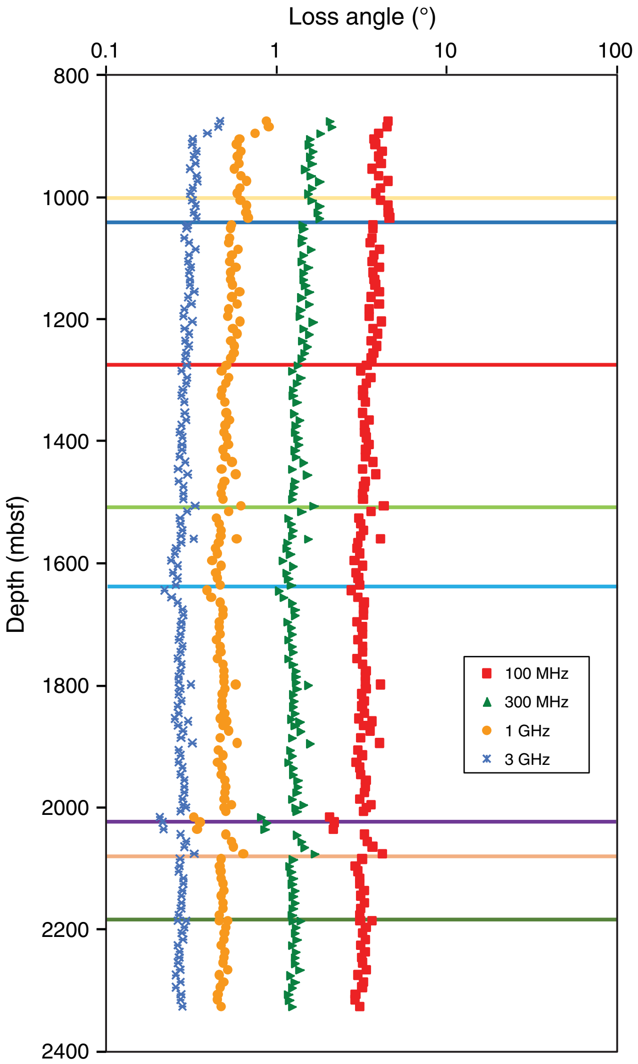

Figure F106. Petrophysical logs from Holes C0002N and C0002P compared with dielectric data for prepared pastes. DGRCC = gamma ray, R39PC = deep resistivity, R27PC = medium resistivity, R15PC = shallow resistivity. ε'_r = real relative dielectric permittivity, ε''_r = imaginary relative dielectric permittivity.

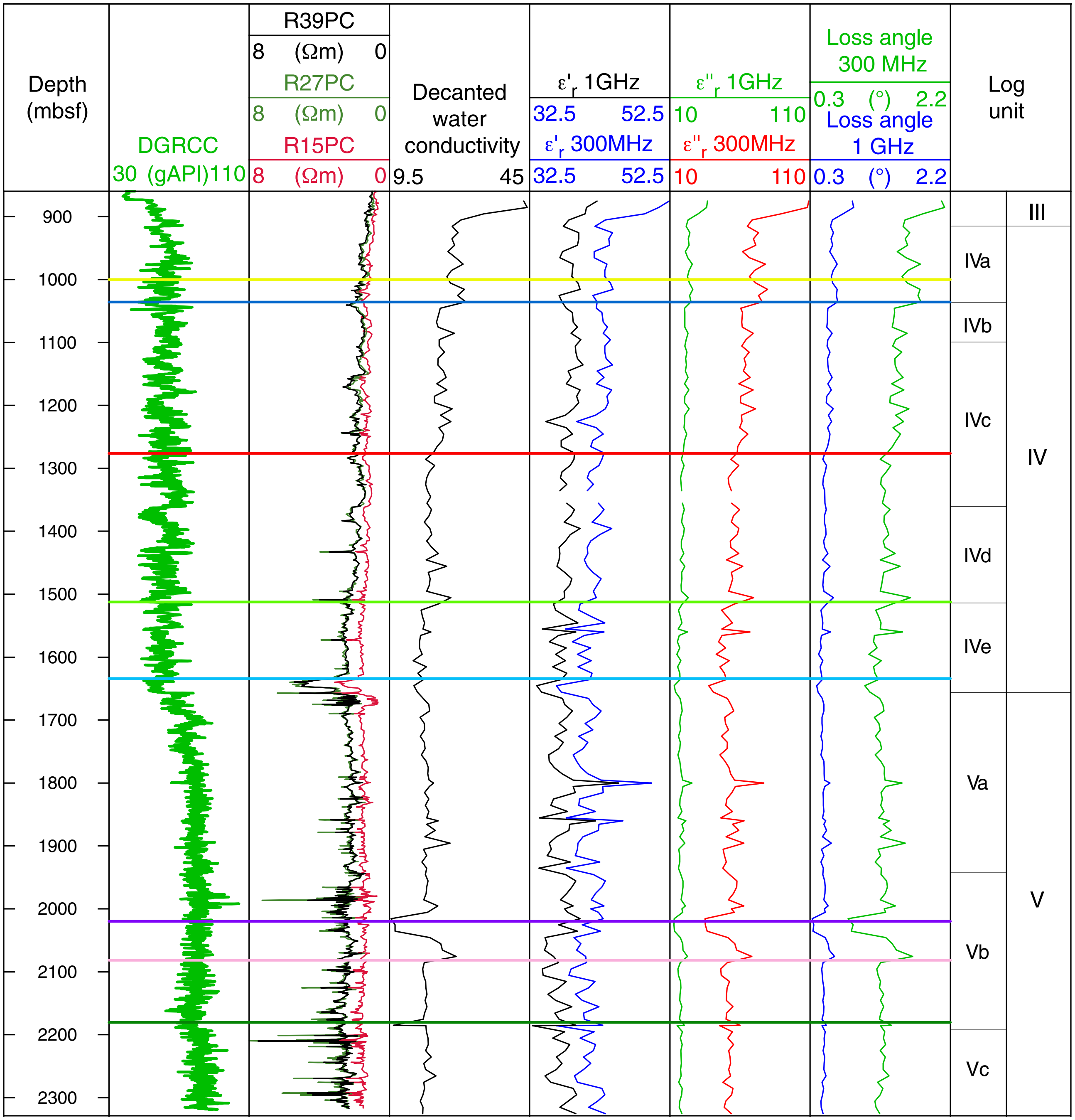

Figure F107. Borehole configuration at the time of the leak-off test, Hole C0002P.

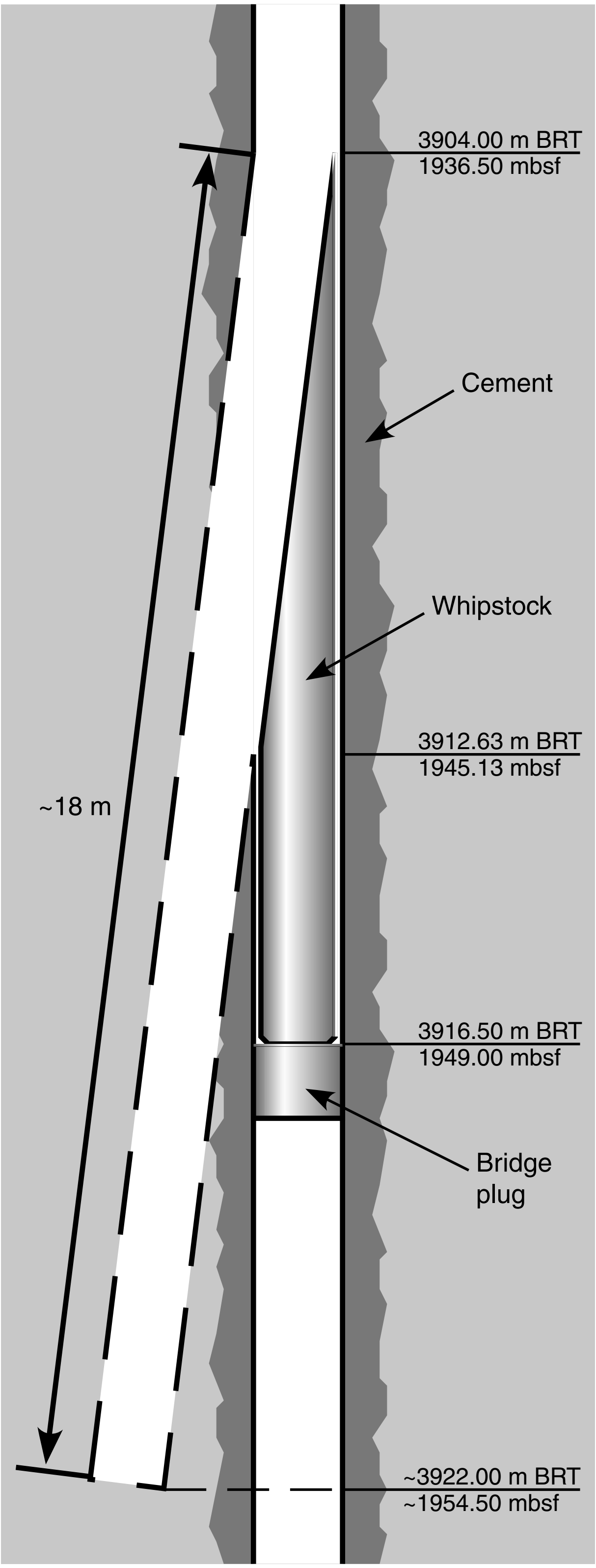

Figure F108. A–C. Calculated downhole pressure and fluid injection rate data from the two leak-off tests plotted against time, Hole C0002P. Downhole pressure was calculated by adding static mud pressure to the surface pressure measurement.

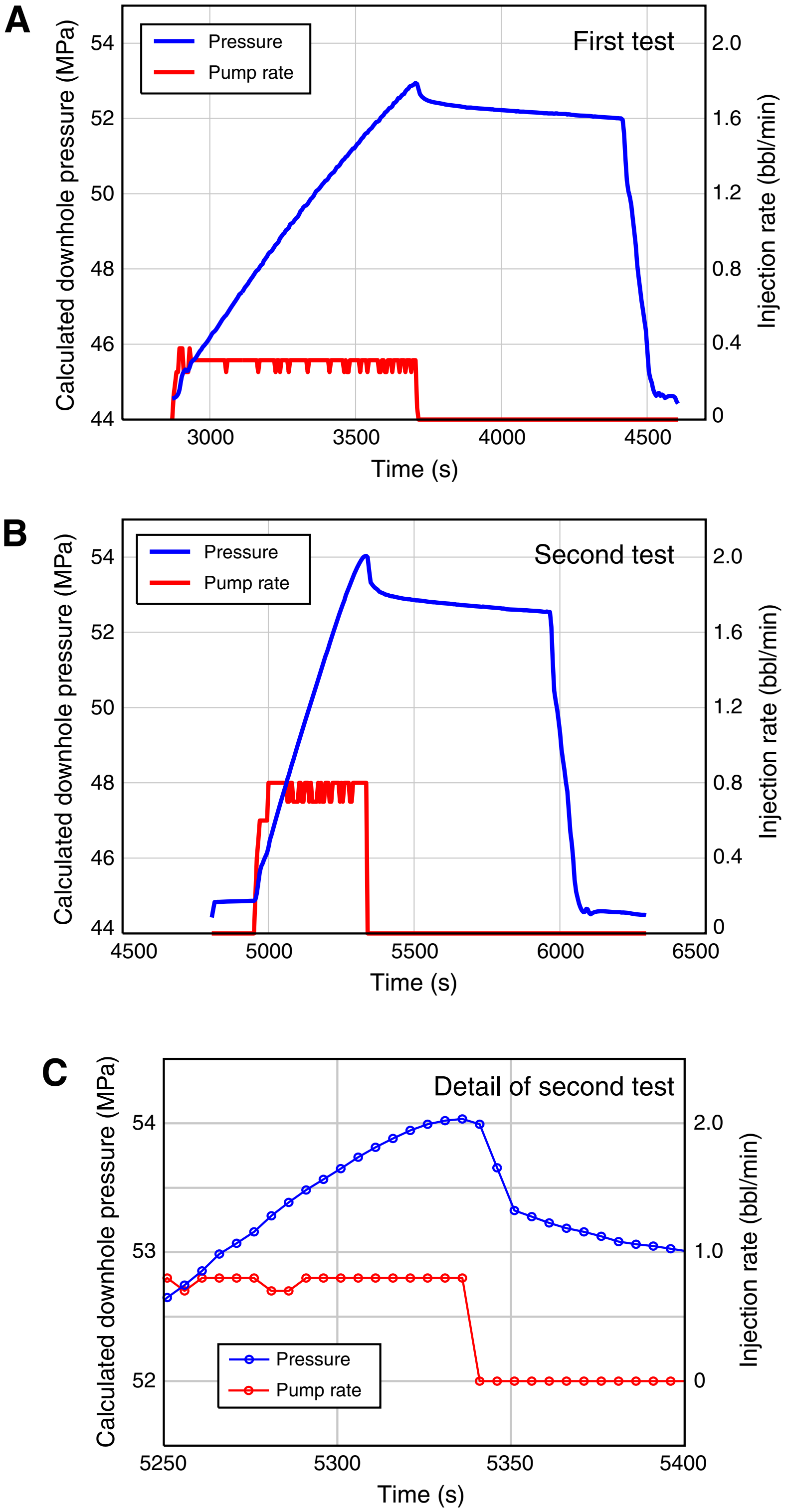

Figure F109. Downhole pressure versus injected volume data, Hole C0002P. **A.** Comparison between the two tests. **B.** Downhole pressure and pressure build-up rate data from the first test. **C.** Downhole pressure and pressure build-up rate data from the second test. Gray curve is the full data set; black curve is smoothed by a moving average over 15 samples, and blue is the downhole pressure. LOP = leak-off point.

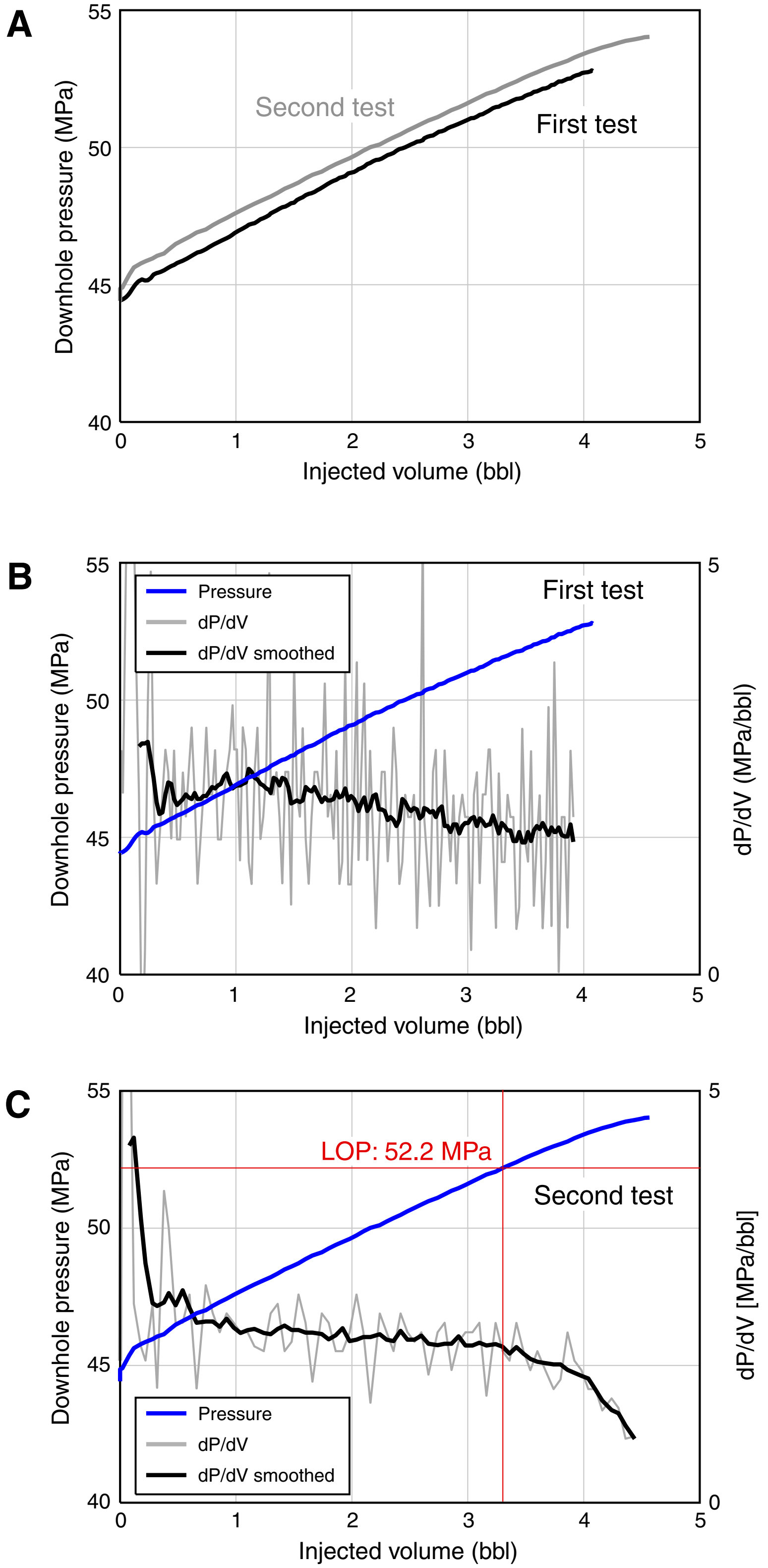

Figure F110. Leak-off point (LOP) pressure data plotted together with hydrostatic and lithostatic pressure gradients, Holes C0002N and C0002P. Hydrostatic pressure is calculated based on seawater density of 1.023 g/cm^3; lithostatic pressure from the seafloor is calculated based on log data (gray curve) and then linearly extrapolated to deeper depth (black line). PWD-N, PWD-P = annular pressure while drilling.

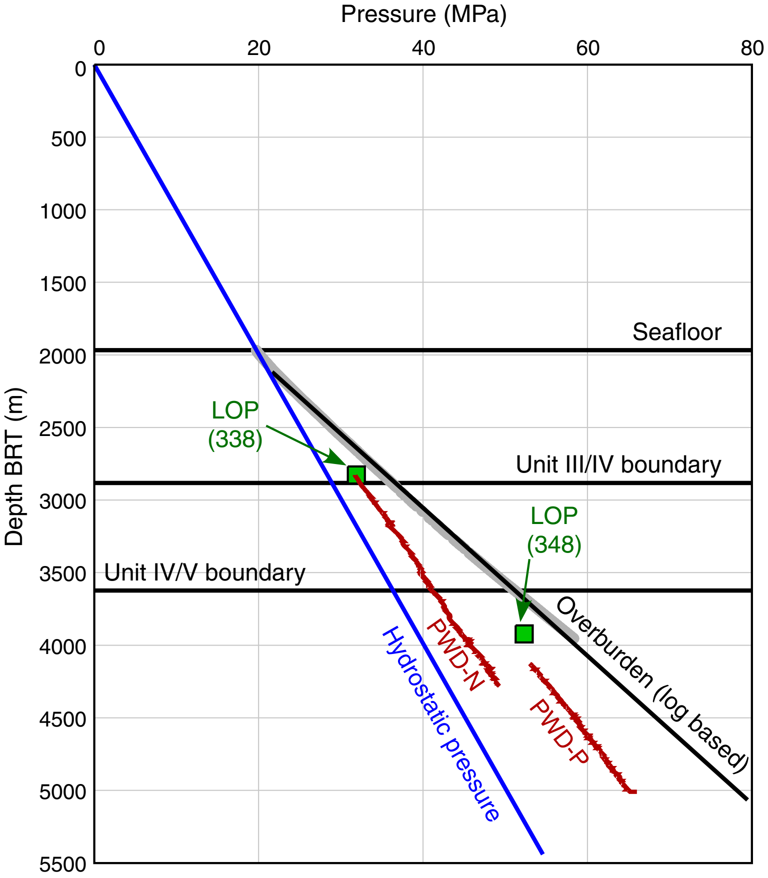

Figure F111. Drilling parameters and selected logs. EWR = electromagnetic wave resistivity tool, PWD = pressure while drilling, Ph. Resis. = phase resistivity. **A.** Hole C0002N. Exposure time data drawn with dashed lines at ~2000 mbsf was reconstructed because data were not recorded during the changeover from Run 1 to Run 2. (Continued on next page.)

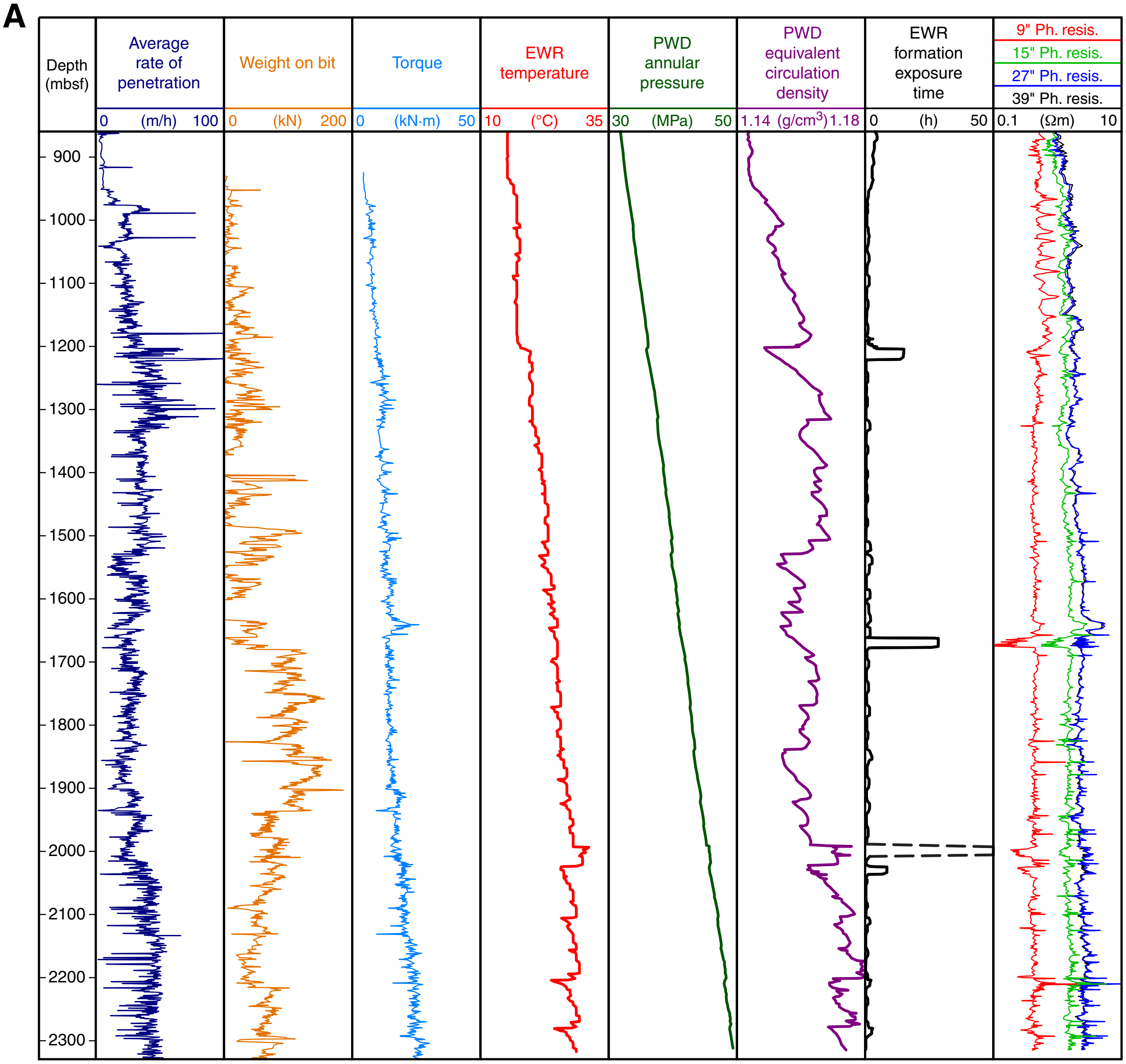

Figure F111 (continued). B. Hole C0002P. The cored depth interval from 2163 to 2218.5 mbsf is shown in gray. Ultrasonic caliper data are shown together with a vertical base line representing the drill bit diameter.

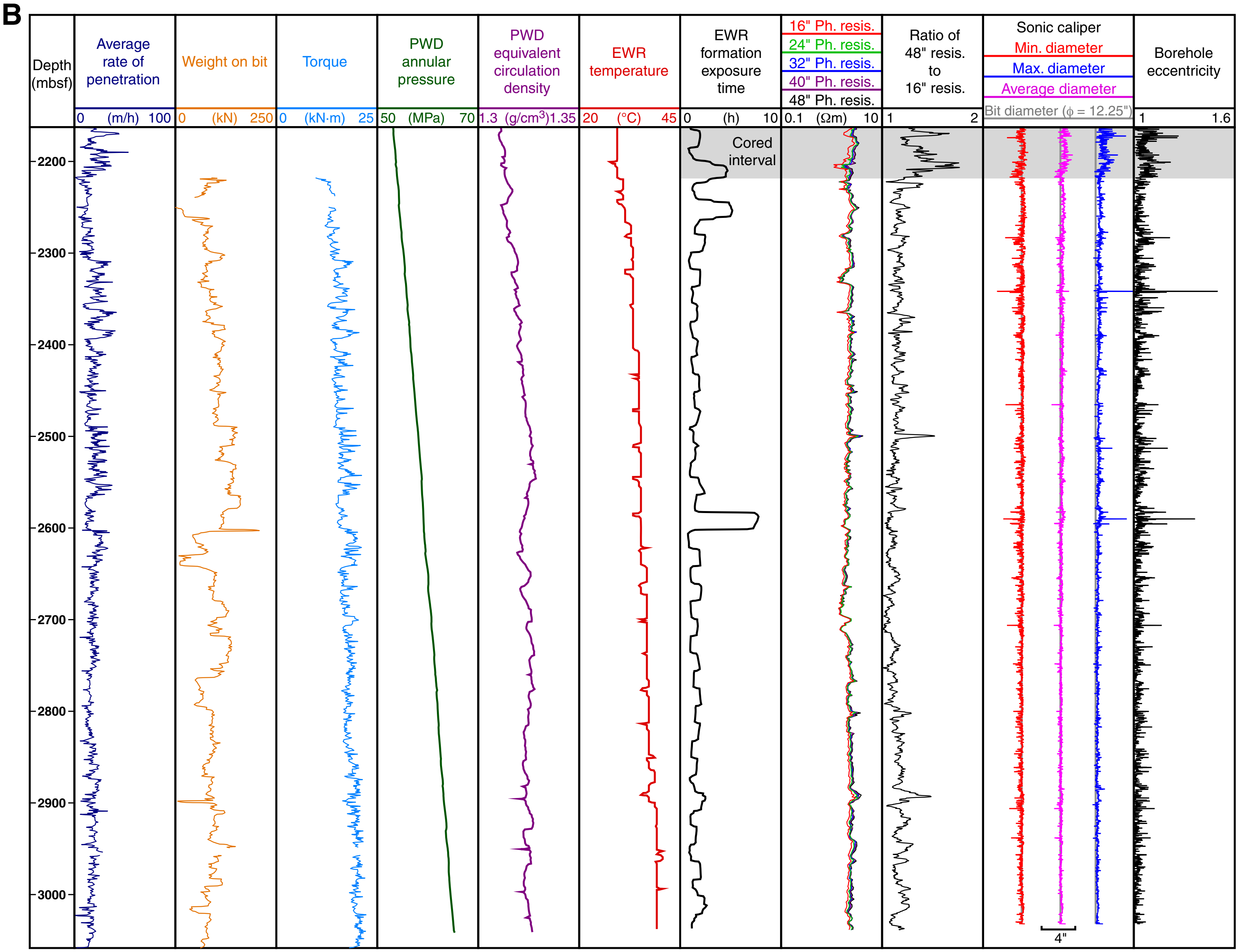

Figure F112. Composite plot of LWD logs, Hole C0002N. The R09PC and R09AC short-spacing phase resistivity and, to a lesser degree, the R15PC and R15AC phase resistivity exhibit low resistivity values compared to those of the deep resistivity readings (R27PC, R39PC, R27AC, and R39PC). Short-spacing receivers record the response of the electromagnetic wave propagation in the mud, and long-spacing receivers provide a measurement of the formation. Only deep resistivities were used in the geological interpretation. DGRCC = dual gamma ray.

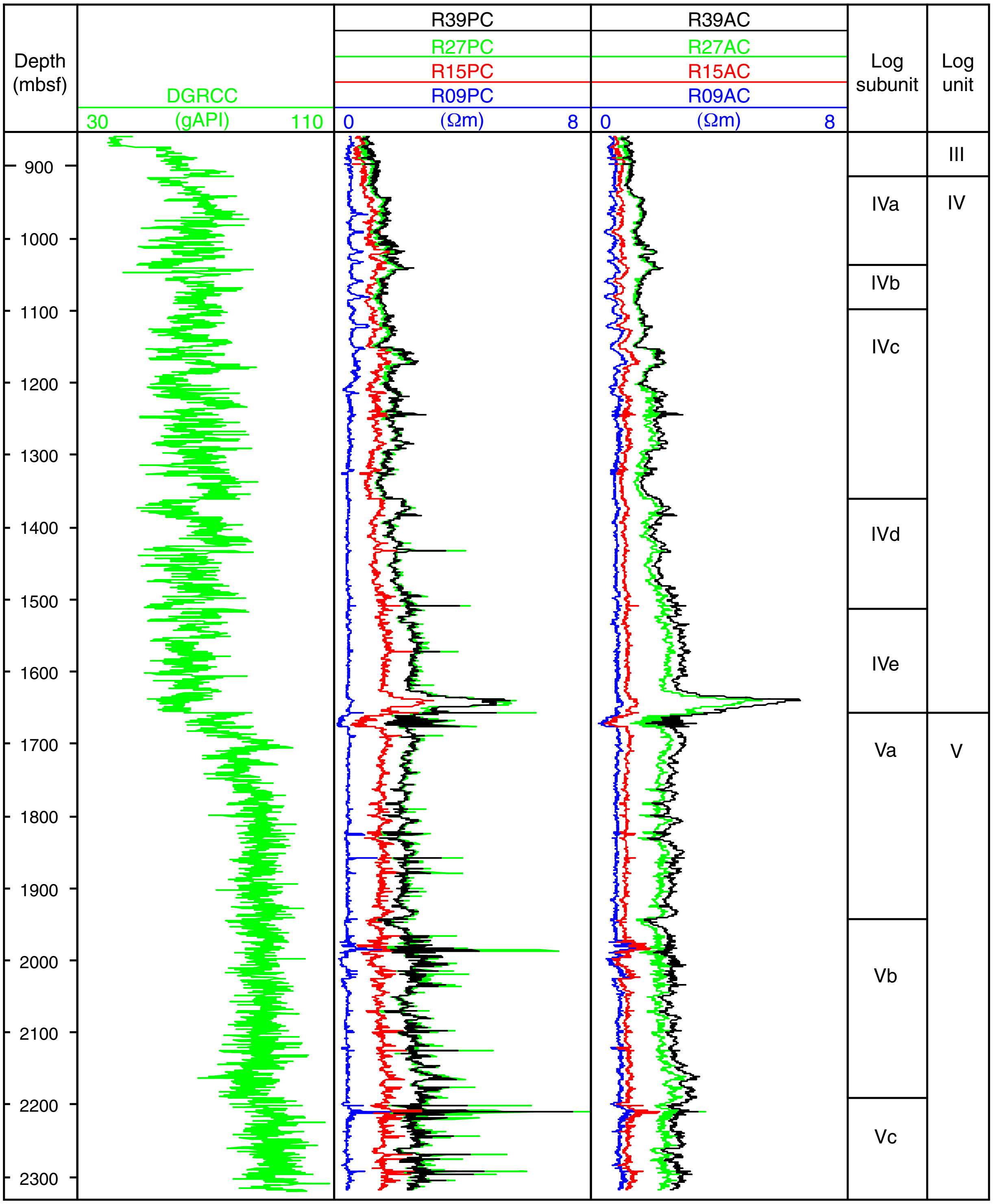

Figure F113. Correlation of log units and subunits between Holes C0002F and C0002N. Log units and subunits defined in Hole C0002F were correlated to Hole C0002N based on the gamma ray and resistivity log response in Hole C0002N. The definition and characterization of units and subunits in Hole C0002F is based on a more complete data set including resistivity images and acoustic logs. Major boundaries and changes in trend or character were identified and correlated. Gamma ray values in Hole C0002N are higher throughout, which may be an artifact (see text for discussion of data quality). RES_BD = resistivity, GR = gamma radiation, R27PC = deep resistivity, DGRCC = dual gamma ray.

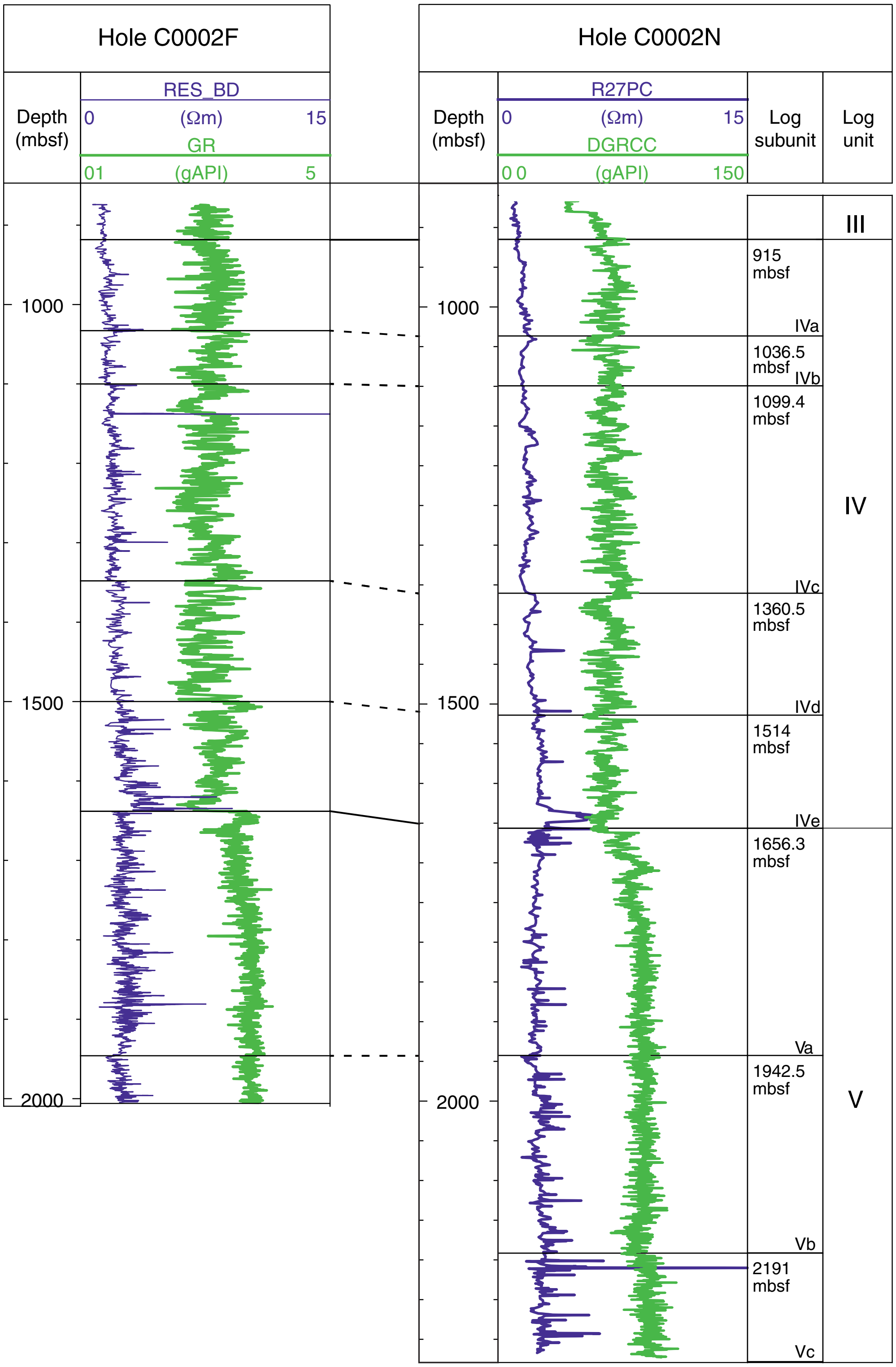

Figure F114. Composite plot of main LWD logs, Hole C0002P. Dotted lines indicate main trends observed on the different log measurements with depth. AGRCC = AGR tool gamma radioactivity; XBCS = XBAT tool compressional slowness and velocity (low XBCS values are equivalent to high velocity); RH16PC, RH24PC, RH48PC = three-phase 2 MHz EWR tool resistivity measurements (shallowest to deepest).

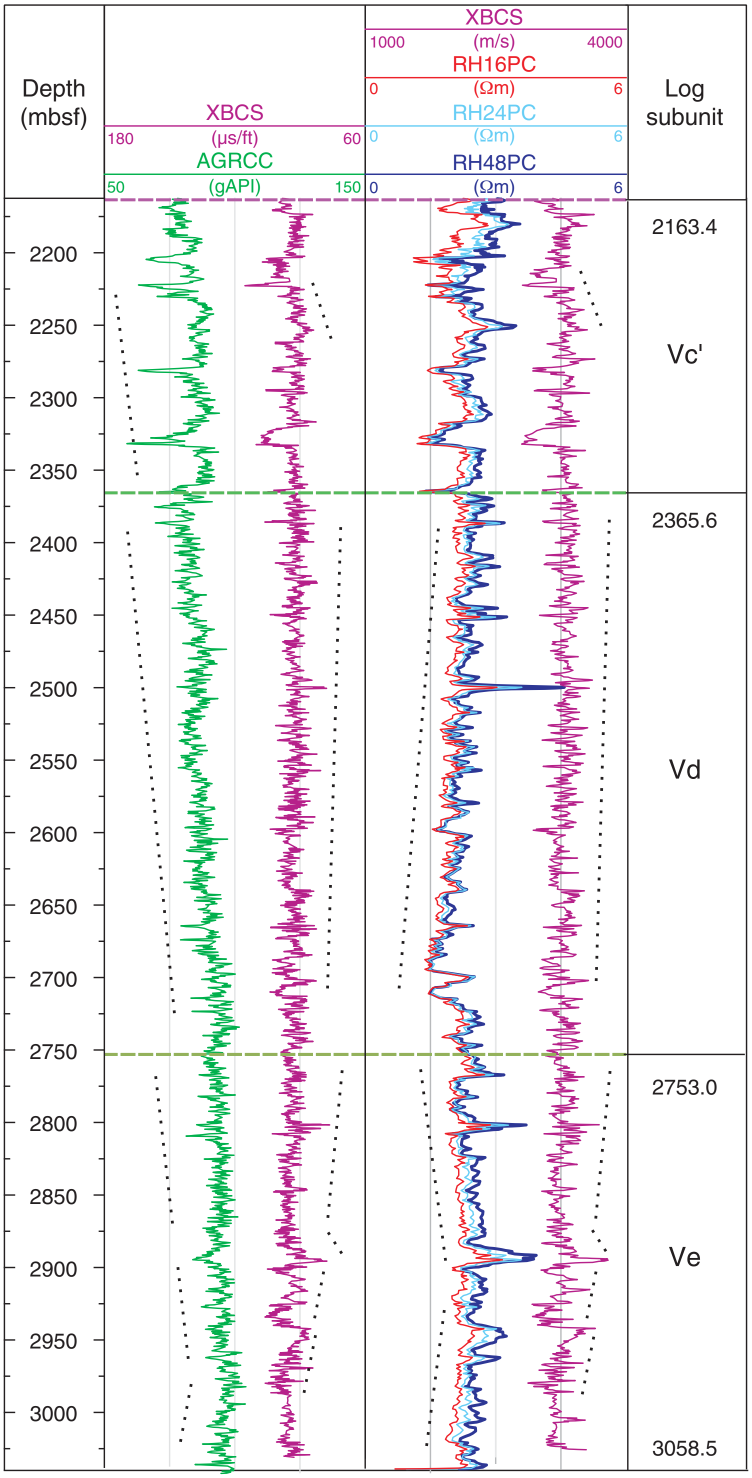

Figure F115. Resistivity data collected using the EWR-M5 tool, Hole C0002P. Each column represents resistivity data from either phase-shift (P) or attenuation (A) resistivity measured using one of the sensor spacings (16, 24, 32, 40, or 48 inch). Black (H) = 2 MHz, blue (M) = 500 kHz, red (L) = 250 kHz. Low-frequency data shows lower resolution than the higher frequency data.

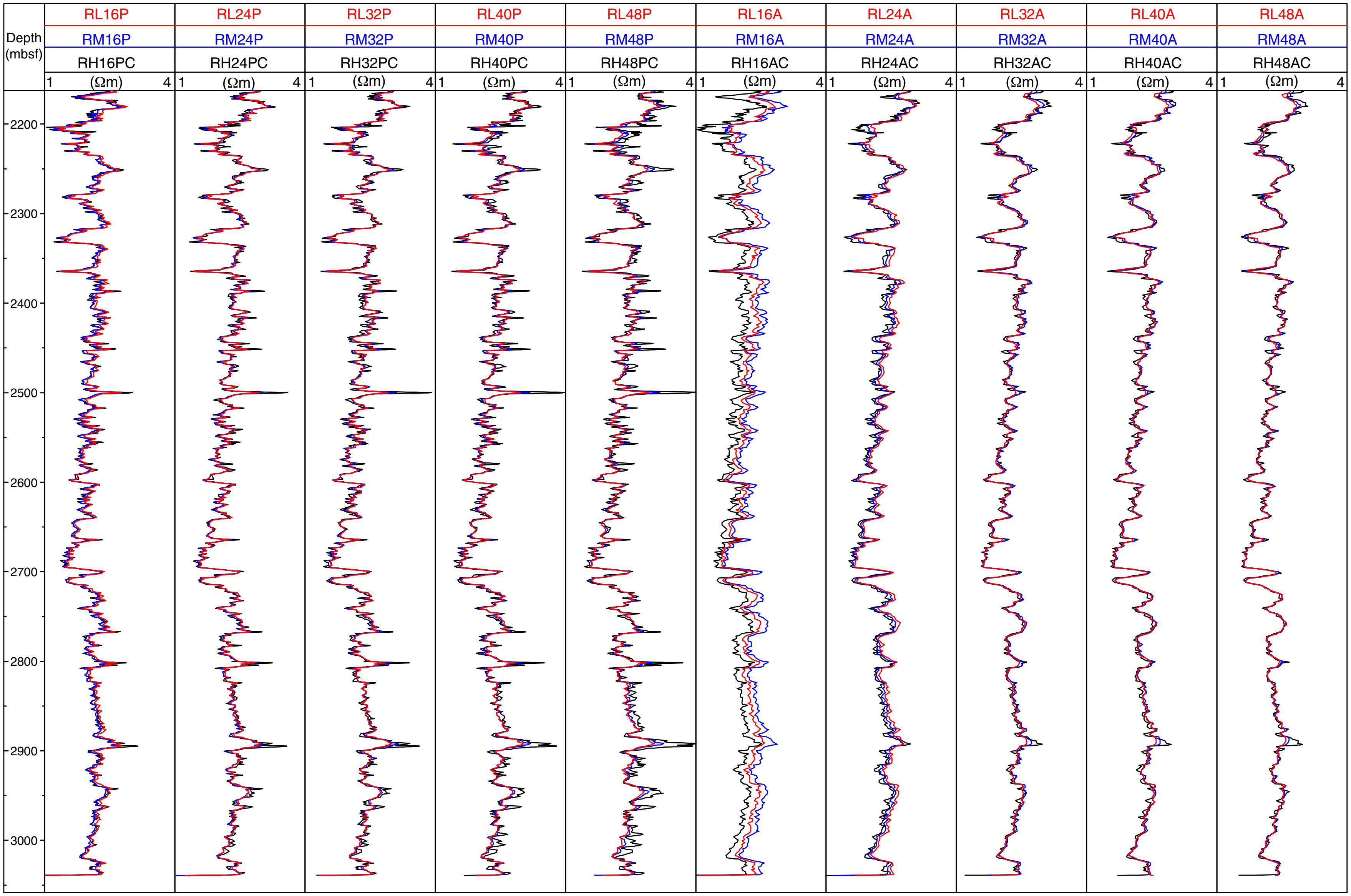

Figure F116. Comparison of phase shift (P) and attenuation (A) resistivity data measured at 2 MHz, Hole C0002P. Each column compares data from 16, 24, 32, 40, and 48 inch sensor spacing. Phase shift data is preferred due to its higher resolution, but both resistivity data record similar log responses.

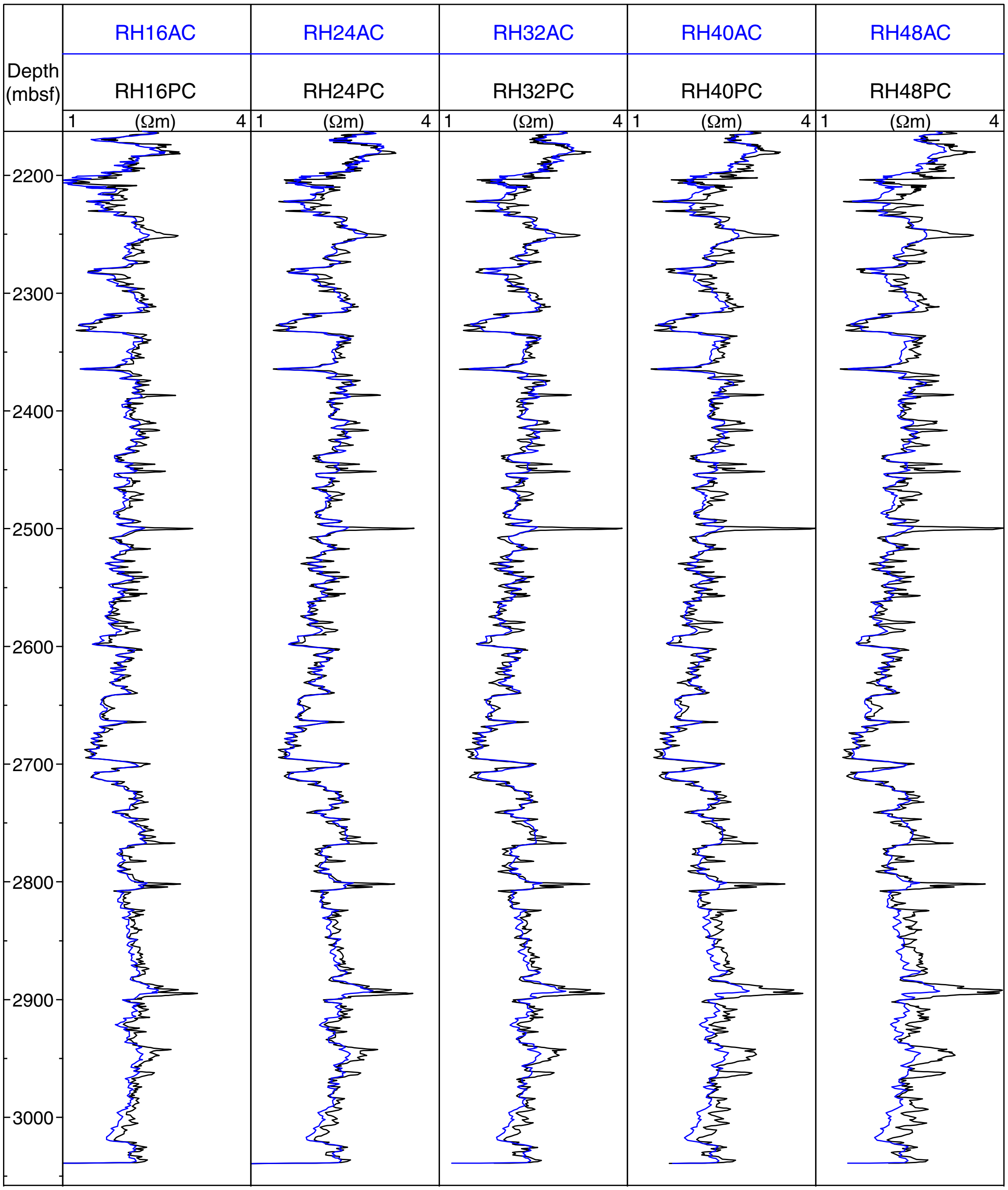

Figure F117. Details of Hole C0002P log responses for intervals and levels described in the text within log Subunits Vc′, Vd, and Ve, respectively. Oriented resistivity images and preliminary interpretation of bedding and structures (green and red tadpoles, respectively) for selected intervals of the different subunits. Arrows connect detailed images to logged sections.

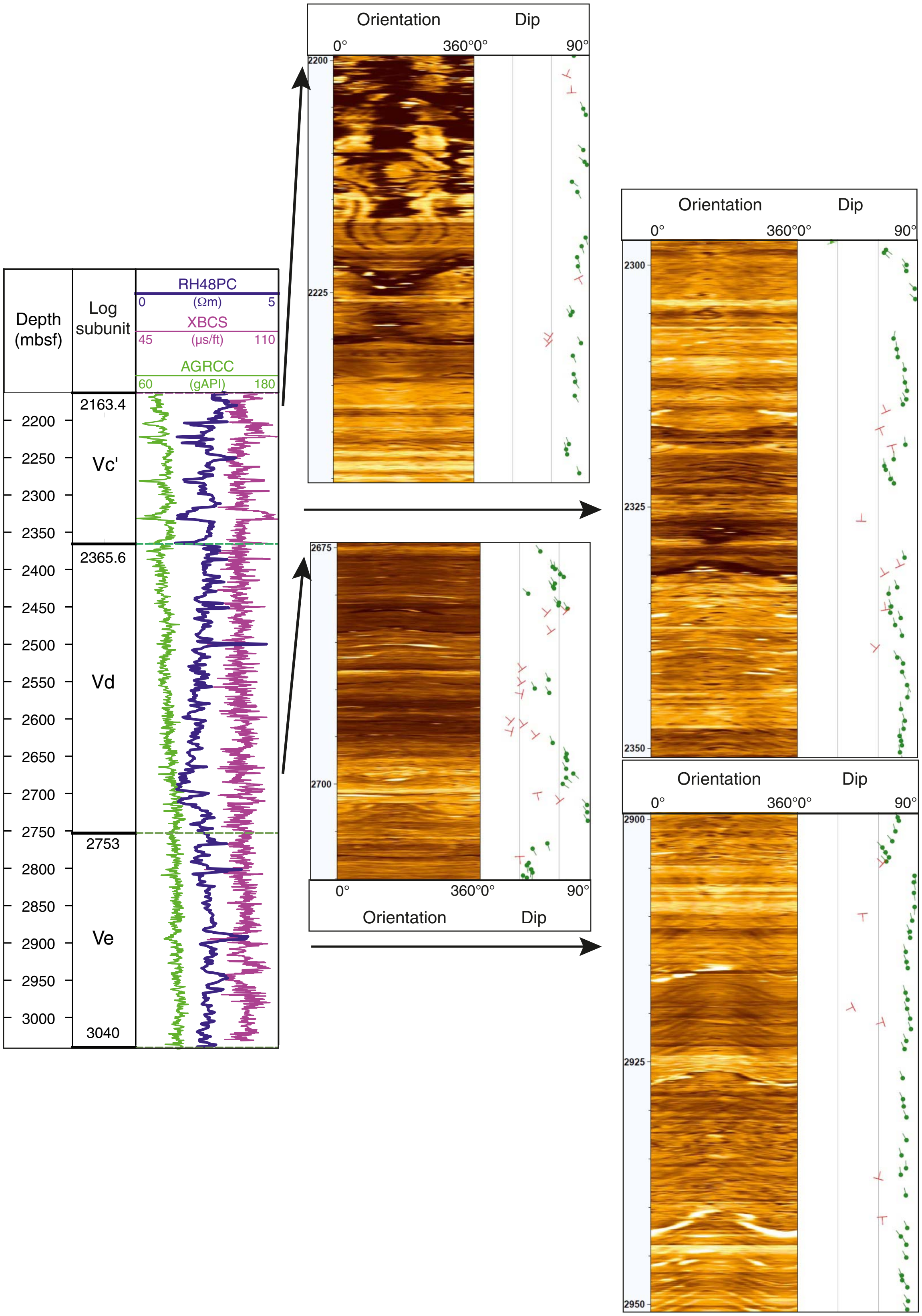

Figure F118. Summary of the preliminary interpretation of azimuthal focused resistivity (AFR) images displayed with velocity, resistivity (RH48PC), and gamma radioactivity (AGRCC). Tadpole plot of downsampled bedding dips (interval = 30 m, step = 15) and shipboard *P*-wave velocity, high-resolution AFR image (static processing), tadpole plot of structures, resistivity, and gamma ray logs.

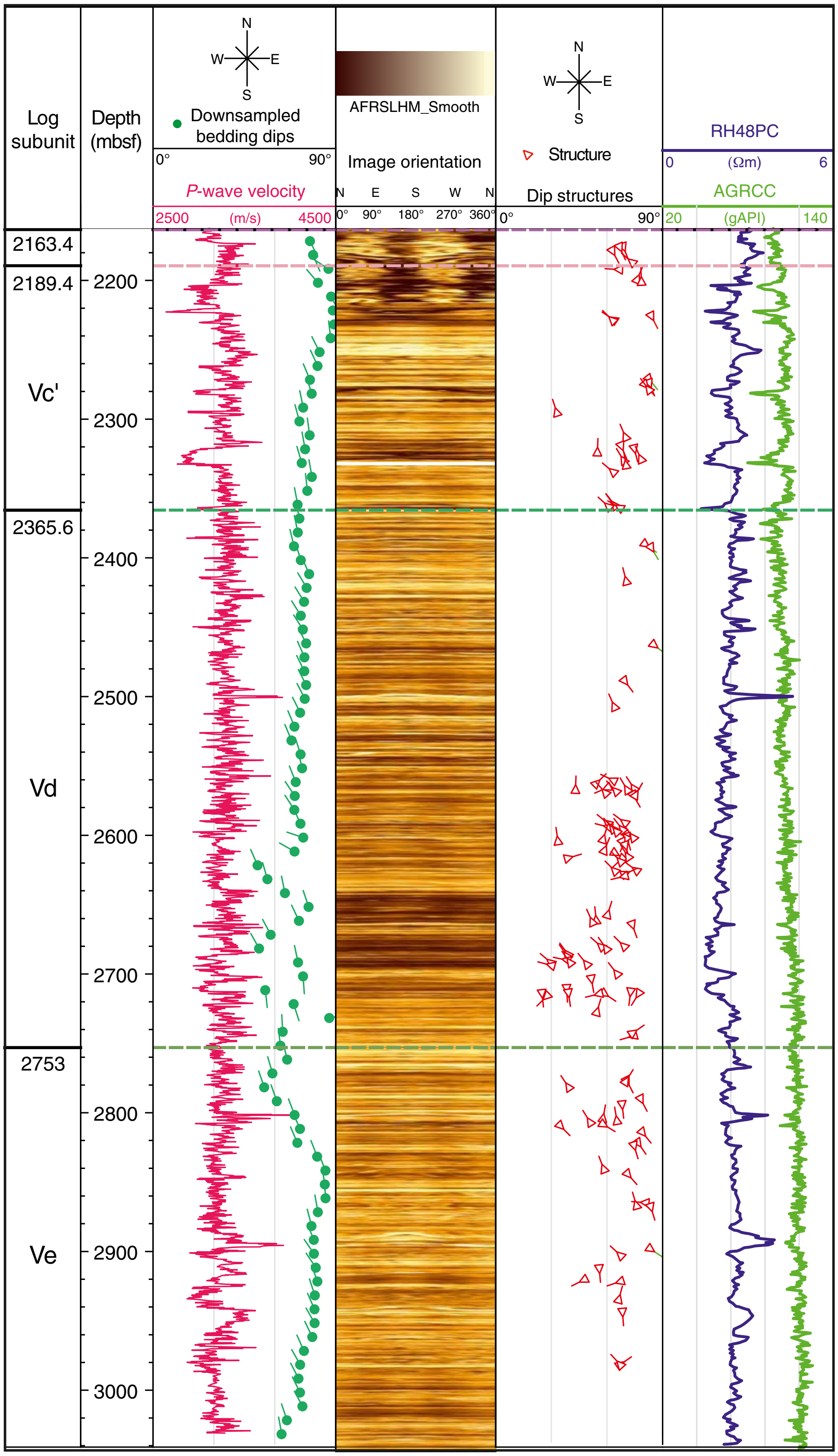

Figure F119. Summary of wellbore failures observed in the resistivity image log shown together with the sonic caliper image, Hole C0002P. AFR = azimuthal focused resistivity.

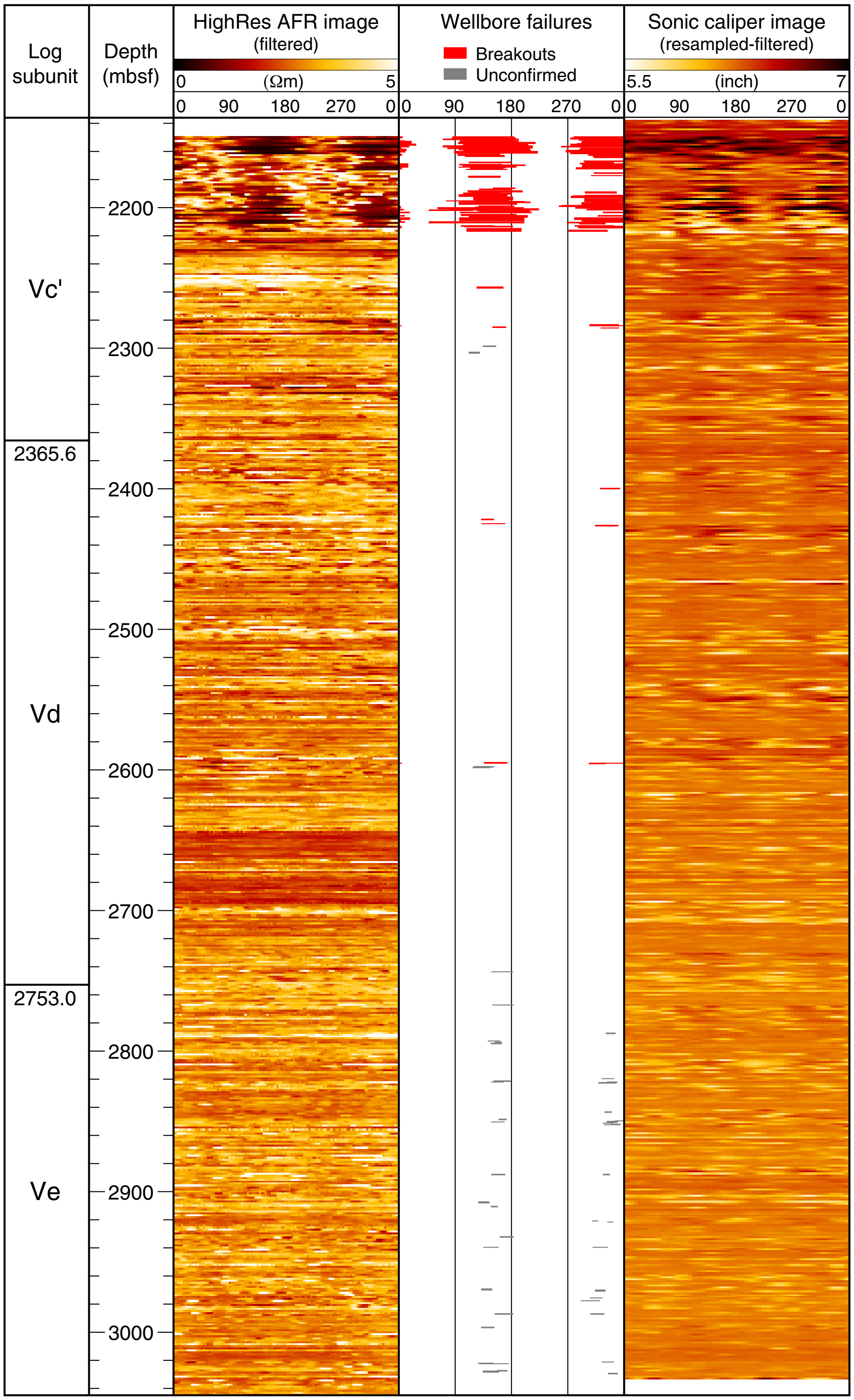

Figure F120. Close-up image examples of the observed wellbore failures, Hole C0002P. The borehole cross-section was constructed from the sonic caliper data within the depth interval shown by the black, vertical bars in the right-hand column.

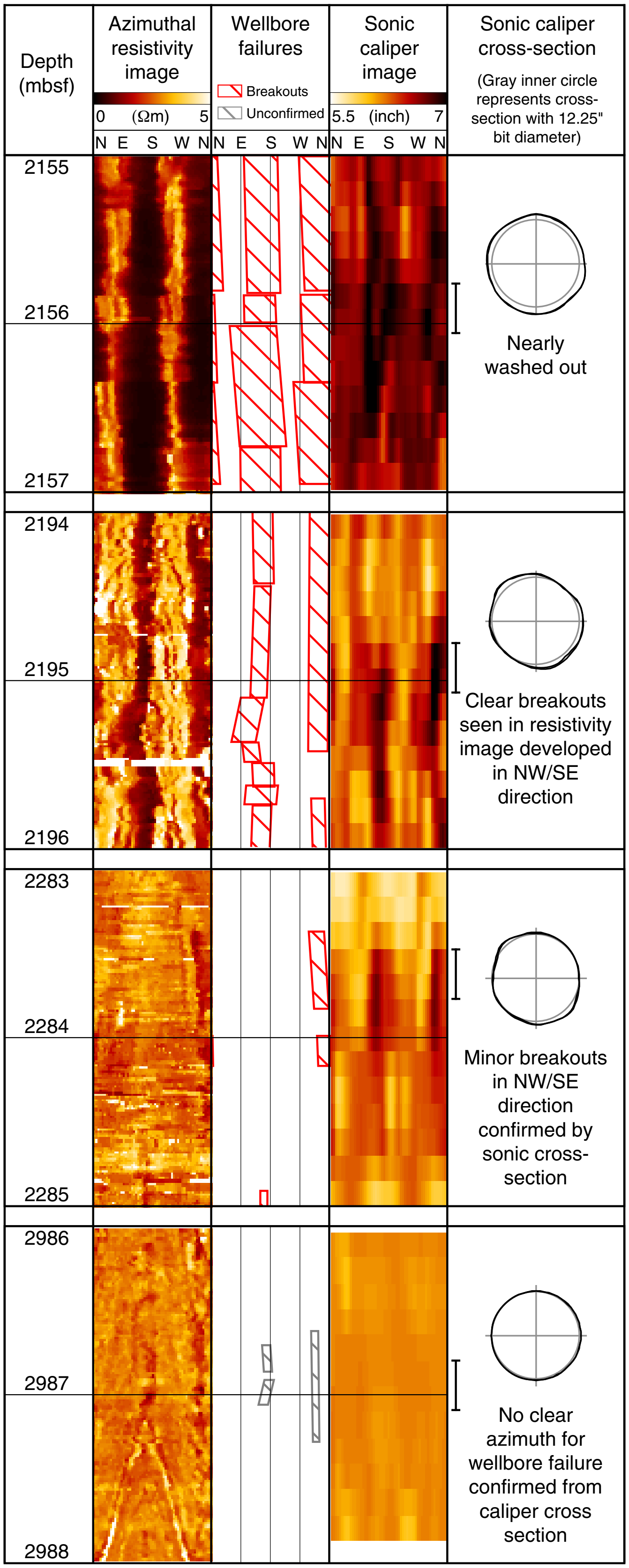

Table T1. Bottom-hole assemblies (BHAs) used for Site C0002.

Hole	Drilling type	Water depth (mbsl)	Top hole depth (mbsf)	Top hole depth BRT (m)	Total depth (mbsf)	Total depth BRT (m)	Bit size (inch)	BHA
C0002M	SD-RCB	1937.5	0.0	1967.5	512.5	2480.0	8-1/2	Bit × near-bit sub (w/float and inner tube stabilizer) × DC sub (w/landing ring) × landing sub × head sub (w/latch sleeve) × 7 inch coring DC (11) × XO × 5.68 inch HWDP (12) × XO × 5 inch DP S-140 (21 stands) × 5-1/2 inch DP S-140 (21 stands) × XO × 5-1/2 inch DP S-150
C0002F	LWD/MWD	1939.0	0.0	1967.5	2005.5	3973.0	12-1/4	Bit × GVR × ARC8 × TeleScope × 12-1/8 inch ILS × sonicVISION × 12-1/8 inch stab × 8-1/2 inch DC (1) × CST × Anderreamer × F/S × 9-1/2 inch DC (2) × 17 inch stab × 9-1/2 inch DC (1) × XO × 8-1/2 inch DC (3) × 7-3/4 inch Jar × 8-1/2 inch DC (3) × XO × 5.68 inch HWDP (12) × XO × 5 inch DP S-140 (46 stands) × 5-1/2 inch DP S-150
C0002N	Sidetrack	1939.0	860.0	2827.5	2330.0	4297.5	17	Bit × sleeve stab × Geopilot9600 w/near-bit stab × flex collar × 16-7/8 inch ILS × 8 inch DGR × 8 inch EWR × 8 inch PWD × 8 inch HCIM × HOC × MWD down screen × float sub (w/float) × 8-1/2 inch DC (12) × 8 inch hydraulic Jar × 8-1/2 inch DC (2) × XO × 5.68 inch HWDP (12) × XO × 5 inch DP S-140 (53 stands) × XO × 5-1/2 inch DP S-150
	Casing run	1939.0	NA	NA	2009.0	3976.5	NA	13-3/8 inch casing PADPRT × XO × 5-1/2 inch DP S-150 (6 m) × XO × XO × 5-7/8 inch DP NK-155 (3) × 5-7/8 inch DP NK-155 (18 stands) × XO × 6-5/8 inch DP UD-165 (1 stand) × 6-5/8 inch DP (6 m) × 6-5/8 inch DP (31 stands) × CMT stand
	Fishing	1939.0	NA	NA	1886.4	3853.9	NA	Screw-in sub (5-3/4 inch DSTJ pin) × XO × 5.68 inch HWDP (2) × XO × drilling jar × 8-1/2 inch DC (2) × XO × 5.68 inch HWDP (12) × 5-1/2 inch DP S-150 (21 stands) × XO × XO × 5-7/8 inch DP NK-155 (19 stands) × XO × 6-5/8 inch DP Z-140 (25 stands) × XO × 6-5/8 inch DP UD-165
	WBRRT	1939.0	NA	NA	NA	NA	NA	Jetting sub × XO × 5-1/2 inch DP S-140 (1stand) × XO × 8-1/2 inch DC (1) × 12-1/4 inch stab × 8-1/2 inch DC (5) × XO × 5-1/2 inch DP S-140 (1 stand) × XO × WBRRT × XO × 5-1/2 inch DP pup (6 m) × 5 inch DP S-140 (44 stands) × 6-5/8 inch DP Z-140
C0002P	Window milling	1939.0	1935.5	3903.0	1954.5	3922.0	12-1/4	Lead mill × 8-1/2 inch DC (1) × 12-1/4 inch stab × secondary mill × flex mandrel × steering mill × 8-1/2 inch DC (9) × XO × 8-1/2 inch coring DC (12) × XO × 5.68 inch HWDP (12) × XO × 5 inch DP S-140 (26 stands) × 5-1/2 inch DP S-140 (21 stands) × XO × 5-1/2 inch DP S-150 (25 stands) × XO × 6-5/8 inch DP Z-140
	Kick-off	1939.0	1936.5	3904.0	2162.5	4130.0	12-1/4	Bit × motor × 12 inch stab × HOC × DH screen × float sub (w/float) × 8-1/2 inch DC (12) × drilling jar × 8-1/2 inch DC (2) × XO × 5.68 inch HWDP (12) × XO × 5 inch DP S-140 (44 stands) × 5-1/2 inch DP S-140 (21 stands) × XO × 5-1/2 inch DP S-150 (25 stands) × XO × 6-5/8 inch DP Z-140
	RCB	1939.0	2162.5	4130.0	2118.0	4085.5	10-5/8	Bit × bit sub w/stab × RCB core barrel × top sub × head sub × 10-5/8 inch stab × 8-1/2- inch coring DC (12) × coring jar × 8-1/2 inch coring DC (3) × XO × 5.68 inch HWDP (12) × XO × 5 inch DP S-140 (44 stands) × 5-1/2 inch DP S-140 (21 stands) × 5-1/2 inch DP S-150 (25 stands) × XO × 6-5/8 inch DP Z-140
	LWD/MWD	1939.0	2100.0	4067.5	3058.5	5026.0	12-1/4	Bit × PDM × float sub (non-ported) × 12-1/4 inch stab × AFR × M5 (AGR + EWR + PWD + HCIM) × XBAT × HOC × 8-1/2 inch DC (12) × drilling jar × XO × 5.68 inch HWDP (12) × XO × 5 inch DP S-140 (65 stands) × 5-1/2 inch DP S-140 (21stands) × XO × 5-1/2 inch DP S-150 (15 stands) × XO × 6-5/8 inch DP Z-140
	Underreamer	1939.0	1936.5	3904.0	2960.5	4928.0	12-1/4, 14-1/2	Bit × bit sub × 14-1/2 inch Anderreamer × float sub (w/flapper-type float) × 8-1/2 inch DC (1) × 12-3/16 inch × 8-1/2 inch DC (11) × drilling jar × XO × 5.68 inch HWDP (12) × XO × 5 inch DP S-140 (67 stands) × 5-1/2 inch DP S-140 (21 stands) × XO × 5-1/2 inch DP S-150 (8 stands) × XO × 6-5/8 inch DP X-140
	Underreamer	1939.0	1936.5	3904.0	2960.5	4928.0	12-1/4, 14-1/2	Bit × bit sub × 14-1/2 inch Anderreamer × float sub (w/flapper-type float) × 8-1/2 inch DC (1) × 12-3/16 inch stab × 8-1/2 inch DC (11) × drilling jar × 8-1/2 inch DC (2) × XO × 5.68 inch HWDP (12) × XO × 5 inch DP S-140 (67 stands) × 5-1/2 inch DP S-140 (21 stands) × XO × 5-1/2 inch DP S-150 (25 stands) × XO × 6-5/8 inch DP Z-140
	Underreamer	1939.0	1936.5	3904.0	2964.5	4932.0	12-1/4, 14-1/2	Bit × bit sub × 14-1/2 inch Anderreamer × float sub (w/flapper-type float) × 8-1/2 inch DC (1) × 12-3/16 inch stab × 8-1/2 inch DC (11) × drilling jar × 8-1/2 inch DC (2) × XO × 5.68 inch HWDP (12) × XO × 5 inch DP S-140 (67 stands) × 5-1/2 inch DP S-140 (21 stands) × XO × 5-1/2 inch DP S-150 (13 stands) × XO × 6-5/8 inch DP Z-140
	Casing run	1939.0	NA	NA	2922.0	4889.5	NA	11-3/4 inch casing (G/S × 1 × F/C × 9 × L/C × 30 × 41, total 82 joints) × liner hanger × 5 inch DP (5 stands) × 5-1/2 inch DP S-140 (21 stands) × XO × 5-1/2 inch DP S-150 (25 stands) × XO × XO × 5-7/8 inch DP NK-155 (19 stands)

NA = not applicable. AFR = azimuthal focused resistivity tool, AGR = azimuthal gamma ray tool, ARC8 = arcVISION array resistivity compensated tool, CMT = drill stand, CST = concentric string tool, DC = drill collar, DGR = dual gamma ray tool, DP = drill pipe, EWR = electromagnetic wave resistivity tool, GVR = geoVISION resistivity tool, HOC = underreamer model, HWDP = heavy-wall drill pipe, ILS = instrument landing system, LWD/MWD = logging while drilling/measurement while drilling, PADPRT = pressure-assisted drill pipe running tool, PDM = positive-displacement motor, PWD = pressure while drilling tool, SD-RCB = small-diameter rotary core barrel system, stab = stabilizer, WBRRT = wear bushing running/retrieving tool, XBAT = azimuthal sonic/ultrasonic tool, XO = crossover sub.

Table T2. Drilling summary, Expedition 348.

Hole	Latitude	Longitude	Water depth (mbsl)	Cores (*N*)	Interval cored (m)	Core recovered (m)	Recovery (%)	Drilled interval (mbsf)	Total penetration (mbsf)	Time on site (days)
348-										
C0002M	33°18.0058′N	136°38.2397′E	1937.50	4	37.5	16.43	43.8	475–512.5	512.5	1
C0002N	33°18.0507′N	136°38.2029′E	1939.00	0	LWD/MWD	—	—	859.5–2329.3	1472.8	
C0002P	33°18.0507′N	136°38.2029′E	1939.00	6	55.5	31.5	56.7	2163–2218.5	55.5	
	33°18.0507′N	136°38.2029′E	1939.00	0	LWD/MWD	—	—	2163–3058.5	840.0	
			Totals:	10	93	47.93	50.3		2880.8	

LWD/MWD = logging while drilling/measurement while drilling. — = not applicable.

Table T3. Coring completed during Expedition 348.

Hole	Longitude	Latitude	Water depth (mbsl)	Core	Time on deck (h UTC)	Date (2013)	Depth (mbsf)	Advanced (m)	Recovered (m)	Recovery (%)	Drilled interval (mbsf)	Cored interval (m)	Core recovered (m)	Recovery (%)
348-														
C0002M	33°18.0058′N	136°38.2397′E	1937.5	1R	1135	21 Sep	475.0	9.5	5.3	56.0	475–512.5	37.5	16.4	43.8
				2R	1442	21 Sep	484.5	9.5	4.0	44.2				
				3R	1726	21 Sep	493.5	9.0	2.5	26.7				
				4R	1953	21 Sep	503.0	9.5	4.6	48.4				
C0002P	33°18.0507′N	136°38.2029′E	1939.0	1R	0513	23 Dec	2163.0	9.5	0.4	4.2	2163–2218.5	55.5	31.5	56.7
				2R	1138	23 Dec	2172.5	9.5	6.1	63.7				
				3R	1842	23 Dec	2182.0	9.5	2.9	30.3				
				4R	0353	24 Dec	2191.5	9.5	8.2	86.2				
				5R	1214	24 Dec	2201.0	8.0	5.5	68.8				
				6R	2015	24 Dec	2209.0	9.5	8.5	89.1				

Table T4. Casing depths, drilling depths, and significant events, Expedition 348.

Event	Time (h UTC)	Date	Measured depth BRT (m)	Measured depth (mbsf)	True vertical depth (mbsf)	Remarks
Sea level			1967.50	0.00	0.00	
36 inch casing			2021.40	53.90	53.90	
20 inch casing			2827.80	860.30	860.30	
Lithologic Unit I/II boundary			2167.50	200.00	200.00	
Lithologic Unit II/III boundary			2843.00	875.50	875.50	
Lithologic Unit III/IV boundary			2943.00	975.50	975.50	
Lithologic Unit IV/V boundary			3633.00	1665.50	1664.40	
TD Hole C0002F			3973.00	2005.50	2005.50	
Hole C0002F side track	0815	4 Nov 2013	2845.00	877.50	877.50	
Hole C0002N	0815	4 Nov 2013	2827.80	860.30	860.30	
Borehole conditioning (top)	1030	6 Nov 2013	2805.90	838.40	838.40	*1205–1221 mbsf; ~15 h
Borehole conditioning (bottom)	2245	5 Nov 2013	3186.50	1219.00	1217.90	*1205–1221 mbsf; ~15 h
WOW #1	2115	7 Nov 2013	3645.00	1677.50	1676.40	POOH to 1939.8 m BRT
WOW #1	2200	8 Nov 2013	3645.00	1677.50	1676.40	*1662–1678 mbsf; ~28.5 h
Lost signal	0815	9 Nov 2013	3823.80	1856.30	1855.20	
WOW #2	0000	10 Nov 2013	3976.00	2008.50	2007.40	POOH to surface
WOW #2	2215	11 Nov 2013	3976.00	2008.50	2007.40	*1992–2008 mbsf; ~50 h
Mud loss #1	2345	11 Nov 2013	4004.00	2036.50	2035.40	*2022–2038 mbsf; ~8.5 h
Mud loss #1	0000	12 Nov 2013	3995.50	2028.00	2026.90	*2022–2038 mbsf; ~8.5 h
Mud loss #2	1100	12 Nov 2013	4085.00	2117.50	2116.40	
Hole C0002N TD	0115	13 Nov 2013	4297.50	2330.00	2328.90	859.5–2329.3 (1962.6–2008.5 overlap zone) mbsf; logged interval
Hole C0002N 13-3/8 inch casing	0645	22 Nov 2013	3977.50	2010.00	2008.90	2013 m total length
13-3/8 inch casing TOC			3320.00	1352.50	1351.41	
Bridge plug	1745	7 Dec 2013	3916.50	1949.00	1947.90	
Top of DC fish			3928.08	1960.58	1959.50	
Window top			3904.00	1936.50	1935.40	
Window bottom			3912.63	1945.13	1944.00	
Hole C0002P sidetrack top	0000	15 Dec 2013	3904.00	1936.50	1935.40	
LOT #1	0630	15 Dec 2013	3922.00	1954.50	1953.40	1130 psi (7.79 MPa)
LOT #2	0700	15 Dec 2013	3922.00	1954.50	1953.40	1280 psi (8.83 MPa)
WOW #3		18–20, Dec 2013	4035.20	2067.70	2066.50	
Bottom of kickoff	1400	20 Dec 2013	4075.00	2107.50	2106.30	
Core prep		20–22 Dec 2013	4130.50	2163.00	2161.70	
Top RCB coring	2045	22 Dec 2013	4130.50	2163.00	2161.70	
Fault zone			4172.50	2205.00		Zone width: 2204.9–2205.8 mbsf
Bottom of RCB coring	1745	24 Dec 2013	4186.00	2218.50	2216.60	
Open hole (top)	1200	27 Dec 2013	4130.00	2162.50	2161.20	*2163–2218.5 mbsf; >66.25 h
Open hole (bottom)	1800	27 Dec 2013	4186.00	2218.50	2217.10	*2163–2218.5 mbsf; >66.25 h
TD 12-1/4 inch LWD	0700	1 Jan 2014	5026.00	3058.50	3056.60	2163.5–3058.5 mbsf; logged interval
Top of open hole 14-1/2 inch	2230	2 Jan 2014	3928.00	1960.50	1959.40	
Stuck pipe	1340	11 Jan 2014	4928.00	2960.50	2959.50	2960.5 mbsf; ~1.75 h
Stuck pipe	0400	14 Jan 2014	4932.00	2964.50	2963.50	2964.5 mbsf; ~17 h; pressure stabilized at 15.2 MPa
Hole C0002P 11-3/4 inch casing shoe	0630	18 Jan 2014	4890.00	2922.50	2920.65	1007.18 m total length
LOT #3	1945	19 Jan 2014				After diverter, before CRT; 650 psi (4.48 MPa) and 530 psi (3.65 MPa)
TD 14-1/2 inch hole			4927.50	2960.00	2958.14	

* = depth intervals with long exposure time before logging-while-drilling tools were able to log after initial drilling. TD = total depth, WOW = waiting on weather, TOC = top of casing/cement, DC = drill collar, LOT = leak-off test, RCB = rotary core barrel, LWD = logging while drilling, POOH = pull out of hole, CRT =casing running tool.

Table T5. Summary of lithologic units, depths, and sample intervals, Holes C0002N and C0002P.

Unit	Subunit	Hole C0002M depth (mbsf)	Hole C0002N depth (mbsf)	Hole C0002P depth (mbsf)	Lithology Major	Lithology Minor	Environmental interpretation
II		475.0–512.5			Silty claystone	Sandstone	Lower forearc succession of the Kumano basin
III			870.5–975.5		Silty claystone	Sandstone	Lower part of the Kumano forearc basin
IV			975.5–1665.5		Silty claystone	Sandstone	Upper accretionary prism slope basin
	A		975.5–1045.5		Silty claystone	Sandstone	
	B		1045.5–1125.5		Silty claystone	Sandstone	Trench, accretionary prism slope basin, or Shikoku Basin submarine fan and related deposits
	C		1125.5–1345.5		Silty claystone	Sandstone	
	D		1345.5–1525.5		Silty claystone	Sandstone	
	E		1525.5–1665.5		Silty claystone	Sandstone	
V			1665.5–2325.5	1960.5–3058.5	Silty claystone	Sandstone	Hemipelagic deposits; trench or lower Shikoku Basin?
	A		1665.5–2325.5	1960.5–2625.5	Silty claystone	Sandstone	
	B		—	2625.5–3058.5	Silty claystone	Sandstone	

Table T6. X-ray diffraction analysis on bulk powder samples from Hole C0002M.

Core, section	Depth (mbsf)	Integrated peak area (total counts)				Absolute mineral abundance calculated from SVD normalization factors (wt%)					Relative abundance (wt%)			
		Total clay	Quartz	Feldspar	Calcite	Total clay	Quartz	Feldspar	Calcite	Sum	Total clay	Quartz	Feldspar	Calcite
348-C0002M-														
1R-1	475.84	2904	47868	23863	5018	43.3	25.8	24.8	1.4	95.3	45.5	27.1	26.0	1.5
1R-2	477.04	3031	48522	19310	5573	42.5	26.5	19.6	2.2	90.8	46.8	29.2	21.6	2.4
1R-3	478.70	2940	32703	12711	12157	38.8	17.7	12.5	12.1	81.2	47.9	21.8	15.5	14.9
2R-2	486.98	2308	60065	27896	3537	38.5	32.9	29.2	0.1	100.6	38.3	32.7	29.0	0.1
2R-3	487.97	3401	40775	14847	2875	44.3	22.2	14.7	0.1	81.3	54.5	27.3	18.0	0.1
3R-1	494.32	3123	45981	18560	3275	43.1	25.1	18.8	0.1	87.0	49.5	28.8	21.6	0.1
3R-1	494.35	4214	35669	11127	4388	51.6	19.3	10.4	0.1	81.4	63.4	23.7	12.7	0.1
3R-2	495.09	3723	33028	11335	4792	46.4	17.8	10.8	1.0	76.0	61.0	23.5	14.2	1.3
4R-2	504.83	3647	32795	12210	6757	46.1	17.7	11.8	3.8	79.3	58.1	22.3	14.9	4.8
4R-2	505.51	3943	35121	13501	5105	49.8	18.9	13.1	1.0	82.9	60.2	22.8	15.8	1.2
4R-3	506.48	2645	49544	20810	10946	39.3	27.1	21.3	10.0	97.7	40.2	27.7	21.8	10.3

SVD = singular value decomposition.

Table T7. X-ray fluorescence analysis on bulk powder samples from Hole C0002M.

Core, section	Top depth (mbsf)	Na_2O (wt%)	MgO (wt%)	Al_2O_3 (wt%)	SiO_2 (wt%)	P_2O_5 (wt%)	K_2O (wt%)	CaO (wt%)	TiO_2 (wt%)	MnO (wt%)	Fe_2O_3 (wt%)	Loss on ignition (wt%)
348-C0002M-												
1R-1	475.84	2.430	1.955	16.336	66.253	0.095	3.069	3.401	0.713	0.075	5.272	6.878
1R-2	477.04	2.525	1.897	15.993	65.962	0.095	3.085	3.629	0.688	0.066	5.034	6.711
1R-3	478.70	2.338	2.481	16.109	59.693	0.207	3.038	7.811	0.686	0.083	6.756	10.578
2R-2	486.98	2.555	1.833	14.877	69.985	0.081	2.92	2.766	0.621	0.064	5.057	5.367
2R-3	487.97	2.409	2.763	17.322	63.94	0.095	3.19	2.183	0.807	0.097	6.733	6.511
3R-1	494.32	2.395	2.017	16.638	65.604	0.103	3.156	2.614	0.719	0.068	5.667	6.704
3R-1	494.35	2.256	2.473	18.063	62.252	0.113	3.361	3.019	0.767	0.082	6.964	7.723
3R-2	495.09	2.212	2.664	17.938	60.609	0.18	3.383	3.405	0.767	0.104	8.112	8.59
4R-2	504.83	2.346	2.588	17.451	61.555	0.124	3.258	3.971	0.736	0.08	7.44	8.483
4R-2	505.51	2.313	2.731	17.325	60.127	0.131	3.231	4.9	0.764	0.094	7.647	9.208
4R-3	506.48	2.243	1.909	14.186	63.915	0.263	2.781	7.432	0.608	0.077	5.619	9.004
	Average:	2.366	2.301	16.567	63.627	0.135	3.134	4.103	0.716	0.081	6.391	7.796

Table T8. Visual lithologic estimations (binocular microscope) of percent silty clay(stone), percent sand(stone), induration, grain shape, and fossil and wood content, Holes C0002N and C0002P. (Continued on next five pages.)

Cuttings sample	Bottom depth (mbsf)	Silty claystone (%)	Silty claystone consolidation	Silty claystone structures	Silty claystone shape	Sandstone (%)	Sandstone consolidation	Sandstone structures	Sandstone shape	Sandstone texture	Wood/Lignite	Fossils
348-C0002N-												
3-SMW	875.5	100	Semi	No	Round	0					Not observed	Not observed
5-SMW	885.5	100	Semi	No	Round	0						
7-SMW	895.5	100	Semi	No	Round	0						
9-SMW	905.5	100	Semi	No	Round	0						
12-SMW	915.5	100	Semi	No	Round	0						
14-SMW	925.5	100	Semi	No	Round	0						
16-SMW	935.5	100	Semi	No	Round	0						
18-SMW	945.5	100	Semi	No	Subangular	0					Not observed	Not observed
20-SMW	955.5	100	Semi	No	Subangular	0					Not observed	Not observed
22-SMW	965.5	100	Semi	No	Subangular	0					Not observed	Not observed
24-SMW	975.5	100	Semi	No	Subangular	0					Not observed	Not observed
26-SMW	985.5	100	Semi	No	Subangular	0					Rare	Not observed
28-SMW	995.5	95	Semi	No	Subangular	5	Loose	No			Rare	Rare
30-SMW	1005.5	95	Semi	No	Subangular	5	Loose	No			Not observed	Not observed
32-SMW	1015.5	95	Semi	No	Subangular	5	Loose	No			Rare	Not observed
34-SMW	1025.5	95	Semi	No	Subangular	5	Loose	No			Not observed	Not observed
36-SMW	1035.5	90	Semi	No	Subangular	10	Loose	No			Rare	Not observed
39-SMW	1045.5	90	Semi	No	Subangular	10	Loose	No			Not observed	Not observed
40-SMW	1052.5	95	Semi	No	Subangular	5	Loose	No			Not observed	Not observed
41-SMW	1067.5	100	Semi	No	Subangular	0		No			Not observed	Not observed
42-SMW	1069.5	100	Semi	No	Subangular	0		No			Not observed	Not observed
43-SMW	1070.5	100	Semi	No	Round	0		No			Not observed	Not observed
44-SMW	1075.5	100	Semi	No	Round	0		No			Not observed	Not observed
46-SMW	1085.5	100	Semi	No	Round	0		No			Not observed	Not observed
48-SMW	1095.5	100	Semi	No	Round	0		No			Not observed	Not observed
50-SMW	1105.5	100	Semi	No	Round	0		No			Not observed	Not observed
52-SMW	1115.5	100	Semi	No	Subangular	0		No			Not observed	Not observed
54-SMW	1125.5	100	Semi	No	Subangular	0		No			Not observed	Not observed
57-SMW	1135.5	90	Semi	No	Subangular	10	Loose	No			Not observed	Not observed
59-SMW	1145.5	80	Semi	No	Round	20	Loose	No			Not observed	Rare
61-SMW	1155.5	90	Semi	No	Round	10	Loose	No			Not observed	Not observed
63-SMW	1165.5	70	Semi	No	Round	30	Loose	No			Not observed	Not observed
65-SMW	1175.5	70	Semi	No	Round	30	Loose	No			Not observed	Not observed
67-SMW	1185.5	75	Semi	No	Subangular	25	Loose	No			Not observed	Not observed
69-SMW	1195.5	70	Semi	No	Round	30	Loose	No			Not observed	Not observed
71-SMW	1205.5	80	Semi	No	Round	20	Loose	No			Not observed	Not observed
73-SMW	1215.5	60	Semi	No	Round	40	Loose	No			Not observed	Not observed
81-SMW	1225.5	80	Semi	No	Subangular	20	Loose	No			Not observed	Not observed
83-SMW	1235.5	90	Semi	No	Subangular	10	Loose	No			Not observed	Not observed
85-SMW	1245.5	85	Semi	No	Subangular	15	Loose	No			Not observed	Not observed
87-SMW	1255.5	80	Semi	No	Round	20	Loose	No			Rare	Not observed
89-SMW	1265.5	80	Semi	No	Round	20	Loose	No			Not observed	Not observed
91-SMW	1275.5	60	Semi	No	Round	40	Loose	No			Not observed	Not observed
93-SMW	1285.5	60	Semi	No	Round	40	Loose	No			Not observed	Rare
95-SMW	1295.5	70	Semi	No	Round	30	Loose	No			Not observed	Not observed
97-SMW	1305.5	80	Semi	No	Subangular	20	Loose	No			Not observed	Rare
99-SMW	1315.5	70	Semi	No	Subangular	30	Loose	No			Not observed	Not observed
101-SMW	1325.5	70	Semi	No	Round	30	Loose	No			Not observed	Not observed

Table T8 (continued). (Continued on next page.)

Cuttings sample	Bottom depth (mbsf)	Silty claystone (%)	Silty claystone consolidation	Silty claystone structures	Silty claystone shape	Sandstone (%)	Sandstone consolidation	Sandstone structures	Sandstone shape	Sandstone texture	Wood/Lignite	Fossils
105-SMW	1335.5	80	Soft	No	Round	20	Loose	No			Not observed	Not observed
107-SMW	1345.5	85	Semi	No	Subangular	15	Loose	No			Not observed	Not observed
109-SMW	1355.5	90	Semi	No	Round	10	Loose	No			Not observed	Not observed
111-SMW	1365.5	90	Semi	No	Round	10	Loose	No			Not observed	Not observed
113-SMW	1375.5	90	Semi	No	Round	10	Loose	No			Not observed	Not observed
115-SMW	1385.5	55	Semi	No	Round	45	Loose	No			Not observed	Not observed
117-SMW	1395.5	90	Semi	No	Subangular	10	Loose	No			Not observed	Not observed
119-SMW	1405.5	80	Semi	No	Subangular	20	Loose	No			Not observed	Not observed
121-SMW	1415.5	80	Semi	No	Subangular	20	Loose	No			Not observed	Not observed
123-SMW	1425.5	90	Semi	No	Round	10	Loose	No			Not observed	Not observed
125-SMW	1435.5	80	Semi	No	Round	20	Loose	No			Rare	Rare
128-SMW	1445.5	70	Semi	No	Subangular	30	Loose	No			Rare	Not observed
130-SMW	1455.5	70	Semi	No	Subangular	30	Loose	No			Not observed	Not observed
132-SMW	1465.5	65	Semi	No	Subangular	35	Loose	No			Rare	Not observed
134-SMW	1475.5	65	Semi	No	Subangular	35	Loose	No			Not observed	Not observed
136-SMW	1485.5	65	Semi	No	Subangular	35	Loose	No			Rare	Not observed
138-SMW	1495.5	60	Semi	No	Subangular	40	Loose	No			Not observed	Not observed
140-SMW	1505.5	75	Semi	No	Subangular	25	Loose	No			Not observed	Rare
142-SMW	1515.5	60	Semi	No	Subangular	40	Loose	No			Not observed	Not observed
146-SMW	1525.5	55	Semi	No	Subangular	45	Loose	No			Not observed	Not observed
148-SMW	1535.5	65	Semi	No	Subangular	35	Loose	No			Not observed	Not observed
150-SMW	1545.5	65	Semi	No	Subangular	35	Loose	No			Not observed	Not observed
152-SMW	1555.5	70	Semi	No	Subangular	30	Loose	No			Not observed	Rare
154-SMW	1565.5	70	Semi	No	Subangular	30	Loose	No			Not observed	Rare
156-SMW	1575.5	65	Semi	No	Subangular	35	Loose	No			Not observed	Not observed
158-SMW	1585.5	60	Semi	No	Subangular	40	Loose	No			Not observed	Not observed
160-SMW	1595.5	70	Semi	No	Subangular	30	Loose	No			Not observed	Not observed
162-SMW	1605.5	55	Semi	No	Subangular	45	Loose	No			Not observed	Not observed
164-SMW	1615.5	60	Semi	No	Subangular	40	Loose	No			Not observed	Not observed
166-SMW	1625.5	70	Semi	Yes	Subangular	30	Loose	No			Not observed	Not observed
169-SMW	1635.5	70	Semi	Yes	Subangular	30	Loose	No			Not observed	Not observed
171-SMW	1645.5	50	Semi	Yes	Subangular	50	Loose	No			Not observed	Not observed
173-SMW	1655.5	40	Semi	Yes	Subangular	60	Loose	No			Not observed	Not observed
175-SMW	1665.5	45	Semi	Yes	Subangular	55	Loose	No			Not observed	Not observed
177-SMW	1677.5	80	Semi	Yes	Subangular	20	Loose	No			Not observed	Not observed
182-SMW	1685.5	95	Semi	Yes	Subangular	5	Loose	No			Not observed	Not observed
184-SMW	1695.5	95	Semi	Yes	Subangular	5		No			Not observed	Not observed
186-SMW	1705.5	100	Semi	Yes	Subangular	0					Not observed	Not observed
188-SMW	1715.5	100	Semi	Yes	Subangular	0					Not observed	Not observed
190-SMW	1725.5	100	Semi	Yes	Subangular	0					Not observed	Not observed
192-SMW	1735.5	100	Semi	Yes	Subangular	0					Not observed	Not observed
195-SMW	1745.5	100	Soft	Yes	Subangular	0					Not observed	Not observed
197-SMW	1755.5	100	Soft	Yes	Subangular	0					Not observed	Not observed
199-SMW	1765.5	100	Soft	No	Subangular	0					Not observed	Not observed
201-SMW	1775.5	100	Semi	No	Angular	0					Not observed	Not observed
203-SMW	1785.5	100	Semi	No	Subangular	0					Not observed	Not observed
205-SMW	1795.5	100	Semi	No	Angular	0					Not observed	Not observed
207-SMW	1805.5	100	Semi	Yes	Angular	0					Not observed	Not observed
209-SMW	1815.5	100	Semi	No	Subangular	0					Not observed	Not observed
211-SMW	1825.5	100	Semi	No	Subangular	0					Not observed	Not observed

Table T8 (continued). (Continued on next page.)

Cuttings sample	Bottom depth (mbsf)	Silty claystone (%)	Silty claystone consolidation	Silty claystone structures	Silty claystone shape	Sandstone (%)	Sandstone consolidation	Sandstone structures	Sandstone shape	Sandstone texture	Wood/Lignite	Fossils
213-SMW	1835.5	100	Semi	Yes	Subangular	0					Not observed	Not observed
216-SMW	1845.5	100	Semi	Yes	Subangular	0					Not observed	Not observed
218-SMW	1855.5	100	Semi	Yes	Subangular	0					Not observed	Not observed
220-SMW	1865.5	90	Semi	No	Subangular	10	Loose	No			Not observed	Not observed
222-SMW	1875.5	95	Semi	No	Subangular	5	Loose	No			Not observed	Not observed
224-SMW	1885.5	95	Semi	No	Subangular	5	Loose	No			Not observed	Not observed
226-SMW	1895.5	100	Semi	Yes	Angular	0					Not observed	Not observed
228-SMW	1905.5	100	Semi	No	Subangular	0					Not observed	Not observed
230-SMW	1915.5	100	Semi	No	Round	0					Not observed	Not observed
232-SMW	1925.5	100	Semi	No	Round	0					Not observed	Not observed
234-SMW	1935.5	100	Semi	Yes	Round	0					Not observed	Not observed
237-SMW	1945.5	100	Semi	No	Subangular	0					Not observed	Not observed
239-SMW	1955.5	100	Semi	No	Round	0					Not observed	Not observed
241-SMW	1965.5	100	Semi	Yes	Round	0					Not observed	Not observed
243-SMW	1975.5	100	Semi	No	Round	0					Not observed	Not observed
248-SMW	1985.5	100	Semi	No	Round	0					Not observed	Not observed
250-SMW	1995.5	100	Semi	No	Round	0					Not observed	Not observed
252-SMW	2005.5	100	Semi	No	Round	0					Not observed	Not observed
259-SMW	2015.5	95	Hard	Yes	Subangular	5	Loose	No			Not observed	Rare
261-SMW	2025.5	95	Hard	Yes	Subangular	5	Loose	No			Not observed	Not observed
264-SMW	2035.5	95	Hard	Yes	Subangular	5	Loose	No			Not observed	Not observed
266-SMW	2045.5	90	Hard	Yes	Subangular	10	Loose	No			Not observed	Not observed
268-SMW	2055.5	90	Hard	Yes	Subangular	10	Loose	No			Not observed	Not observed
270-SMW	2065.5	80	Hard	Yes	Subangular	20	Loose	No			Not observed	Not observed
272-SMW	2075.5	80	Hard	Yes	Subangular	20	Loose	No			Not observed	Not observed
274-SMW	2085.5	80	Hard	Yes	Subangular	20	Loose	No			Not observed	Not observed
276-SMW	2095.5	85	Hard	Yes	Subangular	15	Loose	No			Not observed	Not observed
278-SMW	2105.5	80	Hard	Yes	Subangular	20	Loose	No			Not observed	Not observed
281-SMW	2115.5	85	Hard	Yes	Subangular	15	Loose	No			Not observed	Not observed
283-SMW	2125.5	90	Semi	Yes	Subangular	10	Loose	No			Not observed	Not observed
285-SMW	2135.5	90	Semi	Yes	Subangular	10	Loose	No			Not observed	Not observed
287-SMW	2145.5	90	Semi	Yes	Subangular	10	Loose	No			Not observed	Not observed
289-SMW	2155.5	95	Semi	Yes	Subangular	5	Loose	No			Not observed	Not observed
291-SMW	2165.5	100	Semi	Yes	Subangular	0					Not observed	Not observed
296-SMW	2175.5	100	Semi	Yes	Subangular	0					Not observed	Not observed
298-SMW	2185.5	95	Semi	No	Subangular	0					Not observed	Not observed
300-SMW	2195.5	100	Soft	No	Subangular	0					Not observed	Not observed
302-SMW	2205.5	100	Soft	No	Subangular	0					Not observed	Not observed
304-SMW	2215.5	100	Soft	No	Subangular	0					Not observed	Not observed
306-SMW	2225.5	100	Soft	No	Subangular	0					Not observed	Not observed
308-SMW	2235.5	100	Soft	No	Subangular	0					Not observed	Not observed
310-SMW	2245.5	100	Soft	No	Subangular	0					Not observed	Not observed
312-SMW	2255.5	100	Soft	No	Subangular	0					Not observed	Not observed
314-SMW	2265.5	100	Soft	No	Subangular	0					Not observed	Not observed
316-SMW	2275.5	100	Soft	No	Subangular	0					Not observed	Not observed
318-SMW	2285.5	100	Soft	No	Subangular	0					Not observed	Not observed
321-SMW	2295.5	100	Soft	No	Subangular	0					Not observed	Not observed
323-SMW	2305.5	100	Soft	No	Subangular	0					Not observed	Not observed
325-SMW	2315.5	100	Soft	No	Subangular	0					Not observed	Not observed
327-SMW	2325.5	100	Soft	No	Subangular	0					Not observed	Not observed

Table T8 (continued). (Continued on next page.)

Cuttings sample	Bottom depth (mbsf)	Silty claystone (%)	Silty claystone consolidation	Silty claystone structures	Silty claystone shape	Sandstone (%)	Sandstone consolidation	Sandstone structures	Sandstone shape	Sandstone texture	Wood/Lignite	Fossils
348-C0002P-												
9-SMW	1965.5	100	Semi	Yes	Subangular						Not observed	Not observed
14-SMW	1975.5	100	Semi	No	Subangular						Not observed	Not observed
16-SMW	1985.5	100	Semi	No	Subangular						Not observed	Not observed
18-SMW	1995.5	100	Semi	No	Subangular						Not observed	Not observed
20-SMW	2005.5	100	Semi	No	Subangular						Not observed	Not observed
25-SMW	2015.5	100	Semi	No	Subangular						Not observed	Not observed
28-SMW	2025.5	100	Soft	No	Subangular						Not observed	Not observed
30-SMW	2035.5	100	Soft	No	Subangular						Not observed	Not observed
32-SMW	2045.5	100	Soft	No	Subangular						Not observed	Not observed
34-SMW	2055.5	100	Soft	No	Subangular						Not observed	Not observed
36-SMW	2065.5	100	Soft	No	Subangular						Not observed	Not observed
43-SMW	2075.5	100	Soft	No	Subangular						Not observed	Not observed
45-SMW	2085.5	70	Semi	No	Subangular	30	Soft	No	Round	Crumbly	Not observed	Not observed
47-SMW	2095.5	80	Semi	No	Subangular	20	Soft	No	Round	Crumbly	Not observed	Not observed
49-SMW	2105.5	65	Soft	No	Round	35	Soft	No	Round	Crumbly	Not observed	Not observed
53-SMW	2115.5	100	Soft	Yes	Subangular	0					Not observed	Not observed
56-SMW	2125.5	100	Soft	No	Subangular	0					Not observed	Not observed
58-SMW	2135.5	100	Semi	No	Subangular	0					Not observed	Not observed
61-SMW	2145.5	90	Semi	No	Subangular	10	Soft	No	Round	Crumbly	Not observed	Not observed
63-SMW	2155.5	90	Semi	No	Subangular	10	Soft	No	Round	Crumbly	Not observed	Not observed
71-SMW	2165.5	65	Semi	Yes	Subangular	35	Soft	No	Round	Crumbly	Not observed	Not observed
73-SMW	2175.5	80	Semi	Yes	Subangular	20	Soft	No	Round	Crumbly	Not observed	Not observed
74-SMW	2180.5	85	Semi	Yes	Subangular	15	Soft	No	Round	Crumbly	Not observed	Not observed
76-SMW	2185.5	65	Semi	Yes	Subangular	35	Soft	No	Round	Crumbly	Not observed	Not observed
81-SMW	2195.5	70	Semi	Yes	Subangular	30	Soft	No	Round	Crumbly	Not observed	Not observed
82-SMW	2200.5	85	Semi	Yes	Subangular	15	Soft	No	Round	Crumbly	Not observed	Not observed
83-SMW	2205.5	80	Semi	Yes	Subangular	20	Soft	No	Round	Crumbly	Not observed	Not observed
86-SMW	2215.5	80	Semi	Yes	Subangular	20	Soft	No	Round	Crumbly	Not observed	Not observed
107-SMW	2225.5	90	Semi	Yes	Subangular	10	Semi	No	Round	Crumbly	Not observed	Not observed
109-SMW	2235.5	90	Semi	Yes	Subangular	10	Semi	No	Round	Crumbly	Not observed	Not observed
111-SMW	2245.5	95	Semi	Yes	Subangular	5	Semi	No	Round	Crumbly	Not observed	Not observed
113-SMW	2255.5	100	Semi	Yes	Subangular	0					Not observed	Not observed
115-SMW	2265.5	100	Semi	Yes	Subangular	0					Not observed	Not observed
117-SMW	2275.5	90	Semi	Yes	Subangular	10	Semi	No	Round	Crumbly	Not observed	Not observed
121-SMW	2285.5	90	Semi	Yes	Subangular	10	Semi	No	Round	Crumbly	Not observed	Not observed
123-SMW	2295.5	85	Semi	Yes	Subangular	15	Semi	No	Round	Crumbly	Not observed	Not observed
125-SMW	2305.5	90	Semi	Yes	Subangular	10	Semi	No	Round	Crumbly	Not observed	Not observed
127-SMW	2315.5	90	Semi	Yes	Subangular	10	Semi	No	Round	Crumbly	Not observed	Not observed
129-SMW	2325.5	95	Semi	Yes	Subangular	5	Semi	No	Round	Crumbly	Not observed	Not observed
131-SMW	2335.5	95	Semi	No	Round	5	Semi	No	Round	Crumbly	Not observed	Not observed
133-SMW	2345.5	95	Semi	No	Round	5	Semi	No	Round	Crumbly	Not observed	Not observed
136-SMW	2355.5	95	Semi	Yes	Subangular	10	Semi	No	Round	Crumbly	Not observed	Not observed
138-SMW	2365.5	95	Semi	No	Round	5	Semi	No	Round	Crumbly	Not observed	Not observed
141-SMW	2375.5	95	Semi	No	Round	5	Semi	No	Round	Crumbly	Rare	Not observed
143-SMW	2385.5	90	Semi	Yes	Subangular	10	Semi	No	Round	Crumbly	Not observed	Not observed
145-SMW	2395.5	85	Semi	Yes	Subangular	15	Semi	No	Round	Crumbly	Not observed	Not observed
149-SMW	2405.5	90	Semi	Yes	Subangular	10	Semi	No	Round	Crumbly	Not observed	Not observed
151-SMW	2415.5	85	Semi	No	Subangular	15	Semi	No	Round	Crumbly		
155-SMW	2425.5	85	Semi	No	Subangular	15	Semi	No	Round	Crumbly		

Table T8 (continued). (Continued on next page.)

Cuttings sample	Bottom depth (mbsf)	Silty claystone (%)	Silty claystone consolidation	Silty claystone structures	Silty claystone shape	Sandstone (%)	Sandstone consolidation	Sandstone structures	Sandstone shape	Sandstone texture	Wood/Lignite	Fossils
157-SMW	2435.5	85	Semi	No	Subangular	15	Semi	No	Round	Crumbly		
159-SMW	2445.5	75	Semi	Yes	Subangular	25	Semi	No	Round	Crumbly		
161-SMW	2455.5	80	Semi	Yes	Subangular	20	Semi	No	Round	Crumbly		
163-SMW	2465.5	90	Semi	No	Subangular	10	Semi	No	Round	Crumbly		
165-SMW	2475.5	100	Semi	No	Subangular	0					Not observed	Not observed
168-SMW	2485.5	100	Semi	Yes	Subangular	0					Not observed	Not observed
170-SMW	2495.5	100	Semi	No	Subangular	0					Not observed	Not observed
172-SMW	2505.5	90	Semi	No	Subangular	10	Semi	No	Round	Crumbly	Not observed	Not observed
174-SMW	2515.5	90	Semi	No	Subangular	10	Semi	No	Round	Crumbly	Not observed	Not observed
176-SMW	2525.5	85	Semi	No	Subangular	15	Semi	No	Round	Crumbly	Not observed	Not observed
179-SMW	2535.5	85	Semi	No	Subangular	15	Semi	No	Round	Crumbly	Not observed	Not observed
181-SMW	2545.5	90	Soft	No	Subangular	10	Semi	No	Round	Crumbly	Not observed	Not observed
183-SMW	2555.5	95	Soft	No	Subangular	5	Semi	No	Round	Crumbly	Not observed	Not observed
185-SMW	2565.5	95	Soft	No	Subangular	5	Semi	No	Round	Crumbly	Not observed	Not observed
187-SMW	2575.5	95	Soft	No	Subangular	5	Semi	No	Round	Crumbly	Not observed	Not observed
189-SMW	2585.5	90	Semi	Yes	Subangular	10	Semi	No	Round	Crumbly	Not observed	Not observed
191-SMW	2595.5	90	Semi	Yes	Subangular	10	Semi	No	Round	Crumbly	Not observed	Not observed
196-SMW	2605.5	80	Semi	No	Subangular	20	Semi	No	Round	Crumbly	Not observed	Not observed
198-SMW	2615.5	90	Semi	No	Subangular	10	Semi	No	Round	Crumbly	Not observed	Not observed
200-SMW	2625.5	100	Soft	No	Subangular	0					Not observed	Not observed
202-SMW	2635.5	100	Soft	No	Subangular	0					Not observed	Not observed
204-SMW	2645.5	100	Soft	No	Subangular	0					Not observed	Not observed
208-SMW	2655.5	100	Soft	No	Subangular	0					Not observed	Not observed
210-SMW	2665.5	100	Soft	No	Subangular	0					Not observed	Not observed
213-SMW	2675.5	98	Soft	No	Subangular	2	Semi	No	Round	Crumbly	Not observed	Not observed
215-SMW	2685.5	100	Soft	Yes	Subangular	0					Not observed	Not observed
217-SMW	2695.5	100	Soft	Yes	Subangular	0					Not observed	Not observed
219-SMW	2705.5	100	Soft	Yes	Subangular	0					Not observed	Not observed
221-SMW	2715.5	100	Soft	Yes	Subangular	0					Not observed	Not observed
224-SMW	2725.5	100	Soft	Yes	Subangular	0					Not observed	Not observed
226-SMW	2735.5	100	Soft	Yes	Subangular	0					Not observed	Not observed
229-SMW	2745.5	100	Soft	No	Subangular	0					Not observed	Not observed
231-SMW	2755.5	100	Soft	No	Subangular	0					Not observed	Not observed
233-SMW	2765.5	100	Semi	No	Subangular	0					Not observed	Not observed
235-SMW	2775.5	100	Soft	No	Subangular	0					Not observed	Not observed
237-SMW	2785.5	100	Soft	No	Subangular	0					Not observed	Not observed
240-SMW	2795.5	100	Semi	No	Subangular	0					Not observed	Not observed
242-SMW	2805.5	100	Semi	No	Subangular	0					Not observed	Not observed
244-SMW	2815.5	100	Semi	Yes	Subangular	0					Not observed	Not observed
247-SMW	2825.5	100	Semi	Yes	Subangular	0					Not observed	Not observed
249-SMW	2835.5	100	Semi	Yes	Subangular	0					Not observed	Not observed
251-SMW	2845.5	95	Semi	Yes	Subangular	5	Semi	Yes	Round	Crumbly	Not observed	Not observed
254-SMW	2855.5	95	Semi	Yes	Subangular	5	Soft	No	Round	Crumbly	Not observed	Not observed
256-SMW	2865.5	100	Semi	Yes	Subangular	0					Not observed	Not observed
259-SMW	2875.5	95	Semi	Yes	Subangular	5	Soft	No	Round	Crumbly	Not observed	Not observed
261-SMW	2885.5	100	Semi	No	Subangular	0					Not observed	Not observed
263-SMW	2895.5	100	Semi	Yes	Subangular	0					Not observed	Not observed
265-SMW	2905.5	100	Semi	Yes	Subangular	0					Not observed	Not observed
267-SMW	2915.5	95	Semi	Yes	Subangular	5	Soft	No	Round	Crumbly	Not observed	Not observed
269-SMW	2925.5	100	Semi	Yes	Subangular	0					Not observed	Not observed

Table T8 (continued).

Cuttings sample	Bottom depth (mbsf)	Silty claystone (%)	Silty claystone consolidation	Silty claystone structures	Silty claystone shape	Sandstone (%)	Sandstone consolidation	Sandstone structures	Sandstone shape	Sandstone texture	Wood/Lignite	Fossils
271-SMW	2935.5	95	Semi	Yes	Subangular	5	Soft	No	Round	Crumbly	Not observed	Not observed
273-SMW	2945.5	100	Soft	No	Round	0					Not observed	Not observed
277-SMW	2955.5	100	Soft	No	Round	0					Not observed	Not observed
279-SMW	2965.5	100	Semi	No	Subangular	0					Not observed	Not observed
281-SMW	2975.5	95	Semi	No	Subangular	5	Semi	No	Round	Crumbly	Not observed	Not observed
283-SMW	2985.5	90	Semi	No	Subangular	10	Semi	No	Round	Crumbly	Not observed	Not observed
285-SMW	2995.5	95	Semi	No	Subangular	5	Semi	No	Round	Crumbly	Not observed	Not observed
289-SMW	3005.5	100	Semi	No	Subangular	0					Not observed	Not observed
291-SMW	3015.5	100	Semi	Yes	Subangular	0					Not observed	Not observed
293-SMW	3025.5	100	Semi	Yes	Subangular	0					Not observed	Not observed
296-SMW	3035.5	100	Semi	Yes	Subangular	0					Not observed	Not observed
298-SMW	3045.5	95	Semi	Yes	Subangular	5	Semi	No	Round	Crumbly	Not observed	Not observed
300-SMW	3058.5	90	Semi	Yes	Subangular	10	Semi	No	Round	Crumbly	Not observed	Not observed

Table T9. X-ray diffraction analysis on random bulk powder samples, Holes C0002N and C0002P. (Continued on next seven pages.)

Cuttings sample	Depth (mbsf)	Size fraction (mm)	Integrated peak area (total counts)				Absolute mineral abundance calculated from SVD normalization factors (wt%)					Relative abundance (wt%)			
			Total clay	Quartz	Feldspar	Calcite	Total clay	Quartz	Feldspar	Calcite	Sum	Total clay	Quartz	Feldspar	Calcite
348-C0002N-															
3-SMW	875.5	1–4	280	1321	1549	3153	4.0	0.6	1.6	3.9	10.2	39.4	5.9	15.8	38.9
5-SMW	885.5	1–4	1414	10871	4156	8660	17.9	5.8	3.9	9.9	37.6	47.8	15.4	10.5	26.4
7-SMW	895.5	1–4	985	15366	5552	8829	13.9	8.4	5.5	10.5	38.3	36.2	22.0	14.4	27.4
9-SMW	905.5	1–4	2427	24365	10375	14628	32.3	13.0	10.3	16.4	72.0	44.8	18.1	14.3	22.8
12-SMW	915.5	1–4	2495	25269	8716	15888	32.3	13.7	8.4	18.1	72.5	44.6	18.9	11.5	25.0
14-SMW	925.5	1–4	3281	25574	10255	13058	41.5	13.6	9.9	13.2	78.2	53.1	17.4	12.6	16.9
16-SMW	935.5	1–4	3504	25563	10989	14095	44.4	13.5	10.6	14.3	82.9	53.6	16.3	12.8	17.3
18-SMW	945.5	1–4	4166	28900	10750	10649	51.3	15.3	10.1	8.7	85.5	60.1	18.0	11.8	10.2
20-SMW	955.5	1–4	3400	32298	14822	3437	44.5	17.2	14.8	0.1	76.6	58.0	22.5	19.4	0.1
22-SMW	965.5	1–4	3879	31228	13753	3558	49.2	16.6	13.5	0.1	79.4	62.0	20.9	17.0	0.1
24-SMW	975.5	1–4	3307	32879	14438	4594	43.3	17.6	14.4	1.1	76.4	56.7	23.1	18.9	1.4
26-SMW	985.5	1–4	3592	26753	12053	5593	45.4	14.1	11.8	2.4	73.7	61.6	19.2	16.0	3.2
28-SMW	995.5	1–4	4092	29037	10162	4333	49.9	15.5	9.5	0.1	74.9	66.6	20.7	12.7	0.1
30-SMW	1005.5	1–4	4625	29636	11737	5238	56.6	15.6	11.1	0.6	83.9	67.4	18.6	13.2	0.7
32-SMW	1015.5	1–4	4254	33519	12360	5584	52.8	18.0	11.8	1.4	83.9	62.9	21.4	14.0	1.7
34-SMW	1025.5	1–4	4650	30546	10556	4086	56.2	16.3	9.7	0.1	82.3	68.3	19.8	11.8	0.1
36-SMW	1035.5	1–4	4148	33318	15449	3610	53.0	17.6	15.3	0.1	86.0	61.6	20.5	17.8	0.1
39-SMW	1045.5	1–4	3677	37643	14734	3541	47.4	20.3	14.5	0.1	82.4	57.6	24.7	17.6	0.1
40-SMW	1052.5	1–4	4021	32794	17394	3314	52.6	17.2	17.5	0.1	87.4	60.1	19.7	20.1	0.1
41-SMW	1067.5	1–4	3873	31942	17150	4678	50.9	16.8	17.3	0.4	85.4	59.6	19.6	20.3	0.5
42-SMW	1069.5	1–4	3439	29613	12528	3995	43.8	15.8	12.3	0.2	72.2	60.7	21.9	17.1	0.3
43-SMW	1070.5	1–4	3711	30491	15986	4311	48.5	16.0	16.1	0.2	80.9	60.0	19.8	19.9	0.2
44-SMW	1075.5	1–4	3590	29820	13932	3810	46.2	15.8	13.8	0.1	75.9	60.8	20.8	18.2	0.1
46-SMW	1085.5	1–4	3789	32332	13321	3925	48.0	17.3	13.0	0.1	78.5	61.2	22.0	16.6	0.1
48-SMW	1095.5	1–4	4235	33239	15123	4239	53.8	17.6	14.9	0.1	86.4	62.3	20.4	17.2	0.1
50-SMW	1105.5	1–4	4343	35055	16109	3778	55.5	18.6	15.9	0.1	90.1	61.6	20.6	17.7	0.1
52-SMW	1115.5	1–4	4451	30069	18778	3653	58.0	15.4	19.0	0.1	92.6	62.7	16.7	20.6	0.1
54-SMW	1125.5	1–4	3795	33206	16569	3526	49.7	17.6	16.7	0.1	84.0	59.1	20.9	19.8	0.1
57-SMW	1135.5	1–4	3415	33342	19902	3301	47.1	17.5	20.5	0.1	85.2	55.3	20.5	24.1	0.1
59-SMW	1145.5	1–4	4016	32701	18246	4358	53.0	17.1	18.5	0.1	88.7	59.7	19.3	20.9	0.1
61-SMW	1155.5	1–4	3711	31794	14464	4491	47.8	16.9	14.4	0.5	79.5	60.1	21.3	18.1	0.6
63-SMW	1165.5	1–4	3240	35409	15062	3947	42.8	19.1	15.1	0.2	77.1	55.5	24.7	19.5	0.2
65-SMW	1175.5	1–4	4604	34819	13118	3903	56.9	18.6	12.5	0.1	88.1	64.6	21.1	14.2	0.1
67-SMW	1185.5	1–4	4045	36269	22762	3364	55.4	18.9	23.5	0.1	97.9	56.6	19.3	24.0	0.1
69-SMW	1195.5	1–4	3604	34029	18334	3817	48.4	18.0	18.7	0.1	85.2	56.9	21.1	21.9	0.1
71-SMW	1205.5	1–4	3926	33669	14989	5105	50.4	17.9	14.8	1.0	84.2	59.9	21.3	17.6	1.2
73-SMW	1215.5	1–4	3760	35746	15546	3907	48.8	19.1	15.5	0.1	83.5	58.4	22.9	18.5	0.1
81-SMW	1225.5	1–4	3109	30371	12642	5554	40.3	16.3	12.5	2.8	71.9	56.1	22.7	17.4	3.9
83-SMW	1235.5	1–4	3564	34931	14319	3132	46.0	18.8	14.2	0.1	79.0	58.2	23.8	17.9	0.1
85-SMW	1245.5	1–4	4064	35316	15055	5575	52.0	18.9	14.8	1.5	87.1	59.7	21.6	17.0	1.7
87-SMW	1255.5	1–4	4068	30821	15540	5218	52.3	16.2	15.5	1.0	85.0	61.5	19.0	18.2	1.2
89-SMW	1265.5	1–4	3715	35102	16804	3298	48.9	18.7	16.9	0.1	84.6	57.8	22.1	20.0	0.1
91-SMW	1275.5	1–4	4224	39497	15899	3216	54.0	21.2	15.6	0.1	90.9	59.3	23.4	17.2	0.1
93-SMW	1285.5	1–4	4335	37231	13721	3807	54.2	20.0	13.2	0.1	87.5	61.9	22.9	15.1	0.1
95-SMW	1295.5	1–4	4598	38747	12568	4137	56.5	20.9	11.8	0.1	89.3	63.2	23.5	13.2	0.1
97-SMW	1305.5	1–4	4421	36832	15371	4480	56.0	19.7	15.0	0.1	90.8	61.7	21.7	16.6	0.1
99-SMW	1315.5	1–4	3569	35507	14347	5046	46.1	19.1	14.2	1.3	80.8	57.1	23.7	17.5	1.7
101-SMW	1325.5	1–4	3959	35746	15640	4777	51.0	19.1	15.5	0.4	86.1	59.3	22.2	18.0	0.5
105-SMW	1335.5	1–4	4266	35426	12971	5258	53.1	19.0	12.4	0.9	85.5	62.2	22.3	14.5	1.0
107-SMW	1345.5	1–4	5663	33093	12901	2781	68.4	17.4	12.0	0.1	97.9	69.9	17.8	12.3	0.1
109-SMW	1355.5	1–4	4455	34726	12238	2943	54.7	18.6	11.6	0.1	85.1	64.4	21.9	13.6	0.1
111-SMW	1365.5	1–4	5258	31197	15907	3863	65.5	16.1	15.5	0.1	97.3	67.3	16.6	16.0	0.1
113-SMW	1375.5	1–4	4486	34554	15871	3776	56.9	18.3	15.6	0.1	90.9	62.6	20.1	17.2	0.1
115-SMW	1385.5	1–4	4261	35250	15608	5570	54.4	18.7	15.4	1.2	89.7	60.6	20.9	17.2	1.3
117-SMW	1395.5	1–4	4390	30687	11663	5627	54.0	16.3	11.0	1.4	82.7	65.2	19.7	13.3	1.7
119-SMW	1405.5	1–4	3610	35739	13875	5362	46.4	19.3	13.6	1.7	81.0	57.2	23.8	16.8	2.2
121-SMW	1415.5	1–4	3468	41516	15217	5021	45.4	22.6	15.0	1.2	84.3	53.8	26.8	17.8	1.5
123-SMW	1425.5	1–4	3527	39327	17106	3621	46.9	21.2	17.2	0.1	85.4	54.9	24.8	20.1	0.1
125-SMW	1435.5	1–4	3372	40315	14368	4806	43.9	22.0	14.1	1.1	81.1	54.1	27.1	17.4	1.4
128-SMW	1445.5	1–4	3448	44359	17419	4711	46.2	24.1	17.4	0.7	88.4	52.2	27.3	19.7	0.8
130-SMW	1455.5	1–4	3971	40338	14680	4117	50.6	21.9	14.3	0.1	86.9	58.2	25.2	16.5	0.1
132-SMW	1465.5	1–4	4178	44458	16826	3276	53.8	24.1	16.6	0.1	94.6	56.9	25.5	17.5	0.1
134-SMW	1475.5	1–4	3786	44653	16329	3495	49.3	24.3	16.1	0.1	89.8	54.9	27.1	17.9	0.1
136-SMW	1485.5	1–4	3370	43520	18488	3269	45.8	23.6	18.7	0.1	88.2	51.9	26.8	21.2	0.1
138-SMW	1495.5	1–4	4110	42844	14785	3337	52.1	23.3	14.3	0.1	89.8	58.0	25.9	16.0	0.1

Table T9 (continued). (Continued on next page.)

Cuttings sample	Depth (mbsf)	Size fraction (mm)	Integrated peak area (total counts)				Absolute mineral abundance calculated from SVD normalization factors (wt%)					Relative abundance (wt%)			
			Total clay	Quartz	Feldspar	Calcite	Total clay	Quartz	Feldspar	Calcite	Sum	Total clay	Quartz	Feldspar	Calcite
140-SMW	1505.5	1–4	3822	36385	16899	3691	50.1	19.4	16.9	0.1	86.5	57.9	22.4	19.6	0.1
142-SMW	1515.5	1–4	3299	40549	16311	4462	44.0	22.0	16.3	0.7	83.0	53.0	26.5	19.7	0.8
146-SMW	1525.5	1–4	2958	48963	22287	2646	43.0	26.6	23.0	0.1	92.7	46.4	28.7	24.8	0.1
148-SMW	1535.5	1–4	3568	43745	14676	4161	46.1	23.9	14.3	0.1	84.5	54.6	28.3	17.0	0.1
150-SMW	1545.5	1–4	3602	39413	19295	3281	48.8	21.1	19.6	0.1	89.6	54.5	23.5	21.9	0.1
152-SMW	1555.5	1–4	3647	43908	17020	3281	48.1	23.9	17.0	0.1	89.0	54.0	26.8	19.0	0.1
154-SMW	1565.5	1–4	2989	45204	17738	3706	41.2	24.7	17.9	0.1	83.9	49.1	29.4	21.3	0.1
156-SMW	1575.5	1–4	3058	48252	17770	3782	41.9	26.5	17.9	0.1	86.4	48.6	30.7	20.7	0.1
158-SMW	1585.5	1–4	4286	41920	14299	3846	53.8	22.8	13.8	0.1	90.5	59.5	25.2	15.2	0.1
160-SMW	1595.5	1–4	4155	48722	15944	3262	53.1	26.7	15.5	0.1	95.3	55.7	28.0	16.2	0.1
162-SMW	1605.5	1–4	3301	52589	15742	2508	43.5	29.1	15.4	0.1	88.1	49.3	33.1	17.5	0.1
164-SMW	1615.5	1–4	4931	45247	15275	2734	61.3	24.5	14.6	0.1	100.5	61.0	24.4	14.5	0.1
166-SMW	1625.5	1–4	3442	50598	17995	2852	46.2	27.8	17.9	0.1	92.0	50.2	30.2	19.5	0.1
169-SMW	1635.5	1–4	3901	42154	31623	2813	58.1	21.7	33.3	0.1	113.3	51.3	19.2	29.4	0.1
171-SMW	1645.5	1–4	1621	70825	32940	2346	33.2	39.0	34.8	0.1	107.1	31.0	36.4	32.5	0.1
173-SMW	1655.5	1–4	1843	74810	24275	2814	31.4	41.9	24.9	0.1	98.2	31.9	42.7	25.3	0.1
175-SMW	1665.5	1–4	2913	52036	20816	4987	41.9	28.5	21.2	1.4	93.0	45.0	30.7	22.8	1.5
177-SMW	1677.5	1–4	3619	42212	18030	4796	48.4	22.8	18.1	0.6	89.9	53.8	25.3	20.2	0.7
182-SMW	1685.5	1–4	3924	39124	16303	3805	50.9	21.0	16.2	0.1	88.2	57.7	23.9	18.3	0.1
184-SMW	1695.5	1–4	3544	39830	17706	3480	47.4	21.4	17.9	0.1	86.8	54.6	24.7	20.6	0.1
186-SMW	1705.5	1–4	3998	40828	21783	3237	54.3	21.6	22.3	0.1	98.4	55.3	22.0	22.6	0.1
188-SMW	1715.5	1–4	3708	39464	16306	3763	48.5	21.3	16.2	0.1	86.1	56.3	24.7	18.9	0.1
190-SMW	1725.5	1–4	3579	42300	17836	6304	47.9	22.9	17.9	2.8	91.5	52.4	25.0	19.6	3.0
192-SMW	1735.5	1–4	3682	38974	16885	4211	48.5	21.0	16.9	0.1	86.5	56.1	24.2	19.5	0.1
195-SMW	1745.5	1–4	3122	42323	20359	4865	44.1	22.8	20.9	1.2	89.0	49.5	25.6	23.5	1.4
197-SMW	1755.5	1–4	3367	37645	14905	5293	44.2	20.4	14.8	1.8	81.2	54.4	25.1	18.2	2.3
199-SMW	1765.5	1–4	3542	43713	16740	4573	46.9	23.8	16.7	0.4	87.8	53.4	27.1	19.0	0.5
201-SMW	1775.5	1–4	3662	37893	16447	4341	48.1	20.4	16.4	0.1	85.0	56.6	23.9	19.3	0.1
203-SMW	1785.5	1–4	3998	42353	15831	4671	51.5	23.0	15.5	0.1	90.1	57.2	25.5	17.3	0.1
205-SMW	1795.5	1–4	4195	42557	16087	3597	53.7	23.0	15.8	0.1	92.6	58.0	24.9	17.0	0.1
207-SMW	1805.5	1–4	3910	46118	19353	3573	52.1	24.9	19.4	0.1	96.6	54.0	25.8	20.1	0.1
209-SMW	1815.5	1–4	4173	43360	14420	3772	52.6	23.6	13.9	0.1	90.2	58.3	26.2	15.4	0.1
211-SMW	1825.5	1–4	4821	43081	11301	3610	58.2	23.5	10.2	0.1	92.1	63.2	25.6	11.1	0.1
213-SMW	1835.5	1–4	3761	43766	13502	4643	47.7	24.0	13.0	0.4	85.1	56.1	28.2	15.2	0.5
216-SMW	1845.5	1–4	3853	45438	16260	3572	50.0	24.8	16.0	0.1	90.9	55.0	27.3	17.6	0.1
218-SMW	1855.5	1–4	4449	44000	12399	2820	54.6	24.1	11.5	0.1	90.3	60.5	26.7	12.8	0.1
220-SMW	1865.5	1–4	4430	43027	15853	3536	56.2	23.3	15.4	0.1	95.0	59.1	24.5	16.3	0.1
222-SMW	1875.5	1–4	4047	42211	16662	3787	52.4	22.8	16.5	0.1	91.8	57.1	24.9	18.0	0.1
224-SMW	1885.5	1–4	4008	44640	16068	4139	51.6	24.3	15.8	0.1	91.8	56.3	26.5	17.2	0.1
226-SMW	1895.5	1–4	4105	40124	16455	5633	53.0	21.6	16.3	1.3	92.2	57.5	23.4	17.6	1.4
228-SMW	1905.5	1–4	4439	41034	13856	6008	55.4	22.2	13.2	1.5	92.4	60.0	24.0	14.3	1.7
230-SMW	1915.5	1–4	3757	40472	13344	7294	47.8	22.1	12.9	4.2	86.8	55.0	25.4	14.8	4.8
232-SMW	1925.5	1–4	4529	40228	12690	9112	56.0	21.8	11.9	5.8	95.5	58.7	22.8	12.4	6.1
234-SMW	1935.5	1–4	3983	39621	11287	8016	49.3	21.7	10.5	5.0	86.5	57.0	25.1	12.1	5.8
237-SMW	1945.5	1–4	4347	40438	12713	7150	53.9	22.0	12.0	3.3	91.2	59.2	24.1	13.1	3.6
239-SMW	1955.5	1–4	4874	40023	12770	5001	59.7	21.6	11.9	0.1	93.3	63.9	23.2	12.8	0.1
241-SMW	1965.5	1–4	5408	38697	12887	4424	65.6	20.7	11.9	0.1	98.3	66.7	21.1	12.1	0.1
243-SMW	1975.5	1–4	4741	38418	13345	5349	58.5	20.7	12.6	0.3	92.2	63.5	22.4	13.7	0.4
248-SMW	1985.5	1–4	4757	41145	12524	2915	58.1	22.3	11.6	0.1	92.2	63.0	24.2	12.6	0.1
250-SMW	1995.5	1–4	5028	42253	16196	3550	62.9	22.7	15.7	0.1	101.4	62.1	22.4	15.5	0.1
252-SMW	2005.5	1–4	4907	42704	20647	3165	63.8	22.6	20.7	0.1	107.2	59.5	21.1	19.3	0.1
259-SMW	2015.5	1–4	4119	38365	13789	4190	51.8	20.7	13.3	0.1	86.0	60.3	24.1	15.5	0.1
261-SMW	2025.5	1–4	3835	41295	14831	4157	49.2	22.4	14.5	0.1	86.2	57.0	26.0	16.8	0.1
264-SMW	2035.5	1–4	3873	40713	17710	3543	51.0	21.9	17.7	0.1	90.7	56.2	24.1	19.6	0.1
266-SMW	2045.5	1–4	4158	41781	13779	4247	52.2	22.7	13.2	0.1	88.3	59.2	25.8	15.0	0.1
268-SMW	2055.5	1–4	4254	39702	18418	3035	55.5	21.2	18.5	0.1	95.2	58.3	22.2	19.4	0.1
270-SMW	2065.5	1–4	4421	41795	13366	1744	54.8	22.7	12.7	0.1	90.3	60.7	25.2	14.0	0.1
272-SMW	2075.5	1–4	4677	46320	16425	2466	59.1	25.1	15.9	0.1	100.2	58.9	25.1	15.9	0.1
274-SMW	2085.5	1–4	5114	44694	15007	1961	63.2	24.2	14.2	0.1	101.7	62.1	23.8	14.0	0.1
276-SMW	2095.5	1–4	4928	42908	13175	1594	60.2	23.3	12.3	0.1	95.9	62.8	24.3	12.8	0.1
278-SMW	2105.5	1–4	3774	46559	14478	1531	48.1	25.6	14.0	0.1	87.8	54.8	29.1	15.9	0.1
281-SMW	2115.5	1–4	4046	46658	13993	1987	50.9	25.6	13.4	0.1	90.0	56.6	28.5	14.9	0.1
283-SMW	2125.5	1–4	3962	50726	15707	2033	50.7	27.9	15.2	0.1	94.0	54.0	29.7	16.2	0.1
285-SMW	2135.5	1–4	4380	45183	12659	1965	53.9	24.8	11.8	0.1	90.6	59.5	27.4	13.0	0.1
287-SMW	2145.5	1–4	4401	44552	16332	1913	56.0	24.1	15.9	0.1	96.2	58.2	25.1	16.6	0.1
289-SMW	2155.5	1–4	4337	44476	16192	1790	55.2	24.1	15.8	0.1	95.2	58.0	25.3	16.6	0.1
291-SMW	2165.5	1–4	4783	42257	14277	1643	59.2	22.9	13.6	0.1	95.7	61.8	23.9	14.2	0.1
296-SMW	2175.5	1–4	3819	52296	16417	2067	49.5	28.8	16.0	0.1	94.4	52.4	30.5	17.0	0.1

Table T9 (continued). (Continued on next page.)

Cuttings sample	Depth (mbsf)	Size fraction (mm)	Integrated peak area (total counts)				Absolute mineral abundance calculated from SVD normalization factors (wt%)					Relative abundance (wt%)			
			Total clay	Quartz	Feldspar	Calcite	Total clay	Quartz	Feldspar	Calcite	Sum	Total clay	Quartz	Feldspar	Calcite
298-SMW	2185.5	1–4	5052	45993	17302	2157	63.6	24.8	16.8	0.1	105.3	60.4	23.5	16.0	0.1
300-SMW	2195.5	1–4	4506	45070	15803	2922	56.9	24.5	15.3	0.1	96.8	58.8	25.3	15.8	0.1
302-SMW	2205.5	1–4	4476	45791	16162	2356	56.7	24.9	15.7	0.1	97.4	58.2	25.5	16.1	0.1
304-SMW	2215.5	1–4	3882	47252	17504	2843	50.8	25.8	17.3	0.1	94.0	54.1	27.4	18.4	0.1
306-SMW	2225.5	1–4	3735	43441	12672	4369	47.0	23.9	12.0	0.1	83.0	56.6	28.8	14.5	0.1
308-SMW	2235.5	1–4	4175	42588	18535	3968	54.7	22.9	18.5	0.1	96.2	56.9	23.8	19.3	0.1
310-SMW	2245.5	1–4	3479	43060	15561	2872	45.5	23.5	15.4	0.1	84.5	53.9	27.8	18.2	0.1
312-SMW	2255.5	1–4	4266	43771	13654	3935	53.3	23.9	13.0	0.1	90.3	59.0	26.5	14.4	0.1
314-SMW	2265.5	1–4	3918	44108	13459	2608	49.3	24.2	12.9	0.1	86.4	57.0	28.0	14.9	0.1
316-SMW	2275.5	1–4	4367	44343	11842	4190	53.5	24.3	10.9	0.1	88.9	60.2	27.4	12.3	0.1
318-SMW	2285.5	1–4	4576	42009	13388	3433	56.6	22.8	12.6	0.1	92.1	61.4	24.8	13.7	0.1
321-SMW	2295.5	1–4	4164	44894	14282	3031	52.4	24.5	13.7	0.1	90.7	57.8	27.0	15.1	0.1
323-SMW	2305.5	1–4	4880	43963	11724	3109	59.0	24.0	10.6	0.1	93.8	62.9	25.6	11.3	0.1
325-SMW	2315.5	1–4	4775	43342	13620	2584	58.8	23.5	12.8	0.1	95.3	61.7	24.7	13.5	0.1
327-SMW	2325.5	1–4	4963	43536	11950	3554	60.1	23.7	10.9	0.1	94.8	63.4	25.0	11.5	0.1
3-SMW	875.5	>4	282	1123	868	4597	3.8	0.5	0.8	6.0	11.1	33.9	4.7	7.6	53.8
5-SMW	885.5	>4	402	1346	1018	3590	5.1	0.6	1.0	4.4	11.1	45.9	5.6	8.8	39.8
7-SMW	895.5	>4	361	2485	1596	4591	5.0	1.3	1.6	5.8	13.7	36.5	9.2	11.7	42.6
9-SMW	905.5	>4	696	7409	3880	6630	9.8	3.9	3.9	8.0	25.7	38.2	15.2	15.3	31.2
12-SMW	915.5	>4	1654	21180	10086	13423	23.6	11.3	10.3	15.7	61.0	38.8	18.6	16.8	25.8
14-SMW	925.5	>4	1628	18445	7632	10571	22.0	9.9	7.6	12.0	51.5	42.7	19.3	14.7	23.3
16-SMW	935.5	>4	1817	16909	6020	10439	23.3	9.1	5.8	11.7	49.9	46.8	18.3	11.6	23.4
18-SMW	945.5	>4	1975	19579	7920	9607	25.9	10.5	7.8	10.2	54.4	47.6	19.3	14.3	18.7
20-SMW	955.5	>4	1940	22566	10991	5283	26.7	12.1	11.2	4.0	54.1	49.5	22.3	20.7	7.5
22-SMW	965.5	>4	2713	23535	10197	2825	34.7	12.6	10.1	0.1	57.4	60.4	21.9	17.5	0.2
24-SMW	975.5	>4	3446	27863	12639	3889	44.0	14.8	12.5	0.1	71.4	61.6	20.7	17.5	0.2
26-SMW	985.5	>4	3333	28362	14527	4680	43.7	15.0	14.6	1.3	74.6	58.6	20.1	19.6	1.7
28-SMW	995.5	>4	3382	28055	12414	4367	43.2	14.9	12.2	0.9	71.2	60.6	20.9	17.2	1.2
30-SMW	1005.5	>4	2966	29260	14180	4157	39.5	15.6	14.3	1.0	70.3	56.1	22.2	20.4	1.4
32-SMW	1015.5	>4	3622	26009	10554	4085	44.9	13.8	10.1	0.3	69.2	64.9	19.9	14.6	0.5
34-SMW	1025.5	>4	4060	33996	17155	3479	52.9	17.9	17.2	0.1	88.1	60.0	20.4	19.6	0.1
36-SMW	1035.5	>4	4269	33307	13665	3253	53.4	17.7	13.3	0.1	84.5	63.2	21.0	15.7	0.1
39-SMW	1045.5	>4	2147	25784	11226	3674	29.0	13.9	11.3	1.5	55.7	52.0	25.0	20.3	2.7
40-SMW	1052.5	>4	3686	35123	16804	3332	48.5	18.7	16.9	0.1	84.3	57.6	22.2	20.1	0.1
41-SMW	1067.5	>4	3339	30612	15404	4033	44.1	16.2	15.6	0.3	76.2	57.9	21.3	20.4	0.4
42-SMW	1069.5	>4	3863	31528	16706	4201	50.5	16.6	16.8	0.1	84.0	60.1	19.7	20.0	0.1
43-SMW	1070.5	>4	3916	31994	14637	3839	50.1	17.0	14.5	0.1	81.6	61.3	20.8	17.7	0.1
44-SMW	1075.5	>4	4304	35294	16083	3031	55.0	18.7	15.9	0.1	89.7	61.3	20.9	17.7	0.1
46-SMW	1085.5	>4	3696	33977	15091	3176	47.8	18.1	15.0	0.1	81.1	59.0	22.4	18.5	0.1
48-SMW	1095.5	>4	3893	32901	18357	3850	51.6	17.2	18.7	0.1	87.6	58.9	19.7	21.3	0.1
50-SMW	1105.5	>4	3534	33008	13881	3062	45.4	17.7	13.7	0.1	77.0	59.0	23.0	17.8	0.1
52-SMW	1115.5	>4	3575	33989	18040	3307	47.9	18.0	18.4	0.1	84.4	56.8	21.3	21.8	0.1
54-SMW	1125.5	>4	3738	33647	17172	3262	49.3	17.8	17.4	0.1	84.6	58.3	21.0	20.5	0.1
57-SMW	1135.5	>4	3743	38729	17772	3280	49.6	20.7	17.9	0.1	88.3	56.1	23.5	20.3	0.1
59-SMW	1145.5	>4	3530	38568	15099	2962	45.9	20.9	15.0	0.1	81.9	56.1	25.5	18.3	0.1
61-SMW	1155.5	>4	3297	36334	18552	3324	45.1	19.4	19.0	0.1	83.5	54.0	23.2	22.7	0.1
63-SMW	1165.5	>4	4317	35533	15324	3934	54.8	18.9	15.1	0.1	88.9	61.7	21.3	16.9	0.1
65-SMW	1175.5	>4	4084	36369	17157	3784	53.1	19.3	17.2	0.1	89.7	59.2	21.5	19.1	0.1
67-SMW	1185.5	>4	4206	33924	13689	3377	52.8	18.1	13.3	0.1	84.3	62.6	21.5	15.8	0.1
69-SMW	1195.5	>4	3440	33995	20066	4704	47.5	17.8	20.7	0.8	86.9	54.7	20.5	23.8	0.9
71-SMW	1205.5	>4	3484	34082	20175	3087	48.0	17.9	20.8	0.1	86.8	55.3	20.6	24.0	0.1
73-SMW	1215.5	>4	3098	30421	21512	3211	44.5	15.7	22.5	0.1	82.8	53.7	19.0	27.2	0.1
81-SMW	1225.5	>4	3223	32156	13159	3427	41.7	17.3	13.0	0.1	72.1	57.8	24.0	18.1	0.1
83-SMW	1235.5	>4	3950	34581	14345	2815	50.2	18.5	14.1	0.1	82.9	60.6	22.3	17.0	0.1
85-SMW	1245.5	>4	3739	37022	16951	3362	49.2	19.8	17.0	0.1	86.1	57.1	23.0	19.8	0.1
87-SMW	1255.5	>4	3957	32750	15439	3745	50.9	17.3	15.4	0.1	83.7	60.8	20.7	18.3	0.1
89-SMW	1265.5	>4	2970	36893	16659	3217	40.6	19.9	16.9	0.1	77.5	52.4	25.7	21.8	0.1
91-SMW	1275.5	>4	3517	38193	18968	3291	47.7	20.4	19.3	0.1	87.5	54.5	23.3	22.1	0.1
93-SMW	1285.5	>4	4280	33973	14197	2954	53.8	18.1	13.8	0.1	85.8	62.7	21.1	16.1	0.1
95-SMW	1295.5	>4	4603	31588	13028	3520	56.8	16.7	12.5	0.1	86.1	66.0	19.4	14.5	0.1
97-SMW	1305.5	>4	3651	37373	14605	3774	47.1	20.2	14.4	0.1	81.8	57.6	24.7	17.6	0.1
99-SMW	1315.5	>4	4118	38843	15328	3595	52.5	20.9	15.0	0.1	88.6	59.3	23.6	17.0	0.1
101-SMW	1325.5	>4	3813	33701	14901	3843	49.1	18.0	14.8	0.1	81.9	59.9	21.9	18.0	0.1
105-SMW	1335.5	>4	3690	36711	16225	3615	48.3	19.7	16.2	0.1	84.3	57.3	23.3	19.2	0.1
107-SMW	1345.5	>4	4348	33451	15321	3425	55.1	17.7	15.1	0.1	88.0	62.6	20.1	17.2	0.1
109-SMW	1355.5	>4	4477	32892	14157	3054	56.0	17.4	13.8	0.1	87.2	64.1	20.0	15.8	0.1
111-SMW	1365.5	>4	4199	30475	13461	5343	52.7	16.1	13.1	1.2	83.1	63.5	19.4	15.8	1.4
113-SMW	1375.5	>4	4729	34011	16090	4462	59.8	17.9	15.8	0.1	93.6	63.9	19.1	16.9	0.1

Table T9 (continued). (Continued on next page.)

Cuttings sample	Depth (mbsf)	Size fraction (mm)	Integrated peak area (total counts)				Absolute mineral abundance calculated from SVD normalization factors (wt%)					Relative abundance (wt%)			
			Total clay	Quartz	Feldspar	Calcite	Total clay	Quartz	Feldspar	Calcite	Sum	Total clay	Quartz	Feldspar	Calcite
115-SMW	1385.5	>4	4168	37255	14053	4954	52.6	20.0	13.6	0.5	86.7	60.6	23.1	15.7	0.5
117-SMW	1395.5	>4	3919	30039	12310	5999	49.1	16.0	11.9	2.5	79.5	61.8	20.1	15.0	3.1
119-SMW	1405.5	>4	4216	36568	16385	4380	54.2	19.5	16.2	0.1	90.0	60.2	21.6	18.0	0.1
121-SMW	1415.5	>4	3794	42475	17466	3943	50.0	23.0	17.4	0.1	90.5	55.2	25.4	19.3	0.1
123-SMW	1425.5	>4	3692	43782	22751	3879	51.5	23.4	23.4	0.1	98.3	52.3	23.8	23.8	0.1
125-SMW	1435.5	>4	3975	37844	22093	3831	54.3	19.9	22.7	0.1	97.0	56.0	20.5	23.4	0.1
128-SMW	1445.5	>4	4189	39464	16422	4397	53.9	21.2	16.2	0.1	91.4	59.0	23.2	17.8	0.1
130-SMW	1455.5	>4	3679	37222	14271	2724	47.2	20.1	14.0	0.1	81.4	57.9	24.7	17.2	0.1
132-SMW	1465.5	>4	3732	39522	19960	3519	50.6	21.1	20.3	0.1	92.0	54.9	22.9	22.1	0.1
134-SMW	1475.5	>4	4443	39585	14140	2820	55.5	21.4	13.6	0.1	90.5	61.3	23.6	15.0	0.1
136-SMW	1485.5	>4	4174	38680	16899	2277	53.9	20.7	16.8	0.1	91.4	58.9	22.6	18.4	0.1
138-SMW	1495.5	>4	4339	38070	13427	3002	54.0	20.5	12.9	0.1	87.5	61.7	23.5	14.7	0.1
140-SMW	1505.5	>4	4809	37666	15341	3293	60.1	20.1	14.9	0.1	95.2	63.2	21.1	15.6	0.1
142-SMW	1515.5	>4	3635	40681	17618	4611	48.4	21.9	17.7	0.4	88.4	54.7	24.8	20.0	0.5
146-SMW	1525.5	>4	3879	40016	15504	2505	49.9	21.6	15.3	0.1	86.9	57.4	24.9	17.6	0.1
148-SMW	1535.5	>4	3648	41498	15441	3008	47.3	22.6	15.2	0.1	85.2	55.5	26.5	17.9	0.1
150-SMW	1545.5	>4	3602	41748	15371	2980	46.8	22.7	15.2	0.1	84.8	55.2	26.8	17.9	0.1
152-SMW	1555.5	>4	4134	41763	17536	3110	53.7	22.5	17.4	0.1	93.7	57.3	24.0	18.6	0.1
154-SMW	1565.5	>4	3175	43262	21058	2515	44.9	23.3	21.6	0.1	89.9	49.9	25.9	24.1	0.1
156-SMW	1575.5	>4	3779	43330	13242	3344	47.7	23.8	12.7	0.1	84.2	56.6	28.2	15.1	0.1
158-SMW	1585.5	>4	4313	44055	14828	4450	54.4	24.0	14.3	0.1	92.8	58.7	25.8	15.4	0.1
160-SMW	1595.5	>4	3881	42085	14001	3010	49.2	23.0	13.5	0.1	85.8	57.3	26.8	15.8	0.1
162-SMW	1605.5	>4	3744	43057	17179	2824	49.2	23.3	17.1	0.1	89.8	54.8	26.0	19.1	0.1
164-SMW	1615.5	>4	3036	44930	22733	2927	44.2	24.2	23.5	0.1	92.0	48.0	26.3	25.6	0.1
166-SMW	1625.5	>4	3724	43818	19174	2071	49.9	23.6	19.4	0.1	93.0	53.7	25.4	20.8	0.1
169-SMW	1635.5	>4	3518	45969	21795	3074	49.0	24.8	22.3	0.1	96.2	50.9	25.8	23.2	0.1
171-SMW	1645.5	>4	3321	52921	20470	2333	46.0	29.0	20.7	0.1	95.8	48.0	30.3	21.6	0.1
173-SMW	1655.5	>4	3063	53372	17031	2006	41.5	29.6	16.9	0.1	88.0	47.1	33.6	19.2	0.1
175-SMW	1665.5	>4	3535	41139	20193	4014	48.5	22.0	20.6	0.1	91.2	53.2	24.1	22.6	0.1
177-SMW	1677.5	>4	3477	41979	20978	3942	48.2	22.5	21.5	0.1	92.3	52.3	24.3	23.3	0.1
182-SMW	1685.5	>4	4063	38289	15692	3708	52.1	20.6	15.5	0.1	88.3	59.1	23.3	17.5	0.1
184-SMW	1695.5	>4	3445	37094	16813	4308	45.9	19.9	16.9	0.3	83.1	55.3	24.0	20.4	0.4
186-SMW	1705.5	>4	3950	42122	20941	2513	53.3	22.5	21.3	0.1	97.2	54.9	23.1	21.9	0.1
188-SMW	1715.5	>4	4113	41075	23646	3906	56.6	21.6	24.3	0.1	102.6	55.1	21.1	23.7	0.1
190-SMW	1725.5	>4	3653	42605	16955	5738	48.3	23.1	16.9	1.9	90.2	53.5	25.6	18.7	2.1
192-SMW	1735.5	>4	3411	40440	18033	3858	46.1	21.8	18.2	0.1	86.2	53.4	25.3	21.2	0.1
195-SMW	1745.5	>4	4212	37514	16240	4590	54.1	20.0	16.1	0.1	90.3	59.9	22.2	17.8	0.1
197-SMW	1755.5	>4	3820	40114	18162	4758	50.7	21.5	18.3	0.4	90.9	55.8	23.7	20.1	0.4
199-SMW	1765.5	>4	3866	36163	16625	3377	50.4	19.3	16.6	0.1	86.5	58.3	22.3	19.2	0.1
201-SMW	1775.5	>4	3831	39699	16341	4254	49.9	21.4	16.2	0.1	87.6	56.9	24.4	18.5	0.1
203-SMW	1785.5	>4	4086	40911	15849	3634	52.4	22.1	15.6	0.1	90.2	58.1	24.5	17.3	0.1
205-SMW	1795.5	>4	4326	40711	13572	3616	53.9	22.1	13.0	0.1	89.1	60.5	24.8	14.5	0.1
207-SMW	1805.5	>4	4128	41960	14365	3158	52.1	22.8	13.9	0.1	88.9	58.6	25.7	15.6	0.1
209-SMW	1815.5	>4	4371	41377	15419	3457	55.3	22.3	15.0	0.1	92.8	59.6	24.1	16.2	0.1
211-SMW	1825.5	>4	4256	39748	14947	4381	53.9	21.4	14.5	0.1	90.0	59.9	23.8	16.2	0.1
213-SMW	1835.5	>4	4024	43562	17442	2576	52.4	23.6	17.3	0.1	93.4	56.1	25.2	18.6	0.1
216-SMW	1845.5	>4	4403	43469	17522	1966	56.6	23.4	17.3	0.1	97.4	58.1	24.0	17.8	0.1
218-SMW	1855.5	>4	3279	44275	19803	2697	45.4	24.0	20.2	0.1	89.6	50.6	26.7	22.5	0.1
220-SMW	1865.5	>4	4050	43183	16492	3628	52.3	23.4	16.3	0.1	92.0	56.8	25.4	17.7	0.1
222-SMW	1875.5	>4	4054	40591	17398	2860	52.8	21.8	17.3	0.1	92.0	57.4	23.7	18.8	0.1
224-SMW	1885.5	>4	4266	40940	14543	3959	53.8	22.2	14.1	0.1	90.1	59.7	24.6	15.6	0.1
226-SMW	1895.5	>4	4593	41414	17673	6172	59.0	22.1	17.5	1.4	100.0	59.0	22.1	17.4	1.4
228-SMW	1905.5	>4	4558	36851	13595	6602	56.7	19.8	13.0	2.3	91.8	61.8	21.5	14.2	2.5
230-SMW	1915.5	>4	3926	38346	11123	6733	48.5	20.9	10.4	3.3	83.2	58.4	25.2	12.5	4.0
232-SMW	1925.5	>4	4602	40839	14490	7475	57.6	22.0	13.9	3.4	96.9	59.5	22.7	14.3	3.5
234-SMW	1935.5	>4	4566	37718	13247	6734	56.6	20.3	12.6	2.5	92.0	61.6	22.1	13.7	2.7
237-SMW	1945.5	>4	3927	38729	20447	6174	53.1	20.5	20.8	2.2	96.6	55.0	21.2	21.6	2.2
239-SMW	1955.5	>4	4704	41112	15570	5515	59.2	22.1	15.1	0.5	96.8	61.1	22.8	15.6	0.5
241-SMW	1965.5	>4	4373	41676	15912	5675	55.7	22.5	15.5	1.0	94.8	58.8	23.7	16.4	1.1
243-SMW	1975.5	>4	4725	41721	15979	4661	59.6	22.4	15.5	0.1	97.6	61.0	23.0	15.9	0.1
248-SMW	1985.5	>4	4883	42258	14666	4608	60.6	22.8	14.0	0.1	97.5	62.2	23.4	14.3	0.1
250-SMW	1995.5	>4	5106	42405	13829	3384	62.6	22.9	13.0	0.1	98.6	63.5	23.2	13.2	0.1
252-SMW	2005.5	>4	4791	40176	12915	4026	58.8	21.7	12.1	0.1	92.7	63.4	23.4	13.0	0.1
259-SMW	2015.5	>4	3143	42279	22302	2321	45.1	22.6	23.1	0.1	90.9	49.6	24.9	25.4	0.1
261-SMW	2025.5	>4	3976	40973	15780	4072	51.2	22.2	15.5	0.1	89.0	57.5	24.9	17.5	0.1
264-SMW	2035.5	>4	4040	40009	19531	5306	53.8	21.3	19.7	0.8	95.7	56.2	22.3	20.6	0.9
266-SMW	2045.5	>4	3197	40255	19202	3902	44.3	21.6	19.6	0.1	85.7	51.7	25.3	22.9	0.1
268-SMW	2055.5	>4	3581	45273	29119	3455	53.3	23.8	30.5	0.1	107.8	49.5	22.1	28.3	0.1

Table T9 (continued). (Continued on next page.)

Cuttings sample	Depth (mbsf)	Size fraction (mm)	Integrated peak area (total counts)				Absolute mineral abundance calculated from SVD normalization factors (wt%)					Relative abundance (wt%)			
			Total clay	Quartz	Feldspar	Calcite	Total clay	Quartz	Feldspar	Calcite	Sum	Total clay	Quartz	Feldspar	Calcite
270-SMW	2065.5	>4	3720	46266	27711	1755	54.0	24.5	28.9	0.1	107.5	50.3	22.8	26.9	0.1
272-SMW	2075.5	>4	4519	41153	15116	3742	56.8	22.2	14.6	0.1	93.7	60.6	23.7	15.6	0.1
274-SMW	2085.5	>4	3832	44023	14834	2211	49.0	24.1	14.4	0.1	87.6	55.9	27.5	16.5	0.1
276-SMW	2095.5	>4	4725	43721	12947	1735	57.9	23.8	12.1	0.1	93.9	61.6	25.4	12.9	0.1
278-SMW	2105.5	>4	4522	48296	15091	1447	56.6	26.4	14.4	0.1	97.6	58.0	27.1	14.8	0.1
281-SMW	2115.5	>4	3889	43984	16789	1583	50.5	23.9	16.6	0.1	91.2	55.5	26.2	18.2	0.1
283-SMW	2125.5	>4	4089	46983	23102	2662	55.9	25.1	23.6	0.1	104.7	53.4	24.0	22.5	0.1
285-SMW	2135.5	>4	4318	47321	24340	1507	58.9	25.2	24.9	0.1	109.2	54.0	23.1	22.8	0.1
287-SMW	2145.5	>4	4056	44584	20541	2281	54.3	23.9	20.8	0.1	99.1	54.8	24.2	21.0	0.1
289-SMW	2155.5	>4	4177	44702	15516	1196	53.1	24.3	15.1	0.1	92.6	57.3	26.3	16.3	0.1
291-SMW	2165.5	>4	4957	44643	13421	2296	60.7	24.3	12.5	0.1	97.6	62.2	24.9	12.8	0.1
296-SMW	2175.5	>4	4445	44953	17418	3128	57.1	24.3	17.1	0.1	98.6	57.9	24.6	17.4	0.1
298-SMW	2185.5	>4	3783	44451	13312	4861	47.8	24.4	12.7	0.7	85.6	55.9	28.5	14.9	0.8
300-SMW	2195.5	>4	4099	49161	16338	1915	52.6	26.9	15.9	0.1	95.5	55.0	28.2	16.7	0.1
302-SMW	2205.5	>4	3786	44307	14812	2211	48.5	24.2	14.4	0.1	87.2	55.6	27.8	16.5	0.1
304-SMW	2215.5	>4	4257	46087	18031	2551	55.2	25.0	17.9	0.1	98.1	56.3	25.4	18.2	0.1
306-SMW	2225.5	>4	4363	43717	15919	3703	55.5	23.7	15.5	0.1	94.7	58.5	25.0	16.4	0.1
308-SMW	2235.5	>4	4058	43278	14920	2679	51.6	23.6	14.5	0.1	89.7	57.5	26.3	16.2	0.1
310-SMW	2245.5	>4	4331	42995	13878	3268	54.1	23.4	13.2	0.1	90.8	59.5	25.8	14.6	0.1
312-SMW	2255.5	>4	4748	46388	13578	3183	58.5	25.3	12.7	0.1	96.6	60.5	26.2	13.1	0.1
314-SMW	2265.5	>4	4280	43317	14092	2744	53.6	23.6	13.5	0.1	90.8	59.0	26.0	14.9	0.1
316-SMW	2275.5	>4	4110	48671	14655	2112	51.9	26.7	14.0	0.1	92.8	55.9	28.8	15.1	0.1
318-SMW	2285.5	>4	4934	43616	12423	2110	59.9	23.8	11.4	0.1	95.2	62.9	25.0	12.0	0.1
321-SMW	2295.5	>4	3969	43730	15081	2679	50.7	23.8	14.7	0.1	89.3	56.7	26.7	16.5	0.1
323-SMW	2305.5	>4	5020	43184	12780	2929	61.1	23.5	11.8	0.1	96.5	63.3	24.3	12.2	0.1
325-SMW	2315.5	>4	4509	43067	12701	3284	55.5	23.5	11.9	0.1	90.9	61.0	25.8	13.0	0.1
327-SMW	2325.5	>4	5019	45202	13493	2794	61.4	24.6	12.6	0.1	98.7	62.2	24.9	12.7	0.1
348-C0002P-															
9-SMW	1965.5	1–4	3132	31690	9540	2512	38.9	17.3	9.0	0.1	65.3	59.5	26.5	13.8	0.2
14-SMW	1975.5	1–4	4225	32673	10398	3115	51.3	17.6	9.6	0.1	78.7	65.3	22.4	12.2	0.1
16-SMW	1985.5	1–4	3727	34308	11642	2874	46.4	18.6	11.1	0.1	76.2	60.9	24.4	14.6	0.1
18-SMW	1995.5	1–4	4596	38732	14421	4056	57.4	20.8	13.9	0.1	92.2	62.3	22.6	15.1	0.1
20-SMW	2005.5	1–4	1843	19820	6469	2745	23.3	10.8	6.2	0.9	41.3	56.6	26.2	15.1	2.2
25-SMW	2015.5	1–4	3013	29068	8147	3423	37.0	15.9	7.5	0.2	60.5	61.0	26.3	12.4	0.3
28-SMW	2025.5	1–4	4247	38835	11752	3024	52.2	21.1	11.0	0.1	84.4	61.8	25.0	13.0	0.1
30-SMW	2035.5	1–4	5001	41265	14084	1989	61.5	22.3	13.3	0.1	97.2	63.3	22.9	13.7	0.1
32-SMW	2045.5	1–4	4905	44232	12233	1890	59.5	24.1	11.2	0.1	94.9	62.7	25.4	11.8	0.1
34-SMW	2055.5	1–4	4657	45265	14318	1778	57.8	24.7	13.6	0.1	96.1	60.1	25.7	14.1	0.1
36-SMW	2065.5	1–4	4876	43922	12183	2174	59.2	24.0	11.2	0.1	94.4	62.7	25.4	11.8	0.1
43-SMW	2075.5	1–4	4905	42674	11822	1465	59.3	23.3	10.8	0.1	93.4	63.5	24.9	11.5	0.1
45-SMW	2085.5	1–4	4927	45388	12349	763	59.7	24.8	11.3	0.1	95.9	62.2	25.9	11.8	0.1
47-SMW	2095.5	1–4	4428	46503	15701	1854	55.9	25.3	15.2	0.1	96.5	57.9	26.2	15.7	0.1
49-SMW	2105.5	1–4	3670	44928	14138	1398	46.8	24.7	13.7	0.1	85.3	54.9	28.9	16.1	0.1
53-SMW	2115.5	1–4	4549	45937	15385	2102	57.1	25.0	14.8	0.1	97.0	58.9	25.8	15.3	0.1
56-SMW	2125.5	1–4	4707	43080	20574	1987	61.5	22.9	20.7	0.1	105.1	58.5	21.8	19.7	0.1
58-SMW	2135.5	1–4	3661	45578	15333	2449	47.3	25.0	15.0	0.1	87.4	54.2	28.6	17.2	0.1
61-SMW	2145.5	1–4	4516	47645	16616	2768	57.4	25.9	16.2	0.1	99.5	57.6	26.0	16.2	0.1
63-SMW	2155.5	1–4	4384	46245	16122	3090	55.7	25.2	15.7	0.1	96.6	57.7	26.0	16.2	0.1
71-SMW	2165.5	1–4	4139	47939	15494	3402	52.7	26.2	15.0	0.1	94.0	56.0	27.9	15.9	0.1
73-SMW	2175.5	1–4	3881	46086	15916	2694	50.1	25.2	15.6	0.1	90.9	55.1	27.7	17.1	0.1
76-SMW	2185.5	1–4	3441	47894	15478	2899	45.0	26.4	15.2	0.1	86.6	51.9	30.4	17.5	0.1
81-SMW	2195.5	1–4	2936	49065	16044	2168	39.7	27.1	15.9	0.1	82.8	47.9	32.7	19.2	0.1
83-SMW	2205.5	1–4	3237	49024	15371	1754	42.6	27.1	15.1	0.1	84.9	50.2	31.9	17.8	0.1
86-SMW	2215.5	1–4	3999	45710	14419	2264	50.6	25.0	13.9	0.1	89.6	56.5	27.9	15.5	0.1
107-SMW	2225.5	1–4	4297	44324	18925	2157	56.1	23.8	18.9	0.1	99.0	56.7	24.1	19.1	0.1
109-SMW	2235.5	1–4	4877	46283	19110	2362	62.6	24.9	18.9	0.1	106.4	58.8	23.4	17.7	0.1
111-SMW	2245.5	1–4	4733	38966	10989	2087	57.1	21.2	10.0	0.1	88.3	64.6	24.0	11.3	0.1
113-SMW	2255.5	1–4	4752	44453	13761	2040	58.6	24.2	13.0	0.1	95.8	61.1	25.3	13.5	0.1
115-SMW	2265.5	1–4	3750	44876	14741	2618	48.1	24.6	14.3	0.1	87.1	55.2	28.2	16.5	0.1
117-SMW	2275.5	1–4	3546	43860	12797	3355	44.9	24.2	12.2	0.1	81.4	55.2	29.7	15.0	0.1
121-SMW	2285.5	1–4	4811	43321	14118	3029	59.5	23.5	13.4	0.1	96.4	61.7	24.4	13.9	0.1
123-SMW	2295.5	1–4	4447	44240	13464	2450	55.1	24.2	12.7	0.1	92.1	59.8	26.2	13.8	0.1
125-SMW	2305.5	1–4	4586	43443	15315	2950	57.6	23.5	14.8	0.1	96.0	60.0	24.5	15.4	0.1
127-SMW	2315.5	1–4	5293	45204	12397	3054	63.9	24.6	11.2	0.1	99.9	64.0	24.7	11.3	0.1
129-SMW	2325.5	1–4	4580	44477	16215	2201	57.9	24.1	15.8	0.1	97.8	59.2	24.6	16.1	0.1
131-SMW	2335.5	1–4	5089	41956	12037	2580	61.5	22.8	11.0	0.1	95.4	64.5	23.9	11.5	0.1
133-SMW	2345.5	1–4	3958	41944	15014	1842	50.5	22.8	14.7	0.1	88.0	57.3	25.9	16.7	0.1
136-SMW	2355.5	1–4	4360	46509	13596	1930	54.1	25.5	12.8	0.1	92.6	58.5	27.5	13.9	0.1

Table T9 (continued). (Continued on next page.)

Cuttings sample	Depth (mbsf)	Size fraction (mm)	Integrated peak area (total counts)				Absolute mineral abundance calculated from SVD normalization factors (wt%)					Relative abundance (wt%)			
			Total clay	Quartz	Feldspar	Calcite	Total clay	Quartz	Feldspar	Calcite	Sum	Total clay	Quartz	Feldspar	Calcite
138-SMW	2365.5	1–4	4217	45232	15867	2061	53.7	24.6	15.5	0.1	93.9	57.2	26.2	16.5	0.1
141-SMW	2375.5	1–4	3848	46048	15418	2000	49.4	25.2	15.0	0.1	89.8	55.1	28.1	16.8	0.1
143-SMW	2385.5	1–4	4407	46199	21470	1836	58.5	24.7	21.7	0.1	105.1	55.7	23.6	20.6	0.1
145-SMW	2395.5	1–4	3402	45386	16153	2563	44.9	24.8	16.0	0.1	85.9	52.3	28.9	18.7	0.1
149-SMW	2405.5	1–4	3935	46176	21761	1833	53.5	24.8	22.1	0.1	100.5	53.2	24.7	22.0	0.1
151-SMW	2415.5	1–4	4087	49465	14888	2192	51.7	27.2	14.3	0.1	93.3	55.4	29.1	15.3	0.1
155-SMW	2425.5	1–4	3783	48888	17359	2426	49.6	26.7	17.2	0.1	93.7	53.0	28.6	18.3	0.1
157-SMW	2435.5	1–4	3238	47818	14301	1906	42.1	26.4	13.9	0.1	82.6	51.0	32.0	16.9	0.1
159-SMW	2445.5	1–4	3527	47164	16494	2790	46.4	25.8	16.3	0.1	88.7	52.4	29.1	18.4	0.1
161-SMW	2455.5	1–4	3716	51362	17305	2561	48.8	28.2	17.1	0.1	94.2	51.8	29.9	18.1	0.1
163-SMW	2465.5	1–4	3854	47413	16821	2470	50.2	25.9	16.6	0.1	92.8	54.1	27.9	17.9	0.1
165-SMW	2475.5	1–4	3718	45963	15161	2647	47.9	25.2	14.8	0.1	88.0	54.4	28.6	16.8	0.1
168-SMW	2485.5	1–4	3856	47274	18746	3054	51.2	25.7	18.7	0.1	95.7	53.5	26.8	19.6	0.1
170-SMW	2495.5	1–4	4204	47136	15280	2989	53.3	25.8	14.8	0.1	93.9	56.7	27.4	15.7	0.1
172-SMW	2505.5	1–4	3729	48801	15133	2860	48.0	26.9	14.7	0.1	89.6	53.5	30.0	16.4	0.1
174-SMW	2515.5	1–4	4146	46166	14840	2228	52.4	25.3	14.3	0.1	92.1	56.9	27.4	15.5	0.1
176-SMW	2525.5	1–4	4496	45541	15367	2270	56.5	24.8	14.8	0.1	96.2	58.8	25.7	15.4	0.1
179-SMW	2535.5	1–4	4006	46006	14871	2216	50.9	25.2	14.4	0.1	90.6	56.2	27.8	15.9	0.1
181-SMW	2545.5	1–4	4029	46909	15799	1764	51.6	25.6	15.4	0.1	92.7	55.6	27.7	16.6	0.1
183-SMW	2555.5	1–4	4382	47206	17572	1822	56.3	25.6	17.3	0.1	99.3	56.7	25.8	17.4	0.1
185-SMW	2565.5	1–4	3674	46820	16056	2471	47.8	25.6	15.8	0.1	89.4	53.5	28.7	17.7	0.1
187-SMW	2575.5	1–4	4469	47592	20632	3136	58.9	25.6	20.7	0.1	105.2	55.9	24.3	19.6	0.1
189-SMW	2585.5	1–4	4507	45305	15454	2443	56.7	24.6	14.9	0.1	96.4	58.9	25.6	15.5	0.1
191-SMW	2595.5	1–4	4208	48666	17687	2900	54.5	26.5	17.4	0.1	98.5	55.3	26.9	17.7	0.1
196-SMW	2605.5	1–4	4608	44389	16080	3456	58.2	24.0	15.6	0.1	97.9	59.4	24.5	15.9	0.1
198-SMW	2615.5	1–4	4760	45302	14105	3599	58.9	24.7	13.3	0.1	97.0	60.7	25.4	13.7	0.1
200-SMW	2625.5	1–4	4022	44425	14883	4341	51.2	24.2	14.4	0.1	90.0	56.9	26.9	16.0	0.1
202-SMW	2635.5	1–4	4068	44878	15412	5045	52.0	24.5	15.0	0.5	91.9	56.6	26.6	16.3	0.5
204-SMW	2645.5	1–4	4292	42694	11952	5186	52.8	23.4	11.1	0.6	87.9	60.1	26.6	12.6	0.7
208-SMW	2655.5	1–4	4840	40627	11937	4382	58.8	22.1	11.0	0.1	91.9	64.0	24.0	11.9	0.1
210-SMW	2665.5	1–4	4080	43194	15924	4692	52.4	23.4	15.6	0.0	91.4	57.3	25.6	17.1	0.0
213-SMW	2675.5	1–4	5109	44735	14911	4635	63.2	24.2	14.1	0.1	101.6	62.2	23.8	13.9	0.1
215-SMW	2685.5	1–4	4664	42565	13286	4154	57.5	23.1	12.5	0.1	93.2	61.7	24.8	13.4	0.1
217-SMW	2695.5	1–4	5204	42142	12299	3475	62.9	22.8	11.2	0.1	97.1	64.8	23.5	11.6	0.1
219-SMW	2705.5	1–4	4997	42084	12913	3545	61.0	22.8	12.0	0.1	95.9	63.6	23.8	12.5	0.1
221-SMW	2715.5	1–4	4617	42167	12736	3742	56.7	22.9	11.9	0.1	91.7	61.9	25.0	13.0	0.1
224-SMW	2725.5	1–4	4676	44488	13135	2881	57.5	24.3	12.3	0.1	94.1	61.1	25.8	13.0	0.1
226-SMW	2735.5	1–4	5170	44625	11946	2819	62.3	24.3	10.8	0.1	97.6	63.9	25.0	11.1	0.1
229-SMW	2745.5	1–4	5322	48460	13163	2685	64.5	26.5	12.0	0.1	103.1	62.6	25.7	11.7	0.1
231-SMW	2755.5	1–4	4916	45130	13058	2415	60.0	24.6	12.1	0.1	96.9	62.0	25.4	12.5	0.1
233-SMW	2765.5	1–4	4520	46492	13717	2378	56.0	25.4	12.9	0.1	94.5	59.3	26.9	13.7	0.1
235-SMW	2775.5	1–4	4489	48307	12836	2796	55.2	26.6	11.9	0.1	93.8	58.9	28.3	12.7	0.1
237-SMW	2785.5	1–4	4160	45850	13990	1727	52.1	25.1	13.4	0.1	90.7	57.5	27.7	14.7	0.1
240-SMW	2795.5	1–4	4745	49079	13970	2566	58.6	26.9	13.1	0.1	98.6	59.4	27.3	13.3	0.1
242-SMW	2805.5	1–4	3982	47095	12586	2693	49.5	26.0	11.8	0.1	87.4	56.7	29.7	13.5	0.1
244-SMW	2815.5	1–4	4353	49471	14028	1878	54.2	27.2	13.3	0.1	94.8	57.2	28.7	14.0	0.1
247-SMW	2825.5	1–4	4120	48814	14557	3032	52.0	26.8	13.9	0.1	92.9	56.0	28.9	15.0	0.1
249-SMW	2835.5	1–4	4511	47359	13439	3092	55.8	26.0	12.6	0.1	94.4	59.1	27.5	13.3	0.1
251-SMW	2845.5	1–4	4190	46483	12927	1890	51.9	25.6	12.1	0.1	89.7	57.9	28.5	13.5	0.1
254-SMW	2855.5	1–4	4508	45979	12510	2358	55.3	25.2	11.6	0.1	92.2	60.0	27.4	12.6	0.1
256-SMW	2865.5	1–4	4180	46024	12584	1868	51.7	25.3	11.8	0.1	88.9	58.1	28.5	13.2	0.1
259-SMW	2875.5	1–4	3993	47744	11995	2893	49.4	26.4	11.1	0.1	87.0	56.7	30.4	12.8	0.1
261-SMW	2885.5	1–4	4080	48986	14877	2840	51.7	26.9	14.3	0.1	93.0	55.6	28.9	15.4	0.1
263-SMW	2895.5	1–4	4045	47610	14189	2247	51.0	26.2	13.6	0.1	90.8	56.1	28.8	14.9	0.1
265-SMW	2905.5	1–4	3808	47116	14680	1964	48.6	25.9	14.2	0.1	88.8	54.7	29.2	16.0	0.1
267-SMW	2915.5	1–4	4241	48227	15604	1739	53.8	26.4	15.1	0.1	95.4	56.4	27.7	15.8	0.1
269-SMW	2925.5	1–4	4508	46293	13582	1672	55.8	25.3	12.8	0.1	94.0	59.3	27.0	13.6	0.1
271-SMW	2935.5	1–4	4502	47413	13536	2235	55.7	26.0	12.7	0.1	94.5	58.9	27.5	13.4	0.1
273-SMW	2945.5	1–4	4471	45574	11517	2060	54.4	25.1	10.5	0.1	90.0	60.4	27.9	11.7	0.1
277-SMW	2955.5	1–4	3880	50322	13965	1771	49.0	27.8	13.3	0.1	90.2	54.3	30.8	14.7	0.1
279-SMW	2965.5	1–4	4470	48652	15918	1323	56.4	26.6	15.4	0.1	98.5	57.3	27.0	15.6	0.1
281-SMW	2975.5	1–4	5408	46505	12556	2679	65.2	25.4	11.4	0.1	102.0	63.9	24.9	11.1	0.1
283-SMW	2985.5	1–4	3568	51014	16247	3149	46.7	28.1	15.9	0.1	90.9	51.4	30.9	17.5	0.1
285-SMW	2995.5	1–4	4734	48513	14167	2523	58.5	26.6	13.3	0.1	98.5	59.4	27.0	13.5	0.1
289-SMW	3005.5	1–4	4415	47203	13615	1521	54.7	25.9	12.8	0.1	93.5	58.5	27.7	13.7	0.1
291-SMW	3015.5	1–4	4682	46557	13218	1668	57.5	25.5	12.3	0.1	95.4	60.3	26.7	12.9	0.1
293-SMW	3025.5	1–4	3506	49886	16698	2404	46.3	27.4	16.5	0.1	90.3	51.2	30.4	18.3	0.1
296-SMW	3035.5	1–4	4831	44009	11644	2213	58.4	24.1	10.6	0.1	93.2	62.7	25.8	11.3	0.1

Table T9 (continued). (Continued on next page.)

Cuttings sample	Depth (mbsf)	Size fraction (mm)	Integrated peak area (total counts)				Absolute mineral abundance calculated from SVD normalization factors (wt%)					Relative abundance (wt%)			
			Total clay	Quartz	Feldspar	Calcite	Total clay	Quartz	Feldspar	Calcite	Sum	Total clay	Quartz	Feldspar	Calcite
298-SMW	3045.5	1–4	4664	44475	10844	1312	56.1	24.4	9.7	0.1	90.4	62.1	27.0	10.7	0.1
300-SMW	3058.5	1–4	4213	44840	13420	2297	52.5	24.6	12.7	0.1	89.9	58.4	27.3	14.2	0.1
9-SMW	1965.5	>4	2385	23689	6827	3619	29.5	13.0	6.4	1.4	50.2	58.8	25.8	12.7	2.7
14-SMW	1975.5	>4	4036	35581	11479	2830	49.7	19.3	10.8	0.1	79.9	62.2	24.1	13.5	0.1
16-SMW	1985.5	>4	3853	36148	11565	2663	47.7	19.6	11.0	0.1	78.5	60.9	25.0	14.0	0.1
18-SMW	1995.5	>4	2419	19442	5794	3001	29.4	10.5	5.3	0.6	45.8	64.1	23.0	11.6	1.3
20-SMW	2005.5	>4	4361	36247	9919	3834	52.6	19.7	9.0	0.1	81.4	64.6	24.2	11.0	0.1
25-SMW	2015.5	>4	4086	43132	11591	4658	50.3	23.7	10.7	0.1	84.9	59.3	27.9	12.6	0.1
28-SMW	2025.5	>4	4211	40590	14997	2689	53.3	21.9	14.6	0.1	90.0	59.3	24.4	16.2	0.1
30-SMW	2035.5	>4	4054	45510	13576	2123	50.8	25.0	12.9	0.1	88.8	57.2	28.1	14.6	0.1
34-SMW	2055.5	>4	4576	45059	12802	1588	56.1	24.7	11.9	0.1	92.8	60.5	26.6	12.8	0.1
36-SMW	2065.5	>4	3961	45043	15398	2729	50.7	24.6	15.0	0.1	90.4	56.1	27.2	16.6	0.1
43-SMW	2075.5	>4	4837	43190	14758	2043	60.0	23.4	14.1	0.1	97.6	61.5	23.9	14.4	0.1
45-SMW	2085.5	>4	4449	42729	14198	1667	55.5	23.2	13.6	0.1	92.4	60.0	25.1	14.7	0.1
47-SMW	2095.5	>4	3104	43656	13611	6218	40.6	24.1	13.3	3.4	81.3	50.0	29.6	16.3	4.1
49-SMW	2105.5	>4	3759	40667	11193	2730	46.5	22.4	10.5	0.1	79.4	58.5	28.2	13.2	0.1
53-SMW	2115.5	>4	3442	41355	13191	6376	44.2	22.7	12.8	3.2	82.8	53.3	27.4	15.4	3.9
56-SMW	2125.5	>4	4985	43325	17806	2015	63.1	23.2	17.5	0.1	103.9	60.8	22.3	16.8	0.1
58-SMW	2135.5	>4	3964	43703	14254	2274	50.2	23.9	13.8	0.1	87.9	57.1	27.2	15.7	0.1
61-SMW	2145.5	>4	3432	42658	12788	2832	43.6	23.5	12.3	0.1	79.5	54.9	29.5	15.5	0.1
63-SMW	2155.5	>4	4136	48072	15092	2425	52.4	26.4	14.5	0.1	93.4	56.1	28.2	15.6	0.1
71-SMW	2165.5	>4	3930	44641	14974	4029	50.2	24.4	14.5	0.1	89.3	56.3	27.3	16.3	0.1
73-SMW	2175.5	>4	4323	41378	11796	2138	52.9	22.6	11.0	0.1	86.6	61.1	26.1	12.6	0.1
76-SMW	2185.5	>4	4113	47605	17094	2143	53.1	25.9	16.8	0.1	96.0	55.4	27.0	17.5	0.1
81-SMW	2195.5	>4	3664	46836	17207	1665	48.2	25.6	17.1	0.1	91.0	53.0	28.1	18.8	0.1
83-SMW	2205.5	>4	2891	50721	25412	2403	43.8	27.4	26.4	0.1	97.7	44.8	28.1	27.1	0.1
86-SMW	2215.5	>4	4487	42962	17648	2058	57.6	23.1	17.4	0.1	98.2	58.6	23.5	17.8	0.1
107-SMW	2225.5	>4	4636	42891	14775	2631	57.9	23.2	14.2	0.1	95.3	60.7	24.4	14.9	0.1
109-SMW	2235.5	>4	4333	48009	19935	4018	57.1	25.9	19.9	0.1	103.0	55.4	25.2	19.3	0.1
111-SMW	2245.5	>4	4311	44832	12958	1579	53.3	24.6	12.2	0.1	90.1	59.1	27.3	13.5	0.1
113-SMW	2255.5	>4	2000	30710	14171	1481	28.6	16.6	14.6	0.1	60.0	47.8	27.8	24.3	0.2
115-SMW	2265.5	>4	4101	44757	22744	2472	55.9	23.9	23.2	0.1	103.1	54.2	23.2	22.5	0.1
117-SMW	2275.5	>4	4939	44757	14761	1310	61.1	24.3	14.0	0.1	99.5	61.4	24.4	14.1	0.1
121-SMW	2285.5	>4	4596	46426	16247	2472	58.1	25.2	15.7	0.1	99.1	58.6	25.4	15.9	0.1
123-SMW	2295.5	>4	4171	45321	17328	2082	53.9	24.6	17.1	0.1	95.7	56.3	25.7	17.9	0.1
125-SMW	2305.5	>4	4309	49127	20980	1752	57.2	26.5	21.1	0.1	104.9	54.5	25.3	20.1	0.1
127-SMW	2315.5	>4	3911	46260	21279	1911	53.0	24.9	21.6	0.1	99.6	53.2	25.0	21.7	0.1
129-SMW	2325.5	>4	3588	47834	18309	1585	47.9	26.1	18.3	0.1	92.5	51.8	28.2	19.8	0.1
131-SMW	2335.5	>4	4370	43739	13954	2474	54.5	23.8	13.3	0.1	91.7	59.4	26.0	14.5	0.1
133-SMW	2345.5	>4	3377	49006	24464	2188	48.7	26.4	25.3	0.1	100.4	48.5	26.3	25.2	0.1
136-SMW	2355.5	>4	4243	46207	14021	1775	53.1	25.3	13.4	0.1	91.8	57.8	27.6	14.5	0.1
138-SMW	2365.5	>4	3873	45444	19782	1763	51.8	24.5	20.0	0.1	96.4	53.8	25.4	20.7	0.1
141-SMW	2375.5	>4	4143	45486	17541	2324	53.7	24.7	17.4	0.1	95.9	56.1	25.7	18.1	0.1
143-SMW	2385.5	>4	4032	46486	19567	2170	53.5	25.1	19.6	0.1	98.4	54.4	25.5	20.0	0.1
145-SMW	2395.5	>4	4480	46590	13679	1672	55.5	25.5	12.9	0.1	94.0	59.0	27.1	13.7	0.1
149-SMW	2405.5	>4	4041	48431	18056	1344	52.8	26.4	17.9	0.1	97.1	54.3	27.2	18.4	0.1
151-SMW	2415.5	>4	2830	52384	20795	1922	40.8	28.8	21.2	0.1	90.8	44.9	31.6	23.4	0.1
155-SMW	2425.5	>4	3530	46061	14895	2362	45.7	25.3	14.5	0.1	85.6	53.3	29.6	17.0	0.1
157-SMW	2435.5	>4	3732	46719	14778	1694	47.8	25.7	14.3	0.1	87.9	54.4	29.2	16.3	0.1
159-SMW	2445.5	>4	3323	55562	23107	2026	47.3	30.4	23.6	0.1	101.4	46.7	29.9	23.3	0.1
161-SMW	2455.5	>4	3272	49731	14624	1742	42.6	27.5	14.2	0.1	84.5	50.4	32.6	16.8	0.1
163-SMW	2465.5	>4	3928	53141	18144	2191	51.6	29.2	17.9	0.1	98.7	52.2	29.5	18.1	0.1
165-SMW	2475.5	>4	3555	45743	15030	2011	46.0	25.1	14.7	0.1	85.9	53.5	29.2	17.1	0.1
168-SMW	2485.5	>4	3772	52383	27524	1169	54.4	28.1	28.5	0.1	111.1	49.0	25.3	25.7	0.1
170-SMW	2495.5	>4	3916	46010	14635	2592	49.8	25.2	14.1	0.1	89.3	55.8	28.2	15.8	0.1
172-SMW	2505.5	>4	3428	51220	16661	1097	45.3	28.2	16.4	0.1	90.1	50.3	31.4	18.3	0.1
174-SMW	2515.5	>4	3613	45898	16897	2199	47.6	25.1	16.8	0.1	89.5	53.1	28.0	18.7	0.1
176-SMW	2525.5	>4	4047	46905	15356	1104	51.5	25.7	14.9	0.1	92.2	55.9	27.9	16.2	0.1
179-SMW	2535.5	>4	3859	49737	18684	1086	51.0	27.1	18.6	0.1	96.9	52.7	28.0	19.2	0.1
181-SMW	2545.5	>4	3082	48145	16080	1912	41.3	26.5	16.0	0.1	83.9	49.2	31.6	19.0	0.1
183-SMW	2555.5	>4	3875	52435	21467	1124	52.6	28.5	21.7	0.1	102.9	51.1	27.7	21.1	0.1
185-SMW	2565.5	>4	3688	46826	15485	1793	47.7	25.7	15.1	0.1	88.6	53.8	29.0	17.1	0.1
187-SMW	2575.5	>4	3733	48225	19390	1793	50.1	26.2	19.5	0.1	95.9	52.2	27.3	20.3	0.1
189-SMW	2585.5	>4	4006	45013	16612	3945	51.9	24.5	16.4	0.1	92.8	55.9	26.4	17.6	0.1
191-SMW	2595.5	>4	3772	47064	18278	2866	50.0	25.6	18.3	0.1	94.0	53.2	27.2	19.4	0.1
196-SMW	2605.5	>4	4366	44630	17359	3311	56.2	24.1	17.1	0.1	97.5	57.6	24.7	17.5	0.1
198-SMW	2615.5	>4	4191	51093	23023	3018	56.9	27.6	23.4	0.1	107.9	52.7	25.5	21.6	0.1
200-SMW	2625.5	>4	3669	47282	14860	6362	47.4	26.0	14.4	2.8	90.6	52.3	28.7	15.9	3.0

Table T9 (continued).

Cuttings sample	Depth (mbsf)	Size fraction (mm)	Integrated peak area (total counts)				Absolute mineral abundance calculated from SVD normalization factors (wt%)					Relative abundance (wt%)			
			Total clay	Quartz	Feldspar	Calcite	Total clay	Quartz	Feldspar	Calcite	Sum	Total clay	Quartz	Feldspar	Calcite
202-SMW	2635.5	>4	3618	45083	22185	4693	50.4	24.2	22.7	0.2	97.5	51.7	24.8	23.3	0.3
204-SMW	2645.5	>4	4450	46031	18517	3725	57.7	24.8	18.3	0.1	101.0	57.1	24.6	18.2	0.1
208-SMW	2655.5	>4	4127	42857	15558	3372	52.7	23.3	15.2	0.1	91.2	57.7	25.5	16.7	0.1
210-SMW	2665.5	>4	5150	43134	13806	4471	63.1	23.3	12.9	0.1	99.5	63.5	23.5	13.0	0.1
213-SMW	2675.5	>4	4624	42651	13564	3433	57.2	23.2	12.8	0.1	93.3	61.3	24.8	13.7	0.1
215-SMW	2685.5	>4	4307	43598	14262	3535	54.0	23.7	13.7	0.1	91.5	59.0	25.9	14.9	0.1
217-SMW	2695.5	>4	4728	41895	12259	2156	57.6	22.8	11.3	0.1	91.9	62.7	24.8	12.3	0.1
219-SMW	2705.5	>4	4114	43226	11762	2911	50.6	23.7	10.9	0.1	85.4	59.3	27.8	12.8	0.1
221-SMW	2715.5	>4	4150	45349	12449	2588	51.3	24.9	11.6	0.1	88.0	58.3	28.3	13.2	0.1
224-SMW	2725.5	>4	3935	48542	16042	3019	50.7	26.6	15.7	0.1	93.1	54.5	28.6	16.8	0.1
226-SMW	2735.5	>4	4521	47022	11869	0	54.9	25.9	10.8	0.1	91.8	59.9	28.2	11.8	0.1
229-SMW	2745.5	>4	4078	50113	13211	1614	50.8	27.7	12.4	0.1	91.0	55.8	30.5	13.6	0.1
231-SMW	2755.5	>4	4468	47926	12425	1670	54.7	26.4	11.5	0.1	92.7	59.0	28.5	12.4	0.1
233-SMW	2765.5	>4	3675	50810	16283	1724	47.9	28.0	16.0	0.1	91.9	52.1	30.4	17.4	0.1
235-SMW	2775.5	>4	4597	47004	11608	2004	55.8	25.9	10.5	0.1	92.3	60.4	28.1	11.4	0.1
237-SMW	2785.5	>4	4091	44981	12260	2494	50.6	24.7	11.4	0.1	86.9	58.2	28.5	13.2	0.1
240-SMW	2795.5	>4	3924	50349	14445	1879	49.7	27.8	13.8	0.1	91.4	54.4	30.4	15.1	0.1
242-SMW	2805.5	>4	4016	43163	12472	3925	50.0	23.7	11.7	0.1	85.5	58.4	27.7	13.7	0.1
244-SMW	2815.5	>4	4529	44791	11423	1835	54.9	24.6	10.4	0.1	90.1	61.0	27.3	11.5	0.1
247-SMW	2825.5	>4	4197	50276	13848	830	52.4	27.7	13.1	0.1	93.3	56.1	29.7	14.0	0.1
249-SMW	2835.5	>4	4452	47599	15134	990	55.8	26.0	14.5	0.1	96.5	57.9	27.0	15.0	0.1
251-SMW	2845.5	>4	4375	46366	12314	706	53.6	25.5	11.4	0.1	90.6	59.2	28.2	12.6	0.1
254-SMW	2855.5	>4	3878	48854	14855	768	49.4	26.9	14.3	0.1	90.7	54.4	29.7	15.8	0.1
256-SMW	2865.5	>4	4368	48305	13699	1392	54.2	26.6	12.9	0.1	93.8	57.8	28.3	13.8	0.1
259-SMW	2875.5	>4	4364	46854	13254	1081	54.0	25.7	12.4	0.1	92.2	58.5	27.9	13.5	0.1
261-SMW	2885.5	>4	4212	43348	14613	5144	53.2	23.6	14.1	0.5	91.4	58.2	25.8	15.4	0.6
263-SMW	2895.5	>4	4289	46330	12090	1331	52.6	25.5	11.2	0.1	89.4	58.8	28.6	12.5	0.1
265-SMW	2905.5	>4	4427	47219	12236	1548	54.2	26.0	11.3	0.1	91.6	59.2	28.4	12.3	0.1
267-SMW	2915.5	>4	4213	48807	13944	1163	52.6	26.9	13.2	0.1	92.8	56.7	28.9	14.2	0.1
269-SMW	2925.5	>4	4487	46253	12166	2086	54.8	25.4	11.2	0.1	91.6	59.9	27.8	12.2	0.1
271-SMW	2935.5	>4	4347	48652	15984	1088	55.1	26.6	15.5	0.1	97.3	56.6	27.3	15.9	0.1
273-SMW	2945.5	>4	4926	44507	12391	1782	59.8	24.3	11.4	0.1	95.6	62.6	25.4	11.9	0.1
277-SMW	2955.5	>4	4097	45044	12497	3975	50.8	24.8	11.7	0.1	87.4	58.2	28.3	13.4	0.1
279-SMW	2965.5	>4	3631	49263	15824	1450	47.2	27.1	15.5	0.1	89.8	52.5	30.2	17.2	0.1
281-SMW	2975.5	>4	4436	48275	16456	808	56.3	26.3	16.0	0.1	98.7	57.0	26.7	16.2	0.1
283-SMW	2985.5	>4	3946	51081	16412	1371	50.9	28.1	16.0	0.1	95.1	53.5	29.5	16.8	0.1
285-SMW	2995.5	>4	3930	51291	14122	1420	49.6	28.4	13.4	0.1	91.5	54.2	31.0	14.7	0.1
289-SMW	3005.5	>4	3983	45454	13382	1144	49.9	25.0	12.7	0.1	87.7	56.9	28.5	14.5	0.1
291-SMW	3015.5	>4	4553	46723	15195	1430	57.0	25.5	14.6	0.1	97.2	58.7	26.2	15.0	0.1
293-SMW	3025.5	>4	4162	45374	12629	1588	51.5	24.9	11.8	0.1	88.4	58.3	28.2	13.4	0.1
296-SMW	3035.5	>4	4722	45863	11994	1961	57.3	25.2	10.9	0.1	93.6	61.3	26.9	11.7	0.1
298-SMW	3045.5	>4	4619	44975	15153	1627	57.8	24.4	14.6	0.1	96.9	59.6	25.2	15.0	0.1
300-SMW	3058.5	>4	3718	46267	13910	972	47.2	25.5	13.4	0.1	86.1	54.8	29.6	15.5	0.1

SVD = singular value decomposition.

Table T10. X-ray fluorescence analysis on cuttings samples, Holes C0002N and C0002P. (Continued on next seven pages.)

Cuttings sample	Bottom depth (mbsf)	Bulk fraction size (mm)	Na_2O (wt%)	MgO (wt%)	Al_2O_3 (wt%)	SiO_2 (wt%)	P_2O_5 (wt%)	K_2O (wt%)	CaO (wt%)	TiO_2 (wt%)	MnO (wt%)	Fe_2O_3 (wt%)	Loss on ignition (wt%)
348-C0002N-													
3-SMW	875.5	1–4	1.114	1.746	3.734	27.165	0.147	0.512	59.238	0.174	0.067	4.828	17.794
5-SMW	885.5	1–4	2.1	2.066	8.583	41.017	0.124	1.358	36.723	0.371	0.064	4.784	14.727
7-SMW	895.5	1–4	1.881	2.197	9.68	45.575	0.117	1.252	32.192	0.408	0.062	4.915	13.901
9-SMW	905.5	1–4	2.219	2.248	12.768	55.504	0.101	2.292	18.2	0.565	0.058	4.821	13.239
12-SMW	915.5	1–4	2.291	2.349	13.387	57.559	0.112	2.48	14.602	0.57	0.062	5.311	12.643
14-SMW	925.5	1–4	2.559	2.599	14.212	60.032	0.097	2.87	10.516	0.613	0.057	5.214	12.034
16-SMW	935.5	1–4	2.353	2.387	14.421	60.285	0.088	2.943	10.196	0.575	0.055	5.047	11.295
18-SMW	945.5	1–4	2.657	2.595	15.284	61.804	0.084	3.027	7.718	0.631	0.049	5.176	11.23
20-SMW	955.5	1–4	2.718	2.435	16.11	63.083	0.081	3.108	5.619	0.675	0.061	5.29	8.391
22-SMW	965.5	1–4	2.766	2.417	16.706	63.507	0.079	3.508	4.082	0.684	0.061	5.664	8.384
24-SMW	975.5	1–4	2.706	2.457	16.74	63.48	0.098	3.754	3.706	0.682	0.069	5.829	8.663
26-SMW	985.5	1–4	2.738	2.435	17.001	62.3	0.104	3.572	4.41	0.725	0.072	5.828	21.233
28-SMW	995.5	1–4	2.717	2.492	16.441	63.323	0.1	3.416	4.155	0.7	0.065	5.776	8.098
30-SMW	1005.5	1–4	2.605	2.647	16.675	63.67	0.096	3.369	4.226	0.65	0.075	5.804	8.688
32-SMW	1015.5	1–4	2.678	2.496	16.494	62.901	0.094	3.537	4.198	0.671	0.074	5.728	8.551
34-SMW	1025.5	1–4	2.723	2.542	16.349	63.134	0.086	3.423	3.434	0.66	0.072	5.839	8.068
36-SMW	1035.5	1–4	2.582	2.464	16.45	64.09	0.095	3.463	3.347	0.663	0.066	5.914	7.771
39-SMW	1045.5	1–4	2.605	2.374	16.083	64.327	0.086	3.412	3.63	0.64	0.066	5.676	7.676
40-SMW	1052.5	1–4	2.683	2.389	16.594	63.67	0.087	3.666	3.237	0.66	0.066	5.861	7.296
41-SMW	1067.5	1–4	2.683	2.361	16.938	63.378	0.097	3.44	3.698	0.681	0.065	5.946	7.48
42-SMW	1069.5	1–4	2.612	2.271	16.769	62.993	0.102	3.42	4.094	0.699	0.068	5.897	7.514
43-SMW	1070.5	1–4	2.836	2.26	16.516	63.124	0.104	3.436	3.84	0.691	0.064	5.78	7.577
44-SMW	1075.5	1–4	2.753	2.306	16.212	63.447	0.088	3.457	3.543	0.674	0.065	5.85	7.529
46-SMW	1085.5	1–4	2.897	2.195	16.305	63.833	0.088	3.505	3.561	0.666	0.062	5.689	7.557
48-SMW	1095.5	1–4	2.61	2.415	16.321	64.469	0.086	3.373	3.351	0.661	0.059	5.727	7.664
50-SMW	1105.5	1–4	2.808	2.33	16.231	65.115	0.084	3.329	3.11	0.643	0.055	5.607	7.388
52-SMW	1115.5	1–4	2.617	2.34	16.709	63.429	0.092	3.293	3.586	0.659	0.057	5.846	7.583
54-SMW	1125.5	1–4	2.715	2.405	16.628	64.146	0.087	3.202	3.193	0.673	0.055	5.736	7.079
57-SMW	1135.5	1–4	2.573	2.391	16.391	64.127	0.089	3.121	3.559	0.678	0.061	5.759	7.153
59-SMW	1145.5	1–4	2.75	2.355	16.274	64.387	0.095	3.335	3.693	0.663	0.061	5.698	8.189
61-SMW	1155.5	1–4	2.533	2.392	16.816	64.776	0.089	3.395	3.275	0.682	0.06	5.799	8.15
63-SMW	1165.5	1–4	2.523	2.331	16.273	64.38	0.1	3.354	3.908	0.648	0.069	5.606	8.465
65-SMW	1175.5	1–4	2.588	2.265	16.296	63.94	0.09	3.418	3.478	0.669	0.077	5.583	7.973
67-SMW	1185.5	1–4	2.559	2.435	16.881	64.578	0.075	3.622	2.882	0.669	0.054	5.866	8.021
69-SMW	1195.5	1–4	2.458	2.548	16.305	63.944	0.094	3.358	3.857	0.668	0.071	5.751	8.082
71-SMW	1205.5	1–4	2.619	2.473	16.226	63.894	0.105	3.273	4.344	0.658	0.081	5.657	7.942
73-SMW	1215.5	1–4	2.569	2.34	16.366	64.28	0.094	3.45	3.565	0.66	0.068	5.717	7.984
81-SMW	1225.5	1–4	2.527	2.804	15.469	61.705	0.141	3.063	6.712	0.61	0.106	5.711	10.114
83-SMW	1235.5	1–4	2.556	2.31	16.424	64.641	0.086	3.551	2.875	0.666	0.055	5.73	7.219
85-SMW	1245.5	1–4	2.499	2.33	15.935	63.581	0.129	3.53	4.825	0.656	0.078	5.61	7.984
87-SMW	1255.5	1–4	2.553	2.318	16.103	63.482	0.129	3.389	4.782	0.638	0.078	5.698	8.443
89-SMW	1265.5	1–4	2.593	2.332	16.249	64.488	0.1	3.542	3.362	0.688	0.063	5.729	7.805
91-SMW	1275.5	1–4	2.535	2.254	16.174	64.85	0.092	3.554	3.443	0.662	0.072	5.653	7.553
93-SMW	1285.5	1–4	2.458	2.279	16.065	64.278	0.106	3.464	3.667	0.649	0.07	5.517	7.006
95-SMW	1295.5	1–4	2.486	2.449	16.045	63.812	0.104	3.561	4.069	0.636	0.074	5.641	8.122
97-SMW	1305.5	1–4	2.481	2.302	15.819	64.623	0.105	3.307	3.717	0.65	0.065	5.455	6.881
99-SMW	1315.5	1–4	2.514	2.352	15.713	64.519	0.096	3.257	4.164	0.625	0.071	5.466	7.093
101-SMW	1325.5	1–4	2.515	2.37	15.752	65.022	0.123	3.116	4.159	0.624	0.07	5.339	7.602
105-SMW	1335.5	1–4	2.616	2.421	15.436	65.392	0.097	3.145	4.183	0.609	0.076	5.299	7.892
107-SMW	1345.5	1–4	2.425	2.37	16.591	64.85	0.088	3.622	2.673	0.653	0.05	5.592	7.627
109-SMW	1355.5	1–4	2.643	2.341	16.642	65.375	0.08	3.427	2.606	0.663	0.058	5.459	7.489
111-SMW	1365.5	1–4	2.493	2.342	16.495	65.123	0.094	3.399	3.195	0.642	0.06	5.456	7.686
113-SMW	1375.5	1–4	2.483	2.296	16.081	65.408	0.092	3.205	3.375	0.62	0.062	5.328	7.751
115-SMW	1385.5	1–4	2.49	2.557	15.58	64.375	0.114	3.21	5.038	0.617	0.085	5.257	9.214
117-SMW	1395.5	1–4	2.494	2.54	16.402	63.047	0.098	3.451	4.537	0.641	0.071	5.789	9.048
119-SMW	1405.5	1–4	2.455	2.518	15.595	64.257	0.108	3.404	4.447	0.629	0.075	5.438	8.737
121-SMW	1415.5	1–4	2.605	2.252	15.047	66.007	0.104	3.33	3.933	0.601	0.07	5.029	7.5
123-SMW	1425.5	1–4	2.463	2.182	15.648	65.589	0.081	3.663	3.014	0.641	0.056	5.385	7.312
125-SMW	1435.5	1–4	2.367	2.36	15.137	65.562	0.129	3.243	4.564	0.605	0.08	5.2	8.267
128-SMW	1445.5	1–4	2.423	2.281	15.109	65.099	0.123	3.326	4.458	0.598	0.08	5.134	7.983
130-SMW	1455.5	1–4	2.293	2.284	15.926	65.022	0.111	3.472	3.513	0.633	0.084	5.394	7.484
132-SMW	1465.5	1–4	2.514	2.096	15.624	66.39	0.091	3.575	2.809	0.627	0.07	5.176	7.364
134-SMW	1475.5	1–4	2.496	2.255	15.645	66.015	0.09	3.482	3.08	0.623	0.074	5.419	7.24
136-SMW	1485.5	1–4	2.361	2.039	14.07	62.845	0.1	3.299	3.259	0.566	0.07	4.814	7.315
138-SMW	1495.5	1–4	2.364	2.141	15.325	66.07	0.096	3.422	3.432	0.615	0.078	5.269	6.844
140-SMW	1505.5	1–4	2.497	2.21	16.113	64.667	0.097	3.488	3.251	0.668	0.072	5.665	7.243

Table T10 (continued). (Continued on next page.)

Cuttings sample	Bottom depth (mbsf)	Bulk fraction size (mm)	Na_2O (wt%)	MgO (wt%)	Al_2O_3 (wt%)	SiO_2 (wt%)	P_2O_5 (wt%)	K_2O (wt%)	CaO (wt%)	TiO_2 (wt%)	MnO (wt%)	Fe_2O_3 (wt%)	Loss on ignition (wt%)
142-SMW	1515.5	1–4	2.507	2.048	15.413	65.264	0.087	3.385	3.518	0.641	0.079	5.402	7.417
146-SMW	1525.5	1–4	2.439	1.849	14.406	68.713	0.076	3.173	3.084	0.578	0.073	4.806	6.39
148-SMW	1535.5	1–4	2.294	2.043	15.589	66.437	0.091	3.413	3.248	0.624	0.066	5.265	6.891
150-SMW	1545.5	1–4	2.407	2.085	15.75	66.321	0.097	3.338	3.305	0.627	0.065	5.338	6.658
152-SMW	1555.5	1–4	2.422	2.159	15.798	66.3	0.075	3.292	2.884	0.626	0.07	5.369	7.197
154-SMW	1565.5	1–4	2.386	2.004	15.3	67.709	0.078	3.316	2.841	0.606	0.07	5.174	7.063
156-SMW	1575.5	1–4	2.363	1.885	14.494	68.474	0.082	3.175	2.852	0.566	0.08	5.019	6.462
158-SMW	1585.5	1–4	2.524	2.239	16.097	65.648	0.085	3.429	2.886	0.683	0.077	5.558	6.848
160-SMW	1595.5	1–4	2.43	2.047	15.119	67.293	0.075	3.295	2.52	0.622	0.07	5.126	6.262
162-SMW	1605.5	1–4	2.424	1.953	14.683	69.016	0.077	3.178	2.177	0.589	0.061	4.892	5.854
164-SMW	1615.5	1–4	2.42	2.19	15.993	66.516	0.144	3.568	2.251	0.664	0.064	5.474	6.57
166-SMW	1625.5	1–4	2.463	2.074	15.262	67.696	0.186	3.242	2.417	0.612	0.065	5.146	6.222
169-SMW	1635.5	1–4	2.531	2.121	16.266	66.299	0.114	3.361	2.236	0.645	0.052	5.369	6.226
171-SMW	1645.5	1–4	2.476	1.398	12.852	72.997	0.237	3.185	2.584	0.491	0.064	3.642	4.587
173-SMW	1655.5	1–4	2.386	1.307	11.856	75.323	0.12	3.038	2.086	0.408	0.052	3.141	3.795
175-SMW	1665.5	1–4	2.405	1.86	14.24	68.327	0.097	3.273	3.531	0.568	0.064	4.558	5.925
177-SMW	1677.5	1–4	2.395	2.149	15.811	64.876	0.11	3.467	3.613	0.657	0.057	5.334	6.517
182-SMW	1685.5	1–4	2.572	2.275	16.232	65.309	0.087	3.501	2.901	0.663	0.054	5.594	6.434
184-SMW	1695.5	1–4	2.534	2.24	16.26	65.546	0.101	3.465	2.86	0.672	0.059	5.557	6.485
186-SMW	1705.5	1–4	2.468	2.247	16.266	65.796	0.074	3.604	2.313	0.663	0.054	5.568	6.293
188-SMW	1715.5	1–4	2.473	2.178	16.131	65.604	0.086	3.608	3.007	0.653	0.059	5.513	6.659
190-SMW	1725.5	1–4	2.325	2.101	15.854	65.017	0.094	3.36	4.098	0.66	0.076	5.206	7.009
192-SMW	1735.5	1–4	2.424	2.159	16.141	65.126	0.083	3.566	3.091	0.67	0.063	5.434	7.05
195-SMW	1745.5	1–4	2.487	2.161	16.018	65.322	0.093	3.497	3.387	0.661	0.063	5.363	7.263
197-SMW	1755.5	1–4	2.421	2.119	15.881	64.866	0.115	3.447	3.804	0.673	0.072	5.414	7.173
199-SMW	1765.5	1–4	2.477	2.194	16.294	65.207	0.08	3.634	3.01	0.683	0.061	5.534	7.146
201-SMW	1775.5	1–4	2.478	2.223	16.312	64.811	0.082	3.653	3.201	0.678	0.06	5.499	7.781
203-SMW	1785.5	1–4	2.34	2.05	16.181	65.13	0.09	3.693	2.874	0.703	0.059	5.367	7.444
205-SMW	1795.5	1–4	2.43	2.163	16.248	65.494	0.089	3.691	2.543	0.718	0.06	5.374	7.462
207-SMW	1805.5	1–4	2.319	2.225	16.298	65.826	0.093	3.672	2.241	0.67	0.055	5.49	7.094
209-SMW	1815.5	1–4	2.39	2.016	16.158	66.093	0.112	3.597	2.518	0.687	0.059	5.302	7.248
211-SMW	1825.5	1–4	2.427	2.133	16.448	66.145	0.097	3.71	2.233	0.686	0.054	5.423	6.921
213-SMW	1835.5	1–4	2.319	2.124	16.236	65.823	0.099	3.596	2.815	0.699	0.067	5.379	7.115
216-SMW	1845.5	1–4	2.351	2.093	16.325	66.528	0.086	3.758	2.183	0.704	0.06	5.38	6.507
218-SMW	1855.5	1–4	2.223	2.105	16.258	66.027	0.079	3.686	2.1	0.717	0.057	5.328	6.452
220-SMW	1865.5	1–4	2.287	2.167	16.421	65.771	0.085	3.676	2.415	0.694	0.06	5.406	6.853
222-SMW	1875.5	1–4	2.48	2.049	16.282	65.649	0.087	3.823	2.647	0.691	0.061	5.395	7.176
224-SMW	1885.5	1–4	2.36	2.1	16.475	66.132	0.078	3.671	2.718	0.695	0.057	5.426	6.962
226-SMW	1895.5	1–4	2.261	2.012	16.204	65.379	0.087	3.771	3.263	0.668	0.056	5.26	7.081
228-SMW	1905.5	1–4	2.24	2.156	16.162	65.057	0.088	3.581	3.89	0.666	0.055	5.305	7.466
230-SMW	1915.5	1–4	2.253	2.17	16.209	64.664	0.085	3.664	4.212	0.673	0.061	5.404	7.883
232-SMW	1925.5	1–4	2.227	2.194	16.092	63.463	0.094	3.432	4.941	0.669	0.076	5.45	8.326
234-SMW	1935.5	1–4	2.283	2.2	16.234	63.761	0.086	3.758	4.488	0.653	0.08	5.526	8.026
237-SMW	1945.5	1–4	2.111	2.244	16.224	64.083	0.085	3.643	4.024	0.682	0.084	5.577	7.883
239-SMW	1955.5	1–4	2.213	2.266	16.422	64.721	0.079	3.843	3.114	0.687	0.07	5.553	7.17
241-SMW	1965.5	1–4	2.177	2.305	16.402	64.984	0.08	3.795	2.527	0.674	0.064	5.59	6.809
243-SMW	1975.5	1–4	2.186	2.226	16.367	65.29	0.074	3.888	2.77	0.68	0.066	5.555	7.161
248-SMW	1985.5	1–4	2.122	2.24	16.357	65.976	0.067	3.704	1.998	0.688	0.06	5.514	6.273
250-SMW	1995.5	1–4	2.307	2.202	16.549	66.068	0.077	3.856	1.926	0.673	0.055	5.537	6.744
252-SMW	2005.5	1–4	2.273	2.198	16.173	65.864	0.076	3.731	1.785	0.68	0.061	5.474	6.049
259-SMW	2015.5	1–4	2.272	2.257	16.478	65.505	0.079	3.565	2.807	0.661	0.059	5.612	7.217
261-SMW	2025.5	1–4	2.171	2.186	16.351	65.294	0.088	3.728	2.755	0.665	0.059	5.514	6.953
264-SMW	2035.5	1–4	2.044	2.161	16.225	65.192	0.088	3.762	2.598	0.661	0.058	5.509	6.532
266-SMW	2045.5	1–4	2.331	2.149	16.207	65.791	0.094	3.716	2.801	0.667	0.072	5.301	9.269
268-SMW	2055.5	1–4	2.331	2.126	15.925	64.974	0.072	3.747	2.97	0.666	0.054	5.799	7.66
270-SMW	2065.5	1–4	2.42	2.148	16.364	67.382	0.068	3.891	1.052	0.67	0.044	5.384	6.287
272-SMW	2075.5	1–4	2.335	2.057	16.223	66.909	0.068	3.949	1.132	0.657	0.044	5.276	6.226
274-SMW	2085.5	1–4	2.427	2.092	16.292	66.532	0.072	3.917	1.346	0.671	0.052	5.33	6.191
276-SMW	2095.5	1–4	2.35	2.114	16.484	66.534	0.078	3.966	1.296	0.705	0.051	5.373	6.729
278-SMW	2105.5	1–4	2.23	2.04	16.161	66.95	0.072	3.826	1.233	0.647	0.047	5.25	5.699
281-SMW	2115.5	1–4	2.268	2.043	16.126	66.788	0.081	3.878	1.458	0.634	0.053	5.189	5.832
283-SMW	2125.5	1–4	2.324	1.945	15.941	67.209	0.087	3.794	1.444	0.65	0.049	5.177	6.471
285-SMW	2135.5	1–4	2.333	1.982	16.134	66.74	0.09	3.865	1.548	0.642	0.057	5.213	8.103
287-SMW	2145.5	1–4	2.362	2.054	16.346	66.552	0.079	3.924	1.342	0.684	0.05	5.248	6.855
289-SMW	2155.5	1–4	2.312	2.061	16.357	66.666	0.071	3.839	1.239	0.663	0.051	5.291	6.363
291-SMW	2165.5	1–4	2.245	2.014	16.834	67.649	0.082	3.906	1.025	0.681	0.05	5.294	6.009
296-SMW	2175.5	1–4	2.189	1.913	16.05	66.921	0.069	3.738	1.399	0.649	0.052	5.188	5.974
298-SMW	2185.5	1–4	2.288	1.914	16.193	67.356	0.069	3.749	1.435	0.664	0.047	5.174	6.231

Table T10 (continued). (Continued on next page.)

Cuttings sample	Bottom depth (mbsf)	Bulk fraction size (mm)	Na_2O (wt%)	MgO (wt%)	Al_2O_3 (wt%)	SiO_2 (wt%)	P_2O_5 (wt%)	K_2O (wt%)	CaO (wt%)	TiO_2 (wt%)	MnO (wt%)	Fe_2O_3 (wt%)	Loss on ignition (wt%)
300-SMW	2195.5	1–4	2.307	1.862	15.92	67.197	0.062	3.778	1.591	0.662	0.052	5.153	6.143
302-SMW	2205.5	1–4	2.349	1.946	16.265	67.257	0.06	3.785	1.506	0.684	0.051	5.222	6.624
304-SMW	2215.5	1–4	2.283	1.788	15.694	67.79	0.064	3.708	2.014	0.638	0.057	5.039	6.382
306-SMW	2225.5	1–4	2.108	1.828	15.769	66.482	0.072	3.696	2.638	0.655	0.061	5.212	6.911
308-SMW	2235.5	1–4	2.321	1.855	15.825	66.443	0.073	3.747	2.72	0.653	0.061	5.15	7.742
310-SMW	2245.5	1–4	2.145	2.026	16.625	66.189	0.073	3.792	1.731	0.701	0.057	5.553	6.64
312-SMW	2255.5	1–4	2.33	1.968	16.362	66.135	0.079	3.766	2.404	0.678	0.064	5.62	7.647
314-SMW	2265.5	1–4	2.217	2.034	16.648	66.37	0.081	3.867	1.593	0.692	0.05	5.658	6.984
316-SMW	2275.5	1–4	2.326	1.965	16.325	65.307	0.079	3.891	2.52	0.688	0.064	5.567	7.351
318-SMW	2285.5	1–4	2.063	2.055	16.86	65.895	0.087	3.826	1.837	0.685	0.057	5.643	6.83
321-SMW	2295.5	1–4	2.011	2.061	16.625	66.235	0.068	3.808	1.689	0.679	0.053	5.556	6.691
323-SMW	2305.5	1–4	2.185	2.092	16.619	65.949	0.073	3.799	1.864	0.688	0.054	5.548	7.153
325-SMW	2315.5	1–4	2.155	2.011	16.626	65.564	0.072	3.822	1.609	0.687	0.049	5.618	7.118
327-SMW	2325.5	1–4	2.27	2.004	16.766	65.923	0.073	3.804	1.739	0.694	0.053	5.615	6.966
3-SMW	875.5	>4	0.8	1.094	3.519	27.203	0.137	0.612	60.792	0.134	0.066	4.65	16.119
5-SMW	885.5	>4	0.7	1.25	4.11	27.959	0.149	0.501	58.612	0.181	0.068	4.872	16.612
7-SMW	895.5	>4	0.969	1.217	4.564	29.41	0.137	0.639	57.496	0.164	0.065	4.841	16.933
9-SMW	905.5	>4	1.636	1.51	7.142	37.089	0.128	1.112	44.441	0.285	0.063	4.825	16.544
12-SMW	915.5	>4	2.327	2.047	12.071	53.521	0.105	2.216	20.009	0.502	0.059	4.931	13.017
14-SMW	925.5	>4	1.884	2.095	11.907	52.951	0.104	2.37	21.072	0.511	0.061	5.091	12.887
16-SMW	935.5	>4	2.066	2.211	11.425	51.071	0.117	1.851	23.72	0.511	0.062	5.19	13.105
18-SMW	945.5	>4	2.195	2.084	12.022	52.531	0.1	2.255	20.629	0.484	0.055	5.078	12.666
20-SMW	955.5	>4	2.06	1.929	12.814	55.186	0.096	2.571	17.049	0.527	0.058	5.018	9.824
22-SMW	965.5	>4	2.401	1.995	13.638	55.339	0.095	2.84	14.897	0.563	0.065	5.433	8.932
24-SMW	975.5	>4	2.494	2.151	15.106	59.132	0.089	3.356	9.572	0.609	0.061	5.567	8.525
26-SMW	985.5	>4	2.805	2.152	16.498	62.103	0.099	3.637	5.007	0.67	0.063	5.685	8.076
28-SMW	995.5	>4	2.421	2.077	14.964	59.21	0.104	3.385	8.81	0.615	0.063	5.585	7.741
30-SMW	1005.5	>4	2.448	2.238	15.751	61.464	0.098	3.369	8.178	0.622	0.064	5.533	7.605
32-SMW	1015.5	>4	2.272	2.18	15.114	59.107	0.104	3.309	10.116	0.607	0.072	5.598	8.087
34-SMW	1025.5	>4	2.568	2.395	16.78	64.486	0.087	3.681	2.983	0.694	0.067	5.703	7.662
36-SMW	1035.5	>4	2.474	2.283	16.639	64.485	0.083	3.821	2.794	0.663	0.059	5.768	7.524
39-SMW	1045.5	>4	2.273	2.056	14.078	56.955	0.103	2.792	13.847	0.584	0.064	5.485	9.091
40-SMW	1052.5	>4	2.631	2.227	16.458	64.439	0.088	3.928	3.047	0.67	0.062	5.696	7.544
41-SMW	1067.5	>4	2.7	2.197	16.791	63.621	0.096	3.735	3.644	0.669	0.062	5.763	7.231
42-SMW	1069.5	>4	2.64	2.166	16.736	63.3	0.107	3.712	3.69	0.691	0.062	5.76	7.281
43-SMW	1070.5	>4	2.472	2.19	16.511	63.311	0.089	3.747	3.6	0.67	0.06	5.732	6.73
44-SMW	1075.5	>4	2.536	2.164	16.651	64.862	0.087	3.75	2.942	0.682	0.06	5.734	6.839
46-SMW	1085.5	>4	2.491	2.088	16.309	63.907	0.088	3.909	4.059	0.648	0.059	5.676	7.042
48-SMW	1095.5	>4	2.527	2.284	16.481	64.454	0.083	3.678	3.155	0.662	0.062	5.83	7.266
50-SMW	1105.5	>4	2.542	2.181	16.208	65.057	0.081	3.667	2.942	0.66	0.057	5.703	6.881
52-SMW	1115.5	>4	2.702	2.159	16.302	64.213	0.089	3.609	3.801	0.667	0.059	5.637	6.559
54-SMW	1125.5	>4	2.626	2.181	16.526	64.97	0.083	3.58	2.955	0.683	0.055	5.577	6.391
57-SMW	1135.5	>4	2.499	2.179	15.959	65.13	0.084	3.477	3.213	0.646	0.055	5.449	6.473
59-SMW	1145.5	>4	2.503	2.143	16.23	65.213	0.09	3.766	3.14	0.669	0.056	5.659	7.16
61-SMW	1155.5	>4	2.58	2.334	16.126	64.382	0.089	3.739	3.58	0.645	0.059	5.573	7.66
63-SMW	1165.5	>4	2.364	2.148	16.595	64.323	0.083	3.799	3.089	0.671	0.062	5.734	7.778
65-SMW	1175.5	>4	2.431	2.151	16.737	64.531	0.085	3.744	2.89	0.671	0.083	5.956	7.913
67-SMW	1185.5	>4	2.565	2.271	16.882	64.419	0.087	3.857	3.078	0.683	0.065	5.475	8.213
69-SMW	1195.5	>4	2.612	2.446	15.954	63.094	0.105	3.487	4.421	0.642	0.083	5.661	8.252
71-SMW	1205.5	>4	2.489	2.077	15.271	60.859	0.085	3.373	7.268	0.608	0.065	5.706	7.231
73-SMW	1215.5	>4	2.344	2.019	14.45	58.657	0.092	3.237	10.652	0.591	0.06	5.455	7.723
81-SMW	1225.5	>4	2.262	2.33	15.299	60.426	0.087	3.462	7.517	0.62	0.062	5.789	7.995
83-SMW	1235.5	>4	2.389	2.124	15.987	62.577	0.098	3.662	5.297	0.662	0.06	5.958	7.318
85-SMW	1245.5	>4	2.561	2.224	16.469	65.386	0.097	3.944	3.309	0.681	0.051	4.982	7.533
87-SMW	1255.5	>4	2.447	2.045	15.904	63.793	0.107	3.659	5.231	0.64	0.05	4.933	7.985
89-SMW	1265.5	>4	2.51	2.175	16.436	65.255	0.091	3.853	3.307	0.67	0.056	5.224	7.506
91-SMW	1275.5	>4	2.368	2.16	16.167	64.395	0.088	3.816	3.198	0.645	0.057	5.655	7.405
93-SMW	1285.5	>4	2.363	2.135	16.445	64.78	0.093	3.769	2.854	0.684	0.053	5.694	7.269
95-SMW	1295.5	>4	2.327	2.167	15.296	61.136	0.104	3.485	7.106	0.627	0.061	5.579	7.009
97-SMW	1305.5	>4	2.418	2.218	16.01	64.493	0.103	3.61	3.52	0.66	0.063	5.619	7.204
99-SMW	1315.5	>4	2.503	2.162	16.071	64.939	0.094	3.741	3.101	0.664	0.062	5.561	7.202
101-SMW	1325.5	>4	2.575	2.374	15.606	64.855	0.126	3.284	3.907	0.626	0.067	5.268	7.65
105-SMW	1335.5	>4	2.476	2.179	16.011	65.162	0.082	3.582	3.774	0.647	0.054	5.562	7.353
107-SMW	1345.5	>4	2.444	2.275	16.145	64.619	0.127	3.698	3.256	0.652	0.068	5.521	7.539
109-SMW	1355.5	>4	2.593	2.237	16.366	65.067	0.079	3.593	2.879	0.65	0.055	5.585	7.493
111-SMW	1365.5	>4	2.407	2.248	16.135	64.031	0.117	3.534	4.403	0.642	0.075	5.617	8.411
113-SMW	1375.5	>4	2.399	2.295	16.332	64.333	0.099	3.625	3.442	0.661	0.062	5.603	7.873
115-SMW	1385.5	>4	2.299	2.308	15.845	64.273	0.109	3.708	4.49	0.643	0.072	5.353	8.231

Table T10 (continued). (Continued on next page.)

Cuttings sample	Bottom depth (mbsf)	Bulk fraction size (mm)	Na_2O (wt%)	MgO (wt%)	Al_2O_3 (wt%)	SiO_2 (wt%)	P_2O_5 (wt%)	K_2O (wt%)	CaO (wt%)	TiO_2 (wt%)	MnO (wt%)	Fe_2O_3 (wt%)	Loss on ignition (wt%)
117-SMW	1395.5	>4	2.383	2.528	16.456	62.609	0.105	3.542	4.958	0.652	0.079	5.632	9.021
119-SMW	1405.5	>4	2.371	2.272	16.044	64.704	0.083	3.859	3.703	0.647	0.064	5.595	7.971
121-SMW	1415.5	>4	2.488	2.097	15.412	65.973	0.077	3.662	3.022	0.607	0.063	5.207	6.864
123-SMW	1425.5	>4	2.602	2.136	15.673	66.279	0.079	3.843	2.681	0.655	0.053	5.32	6.672
125-SMW	1435.5	>4	2.439	2.215	16.027	65.188	0.091	3.705	3.258	0.654	0.058	5.474	7.478
128-SMW	1445.5	>4	2.491	2.109	15.993	65.032	0.078	3.783	2.912	0.633	0.055	5.371	7.201
130-SMW	1455.5	>4	2.304	2.289	16.639	64.693	0.075	3.934	2.256	0.676	0.067	5.697	6.816
132-SMW	1465.5	>4	2.329	2.244	16.442	64.827	0.076	3.817	2.593	0.668	0.073	5.546	7.09
134-SMW	1475.5	>4	2.313	2.249	16.521	65.281	0.079	3.8	2.521	0.658	0.059	5.497	7.118
136-SMW	1485.5	>4	2.347	2.241	16.657	65.281	0.078	3.836	2.144	0.679	0.053	5.785	6.858
138-SMW	1495.5	>4	2.33	2.232	16.54	65.158	0.081	3.915	2.49	0.674	0.057	5.696	6.924
140-SMW	1505.5	>4	2.331	2.137	16.24	64.797	0.083	3.722	2.74	0.644	0.06	5.625	6.823
142-SMW	1515.5	>4	2.344	2.114	16.039	64.733	0.082	3.723	3.035	0.675	0.071	5.644	7.435
146-SMW	1525.5	>4	2.398	2.114	16.219	65.475	0.076	3.691	2.693	0.651	0.061	5.58	6.978
148-SMW	1535.5	>4	2.36	2.181	16.352	65.119	0.086	3.715	2.727	0.676	0.053	5.64	7.048
150-SMW	1545.5	>4	2.347	2.1	15.996	65.531	0.092	3.555	3.092	0.633	0.058	5.493	6.603
152-SMW	1555.5	>4	2.413	2.158	16.193	66.024	0.074	3.58	2.485	0.661	0.063	5.596	6.712
154-SMW	1565.5	>4	2.309	2	15.626	66.311	0.075	3.666	2.498	0.641	0.063	5.339	6.258
156-SMW	1575.5	>4	2.35	2.069	15.813	66.493	0.082	3.512	2.476	0.632	0.064	5.376	6.222
158-SMW	1585.5	>4	2.319	2.187	16.132	65.391	0.087	3.623	3.259	0.659	0.083	5.567	6.769
160-SMW	1595.5	>4	2.332	2.096	16.003	66.279	0.074	3.649	2.215	0.655	0.062	5.531	6.555
162-SMW	1605.5	>4	2.359	2.148	16.265	65.939	0.079	3.598	2.308	0.656	0.061	5.609	6.175
164-SMW	1615.5	>4	2.324	2.063	15.829	65.967	0.138	3.694	2.259	0.657	0.065	5.497	6.447
166-SMW	1625.5	>4	2.267	2.105	16.03	66.424	0.081	3.523	2.192	0.659	0.06	5.525	5.897
169-SMW	1635.5	>4	2.3	2.083	15.811	66.89	0.077	3.535	2.253	0.643	0.056	5.423	6.116
171-SMW	1645.5	>4	2.345	1.934	15.061	68.205	0.094	3.514	2.129	0.607	0.057	4.997	5.785
173-SMW	1655.5	>4	2.521	1.865	14.893	69.158	0.072	3.452	1.921	0.582	0.051	4.838	5.433
175-SMW	1665.5	>4	2.39	2.17	16.079	65.637	0.086	3.627	3.126	0.662	0.057	5.447	6.486
177-SMW	1677.5	>4	2.582	2.074	15.853	65.509	0.096	3.651	3.287	0.657	0.055	5.293	6.631
182-SMW	1685.5	>4	2.212	2.161	16.155	65.133	0.087	3.935	2.744	0.673	0.05	5.508	6.389
184-SMW	1695.5	>4	2.255	2.101	15.87	64.935	0.076	3.741	3.42	0.668	0.058	5.523	6.555
186-SMW	1705.5	>4	2.508	2.13	16.507	65.442	0.075	3.72	2.317	0.66	0.052	5.667	6.094
188-SMW	1715.5	>4	2.279	2.078	16.121	65.519	0.084	3.735	2.658	0.671	0.054	5.446	6.43
190-SMW	1725.5	>4	2.284	2.103	15.919	64.986	0.09	3.566	3.786	0.673	0.07	5.27	6.769
192-SMW	1735.5	>4	2.433	2.094	16.152	65.378	0.08	3.655	2.953	0.662	0.057	5.441	6.457
195-SMW	1745.5	>4	2.368	2.146	16.463	64.54	0.086	3.763	3.042	0.688	0.058	5.632	6.958
197-SMW	1755.5	>4	2.347	2.021	15.845	65.227	0.103	3.621	3.356	0.643	0.062	5.326	6.582
199-SMW	1765.5	>4	2.322	2.141	16.285	65.465	0.085	3.899	2.658	0.674	0.052	5.594	6.78
201-SMW	1775.5	>4	2.253	2.045	16.087	65.791	0.078	3.852	2.875	0.655	0.058	5.352	6.846
203-SMW	1785.5	>4	2.418	2.076	16.479	65.987	0.073	3.908	2.36	0.687	0.053	5.486	6.938
205-SMW	1795.5	>4	2.353	2.072	16.548	65.672	0.076	3.988	2.181	0.714	0.056	5.554	6.985
207-SMW	1805.5	>4	2.243	2.155	16.438	65.654	0.085	3.862	2.269	0.707	0.053	5.432	6.87
209-SMW	1815.5	>4	2.241	2.101	16.463	65.609	0.071	3.94	2.315	0.694	0.061	5.456	6.797
211-SMW	1825.5	>4	2.23	2.096	16.349	65.158	0.078	3.891	2.777	0.684	0.071	5.475	6.752
213-SMW	1835.5	>4	2.253	2.066	16.421	66.209	0.091	3.81	1.87	0.692	0.054	5.375	6.432
216-SMW	1845.5	>4	2.189	2.043	16.561	66.413	0.07	3.9	1.631	0.68	0.047	5.559	6.301
218-SMW	1855.5	>4	2.256	2.003	16.333	66.005	0.071	3.857	1.92	0.688	0.05	5.398	6.471
220-SMW	1865.5	>4	2.125	2.095	16.603	65.431	0.075	3.864	2.139	0.706	0.053	5.494	6.57
222-SMW	1875.5	>4	2.197	2.089	16.581	65.021	0.075	3.97	2.19	0.69	0.053	5.816	6.33
224-SMW	1885.5	>4	2.239	2.052	16.397	65.185	0.084	3.854	2.471	0.699	0.052	5.438	6.557
226-SMW	1895.5	>4	2.187	2.005	16.223	65.223	0.076	3.92	3.403	0.68	0.05	5.332	7.347
228-SMW	1905.5	>4	2.14	2.116	15.943	63.627	0.098	3.631	4.564	0.687	0.075	5.38	7.604
230-SMW	1915.5	>4	2.046	2.123	16.299	63.958	0.081	3.878	4.048	0.692	0.06	5.591	7.571
232-SMW	1925.5	>4	2.059	2.091	16.4	64.148	0.081	3.77	4.269	0.682	0.068	5.532	7.838
234-SMW	1935.5	>4	2.15	2.148	16.434	64.077	0.08	3.965	3.859	0.674	0.063	5.602	7.721
237-SMW	1945.5	>4	2.076	2.155	16.423	63.816	0.083	3.929	3.738	0.676	0.074	5.681	7.619
239-SMW	1955.5	>4	2.02	2.155	16.404	64.453	0.085	4.104	3.315	0.689	0.072	5.592	7.135
241-SMW	1965.5	>4	2.155	2.195	16.333	64.93	0.079	3.944	3.016	0.672	0.067	5.474	6.764
243-SMW	1975.5	>4	2.113	2.153	16.41	64.79	0.078	4.03	2.712	0.684	0.061	5.53	6.746
248-SMW	1985.5	>4	2.069	2.205	16.549	65.513	0.078	3.968	2.254	0.683	0.059	5.593	6.489
250-SMW	1995.5	>4	2.231	2.139	16.332	65.177	0.085	4.131	2.071	0.679	0.06	5.551	6.456
252-SMW	2005.5	>4	2.21	2.149	16.338	65.44	0.078	3.954	2.353	0.676	0.066	5.53	6.58
259-SMW	2015.5	>4	2.138	1.969	16.097	66.3	0.07	3.926	2.309	0.665	0.049	5.361	5.785
261-SMW	2025.5	>4	2.057	2.092	16.232	65.249	0.074	3.889	2.614	0.668	0.057	5.491	6.205
264-SMW	2035.5	>4	1.997	2.059	16.216	64.73	0.082	3.913	3.09	0.676	0.07	5.599	6.256
266-SMW	2045.5	>4	2.046	2.038	16.015	65.78	0.1	3.938	2.84	0.657	0.068	5.548	6.118
268-SMW	2055.5	>4	2.124	1.923	15.831	66.57	0.065	3.961	2.2	0.653	0.051	5.26	5.625
270-SMW	2065.5	>4	2.314	2.009	16.231	66.631	0.065	3.915	1.775	0.657	0.051	5.338	5.528

Table T10 (continued). (Continued on next page.)

Cuttings sample	Bottom depth (mbsf)	Bulk fraction size (mm)	Na_2O (wt%)	MgO (wt%)	Al_2O_3 (wt%)	SiO_2 (wt%)	P_2O_5 (wt%)	K_2O (wt%)	CaO (wt%)	TiO_2 (wt%)	MnO (wt%)	Fe_2O_3 (wt%)	Loss on ignition (wt%)
272-SMW	2075.5	>4	2.098	2.053	16.52	65.875	0.077	4.133	2.222	0.678	0.057	5.592	5.887
274-SMW	2085.5	>4	2.177	1.945	16.199	66.938	0.069	4.08	1.475	0.67	0.05	5.322	5.624
276-SMW	2095.5	>4	2.259	2.049	16.603	66.279	0.073	4.214	1.233	0.675	0.049	5.487	5.896
278-SMW	2105.5	>4	2.227	1.975	16.2	67.471	0.066	4.008	0.98	0.653	0.045	5.288	5.412
281-SMW	2115.5	>4	2.187	2.008	16.694	67.479	0.076	4.193	1.263	0.69	0.044	5.438	5.9
283-SMW	2125.5	>4	2.235	2.001	16.246	66.885	0.07	3.959	1.403	0.675	0.057	5.288	6.42
285-SMW	2135.5	>4	2.248	2.012	16.258	66.471	0.064	4.085	0.965	0.667	0.044	5.319	6.326
287-SMW	2145.5	>4	2.155	2.068	16.515	65.976	0.07	4.175	1.275	0.687	0.048	5.463	6.401
289-SMW	2155.5	>4	2.236	1.955	16.466	67.145	0.065	4.122	1.046	0.68	0.047	5.348	5.916
291-SMW	2165.5	>4	2.252	1.992	16.591	66.349	0.069	4.199	1.442	0.689	0.052	5.427	6.116
296-SMW	2175.5	>4	2.165	1.931	16.112	66.486	0.071	3.968	1.733	0.677	0.055	5.352	6.444
298-SMW	2185.5	>4	2.142	1.96	16.247	65.697	0.101	4.007	3.045	0.687	0.071	5.347	6.751
300-SMW	2195.5	>4	2.276	1.801	16.081	67.675	0.068	4.11	1.322	0.67	0.045	5.133	5.984
302-SMW	2205.5	>4	2.213	1.926	16.37	66.641	0.069	4.085	1.271	0.672	0.046	5.29	6.349
304-SMW	2215.5	>4	2.252	1.971	16.535	66.38	0.072	4.25	1.44	0.71	0.051	5.4	6.886
306-SMW	2225.5	>4	2.085	1.982	16.599	65.932	0.079	4.035	2.395	0.679	0.058	5.601	7.457
308-SMW	2235.5	>4	2.173	1.938	16.283	65.868	0.067	4.104	1.567	0.667	0.049	5.373	6.55
310-SMW	2245.5	>4	2.112	1.954	16.573	65.371	0.075	4.071	1.79	0.688	0.051	5.568	6.357
312-SMW	2255.5	>4	2.199	1.884	16.408	66.274	0.067	4.088	1.754	0.685	0.055	5.484	6.633
314-SMW	2265.5	>4	2.217	1.993	16.342	65.763	0.072	4.141	1.46	0.672	0.048	5.507	6.473
316-SMW	2275.5	>4	2.166	2.022	16.93	66.162	0.071	4.099	1.406	0.7	0.052	5.823	7.173
318-SMW	2285.5	>4	2.165	1.937	16.699	66.772	0.061	4.044	1.366	0.669	0.049	5.548	6.704
321-SMW	2295.5	>4	2.228	1.986	16.485	66.22	0.073	4.07	1.594	0.7	0.055	5.603	6.559
323-SMW	2305.5	>4	2.126	2.116	16.817	65.567	0.074	4.02	1.739	0.7	0.05	5.765	6.499
325-SMW	2315.5	>4	2.237	2.035	16.643	66.291	0.068	4.162	1.656	0.681	0.044	5.521	6.87
327-SMW	2325.5	>4	2.207	1.993	16.666	66.427	0.072	3.992	1.632	0.7	0.047	5.551	6.508
348-C0002P-													
9-SMW	1965.5	1–4	2.133	2.163	14.519	60.426	0.09	3.202	9.231	0.532	0.056	5.613	7.23
14-SMW	1975.5	1–4	2.119	2.097	14.964	60.521	0.088	3.168	8.351	0.589	0.06	5.795	6.819
16-SMW	1985.5	1–4	2.104	2.146	15.391	62.368	0.076	3.227	7.085	0.588	0.063	5.997	6.163
18-SMW	1995.5	1–4	2.132	2.054	15.332	62.955	0.09	3.566	6.196	0.588	0.069	5.453	6.714
20-SMW	2005.5	1–4	2.129	2.032	15.051	61.924	0.096	3.439	6.546	0.578	0.074	5.757	6.477
25-SMW	2015.5	1–4	2.071	2.025	13.649	58.159	0.098	2.8	12.956	0.473	0.066	5.47	8.456
28-SMW	2025.5	1–4	2.237	2.049	15.525	63.534	0.081	3.571	4.561	0.605	0.061	5.497	6.688
30-SMW	2035.5	1–4	2.278	2.087	15.862	65.214	0.077	3.571	2.491	0.62	0.053	5.651	6.195
32-SMW	2045.5	1–4	2.318	1.993	16.161	66.451	0.06	3.74	1.403	0.631	0.048	5.476	5.954
34-SMW	2055.5	1–4	2.309	2.01	16.111	66.289	0.067	3.668	1.402	0.65	0.05	5.541	5.975
36-SMW	2065.5	1–4	2.294	1.946	16.361	66.092	0.075	3.733	1.292	0.653	0.057	5.591	5.397
43-SMW	2075.5	1–4	2.389	1.971	16.596	66.961	0.076	3.698	0.94	0.653	0.044	5.325	4.901
45-SMW	2085.5	1–4	2.28	2.023	16.262	66.454	0.058	3.698	1.179	0.66	0.038	5.231	5.205
47-SMW	2095.5	1–4	2.372	1.97	16.016	66.947	0.068	3.587	1.567	0.61	0.05	5.119	5.498
49-SMW	2105.5	1–4	2.349	2.005	16.034	66.885	0.074	3.813	1.392	0.624	0.048	5.158	5.208
53-SMW	2115.5	1–4	2.437	2.027	15.988	67.02	0.079	3.709	1.675	0.622	0.05	5.157	5.642
56-SMW	2125.5	1–4	2.392	1.992	16.244	66.629	0.068	3.657	1.233	0.651	0.045	5.399	5.12
58-SMW	2135.5	1–4	2.513	2.022	16.216	66.737	0.072	3.713	1.323	0.633	0.042	5.224	5.275
61-SMW	2145.5	1–4	2.322	1.867	15.97	66.786	0.072	3.812	1.629	0.617	0.048	5.12	5.599
63-SMW	2155.5	1–4	2.274	1.878	16.002	67.077	0.064	3.832	1.849	0.624	0.051	5.152	6.063
71-SMW	2165.5	1–4	2.219	1.831	15.499	67.057	0.071	3.628	2.536	0.603	0.055	4.983	6.229
73-SMW	2175.5	1–4	2.263	1.84	15.699	67.91	0.063	3.675	1.662	0.587	0.048	4.978	5.98
76-SMW	2185.5	1–4	2.327	1.751	15.373	68.125	0.07	3.7	1.833	0.593	0.055	4.823	5.596
81-SMW	2195.5	1–4	2.239	1.728	15.502	67.977	0.059	3.75	1.574	0.599	0.046	4.947	6.055
83-SMW	2205.5	1–4	2.393	1.821	15.786	67.862	0.064	3.787	1.553	0.612	0.051	5.079	6.374
86-SMW	2215.5	1–4	2.253	1.941	16.005	67.131	0.066	3.78	1.54	0.615	0.047	5.215	6.158
107-SMW	2225.5	1–4	1.988	1.966	16.429	67.121	0.065	3.895	1.376	0.662	0.047	5.394	5.32
109-SMW	2235.5	1–4	2.263	2.033	16.457	66.415	0.072	3.853	1.436	0.66	0.049	5.391	5.807
111-SMW	2245.5	1–4	2.184	2.036	16.722	65.973	0.072	3.956	1.453	0.646	0.049	5.57	6.082
113-SMW	2255.5	1–4	2.193	2.043	16.609	66.499	0.069	3.956	1.351	0.672	0.048	5.477	5.769
115-SMW	2265.5	1–4	2.181	1.87	16.083	67.333	0.065	3.868	1.574	0.633	0.05	5.261	5.905
117-SMW	2275.5	1–4	2.177	1.961	16.203	66.344	0.071	3.903	1.949	0.636	0.054	5.413	6.225
121-SMW	2285.5	1–4	2.254	2.035	16.366	66.516	0.075	3.721	1.801	0.645	0.049	5.419	5.921
123-SMW	2295.5	1–4	2.225	2.028	16.54	66.575	0.073	3.751	1.408	0.675	0.045	5.483	5.888
125-SMW	2305.5	1–4	2.261	2.042	16.573	66.806	0.073	3.797	1.555	0.664	0.049	5.544	6.174
127-SMW	2315.5	1–4	2.221	1.967	16.496	66.689	0.089	3.772	1.686	0.649	0.054	5.397	6.268
129-SMW	2325.5	1–4	2.173	1.992	16.605	66.943	0.069	3.888	1.224	0.66	0.043	5.356	5.809
131-SMW	2335.5	1–4	2.203	2.042	16.309	66.753	0.073	3.834	1.428	0.649	0.046	5.263	5.678
133-SMW	2345.5	1–4	2.257	1.993	16.523	66.305	0.071	3.783	1.31	0.648	0.045	5.555	6.106
136-SMW	2355.5	1–4	2.24	1.967	16.477	66.34	0.069	3.947	1.309	0.642	0.052	5.438	6.157
138-SMW	2365.5	1–4	2.145	2.002	16.414	66.947	0.063	3.98	1.301	0.662	0.044	5.371	6.023

Table T10 (continued). (Continued on next page.)

Cuttings sample	Bottom depth (mbsf)	Bulk fraction size (mm)	Na_2O (wt%)	MgO (wt%)	Al_2O_3 (wt%)	SiO_2 (wt%)	P_2O_5 (wt%)	K_2O (wt%)	CaO (wt%)	TiO_2 (wt%)	MnO (wt%)	Fe_2O_3 (wt%)	Loss on ignition (wt%)
141-SMW	2375.5	1–4	2.192	1.885	16.252	66.976	0.066	3.948	1.251	0.663	0.043	5.241	5.796
143-SMW	2385.5	1–4	2.209	1.942	16.449	67.389	0.066	3.829	1.198	0.652	0.045	5.32	5.914
145-SMW	2395.5	1–4	2.221	1.895	16.213	67.008	0.072	3.905	1.42	0.653	0.051	5.254	6.001
149-SMW	2405.5	1–4	2.174	1.814	16.153	67.553	0.07	3.874	1.24	0.645	0.043	5.173	5.849
151-SMW	2415.5	1–4	2.363	1.823	15.916	67.92	0.067	3.864	1.398	0.618	0.05	5.074	6.138
155-SMW	2425.5	1–4	2.197	1.861	16.046	67.138	0.068	3.824	1.631	0.633	0.051	5.311	6.381
157-SMW	2435.5	1–4	2.201	1.8	15.834	68.103	0.063	3.677	1.368	0.614	0.049	5.058	5.725
159-SMW	2445.5	1–4	2.249	1.81	16.074	67.475	0.077	3.762	1.592	0.86	0.051	6.009	6.024
161-SMW	2455.5	1–4	2.269	1.783	15.691	67.934	0.068	3.683	1.491	0.621	0.052	4.967	5.803
163-SMW	2465.5	1–4	2.255	1.798	15.732	67.084	0.074	3.713	1.518	0.835	0.046	5.941	5.768
165-SMW	2475.5	1–4	2.365	1.831	15.827	67.675	0.07	3.669	1.607	0.633	0.052	5.043	5.588
168-SMW	2485.5	1–4	2.264	1.779	15.748	66.706	0.074	3.607	1.449	0.866	0.048	5.99	5.677
170-SMW	2495.5	1–4	2.211	1.879	15.875	67.531	0.07	3.707	1.597	0.637	0.05	5.057	5.689
172-SMW	2505.5	1–4	2.409	1.911	16.034	66.222	0.072	3.735	1.398	0.884	0.045	6.124	5.697
174-SMW	2515.5	1–4	2.426	1.899	16.085	67.602	0.076	3.807	1.214	0.647	0.044	5.153	5.502
176-SMW	2525.5	1–4	2.34	1.878	15.921	66.476	0.069	3.757	1.357	0.911	0.044	6.081	5.409
179-SMW	2535.5	1–4	2.354	1.903	15.998	67.483	0.072	3.83	1.385	0.646	0.048	5.115	5.649
181-SMW	2545.5	1–4	2.356	1.907	16.105	67.61	0.069	3.845	1.181	0.638	0.044	5.147	5.661
183-SMW	2555.5	1–4	2.316	1.939	16.081	67.287	0.068	3.829	1.073	0.646	0.047	5.199	5.498
185-SMW	2565.5	1–4	2.365	1.917	16.015	67.41	0.071	3.839	1.517	0.633	0.052	5.173	5.673
187-SMW	2575.5	1–4	2.337	2.033	16.045	66.578	0.076	3.791	1.552	0.653	0.054	5.242	5.827
189-SMW	2585.5	1–4	2.305	2.008	16.037	66.807	0.065	3.831	1.491	0.637	0.053	5.276	5.889
191-SMW	2595.5	1–4	2.379	2.003	15.738	66.602	0.072	3.802	1.62	0.63	0.054	5.141	7.078
196-SMW	2605.5	1–4	2.351	2.107	16.136	66.833	0.072	3.746	1.751	0.632	0.055	5.288	6.168
198-SMW	2615.5	1–4	2.387	2.103	15.863	66.291	0.077	3.822	1.98	0.633	0.057	5.234	6.256
200-SMW	2625.5	1–4	2.232	2.082	16.028	66.159	0.072	3.683	2.116	0.627	0.061	5.292	5.997
202-SMW	2635.5	1–4	2.181	2.153	16.162	65.433	0.082	3.709	2.708	0.635	0.066	5.409	6.554
204-SMW	2645.5	1–4	2.19	2.077	16.072	65.595	0.087	3.812	2.65	0.614	0.071	5.404	6.402
208-SMW	2655.5	1–4	2.232	2.137	16.413	65.429	0.084	3.87	2.405	0.647	0.068	5.693	6.609
210-SMW	2665.5	1–4	2.198	2.119	16.485	65.383	0.077	3.656	2.404	0.666	0.064	5.618	6.327
213-SMW	2675.5	1–4	2.219	2.086	16.339	65.397	0.084	3.789	2.339	0.653	0.063	5.502	6.313
215-SMW	2685.5	1–4	2.296	2.079	16.487	65.495	0.078	3.821	2.197	0.642	0.064	5.54	6.47
217-SMW	2695.5	1–4	2.217	2.147	16.784	65.68	0.077	3.822	1.555	0.665	0.051	5.641	5.885
219-SMW	2705.5	1–4	2.255	2.045	16.595	65.853	0.07	3.72	1.653	0.653	0.06	5.543	5.915
221-SMW	2715.5	1–4	2.311	2.094	16.707	65.763	0.082	3.731	1.616	0.66	0.061	5.602	6.174
224-SMW	2725.5	1–4	2.274	1.97	16.762	66.042	0.069	3.757	1.474	0.663	0.059	5.525	6.117
226-SMW	2735.5	1–4	2.279	1.955	16.769	66.625	0.083	3.729	1.325	0.649	0.063	5.491	5.978
229-SMW	2745.5	1–4	2.407	1.9	16.533	67.018	0.066	3.612	1.02	0.658	0.046	5.4	5.728
231-SMW	2755.5	1–4	2.307	1.958	16.301	66.79	0.08	3.682	1.362	0.639	0.055	5.38	5.729
233-SMW	2765.5	1–4	2.326	1.896	16.418	67.08	0.069	3.708	0.988	0.648	0.047	5.376	5.768
235-SMW	2775.5	1–4	2.342	1.9	16.466	67.066	0.074	3.759	1.124	0.666	0.054	5.363	5.583
237-SMW	2785.5	1–4	2.341	1.759	16.291	67.015	0.073	3.829	0.948	0.646	0.051	5.295	5.868
240-SMW	2795.5	1–4	2.39	1.978	16.459	66.601	0.071	3.91	0.804	0.666	0.054	5.488	5.376
242-SMW	2805.5	1–4	2.39	1.752	16.266	67.6	0.07	3.717	1.417	0.617	0.071	5.238	6.263
244-SMW	2815.5	1–4	2.454	1.806	16.232	67.776	0.069	3.821	0.941	0.621	0.05	5.163	5.885
247-SMW	2825.5	1–4	2.402	1.796	16.244	66.944	0.07	3.839	1.086	0.645	0.056	5.269	5.671
249-SMW	2835.5	1–4	2.243	1.859	16.301	67.235	0.071	3.78	1.208	0.657	0.066	5.367	6.165
251-SMW	2845.5	1–4	2.394	1.803	16.309	66.784	0.065	3.9	0.825	0.641	0.051	5.364	5.683
254-SMW	2855.5	1–4	2.268	1.855	16.258	66.74	0.078	3.779	1.065	0.645	0.06	5.269	5.788
256-SMW	2865.5	1–4	2.352	1.815	16.517	66.972	0.073	3.868	0.971	0.649	0.061	5.339	5.765
259-SMW	2875.5	1–4	2.397	1.766	16.025	66.835	0.094	3.734	1.455	0.622	0.076	5.266	5.884
261-SMW	2885.5	1–4	2.258	1.853	16.131	66.702	0.084	3.644	1.521	0.651	0.073	5.222	5.74
263-SMW	2895.5	1–4	2.301	1.887	16.218	67.612	0.079	3.671	1.093	0.638	0.063	5.259	5.82
265-SMW	2905.5	1–4	2.327	1.922	16.445	67.263	0.07	3.715	0.956	0.64	0.056	5.341	5.398
267-SMW	2915.5	1–4	2.259	1.856	16.173	67.518	0.076	3.661	0.958	0.64	0.059	5.264	5.394
269-SMW	2925.5	1–4	2.313	1.875	16.471	67.296	0.074	3.684	0.859	0.642	0.055	5.331	5.665
271-SMW	2935.5	1–4	2.296	1.931	16.517	66.805	0.076	3.868	0.834	0.671	0.053	5.433	5.56
273-SMW	2945.5	1–4	2.271	1.926	16.471	66.817	0.091	3.627	0.959	0.643	0.059	5.512	5.665
277-SMW	2955.5	1–4	2.158	1.891	16.575	67.261	0.068	3.661	0.888	0.662	0.054	5.37	5.226
279-SMW	2965.5	1–4	2.229	1.947	16.684	66.936	0.071	3.737	0.82	0.663	0.056	5.564	5.374
281-SMW	2975.5	1–4	2.257	1.92	16.519	67.212	0.074	3.706	1.037	0.662	0.063	5.437	5.801
283-SMW	2985.5	1–4	2.312	1.888	16.266	67.169	0.066	3.708	1.253	0.634	0.069	5.343	5.535
285-SMW	2995.5	1–4	2.286	1.926	16.422	66.927	0.065	3.68	1.155	0.665	0.066	5.467	5.7
289-SMW	3005.5	1–4	2.291	1.862	16.474	66.788	0.067	3.823	0.956	0.667	0.057	5.512	5.67
291-SMW	3015.5	1–4	2.334	1.74	16.004	67.783	0.071	3.632	1.312	0.643	0.066	5.078	5.697
293-SMW	3025.5	1–4	2.348	1.972	16.509	67.02	0.072	3.856	1.038	0.633	0.059	5.422	5.918
296-SMW	3035.5	1–4	2.278	2.008	16.801	66.135	0.075	3.823	0.844	0.67	0.055	5.547	5.84
298-SMW	3045.5	1–4	2.265	2.065	17.133	66.232	0.068	3.948	0.8	0.679	0.05	5.691	5.998

Table T10 (continued). (Continued on next page.)

Cuttings sample	Bottom depth (mbsf)	Bulk fraction size (mm)	Na_2O (wt%)	MgO (wt%)	Al_2O_3 (wt%)	SiO_2 (wt%)	P_2O_5 (wt%)	K_2O (wt%)	CaO (wt%)	TiO_2 (wt%)	MnO (wt%)	Fe_2O_3 (wt%)	Loss on ignition (wt%)
300-SMW	3058.5	1–4	2.272	2.016	17.081	66.984	0.067	3.859	1.092	0.666	0.061	5.664	6.179
9-SMW	1965.5	>4	1.963	1.743	12.497	52.939	0.108	2.512	19.909	0.381	0.074	5.265	8.542
14-SMW	1975.5	>4	2.229	2.028	15.547	62.774	0.079	3.848	5.202	0.595	0.055	5.431	5.997
16-SMW	1985.5	>4	2.151	1.993	15.621	63.476	0.08	3.736	5.17	0.608	0.057	5.456	5.809
18-SMW	1995.5	>4	1.716	1.576	11.346	49.212	0.142	2.283	25.776	0.408	0.066	5.288	9.362
20-SMW	2005.5	>4	2.17	1.921	14.904	61.973	0.113	3.675	7.811	0.578	0.079	5.297	7.756
25-SMW	2015.5	>4	2.332	2.008	15.64	65.201	0.092	3.833	3.392	0.577	0.079	5.317	7.006
28-SMW	2025.5	>4	2.413	1.976	15.699	65.299	0.078	3.87	3.181	0.598	0.056	5.314	6.505
30-SMW	2035.5	>4	2.47	2.095	15.96	66.03	0.068	3.887	1.446	0.62	0.04	5.423	5.971
34-SMW	2055.5	>4	2.389	1.968	15.842	66.046	0.063	3.943	1.116	0.641	0.043	5.278	5.148
36-SMW	2065.5	>4	2.265	1.894	15.52	65.932	0.068	3.862	2.301	0.62	0.058	5.061	5.502
43-SMW	2075.5	>4	2.147	1.983	16.3	66.259	0.075	3.944	1.264	0.674	0.043	5.421	5.015
45-SMW	2085.5	>4	2.259	1.958	16.191	66.772	0.069	3.912	1.089	0.635	0.041	5.272	4.963
47-SMW	2095.5	>4	2.224	1.791	15.202	65.239	0.071	3.608	4.467	0.561	0.082	4.895	6.481
49-SMW	2105.5	>4	2.25	1.833	15.164	63.183	0.075	3.757	5.357	0.516	0.054	5.141	5.782
53-SMW	2115.5	>4	2.322	1.841	15.286	64.841	0.093	3.82	4.747	0.56	0.078	4.944	7.803
56-SMW	2125.5	>4	2.314	2.003	16.205	66.501	0.068	4.017	1.15	0.614	0.041	5.352	5.077
58-SMW	2135.5	>4	2.342	1.929	16.092	67.243	0.072	3.917	1.408	0.623	0.043	5.198	5.196
61-SMW	2145.5	>4	2.181	1.765	15.123	65.075	0.078	3.668	4.012	0.586	0.062	4.992	5.641
63-SMW	2155.5	>4	2.353	1.817	15.673	66.893	0.094	3.949	1.766	0.602	0.051	5.093	5.899
71-SMW	2165.5	>4	2.003	1.869	15.908	67.055	0.071	4.028	2.108	0.625	0.055	5.221	5.6
73-SMW	2175.5	>4	2.127	1.851	16.203	67.203	0.064	4.066	1.526	0.645	0.048	5.242	5.437
76-SMW	2185.5	>4	2.139	1.699	15.368	68.975	0.067	4.002	1.347	0.635	0.044	4.851	4.833
81-SMW	2195.5	>4	2.084	1.78	15.784	68.365	0.064	4.039	1.254	0.632	0.044	4.904	4.988
83-SMW	2205.5	>4	2.264	1.703	15.297	69.123	0.081	3.903	1.583	0.571	0.05	4.739	5.064
86-SMW	2215.5	>4	2.196	1.858	15.963	67.379	0.077	4.085	1.336	0.626	0.048	5.207	5.873
107-SMW	2225.5	>4	2.097	1.854	16.078	67.484	0.068	3.951	1.456	0.659	0.052	5.073	4.926
109-SMW	2235.5	>4	2.116	1.922	15.822	66.228	0.073	3.953	2.011	0.611	0.053	5.223	5.148
111-SMW	2245.5	>4	2.206	1.821	16.257	67.155	0.075	4.035	1.212	0.646	0.044	5.25	5.238
113-SMW	2255.5	>4	2.067	1.924	16.404	67.146	0.065	4.022	1.187	0.637	0.046	5.445	5.231
115-SMW	2265.5	>4	2.201	1.797	15.735	67.634	0.062	4.009	1.327	0.621	0.045	5.001	5.064
117-SMW	2275.5	>4	2.054	1.983	16.4	66.723	0.064	4.183	0.97	0.663	0.043	5.524	4.9
121-SMW	2285.5	>4	2.336	1.926	16.251	66.49	0.077	4.125	1.411	0.628	0.044	5.354	5.7
123-SMW	2295.5	>4	2.306	1.919	16.16	66.326	0.084	4.085	1.407	0.626	0.043	5.311	5.925
125-SMW	2305.5	>4	2.232	1.788	15.855	68.854	0.071	3.98	1.123	0.626	0.041	5.028	5.161
127-SMW	2315.5	>4	2.225	1.855	16.194	67.758	0.066	4.029	1.046	0.628	0.042	5.273	5.47
129-SMW	2325.5	>4	2.11	1.954	15.986	67.75	0.065	4.108	1.001	0.632	0.043	4.994	5.187
131-SMW	2335.5	>4	2.212	1.826	15.881	67.455	0.066	4.151	1.465	0.626	0.05	4.999	5.639
133-SMW	2345.5	>4	2.196	1.866	16.147	66.806	0.11	3.963	1.464	0.632	0.045	5.273	5.791
136-SMW	2355.5	>4	2.234	1.821	16.032	67.432	0.07	4.015	1.194	0.626	0.045	5.205	5.409
138-SMW	2365.5	>4	2.303	1.829	16.02	67.163	0.068	4.025	1.06	0.637	0.043	5.161	5.413
141-SMW	2375.5	>4	2.329	1.829	15.808	67.709	0.071	4	1.29	0.631	0.044	5.016	5.895
143-SMW	2385.5	>4	2.276	1.837	16.263	66.983	0.056	4.017	1.132	0.625	0.045	5.217	5.778
145-SMW	2395.5	>4	2.224	1.765	15.82	67.895	0.062	3.949	1.167	0.61	0.046	5.018	5.321
149-SMW	2405.5	>4	2.188	1.748	15.816	67.968	0.066	3.906	1.157	0.618	0.043	5.055	5.701
151-SMW	2415.5	>4	2.314	1.581	14.702	69.581	0.061	3.854	1.215	0.547	0.04	4.453	5.1
155-SMW	2425.5	>4	2.205	1.81	15.812	67.172	0.066	3.958	1.307	0.606	0.04	5.122	5.671
157-SMW	2435.5	>4	2.357	1.719	15.486	68.185	0.064	3.91	1.344	0.602	0.043	4.857	5.78
159-SMW	2445.5	>4	2.321	1.541	14.984	69.329	0.061	3.824	1.236	0.792	0.037	5.337	4.61
161-SMW	2455.5	>4	2.323	1.575	14.82	69.744	0.063	3.843	1.314	0.578	0.041	4.444	4.964
163-SMW	2465.5	>4	2.297	1.771	15.689	67.047	0.068	3.933	1.093	0.84	0.038	5.915	5.296
165-SMW	2475.5	>4	2.262	1.857	15.95	67.044	0.075	3.897	1.298	0.64	0.046	5.175	5.601
168-SMW	2485.5	>4	2.235	1.788	15.818	67.253	0.066	3.911	0.91	0.854	0.042	6.007	5.147
170-SMW	2495.5	>4	2.338	1.846	15.956	67.548	0.067	3.887	1.604	0.633	0.051	5.151	5.602
172-SMW	2505.5	>4	2.264	1.754	15.699	67.237	0.065	3.811	0.919	0.873	0.044	5.854	4.876
174-SMW	2515.5	>4	2.38	1.811	15.89	67.611	0.071	3.909	1.231	0.625	0.047	5.07	5.383
176-SMW	2525.5	>4	2.274	1.83	15.957	68.019	0.065	3.955	0.743	0.662	0.035	5.175	4.805
179-SMW	2535.5	>4	2.408	1.745	15.269	69.193	0.066	3.837	1.016	0.577	0.042	4.781	4.737
181-SMW	2545.5	>4	2.461	1.825	15.562	68.113	0.073	3.875	1.056	0.612	0.041	4.923	5.219
183-SMW	2555.5	>4	2.515	1.89	15.633	68.389	0.066	3.926	0.883	0.638	0.04	4.971	4.838
185-SMW	2565.5	>4	2.399	1.823	15.717	67.903	0.073	3.991	1.02	0.587	0.045	5.013	5.334
187-SMW	2575.5	>4	2.155	1.959	16.089	67.427	0.072	3.942	0.87	0.656	0.041	5.289	4.897
189-SMW	2585.5	>4	2.189	1.879	15.826	66.682	0.074	3.822	2.283	0.619	0.07	5.165	6.021
191-SMW	2595.5	>4	2.263	2.012	15.986	66.801	0.072	4.006	1.558	0.63	0.048	5.321	5.678
196-SMW	2605.5	>4	2.06	1.985	16.335	66.427	0.079	3.938	1.632	0.663	0.052	5.515	5.223
198-SMW	2615.5	>4	2.012	1.835	15.697	67.879	0.079	3.805	1.626	0.654	0.052	5.098	4.943
200-SMW	2625.5	>4	2.155	1.799	15.407	65.473	0.082	3.855	3.502	0.599	0.077	5.045	6.011
202-SMW	2635.5	>4	2.121	1.976	15.903	65.633	0.076	3.944	2.79	0.636	0.063	5.269	6.309

Table T10 (continued).

Cuttings sample	Bottom depth (mbsf)	Bulk fraction size (mm)	Na_2O (wt%)	MgO (wt%)	Al_2O_3 (wt%)	SiO_2 (wt%)	P_2O_5 (wt%)	K_2O (wt%)	CaO (wt%)	TiO_2 (wt%)	MnO (wt%)	Fe_2O_3 (wt%)	Loss on ignition (wt%)
204-SMW	2645.5	>4	2.055	1.967	16.334	65.672	0.08	4.063	1.86	0.656	0.053	5.393	5.763
208-SMW	2655.5	>4	2.076	2.053	16.435	65.887	0.085	4.159	1.785	0.663	0.053	5.537	5.64
210-SMW	2665.5	>4	2.068	2.037	16.611	65.49	0.081	3.969	2.339	0.633	0.071	5.582	5.968
213-SMW	2675.5	>4	2.222	2.061	16.351	65.58	0.089	4.006	2.098	0.635	0.065	5.526	5.993
215-SMW	2685.5	>4	2.227	1.942	16.093	65.978	0.072	3.979	1.862	0.62	0.067	5.509	5.919
217-SMW	2695.5	>4	2.296	1.995	16.595	66.551	0.075	3.951	1.16	0.66	0.05	5.595	5.325
219-SMW	2705.5	>4	2.248	1.912	16.21	67.085	0.077	3.93	1.403	0.632	0.054	5.327	5.458
221-SMW	2715.5	>4	2.095	1.847	16.31	67.77	0.069	3.916	1.139	0.643	0.052	5.386	4.987
224-SMW	2725.5	>4	2.235	1.806	16.235	67.033	0.081	3.867	1.302	0.63	0.059	5.285	5.495
226-SMW	2735.5	>4	2.374	1.763	16.252	67.72	0.065	3.867	0.683	0.652	0.041	5.258	5.073
229-SMW	2745.5	>4	2.345	1.689	15.77	68.17	0.065	3.731	0.833	0.627	0.039	5.08	5.184
231-SMW	2755.5	>4	2.307	1.72	15.922	67.55	0.067	3.825	0.976	0.626	0.049	5.184	5.257
233-SMW	2765.5	>4	2.267	1.735	15.863	67.66	0.062	3.822	0.85	0.618	0.042	5.096	5.409
235-SMW	2775.5	>4	2.344	1.775	16.103	67.345	0.076	3.95	1.066	0.638	0.053	5.188	5.474
237-SMW	2785.5	>4	2.353	1.807	16.442	66.477	0.085	4.091	1.278	0.658	0.05	5.498	6.113
240-SMW	2795.5	>4	2.308	1.786	16.171	67.527	0.067	3.933	0.947	0.627	0.053	5.298	5.434
242-SMW	2805.5	>4	2.281	1.736	16.236	66.606	0.089	3.942	2.041	0.619	0.087	5.508	6.063
244-SMW	2815.5	>4	2.287	1.827	16.444	67.117	0.067	3.968	0.932	0.645	0.05	5.426	5.798
247-SMW	2825.5	>4	2.377	1.72	15.88	67.987	0.059	3.966	0.606	0.623	0.041	5.079	5.127
249-SMW	2835.5	>4	2.336	1.854	16.417	67.12	0.066	4.068	0.482	0.637	0.036	5.26	5.34
251-SMW	2845.5	>4	2.417	1.76	16.276	67.038	0.063	4.119	0.363	0.645	0.039	5.272	5.227
254-SMW	2855.5	>4	2.28	1.77	16.203	67.404	0.06	4.027	0.482	0.645	0.037	5.244	5.293
256-SMW	2865.5	>4	2.416	1.792	16.294	67.419	0.07	4.01	0.469	0.636	0.041	5.339	5.103
259-SMW	2875.5	>4	2.342	1.792	16.098	67.168	0.064	3.964	0.727	0.623	0.055	5.374	5.244
261-SMW	2885.5	>4	2.115	1.807	15.945	64.834	0.088	3.92	3.655	0.634	0.142	5.246	6.748
263-SMW	2895.5	>4	2.267	1.838	16.503	67.29	0.07	4.027	0.63	0.635	0.043	5.428	5.26
265-SMW	2905.5	>4	2.303	1.837	16.262	66.683	0.073	3.984	0.922	0.64	0.047	5.495	5.589
267-SMW	2915.5	>4	2.223	1.865	16.2	67.013	0.063	3.968	0.798	0.648	0.045	5.206	5.158
269-SMW	2925.5	>4	2.284	1.823	16.41	67.414	0.073	3.902	0.896	0.634	0.052	5.324	5.374
271-SMW	2935.5	>4	2.249	1.835	16.062	67.48	0.069	3.877	0.425	0.644	0.032	5.342	4.746
273-SMW	2945.5	>4	2.127	1.937	16.625	67.028	0.066	3.992	0.612	0.667	0.043	5.493	4.918
277-SMW	2955.5	>4	2.291	1.82	16.461	66.062	0.072	3.841	1.793	0.637	0.07	5.413	5.593
279-SMW	2965.5	>4	2.287	1.823	16.405	67.058	0.065	3.912	0.669	0.626	0.048	5.459	5.347
281-SMW	2975.5	>4	2.232	1.865	16.771	67.086	0.066	4.025	0.562	0.667	0.041	5.475	5.196
283-SMW	2985.5	>4	2.19	1.759	16.251	68.26	0.063	3.952	0.543	0.641	0.04	5.189	4.758
285-SMW	2995.5	>4	2.296	1.859	16.239	67.205	0.061	3.842	0.681	0.661	0.049	5.298	5.092
289-SMW	3005.5	>4	2.179	1.954	16.839	66.367	0.067	4.138	0.594	0.662	0.038	5.565	5.313
291-SMW	3015.5	>4	2.282	1.937	16.685	67.098	0.068	4.086	0.496	0.665	0.043	5.572	5.347
293-SMW	3025.5	>4	2.287	1.901	16.592	66.644	0.071	4.138	0.815	0.645	0.049	5.52	5.447
296-SMW	3035.5	>4	2.171	1.912	16.744	66.263	0.075	4.032	0.726	0.667	0.046	5.592	5.531
298-SMW	3045.5	>4	2.199	1.954	16.919	66.379	0.068	4.119	0.862	0.678	0.05	5.666	5.906
300-SMW	3058.5	>4	2.106	1.902	16.975	66.396	0.068	4.16	0.647	0.66	0.047	5.636	5.378

Table T11. X-ray diffraction analysis on random bulk powder from core samples, Hole C0002P.

Core, section, interval (cm)	Sample	Depth (mbsf)	Integrated peak area (total counts)				Absolute mineral abundance calculated from SVD normalization factors (wt%)					Relative abundance (wt%)			
			Total clay	Quartz	Feldspar	Calcite	Total clay	Quartz	Feldspar	Calcite	Sum	Total clay	Quartz	Feldspar	Calcite
348-C0002P-															
1R-1, 2.5–5	CKY-6204600	2163.05	4743	44322	13666	3982	58.5	24.1	12.8	0.1	95.6	61.2	25.2	13.4	0.1
2R-1, 35–38	CKY-6205900	2172.88	4417	40696	13291	1777	54.7	22.1	12.6	0.1	89.5	61.1	24.7	14.1	0.1
2R-2, 43–48	CKY-6206800	2174.395	3184	52193	18640	823	43.5	28.7	18.7	0.1	91.1	47.8	31.5	20.5	0.1
2R-3, 137.5–141	CKY-6194700	2176.73	4532	44644	14523	1954	56.5	24.3	13.9	0.1	94.8	59.6	25.6	14.6	0.1
2R-4, 28–31	CKY-6207600	2177.04	2241	59083	21705	726	34.6	32.8	22.3	0.1	89.7	38.5	36.5	24.8	0.1
3R-1, 35–37	CKY-6212900	2182.37	3009	49646	19907	2336	42.4	27.2	20.2	0.1	89.9	47.1	30.2	22.5	0.1
3R-2, 60–63	CKY-6216200	2184.035	3961	44301	16032	2835	51.0	24.1	15.7	0.1	91.0	56.1	26.5	17.3	0.1
4R-1, 39–44	CKY-6218800	2191.94	5784	39866	13248	908	69.7	21.3	12.2	0.1	103.3	67.4	20.6	11.8	0.1
4R-2, 135–142	CKY-6220500	2194.025	3723	39627	15548	2157	48.2	21.4	15.4	0.1	85.1	56.6	25.2	18.1	0.1
4R-3, 73–77	CKY-6222000	2194.82	4221	40334	12622	728	52.2	22.0	11.9	0.1	86.2	60.5	25.5	13.9	0.1
4R-4, 32–37	CKY-6223000	2195.38	5203	38951	11739	1005	62.6	21.0	10.7	0.1	94.4	66.3	22.3	11.3	0.1
4R-5, 125–129	CKY-6223900	2197.675	4794	40313	14365	612	59.3	21.7	13.7	0.1	94.9	62.5	22.9	14.5	0.1
4R-6, 54–60	CKY-6225400	2198.49	4576	40652	17506	792	58.5	21.7	17.3	0.1	97.6	59.9	22.3	17.7	0.1
5R-1, 95–101	CKY-6227800	2202.01	3580	47683	18788	1185	48.1	26.0	18.9	0.1	93.0	51.7	27.9	20.3	0.1
5R-2, 99–104	CKY-6227100	2203.48	3949	38346	11727	625	48.7	20.9	11.1	0.1	80.8	60.3	25.9	13.7	0.1
5R-3, 0–7	CKY-6228500	2203.92	3630	41457	13712	1070	46.2	22.7	13.3	0.1	82.3	56.1	27.6	16.2	0.1
5R-5, 2–6	CKY-6246800	2205.61	7942	29175	22804	2281	98.4	13.9	22.6	0.1	135.0	72.9	10.3	16.7	0.1
6R-1, 77–83	CKY-6236100	2209.83	5852	36076	10565	1527	69.2	19.3	9.3	0.1	97.8	70.7	19.7	9.5	0.1
6R-2, 37–39	CKY-6226100	2210.8	4580	41328	14733	1061	57.1	22.3	14.2	0.1	93.8	60.9	23.8	15.1	0.1
6R-3, 37–41	CKY-6237000	2212.225	4618	44427	15282	1077	57.8	24.1	14.7	0.1	96.7	59.8	24.9	15.2	0.1
6R-4, 103–108	CKY-6237900	2214.31	3364	39853	15333	1124	44.1	21.7	15.3	0.1	81.1	54.4	26.7	18.8	0.1
6R-5, 94–101	CKY-6239200	2215.65	4377	50921	16139	1090	55.5	27.9	15.6	0.1	99.1	56.0	28.2	15.7	0.1
6R-6, 62–64	CKY-6247300	2216.695	3929	43723	15155	448	50.1	23.8	14.8	0.1	88.9	56.4	26.8	16.6	0.1
6R-6, 77–84	CKY-6241800	2216.895	5312	40675	16226	1226	66.0	21.7	15.7	0.1	103.4	63.8	21.0	15.1	0.1

SVD = singular value decomposition.

Table T12. X-ray fluorescence analysis on core samples, Hole C0002P.

Core, section, interval (cm)	Sample	Bottom depth (mbsf)	Na_2O (wt%)	MgO (wt%)	Al_2O_3 (wt%)	SiO_2 (wt%)	P_2O_5 (wt%)	K_2O (wt%)	CaO (wt%)	TiO_2 (wt%)	MnO (wt%)	Fe_2O_3 (wt%)	Loss on ignition (wt%)
348-C0002P-													
1R-1, 2.5–5	CKY-6204700	2163.05	2.122	1.955	16.905	65.389	0.09	3.443	2.467	0.686	0.04	5.301	5.917
2R-1, 35–38	CKY-6206000	2172.88	2.547	1.986	16.832	64.529	0.063	3.719	1.502	0.617	0.05	6.008	7.042
2R-2, 43–48	CKY-6206900	2174.395	2.689	1.76	15.628	67.808	0.05	3.401	0.967	0.487	0.04	5.222	5.556
2R-3, 137.5–141	CKY-6194800	2176.73	2.273	2.106	17.181	65.66	0.076	3.384	1.454	0.687	0.051	5.907	5.605
2R-4, 27–31	CKY-6207800	2177.04	2.802	1.042	12.709	73.855	0.038	3.522	1.439	0.243	0.026	3.203	4.038
3R-1, 35–37	CKY-6213000	2182.37	2.373	1.679	15.676	67.798	0.062	3.45	1.395	0.571	0.04	4.904	5.526
3R-2, 60–63	CKY-6216300	2184.035	2.234	2.089	17.533	69.28	0.115	3.398	1.828	0.675	0.055	5.99	5.399
4R-1, 39–44	CKY-6218900	2191.94	2.231	1.983	17.463	65.735	0.063	3.239	1.131	0.72	0.051	6.044	5.798
4R-2, 135–142	CKY-6220600	2194.025	2.239	2.006	16.836	65.025	0.081	3.496	1.688	0.631	0.054	5.899	6.264
4R-3, 73–77	CKY-6222100	2194.82	2.21	2.177	17.955	64.847	0.07	3.629	0.774	0.714	0.051	6.049	5.746
4R-4, 32–37	CKY-6223100	2195.38	2.409	2.024	17.026	64.943	0.063	3.527	0.973	0.636	0.051	5.86	5.775
4R-5, 125–129	CKY-6224000	2197.675	2.22	2.071	17.393	65.712	0.067	3.512	0.863	0.628	0.045	5.921	5.712
4R-6, 54–60	CKY-6225500	2198.49	2.113	2.092	17.837	66.098	0.073	3.381	0.739	0.735	0.044	5.767	5.047
5R-1, 95–101	CKY-6227900	2202.01	2.507	1.717	15.654	66.934	0.07	3.951	0.865	0.511	0.039	4.981	5.647
5R-2, 99–104	CKY-6227200	2203.48	2.39	2.096	17.317	63.988	0.068	3.649	0.823	0.598	0.044	5.915	6.541
5R-3, 0–7	CKY-6228600	2203.92	2.228	2.147	17.142	65.244	0.064	3.449	0.875	0.659	0.045	5.792	5.536
5R-5, 2–6	CKY-6246900	2205.61	3.063	2.027	17.016	67.29	0.039	1.735	1.601	0.393	0.016	5.024	4.456
6R-1, 77–83	CKY-6236200	2209.83	2.396	2.26	17.169	64.534	0.091	3.524	1.4	0.586	0.042	5.857	6.073
6R-2, 37–39	CKY-6226200	2210.8	2.482	2.057	16.72	66.176	0.086	3.906	0.875	0.636	0.034	5.597	5.551
6R-3, 37–41	CKY-6237100	2212.225	2.313	1.994	16.553	66.398	0.072	3.364	0.931	0.695	0.041	5.756	5.212
6R-4, 103–108	CKY-6238000	2214.31	2.993	1.736	15.773	65.584	0.063	3.88	1.274	0.409	0.031	5.361	7.725
6R-5, 94–101	CKY-6239300	2215.65	2.211	2.013	16.718	67.129	0.076	3.283	0.832	0.697	0.039	5.337	4.554
6R-6, 62–64	CKY-6247400	2216.695	2.615	1.798	15.783	66.413	0.057	3.555	0.99	0.467	0.032	5.09	4.527
6R-6, 77–84	CKY-6241900	2216.895	2.185	2.108	17.468	65.901	0.07	3.285	1.083	0.745	0.046	5.752	5.384

Table T13. Semiquantitative abundance of calcareous nannofossil species, Hole C0002M.

Core, section, interval (cm)	Depth (mbsf)	Age (Ma)	Nannofossil zone	Preservation	Abundance	*Braarudosphaera bigelowii*	*Calcidiscus leptoporus*	*Calcidiscus macintyrei*	*Coccolithus* spp.	*Discoaster quinqueramus*	medium *Gephyrocapsa* I (<3.5–4 µm)	medium *Gephyrocapsa* II (4–5.5 µm)	large *Gephyrocapsa* (≥5.5 µm)	*Helicosphaera carteri*	*Helicosphaera hyalina*	*Helicosphaera selli*	*Pontosphaera japonica*	*Pseudoemiliania lacunosa*	*Reticulofenestra minuta*	*Sphenolithus* spp.	*Umbilicosphaera sibogae*
348-C0002M-																					
1R-1, 9	475.09	>0.44	NN20	G	A	R	F		C		C	C	F	F			F	F	A		F
1R-1, 86	475.86			G	A		F		C		C	C	F	F			F	F	A		F
1R-2, 6	476.47			G	A		F		C		F	F		R			F	F	A		F
1R-2, 16	476.57			G	F		F		C			F		F			F	F	C		F
1R-2, 117	477.58			G	F		F		C		F			F			F		C		F
1R-3, 8	477.91			G	A		F		C	R		F					F	C	C		F
1R-3, 64	478.47	>1.34	NN19	G	A	F	F		C		F			F	F	F	F	C	A		F
1R-4, 7	479.31			G	A		F		C		F			F		F	F	C	A		F
1R-CC, 6	480.12			G	A		F		C			F		F		F	F	C	A		F
2R-1, 6	484.56			G	A		F	F	C		F	F		F			F	C	C		F
2R-1, 54	485.04			G	A		F		C		F	F		F			F	C	A	R	F
2R-2, 7	485.98			G	A		F		C		F	F		F			F	C	A		F
2R-2, 41	486.32			G	A		F	F	C			F		F			F	C	A		F
2R-3, 8	487.40			G	A		F	F	C								F	C	A		F
2R-CC, 8	488.31			G	A		F		C		F	F					F	C	A		F
3R-1, 52	494.02			G	A		F		C								F	C	C		F
3R-1, 84	494.34			G	C		F		C								F	C	C		F
3R-1, 130	494.80			G	C		F		C		F	F					F		C		F
3R-1, 138	494.88			G	C		F		C					F			F		C		F
3R-2, 15	495.06			G	C		F		C		F			F			F	C	C		F
3R-2, 85	495.76			G	F		F		C		F	F				F	F	C	C		F
3R-CC, 8	495.89			G	C		F		C		F	F		F			F		C		F
3R-CC, 20	496.01			G	F		F		C		F	F					F		C		F
4R-3, 67	506.49			G	C		F		C		F	F					F		C		F
4R-3, 86	506.68	<1.67		G	C		F		C		F	F					F		C		F

Preservation: G = good. Abundance: A = abundant, C = common, F = frequent, R = rare.

Table T14. Semiquantative abundance of calcareous nannofossil species, Holes C0002N and C0002P. (Continued on next seven pages.)

Sample	Depth (mbsf)	Age (Ma)	Nannofossil zone	Preservation	Abundance	*Amaurolithus primus*	*Braarudosphaera bigelowii*	*Calcidiscus leptoporus*	*Coccolithus pelagicus*	*Coccolithus* spp.	*Cyclicargolithus floridanus*	*Discoaster asymmetricus*	*Discoaster bellus*	*Discoaster brouweri*	*Discoaster calcaris*	*Discoaster challengeri*	*Discoaster hamatus*	*Discoaster pentaradiatus*	*Discoaster quinqueramus*	*Discoaster* spp.	*Discoaster surculus*	*Discoaster triradiatus*	*Discoaster tristellifer*	*Discoaster variabilis*	*Helicosphaera carteri*	*Helicosphaera hyalina*	*Helicosphaera sellii*	*Pseudoemiliania lacunosa*	*Pseudoemiliania ovata*	*Reticulofenestra haqii* (3–5 µm)	*Reticulofenestra minuta*	*Reticulofenestra pseudoumbilicus* (>7 µm)	*Sphenolithus abies*	*Sphenolithus* spp.	*Umbilicosphaera rotula*
348-																																			
C0002N-3-SMW	875.50	<3.92	NN19	G	C			F																				F			A				
C0002N-5-SMW	885.50			G	C			F		F																F			F		A				
C0002N-7-SMW	895.50			G	C			F		F																F	F		F		A				
C0002N-9-SMW	905.50	≥2.06	NN19	G	C			F		F				F												F					A				
C0002N-12-SMW	915.50			G	A			F						C											F		F	F	F		A				
C0002N-14-SMW	925.50	≥2.343–2.512	NN18	G	C			F						F				F							F		F				C				
C0002N-16-SMW	935.50			G	A			F						F				F							F	F					A	RW			
C0002N-18-SMW	945.50			G	A			F																	F			F	F	F	C				
C0002N-20-SMW	955.50			G	A			F						C				F					F		F		F			F	C			R	
C0002N-22-SMW	965.50			G	C			F		F				F											F	F					A			F	
C0002N-24-SMW	975.50	≥3.6	NN17	G	A			F		C																					C		F	F	
C0002N-26-SMW	985.50			G	A			F		F				C				C			F			F						F	C			F	
C0002N-28-SMW	995.50			M	C			F		F				F																			F	F	
C0002N-30-SMW	1000.50			M	A			F		C				C	RW										F									F	
C0002N-32-SMW	1015.50			M	C			F		C				C												F				C	C			F	
C0002N-34-SMW	1025.50	≥3.79	NN16	M	C			F		C				C				F				R			F					C	A	R		F	
C0002N-36-SMW	1035.50			M	C			F		F				F										F						C	C	F		F	
C0002N-39-SMW	1045.50			M	C			F		C		R		F											F					C	A	F		F	
C0002N-40-SMW	1052.50			M	C			F	F	C		F		F											F					C	A	F		F	
C0002N-41-SMW	1067.50			M	C			F	F	C				F																C	A	F			
C0002N-42-SMW	1069.50			M	C			F		F		F		F											F					F	A	F		F	
C0002N-43-SMW	1070.50			M	C			F	F	C		F		F											F	F				F	A	F		C	
C0002N-44-SMW	1075.50			M	C			F	F	C																					C	F			
C0002N-46-SMW	1085.50	≤4.13	NN14–15	M	C			F	F	C		C		F							F									C	C	F		F	
C0002N-48-SMW	1095.50			M	C			F	F	C				F							F									C	C	F		F	
C0002N-50-SMW	1105.50			M	C			F	F	C				F																C	C	F		F	
C0002N-52-SMW	1115.50			M	C			F	F	F				F																C	C	F		F	
C0002N-54-SMW	1125.50			M	C			F	F	C		F		F																C	C	F		F	
C0002N-57-SMW	1135.50			M	C			F	F	F		F		F																C	C	F	F	F	
C0002N-59-SMW	1145.50			M	C			F		C				F																C	C	F		F	
C0002N-61-SMW	1155.50			M	C			F		C		F		C										C						C	C	F		F	
C0002N-63-SMW	1165.50			M	C			F		C																				C	F	F		F	
C0002N-65-SMW	1175.50			M	C			F		C		F		F										F		F				F	F	F		F	
C0002N-67-SMW	1185.50			M	C			F		C																				F	F				
C0002N-69-SMW	1195.50			M	C			F		F																				F	F			F	
C0002N-71-SMW	1205.50			M	C			F		C																					A		F		
C0002N-73-SMW	1215.50			M	C			F		C																				F	F			F	
C0002N-81-SMW	1225.50			M	F			F		C																				F	F			F	

Table T14 (continued). (Continued on next page.)

Sample	Depth (mbsf)	Age (Ma)	Nannofossil zone	Preservation	Abundance	*Amaurolithus primus*	*Braarudosphaera bigelowii*	*Calcidiscus leptoporus*	*Coccolithus pelagicus*	*Coccolithus* spp.	*Cyclicargolithus floridanus*	*Discoaster asymmetricus*	*Discoaster bellus*	*Discoaster brouweri*	*Discoaster calcaris*	*Discoaster challengeri*	*Discoaster hamatus*	*Discoaster pentaradiatus*	*Discoaster quinqueramus*	*Discoaster* spp.	*Discoaster surculus*	*Discoaster triradiatus*	*Discoaster tristellifer*	*Discoaster variabilis*	*Helicosphaera carteri*	*Helicosphaera hyalina*	*Helicosphaera sellii*	*Pseudoemiliania lacunosa*	*Pseudoemiliania ovata*	*Reticulofenestra haqii* (3–5 µm)	*Reticulofenestra minuta*	*Reticulofenestra pseudoumbilicus* (>7 µm)	*Sphenolithus abies*	*Sphenolithus* spp.	*Umbilicosphaera rotula*
C0002N-83-SMW	1235.50			M	C			F		C																				F	C			F	
C0002N-85-SMW	1245.50	≥4.5	NN14–15	M	C	R		F	F	C		F		F				F												F	C	R		F	
C0002N-87-SMW	1255.50			M	C			F		F		F		F												F				C	C	R	F	F	
C0002N-89-SMW	1265.50				B																														
C0002N-91-SMW	1275.50			M	F			F		F																					F				
C0002N-93-SMW	1285.50			M	B																														
C0002N-95-SMW	1295.50			M	B																														
C0002N-97-SMW	1305.50			M	B																														
C0002N-99-SMW	1315.50			M	B																														
C0002N-101-SMW	1325.50			M	B																														
C0002N-105-SMW	1335.50			M	F			F		F																				C	C	F			
C0002N-107-SMW	1345.50			M	F			F		C		F		F																F	C	F			
C0002N-109-SMW	1355.50			M	F			F		C		F		F																F	C	R			
C0002N-111-SMW	1365.50			M	F			F		C		F																		F	C	R			F
C0002N-113-SMW	1375.50			M	F			F		C																				F	F	R			
C0002N-115-SMW	1385.50			M	F	R		F		C																				F	F	R		F	
C0002N-117-SMW	1395.50			M	F			F		C																				F	C			F	
C0002N-119-SMW	1405.50			P	F			F		C																				F	F	R			
C0002N-121-SMW	1415.50			M	F			F		C																F				F	F	R		F	
C0002N-123-SMW	1425.50			P	F			F		C																				F	F				
C0002N-125-SMW	1435.50	≥5.59	NN12	P	C	R		F	F	C	RW	F	F	F					F						F					F	C	F		F	F
C0002N-128-SMW	1445.50			P	F			F		F		F		F											F					F	C				
C0002N-130-SMW	1455.50			P	F			F		C		F		F					F											F	C				
C0002N-132-SMW	1465.50			P	R			F		C																				F	C				
C0002N-134-SMW	1475.50			P	F			F		C																					F	F		F	
C0002N-136-SMW	1485.50			P	F			F																							R				
C0002N-138-SMW	1495.50			M	F			F		F																					F	F			
C0002N-140-SMW	1505.50			M	C	R		F		C	RW	F		F					F												F				
C0002N-142-SMW	1515.50			P	F			F		C																				F	F	R		R	
C0002N-146-SMW	1525.50			P	F			F		C																					F				
C0002N-148-SMW	1535.50			P	F			F	F	C		F		F					F												F				F
C0002N-150-SMW	1545.50			M	C			F	F	F		F		F																F	C	F		F	
C0002N-152-SMW	1555.50			M	C			F		F		F		F													R				C	R		F	
C0002N-154-SMW	1565.50			M	F			F		C																				F	F	F		F	F
C0002N-156-SMW	1575.50			P	R			F		C																									
C0002N-158-SMW	1585.50			P	F			F		C																				F	C			F	
C0002N-160-SMW	1595.50			P	F			F						F																F	C	F			
C0002N-162-SMW	1605.50			P	F			F																						F	F				
C0002N-164-SMW	1615.50			P	F			F				F		F	F															F	F				

Table T14 (continued). (Continued on next page.)

Sample	Depth (mbsf)	Age (Ma)	Nannofossil zone	Preservation	Abundance	*Amaurolithus primus*	*Braarudosphaera bigelowii*	*Calcidiscus leptoporus*	*Coccolithus pelagicus*	*Coccolithus* spp.	*Cyclicargolithus floridanus*	*Discoaster asymmetricus*	*Discoaster bellus*	*Discoaster brouweri*	*Discoaster calcaris*	*Discoaster challengeri*	*Discoaster hamatus*	*Discoaster pentaradiatus*	*Discoaster quinqueramus*	*Discoaster* spp.	*Discoaster surculus*	*Discoaster triradiatus*	*Discoaster tristellifer*	*Discoaster variabilis*	*Helicosphaera carteri*	*Helicosphaera hyalina*	*Helicosphaera sellii*	*Pseudoemiliania lacunosa*	*Pseudoemiliania ovata*	*Reticulofenestra haqii* (3–5 µm)	*Reticulofenestra minuta*	*Reticulofenestra pseudoumbilicus* (>7 µm)	*Sphenolithus abies*	*Sphenolithus* spp.	*Umbilicosphaera rotula*
C0002N-166-SMW	1625.50	≤7.362–7.424	NN11b	P	F			F																						F	C	F		R	
C0002N-169-SMW	1635.50			M	F			F		F		F		F																F	C	F			
C0002N-171-SMW	1645.50			M	R			F																						R	F	R		R	
C0002N-173-SMW	1655.50				B																														
C0002N-175-SMW	1665.50			P	F	R		F		F	RW	F		F																F	C	F		R	
C0002P-9-SMW	1665.50				B																														
C0002N-177-SMW	1675.50			M	F			F				F		F																F	F	F			
C0002N-182-SMW	1685.50			M	F			F							F															C	C				
C0002N-184-SMW	1695.50			M	F			F																						C	C				
C0002N-186-SMW	1705.50			M	F			F			RW			F																C	C				
C0002N-188-SMW	1715.50			M	F			F		C	RW																			C	C				
C0002N-190-SMW	1725.50			M	F			F		C			F																	C	C	F		F	
C0002N-192-SMW	1735.50			M	F	R		F						F										F						C	C				
C0002N-195-SMW	1745.50			M	F			F		F																				C	C			F	
C0002N-197-SMW	1755.50			M	F			F		C																				C	C	F			
C0002N-199-SMW	1765.50			M	F			F																						C	C			F	
C0002N-201-SMW	1775.50			M	F			F																						C	C	F			
C0002N-203-SMW	1785.50			M	F			F						F																C	C			F	
C0002N-205-SMW	1795.50			M	F			F																						C	C	C			
C0002N-207-SMW	1800.50			M	F			F			RW																			C	C	C			
C0002N-209-SMW	1810.50			M	F			F																	F					C	C				
C0002N-211-SMW	1820.50			M	F			F																						C	C	C			
C0002N-213-SMW	1830.50			M	F			F			RW								R											C	C	C			
C0002N-216-SMW	1840.50			M	F			F																						C	C	C			
C0002N-218-SMW	1850.50			M	F			F																						C	C	C			
C0002N-220-SMW	1860.50			M	F			F																						C	C				
C0002N-222-SMW	1870.50			M	F			F																						C	C				
C0002N-224-SMW	1880.50			M	F			F			RW			F																C	C				
C0002N-226-SMW	1890.50			M	F			F		C	RW																			C	C	C			
C0002N-228-SMW	1905.50			M	F			F		F																				C	C	C		F	
C0002N-230-SMW	1915.50			M	F			F																						C	C	C		F	
C0002N-232-SMW	1925.50			M	F			F		C																				C	C	C		F	
C0002N-234-SMW	1935.50			G	C			F		C																				C	C	C			
C0002N-237-SMW	1945.50			M	C			F		F															F					C	C	C		F	
C0002N-239-SMW	1955.50			M	F			F						F																C	C	C			
C0002N-241-SMW	1965.50			M	F			F		C																				C	C	C		F	
C0002P-9-SMW	1965.50				B																														
C0002N-243-SMW	1975.50			M	F			F																						C	C	C		F	
C0002P-14-SMW	1975.50			P	R																										R	R			

Table T14 (continued). (Continued on next page.)

Sample	Depth (mbsf)	Age (Ma)	Nannofossil zone	Preservation	Abundance	*Amaurolithus primus*	*Braarudosphaera bigelowii*	*Calcidiscus leptoporus*	*Coccolithus pelagicus*	*Coccolithus* spp.	*Cyclicargolithus floridanus*	*Discoaster asymmetricus*	*Discoaster bellus*	*Discoaster brouweri*	*Discoaster calcaris*	*Discoaster challengeri*	*Discoaster hamatus*	*Discoaster pentaradiatus*	*Discoaster quinqueramus*	*Discoaster* spp.	*Discoaster surculus*	*Discoaster triradiatus*	*Discoaster tristellifer*	*Discoaster variabilis*	*Helicosphaera carteri*	*Helicosphaera hyalina*	*Helicosphaera sellii*	*Pseudoemiliania lacunosa*	*Pseudoemiliania ovata*	*Reticulofenestra haqii* (3–5 µm)	*Reticulofenestra minuta*	*Reticulofenestra pseudoumbilicus* (>7 µm)	*Sphenolithus abies*	*Sphenolithus* spp.	*Umbilicosphaera rotula*
C0002N-248-SMW	1985.50			G	F			F	F	C		F							F											C	C	C		F	
C0002P-16-SMW	1985.50			P	R																				R					F	F				
C0002N-250-SMW	1995.50			M	F			F						F																C	C	C			
C0002P-18-SMW	1995.50			M	R									R																R	F				
C0002N-252-SMW	2000.50			M	F			F																						C	C	C		F	
C0002P-20-SMW	2000.50			M	R																									R	F				
C0002N-259-SMW	2015.50			G	C			F	F	F	RW	F	F	F					F											C	C	C			
C0002P-25-SMW	2015.50			P	R																									R	C				
C0002N-261-SMW	2025.50			G	C			F		C		F		F					F											C	C	C		F	
C0002P-28-SMW	2025.50			M	R																										R				
C0002N-264-SMW	2035.50			G	F			F		C				F					F											C	C	C			
C0002P-30-SMW	2035.50			M	R																										R				
C0002N-266-SMW	2045.50			G	F			F																						C	C	C			
C0002P-32-SMW	2045.50			M	R																									R					
C0002N-268-SMW	2055.50			G	F			F																						C	C				
C0002P-34-SMW	2055.50			M	R																										R				
C0002N-270-SMW	2065.50			M	R			F																							C				
C0002P-36-SMW	2065.50			M	R																									R	R				
C0002N-272-SMW	2075.50			M	R			F																							C				
C0002P-43-SMW	2075.50				B																														
C0002N-274-SMW	2085.50			M	F			F		C																				C	C	C			
C0002P-45-SMW	2085.50				B																														
C0002N-276-SMW	2095.50			G	F			F		C									F												C			F	
C0002P-47-SMW	2095.50			M	R																									F	F				
C0002N-278-SMW	2105.50			G	C			F		C																				C	C				
C0002P-49-SMW	2105.50			M	R																									F	F				
C0002N-281-SMW	2115.50			G	R			F		F																					C				
C0002P-53-SMW	2115.50			P	R																										R				
C0002N-283-SMW	2125.50			P	R			F		C																					C				
C0002P-56-SMW	2125.50			P	R			F																											
C0002N-285-SMW	2135.50			G	F			F		C									F												C	C			
C0002P-58-SMW	2135.50			P	R																									R	R				
C0002N-287-SMW	2145.50	≤9.35	NN9	G	C			F		C				F			F														C	C			F
C0002P-61-SMW	2145.50				B																														
C0002N-289-SMW	2155.50			P	R			F		C																					C	C			
C0002P-63-SMW	2155.50			M	F					R															R					F	F				
C0002P-1R-CC, 20	2163.36			M	F																										F				
C0002P-1R-CC, 23	2163.39			M	F															R										F	F			R	
C0002P-71-SMW	2165.50			M	C					F	RW															F				C	C				

Table T14 (continued). (Continued on next page.)

Sample	Depth (mbsf)	Age (Ma)	Nannofossil zone	Preservation	Abundance	*Amaurolithus primus*	*Braarudosphaera bigelowii*	*Calcidiscus leptoporus*	*Coccolithus pelagicus*	*Coccolithus* spp.	*Cyclicargolithus floridanus*	*Discoaster asymmetricus*	*Discoaster bellus*	*Discoaster brouweri*	*Discoaster calcaris*	*Discoaster challengeri*	*Discoaster hamatus*	*Discoaster pentaradiatus*	*Discoaster quinqueramus*	*Discoaster* spp.	*Discoaster surculus*	*Discoaster triradiatus*	*Discoaster tristellifer*	*Discoaster variabilis*	*Helicosphaera carteri*	*Helicosphaera hyalina*	*Helicosphaera sellii*	*Pseudoemiliania lacunosa*	*Pseudoemiliania ovata*	*Reticulofenestra haqii* (3–5 µm)	*Reticulofenestra minuta*	*Reticulofenestra pseudoumbilicus* (>7 µm)	*Sphenolithus abies*	*Sphenolithus* spp.	*Umbilicosphaera rotula*
C0002N-291-SMW	2165.50			M	F			F						F					F											C	C				F
C0002P-72-SMW	2170.50			M	F					F										F										F	F			F	
C0002P-2R-1, 135	2173.85			M	F																										F				
C0002P-2R-3, 40	2175.72			M	F															F										F	C			F	
C0002N-296-SMW	2175.50			M	R			F																						C	C				
C0002P-73-SMW	2175.50				B																														
C0002P-2R-4, 15	2176.88			M	F					F										R										F	F				
C0002P-2R-4, CC, 25	2178.47			G	C					F										R										F	F				
C0002P-74-SMW	2180.50			M	F					F										F					F	F					F			F	
C0002N-298-SMW	2185.50			M	R			F		C																					C	C			
C0002P-76-SMW	2185.50			M	F											F				F						F				F	C				
C0002P-3R-1, 42	2182.42			M	F					F	RW									F										F	C				
C0002P-3R-1, 91	2182.91			M	F															R											F				
C0002P-3R-2, 120	2184.61			—	B																														
C0002P-3R-2, 120	2184.61			M	F															F						F					C			F	
C0002P-3R-2, 120	2184.61			M	F						RW																				C				
C0002P-3R-CC, 25	2184.90			M	R																									R	R				
C0002P-77-SMW	2190.50			M	R																									R	F			F	
C0002P-4R-1, 20	2191.70			M	C					F	RW									F						F				F	C			F	
C0002P-4R-1, 81	2192.31			M	F					F																					F				
C0002P-4R-2, 8	2192.69			M	F					F	RW																			R	F			R	
C0002N-300-SMW	2195.50			P	R			F																							C	C			
C0002P-81-SMW	2195.50			M	R					R																F				F	F				
C0002P-4R-4, 96	2195.97			M	F																									R	F				
C0002P-4R-6, 87	2198.76			P	F																									F	F				
C0002P-82-SMW	2200.50			M	F																									F	F			C	
C0002P-5R-2, 127	2203.71			—	B																														
C0002P-5R-4, 65	2205.29			P	F															F										F	F				
C0002N-302-SMW	2205.50			M	R			F		F																				C	C				
C0002P-83-SMW	2205.50			M	F					F										R										F	F			R	
C0002P-6R-1, 12	2209.12			M	F															F										R	C				
C0002P-6R-1, 39	2209.39			M	R																									R	F				
C0002P-6R-1, 93	2209.93			M	F					F																F					C				
C0002P-85-SMW	2210.50			—	B																														
C0002P-6R-4, 76	2213.99			M	F																									R	F				
C0002N-304-SMW	2215.50			G	F			F		F																				C	C				
C0002P-86-SMW	2215.50			M	R																					R				R	R				
C0002P-6R-6 64	2216.70			M	R																										F				
C0002P-6R-CC, 10	2217.30			M	F																										F			F	

Table T14 (continued). (Continued on next page.)

Sample	Depth (mbsf)	Age (Ma)	Nannofossil zone	Preservation	Abundance	*Amaurolithus primus*	*Braarudosphaera bigelowii*	*Calcidiscus leptoporus*	*Coccolithus pelagicus*	*Coccolithus* spp.	*Cyclicargolithus floridanus*	*Discoaster asymmetricus*	*Discoaster bellus*	*Discoaster brouweri*	*Discoaster calcaris*	*Discoaster challengeri*	*Discoaster hamatus*	*Discoaster pentaradiatus*	*Discoaster quinqueramus*	*Discoaster* spp.	*Discoaster surculus*	*Discoaster triradiatus*	*Discoaster tristellifer*	*Discoaster variabilis*	*Helicosphaera carteri*	*Helicosphaera hyalina*	*Helicosphaera sellii*	*Pseudoemiliania lacunosa*	*Pseudoemiliania ovata*	*Reticulofenestra haqii* (3–5 µm)	*Reticulofenestra minuta*	*Reticulofenestra pseudoumbilicus* (>7 µm)	*Sphenolithus abies*	*Sphenolithus* spp.	*Umbilicosphaera rotula*
C0002N-306-SMW	2225.50			M	F			F		F																				C	C				
C0002P-107-SMW	2225.50			M	R																										F			R	
C0002N-308-SMW	2235.50			M	R			F		C																					C				
C0002P-109-SMW	2235.50			M	F					F	RW									F						F					F			C	
C0002N-310-SMW	2245.50			M	R			F																							C				
C0002P-111-SMW	2245.50	≤10.541	NN9	M	F									F			F			F											F			C	
C0002N-312-SMW	2255.50			M	F			F																						C	C				
C0002P-113-SMW	2255.50			M	F								F																		F			F	
C0002N-314-SMW	2265.50			G	F			F																						C	C			F	
C0002P-115-SMW	2265.50			M	F																					F					F			F	
C0002N-316-SMW	2275.50			G	F			F		C	RW																			C	C				
C0002P-117-SMW	2275.50			M	F									F						F											F			F	
C0002N-318-SMW	2285.50			M	F			F																						C	C			F	
C0002P-121-SMW	2285.50			M	F					F			F	F						F						F					F			F	
C0002N-321-SMW	2295.50			M	F			F		C																					C				
C0002P-123-SMW	2295.50			M	F								F	F						F											F			F	
C0002N-323-SMW	2305.50			M	F			F		F																					C				
C0002P-125-SMW	2305.50			M	F								F	F						F											F			F	
C0002N-325-SMW	2315.50			M	F			F						F																	C				
C0002P-127-SMW	2315.50			M	C					F			F	F		F				F						F					C			C	
C0002N-327-SMW	2325.50			M	F			F																						C	C				
C0002P-129-SMW	2325.50			M	F		F			F	RW			F		F				F					F	F					F			C	
C0002P-131-SMW	2335.50			M	F					F				F		F				F						F					F			C	
C0002P-133-SMW	2345.50			M	F								F	F						F						F					F			F	
C0002P-136-SMW	2355.50			M	F									F						F						F					F			F	
C0002P-138-SMW	2365.50			M	F																					F					F			C	
C0002P-141-SMW	2375.50			M	F																										F			F	
C0002P-143-SMW	2385.50			M	F		F																								F			F	
C0002P-145-SMW	2395.50			M	F																										F			F	
C0002P-149--SMW	2405.50			M	F																										F			F	
C0002P-151-SMW	2415.50			M	F																										F			F	
C0002P-155-SMW	2425.50			M	F																									F	F			F	
C0002P-157-SMW	2435.50			M	R																										F				
C0002P-159-SMW	2445.50			M	F					F																					F			F	
C0002P-161-SMW	2455.50			M	F																										F			F	
C0002P-163-SMW	2465.50			M	F					F			F	F						F					F	F					F			F	
C0002P-165-SMW	2475.50			G	F					F			F	F																	F			F	
C0002P-168-SMW	2485.50			M	F																										F			F	
C0002P-170-SMW	2495.50			—	B																														

Table T14 (continued). (Continued on next page.)

Sample	Depth (mbsf)	Age (Ma)	Nannofossil zone	Preservation	Abundance	*Amaurolithus primus*	*Braarudosphaera bigelowii*	*Calcidiscus leptoporus*	*Coccolithus pelagicus*	*Coccolithus* spp.	*Cyclicargolithus floridanus*	*Discoaster asymmetricus*	*Discoaster bellus*	*Discoaster brouweri*	*Discoaster calcaris*	*Discoaster challengeri*	*Discoaster hamatus*	*Discoaster pentaradiatus*	*Discoaster quinqueramus*	*Discoaster* spp.	*Discoaster surculus*	*Discoaster triradiatus*	*Discoaster tristellifer*	*Discoaster variabilis*	*Helicosphaera carteri*	*Helicosphaera hyalina*	*Helicosphaera sellii*	*Pseudoemiliania lacunosa*	*Pseudoemiliania ovata*	*Reticulofenestra haqii* (3–5 µm)	*Reticulofenestra minuta*	*Reticulofenestra pseudoumbilicus* (>7 µm)	*Sphenolithus abies*	*Sphenolithus* spp.	*Umbilicosphaera rotula*
C0002P-172-SMW	2505.50			M	F																										F			F	
C0002P-174-SMW	2515.50			G	C		F			F	RW		F													F					F		F	C	
C0002P-176-SMW	2525.50			G	C				F	F			F	F																	F			C	
C0002P-179-SMW	2535.50			M	F																													F	
C0002P-181-SMW	2545.50			M	F					F																					F			F	
C0002P-183-SMW	2555.50			M	F				F	F	RW																				F			F	
C0002P-185-SMW	2565.50			M	F									F																	F			F	
C0002P-187-SMW	2575.50			M	F					F																					F			F	
C0002P-189-SMW	2585.50			M	F																										F			F	
C0002P-191-SMW	2595.50			M	F																										F			F	
C0002P-196-SMW	2605.50			M	F																										F				
C0002P-198-SMW	2615.50			M	F																										F			F	
C0002P-200-SMW	2625.50			M	F					F																F					F			C	
C0002P-202-SMW	2635.50			M	F					F				F																	F			C	
C0002P-204-SMW	2645.50			M	F					F				F																				F	
C0002P-208-SMW	2655.50			M	F					F				F																	F			F	
C0002P-210-SMW	2665.50			M	R																													F	
C0002P-213-SMW	2675.50			M	F					F				F																	F			C	
C0002P-215-SMW	2685.50			M	F					F	RW			F						F											F			F	
C0002P-217-SMW	2695.50			M	F															F											F			F	
C0002P-219-SMW	2705.50			M	F					F																F					F			F	
C0002P-221-SMW	2715.50			M	F					F				F																				F	
C0002P-224-SMW	2725.50			M	R					F																								F	
C0002P-226-SMW	2735.50			M	C					F			F	F												F					C			C	
C0002P-229-SMW	2745.50			M	F																										F		F	F	
C0002P-231-SMW	2755.50			M	F			F		F	RW															F					F			F	
C0002P-233-SMW	2765.50			M	F						RW																				F			F	
C0002P-235-SMW	2775.50			M	F			F																							R			F	
C0002P-237-SMW	2785.50			M	F																													F	
C0002P-240-SMW	2795.50			M	F																													F	
C0002P-242-SMW	2805.50			M	F															F											F			F	
C0002P-244-SMW	2815.50			M	F					F																					F			F	
C0002P-249-SMW	2835.50			M	F											F																		F	
C0002P-251-SMW	2845.50			M	F					F	RW														F	F					F			F	
C0002P-254-SMW	2855.50			M	F																													F	
C0002P-256-SMW	2865.50			M	F																													F	
C0002P-259-SMW	2875.50			M	F						RW			F		F				F						F								F	
C0002P-261-SMW	2885.50			M	F					F			F			F																		F	
C0002P-263-SMW	2895.50			M	F					F	RW		F							F											F			F	

Table T14 (continued).

Sample	Depth (mbsf)	Age (Ma)	Nannofossil zone	Preservation	Abundance	*Amaurolithus primus*	*Braarudosphaera bigelowii*	*Calcidiscus leptoporus*	*Coccolithus pelagicus*	*Coccolithus* spp.	*Cyclicargolithus floridanus*	*Discoaster asymmetricus*	*Discoaster bellus*	*Discoaster brouweri*	*Discoaster calcaris*	*Discoaster challengeri*	*Discoaster hamatus*	*Discoaster pentaradiatus*	*Discoaster quinqueramus*	*Discoaster* spp.	*Discoaster surculus*	*Discoaster triradiatus*	*Discoaster tristellifer*	*Discoaster variabilis*	*Helicosphaera carteri*	*Helicosphaera hyalina*	*Helicosphaera sellii*	*Pseudoemiliania lacunosa*	*Pseudoemiliania ovata*	*Reticulofenestra haqii* (3–5 µm)	*Reticulofenestra minuta*	*Reticulofenestra pseudoumbilicus* (>7 µm)	*Sphenolithus abies*	*Sphenolithus* spp.	*Umbilicosphaera rotula*
C0002P-265-SMW	2905.50	≤10.72		M	F																													F	
C0002P-267-SMW	2915.50			M	F																										F			F	
C0002P-269-SMW	2925.50			M	R																													F	
C0002P-271-SMW	2935.50			M	F			F		F			F													F					F		F	C	
C0002P-273-SMW	2945.50			G	C					F			F	F						F											C		F	C	
C0002P-277-SMW	2955.50			M	F					F	RW																							F	
C0002P-279-SMW	2965.50			M	F				F	F																				F	F				
C0002P-281-SMW	2975.50			M	F				F																						F			F	
C0002P-283-SMW	2985.50			M	F																										F				
C0002P-285-SMW	2995.50			M	R																										F				
C0002P-289-SMW	3005.50			M	R																										F				
C0002P-291-SMW	3015.50			M	R																										F				
C0002P-293-SMW	3025.50			M	F																									F	F				
C0002P-296-SMW	3035.50			M	F					F																				F	F				
C0002P-298-SMW	3045.50			M	F					F										F										F	F				
C0002P-300-SMW	3055.50			M	F																									F	F				

Preservation: G = good, M = moderate, P = poor. Abundance: A = abundant, C = common, F = frequent, R = rare, B = barren. RW = reworked.

Table T15. Biostratigraphic events, Holes C0002N and C0002P.

Depth (mbsf)	Age (Ma)	Nannofossil event	Nannofossil zone
905.50	>2.06	LO *Discoaster brouweri*	NN19
925.50	2.393–2.512	LO *Discoaster pentaradiatus*	NN18
975.50	>3.6	LO *Sphenolithus* spp.	NN17
1025.50	>3.79	LO *Reticulofenestra pseudoumbilicus*	NN16
1085.50	>4.13	FCO *Discoaster asymmetricus*	NN14–NN15
1245.50	>4.5	LO *Amaurolithus primus*	NN14–NN15
1435.50	>5.59	LO *Discoaster quinqueramus*	NN12
1735.50	<7.362–7.424	FO *Amaurolithus primus*	NN11b
2145.50	>9.56	LO *Discoaster hamatus*	NN10a
2245.50	<10.54	FO *Discoaster hamatus*	NN9
2945.50	≤10.734–10.764	FO *Discoaster brouweri*	NN9

LO = first occurrence, FCO = first common occurrence, FO = first occurrence.

Table T16. Chlorinity from pressure experiments, Hole C0002M.

Core, section, interval (cm)	Depth (mbsf)	Water aliquot	Applied pressure steps and time (lb/min)	Applied maximum force (lb)	Applied maximum pressure (MPa)	Chlorinity (mM)
348-C0002M-						
1R-1, 87–107	475.00	A	15,000/5; 17,000/7; 20,000/10	20,000	37	399
		B	21,500/10; 23,000/10; 25,000/10	25,000	47	402
		C	30,000/10; 40,000/10; 50,000/10; 60,000/720	60,000	112	389
2R-2, 111–131	485.91	A		20,000	37	409
		B		25,000	47	412
		C		60,000	112	400
3R-1, 90–110	493.50	A		20,000	37	397
		B		25,000	47	396
		C′	30,000/10; 40,000/10; 50,000/10	50,000	94	391
		C″	60,000/720	60,000	112	371
4R-2, 113–133	504.41	A		20,000	37	419
		B		25,000	47	418
		C′		50,000	94	415
		C″		60,000	112	404

Table T17. Carbon and nitrogen data, Hole C0002M.

Core, section, interval (cm)	Depth (mbsf)	IC (wt%)	$CaCO_3$ (wt%)	TN (wt%)	TC (wt%)	TOC (wt%)	TOC/TN
348-C0002M-							
1R-1, 84–87	475.84	0.66	5.50	0.08	1.35	0.69	9.14
1R-1, 87–107	475.87	0.73	6.10	0.08	1.35	0.62	7.38
1R-2, 63–65	477.04	0.67	5.55	0.07	1.28	0.61	8.30
1R-3, 87–90	478.70	1.64	13.67	0.10	2.31	0.67	6.93
2R-2, 107–109	486.98	0.55	4.61	0.06	1.11	0.56	9.79
2R-2, 111–131	487.02	0.75	6.24	0.07	1.28	0.54	7.20
2R-3, 65–68	487.97	0.51	4.26	0.08	1.03	0.52	6.94
3R-1, 82–84	494.32	0.55	4.56	0.07	1.37	0.82	11.14
3R-1, 85–87	494.35	0.79	6.56	0.08	1.32	0.53	6.88
3R-1, 90–110	494.40	0.75	6.23	0.08	1.29	0.54	7.07
3R-2, 18–20	495.09	1.06	8.85	0.08	1.60	0.54	6.85
4R-2, 42–45	504.83	1.06	8.82	0.08	1.57	0.51	6.20
4R-2, 110.5–113	505.51	1.20	10.00	0.09	1.81	0.61	6.79
4R-2, 113–133	505.54	1.22	10.19	0.09	1.84	0.62	6.85
4R-3, 66–69	506.48	1.56	12.96	0.06	2.02	0.46	7.29

IC = inorganic carbon, TN = total nitrogen, TC = total carbon, TOC = total organic carbon.

Table T18. Headspace gas concentrations, Hole C0002M.

Core, section	Depth (mbsf)	Headspace gas (ppmv)			C_1/C_2	Headspace gas (µM)		
		Methane	Ethane	Propane		Methane	Ethane	Propane
348-C0002M-								
1R-2	477.8	3885.0	5.6	ND	689	2041.7	2.9	ND
1R-4	480.0	2532.4	5.4	ND	465	1188.7	2.5	ND
2R-2	487.3	6187.5	8.7	ND	713	1582.7	2.2	ND
3R-1	494.9	2829.5	8.1	ND	350	971.6	2.8	ND
4R-2	505.8	7354.7	9.9	ND	739	2059.1	2.8	ND

ND = not detected.

Table T19. Total organic carbon (TOC) data and estimated temperatures using TOC and C_1/C_2 ratios, Hole C0002M.

Core, section, interval (cm)	Depth	TOC (wt%)	C_1/C_2	Estimated temperature (°C)
348-C0002M-				
1R-2, 63–65	477.79	0.61	689.4	61
1R-3, 87–90	480.02	0.66	465.5	70
2R-2, 111–131	487.28	0.54	712.5	63
3R-1, 90–110	494.86	0.54	349.5	82
4R-2, 113–133	505.78	0.62	739.3	62

Table T20. Interstitial water data determined by the ground rock interstitial normative determination (GRIND) method, Hole C0002P.

Core, section, interval (cm)	Depth (mbsf)	pH*	Salinity*	Chlorinity (mM)	Br^- (mM)	SO_4^{2-} (mM)	PO_4^{3-} (µM)	NH_4^+ (mM)	Na^+ (mM)	K^+ (mM)	Mg^{2+} (mM)	Ca^{2+} (mM)	B (µM)	Ba (µM)	Fe (µM)	Li (µM)	Mn (µM)	Si (µM)	Sr (µM)	V (nM)	Cu (nM)
Dilution ratio based on 60°C wet-dry determination of pore water																					
348-C0002P-																					
2R-3, 96–137.5	2176.3	7.85	1.3359	1,129	0.7	8.8	33.0	5.2	1,041	47.1	9.5	33.2	1,816	102.6	ND	485	3.2	564	349.3	79.4	7,698
3R-2, 84–104	2184.2	7.62	1.3347	459	0.4	4.8	ND	1.8	446	4.3	1.6	7.7	1,004	57.4	ND	205	1.1	387	83.8	28.4	6,385
4R-2 47–57	2193.1	7.29	1.3363	947	0.6	4.5	ND	3.9	869	20.1	7.5	29.6	917	160.4	ND	321	2.7	382	344.3	44.6	4,206
5R-2, 89–99	2203.3	7.35	1.3348	413	0.4	3.8	ND	1.3	409	2.2	1.2	7.1	780	54.8	ND	153	0.8	268	81.1	62.4	694
6R-2, 80–90 (Split 1)	2211.2	7.27	1.3359	694	0.4	3.5	32.4	2.4	653	8.3	4.6	18.8	722	120.4	ND	282	1.7	261	219.0	52.9	3,629
6R-2, 80–90 (Split 2)	2211.2	7.39	1.3363	814	0.5	3.8	ND	2.4	763	10.4	6.5	25.4	697	144.6	2.0	323	1.8	238	296.4	30.4	2,915
Dilution ratio based on 105°C wet-dry determination of pore water																					
348-C0002P-																					
2R-3, 96–137.5	2176.3	7.85	1.3359	734	21.5	3.4	0.5	5.7	677	30.6	6.2	21.6	1,181	66.7	ND	315	2.1	367	227.2	51.6	5,007
3R-2, 84–104	2184.2	7.62	1.3347	428	ND	1.6	0.3	4.5	416	4.0	1.5	7.1	936	53.5	ND	191	1.1	361	78.2	26.5	5,954
4R-2 47–57	2193.1	7.29	1.3363	848	ND	3.5	0.5	4.1	778	18.0	6.7	26.5	821	143.6	ND	288	2.4	342	308.2	39.9	3,765
5R-2, 89–99	2203.3	7.35	1.3348	387	ND	1.2	0.4	3.6	383	2.1	1.1	6.6	729	51.3	ND	143	0.7	251	75.9	58.3	649
6R-2, 80–90 (Split 1)	2211.2	7.27	1.3359	629	29.3	2.2	0.4	3.2	592	7.5	4.2	17.0	655	109.2	ND	256	1.5	237	198.6	48.0	3,291
6R-2, 80–90 (Split 2)	2211.2	7.39	1.3363	733	ND	2.2	0.5	3.4	686	9.3	5.8	22.8	627	130.2	ND	291	1.6	214	266.8	27.4	2,624

* = values not corrected for 10× dilution. ND = not detected.

Core, section, interval (cm)	Depth (mbsf)	Zn (nM)	As (nM)	Rb (nM)	Mo (nM)	Cs (nM)	Pb (nM)	U (nM)
Dilution ratio based on 60°C wet-dry determination of pore water								
348-C0002P-								
2R-3, 96–137.5	2176.3	3,286	350	6,397	20,594	55.8	22.9	19.5
3R-2, 84–104	2184.2	1,700	400	883	6,067	11.8	14.0	3.7
4R-2 47–57	2193.1	2,037	472	2,319	11,399	26.5	10.7	8.4
5R-2, 89–99	2203.3	286	758	499	20,155	9.3	ND	5.9
6R-2, 80–90 (Split 1)	2211.2	1,434	342	1,107	19,010	17.2	ND	1.8
6R-2, 80–90 (Split 2)	2211.2	566	274	1,138	19,262	14.2	10.0	2.2
Dilution ratio based on 105°C wet-dry determination of pore water								
348-C0002P-								
2R-3, 96–137.5	2176.3	2,138	228	4,161	13,396	36.3	14.9	12.7
3R-2, 84–104	2184.2	1,585	373	823	5,657	11.0	13.1	3.4
4R-2 47–57	2193.1	1,823	423	2,076	10,204	23.8	9.6	7.6
5R-2, 89–99	2203.3	268	709	467	18,848	8.7	ND	5.6
6R-2, 80–90 (Split 1)	2211.2	1,300	310	1,004	17,238	15.6	ND	1.7
6R-2, 80–90 (Split 2)	2211.2	566	246	1,024	17,338	12.8	9.0	1.9

Table T21. Chemical analyses of drilling mud water, corrected for dilution during analysis, Holes C0002N and C0002P. (Continued on next page.)

Mud-water sample	Depth (mbsf)	Date of collection (2013)	Time of collection (h UTC)	Wet mud (cm^3)	Wet mud (g)	Dry mud (g)	Water in wet mud (g)	Water content (%)	Refractive index of dilution	Salinity of diluted water (‰)	Alkalinity (mM)	Chlorinity (mM)	PO_4^{3-} (µM)	Br^- (mM)	SO_4^{2-} (mM)	Na^+ (mM)	Mg^{2+} (mM)	K^+ (mM)	Ca^{2+} (mM)
348-C0002N-																			
75-LMW	896.5	4 Nov	1800	20	23.0877	5.0094	18.0783	78.30	1.33623	17.31		2820.05	ND	1.56	36.53	1,928.56	ND	1,039.19	84.27
77-LMW	1140.5	5 Nov	1800	20	22.7834	4.8678	17.9156	78.63	1.33612	16.70		2,760.11	ND	1.50	35.87	1,902.36	ND	1,003.36	71.35
143-LMW	1333.5	6 Nov	1800	20	22.2836	5.0481	17.2355	77.35	1.33608	16.47		2,802.50	ND	1.90	37.18	1,946.80	ND	1,042.44	66.00
179-LMW	1675.5	7 Nov	1800	20	22.8675	5.0681	17.7994	77.84	1.33596	15.80		2,588.67	ND	1.38	34.98	1,763.85	ND	995.56	52.81
245-LMW	1677.5	8 Nov	1800	20	22.4445	5.0960	17.3485	77.30	1.33597	15.86		2,703.87	ND	1.59	35.68	1,820.95	ND	1,005.00	50.72
246-LMW	1978.5	9 Nov	1800	20	22.5194	4.9960	17.5234	77.81	1.33595	15.75		2,651.84	ND	1.57	35.73	1,768.83	ND	988.93	47.30
255-LMW	2008.5	10 Nov	1800	20	22.8669	5.1097	17.7572	77.65	1.33588	15.36		2,543.11	ND	1.35	35.12	1,684.72	ND	953.71	44.60
256-LMW	2008.5	11 Nov	1800	20	22.8145	5.1122	17.7023	77.59	1.33588	15.36		2,546.37	ND	1.46	35.34	1,688.10	ND	959.79	45.05
293-LMW	2215.5	12 Nov	1800	20	22.2584	5.1776	17.0808	76.74	1.33590	15.47		2,591.27	ND	1.49	37.01	1,732.03	ND	1,000.00	41.48
331-LMW	2329.5	13 Nov	1800	20	21.5940	4.9908	16.6032	76.89	1.33577	14.74		2,555.01	ND	1.56	36.19	1,693.30	ND	981.77	35.44
348-C0002P-																			
4-LMW	1939.5	14 Dec	1800	10	11.31	2.75	8.56	75.65	1.33566		47.23	1,871.15	21.66	1.05	34.18	1,185.31	ND	768.11	31.68
7-LMW	1954.5	16 Dec	1600	10	11.45	3.11	8.33	72.79	1.33563		41.08	1,895.49	16.96	1.23	29.66	1,246.25	ND	771.04	28.36
13-LMW	1974.5	17 Dec	0600	10	12.45	4.15	8.31	66.69	1.33625		46.86	2,474.58	12.80	1.30	32.43	1,770.54	ND	859.06	33.87
21-LMW	1991.5	17 Dec	1800	10	12.68	4.64	8.04	63.43	1.33556		34.40	1,888.39	12.62	1.05	26.24	1,348.49	ND	606.91	23.51
22-LMW	2012.5	18 Dec	0600	10	12.51	4.50	8.00	63.99	1.33621		45.12	2,415.76	8.64	1.20	31.71	1,730.39	ND	781.84	30.02
37-LMW	2061.5	18 Dec	1800	10	12.64	4.65	8.00	63.24	1.33648		47.18	2,618.60	17.60	1.26	36.54	1,903.90	ND	828.78	33.48
41-LMW	2067.5	20 Dec	0600	10	12.42	4.20	8.22	66.17	1.33629		38.27	2,471.54	24.92	1.29	34.39	1,779.17	ND	872.59	32.03
55-LMW	2128.5	20 Dec	1800	10	12.38	4.46	7.92	63.98	1.33628		41.14	2,466.47	38.48	1.41	33.52	1,755.79	ND	863.72	31.58
67-LMW	?	22 Dec	0600	10	12.43	4.53	7.90	63.53	1.33494		27.35	1,485.06	22.21	ND	22.12	973.28	ND	532.08	18.23
68-LMW	2107.5	22 Dec	1800	10	12.28	4.47	7.81	63.61	1.33475		22.60	1,355.96	10.00	ND	20.42	888.03	ND	490.88	16.25
70-LMW	2172.5	23 Dec	0600	10	12.49	4.58	7.91	63.31	1.33569		35.60	2,004.01	38.75	ND	29.05	1,353.66	ND	716.27	25.56
75-LMW	2191.5	23 Dec	1800	10	12.44	4.52	7.91	63.62	1.33571		34.73	2,046.60	25.64	1.01	28.75	1,352.99	ND	748.43	24.98
80-LMW	2200.5	24 Dec	0600	10	12.47	4.53	7.94	63.65	1.33549		30.11	1,897.52	17.50	1.03	27.01	1,223.34	ND	687.25	21.96
84-LMW	2217.5	25 Dec	1800	10	12.72	4.64	8.08	63.50	1.33559		31.60	1,964.45	18.14	ND	27.59	1,287.35	ND	738.79	22.53

Table T21 (continued).

Hole/Misc sample number	Depth (mbsf)	B (µM)	Ba (µM)	Fe (µM)	Li (µM)	Mn (µM)	Si (µM)	Sr (µM)	V (nM)	Cu (nM)	Zn (nM)	Rb (nM)	Mo (nM)	Cs (nM)	Pb (nM)	U (nM)
348-C0002N-																
75-LMW	896.5															
77-LMW	1140.5															
143-LMW	1333.5															
179-LMW	1675.5															
245-LMW	1677.5															
246-LMW	1978.5															
255-LMW	2008.5															
256-LMW	2008.5															
293-LMW	2215.5															
331-LMW	2329.5															
348-C0002P-																
4-LMW	1939.5	235.65	47.71	199.75	ND	ND	3,162.78	77.13	2,019.56	5,203.06	8,603.71	4,1876.42	18,380.77	99.25	125.08	8.24
7-LMW	1954.5	175.13	28.85	109.24	ND	ND	2,452.24	69.28	1,407.10	4,219.48	5,823.44	4,3141.97	15,353.30	88.21	79.36	7.19
13-LMW	1974.5	216.70	110.44	189.35	ND	ND	3,341.18	85.25	1,825.16	5,387.28	8,525.28	4,7409.81	17,108.30	103.74	122.43	7.48
21-LMW	1991.5	145.15	25.85	70.58	ND	ND	1,909.46	56.70	1,144.02	ND	3,785.31	3,3502.24	11,743.19	73.99	52.57	5.16
22-LMW	2012.5	183.29	98.39	172.57	ND	ND	2,981.15	75.65	1,624.28	4,696.49	7,178.63	4,2680.28	15,331.77	93.45	98.28	7.49
37-LMW	2061.5	236.05	314.14	268.82	ND	2.90	4,999.84	108.43	2,384.33	5,211.62	7,761.10	4,5474.83	17,127.07	105.06	123.21	9.47
41-LMW	2067.5	218.03	142.28	213.52	ND	ND	3,930.01	84.31	2,067.40	4,539.78	7,107.13	4,7694.01	15,136.11	96.37	97.78	7.72
55-LMW	2128.5	239.53	182.89	263.25	ND	2.73	4,421.05	94.14	2,445.14	4,686.84	7,379.39	4,7742.67	15,700.75	103.13	109.54	7.23
67-LMW	?	ND	26.31	57.65	ND	ND	1,707.47	47.46	1,069.62	ND	2,867.14	3,0232.83	8,614.10	60.87	39.51	3.89
68-LMW	2107.5	ND	26.94	49.52	ND	ND	1,448.46	40.97	896.27	ND	2,332.36	2,7537.93	8,203.57	53.63	34.84	3.43
70-LMW	2172.5	155.53	93.11	219.03	ND	ND	3,898.78	69.11	2,253.23	ND	6,416.44	3,9580.69	13,104.22	85.86	92.02	4.62
75-LMW	2191.5	152.06	190.13	311.39	ND	ND	4,888.91	79.54	2,602.76	4,275.18	6,741.38	4,0606.13	12,826.17	95.52	114.57	6.12
80-LMW	2200.5	121.07	79.94	179.70	ND	ND	3,290.31	64.17	1,858.21	ND	4,790.15	3,7199.09	11,373.84	81.83	78.57	5.48
84-LMW	2217.5	159.68	44.23	146.99	ND	ND	2,863.69	62.27	1,764.20	ND	6,091.36	4,0721.25	11,959.60	82.76	73.12	5.39

Table T22. Perfluorocarbon (PFC) concentrations in liquid of core liner (LCL) and core samples, Hole C0002P.

Core, section	PFC concentration (µg/L)
348-C0002P-	
LCL	
1R-1	56.30
2R-1	7.49
3R-1	5.77
4R-1	12.84
5R-1	6.10
6R-1	5.33
Cores	
2R-3	0.49
3R-2	0.21
4R-2	0.02
5R-2	0.05
6R-2	0.04

Table T23. Ground rock interstitial normative determination (GRIND) water concentrations normalized to chlorinity, Hole C0002P.

Core, section, interval (cm)	Depth (mbsf)	Br/Cl	SO_4^{2-}/Cl	PO_4^{3-}/Cl	NH_4/Cl	Na/Cl	K/Cl	Mg/Cl	Ca/Cl	B/Cl	Ba/Cl	Fe/Cl	Li/Cl	Mn/Cl	Si/Cl	Sr/Cl	Rb/Cl	Cs/Cl
348-C0002P-																		
2R-3, 96–137.5	2176.3	0.000660	0.0078	0.0292	0.00460	0.922	0.0417	0.00845	0.0294	1.61	0.09	ND	0.429	0.00287	0.500	0.309	5.667	0.0494
3R-2, 84–104	2184.2	0.000781	0.0106	ND	0.00382	0.972	0.0093	0.00344	0.0167	2.19	0.13	ND	0.447	0.00246	0.843	0.183	1.925	0.0258
4R-2 47–57	2193.1	0.000615	0.0048	ND	0.00412	0.917	0.0212	0.00793	0.0313	0.97	0.17	ND	0.339	0.00281	0.403	0.363	2.449	0.0280
5R-2, 89–99	2203.3	0.000914	0.0093	ND	0.00313	0.990	0.0054	0.00297	0.0171	1.89	0.13	ND	0.371	0.00187	0.650	0.196	1.207	0.0226
6R-2, 80–90 (Split 1)	2211.2	0.000597	0.0051	0.0466	0.00347	0.941	0.0119	0.00665	0.0271	1.04	0.17	ND	0.407	0.00239	0.376	0.316	1.596	0.0248
6R-2, 80–90 (Split 2)	2211.2	0.000632	0.0047	ND	0.00299	0.937	0.0127	0.00792	0.0312	0.86	0.18	ND	0.396	0.00223	0.292	0.364	1.397	0.0175

ND = not detected.

Table T24. Carbon and nitrogen data for cuttings, Holes C0002N and C0002P. (Continued on next seven pages.)

Cutting sample number	Depth (mbsf)	IC (wt%)	$CaCO_3$ (wt%)	TN (wt%)	TC (wt%)	TOC (wt%)	C/N	Remarks
348-C0002N-								
3-SMW	870.5	0.42	3.48	0.01	1.75	1.33	206.65	1–4 mm bulk
3-SMW	870.5	0.15	1.25	0.01	1.20	1.05	146.86	>4 mm bulk
5-SMW	880.5	1.15	9.58	0.02	2.24	1.09	50.88	1–4 mm bulk
5-SMW	880.5	0.23	1.89	0.01	1.06	0.83	129.02	>4 mm bulk
7-SMW	890.5	1.09	9.11	0.02	1.98	0.89	36.48	1–4 mm bulk
7-SMW	890.5	0.29	2.42	0.01	1.21	0.92	140.82	>4 mm bulk
9-SMW	900.5	1.85	15.39	0.04	3.05	1.20	30.10	1–4 mm bulk
9-SMW	900.5	0.72	5.99	0.02	2.09	1.37	76.55	>4 mm bulk
12-SMW	910.5	1.99	16.58	0.05	3.11	1.12	22.84	1–4 mm bulk
12-SMW	910.5	1.73	14.45	0.04	2.94	1.21	32.03	>4 mm bulk
14-SMW	920.5	1.59	13.28	0.06	3.02	1.42	22.51	1–4 mm bulk
14-SMW	920.5	1.35	11.27	0.04	2.71	1.36	32.85	>4 mm bulk
16-SMW	930.5	1.58	13.17	0.05	2.85	1.27	23.31	1–4 mm bulk
16-SMW	930.5	1.22	10.13	0.04	2.33	1.12	31.41	>4 mm bulk
18-SMW	940.5	1.22	10.19	0.07	2.75	1.53	22.99	1–4 mm bulk
18-SMW	940.5	1.27	10.61	0.05	2.52	1.25	27.14	>4 mm bulk
20-SMW	950.5	0.40	3.31	0.05	1.71	1.32	25.40	1–4 mm bulk
20-SMW	950.5	0.64	5.36	0.04	1.92	1.28	32.79	>4 mm bulk
22-SMW	960.5	0.40	3.35	0.05	1.75	1.35	25.21	1–4 mm bulk
22-SMW	960.5	0.42	3.47	0.04	1.72	1.30	30.43	>4 mm bulk
24-SMW	970.5	0.49	4.07	0.05	1.86	1.37	25.51	1–4 mm bulk
24-SMW	970.5	0.42	3.51	0.05	1.71	1.29	27.89	>4 mm bulk
26-SMW	980.5	0.53	4.45	0.05	1.75	1.22	24.23	1–4 mm bulk
26-SMW	980.5	0.51	4.24	0.05	1.74	1.24	24.28	>4 mm bulk
28-SMW	990.5	0.49	4.08	0.05	1.55	1.06	23.32	1–4 mm bulk
28-SMW	990.5	0.52	4.31	0.05	1.70	1.18	24.68	>4 mm bulk
30-SMW	1000.5	0.70	5.80	0.05	1.73	1.03	19.83	1–4 mm bulk
30-SMW	1000.5	0.52	4.36	0.05	1.78	1.26	23.60	>4 mm bulk
32-SMW	1010.5	0.67	5.58	0.05	1.94	1.27	23.69	1–4 mm bulk
32-SMW	1010.5	0.52	4.32	0.05	1.72	1.21	25.43	>4 mm bulk
34-SMW	1020.5	0.53	4.39	0.05	1.71	1.18	24.20	1–4 mm bulk
34-SMW	1020.5	0.48	4.03	0.06	1.66	1.18	20.84	>4 mm bulk
35-SMW	1025.5	0.68	5.68	0.05	1.69	1.01	19.27	>4 mm handpicked
36-SMW	1030.5	0.56	4.64	0.05	1.75	1.19	24.14	1–4 mm bulk
36-SMW	1030.5	0.46	3.80	0.05	1.72	1.26	23.07	>4 mm bulk
39-SMW	1040.5	0.54	4.50	0.05	1.75	1.21	24.12	1–4 mm bulk
39-SMW	1040.5	0.52	4.33	0.04	1.69	1.17	29.39	>4 mm bulk
40-SMW	1045.5	0.42	3.46	0.05	1.65	1.23	22.53	1–4 mm bulk
40-SMW	1045.5	0.43	3.58	0.06	1.64	1.21	21.81	>4 mm bulk
41-SMW	1052.5	0.46	3.86	0.05	1.62	1.16	22.86	1–4 mm bulk
41-SMW	1052.5	0.47	3.91	0.05	1.60	1.14	21.29	>4 mm bulk
42-SMW	1067.5	0.46	3.80	0.05	1.57	1.11	23.28	1–4 mm bulk
42-SMW	1067.5	0.46	3.85	0.05	1.60	1.14	22.73	>4 mm bulk
43-SMW	1069.5	0.47	3.88	0.05	1.58	1.12	22.31	1–4 mm bulk
43-SMW	1069.5	0.44	3.65	0.05	1.54	1.10	21.27	>4 mm bulk
44-SMW	1070.5	0.42	3.47	0.05	1.46	1.05	22.34	1–4 mm bulk
44-SMW	1070.5	0.38	3.16	0.05	1.47	1.09	20.97	>4 mm bulk
46-SMW	1080.5	0.45	3.72	0.05	1.68	1.24	23.22	1–4 mm bulk
46-SMW	1080.5	0.42	3.53	0.05	1.62	1.19	23.21	>4 mm bulk
48-SMW	1090.5	0.42	3.50	0.05	1.54	1.12	20.58	1–4 mm bulk
48-SMW	1090.5	0.44	3.68	0.06	1.57	1.12	20.38	>4 mm bulk
50-SMW	1100.5	0.38	3.13	0.05	1.54	1.16	22.53	1–4 mm bulk
50-SMW	1100.5	0.40	3.30	0.06	1.50	1.11	20.09	>4 mm bulk
52-SMW	1110.5	0.42	3.53	0.05	1.57	1.15	24.45	1–4 mm bulk
52-SMW	1110.5	0.44	3.63	0.05	1.54	1.11	22.66	>4 mm bulk
54-SMW	1120.5	0.34	2.82	0.05	1.39	1.05	21.79	1–4 mm bulk
54-SMW	1120.5	0.36	2.97	0.05	1.40	1.04	20.38	>4 mm bulk
57-SMW	1130.5	0.40	3.31	0.05	1.40	1.00	21.72	1–4 mm bulk
57-SMW	1130.5	0.41	3.45	0.05	1.35	0.93	19.59	>4 mm bulk
59-SMW	1140.5	0.48	3.97	0.05	1.69	1.21	23.71	1–4 mm bulk
59-SMW	1140.5	0.41	3.44	0.05	1.54	1.12	22.79	>4 mm bulk
61-SMW	1150.5	0.42	3.54	0.05	1.69	1.27	24.53	1–4 mm bulk
61-SMW	1150.5	0.53	4.44	0.05	1.71	1.18	21.62	>4 mm bulk
63-SMW	1160.5	0.56	4.63	0.05	1.92	1.36	28.21	1–4 mm bulk
63-SMW	1160.5	0.45	3.76	0.05	1.71	1.26	25.32	>4 mm bulk
65-SMW	1170.5	0.53	4.44	0.05	1.78	1.25	25.63	1–4 mm bulk

Table T24 (continued). (Continued on next page.)

Cutting sample number	Depth (mbsf)	IC (wt%)	$CaCO_3$ (wt%)	TN (wt%)	TC (wt%)	TOC (wt%)	C/N	Remarks
65-SMW	1170.5	0.51	4.28	0.05	1.72	1.21	24.17	>4 mm bulk
67-SMW	1180.5	0.38	3.17	0.05	1.83	1.45	27.65	1–4 mm bulk
67-SMW	1180.5	0.48	3.98	0.05	1.86	1.38	26.46	>4 mm bulk
69-SMW	1190.5	0.54	4.49	0.05	1.85	1.31	27.10	1–4 mm bulk
69-SMW	1190.5	0.74	6.13	0.05	1.95	1.22	26.25	>4 mm bulk
71-SMW	1200.5	0.63	5.23	0.05	1.88	1.25	26.23	1–4 mm bulk
71-SMW	1200.5	0.45	3.74	0.05	1.74	1.29	27.64	>4 mm bulk
73-SMW	1210.5	0.52	4.32	0.05	1.78	1.26	26.23	1–4 mm bulk
73-SMW	1210.5	0.47	3.88	0.04	1.66	1.20	30.57	>4 mm bulk
81-SMW	1218.5	1.15	9.61	0.05	2.70	1.55	31.48	1–4 mm bulk
81-SMW	1218.5	0.58	4.85	0.05	1.87	1.29	27.19	>4 mm bulk
82-SMW	1225.5	0.52	4.30	0.05	1.82	1.31	25.94	>4 mm handpicked DICAs
82-SMW	1225.5	0.29	2.39	0.02	1.06	0.77	34.61	>4 mm handpicked
83-SMW	1230.5	0.39	3.28	0.05	1.58	1.19	22.20	1–4 mm bulk
83-SMW	1230.5	0.46	3.86	0.05	1.46	1.00	19.81	>4 mm bulk
85-SMW	1240.5	0.78	6.47	0.04	1.94	1.16	26.34	1–4 mm bulk
85-SMW	1240.5	0.51	4.22	0.05	1.57	1.06	22.37	>4 mm bulk
87-SMW	1250.5	0.74	6.18	0.04	2.00	1.26	31.87	1–4 mm bulk
87-SMW	1250.5	0.54	4.50	0.05	1.62	1.08	23.09	>4 mm bulk
89-SMW	1260.5	0.54	4.49	0.05	1.71	1.17	24.15	1–4 mm bulk
89-SMW	1260.5	0.48	3.98	0.05	1.50	1.02	20.40	>4 mm bulk
91-SMW	1270.5	0.53	4.44	0.05	1.73	1.20	25.43	1–4 mm bulk
91-SMW	1270.5	0.51	4.28	0.05	1.52	1.01	21.05	>4 mm bulk
93-SMW	1280.5	0.58	4.83	0.05	1.72	1.14	24.41	1–4 mm bulk
93-SMW	1280.5	0.41	3.42	0.05	1.45	1.04	21.26	>4 mm bulk
95-SMW	1290.5	0.67	5.61	0.05	1.91	1.24	26.13	1–4 mm bulk
95-SMW	1290.5	0.55	4.60	0.04	1.55	1.00	22.56	>4 mm bulk
97-SMW	1300.5	0.55	4.56	0.05	1.61	1.06	23.39	1–4 mm bulk
97-SMW	1300.5	0.52	4.35	0.05	1.49	0.96	18.71	>4 mm bulk
99-SMW	1310.5	0.62	5.15	0.04	1.75	1.13	25.32	1–4 mm bulk
99-SMW	1310.5	0.45	3.74	0.05	1.52	1.07	21.82	>4 mm bulk
101-SMW	1320.5	0.61	5.12	0.05	1.66	1.04	21.46	1–4 mm bulk
101-SMW	1320.5	0.64	5.34	0.05	1.65	1.01	20.47	>4 mm bulk
105-SMW	1330.5	0.65	5.40	0.05	1.79	1.14	24.14	1–4 mm bulk
105-SMW	1330.5	0.48	4.02	0.05	1.58	1.10	22.47	>4 mm bulk
107-SMW	1340.5	0.37	3.08	0.05	1.74	1.37	25.28	1–4 mm bulk
107-SMW	1340.5	0.47	3.92	0.05	1.66	1.19	23.24	>4 mm bulk
109-SMW	1350.5	0.34	2.83	0.05	1.61	1.27	24.39	1–4 mm bulk
109-SMW	1350.5	0.38	3.18	0.06	1.55	1.17	21.11	>4 mm bulk
111-SMW	1360.5	0.43	3.56	0.05	1.80	1.37	27.91	1–4 mm bulk
111-SMW	1360.5	0.68	5.63	0.05	1.99	1.32	25.87	>4 mm bulk
113-SMW	1370.5	0.46	3.85	0.05	1.98	1.51	32.35	1–4 mm bulk
113-SMW	1370.5	0.52	4.37	0.05	1.66	1.14	21.59	>4 mm bulk
115-SMW	1380.5	0.89	7.38	0.05	2.18	1.30	27.14	1–4 mm bulk
115-SMW	1380.5	0.76	6.33	0.05	1.91	1.15	23.80	>4 mm bulk
117-SMW	1390.5	0.73	6.10	0.05	2.07	1.34	26.65	1–4 mm bulk
117-SMW	1390.5	0.84	6.99	0.05	2.08	1.24	23.36	>4 mm bulk
118-SMW	1395.5	0.67	5.59	0.05	2.38	1.71	32.17	>4 mm PP washed DICAs
119-SMW	1400.5	0.79	6.55	0.05	2.13	1.34	27.80	1–4 mm bulk
119-SMW	1400.5	0.63	5.29	0.06	1.87	1.23	21.50	>4 mm bulk
121-SMW	1410.5	0.66	5.50	0.04	1.88	1.22	29.92	1–4 mm bulk
121-SMW	1410.5	0.47	3.91	0.05	1.57	1.10	24.07	>4 mm bulk
123-SMW	1420.5	0.46	3.85	0.05	1.65	1.19	24.19	1–4 mm bulk
123-SMW	1420.5	0.40	3.34	0.05	1.47	1.07	21.18	>4 mm bulk
125-SMW	1430.5	0.79	6.59	0.05	1.95	1.16	25.73	1–4 mm bulk
125-SMW	1430.5	0.52	4.34	0.05	1.64	1.12	22.61	>4 mm bulk
128-SMW	1440.5	0.79	6.60	0.04	1.93	1.14	26.08	1–4 mm bulk
128-SMW	1440.5	0.44	3.67	0.05	1.53	1.09	22.37	>4 mm bulk
130-SMW	1450.5	0.64	5.33	0.05	1.77	1.13	23.80	1–4 mm bulk
130-SMW	1450.5	0.39	3.23	0.06	1.52	1.13	19.56	>4 mm bulk
132-SMW	1460.5	0.45	3.78	0.05	1.72	1.26	26.72	1–4 mm bulk
132-SMW	1460.5	0.44	3.68	0.05	1.57	1.12	22.17	>4 mm bulk
134-SMW	1470.5	0.51	4.25	0.05	1.76	1.25	25.05	1–4 mm bulk
134-SMW	1470.5	0.39	3.23	0.05	1.53	1.15	22.01	>4 mm bulk
136-SMW	1480.5	0.57	4.79	0.05	1.83	1.25	26.64	1–4 mm bulk
136-SMW	1480.5	0.31	2.61	0.06	1.42	1.11	20.05	>4 mm bulk
138-SMW	1490.5	0.57	4.73	0.05	1.67	1.10	22.57	1–4 mm bulk
138-SMW	1490.5	0.39	3.27	0.05	1.44	1.04	19.39	>4 mm bulk
140-SMW	1500.5	0.50	4.13	0.05	1.69	1.20	23.14	1–4 mm bulk

Table T24 (continued). (Continued on next page.)

Cutting sample number	Depth (mbsf)	IC (wt%)	$CaCO_3$ (wt%)	TN (wt%)	TC (wt%)	TOC (wt%)	C/N	Remarks
140-SMW	1500.5	0.42	3.49	0.06	1.46	1.04	18.76	>4 mm bulk
142-SMW	1510.5	0.58	4.80	0.05	1.70	1.13	22.96	1–4 mm bulk
142-SMW	1510.5	0.52	4.31	0.05	1.63	1.12	22.24	>4 mm bulk
146-SMW	1520.5	0.50	4.15	0.04	1.57	1.07	26.16	1–4 mm bulk
146-SMW	1520.5	0.42	3.52	0.05	1.54	1.12	21.49	>4 mm bulk
147-SMW	1525.5	0.35	2.91	0.05	1.26	0.91	18.13	>4 mm handpicked
148-SMW	1530.5	0.52	4.31	0.05	1.60	1.08	22.35	1–4 mm bulk
148-SMW	1530.5	0.42	3.54	0.05	1.50	1.07	20.06	>4 mm bulk
150-SMW	1540.5	0.49	4.05	0.04	1.48	0.99	22.11	1–4 mm bulk
150-SMW	1540.5	0.39	3.27	0.05	1.37	0.97	20.11	>4 mm bulk
152-SMW	1550.5	0.47	3.91	0.05	1.76	1.29	24.68	1–4 mm bulk
152-SMW	1550.5	0.39	3.28	0.05	1.38	0.99	18.04	>4 mm bulk
153-SMW	1555.5	0.45	3.71	0.05	1.82	1.37	27.50	>4 mm PP washed DICAs
154-SMW	1560.5	0.46	3.82	0.05	1.55	1.09	23.20	1–4 mm bulk
154-SMW	1560.5	0.41	3.41	0.05	1.38	0.97	19.55	>4 mm bulk
156-SMW	1570.5	0.49	4.09	0.05	1.49	1.00	21.67	1–4 mm bulk
156-SMW	1570.5	0.40	3.34	0.05	1.23	0.83	16.26	>4 mm bulk
158-SMW	1580.5	0.50	4.20	0.05	1.46	0.95	17.78	1–4 mm bulk
158-SMW	1580.5	0.57	4.72	0.05	1.47	0.90	17.22	>4 mm bulk
160-SMW	1590.5	0.42	3.53	0.05	1.39	0.97	19.68	1–4 mm bulk
160-SMW	1590.5	0.39	3.21	0.05	1.36	0.98	18.92	>4 mm bulk
162-SMW	1600.5	0.36	3.02	0.05	1.23	0.87	18.68	1–4 mm bulk
162-SMW	1600.5	0.50	4.14	0.05	1.28	0.78	14.65	>4 mm handpicked
162-SMW	1600.5	0.38	3.17	0.06	1.30	0.92	16.33	>4 mm bulk
164-SMW	1610.5	0.44	3.65	0.05	1.33	0.89	19.07	1–4 mm bulk
164-SMW	1610.5	0.45	3.75	0.05	1.31	0.86	18.18	>4 mm bulk
166-SMW	1620.5	0.43	3.55	0.04	1.19	0.77	17.37	1–4 mm bulk
166-SMW	1620.5	0.37	3.07	0.05	1.16	0.79	16.67	>4 mm bulk
169-SMW	1630.5	0.36	2.99	0.04	1.23	0.87	19.65	1–4 mm bulk
169-SMW	1630.5	0.41	3.40	0.05	1.25	0.84	18.35	>4 mm bulk
171-SMW	1640.5	0.38	3.18	0.03	1.01	0.63	21.92	1–4 mm bulk
171-SMW	1640.5	0.35	2.92	0.04	1.18	0.83	19.66	>4 mm bulk
173-SMW	1650.5	0.28	2.35	0.02	0.78	0.50	21.15	1–4 mm bulk
173-SMW	1650.5	0.31	2.61	0.05	1.02	0.71	15.61	>4 mm bulk
175-SMW	1660.5	0.57	4.73	0.04	1.28	0.71	19.34	1–4 mm bulk
175-SMW	1660.5	0.47	3.93	0.05	1.28	0.80	17.01	>4 mm bulk
177-SMW	1670.5	0.55	4.55	0.05	1.44	0.90	19.56	1–4 mm bulk
177-SMW	1670.5	0.48	4.02	0.05	1.36	0.88	18.72	>4 mm bulk
182-SMW	1680.5	0.40	3.32	0.05	1.36	0.96	19.50	1–4 mm bulk
182-SMW	1680.5	0.39	3.28	0.05	1.13	0.74	14.41	>4 mm bulk
184-SMW	1690.5	0.39	3.29	0.05	1.39	1.00	20.06	1–4 mm bulk
184-SMW	1690.5	0.55	4.58	0.05	1.34	0.79	16.30	>4 mm bulk
185-SMW	1695.5	0.30	2.53	0.05	1.56	1.25	24.73	>4 mm PP washed DICAs
186-SMW	1700.5	0.34	2.82	0.05	1.30	0.96	18.96	1–4 mm bulk
186-SMW	1700.5	0.47	3.95	0.05	1.10	0.63	12.85	>4 mm handpicked
186-SMW	1700.5	0.33	2.71	0.05	1.13	0.81	14.82	>4 mm bulk
188-SMW	1710.5	0.47	3.89	0.05	1.43	0.97	19.66	1–4 mm bulk
188-SMW	1710.5	0.41	3.43	0.05	1.22	0.81	16.24	>4 mm bulk
190-SMW	1720.5	0.70	5.81	0.04	1.62	0.92	20.63	1–4 mm bulk
190-SMW	1720.5	0.64	5.34	0.05	1.45	0.81	17.87	>4 mm bulk
192-SMW	1730.5	0.50	4.15	0.05	1.41	0.91	18.99	1–4 mm bulk
192-SMW	1730.5	0.45	3.77	0.05	1.21	0.75	15.63	>4 mm bulk
195-SMW	1740.5	0.54	4.54	0.05	1.53	0.99	20.47	1–4 mm bulk
195-SMW	1740.5	0.49	4.09	0.05	1.38	0.89	17.57	>4 mm bulk
197-SMW	1750.5	0.62	5.16	0.05	1.54	0.92	19.57	1–4 mm bulk
197-SMW	1750.5	0.56	4.70	0.05	1.32	0.76	14.45	>4 mm bulk
199-SMW	1760.5	0.49	4.12	0.05	1.51	1.02	19.80	1–4 mm bulk
199-SMW	1760.5	0.43	3.55	0.05	1.36	0.93	18.32	>4 mm bulk
201-SMW	1770.5	0.53	4.41	0.05	1.55	1.02	20.21	1–4 mm bulk
201-SMW	1770.5	0.49	4.11	0.05	1.37	0.88	17.74	>4 mm bulk
203-SMW	1780.5	0.51	4.22	0.05	1.54	1.03	20.78	1–4 mm bulk
203-SMW	1780.5	0.41	3.43	0.05	1.35	0.94	17.69	>4 mm bulk
205-SMW	1790.5	0.46	3.84	0.05	1.53	1.07	20.03	1–4 mm bulk
205-SMW	1790.5	0.41	3.42	0.06	1.42	1.01	18.13	>4 mm bulk
207-SMW	1800.5	0.41	3.38	0.05	1.44	1.03	19.41	1–4 mm bulk
207-SMW	1800.5	0.44	3.63	0.06	1.45	1.01	17.28	>4 mm bulk
209-SMW	1810.5	0.46	3.83	0.05	1.50	1.04	20.67	1–4 mm bulk
209-SMW	1810.5	0.45	3.72	0.05	1.39	0.94	18.18	>4 mm bulk
211-SMW	1820.5	0.41	3.42	0.05	1.41	1.00	18.15	1–4 mm bulk

Table T24 (continued). (Continued on next page.)

Cutting sample number	Depth (mbsf)	IC (wt%)	$CaCO_3$ (wt%)	TN (wt%)	TC (wt%)	TOC (wt%)	C/N	Remarks
211-SMW	1820.5	0.52	4.33	0.06	1.46	0.94	16.89	>4 mm bulk
213-SMW	1830.5	0.52	4.36	0.05	1.45	0.93	18.41	1–4 mm bulk
213-SMW	1830.5	0.35	2.93	0.05	1.23	0.88	16.24	>4 mm bulk
216-SMW	1840.5	0.40	3.34	0.05	1.37	0.97	18.80	1–4 mm bulk
216-SMW	1840.5	0.29	2.43	0.05	1.16	0.87	16.19	>4 mm bulk
218-SMW	1850.5	0.39	3.23	0.05	1.27	0.89	16.48	1–4 mm bulk
218-SMW	1850.5	0.35	2.95	0.06	1.17	0.81	14.29	>4 mm bulk
219-SMW	1855.5	0.37	3.12	0.05	1.66	1.29	25.15	>4 mm PP washed DICAs
220-SMW	1860.5	0.45	3.74	0.05	1.27	0.83	16.35	1–4 mm bulk
220-SMW	1860.5	0.40	3.34	0.05	1.21	0.80	14.92	>4 mm bulk
222-SMW	1870.5	0.48	4.00	0.05	1.35	0.87	17.39	1–4 mm bulk
222-SMW	1870.5	0.38	3.19	0.05	1.11	0.73	14.41	>4 mm bulk
224-SMW	1880.5	0.50	4.16	0.05	1.32	0.82	16.09	1–4 mm bulk
224-SMW	1880.5	0.47	3.90	0.05	1.22	0.76	13.90	>4 mm bulk
226-SMW	1890.5	0.60	4.98	0.05	1.44	0.85	17.28	1–4 mm bulk
226-SMW	1890.5	0.63	5.22	0.05	1.44	0.82	16.44	>4 mm bulk
228-SMW	1900.5	0.72	5.99	0.05	1.42	0.71	13.97	1–4 mm bulk
228-SMW	1900.5	0.88	7.30	0.06	1.59	0.72	12.73	>4 mm bulk
230-SMW	1910.5	0.80	6.67	0.05	1.55	0.75	14.70	1–4 mm bulk
230-SMW	1910.5	0.76	6.36	0.05	1.53	0.77	14.98	>4 mm bulk
232-SMW	1920.5	0.95	7.94	0.05	1.65	0.70	14.27	1–4 mm bulk
232-SMW	1920.5	0.82	6.85	0.05	1.53	0.71	14.09	>4 mm bulk
234-SMW	1930.5	0.86	7.16	0.05	1.63	0.77	14.62	1–4 mm bulk
234-SMW	1930.5	0.75	6.22	0.06	1.51	0.77	13.81	>4 mm bulk
237-SMW	1940.5	0.79	6.55	0.06	1.55	0.76	13.61	1–4 mm bulk
237-SMW	1940.5	0.72	6.02	0.06	1.48	0.75	13.41	>4 mm bulk
239-SMW	1950.5	0.59	4.89	0.06	1.35	0.77	13.03	1–4 mm bulk
239-SMW	1950.5	0.63	5.25	0.06	1.38	0.75	12.12	>4 mm bulk
240-SMW	1955.5	0.52	4.37	0.06	1.87	1.35	23.91	>4 mm PP washed DICAs
241-SMW	1960.5	0.47	3.90	0.06	1.25	0.78	13.85	1–4 mm bulk
241-SMW	1960.5	0.57	4.77	0.06	1.27	0.70	12.56	>4 mm bulk
243-SMW	1970.5	0.51	4.22	0.06	1.34	0.83	15.02	1–4 mm bulk
243-SMW	1970.5	0.50	4.18	0.06	1.26	0.76	13.42	>4 mm bulk
248-SMW	1980.5	0.35	2.93	0.06	1.12	0.77	13.31	1–4 mm bulk
248-SMW	1980.5	0.41	3.42	0.06	1.10	0.69	11.94	>4 mm bulk
250-SMW	1990.5	0.33	2.78	0.06	1.11	0.78	13.83	1–4 mm bulk
250-SMW	1990.5	0.38	3.16	0.06	1.15	0.77	13.54	>4 mm bulk
252-SMW	2000.5	0.16	1.36	0.06	1.08	0.92	15.02	1–4 mm bulk
252-SMW	2000.5	0.45	3.77	0.06	1.20	0.74	12.02	>4 mm bulk
259-SMW	2010.5	0.46	3.84	0.05	1.45	0.99	20.15	1–4 mm bulk
259-SMW	2010.5	0.34	2.86	0.06	1.06	0.72	12.11	>4 mm bulk
261-SMW	2020.5	0.46	3.85	0.05	1.45	0.99	19.03	1–4 mm bulk
261-SMW	2020.5	0.46	3.83	0.04	1.17	0.71	17.65	>4 mm bulk
264-SMW	2030.5	0.44	3.71	0.05	1.37	0.93	17.90	1–4 mm bulk
264-SMW	2030.5	0.53	4.45	0.04	1.35	0.82	19.18	>4 mm bulk
266-SMW	2040.5	0.47	3.91	0.06	2.54	2.07	35.58	1–4 mm bulk
266-SMW	2040.5	0.49	4.06	0.04	1.10	0.62	14.18	>4 mm bulk
268-SMW	2050.5	0.33	2.73	0.06	1.89	1.56	27.37	1–4 mm bulk
268-SMW	2050.5	0.37	3.11	0.05	0.91	0.54	9.89	>4 mm bulk
270-SMW	2060.5	0.14	1.20	0.06	1.14	0.99	17.10	1–4 mm bulk
270-SMW	2060.5	0.27	2.21	0.05	0.91	0.65	12.12	>4 mm bulk
272-SMW	2070.5	0.18	1.47	0.05	1.13	0.96	17.45	1–4 mm bulk
272-SMW	2070.5	0.40	3.35	0.06	1.04	0.63	11.31	>4 mm bulk
274-SMW	2080.5	0.23	1.90	0.05	1.16	0.93	17.27	1–4 mm bulk
274-SMW	2080.5	0.26	2.14	0.05	0.98	0.72	13.89	>4 mm bulk
276-SMW	2090.5	0.24	2.02	0.05	1.34	1.09	20.10	1–4 mm bulk
276-SMW	2090.5	0.23	1.94	0.06	1.05	0.81	14.41	>4 mm bulk
278-SMW	2100.5	0.21	1.76	0.06	1.11	0.90	15.80	1–4 mm bulk
278-SMW	2100.5	0.16	1.32	0.06	0.99	0.84	14.37	>4 mm bulk
281-SMW	2110.5	0.25	2.11	0.05	1.18	0.93	17.52	1–4 mm bulk
281-SMW	2110.5	0.21	1.74	0.06	1.03	0.82	14.46	>4 mm bulk
283-SMW	2120.5	0.26	2.13	0.05	1.52	1.26	23.37	1–4 mm bulk
283-SMW	2120.5	0.26	2.13	0.06	1.15	0.90	15.45	>4 mm bulk
285-SMW	2130.5	0.27	2.26	0.06	2.29	2.02	34.07	1–4 mm bulk
285-SMW	2130.5	0.17	1.42	0.06	1.17	1.00	16.49	>4 mm bulk
287-SMW	2140.5	0.24	2.01	0.06	1.61	1.37	23.66	1–4 mm bulk
287-SMW	2140.5	0.22	1.84	0.06	1.14	0.92	14.49	>4 mm bulk
289-SMW	2150.5	0.44	3.69	0.06	1.32	0.88	14.01	1–4 mm bulk
289-SMW	2150.5	0.17	1.37	0.06	1.10	0.94	15.60	>4 mm bulk

Table T24 (continued). (Continued on next page.)

Cutting sample number	Depth (mbsf)	IC (wt%)	$CaCO_3$ (wt%)	TN (wt%)	TC (wt%)	TOC (wt%)	C/N	Remarks
291-SMW	2160.5	0.19	1.58	0.06	1.22	1.03	17.76	1–4 mm bulk
291-SMW	2160.5	0.26	2.20	0.06	1.12	0.85	14.23	>4 mm bulk
296-SMW	2170.5	0.27	2.27	0.05	1.26	0.98	18.54	1–4 mm bulk
296-SMW	2170.5	0.32	2.70	0.05	1.19	0.86	15.83	>4 mm bulk
298-SMW	2180.5	0.29	2.41	0.05	1.24	0.95	18.12	1–4 mm bulk
298-SMW	2180.5	0.18	1.50	0.05	0.80	0.62	11.70	>4 mm handpicked
298-SMW	2180.5	0.58	4.85	0.04	1.41	0.82	18.75	>4 mm bulk
300-SMW	2190.5	0.33	2.74	0.05	1.30	0.97	19.04	1–4 mm bulk
300-SMW	2190.5	0.27	2.25	0.05	1.18	0.91	17.34	>4 mm bulk
302-SMW	2200.5	0.32	2.63	0.05	1.30	0.99	18.15	1–4 mm bulk
302-SMW	2200.5	0.26	2.18	0.06	1.23	0.97	16.94	>4 mm bulk
304-SMW	2210.5	0.41	3.42	0.05	1.38	0.97	20.95	1–4 mm bulk
304-SMW	2210.5	0.29	2.45	0.05	1.04	0.75	13.66	>4 mm handpicked
304-SMW	2210.5	0.31	2.58	0.05	1.29	0.98	17.85	>4 mm bulk
306-SMW	2220.5	0.55	4.60	0.05	1.56	1.00	19.78	1–4 mm bulk
306-SMW	2220.5	0.51	4.27	0.06	1.52	1.01	17.28	>4 mm bulk
308-SMW	2230.5	0.56	4.70	0.05	1.76	1.20	23.71	1–4 mm bulk
308-SMW	2230.5	0.47	3.95	0.05	1.13	0.66	13.08	>4 mm handpicked
308-SMW	2230.5	0.34	2.84	0.06	1.37	1.03	18.37	>4 mm bulk
310-SMW	2240.5	0.37	3.11	0.05	1.35	0.98	17.85	1–4 mm bulk
310-SMW	2240.5	0.37	3.08	0.06	1.23	0.86	14.37	>4 mm bulk
312-SMW	2250.5	0.50	4.13	0.06	1.60	1.10	19.86	1–4 mm bulk
312-SMW	2250.5	0.37	3.12	0.06	1.30	0.93	16.01	>4 mm bulk
314-SMW	2260.5	0.35	2.92	0.06	1.37	1.02	18.23	1–4 mm bulk
314-SMW	2260.5	0.33	2.78	0.06	1.29	0.96	16.20	>4 mm bulk
316-SMW	2270.5	0.54	4.52	0.05	1.54	1.00	18.80	1–4 mm bulk
316-SMW	2270.5	0.33	2.73	0.06	1.39	1.06	16.71	>4 mm bulk
318-SMW	2280.5	0.41	3.40	0.06	1.38	0.97	17.12	1–4 mm bulk
318-SMW	2280.5	0.31	2.59	0.06	1.23	0.92	15.14	>4 mm bulk
321-SMW	2290.5	0.38	3.13	0.06	1.34	0.96	16.51	1–4 mm bulk
321-SMW	2290.5	0.35	2.90	0.06	1.28	0.93	15.59	>4 mm bulk
323-SMW	2300.5	0.40	3.32	0.06	1.51	1.11	17.99	1–4 mm bulk
323-SMW	2300.5	0.39	3.22	0.06	1.21	0.83	13.04	>4 mm bulk
325-SMW	2310.5	0.35	2.94	0.05	1.55	1.20	22.82	1–4 mm bulk
325-SMW	2310.5	0.36	2.97	0.06	1.23	0.87	14.13	>4 mm bulk
327-SMW	2320.5	0.37	3.09	0.06	1.37	1.00	16.17	1–4 mm bulk
327-SMW	2320.5	0.36	2.98	0.06	1.19	0.83	13.76	>4 mm bulk
348-C0002P-								
9-SMW	1960.5	0.43	3.57	0.04	1.13	0.70	20.11	>4 mm bulk
9-SMW	1960.5	0.31	2.60	0.05	1.34	1.03	21.50	1–4 mm bulk
14-SMW	1970.5	0.36	3.04	0.05	0.99	0.63	11.87	>4 mm bulk
14-SMW	1970.5	0.39	3.22	0.05	1.26	0.87	18.25	1–4 mm bulk
16-SMW	1980.5	0.35	2.87	0.05	0.94	0.59	11.13	>4 mm bulk
16-SMW	1980.5	0.38	3.15	0.05	1.17	0.79	15.28	1–4 mm bulk
18-SMW	1990.5	0.47	3.92	0.03	0.96	0.49	16.91	>4 mm bulk
18-SMW	1990.5	0.43	3.58	0.05	1.37	0.94	17.70	1–4 mm bulk
20-SMW	2000.5	0.55	4.57	0.05	1.23	0.68	13.43	>4 mm bulk
20-SMW	2000.5	0.52	4.34	0.05	1.31	0.79	15.52	1–4 mm bulk
25-SMW	2010.5	0.49	4.07	0.06	1.13	0.64	11.27	>4 mm bulk
25-SMW	2010.5	0.50	4.17	0.04	1.41	0.91	22.01	1–4 mm bulk
28-SMW	2020.5	0.35	2.91	0.06	0.93	0.58	10.45	>4 mm bulk
28-SMW	2020.5	0.38	3.16	0.05	1.05	0.67	12.65	1–4 mm bulk
30-SMW	2030.5	0.19	1.57	0.06	0.73	0.54	8.96	>4 mm bulk
30-SMW	2030.5	0.26	2.15	0.06	0.89	0.64	10.52	1–4 mm bulk
32-SMW	2040.5	0.18	1.49	0.06	0.79	0.62	9.83	1–4 mm bulk
34-SMW	2050.5	0.18	1.51	0.06	0.75	0.56	9.83	>4 mm bulk
34-SMW	2050.5	0.20	1.63	0.06	0.81	0.61	10.54	1–4 mm bulk
36-SMW	2060.5	0.33	2.74	0.05	0.81	0.48	9.30	>4 mm bulk
36-SMW	2060.5	0.24	1.98	0.06	0.76	0.53	9.06	1–4 mm bulk
43-SMW	2070.5	0.19	1.61	0.06	0.64	0.45	7.58	>4 mm bulk
43-SMW	2070.5	0.14	1.14	0.06	0.66	0.53	8.94	1–4 mm bulk
45-SMW	2080.5	0.16	1.35	0.06	0.63	0.47	7.97	>4 mm bulk
45-SMW	2080.5	0.11	0.92	0.06	0.69	0.58	9.72	1–4 mm bulk
47-SMW	2090.5	0.71	5.95	0.05	1.22	0.50	10.26	>4 mm bulk
47-SMW	2090.5	0.24	2.01	0.06	0.83	0.59	10.57	1–4 mm bulk
49-SMW	2100.5	0.37	3.05	0.05	1.03	0.67	12.23	>4 mm bulk
49-SMW	2100.5	0.20	1.69	0.06	0.90	0.69	12.18	1–4 mm bulk
53-SMW	2110.5	0.73	6.09	0.06	1.69	0.96	17.17	>4 mm bulk
53-SMW	2110.5	0.27	2.22	0.06	0.99	0.73	12.34	1–4 mm bulk

Table T24 (continued). (Continued on next page.)

Cutting sample number	Depth (mbsf)	IC (wt%)	$CaCO_3$ (wt%)	TN (wt%)	TC (wt%)	TOC (wt%)	C/N	Remarks
56-SMW	2120.5	0.17	1.44	0.06	0.74	0.57	9.48	>4 mm bulk
56-SMW	2120.5	0.17	1.45	0.06	0.82	0.65	10.76	1–4 mm bulk
58-SMW	2130.5	0.21	1.78	0.06	0.78	0.57	9.93	>4 mm bulk
58-SMW	2130.5	0.19	1.58	0.06	0.83	0.64	10.82	1–4 mm bulk
61-SMW	2140.5	0.44	3.63	0.05	1.09	0.66	12.76	>4 mm bulk
61-SMW	2140.5	0.29	2.38	0.05	1.02	0.74	13.48	1–4 mm bulk
63-SMW	2150.5	0.34	2.86	0.05	0.99	0.64	12.17	>4 mm bulk
63-SMW	2150.5	0.34	2.87	0.06	1.13	0.79	14.26	1–4 mm bulk
71-SMW	2162.5	0.42	3.49	0.05	1.12	0.70	13.28	>4 mm bulk
71-SMW	2162.5	0.42	3.53	0.05	1.41	0.99	19.81	1–4 mm bulk
72-SMW	2165.5	0.23	1.89	0.05	0.84	0.62	11.49	>4 mm bulk
72-SMW	2165.5	0.35	2.95	0.05	1.32	0.97	18.69	1–4 mm bulk
73-SMW	2170.5	0.30	2.47	0.05	1.09	0.79	14.91	>4 mm bulk
73-SMW	2170.5	0.32	2.68	0.05	1.27	0.95	18.96	1–4 mm bulk
74-SMW	2175.5	0.21	1.74	0.05	0.87	0.66	12.25	>4 mm bulk
74-SMW	2175.5	0.31	2.59	0.04	1.18	0.87	20.17	1–4 mm bulk
76-SMW	2180.5	0.23	1.95	0.05	0.91	0.67	13.91	>4 mm bulk
76-SMW	2180.5	0.34	2.87	0.05	1.30	0.95	19.65	1–4 mm bulk
77-SMW	2185.5	0.24	1.96	0.05	0.89	0.65	12.38	>4 mm bulk
77-SMW	2185.5	0.34	2.84	0.05	1.25	0.91	17.53	1–4 mm bulk
81-SMW	2190.5	0.23	1.88	0.05	0.85	0.63	13.33	>4 mm bulk
81-SMW	2190.5	0.30	2.53	0.05	1.35	1.05	20.91	1–4 mm bulk
82-SMW	2195.5	0.30	2.50	0.05	1.00	0.70	15.41	>4 mm bulk
82-SMW	2195.5	0.28	2.34	0.06	1.31	1.02	18.59	1–4 mm bulk
83-SMW	2200.5	0.28	2.33	0.05	0.94	0.66	13.83	>4 mm bulk
83-SMW	2200.5	0.29	2.45	0.05	1.36	1.06	20.67	1–4 mm bulk
85-SMW	2205.5	0.49	4.05	0.05	1.30	0.81	16.61	>4 mm bulk
85-SMW	2205.5	0.26	2.18	0.05	1.33	1.07	22.61	1–4 mm bulk
86-SMW	2210.5	0.25	2.11	0.05	1.07	0.82	15.67	>4 mm bulk
86-SMW	2210.5	0.29	2.38	0.05	1.37	1.09	20.42	1–4 mm bulk
107-SMW	2220.5	0.27	2.29	0.05	0.75	0.48	9.07	>4 mm bulk
107-SMW	2220.5	0.24	1.99	0.05	0.91	0.67	12.39	1–4 mm bulk
109-SMW	2230.5	0.39	3.21	0.05	0.95	0.56	11.10	>4 mm bulk
109-SMW	2230.5	0.29	2.40	0.06	1.03	0.74	12.97	1–4 mm bulk
111-SMW	2240.5	0.25	2.05	0.06	0.86	0.62	10.83	>4 mm bulk
111-SMW	2240.5	0.31	2.61	0.06	1.12	0.81	13.89	1–4 mm bulk
113-SMW	2250.5	0.25	2.06	0.05	0.88	0.63	11.60	>4 mm bulk
113-SMW	2250.5	0.28	2.32	0.05	1.08	0.81	14.71	1–4 mm bulk
115-SMW	2260.5	0.24	1.99	0.05	0.83	0.59	11.44	>4 mm bulk
115-SMW	2260.5	0.32	2.66	0.05	1.16	0.84	15.50	1–4 mm bulk
117-SMW	2270.5	0.18	1.54	0.05	0.76	0.57	10.60	>4 mm bulk
117-SMW	2270.5	0.40	3.37	0.05	1.23	0.83	15.46	1–4 mm bulk
121-SMW	2280.5	0.28	2.36	0.06	1.00	0.72	12.39	>4 mm bulk
121-SMW	2280.5	0.37	3.07	0.06	1.09	0.72	12.32	1–4 mm bulk
123-SMW	2290.5	0.27	2.29	0.06	1.06	0.78	13.75	>4 mm bulk
123-SMW	2290.5	0.29	2.41	0.06	1.04	0.75	13.00	1–4 mm bulk
125-SMW	2300.5	0.22	1.86	0.05	0.87	0.64	12.00	>4 mm bulk
125-SMW	2300.5	0.32	2.67	0.06	1.13	0.81	13.47	1–4 mm bulk
127-SMW	2310.5	0.21	1.74	0.05	0.92	0.71	13.74	>4 mm bulk
127-SMW	2310.5	0.35	2.90	0.05	1.13	0.78	14.76	1–4 mm bulk
129-SMW	2320.5	0.18	1.52	0.05	0.88	0.70	13.21	>4 mm bulk
129-SMW	2320.5	0.25	2.09	0.06	1.06	0.81	14.61	1–4 mm bulk
131-SMW	2330.5	0.28	2.36	0.05	1.07	0.79	14.77	>4 mm bulk
131-SMW	2330.5	0.28	2.37	0.06	1.10	0.82	14.64	1–4 mm bulk
133-SMW	2340.5	0.31	2.57	0.05	1.02	0.71	13.14	>4 mm bulk
133-SMW	2340.5	0.30	2.47	0.06	1.12	0.82	14.27	1–4 mm bulk
136-SMW	2350.5	0.25	2.05	0.05	1.00	0.75	14.24	>4 mm bulk
136-SMW	2350.5	0.28	2.31	0.06	1.21	0.94	16.80	1–4 mm bulk
138-SMW	2360.5	0.21	1.78	0.05	0.98	0.77	14.41	>4 mm bulk
138-SMW	2360.5	0.27	2.28	0.06	1.18	0.91	15.54	1–4 mm bulk
141-SMW	2370.5	0.26	2.15	0.05	1.01	0.75	14.49	>4 mm bulk
141-SMW	2370.5	0.26	2.16	0.05	1.16	0.90	16.76	1–4 mm bulk
143-SMW	2380.5	0.24	1.99	0.05	0.97	0.73	13.47	>4 mm bulk
143-SMW	2380.5	0.26	2.16	0.06	1.15	0.89	15.89	1–4 mm bulk
145-SMW	2390.5	0.24	2.03	0.05	0.99	0.75	14.41	>4 mm bulk
145-SMW	2390.5	0.30	2.47	0.05	1.20	0.90	16.87	1–4 mm bulk
149-SMW	2400.5	0.25	2.08	0.05	1.06	0.81	15.62	>4 mm bulk
149-SMW	2400.5	0.27	2.21	0.05	1.15	0.88	16.28	1–4 mm bulk
151-SMW	2410.5	0.23	1.88	0.04	0.89	0.67	15.93	>4 mm bulk

Table T24 (continued). (Continued on next page.)

Cutting sample number	Depth (mbsf)	IC (wt%)	$CaCO_3$ (wt%)	TN (wt%)	TC (wt%)	TOC (wt%)	C/N	Remarks
151-SMW	2410.5	0.29	2.42	0.05	1.22	0.93	18.46	1–4 mm bulk
155-SMW	2420.5	0.26	2.16	0.06	1.10	0.85	15.32	>4 mm bulk
155-SMW	2420.5	0.33	2.77	0.05	1.30	0.96	18.45	1–4 mm bulk
157-SMW	2430.5	0.26	2.13	0.05	1.09	0.84	17.20	>4 mm bulk
157-SMW	2430.5	0.28	2.31	0.05	1.15	0.88	17.23	1–4 mm bulk
159-SMW	2440.5	0.22	1.83	0.04	0.80	0.58	13.33	>4 mm bulk
159-SMW	2440.5	0.33	2.75	0.05	1.20	0.87	16.56	1–4 mm bulk
161-SMW	2450.5	0.21	1.79	0.04	0.90	0.69	17.10	>4 mm bulk
161-SMW	2450.5	0.30	2.48	0.05	1.14	0.85	17.26	1–4 mm bulk
163-SMW	2460.5	0.20	1.69	0.05	0.96	0.76	14.46	>4 mm bulk
163-SMW	2460.5	0.29	2.45	0.05	1.14	0.84	16.31	1–4 mm bulk
165-SMW	2470.5	0.23	1.93	0.05	1.01	0.78	14.78	>4 mm bulk
165-SMW	2470.5	0.30	2.51	0.05	1.10	0.79	15.57	1–4 mm bulk
168-SMW	2480.5	0.14	1.15	0.05	0.89	0.75	14.04	>4 mm bulk
168-SMW	2480.5	0.27	2.25	0.05	1.05	0.78	14.72	1–4 mm bulk
170-SMW	2490.5	0.29	2.37	0.05	1.01	0.73	14.39	>4 mm bulk
170-SMW	2490.5	0.29	2.39	0.05	1.08	0.80	15.08	1–4 mm bulk
172-SMW	2500.5	0.14	1.20	0.05	0.80	0.65	12.51	>4 mm bulk
172-SMW	2500.5	0.25	2.06	0.05	1.04	0.79	14.49	1–4 mm bulk
174-SMW	2510.5	0.22	1.82	0.05	0.92	0.70	13.99	>4 mm bulk
174-SMW	2510.5	0.20	1.66	0.05	1.01	0.81	15.65	1–4 mm bulk
176-SMW	2520.5	0.10	0.84	0.06	0.72	0.62	11.24	>4 mm bulk
176-SMW	2520.5	0.23	1.91	0.06	1.03	0.80	14.03	1–4 mm bulk
179-SMW	2530.5	0.16	1.31	0.05	0.76	0.60	12.70	>4 mm bulk
179-SMW	2530.5	0.24	2.00	0.05	1.04	0.80	15.07	1–4 mm bulk
181-SMW	2540.5	0.16	1.30	0.05	0.90	0.74	14.48	>4 mm bulk
181-SMW	2540.5	0.19	1.61	0.05	1.06	0.87	15.75	1–4 mm bulk
183-SMW	2550.5	0.23	1.94	0.05	0.77	0.54	10.90	>4 mm bulk
183-SMW	2550.5	0.18	1.47	0.05	0.94	0.76	14.18	1–4 mm bulk
185-SMW	2560.5	0.16	1.37	0.05	0.87	0.71	13.53	>4 mm bulk
185-SMW	2560.5	0.25	2.05	0.05	1.07	0.83	15.12	1–4 mm bulk
187-SMW	2570.5	0.12	0.98	0.06	0.75	0.63	11.41	>4 mm bulk
187-SMW	2570.5	0.27	2.23	0.05	1.06	0.80	15.02	1–4 mm bulk
189-SMW	2580.5	0.41	3.45	0.05	1.10	0.69	12.85	>4 mm bulk
189-SMW	2580.5	0.25	2.05	0.06	1.08	0.84	15.11	1–4 mm bulk
191-SMW	2590.5	0.30	2.49	0.05	1.01	0.71	13.29	>4 mm bulk
191-SMW	2590.5	0.12	1.01	0.05	1.13	1.00	19.65	1–4 mm bulk
196-SMW	2601.5	0.31	2.56	0.06	0.82	0.51	8.97	>4 mm bulk
196-SMW	2601.5	0.29	2.44	0.06	1.20	0.91	15.82	1–4 mm bulk
198-SMW	2610.5	0.30	2.51	0.05	0.77	0.47	9.35	>4 mm bulk
198-SMW	2610.5	0.34	2.83	0.05	1.26	0.92	17.26	1–4 mm bulk
200-SMW	2620.5	0.70	5.80	0.05	1.27	0.58	11.23	>4 mm bulk
200-SMW	2620.5	0.38	3.14	0.06	1.20	0.83	14.63	1–4 mm bulk
202-SMW	2630.5	0.52	4.37	0.05	1.17	0.64	11.86	>4 mm bulk
202-SMW	2630.5	0.50	4.13	0.06	1.27	0.77	13.59	1–4 mm bulk
204-SMW	2640.5	0.34	2.85	0.06	1.00	0.66	11.37	>4 mm bulk
204-SMW	2640.5	0.49	4.07	0.06	1.25	0.76	13.12	1–4 mm bulk
208-SMW	2650.5	0.32	2.67	0.06	0.91	0.59	10.61	>4 mm bulk
208-SMW	2650.5	0.43	3.59	0.06	1.16	0.72	12.10	1–4 mm bulk
210-SMW	2660.5	0.44	3.69	0.05	1.01	0.56	10.44	>4 mm bulk
210-SMW	2660.5	0.43	3.60	0.06	1.09	0.66	11.04	1–4 mm bulk
213-SMW	2670.5	0.38	3.17	0.06	1.09	0.71	12.06	>4 mm bulk
213-SMW	2670.5	0.43	3.54	0.06	1.17	0.74	12.73	1–4 mm bulk
215-SMW	2680.5	0.34	2.83	0.06	1.05	0.71	12.29	>4 mm bulk
215-SMW	2680.5	0.39	3.21	0.06	1.15	0.77	12.94	1–4 mm bulk
217-SMW	2690.5	0.19	1.60	0.06	0.83	0.64	11.06	>4 mm bulk
217-SMW	2690.5	0.26	2.16	0.06	1.00	0.74	12.29	1–4 mm bulk
219-SMW	2700.5	0.23	1.94	0.06	0.84	0.61	10.10	>4 mm bulk
219-SMW	2700.5	0.29	2.44	0.06	1.01	0.71	11.58	1–4 mm bulk
221-SMW	2710.5	0.19	1.56	0.05	0.69	0.51	9.54	>4 mm bulk
221-SMW	2710.5	0.27	2.29	0.06	1.07	0.80	13.62	1–4 mm bulk
224-SMW	2720.5	0.21	1.79	0.06	0.83	0.61	10.34	>4 mm bulk
224-SMW	2720.5	0.25	2.12	0.06	0.95	0.70	11.52	1–4 mm bulk
226-SMW	2730.5	0.09	0.72	0.06	0.74	0.65	11.50	>4 mm bulk
226-SMW	2730.5	0.21	1.78	0.06	0.92	0.71	11.87	1–4 mm bulk
229-SMW	2740.5	0.12	1.01	0.06	0.78	0.66	11.42	>4 mm bulk
229-SMW	2740.5	0.16	1.36	0.06	0.83	0.67	10.80	1–4 mm bulk
231-SMW	2750.5	0.16	1.29	0.06	0.85	0.70	11.96	>4 mm bulk
231-SMW	2750.5	0.23	1.91	0.06	1.00	0.77	12.76	1–4 mm bulk

Table T24 (continued).

Cutting sample number	Depth (mbsf)	IC (wt%)	CaCO$_3$ (wt%)	TN (wt%)	TC (wt%)	TOC (wt%)	C/N	Remarks
233-SMW	2760.5	0.13	1.06	0.06	0.85	0.72	12.26	>4 mm bulk
233-SMW	2760.5	0.15	1.25	0.06	0.92	0.77	12.45	1–4 mm bulk
235-SMW	2770.5	0.18	1.46	0.06	0.92	0.75	12.72	>4 mm bulk
235-SMW	2770.5	0.19	1.55	0.06	0.94	0.75	12.46	1–4 mm bulk
237-SMW	2780.5	0.22	1.85	0.06	1.00	0.78	12.78	>4 mm bulk
237-SMW	2780.5	0.15	1.24	0.06	0.96	0.81	13.43	1–4 mm bulk
240-SMW	2790.5	0.16	1.31	0.06	0.84	0.68	12.27	>4 mm bulk
240-SMW	2790.5	0.23	1.92	0.05	1.01	0.78	14.45	1–4 mm bulk
242-SMW	2800.5	0.42	3.48	0.06	1.14	0.72	12.24	>4 mm bulk
242-SMW	2800.5	0.25	2.07	0.06	1.11	0.86	14.39	1–4 mm bulk
244-SMW	2810.5	0.15	1.29	0.06	0.93	0.78	13.33	>4 mm bulk
244-SMW	2810.5	0.15	1.25	0.06	1.01	0.86	15.49	1–4 mm bulk
247-SMW	2820.5	0.08	0.70	0.06	0.81	0.73	13.13	>4 mm bulk
247-SMW	2820.5	0.19	1.57	0.06	1.00	0.82	13.25	1–4 mm bulk
249-SMW	2830.5	0.06	0.50	0.06	0.85	0.79	13.26	>4 mm bulk
249-SMW	2830.5	0.23	1.91	0.06	1.08	0.85	14.39	1–4 mm bulk
251-SMW	2840.5	0.05	0.43	0.06	0.84	0.78	13.18	>4 mm bulk
251-SMW	2840.5	0.15	1.21	0.06	0.96	0.81	13.98	1–4 mm bulk
254-SMW	2850.5	0.06	0.54	0.06	0.82	0.75	12.83	>4 mm bulk
254-SMW	2850.5	0.21	1.74	0.06	1.00	0.79	13.54	1–4 mm bulk
256-SMW	2860.5	0.08	0.66	0.06	0.80	0.72	12.02	>4 mm bulk
256-SMW	2860.5	0.18	1.46	0.06	0.98	0.80	13.16	1–4 mm bulk
259-SMW	2870.5	0.14	1.20	0.06	0.92	0.78	13.95	>4 mm bulk
259-SMW	2870.5	0.28	2.36	0.05	1.11	0.83	15.30	1–4 mm bulk
261-SMW	2880.5	0.73	6.05	0.06	1.47	0.74	13.32	>4 mm bulk
261-SMW	2880.5	0.29	2.43	0.06	1.08	0.79	13.61	1–4 mm bulk
263-SMW	2890.5	0.11	0.88	0.06	0.84	0.74	12.55	>4 mm bulk
263-SMW	2890.5	0.21	1.72	0.05	0.96	0.75	13.83	1–4 mm bulk
265-SMW	2900.5	0.17	1.39	0.06	0.83	0.66	10.81	>4 mm bulk
265-SMW	2900.5	0.17	1.40	0.06	0.86	0.69	11.33	1–4 mm bulk
267-SMW	2910.5	0.12	0.97	0.06	0.85	0.73	12.87	>4 mm bulk
267-SMW	2910.5	0.19	1.56	0.06	0.90	0.72	12.66	1–4 mm bulk
269-SMW	2920.5	0.16	1.37	0.06	0.83	0.66	11.09	>4 mm bulk
269-SMW	2920.5	0.15	1.28	0.06	0.89	0.74	11.99	1–4 mm bulk
271-SMW	2930.5	0.06	0.46	0.06	0.70	0.64	10.96	>4 mm bulk
271-SMW	2930.5	0.15	1.25	0.06	0.95	0.80	12.94	1–4 mm bulk
273-SMW	2940.5	0.10	0.81	0.06	0.64	0.54	8.95	>4 mm bulk
273-SMW	2940.5	0.18	1.50	0.06	0.85	0.67	10.69	1–4 mm bulk
277-SMW	2950.5	0.36	3.03	0.06	1.01	0.64	11.32	>4 mm bulk
277-SMW	2950.5	0.17	1.44	0.06	0.85	0.68	11.64	1–4 mm bulk
279-SMW	2960.5	0.15	1.22	0.06	0.83	0.68	11.26	>4 mm bulk
279-SMW	2960.5	0.18	1.50	0.06	0.85	0.67	10.82	1–4 mm bulk
281-SMW	2970.5	0.10	0.81	0.06	0.79	0.70	11.61	>4 mm bulk
281-SMW	2970.5	0.22	1.86	0.06	0.96	0.73	12.46	1–4 mm bulk
283-SMW	2980.5	0.09	0.76	0.06	0.72	0.63	10.73	>4 mm bulk
283-SMW	2980.5	0.26	2.18	0.06	0.98	0.72	12.14	1–4 mm bulk
285-SMW	2990.5	0.13	1.10	0.06	0.81	0.68	11.62	>4 mm bulk
285-SMW	2990.5	0.24	2.01	0.06	0.97	0.73	12.38	1–4 mm bulk
289-SMW	3000.5	0.10	0.81	0.06	0.88	0.78	13.46	>4 mm bulk
289-SMW	3000.5	0.19	1.54	0.06	0.98	0.79	13.61	1–4 mm bulk
291-SMW	3010.5	0.08	0.68	0.06	0.82	0.73	11.81	>4 mm bulk
291-SMW	3010.5	0.15	1.28	0.06	0.94	0.78	13.60	1–4 mm bulk
293-SMW	3020.5	0.15	1.25	0.06	0.89	0.74	12.68	>4 mm bulk
293-SMW	3020.5	0.19	1.60	0.06	1.03	0.84	14.83	1–4 mm bulk
296-SMW	3030.5	0.15	1.28	0.06	0.89	0.73	11.75	>4 mm bulk
296-SMW	3030.5	0.17	1.40	0.06	0.98	0.81	13.54	1–4 mm bulk
298-SMW	3040.5	0.17	1.40	0.06	0.93	0.76	13.01	>4 mm bulk
298-SMW	3040.5	0.15	1.23	0.06	1.02	0.88	14.33	1–4 mm bulk
300-SMW	3050.5	0.13	1.05	0.06	0.88	0.75	12.60	>4 mm bulk
300-SMW	3050.5	0.22	1.86	0.06	1.10	0.88	15.85	1–4 mm bulk

IC = inorganic carbon, TN = total nitrogen, TC = total carbon, TOC = total organic carbon. DICA = drilling-induced cohesive aggregate, PP = physical properties.

Table T25. Carbon, nitrogen, and sulfur data, Holes C0002M and C0002P.

Core, section, interval (cm)	Depth (mbsf)	IC (wt%)	$CaCO_3$ (wt%)	TN (wt%)	TC (wt%)	TS (wt%)	TOC (wt%)	TOC/TN	TOC/TS	Remarks
348-C0002M-										
1R-1W, 84–87	475.8	0.7	5.5	0.08	1.3	NA	0.7	9.1	NA	
1R-1WR, 87–107	475.9	0.7	6.1	0.08	1.3	NA	0.6	7.4	NA	From IW
1R-2W, 63–65	477.0	0.7	5.5	0.07	1.3	NA	0.6	8.3	NA	
1R-3W 87–90	478.7	1.6	13.7	0.10	2.3	NA	0.7	6.8	NA	
2R-2W, 107–109	487.0	0.6	4.6	0.06	1.1	NA	0.6	9.8	NA	
2R-2WR, 111–131	487.0	0.7	6.2	0.07	1.3	NA	0.5	7.2	NA	From IW
2R-3W, 65–68	488.0	0.5	4.3	0.08	1.0	NA	0.5	6.9	NA	
3R-1W, 82–84	494.3	0.5	4.6	0.07	1.4	NA	0.8	11.1	NA	
3R-1W, 85–87	494.4	0.8	6.6	0.08	1.3	NA	0.5	6.9	NA	
3R-1WR, 90–110	494.4	0.7	6.2	0.08	1.3	NA	0.5	7.1	NA	From IW
3R-2W, 18–20	495.1	1.1	8.9	0.08	1.6	NA	0.5	6.8	NA	
4R-2W, 42–45	504.8	1.1	8.8	0.08	1.6	NA	0.5	6.2	NA	
4R-2W, 110.5–113	505.5	1.2	10.0	0.09	1.8	NA	0.6	6.8	NA	
4R-2WR, 113–133	505.5	1.2	10.2	0.09	1.8	NA	0.6	6.8	NA	From IW
4R-3W, 66–69	506.5	1.6	13.0	0.06	2.0	NA	0.5	7.3	NA	
348-C0002P-										
1R-1W, 2–5	2163.0	0.5	3.8	0.06	0.9	0.3	0.4	7.2	1.5	
2R-1W, 35–38	2172.9	0.4	3.0	0.06	1.2	0.4	0.8	14.0	1.8	
2R-2W, 43–48	2174.3	0.2	1.4	0.05	0.7	0.2	0.6	11.1	3.3	
2R-3WR, 137.5–141	2176.7	0.3	2.5	0.07	0.9	0.5	0.6	8.6	1.1	IW cluster
2R-4W, 27–31	2177.0	0.2	1.6	0.03	0.7	0.6	0.5	20.1	0.8	Sandy
3R-1W, 35–37	2182.4	0.3	2.1	0.06	1.1	0.4	0.8	14.1	2.1	
3R-2W, 60–63	2184.0	0.4	3.2	0.06	0.9	0.4	0.5	8.1	1.3	
4R-1W, 39–44	2191.9	0.3	2.3	0.07	0.9	0.3	0.7	9.7	2.0	
4R-2W, 135–142	2194.0	0.4	3.3	0.06	1.0	0.4	0.6	10.0	1.4	
4R-3W, 73–77	2194.8	0.2	1.5	0.07	0.7	0.3	0.6	8.2	1.8	
4R-4W, 32–37	2195.3	0.2	1.8	0.07	0.8	0.4	0.6	9.1	1.7	
4R-5W, 125–129	2197.6	0.2	1.7	0.06	0.7	0.4	0.5	8.4	1.3	
4R-6W, 54–60	2198.4	0.1	1.1	0.06	0.5	0.3	0.4	6.2	1.4	
5R-1W, 95–101	2202.0	0.2	1.4	0.06	0.9	0.4	0.7	12.9	2.1	
5R-2W, 99–104	2203.4	0.2	1.6	0.07	1.1	0.5	0.9	12.6	1.6	
5R-3W, 0–7	2203.9	0.2	1.5	0.07	0.7	0.4	0.5	7.8	1.4	
5R-5W, 2–6	2205.6	0.1	0.9	0.02	0.3	0.3	0.2	8.3	0.7	
6R-1W, 77–83	2209.8	0.3	2.2	0.07	0.9	0.4	0.7	9.3	1.8	
6R-2WR, 37–39	2210.8	0.1	1.1	0.07	0.8	0.5	0.6	9.6	1.4	
6R-3W, 37–41	2212.2	0.1	1.2	0.07	0.8	0.6	0.6	9.5	1.0	
6R-4W, 103–108	2214.3	0.2	1.6	0.06	1.4	1.0	1.2	20.2	1.2	
6R-5W, 94–101	2215.6	0.1	0.9	0.06	0.6	0.4	0.5	7.5	1.4	
6R-6W, 62–64	2216.7	0.0	0.2	0.06	0.7	0.6	0.7	11.7	1.2	
6R-6W, 77–84	2216.8	0.2	1.6	0.07	0.8	0.4	0.6	8.8	1.8	

IC = inorganic carbon, TN = total nitrogen, TC = total carbon, TS = total sulfur, TOC = total organic carbon. NA = not analyzed. IW = interstitial water.

Table T26. Hydrocarbon gas composition in headspace gas samples taken from cored material, Hole C0002P.

Core, section	Depth (mbsf)	Headspace gas (ppmv)			$C_1/(C_2 + C_3)$	Headspace gas (µM)		
		Methane	Ethane	Propane		Methane	Ethane	Propane
348-C0002P-								
1R-1	2163.0	6,350.7	191.0	100.5	22	6,932.5	208.5	109.7
2R-1	2173.9	2,271.7	105.8	85.9	12	2,653.5	123.6	100.4
2R-2	2175.3	3,855.2	57.5	24.6	47	5,545.2	82.7	35.4
2R-3	2176.7	20,183.1	221.1	94.5	64	28,068.2	307.4	131.4
2R-4	2178.2	3,511.1	99.9	55.8	23	4,510.6	128.3	71.7
3R-1	2183.4	23,455.2	215.0	95.3	76	33,447.4	306.6	135.9
3R-2	2184.6	6,954.3	283.0	198.7	14	8,770.1	356.9	250.6
4R-1	2192.6	10,675.7	247.5	170.2	26	12,695.2	294.3	202.4
4R-2	2194.0	2,906.6	153.0	135.6	10	3,106.0	163.5	144.9
4R-3	2195.0	3,292.2	238.4	148.0	9	4,052.1	293.5	182.1
4R-4	2196.3	2,527.6	110.0	77.9	13	3,742.5	162.9	115.4
4R-5	2197.9	2,024.8	83.2	61.4	14	2,763.3	113.5	83.8
4R-6	2199.4	2,024.4	92.1	77.0	12	1,307.6	59.5	49.7
5R-1	2202.4	3,835.2	182.1	141.0	12	3,741.5	177.7	137.5
5R-2	2203.8	5,136.2	183.0	139.2	16	5,997.5	213.7	162.6
5R-3	2204.6	8,412.4	90.6	33.0	68	4,987.8	53.7	19.6
5R-4	2205.5	4,548.9	73.0	59.6	34	1,134.4	18.2	14.9
6R-1	2210.4	4,816.4	258.7	211.0	10	3,023.9	162.4	132.5
6R-2	2211.8	4,219.1	197.1	143.7	12	5,739.0	268.1	195.5
6R-3	2213.2	1,703.7	115.7	135.8	7	2,271.2	154.2	181.0
6R-4	2214.6	7,526.9	344.1	246.7	13	5,355.3	244.8	175.5
6R-5	2216.0	4,283.2	155.0	112.5	16	4,996.0	180.8	131.2
6R-6	2217.2	5,130.7	346.9	351.3	7	5,640.7	381.4	386.2

Table T27. Data used for estimating temperature (see Fig. F86), Holes C0002F, C0002N, and C0002P.

Cuttings sample	Depth (m)	TOC (%)	C_1 (%)	C_2 (%)	C_1/C_2	Remarks
348-C0002N-						
14-SMW	925.2	1.36	0.27174	0.00017	1556.9	
166-SMW	1623.2	0.79	0.08943	0.00025	364.9	
177-SMW	1677.8	0.88	0.08828	0.00015	598.0	
222-SMW	1868.4	0.73	0.11698	0.00034	343.4	
259-SMW	2008.6	0.72	0.16064	0.00040	404.8	
276-SMW	2089.2	0.81	0.09153	0.00048	190.9	
348-C0002P-						
16-SMW	1981	0.59	0.02489	0.00014	184.35	
30-SMW	2031	0.54	0.10573	0.00030	352.43	
45-SMW	2081	0.47	0.24647	0.00123	200.38	
58-SMW	2131	0.57	0.08183	0.00041	201.06	
76-SMW	2181	0.67	0.06675	0.00068	98.16	Not plotted
109-SMW	2231	0.56	0.14511	0.00065	222.35	
121-SMW	2281	0.72	0.24548	0.00120	203.85	
131-SMW	2337	0.79	0.10129	0.00074	136.41	
143-SMW	2381	0.73	0.32703	0.00202	161.69	
159-SMW	2441	0.58	0.21806	0.00200	108.77	
348-C0002F-						
40-SMW	1006	1.31	0.70504	0.00059	1194.67	
50-SMW	1051	1.75	0.82581	0.00098	842.03	
64-SMW	1101	1.54	2.90425	0.00439	660.83	
73-SMW	1151	1.60	1.40358	0.00282	498.11	
84-SMW	1201	1.68	1.22606	0.00289	424.85	
96-SMW	1251	1.90	0.10040	0.00021	476.57	1–4 mm fraction
106-SMW	1301	1.85	0.42457	0.00093	455.62	1–4 mm fraction
116-SMW	1351	1.81	1.16992	0.00208	562.05	1–4 mm fraction
130-SMW	1401	1.62	0.25119	0.00043	590.95	
140-SMW	1451	1.62	1.00988	0.00160	632.37	1–4 mm fraction
153-SMW	1501	1.61	0.73485	0.00133	553.62	
167-SMW	1551	1.18	0.42679	0.00077	553.53	
182-SMW	1601	1.43	0.66042	0.00129	513.56	
195-SMW	1651	1.00	0.65044	0.00117	554.25	
207-SMW	1701	1.09	0.36814	0.00079	467.31	
217-SMW	1751	1.16	0.55545	0.00131	424.54	1–4 mm fraction
231-SMW	1801	1.06	0.04306	0.00011	385.09	
250-SMW	1851	1.42	0.31968	0.00085	376.69	
263-SMW	1901	1.00	0.11708	0.00038	305.84	1–4 mm fraction
274-SMW	1951	0.94	0.10245	0.00035	292.02	1–4 mm fraction
289-SMW	2001	1.08	0.15449	0.00069	222.59	

C_1/C_2 ratios are based on GC-NGA data from the SciGas system. TOC = total organic carbon.

Table T28. Moisture and density measurements of bulk cuttings, Holes C0002N and C0002P. (Continued on next four pages.)

Cuttings sample	Depth (mbsf) Top	Depth (mbsf) Bottom	Density (g/cm³) 1–4 mm bulk	Density (g/cm³) 1–4 mm grain	Density (g/cm³) >4 mm bulk	Density (g/cm³) >4 mm grain	Porosity (%) 1–4 mm	Porosity (%) >4 mm	Void ratio 1–4 mm	Void ratio >4 mm
348-C0002N-										
3-SMW	870.5	875.5	1.605	2.348	1.394	2.244	56.09	69.69	1.277	2.299
5-SMW	880.5	885.5	1.676	2.469	1.658	2.326	54.87	51.33	1.216	1.055
7-SMW	890.5	895.5	1.749	2.494	1.716	2.340	50.72	47.38	1.029	0.900
9-SMW	900.5	905.5	1.811	2.577	1.744	2.375	49.36	46.73	0.975	0.877
12-SMW	910.5	915.5	1.827	2.618	1.822	2.529	49.61	46.95	0.985	0.885
14-SMW	920.5	925.5	1.789	2.609	1.793	2.549	51.72	49.56	1.071	0.983
16-SMW	930.5	935.5	1.816	2.629	1.794	2.548	50.66	49.48	1.027	0.979
18-SMW	940.5	945.5	1.846	2.648	1.786	2.544	49.39	49.84	0.976	0.994
20-SMW	950.5	955.5	1.887	2.688	1.848	2.624	48.14	48.47	0.928	0.941
22-SMW	960.5	965.5	1.926	2.691	1.920	2.631	45.92	44.21	0.849	0.792
24-SMW	970.5	975.5	1.920	2.656	1.928	2.640	45.07	44.10	0.821	0.789
26-SMW	980.5	985.5	1.933	2.706	1.888	2.628	45.96	46.14	0.851	0.857
28-SMW	990.5	995.5	1.885	2.650	1.908	2.706	47.03	47.44	0.888	0.903
30-SMW	1000.5	1005.5	1.896	2.664	1.905	2.674	46.82	46.58	0.880	0.872
32-SMW	1010.5	1015.5	1.919	2.675	1.900	2.652	45.82	46.19	0.846	0.858
34-SMW	1020.5	1025.5	1.901	2.680	1.918	2.675	47.04	45.83	0.888	0.846
36-SMW	1030.5	1035.5	1.918	2.681	1.930	2.656	46.09	44.51	0.855	0.802
39-SMW	1040.5	1045.5	1.937	2.678	1.933	2.660	44.79	44.41	0.811	0.799
40-SMW	1045.5	1052.5	1.944	2.665	1.954	2.680	43.95	43.83	0.784	0.780
41-SMW	1052.5	1067.5	1.922	2.673	1.938	2.671	45.54	44.51	0.836	0.802
42-SMW	1067.5	1069.5	1.931	2.668	1.935	2.674	44.82	44.82	0.812	0.812
43-SMW	1069.5	1070.5	1.929	2.683	1.947	2.693	45.46	44.68	0.833	0.808
44-SMW	1070.5	1075.5	1.918	2.663	1.936	2.674	45.45	44.74	0.833	0.810
46-SMW	1080.5	1085.5	1.910	2.664	1.931	2.658	46.02	44.47	0.853	0.801
48-SMW	1090.5	1095.5	1.907	2.673	1.922	2.660	46.46	45.12	0.868	0.822
50-SMW	1100.5	1105.5	1.908	2.672	1.904	2.644	46.38	45.66	0.865	0.840
52-SMW	1110.5	1115.5	1.935	2.702	1.946	2.672	45.71	44.05	0.842	0.787
54-SMW	1120.5	1125.5	1.923	2.659	1.930	2.673	45.01	45.05	0.819	0.820
57-SMW	1130.5	1135.5	1.930	2.669	1.930	2.677	44.96	45.18	0.817	0.824
59-SMW	1140.5	1145.5	1.921	2.643	1.944	2.663	44.62	43.91	0.806	0.783
61-SMW	1150.5	1155.5	1.913	2.673	1.937	2.650	46.08	43.81	0.855	0.780
63-SMW	1160.5	1165.5	1.928	2.678	1.961	2.694	45.35	43.90	0.830	0.783
65-SMW	1170.5	1175.5	1.942	2.663	1.950	2.665	44.00	43.55	0.786	0.771
67-SMW	1180.5	1185.5	1.952	2.648	1.963	2.663	42.85	42.75	0.750	0.747
69-SMW	1190.5	1195.5	1.941	2.674	1.954	2.655	44.41	42.95	0.799	0.753
71-SMW	1200.5	1205.5	1.962	2.675	1.963	2.678	43.17	43.24	0.760	0.762
73-SMW	1210.5	1215.5	1.977	2.674	1.964	2.661	42.22	42.56	0.731	0.741
81-SMW	1218.5	1225.5	1.988	2.653	1.983	2.651	40.84	41.06	0.691	0.697
82-SMW	1225.5	1230.5	1.963	2.683	2.005	2.677	43.42	40.63	0.767	0.684
85-SMW	1240.5	1245.5	1.982	2.676	2.011	2.667	42.00	39.94	0.724	0.665
87-SMW	1250.5	1255.5	1.961	2.642	1.983	2.669	42.10	41.68	0.727	0.715
89-SMW	1260.5	1265.5	1.976	2.665	1.982	2.656	41.97	41.30	0.723	0.704
91-SMW	1270.5	1275.5	1.974	2.654	1.983	2.651	41.74	41.05	0.716	0.696
93-SMW	1280.5	1285.5	2.002	2.691	1.999	2.692	41.37	41.52	0.706	0.710
95-SMW	1290.5	1295.5	1.976	2.671	2.001	2.688	42.21	41.24	0.730	0.702
97-SMW	1300.5	1305.5	1.980	2.687	1.982	2.672	42.53	41.87	0.740	0.720
99-SMW	1310.5	1315.5	1.994	2.664	1.975	2.666	40.87	42.09	0.691	0.727
101-SMW	1320.5	1325.5	1.975	2.689	1.946	2.647	42.89	43.18	0.751	0.760
105-SMW	1330.5	1335.5	1.987	2.701	1.959	2.669	42.56	43.14	0.741	0.759
107-SMW	1340.5	1345.5	1.933	2.633	1.961	2.670	43.54	43.11	0.771	0.758
109-SMW	1350.5	1355.5	1.971	2.665	1.932	2.658	42.29	44.44	0.733	0.800
111-SMW	1360.5	1365.5	1.947	2.653	1.961	2.642	43.35	42.11	0.765	0.727
113-SMW	1370.5	1375.5	1.946	2.624	1.950	2.652	42.39	43.15	0.736	0.759
115-SMW	1380.5	1385.5	2.002	2.683	1.982	2.667	41.04	41.66	0.696	0.714
117-SMW	1390.5	1395.5	1.984	2.647	1.991	2.652	40.82	40.61	0.690	0.684
119-SMW	1400.5	1405.5	1.996	2.645	2.011	2.674	40.06	40.16	0.668	0.671
121-SMW	1410.5	1415.5	1.975	2.628	2.003	2.664	40.71	40.34	0.687	0.676
123-SMW	1420.5	1425.5	2.000	2.672	2.006	2.664	40.76	40.13	0.688	0.670
125-SMW	1430.5	1435.5	2.021	2.685	2.012	2.679	39.99	40.31	0.666	0.675
128-SMW	1440.5	1445.5	2.020	2.663	2.013	2.664	39.23	39.73	0.646	0.659
130-SMW	1450.5	1455.5	2.015	2.641	2.018	2.671	38.68	39.65	0.631	0.657
132-SMW	1460.5	1465.5	2.012	2.676	2.006	2.666	40.19	40.21	0.672	0.673
134-SMW	1470.5	1475.5	2.011	2.661	2.016	2.673	39.70	39.88	0.658	0.663
136-SMW	1480.5	1485.5	2.035	2.670	2.025	2.674	38.57	39.32	0.628	0.648
138-SMW	1490.5	1495.5	2.023	2.674	2.029	2.679	39.43	39.29	0.651	0.647

Table T28 (continued). (Continued on next page.)

Cuttings sample	Depth (mbsf)		Density (g/cm^3)				Porosity (%)		Void ratio	
	Top	Bottom	1–4 mm bulk	1–4 mm grain	>4 mm bulk	>4 mm grain	1–4 mm	>4 mm	1–4 mm	>4 mm
140-SMW	1500.5	1505.5	2.008	2.649	2.023	2.651	39.48	38.62	0.652	0.629
142-SMW	1510.5	1515.5	2.001	2.655	2.031	2.674	40.11	38.98	0.670	0.639
146-SMW	1520.5	1525.5	2.027	2.667	2.012	2.676	38.94	40.19	0.638	0.672
148-SMW	1530.5	1535.5	2.032	2.677	2.044	2.702	39.01	39.20	0.640	0.645
150-SMW	1540.5	1545.5	2.020	2.667	2.038	2.685	39.41	38.97	0.650	0.639
152-SMW	1550.5	1555.5	2.002	2.673	2.033	2.688	40.68	39.35	0.686	0.649
154-SMW	1560.5	1565.5	2.019	2.652	2.073	2.675	38.89	36.48	0.637	0.574
156-SMW	1570.5	1575.5	2.027	2.663	2.040	2.694	38.79	39.17	0.634	0.644
158-SMW	1580.5	1585.5	2.017	2.671	2.046	2.680	39.73	38.27	0.659	0.620
160-SMW	1590.5	1595.5	2.023	2.683	2.026	2.668	39.79	39.02	0.661	0.640
162-SMW	1600.5	1605.5	2.059	2.668	2.018	2.661	37.07	39.28	0.589	0.647
164-SMW	1610.5	1615.5	2.030	2.702	2.052	2.690	40.02	38.31	0.667	0.621
166-SMW	1620.5	1625.5	2.028	2.680	2.037	2.690	39.37	39.17	0.649	0.644
169-SMW	1630.5	1635.5	2.019	2.693	2.030	2.683	40.42	39.34	0.678	0.649
171-SMW	1640.5	1645.5	2.087	2.656	2.081	2.656	34.88	35.26	0.536	0.545
173-SMW	1650.5	1655.5	2.062	2.650	2.053	2.675	36.19	37.66	0.567	0.604
175-SMW	1660.5	1665.5	2.005	2.676	2.028	2.672	40.62	39.06	0.684	0.641
177-SMW	1670.5	1677.5	1.991	2.681	2.042	2.683	41.68	38.61	0.715	0.629
182-SMW	1680.5	1685.5	2.008	2.693	2.148	2.679	41.02	32.06	0.696	0.472
184-SMW	1690.5	1695.5	2.028	2.677	2.069	2.618	39.25	34.45	0.646	0.526
186-SMW	1700.5	1705.5	2.013	2.673	2.060	2.677	40.02	37.32	0.667	0.595
188-SMW	1710.5	1715.5	2.036	2.682	2.126	2.717	38.98	34.96	0.639	0.538
190-SMW	1720.5	1725.5	2.019	2.695	2.047	2.664	40.49	37.61	0.680	0.603
192-SMW	1730.5	1735.5	2.010	2.687	2.087	2.674	40.67	35.59	0.686	0.553
195-SMW	1740.5	1745.5	2.017	2.682	2.041	2.694	40.13	39.12	0.670	0.643
197-SMW	1750.5	1755.5	2.018	2.680	2.072	2.670	39.98	36.33	0.666	0.571
199-SMW	1760.5	1765.5	2.011	2.687	2.041	2.680	40.65	38.61	0.685	0.629
201-SMW	1770.5	1775.5	2.005	2.687	2.057	2.681	41.03	37.69	0.696	0.605
203-SMW	1780.5	1785.5	2.005	2.667	2.033	2.675	40.29	38.88	0.675	0.636
205-SMW	1790.5	1795.5	2.002	2.670	2.042	2.684	40.55	38.68	0.682	0.631
207-SMW	1800.5	1805.5	1.988	2.682	2.045	2.713	41.83	39.56	0.719	0.655
209-SMW	1810.5	1815.5	2.007	2.700	2.024	2.709	41.32	40.64	0.704	0.685
211-SMW	1820.5	1825.5	2.012	2.715	2.216	2.817	41.58	33.55	0.712	0.505
213-SMW	1830.5	1835.5	2.010	2.687	2.031	2.677	40.68	39.08	0.686	0.641
216-SMW	1840.5	1845.5	2.010	2.679	2.047	2.703	40.44	39.07	0.679	0.641
218-SMW	1850.5	1855.5	1.996	2.680	2.017	2.676	41.31	39.89	0.704	0.664
220-SMW	1860.5	1865.5	2.005	2.713	2.045	2.694	41.91	38.86	0.721	0.636
222-SMW	1870.5	1875.5	2.013	2.705	2.050	2.687	41.14	38.27	0.699	0.620
224-SMW	1880.5	1885.5	2.014	2.732	2.040	2.709	42.08	39.69	0.727	0.658
226-SMW	1890.5	1895.5	1.947	2.668	2.037	2.689	43.90	39.17	0.782	0.644
228-SMW	1900.5	1905.5	1.990	2.709	2.041	2.712	42.69	39.73	0.745	0.659
230-SMW	1910.5	1915.5	1.998	2.717	2.020	2.700	42.48	40.56	0.739	0.682
232-SMW	1920.5	1925.5	1.991	2.714	2.019	2.720	42.76	41.34	0.747	0.705
234-SMW	1930.5	1935.5	1.998	2.699	2.026	2.717	41.84	40.85	0.719	0.691
237-SMW	1940.5	1945.5	1.994	2.730	2.009	2.692	43.16	40.96	0.759	0.694
239-SMW	1950.5	1955.5	1.990	2.718	2.027	2.705	42.98	40.34	0.754	0.676
241-SMW	1960.5	1965.5	2.009	2.722	2.025	2.734	41.96	41.45	0.723	0.708
243-SMW	1970.5	1975.5	1.986	2.689	2.041	2.720	42.19	40.03	0.730	0.668
248-SMW	1980.5	1985.5	1.992	2.686	2.015	2.689	41.80	40.47	0.718	0.680
250-SMW	1990.5	1995.5	1.961	2.681	2.002	2.672	43.48	40.62	0.769	0.684
252-SMW	2000.5	2005.5	1.999	2.721	2.023	2.733	42.54	41.54	0.740	0.711
259-SMW	2010.5	2015.5	2.260	2.689	2.263	2.678	25.75	25.06	0.347	0.334
261-SMW	2020.5	2025.5	2.253	2.663	2.280	2.688	25.04	24.50	0.334	0.325
264-SMW	2030.5	2035.5	2.249	2.672	2.263	2.703	25.68	26.23	0.346	0.356
266-SMW	2040.5	2045.5	2.096	2.631	2.292	2.707	33.26	24.66	0.498	0.327
268-SMW	2050.5	2055.5	2.038	2.623	2.333	2.712	36.59	22.45	0.577	0.289
270-SMW	2060.5	2065.5	2.030	2.683	2.164	2.684	39.36	31.33	0.649	0.456
272-SMW	2070.5	2075.5	2.058	2.703	2.252	2.694	38.44	26.49	0.624	0.360
274-SMW	2080.5	2085.5	2.051	2.687	2.158	2.673	38.22	31.23	0.619	0.454
276-SMW	2090.5	2095.5	2.046	2.675	2.151	2.686	38.10	32.18	0.615	0.474
278-SMW	2100.5	2105.5	2.039	2.691	2.063	2.671	39.14	36.90	0.643	0.585
281-SMW	2110.5	2115.5	2.047	2.681	2.089	2.688	38.28	36.00	0.620	0.563
283-SMW	2120.5	2125.5	2.010	2.655	2.081	2.683	39.56	36.30	0.655	0.570
285-SMW	2130.5	2135.5	2.002	2.640	2.047	2.681	39.50	38.25	0.653	0.619
287-SMW	2140.5	2145.5	2.028	2.672	2.098	2.698	39.05	35.83	0.641	0.558
289-SMW	2150.5	2155.5	2.023	2.693	2.068	2.682	40.11	37.06	0.670	0.589
291-SMW	2160.5	2165.5	2.045	2.722	2.082	2.689	39.87	36.47	0.663	0.574
296-SMW	2170.5	2175.5	2.043	2.705	2.073	2.703	39.39	37.50	0.650	0.600

Table T28 (continued). (Continued on next page.)

Cuttings sample	Depth (mbsf)		Density (g/cm^3)				Porosity (%)		Void ratio	
	Top	Bottom	1–4 mm bulk	1–4 mm grain	>4 mm bulk	>4 mm grain	1–4 mm	>4 mm	1–4 mm	>4 mm
298-SMW	2180.5	2185.5	2.030	2.701	2.093	2.685	40.01	35.64	0.667	0.554
300-SMW	2190.5	2195.5	2.029	2.672	2.065	2.681	39.04	37.19	0.641	0.592
302-SMW	2200.5	2205.5	2.017	2.680	2.059	2.678	40.01	37.45	0.667	0.599
304-SMW	2210.5	2215.5	2.046	2.694	2.143	2.697	38.78	33.13	0.634	0.495
306-SMW	2220.5	2225.5	2.057	2.689	2.062	2.678	37.95	37.25	0.612	0.594
308-SMW	2230.5	2235.5	2.008	2.669	2.036	2.687	40.19	39.14	0.672	0.643
310-SMW	2240.5	2245.5	2.037	2.671	2.065	2.691	38.46	37.54	0.625	0.601
312-SMW	2250.5	2255.5	2.036	2.684	2.073	2.669	39.02	36.24	0.640	0.568
314-SMW	2260.5	2265.5	2.044	2.687	2.108	2.676	38.66	34.36	0.630	0.523
316-SMW	2270.5	2275.5	2.030	2.690	2.062	2.682	39.59	37.41	0.656	0.598
318-SMW	2280.5	2285.5	2.016	2.673	2.081	2.692	39.83	36.65	0.662	0.579
348-C0002P-										
9-SMW	1960.5	1965.5	1.859	2.673	2.117	2.671	49.34	33.63	0.974	0.507
14-SMW	1970.5	1975.5	1.876	2.655	1.945	2.694	47.79	44.81	0.915	0.812
16-SMW	1980.5	1985.5	1.911	2.678	2.020	2.742	46.38	42.03	0.865	0.725
18-SMW	1990.5	1995.5	1.969	2.691	2.039	2.640	43.29	37.22	0.763	0.593
20-SMW	2000.5	2005.5	1.966	2.678	2.034	2.677	43.03	38.91	0.755	0.637
25-SMW	2010.5	2015.5	1.934	2.634	1.986	2.700	43.46	42.59	0.769	0.742
28-SMW	2020.5	2025.5	1.911	2.681	1.988	2.692	46.47	42.21	0.868	0.730
30-SMW	2030.5	2035.5	1.946	2.729	1.967	2.697	45.95	43.62	0.850	0.774
32-SMW	2040.5	2045.5	2.001	2.709	2.016	2.734	42.01	41.99	0.724	0.724
34-SMW	2050.5	2055.5	1.953	2.684	2.058	2.729	44.03	39.39	0.787	0.650
36-SMW	2060.5	2065.5	1.977	2.727	2.043	2.693	44.02	38.93	0.786	0.638
43-SMW	2070.5	2075.5	1.947	2.708	2.148	2.735	45.23	34.34	0.826	0.523
45-SMW	2080.5	2085.5	1.981	2.718	2.051	2.733	43.50	39.89	0.770	0.664
47-SMW	2090.5	2095.5	1.948	2.758	2.041	2.750	46.70	41.08	0.876	0.697
49-SMW	2100.5	2105.5	2.027	2.731	2.064	2.706	41.26	38.18	0.702	0.618
53-SMW	2110.5	2115.5	1.924	2.737	2.046	2.714	47.43	39.54	0.902	0.654
56-SMW	2120.5	2125.5	1.943	2.715	2.047	2.707	45.68	39.18	0.841	0.644
58-SMW	2130.5	2135.5	1.963	2.720	2.191	2.719	44.61	31.15	0.806	0.452
61-SMW	2140.5	2145.5	1.984	2.706	2.055	2.707	42.88	38.73	0.751	0.632
63-SMW	2150.5	2155.5	1.992	2.690	2.066	2.704	41.89	37.94	0.721	0.611
71-SMW	2162.5	2165.5	2.082	2.720	2.298	2.681	37.61	23.11	0.603	0.301
92-SMW	2162.5	2165.5	2.233	2.672	2.344	2.693	26.61	20.94	0.363	0.265
72-SMW	2165.5	2170.5	2.070	2.680	2.270	2.686	36.85	25.02	0.584	0.334
73-SMW	2170.5	2175.5	2.031	2.681	2.229	2.686	39.24	27.49	0.646	0.379
94-SMW	2170.5	2175.5	2.199	2.689	2.364	2.704	29.44	20.27	0.417	0.254
74-SMW	2175.5	2180.5	2.059	2.697	2.261	2.678	38.16	25.17	0.617	0.336
76-SMW	2180.5	2185.5	2.071	2.698	2.340	2.683	37.46	20.66	0.599	0.260
96-SMW	2180.5	2185.5	2.259	2.695	2.339	2.683	26.08	20.72	0.353	0.261
77-SMW	2185.5	2190.5	1.963	2.688	2.202	2.684	43.58	29.00	0.772	0.408
81-SMW	2190.5	2195.5	2.039	2.680	2.315	2.687	38.68	22.39	0.631	0.288
98-SMW	2190.5	2195.5	2.245	2.682	2.358	2.702	26.36	20.50	0.358	0.258
82-SMW	2195.5	2200.5	1.993	2.701	2.235	2.696	42.20	27.54	0.730	0.380
83-SMW	2200.5	2205.5	1.988	2.680	2.293	2.676	41.77	23.22	0.717	0.302
100-SMW	2200.5	2205.5	2.214	2.679	2.352	2.688	28.06	20.18	0.390	0.253
85-SMW	2205.5	2210.5	1.983	2.715	2.155	2.674	43.29	31.49	0.763	0.460
86-SMW	2210.5	2215.5	1.992	2.686	2.287	2.709	41.73	25.05	0.716	0.334
102-SMW	2210.5	2215.5	2.221	2.719	2.331	2.681	29.37	21.11	0.416	0.268
107-SMW	2220.5	2225.5	2.227	2.708	2.349	2.704	28.53	21.17	0.399	0.269
109-SMW	2230.5	2235.5	2.048	2.753	2.190	2.707	40.77	30.74	0.688	0.444
111-SMW	2240.5	2245.5	2.010	2.707	2.081	2.697	41.40	36.82	0.707	0.583
113-SMW	2250.5	2255.5	2.039	2.708	2.182	2.745	39.73	32.70	0.659	0.486
115-SMW	2260.5	2265.5	2.054	2.731	2.206	2.704	39.68	29.64	0.658	0.421
117-SMW	2270.5	2275.5	2.030	2.689	2.091	2.705	39.62	36.52	0.656	0.575
121-SMW	2280.5	2285.5	1.952	2.735	2.090	2.705	45.77	36.60	0.844	0.577
123-SMW	2290.5	2295.5	1.947	2.701	2.052	2.684	44.99	38.11	0.818	0.616
125-SMW	2300.5	2305.5	1.990	2.767	2.040	2.680	44.60	38.65	0.805	0.630
127-SMW	2310.5	2315.5	1.987	2.697	2.081	2.677	42.47	36.06	0.738	0.564
129-SMW	2320.5	2325.5	2.011	2.758	2.060	2.706	43.07	38.37	0.756	0.623
131-SMW	2330.5	2335.5	1.972	2.688	2.058	2.674	43.02	37.35	0.755	0.596
133-SMW	2340.5	2345.5	1.987	2.718	2.015	2.704	43.13	41.03	0.758	0.696
136-SMW	2350.5	2355.5	2.003	2.686	2.047	2.712	41.08	39.42	0.697	0.651
138-SMW	2360.5	2365.5	2.024	2.681	2.030	2.653	39.64	38.22	0.657	0.619
141-SMW	2370.5	2375.5	2.025	2.686	2.054	2.671	39.73	37.47	0.659	0.599
143-SMW	2380.5	2385.5	2.019	2.717	2.071	2.697	41.21	37.44	0.701	0.599
145-SMW	2390.5	2395.5	2.007	2.705	2.051	2.681	41.53	38.01	0.710	0.613
149-SMW	2400.5	2405.5	2.004	2.666	2.047	2.683	40.32	38.31	0.676	0.621

Table T28 (continued). (Continued on next page.)

Cuttings sample	Depth (mbsf)		Density (g/cm^3)				Porosity (%)		Void ratio	
	Top	Bottom	1–4 mm bulk	1–4 mm grain	>4 mm bulk	>4 mm grain	1–4 mm	>4 mm	1–4 mm	>4 mm
151-SMW	2410.5	2415.5	2.028	2.682	2.074	2.682	39.40	36.69	0.650	0.580
155-SMW	2420.5	2425.5	2.020	2.701	2.077	2.675	40.58	36.21	0.683	0.568
157-SMW	2430.5	2435.5	2.012	2.686	2.081	2.687	40.57	36.44	0.683	0.573
159-SMW	2440.5	2445.5	2.000	2.644	2.088	2.675	39.74	35.57	0.660	0.552
161-SMW	2450.5	2455.5	2.002	2.681	2.088	2.699	40.98	36.46	0.694	0.574
163-SMW	2460.5	2465.5	1.998	2.664	2.075	2.689	40.62	36.85	0.684	0.584
165-SMW	2470.5	2475.5	2.007	2.685	2.095	2.700	40.83	36.08	0.690	0.564
168-SMW	2480.5	2485.5	2.003	2.698	2.062	2.698	41.51	38.00	0.710	0.613
170-SMW	2490.5	2495.5	2.010	2.709	2.083	2.701	41.46	36.81	0.708	0.583
172-SMW	2500.5	2505.5	1.986	2.696	2.033	2.688	42.45	39.34	0.738	0.649
174-SMW	2510.5	2515.5	1.972	2.700	2.053	2.728	43.43	39.61	0.768	0.656
176-SMW	2520.5	2525.5	1.996	2.710	2.040	2.687	42.37	38.89	0.735	0.636
179-SMW	2530.5	2535.5	2.029	2.697	2.125	2.733	39.90	35.61	0.664	0.553
181-SMW	2540.5	2545.5	2.029	2.708	2.053	2.686	40.30	38.11	0.675	0.616
183-SMW	2550.5	2555.5	2.030	2.692	2.119	2.716	39.72	35.29	0.659	0.545
185-SMW	2560.5	2565.5	2.035	2.726	2.102	2.719	40.62	36.41	0.684	0.573
187-SMW	2570.5	2575.5	2.000	2.698	2.138	2.692	41.67	33.23	0.714	0.498
189-SMW	2580.5	2585.5	2.040	2.758	2.055	2.704	41.42	38.62	0.707	0.629
191-SMW	2590.5	2595.5	1.982	2.712	2.063	2.699	43.22	37.97	0.761	0.612
196-SMW	2601.5	2605.5	1.983	2.700	2.339	2.713	42.79	22.16	0.748	0.285
198-SMW	2610.5	2615.5	1.942	2.703	2.128	2.689	45.35	33.68	0.830	0.508
200-SMW	2620.5	2625.5	2.002	2.702	2.105	2.687	41.73	35.02	0.716	0.539
202-SMW	2630.5	2635.5	1.994	2.735	2.026	2.702	43.29	40.28	0.763	0.675
204-SMW	2640.5	2645.5	1.982	2.701	2.121	2.693	42.91	34.25	0.752	0.521
208-SMW	2650.5	2655.5	2.004	2.716	2.095	2.729	42.08	37.21	0.726	0.593
210-SMW	2660.5	2665.5	1.944	2.729	2.032	2.693	46.03	39.63	0.853	0.657
213-SMW	2670.5	2675.5	1.956	2.703	2.025	2.688	44.49	39.84	0.802	0.662
215-SMW	2680.5	2685.5	1.958	2.709	2.120	2.719	44.59	35.30	0.805	0.546
217-SMW	2690.5	2695.5	1.948	2.751	2.019	2.689	46.48	40.25	0.868	0.674
219-SMW	2700.5	2705.5	1.888	2.692	2.034	2.707	48.20	40.03	0.931	0.667
221-SMW	2710.5	2715.5	1.863	2.712	2.057	2.729	50.28	39.44	1.011	0.651
224-SMW	2720.5	2725.5	1.884	2.726	2.032	2.717	49.46	40.48	0.979	0.680
226-SMW	2730.5	2735.5	1.918	2.779	1.966	2.693	49.06	43.54	0.963	0.771
229-SMW	2740.5	2745.5	1.834	2.750	2.028	2.720	53.09	40.79	1.132	0.689
231-SMW	2750.5	2755.5	1.922	2.738	2.059	2.731	47.62	39.38	0.909	0.650
233-SMW	2760.5	2765.5	1.920	2.707	2.015	2.690	46.75	40.51	0.878	0.681
235-SMW	2770.5	2775.5	1.875	2.695	1.997	2.705	49.08	42.16	0.964	0.729
237-SMW	2780.5	2785.5	1.947	2.734	2.008	2.712	46.03	41.73	0.853	0.716
240-SMW	2790.5	2795.5	1.908	2.700	2.015	2.755	47.26	42.75	0.896	0.747
242-SMW	2800.5	2805.5	1.925	2.683	1.982	2.709	45.68	43.14	0.841	0.759
244-SMW	2810.5	2815.5	1.936	2.715	1.988	2.711	46.10	42.84	0.855	0.749
247-SMW	2820.5	2825.5	1.885	2.707	1.992	2.701	48.81	42.28	0.954	0.732
249-SMW	2830.5	2835.5	1.953	2.713	2.027	2.707	44.99	40.42	0.818	0.678
251-SMW	2840.5	2845.5	1.922	2.691	2.087	2.700	46.11	36.57	0.856	0.576
254-SMW	2850.5	2855.5	1.873	2.700	1.980	2.697	49.36	42.84	0.975	0.750
256-SMW	2860.5	2865.5	1.926	2.727	1.995	2.705	47.05	42.25	0.888	0.732
259-SMW	2870.5	2875.5	1.922	2.703	2.000	2.680	46.53	41.08	0.870	0.697
261-SMW	2880.5	2885.5	1.944	2.680	2.022	2.706	44.42	40.63	0.799	0.684
263-SMW	2890.5	2895.5	1.901	2.716	2.056	2.698	48.16	38.34	0.929	0.622
265-SMW	2900.5	2905.5	1.885	2.704	2.003	2.707	48.74	41.82	0.951	0.719
267-SMW	2910.5	2915.5	1.933	2.685	2.048	2.702	45.25	38.99	0.827	0.639
269-SMW	2920.5	2925.5	1.876	2.693	2.157	2.708	48.95	32.70	0.959	0.486
271-SMW	2930.5	2935.5	1.924	2.712	1.987	2.684	46.68	41.97	0.876	0.723
273-SMW	2940.5	2945.5	1.921	2.747	2.135	2.712	47.97	34.17	0.922	0.519
279-SMW	2960.5	2965.5	1.946	2.713	2.117	2.708	45.44	35.08	0.833	0.540
281-SMW	2970.5	2975.5	1.915	2.717	2.008	2.710	47.40	41.66	0.901	0.714
283-SMW	2980.5	2985.5	1.935	2.717	2.101	2.745	46.20	37.43	0.859	0.598
285-SMW	2990.5	2995.5	1.884	2.706	2.107	2.716	48.86	35.97	0.955	0.562
289-SMW	3000.5	3005.5	1.984	2.732	2.007	2.723	43.76	42.16	0.778	0.729
291-SMW	3010.5	3015.5	1.917	2.705	2.023	2.728	46.85	41.37	0.882	0.706
293-SMW	3020.5	3025.5	1.938	2.701	1.993	2.691	45.48	41.84	0.834	0.720
296-SMW	3030.5	3035.5	1.884	2.702	2.019	2.707	48.77	40.89	0.952	0.692
298-SMW	3040.5	3045.5	1.926	2.714	1.985	2.703	46.63	42.74	0.874	0.746
300-SMW	3050.5	3058.5	1.933	2.684	2.006	2.721	45.21	42.11	0.825	0.727
348-C0002P- (reaming)										
321-SMW	2105.5	2115.5	2.269	2.191	2.710	2.685	26.16	29.73	0.354	0.423
325-SMW	2145.5	2155.5	2.280	2.286	2.691	2.688	24.70	24.12	0.328	0.318
331-SMW	2185.5	2195.5	2.210	2.345	2.666	2.695	27.79	20.95	0.385	0.265

Table T28 (continued).

Cuttings sample	Depth (mbsf)		Density (g/cm^3)				Porosity (%)		Void ratio	
	Top	Bottom	1–4 mm bulk	1–4 mm grain	>4 mm bulk	>4 mm grain	1–4 mm	>4 mm	1–4 mm	>4 mm
335-SMW	2225.5	2235.5	2.247	2.341	2.705	2.715	27.29	22.15	0.375	0.285
340-SMW	2265.5	2275.5	2.161	2.324	2.708	2.693	32.51	22.12	0.482	0.284
345-SMW	2305.5	2315.5	2.273	2.354	2.697	2.680	25.37	19.68	0.340	0.245
349-SMW	2345.5	2355.5	2.320	2.324	2.697	2.663	22.54	20.69	0.291	0.261
356-SMW	2385.5	2395.5	2.207	2.348	2.686	2.704	28.82	21.16	0.405	0.268
360-SMW	2425.5	2435.5	2.273	2.367	2.691	2.690	25.11	19.41	0.335	0.241
365-SMW	2465.5	2475.5	2.265	2.339	2.696	2.683	25.79	20.75	0.348	0.262
370-SMW	2505.5	2515.5	2.297	2.376	2.697	2.698	23.89	19.23	0.314	0.238
374-SMW	2545.5	2555.5	2.282	2.393	2.685	2.685	24.25	17.57	0.320	0.213
381-SMW	2585.5	2595.5	2.312	2.368	2.695	2.702	22.93	19.88	0.298	0.248
383-SMW	2605.5	2615.5	2.329	2.688	2.402	2.708	21.59	18.20	0.275	0.223
387-SMW	2625.5	2635.5	2.314	2.732	2.410	2.744	24.43	19.42	0.323	0.241
389-SMW	2645.5	2655.5	2.325	2.711	2.404	2.708	22.88	18.05	0.297	0.220
391-SMW	2665.5	2675.5	2.357	2.703	2.432	2.731	20.59	17.53	0.259	0.213
393-SMW	2685.5	2695.5	2.380	2.703	2.431	2.719	19.24	16.98	0.238	0.205
399-SMW	2725.5	2735.5	2.360	2.689	2.434	2.702	19.73	15.99	0.246	0.190
403-SMW	2765.5	2775.5	2.393	2.696	2.426	2.689	18.12	15.80	0.221	0.188
407-SMW	2805.5	2815.5	2.402	2.707	2.434	2.718	18.10	21.59	18.20	0.275
413-SMW	2845.5	2855.5	2.427	2.711	2.442	2.718	16.82	24.43	19.42	0.323

Table T29. Moisture and density measurements of >4 mm handpicked intact cuttings for Holes C0002N and C0002P. (Continued on next page.)

Cuttings sample	Depth (mbsf)		Density (g/cm^3)		Porosity (%)	Void ratio	Comment
	Top	Bottom	bulk	grain			
348-C0002N-							
82-SMW	1225.5	1230.5	2.059	2.667	37.03	0.588	
89-SMW	1260.5	1265.5	2.048	2.572	33.87	0.512	
140-SMW	1500.5	1505.5	2.094	2.635	33.55	0.505	
153-SMW	1555.5	1560.5	2.208	2.631	26.34	0.358	
156-SMW	1570.5	1575.5	2.183	2.717	31.57	0.462	
163-SMW	1605.5	1610.5	2.172	2.684	30.84	0.446	
176-SMW	1665.5	1670.5	2.152	2.630	29.75	0.424	
185-SMW	1695.5	1700.5	2.198	2.718	30.70	0.443	
186-SMW	1700.5	1705.5	2.195	2.638	27.44	0.378	
196-SMW	1745.5	1750.5	2.202	2.672	28.52	0.399	
206-SMW	1795.5	1800.5	2.229	2.672	26.89	0.368	
219-SMW	1855.5	1860.5	2.217	2.648	26.54	0.361	
227-SMW	1895.5	1900.5	2.209	2.651	27.15	0.373	
374-SMW	1945.5	1960.5	2.251	2.680	25.91	0.350	
251-SMW	1995.5	2000.5	2.219	2.663	27.02	0.370	
264-SMW	2030.5	2035.5	2.287	2.717	25.40	0.340	
268-SMW	2050.5	2055.5	2.307	2.716	24.20	0.319	
272-SMW	2070.5	2075.5	2.317	2.695	22.60	0.292	
276-SMW	2090.5	2095.5	2.321	2.713	23.16	0.301	
281-SMW	2110.5	2115.5	2.298	2.727	25.21	0.337	
291-SMW	2160.5	2165.5	2.323	2.719	23.36	0.305	
298-SMW	2180.5	2185.5	2.322	2.706	22.82	0.296	
300-SMW	2190.5	2195.5	2.369	2.744	21.81	0.279	
310-SMW	2240.5	2245.5	2.338	2.714	22.23	0.286	
348-C0002P-							
9-SMW	1960.5	1965.5	2.316	2.696	22.70	0.294	
16-SMW	1980.5	1985.5	2.292	2.691	23.94	0.315	
18-SMW	1990.5	1995.5	2.340	2.747	23.61	0.309	
25-SMW	2010.5	2015.5	2.297	2.730	25.42	0.341	
28-SMW	2020.5	2025.5	2.346	2.735	22.75	0.295	
34-SMW	2050.5	2055.5	2.334	2.719	22.66	0.293	
36-SMW	2060.5	2065.5	2.321	2.698	22.53	0.291	
43-SMW	2070.5	2075.5	2.344	2.744	23.26	0.303	
45-SMW	2080.5	2085.5	2.319	2.711	23.27	0.303	
49-SMW	2100.5	2105.5	2.304	2.720	24.50	0.325	
56-SMW	2120.5	2125.5	2.335	2.754	24.23	0.320	
58-SMW	2130.5	2135.5	2.370	2.742	21.65	0.276	
61-SMW	2140.5	2145.5	2.329	2.715	22.79	0.295	
63-SMW	2150.5	2155.5	2.388	2.798	23.09	0.300	
71-SMW	2162.5	2165.5	2.342	2.678	20.30	0.255	
72-SMW	2165.5	2170.5	2.301	2.679	22.85	0.296	Sand
72-SMW	2165.5	2170.5	2.361	2.700	20.26	0.254	Mud
73-SMW	2170.5	2175.5	2.372	2.693	19.25	0.238	
74-SMW	2175.5	2180.5	2.375	2.692	19.02	0.235	Sand
74-SMW	2175.5	2180.5	2.368	2.700	19.78	0.247	Mud
76-SMW	2180.5	2185.5	2.339	2.690	21.05	0.267	
77-SMW	2185.5	2190.5	2.391	2.715	19.14	0.237	Sand
77-SMW	2185.5	2190.5	2.365	2.712	20.56	0.259	Mud
81-SMW	2190.5	2195.5	2.332	2.706	22.24	0.286	
82-SMW	2195.5	2200.5	2.325	2.682	21.51	0.274	Sand
82-SMW	2195.5	2200.5	2.369	2.710	20.00	0.253	Mud
83-SMW	2200.5	2205.5	2.372	2.726	20.83	0.263	
83-SMW	2200.5	2205.5	2.355	2.705	20.84	0.263	
85-SMW	2205.5	2210.5	2.317	2.674	21.60	0.276	Sand
85-SMW	2205.5	2210.5	2.356	2.706	20.82	0.263	Mud
86-SMW	2210.5	2215.5	2.366	2.718	20.78	0.262	
86-SMW	2210.5	2215.5	2.333	2.687	21.26	0.270	
107-SMW	2220.5	2225.5	2.373	2.712	20.10	0.252	
109-SMW	2230.5	2235.5	2.365	2.715	20.68	0.261	
111-SMW	2240.5	2245.5	2.371	2.737	21.38	0.272	
113-SMW	2250.5	2255.5	2.356	2.707	20.81	0.263	
115-SMW	2260.5	2265.5	2.327	2.694	21.95	0.281	
117-SMW	2270.5	2275.5	2.364	2.742	22.01	0.282	Mud
121-SMW	2280.5	2285.5	2.370	2.733	21.22	0.269	Sand
123-SMW	2290.5	2295.5	2.368	2.719	20.73	0.262	Mud
125-SMW	2300.5	2305.5	2.355	2.714	21.22	0.269	Sand

Table T29 (continued).

Cuttings sample	Depth (mbsf)		Density (g/cm^3)		Porosity (%)	Void ratio	Comment
	Top	Bottom	bulk	grain			
129-SMW	2320.5	2325.5	2.379	2.763	22.08	0.283	Mud
133-SMW	2340.5	2345.5	2.341	2.711	21.97	0.282	Sand
138-SMW	2360.5	2365.5	2.371	2.726	20.87	0.264	Mud
143-SMW	2380.5	2385.5	2.337	2.708	22.01	0.282	Sand
155-SMW	2420.5	2425.5	2.327	2.690	21.80	0.279	
159-SMW	2440.5	2445.5	2.327	2.699	22.20	0.285	Mud
163-SMW	2460.5	2465.5	2.381	2.726	20.28	0.254	Sand
163-SMW	2460.5	2465.5	2.354	2.712	21.20	0.269	Silt
168-SMW	2480.5	2485.5	2.367	2.704	20.03	0.250	Sand
168-SMW	2480.5	2485.5	2.333	2.684	21.13	0.268	Sand
172-SMW	2500.5	2505.5	2.399	2.743	19.98	0.250	Mud
172-SMW	2500.5	2505.5	2.276	2.680	24.36	0.322	Mud
176-SMW	2520.5	2525.5	2.375	2.713	19.98	0.250	Sand
176-SMW	2520.5	2525.5	2.313	2.687	22.48	0.290	
181-SMW	2540.5	2545.5	2.373	2.721	20.52	0.258	Sand
185-SMW	2560.5	2565.5	2.364	2.701	20.12	0.252	Mud
185-SMW	2560.5	2565.5	2.301	2.673	22.58	0.292	
189-SMW	2580.5	2585.5	2.362	2.720	21.10	0.267	Silt
189-SMW	2580.5	2585.5	2.331	2.709	22.44	0.289	
196-SMW	2601.5	2605.5	2.356	2.712	21.09	0.267	Mud
196-SMW	2601.5	2605.5	2.376	2.724	20.52	0.258	
200-SMW	2620.5	2625.5	2.382	2.718	19.83	0.247	
200-SMW	2620.5	2625.5	2.349	2.699	20.90	0.264	
204-SMW	2640.5	2645.5	2.372	2.714	20.24	0.254	Mud
210-SMW	2660.5	2665.5	2.376	2.743	21.34	0.271	Sand
210-SMW	2660.5	2665.5	2.398	2.700	18.03	0.220	
215-SMW	2680.5	2685.5	2.394	2.697	18.12	0.221	
224-SMW	2720.5	2725.5	2.417	2.738	18.72	0.230	
231-SMW	2750.5	2755.5	2.392	2.720	19.38	0.240	Sand
235-SMW	2770.5	2775.5	2.387	2.719	19.60	0.244	Mud
240-SMW	2790.5	2795.5	2.411	2.717	18.11	0.221	
244-SMW	2810.5	2815.5	2.398	2.714	18.69	0.230	
247-SMW	2820.5	2825.5	2.407	2.723	18.61	0.229	
249-SMW	2830.5	2835.5	2.416	2.703	17.11	0.207	Sand
249-SMW	2830.5	2835.5	2.418	2.728	18.21	0.223	Mud
256-SMW	2860.5	2865.5	2.412	2.711	17.69	0.215	
263-SMW	2890.5	2895.5	2.378	2.740	21.12	0.268	
267-SMW	2910.5	2915.5	2.433	2.743	18.05	0.220	
269-SMW	2920.5	2925.5	2.399	2.708	18.34	0.225	Sand
269-SMW	2920.5	2925.5	2.458	2.756	17.19	0.208	Mud
273-SMW	2940.5	2945.5	2.441	2.743	17.56	0.213	
279-SMW	2960.5	2965.5	2.421	2.748	18.95	0.234	
289-SMW	3000.5	3005.5	2.451	2.756	17.59	0.214	
293-SMW	3020.5	3025.5	2.425	2.729	17.79	0.217	
298-SMW	3040.5	3045.5	2.407	2.717	18.29	0.224	
300-SMW	3050.5	3058.5	2.410	2.698	17.25	0.208	Silt
348-C0002P- (reaming)							
321-SMW	2105.5	2115.5	2.373	2.737	21.24	0.270	
325-SMW	2145.5	2155.5	2.341	2.676	20.31	0.255	
331-SMW	2185.5	2195.5	2.406	2.744	19.65	0.245	
335-SMW	2225.5	2235.5	2.365	2.702	20.09	0.251	
340-SMW	2265.5	2275.5	2.363	2.689	19.61	0.244	
345-SMW	2305.5	2315.5	2.387	2.705	18.90	0.233	
349-SMW	2345.5	2355.5	2.384	2.709	19.27	0.239	
356-SMW	2385.5	2395.5	2.360	2.696	20.09	0.251	
360-SMW	2425.5	2435.5	2.377	2.713	19.92	0.249	
365-SMW	2465.5	2475.5	2.412	2.726	18.46	0.226	
374-SMW	2545.5	2555.5	2.437	2.733	17.36	0.210	
381-SMW	2585.5	2595.5	2.397	2.705	18.35	0.225	
383-SMW	2605.5	2615.5	2.398	2.698	17.88	0.218	
387-SMW	2625.5	2635.5	2.426	2.727	17.69	0.215	
389-SMW	2645.5	2655.5	2.419	2.707	17.12	0.207	
391-SMW	2665.5	2675.5	2.413	2.698	17.03	0.205	
393-SMW	2685.5	2695.5	2.432	2.715	16.74	0.201	
399-SMW	2725.5	2735.5	2.428	2.697	16.04	0.191	
403-SMW	2765.5	2775.5	2.438	2.698	15.50	0.184	
407-SMW	2805.5	2815.5	2.428	2.705	16.47	0.197	
413-SMW	2845.5	2855.5	2.459	2.719	14.94	0.176	

Table T30. Moisture and density measurements of >4 mm DICAs/pillow cuttings, Hole C0002N.

Cuttings sample	Depth (mbsf)		Density (g/cm^3)		Porosity (%)	Void ratio
	Top	Bottom	bulk	grain		
348-C0002N-						
82-5MW	1225.5	1230.5	1.962	2.660	42.69	0.745
141-SMW	1505.5	1510.5	2.032	2.665	38.55	0.627
276-SMW	2090.5	2095.5	1.962	2.660	42.64	0.743

DICA = drilling-induced cohesive aggregate.

Table T31. Moisture and density measurements of cavings, Holes C0002N and Hole C0002P.

Cavings sample	Depth (mbsf)		Density (g/cm^3)		Porosity (%)	Void ratio
	Top	Bottom	bulk	grain		
348-C0002N-						
353-SMW	870.5	2330	2.292	2.700	24.33	0.322
353-SMW	870.5	2330	2.336	2.697	21.55	0.275
353-SMW	870.5	2330	2.309	2.693	22.99	0.299
348-C0002P-						
309-SMW	2163	3057.5	2.432	2.721	17.04	0.205
309-SMW	2163	3057.5	2.421	2.720	17.66	0.215
309-SMW	2163	3057.5	2.370	2.676	18.53	0.228
309-SMW	2163	3057.5	2.407	2.712	18.08	0.221
309-SMW	2163	3057.5	2.393	2.712	18.90	0.233
309-SMW	2163	3057.5	2.445	2.710	15.73	0.187
309-SMW	2163	3057.5	2.430	2.727	17.42	0.211
309-SMW	2163	3057.5	2.443	2.722	16.45	0.197
309-SMW	2163	3057.5	2.422	2.724	17.78	0.216
309-SMW	2163	3057.5	2.446	2.729	16.58	0.199
316-SMW	2163	3057.5	2.423	2.733	18.14	0.222
317-SMW	2163	3057.5	2.429	2.711	16.15	0.201

Table T32. Moisture and density measurements of discrete core samples, Holes C0002M and C0002P. (Continued on next page.)

Core, section, interval (cm)	Depth (mbsf)		Density (g/cm^3)		Porosity (%)	Void ratio
	Top	Bottom	bulk	grain		
348-C0002M-						
1R-1, 85–86	475.85	475.86	1.933	2.676	44.96	0.816
1R-1, 136–138	476.36	476.38	1.906	2.720	47.97	0.921
1R-2, 63–65	477.04	477.06	1.920	2.685	46.07	0.854
1R-2, 130–131	477.71	477.72	1.972	2.690	43.09	0.757
1R-3, 24–27	478.07	478.10	1.884	2.717	49.17	0.967
1R-3, 87–90	478.70	478.73	1.907	2.717	47.84	0.917
1R-4, 43–45	479.67	479.69	1.867	2.705	49.81	0.992
2R-1, 26–29	484.76	484.79	1.939	2.784	47.98	0.922
2R-1, 106–108	485.56	485.58	1.957	2.763	46.33	0.863
2R-2, 46–48	486.37	486.39	1.915	2.740	48.07	0.925
2R-2, 107–109	486.98	487.00	2.033	2.751	41.58	0.711
2R-3, 13–15	487.45	487.47	1.949	2.762	46.76	0.878
2R-3, 65–68	487.97	488.00	1.976	2.765	45.32	0.828
3R-1, 9–11	493.59	493.61	1.999	2.768	44.12	0.789
3R-1, 85–87	494.35	494.37	1.949	2.775	47.18	0.893
3R-2, 18—20	495.08	495.11	1.968	2.769	45.88	0.847
3R-2, 77–79	495.67	495.70	2.023	2.803	43.82	0.779
4R-1, 31–33	503.31	503.33	1.911	2.742	48.37	0.936
4R-1, 114–116	504.14	504.16	1.946	2.758	46.80	0.879
4R-2, 86–88	505.26	505.29	1.911	2.788	49.67	0.986
4R-2, 111–113	505.51	505.54	1.929	2.816	49.46	0.978
4R-3, 17.5–20	505.99	506.02	1.939	2.739	46.64	0.874
4R-3, 136–139	507.18	507.21	1.991	2.800	45.51	0.835

Table T32 (continued).

Core, section, interval (cm)	Depth (mbsf)		Density (g/cm^3)		Porosity (%)	Void ratio
	Top	Bottom	bulk	grain		
348-C0002P-						
1R-1, 5–7.5	2163.05	2163.08	2.377	2.718	20.12	0.252
2R-1, 29.5–33	2172.80	2172.83	2.161	2.710	32.57	0.483
2R-1, 112–115	2173.62	2173.65	2.296	2.723	25.09	0.335
2R-2, 59–61	2174.51	2174.53	2.256	2.737	28.06	0.390
2R-2, 104–106	2174.96	2174.98	2.420	2.745	18.88	0.233
2R-3, 19–21	2175.51	2175.53	2.325	2.701	22.46	0.290
2R-3, 137.5–141	2176.70	2176.73	2.381	2.734	20.61	0.260
2R-4, 73–77	2177.46	2177.50	2.310	2.742	25.14	0.336
2R-4, 130–133	2178.03	2178.06	2.394	2.771	21.58	0.275
3R-1, 24–27.5	2182.24	2182.28	2.375	2.723	20.52	0.258
3R-1, 93–96	2182.93	2182.96	2.407	2.743	19.56	0.243
3R-2, 62–64	2184.03	2184.05	2.424	2.732	18.02	0.220
3R-2, 106–108	2184.47	2184.49	2.362	2.737	21.89	0.280
4R-1, 39–44	2191.89	2191.94	2.407	2.743	19.55	0.243
4R-1, 75–77	2192.25	2192.27	2.370	2.709	20.11	0.252
4R-2, 39–41	2193.00	2193.02	2.374	2.721	20.44	0.257
4R-2, 96–98	2193.57	2193.59	2.364	2.715	20.79	0.262
4R-2, 135–142	2193.96	2194.03	2.252	2.708	27.10	0.372
4R-3, 9–12	2194.14	2194.17	2.397	2.737	19.85	0.248
4R-3, 73–77	2194.78	2194.82	2.346	2.718	21.96	0.281
4R-4, 32–35	2195.33	2195.36	2.235	2.730	29.03	0.409
4R-4, 111–113	2196.12	2196.14	2.379	2.735	20.77	0.262
4R-5, 27–31	2196.66	2196.70	2.291	2.715	25.06	0.335
4R-5, 128–129	2197.67	2197.68	2.299	2.702	24.00	0.316
4R-6, 17–24	2198.06	2198.13	2.380	2.700	19.10	0.236
4R-6, 54–60	2198.43	2198.49	2.363	2.714	20.73	0.262
5R-1, 95–101	2201.95	2202.01	2.342	2.718	22.17	0.285
5R-1, 127–129	2202.27	2202.29	2.312	2.768	26.11	0.353
5R-2, 10–15	2202.54	2202.59	2.302	2.750	25.92	0.350
5R-2, 99–104	2203.43	2203.48	2.302	2.728	24.99	0.333
5R-3, 0–7	2203.85	2203.92	2.317	2.724	23.96	0.315
6R-1, 4–6	2209.04	2209.06	2.287	2.731	25.98	0.351
6R-1, 77–79	2209.77	2209.79	2.266	2.741	27.66	0.382
6R-2, 37–39	2210.78	2210.80	2.326	2.713	22.93	0.298
6R-2, 38–41	2210.79	2210.82	2.313	2.709	23.52	0.308
6R-2, 104–106	2211.45	2211.47	2.355	2.719	21.50	0.274
6R-3, 37–39	2212.19	2212.21	2.320	2.708	23.07	0.300
6R-3, 138–141	2213.20	2213.23	2.321	2.704	22.80	0.295
6R-4, 15–20	2213.38	2213.43	2.314	2.722	24.01	0.316
6R-4, 103–108	2214.26	2214.31	2.160	2.683	31.52	0.460
6R-5, 27–30	2214.91	2214.94	2.264	2.729	27.29	0.375
6R-5, 94–101	2215.58	2215.65	2.350	2.745	22.93	0.298
6R-6, 18–20	2216.24	2216.26	2.294	2.700	24.23	0.320
6R-6, 77–81	2216.83	2216.87	2.347	2.712	21.66	0.276

Table T33. Electrical conductivity (10 kHz)and *P*-wave velocity measurements (230 kHz) on discrete samples, Site C0002. (Continued on next page.)

Core, section, interval (cm)	Depth (mbsf)		Temperature (°C)	Conductivity (S/m)			Conductivity anisotropy (%)		*P*-wave velocity (m/s)			*P*-wave anisotropy (%)	
	Top	Bottom		*x*	*y*	*z*	V	H	*x*	*y*	*z*	V	H
348-C0002M-													
1R-1, 136–138	476.36	476.38	21.3	0.690	0.727	0.548	25.6	–5.1		*1495*	*1474*		
1R-3, 24–26	478.05	478.07	21.4	0.687	0.688	0.544	23.3	–0.0	*1840*	*1839*			
2R-1, 26–28	484.76	484.79	20.8	0.716	0.735	0.486	39.6	–2.5			*1520*		
2R-2, 46–48	486.37	486.39	20.8	0.683	0.700	0.513	29.6	–2.4	*1526*		*1534*		
2R-3, 13–15	487.45	487.47	20.9	0.611	0.619	0.502	20.2	–1.2	*1949*	*1856*	*1738*	9.0	4.9
3R-1, 87–89	494.37	494.39	20.9	0.645	0.651	0.457	34.5	–1.0	*1443*	*1441*	*1469*		
3R-2, 14–16	495.045	495.065	21.0	0.588	0.613	0.515	15.2	–4.1	*1830*	*1872*	*1583*	15.6	–2.3
4R-3, 94–96	506.76	506.78	20.7	0.614	0.598	0.409	38.8	2.7			*1286*		
315-C0002B-													
17R-4, 16–18	622.89	622.91	21.4	0.717	0.729	0.562	25.0	–1.7	1863	1856	1751	6.0	0.4
19R-4, 71–73	641.44	641.46	21.6	0.929	1.006	0.847	13.2	–8.0					
20R-1, 99–101	647.99	648.01	21.2	0.589	0.657	0.559	10.8	–11.0	2021	1991	1913	4.7	1.5
20R-3, 124–126	651.07	651.09	21.5	0.563	0.571	0.463	20.2	–1.4	1956	1951	1867	4.5	0.2
21R-2, 92–94	658.83	658.85	21.6	0.723	0.726	0.552	26.9	–0.5	1948	1938	1795	7.9	0.5
21R-4, 122–124	660.53	660.55							1819	1877	1772	4.2	–3.1
22R-1, 6–8	666.06	666.08	21.4	0.606	0.625	0.543	12.6	–3.1	1994	2006	1913	4.5	–0.6
23R-2, 126–128	677.67	677.69	21.3	0.641	0.648	0.557	14.6	–1.0	2004	2015	1924	4.4	–0.5
23R-4, 60–62	678.84	678.86	21.5	0.655	0.652	0.484	29.9	0.4	2024	2047	1940	4.8	–1.1
24R-3, 68–70	687.01	687.03	21.3	0.683	0.731	0.604	15.7	–6.8	2017	1996	1931	3.8	1.1
24R-1, 87–89	685.37	685.39	21.3	0.707	0.714	0.581	20.1	–1.0	1955	1983	1876	4.8	–1.4
25R-1, 126–128	695.26	695.28	21.3	0.737	0.747	0.513	36.6	–1.3	1965	1981	1847	6.6	–0.8
26R-1, 122–124	704.72	704.74	21.2	0.721	0.747	0.540	30.5	–3.6	1936	1962	1869	4.2	–1.3
27R-1, 19–21	713.19	713.21	21.3	0.588	0.623	0.536	12.2	–5.9	1850	1869	1843	0.9	–1.0
27R-3, 63–65	715.06	715.08	21.4	0.531	0.550	0.438	20.9	–3.6	1858	1883	1789	4.4	–1.3
28R-1, 36–38	722.86	722.88	21.4	0.567	0.528	0.450	19.5	7.1	2182	2123	1973	8.7	2.7
28R-2, 47–49	724.38	724.40	21.4	0.631	0.640	0.534	17.3	–1.5	2024	2027	1907	6.0	–0.1
29R-1, 86–88	732.86	732.88	21.4	0.643	0.653	0.561	14.3	–1.5	2018	2025	1911	5.6	–0.3
30R-1, 106–108	742.56	742.58	21.2	0.545	0.551	0.491	11.0	–1.1	2059	1997	1912	5.9	3.0
31R-1, 102–104	752.02	752.04	21.3	0.609	0.548	0.470	20.6	10.6	2081	2010	1894	7.7	3.4
32R-2, 51–53	762.42	762.44	21.4	0.677	0.684	0.561	19.3	–1.0	2102	2124	1938	8.6	–1.0
32R-4, 75–77	764.06	764.08	21.5	0.714	0.746	0.601	19.5	–4.4	1990	2023	1918	4.5	–1.6
32R-6, 120–122	765.91	765.93	21.2	0.694	0.699	0.552	23.1	–0.7	2048	2072	1924	6.8	–1.2
33R-1, 53–55	770.53	770.55	21.3	0.769	0.760	0.521	37.9	1.1	2112	2125	1918	10.0	–0.6
37R-1, 133–135	806.83	806.85	21.5	0.627	0.697	0.519	24.2	–10.6	2179	2273	1995	10.9	–4.3
38R-1, 16–18	815.16	815.18	21.7	0.702	0.695	0.553	23.3	0.9	2097	2112	1969	6.7	–0.7
38R-5, 54–56	819.77	819.79	21.6	0.690	0.673	0.530	25.0	2.4	2203	2186	2025	8.0	0.8
40R-1, 130–132	835.30	835.32	21.3	0.606	0.620	0.468	26.9	–2.3	2053	2030	1831	10.9	1.1
40R-4, 5–7	836.87	836.89							2072	2054	1869	9.9	0.9
41R-2, 47–49	845.38	845.40	21.7	0.699	0.680	0.633	8.5	2.7	2066	2044	1996	2.9	1.1
42R-2, 117–119	855.58	855.60	21.4	0.633	0.649	0.549	15.5	–2.6	2064	2121	1960	6.5	–2.7
42R-5, 23–25	858.855	858.875							2112	2143	1910	10.8	–1.5
44R-2, 63–65	874.04	874.06	21.3	0.609	0.608	0.485	22.5	0.3	2217	2191	2011	9.1	1.2
44R-5, 12–14	877.76	877.78	21.6	0.652	0.657	0.523	22.4	–0.8	2087	2125	1972	6.6	–1.8
45R-4, 53–55	884.86	884.88	21.3	0.659	0.681	0.573	15.6	–3.3	2065	2056	1977	4.1	0.4
46R-1, 23–25	891.23	891.25	21.5	0.562	0.548	0.491	12.1	2.5	2163	2152	2029	6.1	0.5
46R-5, 78–80	896.00	896.02	21.4	0.563	0.559	0.474	16.8	0.6	2144	2155	2037	5.4	–0.5
47R-1, 121–123	901.71	901.73	21.4	0.611	0.583	0.504	16.9	4.7	2099	2109	1989	5.6	–0.5
47R-5, 59–61	906.73	906.75	21.3	0.586	0.624	0.481	22.8	–6.2	2132	2143	2020	5.7	–0.5
48R-1, 13–15	910.13	910.15	21.2	0.652	0.604	0.557	12.1	7.6	2098	2067	1955	6.3	1.5
48R-3, 124–126	914.07	914.09	21.3	0.593	0.677	0.594	6.7	–13.2	2053	2062	1934	6.2	–0.4
49R-1, 43–45	919.93	919.95	21.4	0.587	0.603	0.489	19.6	–2.5	2144	2137	2017	6.0	0.3
49R-4, 63–65	922.95	922.97	21.2	0.617	0.487	0.480	13.9	23.5	2147	2070	1996	5.5	3.6
51R-1, 92–94	939.42	939.44	21.5	0.751	0.732	0.598	21.4	2.5	1938	1917	1843	4.5	1.1
51R-7, 63–65	946.16	946.18	21.4	0.515	0.512	0.489	4.8	0.7	2236	2235	2208	1.3	0.0
56R-3, 55–57	987.61	987.63	21.6	0.366	0.377	0.341	8.5	–3.0	2872	2989	2618	11.3	–4.0
57R-1, 6–8	995.56	995.58							5548	5523	5542	–0.1	0.5
59R-3, 83–85	1012.16	1012.18	21.6	0.476	0.487	0.437	9.8	–2.2	2086	2042	1989	3.7	2.1
60R-2, 96–98	1016.37	1016.39	21.4	0.514	0.493	0.471	6.6	4.0	2109	2052	2048	1.5	2.7
61R-1, 96–98	1019.46	1019.48	21.7	0.513	0.529	0.455	13.6	–3.0	1867	1878	1872	0.0	–0.6
61R-5, 33–35	1023.06	1023.08	21.8	0.502	0.536	0.464	11.2	–6.4	2092	2074	2040	2.1	0.9
62R-1, 35–37	1023.35	1023.37	21.5	0.491	0.471	0.408	16.4	4.1	1981	1958	1961	0.4	1.1
62R-CC, 14–16	1026.13	1026.15	21.6	0.412	0.491	0.421	6.9	–17.4	2033	2097	1992	3.6	–3.1
63R-2, 17–19	1034.08	1034.10	21.5	0.444	0.468	0.390	15.6	–5.3	2141	2114	2010	5.7	1.3
63R-2, 67–69	1034.58	1034.60	21.5	0.533	0.542	0.461	15.2	–1.8	2167	2167	2084	3.9	0.0
64R-1, 68–70	1042.68	1042.70	21.9	0.564	0.563	0.490	14.0	0.3	2114	2177	2035	5.3	–2.9

Table T33 (continued).

Core, section, interval (cm)	Depth (mbsf)		Temperature (°C)	Conductivity (S/m)			Conductivity anisotropy (%)		*P*-wave velocity (m/s)			*P*-wave anisotropy (%)	
	Top	Bottom		*x*	*y*	*z*	V	H	*x*	*y*	*z*	V	H
65R-CC, 9–11	1049.45	1049.47	21.5	0.499	0.518	0.486	4.6	–3.9	2078	2125	2006	4.6	–2.3
65R-1, 68–70	1047.18	1047.20	21.4	0.637	0.630	0.559	12.5	1.1	2062	2000	1977	2.7	3.1
66R-1, 32–34	1051.32	1051.34	21.5	0.518	0.486	0.477	5.1	6.4	2228	2197	2164	2.2	1.4
338-C0002H-													
2R-1, 13–15	1100.63	1100.65	22.68	0.497	0.621	0.588	–5.1	–22.2	*2122*	*2225*	*2302*	–4.7	–5.7
2R-1, 26–28	1110.76	1110.78	22.2	0.569	0.642	0.444	30.7	–12.0	*2271*	*2307*	*2081*	–1.6	9.5
338-C0002J-													
1R-1, 12–15	902.12	902.15	21.7	0.712	0.507	0.468	26.3	33.6	*2111*	*2142*	*1966*	–1.5	7.8
1R-1, 45–52	902.45	902.52	21.9	0.459	0.464	0.506	–9.3	–1.1	*2016*	*2082*	*1927*	–3.2	6.2
1R-7, 87–90	904.67	904.7	21.8	0.587	0.411	0.355	33.8	35.4	*2074*	*2076*	*2051*	–0.1	1.1
1R-8, 0–2	904.99	905.01	21.8	0.617	0.373	0.309	46.4	49.4	*2040*	*2059*	*1922*	–0.9	6.4
2R-1, 53–55	907.53	907.55	21.8	0.399	0.325	0.569	–44.6	20.6	*2115*	*2175*	*2059*	–2.8	4.1
3R-1, 0–3	912	912.02	22.7	0.725	0.751	0.492	40.0	–3.5	*2143*	*2034*	*2100*	5.2	–0.5
4R-3, 85–87	918.61	918.63	22.7	0.799	0.793	0.708	11.6	0.7	*2004*	*2079*	*1963*	–3.7	3.9
5R-6, 91–94	924.09	924.12	22.6	0.436	0.580	0.332	42.0	–28.3	*2277*	*2290*	*2116*	–0.6	7.6
5R-8, 75–77	926.43	926.45	22.6	0.659	0.614	0.543	15.9	7.0	*2291*	*2196*	*2207*	4.2	1.6
348-C0002P-													
2R-2, 59–61	2174.51	2174.53	20.1	0.764	0.640	0.885	–23.0	17.7	2233	2266	2384	–5.8	–1.4
2R-2, 104–106	2174.96	2174.98	20.2	0.458	0.254	0.390	–9.0	57.4	2481	2406	2558	–4.6	3.1
2R-3, 137.5–139.5*	2176.70	2176.73	20						2021	2238	2020	5.3	–10.2
2R-3, 139.5–141*	2176.71	2176.73	19.7							2107	2249	–6.5	
2R-4, 73–77	2177.46	2177.50	20.3	0.351	0.418	0.406	–5.6	–17.5	1922	2095	2191	–8.7	–8.6
2R-4, 134–136	2178.07	2178.09	20.2	0.175	0.345	0.336	–25.5	–65.1	2256	2545	2509	–4.4	–12.1
3R-1, 92–94	2182.92	2182.94	20.2	0.272	0.150	0.249	–16.3	57.7	2818	2494	2827	–6.2	12.2
3R-2, 104–106	2184.45	2184.47	20.2	0.297	0.228	0.347	–27.6	25.9	2584	2100	2751	–16.1	20.7
4R-1, 73–75	2192.23	2192.25	19.9	0.239	0.222	0.248	–7.2	7.1	2425	2453	2592	–6.1	–1.2
4R-2, 39–41	2193.00	2193.02	20.3	0.291	0.192	0.307	–24.0	41.2	2656	2300	2612	–5.3	14.3
4R-4, 111–113	2196.12	2196.14	20.5	0.323	0.227	0.344	–22.2	34.7	2521	2431	2505	–1.2	3.6
4R-6, 22–24	2198.11	2198.13	20.9	0.243	0.247	0.338	–31.8	–1.4	2366	2547	2895	–16.4	–7.4
5R-1, 99–101	2201.99	2202.01	21.9						2035		2264	–10.7	
5R-4, 10–12†	2204.74	2204.76	20.3	0.307	0.325	0.376	–17.3	–5.8	2702	2738	2884	–5.9	–1.3
6R-2, 39–41	2210.80	2210.82	21.2	0.394	0.433	0.441	–6.3	–9.5	2411	2404	2341	2.8	0.3
6R-2, 125–127	2211.66	2211.68	20.8						1976	2380	2410	–10.1	–18.6
6R-3, 48–50	2212.30	2212.32	21.4	0.394	0.357	0.441	–16.0	10.0	2365	2499	2422	0.4	–5.5
6R-3, 138–140	2213.20	2213.22	21.5	0.440	0.289	0.403	–10.1	41.6	2319	2169	2253	–0.4	6.7
6R-4, 15–20	2213.38	2213.43	21.7	0.539	0.445	0.551	–11.3	19.0	2320	2362	2312	1.2	–1.8
6R-5, 103–105	2215.67	2215.69	21.7	0.233	0.427	0.409	–21.3	–58.8	2304	2705	2658	–6.0	–16.0
6R-6, 11–13	2216.17	2216.19	21.5	0.325	0.395	0.403	–11.3	–19.5	1927	2278	2251	–6.9	–16.7
6R-6, 82–84	2216.88	2216.90	21.4	0.265	0.183	0.262	–15.5	36.4	2344	2109	2391	–7.1	10.6
Cuttings cubes													
348-C0002P-													
107-SMW-1†	2220.5	2225.5	19.6	0.345	0.346	0.330	4.5	–0.3	2365				
109-SMW-1†	2230.5	2235.5	19.5	0.354	0.341	0.246	34.2	3.8	2530				
163-SMW-1†	2460.5	2465.5	20.1	0.279	0.276	0.196	–14.9	–35.1			2679		

* = sample oriented relative to fabric: *z* = across fabric, *x* = along slickenlines, *y* = orthogonal to *x* and *z*. † = *P*-wave measurements performed at 500 kHz. ‡ = sample oriented relative to bedding: *z* = across bedding, *x* and *y* in bedding plane. V = vertical, H = horizontal. Autopick values are indicated in italic.

Table T34. Electrical conductivity measurements (10 kHz) on cuttings, Holes C0002N and C0002P.

Cuttings sample	Piece	Depth (mbsf)		Lithology	Temperature (°C)	Conductivity (S/m)	Porosity (%)
		Top	Bottom				
348-C0002N-							
268-SMW	8	2050.5	2055.5	Siltstone	18.0	0.467	21.02
268-SMW	9	2050.5	2055.5	Claystone	18.0	0.753	38.25
268-SMW	10	2050.5	2055.5	Sandstone, fine	18.0	0.554	16.62
272-SMW	4	2070.5	2075.5	Sandstone	19.6	0.314	24.97
276-SMW	4	2090.5	2095.5	Mudstone	19.6	0.353	25.16
276-SMW	5	2090.5	2095.5	Sandstone, fine	19.6	0.321	22.42
348-C0002P-							
43-SMW	1	2070.5	2075.5	Mustone, silty	19.7	0.349	22.80
45-SMW	2	2080.5	2085.5	Mustone, silty	19.7	0.228	21.96
49-SMW	2	2100.5	2105.5	Mudstone	20.0	0.216	21.02
56-SMW	3	2120.5	2125.5	Sandstone, fine	20.0	0.303	23.22
58-SMW	3	2130.5	2135.5	Mudstone	19.9	0.180	18.90
72-SMW	4	2165.5	2170.5	Sandstone	20.1	0.274	19.91
73-SMW	2	2170.5	2175.5	Mudstone, silty	19.5	0.183	22.22
74-SMW	5	2175.5	2180.5	Mudstone	20.1	0.245	19.04
77-SMW	1	2185.5	2190.5	Mudstone	20.1	0.312	19.87
77-SMW	5	2185.5	2190.5	Mudstone, sandy	20.1	0.274	17.26
77-SMW	6	2185.5	2190.5	Sandstone	20.1	0.305	16.37
81-SMW	3	2190.5	2195.5	Mudstone	19.5	0.222	21.52
82-SMW	5	2195.5	2200.5	Mudstone	20.1	0.402	18.77
82-SMW	6	2195.5	2200.5	Sandstone	20.1	0.330	20.66
83-SMW	3	2200.5	2205.5	Mudstone, silty	19.6	0.171	23.17
83-SMW	4	2200.5	2205.5	Mudstone, silty	19.6	0.280	21.89
85-SMW	3	2205.5	2210.5	Mudstone	20.1	0.213	18.24
86-SMW	3	2210.5	2215.5	Mudstone	19.5	0.150	23.02
113-SMW	3	2250.5	2255.5	Sandstone	18.9	0.193	23.31
117-SMW	3	2270.5	2275.5	Mudstone, silty	18.9	0.230	22.48
125-SMW	3	2300.5	2305.5	Mudstone, sandy	18.9	0.316	25.74
138-SMW	3	2360.5	2365.5	Mudstone	19.0	0.203	24.70
143-SMW	3	2380.5	2385.5	Mudstone	19.1	0.228	23.38
155-SMW	3	2420.5	2425.5	Sandstone	20.3	0.532	25.20
163-SMW	1	2460.5	2465.5	Mudstone	20.0	0.184	17.99
168-SMW	2	2480.5	2485.5	Siltstone	20.3	0.216	17.71
172-SMW	1	2500.5	2505.5	Sandstone	21.2	0.475	25.33
174-SMW	1	2510.5	2515.5	Mudstone	21.3	0.211	21.18
174-SMW	3	2510.5	2515.5	Sandstone	21.4	0.324	24.48
185-SMW	5	2560.5	2565.5	Mudstone	21.5	0.276	19.16
185-SMW	6	2560.5	2565.5	Sandstone	21.5	0.335	21.01
198-SMW	3	2610.5	2615.5	Mudstone	21.1	0.256	18.97
198-SMW	5	2610.5	2615.5	Sandstone	21.1	0.511	26.19
204-SMW	3	2640.5	2645.5	Mudstone	21.1	0.213	16.10
213-SMW	1	2670.5	2675.5	Sandstone	21.2	0.332	21.52
213-SMW	2	2670.5	2675.5	Mudstone	21.0	0.285	20.44
221-SMW	4	2710.5	2715.5	Mudstone	21.1	0.152	17.81
229-SMW	3	2740.5	2745.5	Sandstone	21.1	0.249	16.42
231-SMW	1	2750.5	2755.5	Mudstone	20.8	0.208	18.01
240-SMW	1	2790.5	2795.5	Sandstone, silty	20.8	0.287	18.63
240-SMW	3	2790.5	2795.5	Mudstone	20.9	0.164	18.15
247-SMW	5	2820.5	2825.5	Mudstone	20.9	0.101	08.18
249-SMW	3	2830.5	2835.5	Mudstone	21.1	0.184	15.41
256-SMW	1	2860.5	2865.5	Mudstone	20.0	0.215	18.43
263-SMW	1	2890.5	2895.5	Mudstone, silty	21.0	0.187	16.98
267-SMW	1	2910.5	2915.5	Sandstone, silty	21.0	0.186	15.44
269-SMW	2	2920.5	2925.5	Sandstone	21.1	0.243	15.78
273-SMW	1	2940.5	2945.5	Siltstone	21.0	0.178	17.99
273-SMW	3	2940.5	2945.5	Siltstone	21.0	0.155	13.52
281-SMW	1	2970.5	2975.5	Mudstone, silty	21.1	0.195	15.56
283-SMW	1	2980.5	2985.5	Sandstone	21.1	0.172	13.72
289-SMW	3	3000.5	3005.5	Mudstone	21.1	0.121	14.11
293-SMW	3	3020.5	3025.5	Mudstone	21.0	0.245	19.35
298-SMW	1	3040.5	3045.5	Mudstone	21.1	0.241	17.27
298-SMW	3	3040.5	3045.5	Mudstone	21.0	0.190	16.88
300-SMW	1	3050.5	3058.5	Siltstone	21.0	0.141	17.37

Table T35. *P*-wave velocity measured on cuttings with autopick and manual first arrival pick, Holes C0002N and C0002P. (Continued on next two pages.)

Cuttings sample	Piece	Depth (mbsf)		Lithology	Frequency (kHz)	Velocity (m/s)		
		Top	Bottom			Autopick	Manual pick	Uncertainty
348-C0002N-								
196-SMW	1	1745.5	1750.5		500	2524	2484	266
196-SMW	1	1745.5	1750.5		230	2465	2408	251
196-SMW	2	1745.5	1750.5		500	3061	2890	284
196-SMW	2	1745.5	1750.5		230	2984	2951	294
196-SMW	3	1745.5	1750.5		500	3030	2956	318
196-SMW	3	1745.5	1750.5		230	2797	2889	306
268-SMW	1	2050.5	2055.5		230	2465	2914	278
268-SMW	2	2050.5	2055.5		230	2984	2804	254
268-SMW	3	2050.5	2055.5	Sandstone	230	2797	2669	276
268-SMW	4	2050.5	2055.5		500	2708	2605	199
268-SMW	4	2050.5	2055.5		230	2577	2672	206
268-SMW	5	2050.5	2055.5		500	2936	2960	395
268-SMW	5	2050.5	2055.5		230	2540	2980	398
268-SMW	6	2050.5	2055.5		500	2858	2586	229
268-SMW	6	2050.5	2055.5		230	2590	2785	263
268-SMW	7	2050.5	2055.5		500	2553	2467	181
268-SMW	7	2050.5	2055.5		230	2437	2539	192
272-SMW	1	2070.5	2075.5		500	3116	2888	241
272-SMW	2	2070.5	2075.5		500	2769	2682	188
272-SMW	3	2070.5	2075.5		500	2862	2644	222
276-SMW	1	2090.5	2095.5		500	2952	2823	305
276-SMW	2	2090.5	2095.5		500	2631	2484	182
276-SMW	3	2090.5	2095.5		500	2981	2848	227
348-C0002P-								
18-SMW	1	1990.5	1995.5	Cement	230	3821		
43-SMW	2	2070.5	2075.5		500	2532	2770	251
43-SMW	3	2070.5	2075.5		500	2333	2738	296
45-SMW	1a	2080.5	2085.5		500	2555	2664	206
45-SMW	1b	2080.5	2085.5		500	2798	2846	244
49-SMW	1	2100.5	2105.5		500	3138	2948	256
56-SMW	1	2120.5	2125.5		500	2912	2803	361
56-SMW	2	2120.5	2125.5		500	3396	2985	398
58-SMW	1	2130.5	2135.5		500	4526	4000	772
58-SMW	2	2130.5	2135.5		500	3712	3680	758
61-SMW	1	2140.5	2145.5		500	3265	3206	532
63-SMW	1	2150.5	2155.5		500	2892	2822	236
71-SMW	1	2162.5	2165.5		230	2805	2847	254
71-SMW	2	2162.5	2165.5		230	3200	3294	352
72-SMW	1	2165.5	2170.5	Mudstone	500	3824	3093	381
72-SMW	2	2165.5	2170.5	Sandstone	500	3259	2870	369
72-SMW	3	2165.5	2170.5	Sandstone	500	3394	2823	326
73-SMW	1	2170.5	2175.5		230		2924	349
74-SMW	1	2175.5	2180.5	Mudstone	500	2962	2484	271
74-SMW	2	2175.5	2180.5	Mudstone	500	3485	3088	403
74-SMW	3	2175.5	2180.5	Sandstone	500	2515	2440	199
74-SMW	4	2175.5	2180.5	Sandstone	500	3066	2782	239
76-SMW	1	2180.5	2185.5		230	3134	2938	258
76-SMW	2	2180.5	2185.5		230	2793	2551	175
77-SMW	1	2185.5	2190.5	Mudstone	500	2956	2586	229
77-SMW	2	2185.5	2190.5	Mudstone	500	3166	2848	207
77-SMW	3	2185.5	2190.5	Sandstone	500	3077	2951	243
77-SMW	4	2185.5	2190.5	Sandstone	500	3657	3476	442
81-SMW	1	2190.5	2195.5		230	2581	2571	177
81-SMW	2	2190.5	2195.5		230	2861	2808	313
82-SMW	1	2195.5	2200.5	Mudstone	500	3002	2855	187
82-SMW	2	2195.5	2200.5	Mudstone	500	3263	2851	248
82-SMW	3	2195.5	2200.5	Mudstone	500	3096	2937	276
82-SMW	4	2195.5	2200.5	Sandstone	500	2716	2513	283
83-SMW	1	2200.5	2205.5		230	2818	2875	228
83-SMW	2	2200.5	2205.5		230	3200	3296	364
85-SMW	1	2205.5	2210.5	Mudstone	500	2947	2691	189
85-SMW	2	2205.5	2210.5	Mudstone	500	3096	2836	296
86-SMW	1	2210.5	2215.5		230	2793	2794	183
86-SMW	2	2210.5	2215.5		230		2271	212
107-SMW	1x	2220.5	2225.5		230	2045	2365	103
107-SMW	1y	2220.5	2225.5		230	1840	2362	77

Table T35 (continued). (Continued on next page.)

Cuttings sample	Piece	Depth (mbsf)		Lithology	Frequency (kHz)	Velocity (m/s)		
		Top	Bottom			Autopick	Manual pick	Uncertainty
107-SMW	1z	2220.5	2225.5		230	1996	2371	124
109-SMW	1x	2230.5	2235.5		230	2061	2530	120
109-SMW	1y	2230.5	2235.5		230	1852	2590	94
109-SMW	1z	2230.5	2235.5		230	1712	2386	113
111-SMW	1	2240.5	2245.5		230	1869	2084	81
111-SMW	2	2240.5	2245.5		230	2701	2742	198
113-SMW	1	2250.5	2255.5		230	2338	2449	140
113-SMW	2	2250.5	2255.5		230	2186	2634	158
115-SMW	2	2260.5	2265.5		230	2033	2333	110
115-SMW	1	2260.5	2265.5		230	2254	2618	163
117-SMW	1	2270.5	2275.5		230		1824	83
117-SMW	2	2270.5	2275.5		230	2177	2771	198
121-SMW	1	2280.5	2285.5		230	2743	2759	231
121-SMW	2	2280.5	2285.5		230	2209	2638	163
123-SMW	1	2290.5	2295.5	Sandstone	230	4567	4521	404
125-SMW	1	2300.5	2305.5		230	2069	2165	122
125-SMW	2	2300.5	2305.5		230	2024	2199	117
129-SMW	1	2320.5	2325.5		230		2267	96
129-SMW	2	2320.5	2325.5		230	2060	2379	128
133-SMW	1x	2340.5	2345.5		230	2986	3101	193
133-SMW	1y	2340.5	2345.5		230	2320	2919	176
138-SMW	1	2360.5	2365.5		230		2193	119
138-SMW	2	2360.5	2365.5		230	2546	2461	154
143-SMW	2	2380.5	2385.5	Sandstone	230	1358	1969	99
143-SMW	1x	2380.5	2385.5		230		1853	49
143-SMW	1y	2380.5	2385.5		230		1840	42
143-SMW	1z	2380.5	2385.5		230		1753	66
155-SMW	1	2420.5	2425.5		500	2721	2581	152
155-SMW	1	2420.5	2425.5		230	2287	2511	145
155-SMW	2	2420.5	2425.5		500	1388	2198	125
155-SMW	2	2420.5	2425.5		230	1252	1817	87
163-SMW	1	2460.5	2465.5		500	2392	2679	176
163-SMW	1	2460.5	2465.5		230	2040	2375	139
163-SMW	2	2460.5	2465.5		230	1933	2168	93
168-SMW	1	2480.5	2485.5		500	1743	2412	126
168-SMW	1	2480.5	2485.5		230	1887	2230	108
172-SMW	1	2500.5	2505.5	Sandstone	500	2661	2446	223
174-SMW	1	2510.5	2515.5	Mudstone	500		2315	132
174-SMW	2	2510.5	2515.5	Sandstone	500	2231	2358	182
176-SMW	2	2520.5	2525.5	Sandstone	500	3221	2777	332
176-SMW	3	2520.5	2525.5	Sandstone	500	2972	2840	380
176-SMW	4	2520.5	2525.5	Mudstone	500	3394	3129	297
176-SMW	5	2520.5	2525.5	Mudstone	500	3212	2987	262
185-SMW	1	2560.5	2565.5	Mudstone	500	3002	2735	224
185-SMW	2	2560.5	2565.5	Mudstone	500	2778	2638	181
185-SMW	3	2560.5	2565.5	Sandstone	500		2405	119
185-SMW	4	2560.5	2565.5	Sandstone	500		2790	199
189-SMW	1	2580.5	2585.5	Mudstone	500	2267	2450	125
196-SMW	1	2601.5	2605.5	Mudstone	500	3150	2718	231
196-SMW	2	2601.5	2605.5	Sandstone	500	3083	2775	266
196-SMW	3	2601.5	2605.5	Sandstone	500	2732	2604	250
198-SMW	1	2610.5	2615.5	Mudstone	500	3084	2902	303
198-SMW	2	2610.5	2615.5	Mudstone	500		2503	176
198-SMW	3	2610.5	2615.5	Mudstone	500	2767	2833	226
198-SMW	4	2610.5	2615.5	Sandstone	500	2920	2680	187
198-SMW	5	2610.5	2615.5	Sandstone	500	2620	2466	252
200-SMW	1	2620.5	2625.5	Sandstone	500	3265	2962	335
202-SMW	1	2630.5	2635.5	Mudstone	500	4508	3875	606
202-SMW	2	2630.5	2635.5	Mudstone	500	4595	3680	758
204-SMW	1	2640.5	2645.5	Mudstone	500	2654	2546	121
204-SMW	2	2640.5	2645.5	Mudstone	500		2237	117
204-SMW	3	2640.5	2645.5	Mudstone	500	2566	2865	235
210-SMW	1	2660.5	2665.5	Mudstone	500	2349	2487	221
210-SMW	2	2660.5	2665.5	Mudstone	500		2313	187
213-SMW	1	2670.5	2675.5	Sandstone	500	4434	3813	896
213-SMW	2	2670.5	2675.5	Mudstone	500	2444	2646	160
215-SMW	1	2680.5	2685.5	Sandstone	500	2363	2419	100
217-SMW	1	2690.5	2695.5	Mudstone	500	3689	3063	463
219-SMW	1	2700.5	2705.5	Sandstone	500	3337	2870	369

Table T35 (continued).

Cuttings sample	Piece	Depth (mbsf)		Lithology	Frequency (kHz)	Velocity (m/s)		
		Top	Bottom			Autopick	Manual pick	Uncertainty
221-SMW	1	2710.5	2715.5	Mudstone	500	5315	4049	1041
221-SMW	2	2710.5	2715.5	Sandstone	500	2529	2317	144
221-SMW	3	2710.5	2715.5	Sandstone	500	3136	2579	276
224-SMW	1	2720.5	2725.5	Mudstone	500	3372	2717	255
229-SMW	1	2740.5	2745.5	Sandstone	500	5283	4462	633
229-SMW	2	2740.5	2745.5	Sandstone	500	3270	3000	500
231-SMW	1	2750.5	2755.5	Mudstone	500	3192	3060	408
233-SMW	1	2760.5	2765.5	Siltstone	500	2971	2598	312
233-SMW	2	2760.5	2765.5	Siltstone	500	3571	3365	464
235-SMW	1	2770.5	2775.5	Mudstone	500	2471	2519	218
235-SMW	2	2770.5	2775.5	Mudstone	500	3856	3114	450
237-SMW	1	2780.5	2785.5	Mudstone	500	3156	2797	317
240-SMW	1	2790.5	2795.5	Sandstone	500	3622	3429	493
240-SMW	2	2790.5	2795.5	Sandstone	500	4633	3819	405
240-SMW	3	2790.5	2795.5	Mudstone	500	3025	2747	242
240-SMW	4	2790.5	2795.5	Siltstone	500	3575	3238	336
240-SMW	5	2790.5	2795.5	Mudstone	500	3750	3362	384
240-SMW	6	2790.5	2795.5	Mudstone	500	3171	2960	395
244-SMW	1	2810.5	2815.5	Mudstone	500	3971	3099	543
247-SMW	1	2820.5	2825.5	Mudstone	500	2217	2829	182
247-SMW	2	2820.5	2825.5	Mudstone	500	2933	2641	222
247-SMW	3	2820.5	2825.5	Mudstone	500	3195	3016	324
247-SMW	4	2820.5	2825.5	Sandstone	500	3460	3164	246
249-SMW	1	2830.5	2835.5	Mudstone	500	3240	2986	216
249-SMW	2	2830.5	2835.5	Mudstone	500	3809	3274	350
251-SMW	1	2840.5	2845.5	Mudstone	500	3900	3546	616
251-SMW	2	2840.5	2845.5	Sandstone	500	5761	4094	671
254-SMW	1	2850.5	2855.5	Sandstone	500	4071	3813	896
256-SMW	1	2860.5	2865.5	Mudstone	500	2266	2722	216
259-SMW	1	2870.5	2875.5	Sandstone	500	2918	2825	270
261-SMW	1	2880.5	2885.5	Mudstone	500	5342	4211	862
261-SMW	2	2880.5	2885.5	Sandstone	500	4231	4172	1708
263-SMW	1	2890.5	2895.5	Mudstone	500	2779	2946	351
267-SMW	1	2910.5	2915.5	Siltstone	500	3316	3218	388
269-SMW	1	2920.5	2925.5	Sandstone	500	3822	3286	454
269-SMW	2	2920.5	2925.5	Siltstone	500	3894	3581	591
269-SMW	3	2920.5	2925.5	Mudstone	500	3855	3353	653
273-SMW	1	2940.5	2945.5	Siltstone	500	2428	2668	168
273-SMW	2	2940.5	2945.5	Siltstone	500	4386	3750	705
279-SMW	1	2960.5	2965.5	Sandstone	500	3496	3076	476
279-SMW	2	2960.5	2965.5	Sandstone	500	3078	2902	421
281-SMW	1	2970.5	2975.5	Mudstone	500	4991	3926	759
281-SMW	2	2970.5	2975.5	Sandy mudstone	500	3501	3098	279
283-SMW	1	2980.5	2985.5	Sandy mudstone	500	3237	3167	390
283-SMW	2	2980.5	2985.5	Sandstone	500			
289-SMW	1	3000.5	3005.5	Mudstone	500	3144	3271	603
289-SMW	2	3000.5	3005.5	Mudstone	500	5051	3828	787
293-SMW	1	3020.5	3025.5	Mudstone	500	2937	2680	265
293-SMW	2	3020.5	3025.5	Mudstone	500	4387	3945	810
293-SMW	3	3020.5	3025.5	Mudstone	500	3533	3141	454
298-SMW	1	3040.5	3045.5	Mudstone	500	4558	4024	629
298-SMW	2	3040.5	3045.5	Mudstone	500	3582	3321	404
300-SMW	2	3050.5	3055.5	Siltstone	500	3603	3287	531

Table T36. Thermal conductivity measurements, Holes C0002M and C0002P.

Core, section, interval (cm)	Depth (mbsf)	Thermal conductivity (W/[m·K])
348-C0002M-		
1R-2, 108.0	477.49	1.53
1R-4, 23.0	479.47	1.47
2R-1, 110.0	485.60	1.44
3R-1, 23.0	493.73	1.49
3R-2, 61.5	495.52	1.58
4R-3, 113.0	506.95	1.56
348-C0002P-		
2R-1, 50.0	2173.00	1.59
3R-2, 109.0	2184.50	1.82
4R-2, 105.0	2193.66	1.73
4R-4, 1.0	2195.02	1.78
5R-3, 10.0	2203.95	1.80
6R-2, 111.0	2211.52	1.63
6R-5, 0.0	2214.64	1.74

Table T37. Comparison of natural gamma radiation (NGR) measurements (uncorrected for background) between Expeditions 348 and 338.

Material	NGR (counts/s)	
	Expedition 348	Expedition 338
Water-filled liner (background)	34.89	32.63
Granite	139.06	133.21
Mud water	51.93	50.66

Table T38. Summary of LWD/MWD data files and included parameters, Hole C0002N.

Data	Raw	Processed	Depth reference	Logs included	Data included	Available formats
Real time	X		BRT	Run 1 (2840–3976 m BRT) Run 2 (3976–4297 m BRT) Trip out (3531–3770 m BRT)	Depth, rate of penetration, gamma radiation, 27 and 39 inch phase resistivity, EWR formation exposure time, EWR tool temperature, annular pressure, annular equivalent circulation density, true vertical depth	LAS
Memory data	X	X	Raw: BRT Processed: mbsf	Run 1 (2840–3976 m BRT) Run 2 (3976–4297 m BRT) Trip out (3531–3770 m BRT)	Depth; rate of penetration; gamma radiation; uncorrected gamma radiation; 9, 15, 27, and 39 inch phase and attenuation resistivity; EWR tool temperature; EWR data density; EWR formation exposure time; annular pressure; annular equivalent circulation density; true vertical depth	LAS
Time	X		BRT	Run 1 (2840–3976 m BRT) Run 2 (3976–4297 m BRT) Trip out (3531–3770 m BRT)	Time, depth, rate of penetration, 27 and 39 inch phase resistivity, EWR exposure time, EWR tool temperature, gamma radiation, annular pressure, annular equivalent circulation density, true vertical depth	ASCII
Geopilot	X		BRT	Run 1 (2840–3976 m BRT)	Depth, true vertical depth, inclination	LAS

BRT = below rig table. EWR = electromagnetic wave resistivity. LAS = log ASCII standard.

Table T39. Summary of LWD/MWD data files and included parameters, Hole C0002P.

Data	Raw	Processed	Processing by	Depth reference	Logs included	Data included	Available formats
Real time	X			BRT	Main (4130–4266.4 m BRT)	Depth; at-bit resistivity; shallow resistivity; gamma radiation; rotations per minute; torque, EWR tool temperature; EWR formation exposure time; 16, 24, 40, and 48 inch phase resistivity; rate of penetration; weight on bit; true vertical depth; compressional slowness	LAS/DLIS
Memory data	X	X	LSS	BRT, mbsf	Main (4130–5026 m BRT)	Depth; gamma radiation; rotations per minute; torque; EWR tool temperature; EWR formation exposure time; annular pressure; annular equivalent circulation density; 16, 24, 32, 40, and 48 inch phase and attenuation resistivity (2 MHz, 500 kHz, and 250 kHz); rate of penetration; weight on bit	LAS/DLIS
Sonic		X	Halliburton	BRT, mbsf	Main (4130–5026 m BRT)	Depth, compressional slowness, reference shear slowness, V_P/V_S ratio, compressional velocity, shear velocity, sonic caliper (minimum, maximum, and average ellipse diameter)	LAS/DLIS
Image Log		X	Halliburton, LSS	BRT, mbsf	Main (4130–5026 m BRT)	At-bit resistivity, ring resistivity, borehole electrical resistivity image	LAS/DLIS/PDF
Time	X			BRT	Main (4130–5026 m BRT)	Time, depth, rate of penetration, 27 and 39 inch phase resistivity, EWR exposure time, EWR tool temperature, gamma radiation, annular pressure, annular equivalent circulation density, true vertical depth	ASCII
Survey	X			BRT	Main (3904–5026 m BRT)	Depth, true vertical depth, inclination	PDF

BRT = below rig table. LSS = logging staff scientist, EWR = electromagnetic wave resistivity. DLIS = digital log information standard, LAS = log ASCII standard.

Table T40. Long borehole exposure events, Holes C0002N and C0002P.

Hole	Depth (mbsf)	EWR exposure time (h)	Reason for long exposure
348-			
C0002N	1205–1221	15	Borehole conditioning
	1662–1678	28.5	Maintenance
	1992–2008	50	Wait on weather/maintenance
	2022–2038	8.5	Mud-loss treatment
C0002P	2163–2218.5	>66.25	Cored interval exposed before reaming
	2601.5–2619	5.5	Borehole conditioning

EWR = electromagnetic wave resistivity.

Table T41. Low, high, and average gamma ray and R39PC resistivity values by units and subunits, Hole C0002N.

Log unit	Depth (mbsf)	Log subunit	Depth (mbsf)	Gamma radiation (gAPI) Low	High	Average	R39PC resistivity (Ωm) Low	High	Average
III	872.0–915.0			40.1	78.7	61.6	0.86	1.5	1.2
IV	915.0–1656.3	IVa	915.0–1036.5	48.9	83.5	66.6	1.1	2.2	1.6
		IVb	1036.5–1099.4	44.3	84.7	67.2	1.3	2.5	1.6
		IVc	1099.4–1360.5	49.7	86.4	67.4	1.3	2.9	1.8
		IVd	1360.5–1514.0	48.7	84.8	65.8	1.5	4.0	2.0
		IVe	1514.0–1656.3	50.9	83.2	65.3	2.0	5.5	2.7
V	1656.3–total depth	Va	1656.3–1942.5	63.6	100.7	84.0	1.4	5.1	2.2
		Vb	1942.5–2191.0	67.7	102.0	87.0	1.4	4.7	2.5
		Vc	2191.0–total depth	76.6	108.6	91.0	1.8	7.5	2.6

Table T42. Depth ranges and minimum, maximum, and mean values for gamma radiation, acoustic *P*-wave, and resistivity (RH48PC), Hole C0002P.

Log unit	Depth (mbsf)	Log subunit	Depth (mbsf)	Gamma radiation (gAPI) Low	High	Mean	Acoustic *P*-wave (µs/ft) Low	High	Mean	RH48PC resistivity (Ωm) Low	High	Mean
V	2163–total depth	Vc′	2163.0–2365.6	58	94	84	83.7	109.8	94.3	1.4	3.6	2.5
		Vd	2365.6–2753.0	69	102	87	84.4	104.1	92.9	1.4	4.6	2.2
		Ve	2753.0–3058.5	81	104	95	79.7	106.2	94.2	1.9	4.0	2.6